MODULATION OF MOLECULAR MOBILITY IN SUCROSE-BASED AMORPHOUS SOLIDS DETECTED BY PHOSPHORESCENCE OF ERYTHROSIN B

by

YUMIN YOU

A Dissertation submitted to the

Graduate School-New Brunswick

Rutgers, The State University of New Jersey

in partial fulfillment of the requirements

for the degree of

Doctor of Philosophy

Graduate Program in Food Science

Written under the direction of

Professor Richard D. Ludescher

And approved by

_____

_____

_____

_____

New Brunswick, New Jersey

October, 2007

ABSTRACT OF THE DISSERTATION

MODULATION OF MOLECULAR MOBILITY IN SUCROSE-BASED AMORPHOUS SOLIDS DETECTED BY PHOSPHORESCENCE OF ERYTHROSIN B

by YUMIN YOU

Dissertation Director:

Dr. Richard D. Ludescher

This project studied the temperature and composition dependence of molecular mobility in amorphous sucrose. Phosphorescence of erythrosin B provided parameters sensitive to localized molecular mobility in the glass and to more global modes of mobility activated at the glass transition and provided evidence of dynamic site heterogeneity in amorphous sucrose solids. In sucrose-based binary matrices, plasticizer (glycerol), salts (NaCl, $CaCl_2$, $MgCl_2$, Na-citrate, Na-acetate, Na-phosphates), maltodextrins (DE 5 to 18), protein (gelatin), and polysaccharides (xanthan and high amylose starch) were selected to investigate how variations in nature and content of each additive influence the molecular mobility as well as dynamic site heterogeneity in amorphous sucrose matrix.

Measurements of phosphorescence intensity, lifetime, and emission energy were made in amorphous sucrose-additive films containing the probe erythrosin B. Results

showed the complex effects of additives on the mobility in a hydrogen-bonded sugar matrix. Glycerol exhibited an antiplasticization effect shown as decreased mobility at glycerol/sucrose mole ratio ≤ 0.27 and at temperature ≤ 45°C. On the contrary, all the polymers studied, including gelatin, xanthan and high amylose starch, displayed a 'plasticization' effect (increasing mobility) at very low while a rigidification effect (decreasing mobility) at higher concentration without significant change in T_g. Maltodextrins, mixtures of molecules with a variety of molecular weights, increase the mobility in spite of their high T_g. Sodium chloride showed a strong rigidification effect on the sucrose matrix; however, this effect was weakened at mole ratio NaCl/sucrose above 0.5. Other salts showed effects resulting from a compromise between two opposite actions (decreasing mobility due to salt itself and increasing mobility due to absorbed moisture). All above behaviors are difficult to interpret using T_g alone. Molecular mobility appears to be more accurate to evaluate the physical stability of the matrix.

Phosphorescence of erythrosin B was also able to report dynamic site heterogeneity that is an intrinsic property of the amorphous solid state. The heterogeneity was be evaluated by the variation of lifetime and lifetime heterogeneity across the excitation and emission band and the temperature dependence of bandwidth and lifetime heterogeneity. The composition influence on the dynamic site heterogeneity was discussed as well.

ACKNOWLEDGEMENTS

I am deeply indebted to my major advisor, Dr. Richard D. Ludescher, for his guidance and support throughout the course of my studies at Rutgers University. He plays an important role in switching my interests to this difficult research area. He opens the door for me and leads me to explore new viewpoints of food science. During the period of working in his lab, he always generously spares his time to discuss the complicated results and explain abstract concepts with great patience. His flexibility and open-door policy in offering advice are tremendously helpful in completing this dissertation. I would like to say Dr. Ludescher is not only my advisor but also my mentor.

I would like to thank Dr. Paul Takhistov, Dr. Qingrong Huang, and Dr. Koushik Seetharaman, for their willingness to be my committee members, and for their valuable suggestions and help on this project. Their input made this work more interesting and challenging, and undoubtedly contributed to the comprehensiveness of the project.

I would also like to thank USDA for financial support.

I would like to express my appreciation to Kristine Lukasik, Sonali Shirke, Tom Nack, Kasi Sundaresan, Rashmi Tiwari, Melinda Ligneres and Sanaz Jalalian for their help on the lab work.

Lastly, I would like to express my gratitude for my husband, Qingbin Yuan, my daughter, Xiaochen Yuan, my mother, Huiqin Zhou, and my sister's family for their constant love and strong support that made the four-year life in Rutgers much easier to go through.

To all my friends, I would like to say thank you for sharing my joys and hardships.

TABLE OF CONTENTS

LIST OF TABLES

LIST OF FIGURES

Figure **Page**

Figure **Page**

Figure **Page**

Figure **Page**

Introduction

1. Why study molecular mobility?

Due to its unique physical properties, amorphous phase modulates the functional properties of a lot of biomaterials including foods (Slade and Levine, 1995; Roos, 1995; Fennema, 1996; Peleg, 1996), pharmaceuticals (Towns, 1995; Craig et al., 1999), hydrated seed tissues and even whole organisms (Crowe et al., 1998; Buitink et al., 1999, 2000; Walters, 2004). Amorphous solids can be obtained through physical processes such as rapid cooling, extrusion and drying. They can also be introduced unintentionally by routine manufacturing operations, such as coating, granulation, milling and lyophilization (Hancock and Zografi, 1997). The latter phenomena may be even more common. Amorphous solids thus have prevalent influence on the physical and chemical properties of most of biological materials.

It is now generally recognized that molecular mobility is associated with the stability of amorphous biomaterials. The stability and quality of amorphous solids are modulated by specific physical processes and chemical reactions involving the translational diffusion, rotational motions or intramolecular motions (Shalaev and Zografi, 1996). For instance, the occurrence of crystallization, one typical physical process, requires molecules to diffuse and orient to form an orderly crystalline structure. In fluid solutions with low viscosity, diffusion is much faster than reaction rate and thus exerts no effect on reaction rate; while in the amorphous solids of extremely high viscosity, change in viscosity influences diffusion significantly and thus diffusion becomes the rate-limiting step in the reactions.

2. What is the advantage and limitations of T_g?

Compared with crystals, amorphous region in foods is metastable and subject to physical, chemical and biological deteriorations affected by chemical structure and composition, environment factors and molecular mobility (Ludescher et al., 2001). For almost 30 years, the influence of molecular mobility on the degradative reactions is simply incorporated into the thermodynamic phase transition phenomena. The glass transition temperature T_g for pure matrix or T_g' for freeze-dried matrix is taken as a useful index temperature to indicate food stability: foods are thought stable at $T<T_g$; above T_g, physical changes or chemical reactions take place at a rate varied with temperature difference ($\Delta T=T-T_g$). Plasticizers such as water and other small molecules modulate reaction rates by lowering T_g.

Undoubtedly T_g, as a simple and direct protocol for food stability, has significant impact on food industry: providing a straightforward method to evaluate the stability of food systems. Thus the complicated issue about food quality attributes change during processing and storage is simplified to a process of determining T_g and storing the food at temperature below T_g to obtain a desirable shelf-life. Several excellent reviews have described the effort made in this field (Slade et al., 1989; Slade & Levine, 1991, 1995; Fennema, 1996).

Recently, however, the increasing studies come to a different conclusion. Hancock and Zografi (1997) proposed that "the attempts to scale reaction kinetics to T_g may be inappropriate" since some reactions still happen below T_g. Also Le Meste and colleagues concluded that "these results have been interpreted and extrapolated to suggest that the T_g is not a universal predictive parameter of the physical stability of glassy food"

(Roudaut et al., 1999a). And "the mobility changes related to the glass transition can be regarded as either suitable or inadequate predictors depending on the processes considered" (Roudaut et al., 2004). Some researchers considered that Kauzmann temperature T_k, a temperature at which the degree of molecular motion is reduced to a level equivalent to that of the crystalline state, was a better benchmark for safe storage (Shamblin et al., 1999; Walters, 2004). And it was also proposed that more parameters such as T_g, T_k, molecular mobility and configurational entropy need to be examined rather than individual one (Zhou et al., 2002).

For physical processes such as crystallization of amorphous sucrose (Saleki-Gerhardt and Zografi, 1994) or cornstarch (Jouppila and Roos, 1997), T_g acts as a relatively trustworthy index temperature for stability: reflecting the onset temperature for translational motion of the molecules engaged in the degradative process. Zografi and colleagues reported one exception, however. They found significant crystallization of indomethacin from dry amorphous powders over several days at $T<T_g$ (Yoshioka et al., 1994). Aso et al. have studied the correlation between the crystallization rates of amorphous nifedipine, phenobarbital, and flopropione, and their molecular mobility below T_g using both NMR and enthalpy relaxation (Aso et al., 2000).

For those food systems in which small solute molecules embedded in an amorphous polymer matrix, T_g may not work appropriately to indicate stability. Le Meste et al. studied the molecular mobility in low-moisture white bread based on a multispectroscopy method (Roudaut et al., 1999b). They found that sub-T_g relaxation existed in the polymer matrix; water remained mobility even in glassy samples and the secondary relaxation was sensitive to the water content. It seemed that molecular

mobility rather than T_g modulated the physical properties such as the texture and mechanical behavior and thus influenced stability during storage. This phenomenon may be interpreted theoretically based on the characteristics of polymer matrix. In the glassy state, a polymer matrix may have insufficient free volume for translational motion of the entire molecule, however, it may have sufficient free volume for local conformation changes that allow small solute molecules to diffuse and react.

More evidences were obtained from chemical reactions occurred in the glassy state. Bell and Hageman (1994) investigated aspartame degradation in amorphous poly (vinyl pyrrolidone) with different molecular weights and found that reaction rate was primarily dependent on water activity rather than T_g. Franks and colleagues (Streefland et al. 1998) studied the kinetics of two reactions: Asn-Pro peptide bond hydrolysis and unimolecular dissociation of 2-(4-nitrophenocy) tetrahydrofuran in freeze-concentrated carbohydrates below and above T_g'. Results showed these two different types of reactions involving a covalent bond cleavage occurred below T_g but exhibited no significant enhancement in rate near T_g. In the latter reaction excipients with low T_gs unexpectedly exhibited the best stabilization. The authors considered matrix density as the major factor responsible for the differences. Lai et al. (1999a,b) investigated the effects of water, plasticizer glycerol content, and T_g on the rate of hydrolytic deamidation of asparagines in the hexapeptide VYPNGA in lyophilized amorphous solids of poly(vinyl alcohol)(PVA) and poly(vinyl pyrrolidone)(PVP). They also found clear evidence for deamidation of the peptide in the glassy state of both polymers. In the glassy polymers with similar T_gs, the rate increased with water content, indicating that water mobility in the glassy state contributed to deamidation reactivity.

Similar evidences were also observed in carbohydrate-based matrixes. Lim and Reid (1991) examined the cryostabilization potential of maltodextrin and CMC in a frozen system. Although CMC provided a T_g' as same as maltodextrin (DE10), it did not show any stabilizing effect in protein aggregation and non-enzymatic oxidation while maltodextrin showed significant cryostabilization behavior in the same chemical reactions. Duddo et al. (1997a, 1997b) compared the protein stability in sucrose and trehalose glasses and found that the mobility in trehalose glass below T_g is greater than that in sucrose glass although trehalose has a higher T_g than sucrose. Biliaderis et al. (1999) studied the rate of oxidation of ascorbic acid in the presence of starch hydrolyzates and unexpectedly found that the reaction rate increased with decreasing DE of the starch hydrolyzates matrix in spite of the inverse relationship between T_g' and DE.

Extra available data about stability in glassy amorphous solids do not show a clear relationship with T_g, either. Chang et al. (1996) examined stability of freeze-dried recombinant human interleukin-1 receptor antagonist in a variety of matrixes and found that protein deamidation and aggregation occurred in some formulations below T_g. Strickley & Anderson (1996, 1997) studied the mechanism of insulin stability in amorphous freeze-dried powders. They found that hydrolytic deamidation and dimerization proceeded in both the glassy and rubbery states; however, these two kinds of reactions showed different sensitivity to the mobility. The deamidation reaction via unimolecular processes required very low mobility and predominated in the glassy solids while the bimolecular dimerization reaction need more mobility and higher energy to react and then predominated in more mobile environment above T_g.

In a study of enzyme stabilization in different amorphous matrixes, Schebor et al. (1997) found that lactase and invertase lost their activities in the glassy state; and enzyme thermal stability appeared to be dependent on the heating temperature per se rather than ΔT (=T- T_g). The authors concluded that T_g was limited as a threshold temperature to predict enzyme inactivation. Sun and Davidson (1998) reported that the stability of glucose-6-phosphate dehydrogenase in glass sugar matrixes was modulated by the chemical composition rather than T_g. In spite of their similar T_g's, enzyme in glucose: trehalose (1:10) glassy matrix showed more stability than in glucose: sucrose (1:10) glassy matrix, which might be resulted from the lower free volume and lower molecular mobility of the trehalose glass.

All the above evidences demonstrate that there is a restriction in application of T_g as a predictive index temperature for stability. For those uniformly diffusion-dependent processes, such as most of physical processes and some chemical reactions with low activation energies (8-25kJ/mol, Fennema, 1996), T_g may be a trustworthy tool to indicate stability. However, for some diffusion-limited processes such as Maillard reaction, crystallization and recrystallization, moisture migration, enzymatic activity, sugar bloom in chocolate, cracking of foods during drying, staling of breads, and collapse of structure (Fennema, 1996), along with many reactions that are complicated and not diffusion-limited, T_g should not be considered as a reliable approach to predict stability.

As a bulk property, the glass transition temperature T_g may well account for the thermomechanical behavior of amorphous solid foods, but it can not map the overall molecular mobility in the glassy matrix and always underestimate the molecule motions. For real amorphous solid foods, composition variety and structural heterogeneity make

them dynamically complex. A variety of components result in a wide T_g range instead of a single value. The highly heterogeneous structure exhibits the length scale from nanometers to centimeters; and the structural elements may exist in different kinds of states, such as glassy/crystalline state, rubbery/melting states, and liquid states, even at a uniform temperature and a_w (Ludescher et al., 2001). Therefore it is not appropriate to use a single index temperature T_g to describe molecular mobility.

3. Molecular mobility in carbohydrate-based glassy solids

Carbohydrates can be found in almost all foods and sugars with low molecular weight play an important role in manufacturing of various sweet foods and stabilization of frozen foods. Molecular mobility in sugar glasses is particularly important in controlling stability of amorphous foods with low moisture content. There is some evidence of mobility in sugars at temperature below T_g. For instance, sucrose was found to have significant molecular mobility in glass down to T_g-50K from enthalpy relaxation (Hancock et al., 1995). And sucrose mobility in glass was also found to decrease upon addition of molecules (trehalose, PVP, dextran) with higher T_g (Shamblin & Zografi, 1998). Its zero-mobility temperature (T_0), estimated as 3.5ºC from width of glass transition, is much lower than the T_g of 64ºC. Similarly, trehalose has T_0 estimated as 44ºC, a value significantly lower than the T_g of 101ºC (Hatley, 1997).

3.1. Molecular mobility and molecular structure & interaction

A study of carbohydrate glasses using Fourier transform infrared microspectroscopy (FTIR) showed that the glass transition is associated with hydrogen bonding interaction between the sugar OH groups rather than the Van der Waals' interactions between CH groups (Wolkers et al., 1997). Another study of mobility of

maltose-water mixture with ^{1}H NMR suggested the formation of a stable hydrogen-bond network between sugar molecules in the glassy state; while water molecules weaken this network and increase the mobility of the hydroxyl protons of maltose (Van den Dries et al., 1998). Ekdawi-Sever et al. (2003) compared the diffusive behavior of sucrose and α, α-trehalose in aqueous solutions by means of pulsed-gradient-spin-echo NMR, and they found that when dissolved in water, sucrose shows higher mobility due to its small hydration number and more compact shape. These interactions present in aqueous solutions may also exist in amorphous glasses and influence the mobility.

3.2. Molecular mobility and relaxation

Molecular mobility is a complicated event associated with relaxation process. According to Crankshaft model applied in polymers, molecule is a collection of mobile segments that have some degree of free movement. When the free volume is restricted at very low temperature, only localized bond movements (bending and stretching) occur within the scale of a single repeat unit. This so called γ transition is mainly studied in polymers and is limited to very small motions within the molecule or with bound water (Schartel and Wendorff, 1995). As free volume increases along with temperature, the whole side chains and localized groups have enough space to move, resulting in the β transition. This transition "is considered as the activation barrier for solid-phase reactions, deformation, flow or creep, acoustic damping, physical aging changes, and gas diffusion into polymers when the activation energy for the transition and these processes are usually similar" (Menard). Compared with primary α- relaxation with higher activation energy which is usually associated with the cooperative global translational

motions of the matrix molecule, β-relaxation is a secondary relaxation which requires less activation energy (Champion et al., 2003).

Similar relaxation phenomena are also found in amorphous food solids: α-relaxation and β-relaxation have been reported in small carbohydrate matrixes (Chan et al., 1986; Gangasharan and Murthy, 1995; Noel et al., 1996; Moran, 2000). However, there is no agreement in the origin and nature of two relaxations. Gangasharan and Murthy (1995) identified the α-relaxation as a non-Arrhenius process while Noel et al. (1992) considered it Arrhenius in all sugar systems. As for the β-relaxation, several models have been proposed for its occurrence, including Johari model related to lower density region and William model related to small angle rotation (Gangasharan and Murthy, 1995).

There are additional evidence of β-relaxation existing in carbohydrates: β-relaxations at sub-Tg temperatures of D-glucose (T_β= -62ºC), D-fructose (T_β= -50ºC), D-mannose (T_β= -63ºC), L-rhamnose (T_β= -70ºC), glucitol (T_β= -30ºC) and maltose (T_β= -50ºC) from dielectric relaxation (Noel et al., 2000); β-relaxations in the glass of maltitiol (T_β ranged from -160 to 0°C) (Correia et al., 2000) and D-sorbitol (T_β ranged from -160 to -50°C) from thermally stimulated depolarization currents (TSDC) (Correia et al., 2001); β-relaxations in the glass of dextran (T_β= -94ºC), pullulan (T_β= -73ºC), and amylose (T_β= -59ºC) from dynamic mechanical and dielectric relaxation spectroscopy (Scandola et al., 1991); β –transition in glassy bread and wheat starch (T_β= -53ºC) from dielectric relaxation (Roudaut et al., 1999b).

3.3. Molecular mobility motions

Although the sugar matrix may be "frozen" in the glassy state and translational motions are severely restricted, there are still some motions to be considered, including the vibrational modes of the three dimensional sugar lattice, and internal rotational modes of side chains. Based on the results of normal mode analysis, an asymmetric molecule has three modes of translational mobility, three modes of rotational mobility and 3N-6 modes of vibrational mobility where N is the number of atoms in the molecule (McCammon & Harvey, 1987). Food molecules, especially macromolecules, consist of a large number of groups linked by different forces and interactions, and the complexity of the molecule motion is thus enormous. If only vibrational mobility is considered, monosaccharide glucose (N=24) has 66 normal modes, disaccharide sucrose (N=45) has 129, oligosaccharide raffinose (N=66) has 192, and polysaccharide amylose ($N \geq 10^5$) has more than 3×10^5.

Vibrational modes may have little impact on the overall mobility of an amorphous matrix; however, it may play an important role in modulating local matrix mobility via rotation of side groups and side chains, and conformation interconversion. At low temperature ($T<T_g$) or lower plasticizer concentration, the localized modes of vibrational mobility that require little free volume may be predominant. For small carbohydrate molecules, they are ranged from localized bond vibrations (stretching and bending) or hydroxyl group and hydroxymethyl group rotations to larger region or segmental vibrations of the molecule. For large molecules, more bond vibrations (e.g. glycosidic bonds) and side group rotations (e.g. side chain structure) get involved. At higher temperatures ($T \geq T_g$) or higher plasticizer content, the free volume increases to allow translational mobility modes (large scale motion) being activated and the glass transition

occurs (Zallen, 1998). Different type of motions activates different transitions with corresponding onset temperature of T_g/T_α, T_β and T_γ (less important).

4. Hypothesis and research model

In this proposal, we hypothesize that physical properties of amorphous solids are modulated by specific modes of molecular mobility above and below the glass transition temperature T_g. Phosphorescence of the triplet probe erythrosin B can provide information about sucrose matrix mobility (dipolar relaxation and collisional quenching mobility) as well as dynamic site heterogeneity due to its high sensitivity and site selectivity. Amorphous sucrose is selected as a major model to investigate the temperature-dependence, plasticizer-dependence, salt-dependence, polymer-dependence of molecular mobility.

Sucrose is one of the most widely used disaccharides in foods, biomaterials and pharmaceuticals for long-term storage (Noel et al., 2000). Sucrose is also the major compound in foods responsible for many degradation reactions including crystallization, caking/lumping, structural collapse, and stickiness (Roos, 1995; Fennema, 1996; Goff and Sahagian, 1996; Labuza et al., 2004). In most low moisture and frozen foods, sucrose always exists in an amorphous or partially amorphous state. By forming amorphous, non-crystalline solids, sucrose acts as an effective protectant for biological materials as well as building a basis for the confection industry (Crowe et al., 1998). Investigation of mobility in amorphous sucrose is of fundamental interest because it relates to questions of stabilization in the biological materials as well as degradation phenomena in amorphous foods.

5. How to measure molecular mobility?

A number of techniques have been applied to measure the properties and molecular mobility of amorphous materials. Spectroscopic techniques such as nuclear magnetic resonance (NMR) (Karger and Ludemann, 1991; Hills and Pardoe, 1995; van den Dries et al., 2000; Hills et al., 2001; Margulies et al., 2000; Richert, 2001; Suihko et al., 2005), Fourier transform infrared (FTIR) (Wolkers et al., 1998; Ottenhof, et al., 2003), Raman (Tsujimi et al., 1999), and electron spin resonance (ESR) (Contreras-Lopez et al., 2000) and fluorescence recovery after photobleaching (FRAP) (Champion et al., 1997), are valuable in the characterization of amorphous systems due to their high structural resolution. Usually they are used to determine the glass transition temperature T_g, the temperature-dependent mean molecular relaxation times, and the percent of amorphous content; and they can provide information about different modes of motion. Thermal analytical methods including differential scanning calorimetry (DSC) are simply used to measure the glass transition temperature T_g and other fundamental thermodynamic properties (e.g. enthalpy changes and heat capacity) (Shamblin et al., 1999; Baek et al., 2004). Thermomechanical analysis (TMA) can be used to study the relaxation processes and measure the initial crystallinity of an amorphous sample. Dielectric relaxation and dynamic mechanical spectroscopy are widely used to study the glass transition and secondary thermal transitions because of their high sensitivity to the lower order molecular mobility (Noel et al., 1996, 2000; Champion, et al., 2003). Recently a dielectric related technique thermally stimulated depolarization currents (TSDC) has been used to resolve a broad global relaxation into its different individual components, fractions or segments (Correia et al., 2000, 2001).

Luminescence using molecular probe to determine the physical properties of amorphous materials becomes more and more common. The probe with well-characterized spectroscopic properties can indirectly report the properties of the molecular environment around the probe (Slavik, 1994). Probe techniques have the advantage of providing information on a molecular level. Luminescence, both fluorescence and phosphorescence, can provide site-specific information about molecular mobility in different time regimes. Recently phosphorescence spectroscopy has been used to monitor the rate of dielectric relaxation around the excited triplet state of luminescent probes doped within supercooled liquids and amorphous solids (Richert, 2000). Phosphorescence spectroscopy is a sensitive, site-specific method. Those fully characterized molecular probes, such as tryptophan, fluorescein-isothiocyanate (FITC), 1-anilino-8-naphthalene sulfonic acid (ANS), and cis-parinaric acid (CPA), are able to provide detailed information about chemical and physical environments and therefore they are currently used in biophysical and biochemical research. Erythrosin B is perhaps the most commonly used phosphorescent probe of the molecular mobility of water-soluble and membrane-bound proteins. For instance, incorporation of erythrosin B in amorphous gelatin films can provide information about molecular mobility and oxygen diffusion (Simon-Lukasik and Ludescher, 2004). Erythrosin B has also been used to monitor the molecular mobility and dynamic heterogeneity in amorphous sucrose (Shah and Ludescher, 1995; Pravinata et al., 2005), maltose and maltitol (Shirke et al., 2005), and lactose and lactitol (Shirke, 2005). In this project phosphorescent probe erythrosin B is selected to monitor the molecular mobility in amorphous sucrose and sucrose-based solids.

6. Basic Photophysics

Probe luminescence (fluorescence and phosphorescence) is fully characterized by its intensity, energy (wavelength), and polarization (Strasburg and Ludescher, 1995). Each of these signals can provide information about the rate of molecular mobility of either the probe or its immediate local environment (Wehry, 1990; Ludescher, 1990; Lakowicz, 1999). In this project emission intensity and emission energy will be explored to characterize the molecular mobility in amorphous solids.

Figure 1 shows the Jablonski energy level diagram which depicts the photophysical events occurring during luminescence. Fluorescence emission from an excited singlet state usually occurs with a lifetime of 10^{-9} to 10^{-8} s while phosphorescence emission from an excited triplet state occurs with a longer lifetime ranging from 10^{-5} to 1 s. Phosphorescence is thus more suited to monitor slower molecular motions characteristic of amorphous solids. Along with fluorescence (rate k_{RF}), there are other de-excitation pathways including internal conversion from S_1 to S_0 (rate k_{IC}), intersystem crossing from S_1 to T_1 (rate k_{ST1}) and collisional quenching by oxygen (rate $k_{O_2}[O_2]$, where $[O_2]$ is the concentration of quencher oxygen). Along with phosphorescence (rate k_{RP}), occurs the de-excitation processes including non-radiative decay from T_1 to S_0 (rate k_{TS0}), reverse intersystem crossing from T_1 to S_1 (rate k_{TS1}) and collisional quenching by oxygen (rate $k'_{O_2}[O_2]$).

6.1. Emission Energy (Wavelength)

The energy (inverse of wavelength) of the excited state is modulated by dipolar interaction between the probe and the matrix as well as by the molecular structure of

probe. Prior to excitation, the ground state of the probe is effectively stabilized by dipolar (or more generally dielectric) interactions between the probe and the matrix (Lakowicz, 1999). Upon photo-excitation, a new excited state with novel electronic distribution is rapidly (10^{-15} s) created within an environment optimized for the ground state. The newly formed excited state, which is at higher energy due to these unfavorable interactions, can be stabilized by dipolar reorientation (dipolar relaxation) in the matrix that generates new interactions that specifically stabilize the excited state (Demchenko, 1988a, b). This dipolar relaxation, however, can only influence the emission energy if it occurs on the time scale of the excited state lifetime. Therefore, a fluorescence spectrum is only affected by fast dipolar relaxation while a phosphorescence spectrum is affected by much slow dipolar relaxation rates.

The occurrence of dipolar relaxation on the time scale of probe luminescence is most easily measured using red-edge excitation (described below) (Demchenko, 1988b). By using red-edge excitation (at 530 and 560nm), the difference in emission energy indicates that some erythrosin B molecules reside in the low energy environments and stay for periods of time longer than the triplet state lifetime due to the slow relaxation around the excited triplet state. Figure 5 in Chapter 1 shows the red-edge effect of phosphorescence emission of erythrosin B as a function of temperature in amorphous sucrose film and in 66% sucrose solution. The decrease in energy difference with increasing temperature reflects a faster relaxation at $T>T_g$, indicating the rate of dipolar relaxation increased significantly in the sucrose melt. The red-edge effect for erythrosin B in 66% sucrose solution was insignificant and close to zero, indicating a fast solvent

relaxation within the viscous solution. Dipolar relaxation in sucrose matrix may result from reorientation of hydroxyl groups in sucrose molecules.

In a summary, an analysis of probe fluorescence or phosphorescence emission spectra as a function of excitation wavelength (red-edge excitation) can indicate the presence of matrix dipolar relaxation on the time scale of the probe emission lifetime. And analysis of emission spectra as a function of temperature, along with the phosphorescence intensity decay (following a stretched exponential function with time constant τ and stretching factor β) provides a direct quantitative measurement of the rate of matrix dipolar relaxation (1/φ) due to hydroxyl group reorientation around the probe excited state.

6.2. Emission intensity

The emission intensity is described by the emission quantum yield (Q), the probability that a molecule will emit a photon following photo excitation to S_1. For fluorescence, the quantum yield is a simple ratio of the rate for fluorescence (k_{RF}) divided by the sum of all deexcitation rates for the singlet state (Lakowicz, 1999):

$$Q_F = \frac{k_{RF}}{k_{RF} + k_{IC} + k_{ST1} + k_{O_2}[O_2]} \quad (1)$$

The quantum yield for phosphorescence emission (Q_p) is the product of the quantum yield for T_1 formation (Q_T) times the probability of emission from T_1 (q_P) (Birks, 1970):

$$Q_p = Q_T q_P = \{\frac{k_{ST1}}{k_{RF} + k_{IC} + k_{ST1} + k_{O_2}[O_2]}\}\{\frac{k_{RP}}{k_{RP} + k_{TS0} + k_{TS1} + k'_{O_2}[O_2]}\} \quad (2)$$

Where in the absence of oxygen, an efficient quencher of the triplet state, equation 2 simplifies to:

$$Q_P = \{\frac{k_{ST1}}{k_{RF} + k_{IC} + k_{ST1}}\}\{\frac{k_{RP}}{k_{RP} + k_{TS0} + k_{TS1}}\} \quad (3)$$

The quantum yield for delayed fluorescence (Q_{DF}) is the product of the quantum yield for fluorescence (Q_F) times the probability of intersystem crossing from S_1 to T_1 and the probability of reverse intersystem crossing from T_1 to S_1(Duchowicz et al., 1998):

$$Q_{DF} = Q_F\{\frac{k_{ST1}}{k_{RF} + k_{IC} + k_{ST1}}\}\{\frac{k_{TS1}}{k_{RP} + k_{TS0} + k_{TS1}}\} \quad (4)$$

Comparison of emission intensities for delayed fluorescence (I_{DF}) and phosphorescence (I_P) provides information about the rate constant for reverse intersystem crossing (k_{TS1}):

$$\frac{I_{DF}}{I_P} = \frac{Q_F\{\frac{k_{ST1}}{k_F}\}\{\frac{k_{TS1}}{k_P}\}}{\{\frac{k_{ST1}}{k_F}\}\{\frac{k_{RP}}{k_P}\}} = Q_F\frac{k_{TS1}}{k_{RP}} \quad (5)$$

This ratio is highly temperature-dependent and can be described by the following equation:

$$\frac{I_{DF}}{I_P} = Q_F\frac{k_{TS1}}{k_{RP}} = \{\frac{Q_F}{k_{RP}}\}k_{TS1}{}^0\exp(-\frac{\Delta E_{TS}}{RT}) \quad (6)$$

A plot of ln (I_{DF}/I_P) versus 1/T has slope of - ΔE_{TS}/R. The energy gap between S_1 and T_1 ΔE_{TS} can be calculated from the slope.

The rate constants k_{RF}, k_{RP} and k_{ST1} are fixed by the probe structure and largely unaffected by environment (Birks, 1970; Turro, 1991). Increase in non-radiative decay will result in lower luminescence intensity.

Phosphorescence intensity decays are non-exponential, a stretched exponential function, or Kohlrausch-Williams-Watts decay function is selected to analyze the intensity decay (Richert, 2000; Lee, et al., 2001).

$$I(t) = I_0 \exp(-(t/\tau)^{\beta}) + \text{constant} \quad (7)$$

Where I_0 is the initial amplitude, τ is the stretched exponential lifetime, and β is an exponent varying from 0~1 and characterizing the distribution of lifetime. The use of a stretched exponential model provides a direct measurement of continuous distribution of lifetimes, which is appropriate for describing a complex glass possessing a distribution of relaxation times for the dynamic molecular processes. The smaller the β value, the more non-exponential the intensity decays and the broader the distribution of lifetimes.

Rate constants are determined in part from analysis of time-resolved measurements of the luminescence emission decay (Lakowicz, 1991). The excited state lifetime for phosphorescence is directly related to the de-excitation rate constant.

$$\tau_P = (k_P)^{-1} = (k_{RP} + k_{TS0} + k_{TS1} + k_{O_2}[O_2])^{-1} \quad (8)$$

$$k_{TS1} = k_{TS1}{}^{0} \exp(-\frac{\Delta E_{TS}}{RT}) \quad (9)$$

It is simple (Parker, 1968; McCaul & Ludescher, 1999) to determine rates for phosphorescence emission, non-radiative decay, and oxygen quenching using equation 8: the total decay rate k_P is inversely proportional to lifetime; k_{RP} can be calculated from emission lifetime at very low temperature when non-radiative rates are negligible, for erythrosin B the value is fixed at $41 s^{-1}$(Duchowicz et al., 1998; Lettinga et al, 2000); k_{TS1} is calculated using Arrhenius expression (Eq. 9) (ΔE_{TS} is obtained from Eq. 6). k_{TS0} is then calculated from the emission lifetime in the absence of O_2; and $k_{O_2}[O_2]$ is calculated

from emission lifetime in the presence of O_2. Rate k_{TS0} consists of two terms: one for processes internal to the molecule itself (e.g. vibrational coupling between the excited state and the ground state) and the other for processes due to interaction between the probe molecule and its environment (e.g. energy dissipated from the excited state to the surrounding matrix). The magnitude of k_{TS0} thus provides a measure of matrix mobility.

In summary, analysis of the probe phosphorescence lifetimes thus provides a direct measurement of the rate of collisional quenching (k_{TS0}) between the matrix and the solute probe. A comparison of lifetimes in the presence and absence of oxygen provides a direct measurement of the rate of oxygen quenching ($k_{O2}[O_2]$).

7. Research Methods

7.1. Preparation of amorphous thin films

Thin films of amorphous solid sucrose and sucrose mixtures will be used as model systems for amorphous solid sucrose-based foods (candies, materials used for flavor encapsulation, etc). They are optically clear to provide an excellent medium for optical spectroscopy. Sucrose solution is prepared by dissolving the purified sucrose with a high concentration in the water. Luminescent probe is added at a molar ratio of 1 part in10^4. A drop of solution is placed on a quartz slide and another identical slide is placed on top of the drop. After drawing two slides horizontally to opposite directions, two films are generated with a thickness ranging from 10μm to 40μm. The slides are gently dried using a heat gun and stored over P_2O_5 for at least 7 days. The slide with film is fit diagonally in a standard 1cm x 1cm fluorescence cuvette for luminescence measurement. The transparent thin films are non-porous and thus facilitate measurement of bulk

amorphous phase properties without interference of surface effects. Glassy films of sucrose mixtures such as sucrose-glycerol and sucrose-salt binary systems are made using this technique as well.

7.2. Optical probe

Erythrosin B (tetra-iodofluorescein), containing xanthene structure, is selected as probe of mobility on the 10^{-5}-10^{-3} s phosphorescence time scale due to its large extinction coefficient and high phosphorescence quantum yield in solution. Previous studies (Shah and Ludescher, 1995; Ludescher et al., 2001; Pravinata et al., 2005; Shirke, 2005) have shown its effectiveness as a probe to provide insight into both the overall molecular mobility and dynamic site heterogeneity within amorphous sucrose and other biomaterials.

8. Research Objectives

In this project, a single-component model (pure sucrose) and a series of binary system models have been established to investigate how temperature and various co-existing components affect the molecular mobility in hydrogen bonded sucrose matrix. The research objectives were listed as follows:

Objective 1: Temperature dependence of molecular mobility in pure sucrose;

Objective 2. Investigate the factors that may influence the luminescence measurement;

Objective 3. Influence of plasticizer (glycerol) on molecular mobility;

Objective 4. Influence of salts on molecular mobility;

Objective 5. Influence of maltodextrin on molecular mobility;

Objective 6. Influence of polymers on molecular mobility.

9. Summary

This project will provide a novel set of luminescence methods useful for measuring the rates of specific modes of matrix vibrational molecular mobility in amorphous solid foods. It will provide a series of mobility maps in which the rates of these modes of molecular mobility are plotted on a temperature versus composition state diagram for sucrose, sucrose-plasticizer, sucrose-salt, sucrose-maltodextrin, sucrose-protein and sucrose-hydrocolloids. Results may bring out a more reliable tool to evaluate food stability. This project also provides the background for developing a novel class of optical sensors useful for measuring food mobility in a rapid and non-invasive manner.

References

Aso, Y., Yoahiok, S., and Kojima, S. 2000. Relationship between the crystallization rate of amorphous nifedipine, phenobarbital, and flopropione, and their molecular mobility as measured by their enthalpy relaxation and ^{1}H NMR relaxation times. *J. Pharm. Sci.* 89,408-416.

Baek, M.H., Yoo, B., and Lim, S.T. 2004. Effects of sugars and sugar alcohols on thermal transition and cold stability of corn starch gel. *Food Hydrocolloids.* 18, 133-142.

Bell, L.N. and Hageman, M.J. 1994. Differentiating between the effects of water activity and glass transition dependent mobility on a solid state chemical reaction: aspartame degradation. *J. Agric. Food Chem.* 42, 2398-2401.

Biliaderis, C.G., Swan, R.S. and Arvanitoyannis, I. 1999. Physicochemical properties of commercial starch hydrolyzates in the frozen state. *Food Chem*. 64, 537-546.

Birks, J.B. 1970. *Photophysics of aromatic molecules*. John Wiley & Sons, NY.

Buitink, J., Hemminga, M.A. & Hoekstra, F.A. 1999. Characterization of molecular mobility in seed tissues: an electron paramagnetic resonance spin probe study. *Biophysical J*. 76, 3315-3322.

Buitink, J., Leprince, O., Hemminga, M.A., and Hoekstra, F.A. 2000. Molecular mobility in the cytoplasm: an approach to describe and predict lifespan of dry germplasm. *Plant Biology*. 97 (5), 2385-2390

Champion, D., Hervet, H., Blond, G., Le Meste, M. and Simatos, D. 1997. Translational diffusion in sucrose solutions in the vicinity of their glass transition temperature. *J. Phys. Chem. B.* 101, 10674-10679.

Champion, D., Maglione, M., Niquet, G., Simatos, D., and Le Meste, M. 2003. Study of α- and β-relaxation processes in supercooled sucrose liquids. J. *Therm. Anal. Cal*. 71, 249-261.

Chan, R.K., Pathmanthan, K. and Johari, G.P. 1986. Dielectric relaxations in the liquid and glassy states of glucose and its water mixtures. *J. Phys. Chem.* 90, 6358-6362.

Chang, B.S., Beauvais, R.M., Dong, A., and Carpenter, J.F. 1996. Physical factors affecting storage stability of freeze-dried interleukin-1 receptor antagonist: glass transition and protein conformation. *Arch. Biochem. Biophys*. 331, 249-258.

Contreras-Lopez, E., Champion, D., Hervet, H., Blond, G., and Le Meste, M. 2000. Rotational and translational mobility of small molecules in sucrose plus polysaccharide solutions. *J. Agric. Food Chem.* 48, 1009-1015.

Correia, N.T., Alvarez, C., Ramos, J.J.M., & Descamps, M. 2000. Molecular motions in molecular glasses as studied by thermally simulated depolarization currents (TSDC). *Chem. Phys.* 252, 151-163.

Correia, N.T., Alvarez, C., Ramos, J.J.M., & Descamps, M. 2001. The β-α branching in D-sorbitol as studied by thermally stimulated depolarization currents (TSDC). *J. Phys. Chem. B.* 105, 5663-5669.

Craig, D.Q., Royall, P.G., Kett, V.L., & Hopton, M.L. 1999. The relevance of the amorphous state to pharmaceutical dosage forms: glassy drugs and freeze-dried systems. *Intl. J. Pharma.* 179, 179-207.

Crowe, J.H., Carpenter, J.F. and Crowe, L.M. 1998. The role of vitrification in anhydrobiosis. *Ann. Rev. Physiol.* 60, 73-103.

Demchenko, A.P. 1988a. Site-selective excitation: a new dimension in protein and membrane spectroscopy. *Trends Biochem. Sci.* 13,374-377.

Demchenko, A.P. 1988b. Red-edge excitation fluorescence spectroscopy of single-tryptophan proteins. *Eur. J. Biophys.* 16, 121-129.

Duchowicz, R., Ferrer, M.L., and Acuna, A.U. 1998. Kinetic spectroscopy of erythrosin phosphorescence and delayed fluorescence in aqueous solution at room temperature. *Photochem. Photobiol.* 68, 494-501.

Duddu, S.P., and Dal Monte, P.R. 1997a. Effect of glass transition temperature on the stability of lyophilized formulations containing a chimeric therapeutic monoclonal antibody. *Pharm. Res.* 14(5), 591-595.

Duddu, S.P., Zhang, G., and Dal Monte, P.R. 1997b. The relationship between protein aggregation and molecular mobility below the glass transition temperature of lyophilized formulations containing monoclonal antibody. *Pharm. Res.* 14(5), 596-600.

Ekdawi-Sever, N, de Pablo, J.J., Feick, E., and von Meerwall, E. 2003. Diffusion of sucrose and α, α-trehalose in aqueous solutions. *J. Phys. Chem. A.* 107, 936-943.

Fennema, O. 1996. Water and Ice. In *Food Chemistry*, 3rd Edition (O. Fennema, editor). Marcel Dekker, Inc. N.Y.

Gangasharan and Murthy, S.S.N. 1995. Nature of relaxation processes in the supercooled liquid and glassy states of some carbohydrates. *J. Phys. Chem.* 99, 12349-12354.

Goff, H.D., & Sahagian, M.E. 1996. Glass transition in aqueous carbohydrate solutions and their relevance to frozen food stability. *Thermocchim. Acta.* 280/281, 449-464.

Hancock, B.C., Shamblin, S.L. and Zografi, G. 1995. Molecular mobility of amorphous pharmaceutical solids below their glass transition temperatures. *Pharm. Res.* 12, 799-806

Hancock, B.C. and Zogarfi, G. 1997. Characteristics and significance of the amorphous state in pharmaceutical systems. *J. Pharma Sci.* 86 (1), 1-12.

Hatley, R.H. 1997. Glass fragility and the stability of pharmaceutical preparations-excipient selection. *Pharm. Develop. Tech.* 2, 257-264.

Hills, B.P. and Pardoe, k. 1995. Proton and deuterium NMR studies of the glass transition in a 10% water-maltose solution. *J. Molec. Liquids.* 63, 229-237.

Hills, B.P., Wang, Y.L., and Tang, H.R. 2001. Molecular dynamics in concentrated sugar solutions and glasses: an NMR field cycling study. *Molec. Phys.* 99(19), 1679-1687.

Jouppila, K. and Roos, Y.H. 1997. The physical state of amorphous cornstarch and its impact on crystallization. *Carbohydr. Polym.* 32, 95-104.

Karger, N. and Ludemann, H.D. 1991. Temperature dependence of the rotational mobility of the sugar and water molecules in concentrated aqueous trehalose and sucrose solutions. *Z. Naturforsch.* 46c, 313-317.

Labuza, T., Roe, K., Payne, C., Panda, F., Labuza, T.J., Labuza, P.S., and Krusch, L. 2004. Storage stability of dry food systems: influence of state changes during drying and storage. Proceedings of the 14th international drying symposium (IDS 2004) Sao Paulo Brazil. 22-25 August. Vol A. pp. 48-68.

Lai, M.C., Hageman, M.J., Schowen, R.L., Borchardt, R.T., and Topp, E.M. 1999a. Chemical stability of peptides in polymers. 1. Effect of water on peptide deamidation in poly(vinyl alcohol) and poly(vinyl pyrrolidone) matrixes. *J. Pharm. Sci.* 88, 1073-1080.

Lai, M.C., Hageman, M.J., Schowen, R.L., Borchardt, R.T., Laiard, B.B., and Topp, E.M. 1999b. Chemical stability of peptides in polymers. 2. Discriminating between solvent and plasticizing effects of water on peptide deamidation in poly (vinyl pyrrolidone). *J. Pharm. Sci.* 88, 1081-1089.

Lakowicz, J.R. 1999. *Principles of Fluorescence Spectroscopy*. Plenum Press, NY.

Lee, K.C.B., J. Siegel, S.E. D.Webb, S.Leveque-Fort, M.J.Cole, R.Jones, K. Dowling, M.J.Lever and P.M.W. French. 2001. Application of the stretched exponential function to fluorescence lifetime imaging. *Biophys. J.* 81, 1265-1274.

Lettinga, M.P., Zuilhof, H., and van Zandvoort, M.A.M.J. 2000. Phosphorescence and fluorescence characterization of fluorescein derivatives immobilized in various polymer matrices. *Phys. Chem. Chem. Phys.,* 2: 3697-3707.

Lim, M.H. & Reid, D.S. 1991. Studies of reaction kinetics in relation to the Tg' of polymers in frozen model systems. *Adv. Exp. Med. Biol.* 302:103-22.

Ludescher, R.D. 1990. Triplet anisotropy as a probe of the rotational motion of soluble proteins. *Spectroscopy.* 5(3), 20-31.

Ludescher, R.D., Shah, N.K., McCaul, C.P., & Simon, K.V. 2001. Beyond T_g: optical luminescence measurements of molecular mobility in amorphous solid foods. *Food Hydrocolloids.* 15, 331-339.

Margulies, M.M., Sixou, B., David, L., Vigier, G., Dolmazon, R., and Albrand, M. 2000. Molecular mobility of sorbitol and maltitol: A ^{13}C NMR and molecular dynamics approach. *Eur. Phys. J.E.* 3, 55-62.

McCammon, J.A. and Harvey, S.C. 1987. *Dynamics of proteins and nucleic acids*. Cambridge Univeristy Press, Cambridge.

McCaul, C.P. and Ludescher, R.D. 1999. Room temperature phosphorescence from tryptophan and halogenated tryptophan analogs in amorphous sucrose. *Photochem Photobiology*, 70, 166-171.

Menard, K.P. Dynamic mechanical analysis basics: part 2 thermoplastic transitions and properties.(http://las.perkinelmer.com/content/ApplicationNotes/ThermomechanicalAnalysis%20PETech-91.PDF)

Moran, G.R., Jeffrey, K.R., Thomas, J.M., and Stevens, J.R. 2000. A dielectric analysis of liquid and glassy solid of glucose/water solutions. *Carbohydr. Res.* 328, 573-584.

Noel, T.R., Ring, S.G., and Whittam, M.A. 1992. Dielectric relaxations of small carbohydrate molecules in the liquid and glassy states. *J. Phys. Chem.* 96, 5662-5667.

Noel, T.R., Parker, R, and Ring, S.G. 1996. A comparative study of the dielectric relaxation behaviour of glucose, maltose, and their mixtures with water in the liquid and glassy states. *Carbohydr. Res.* 282, 193-206.

Noel, T.R., Parker, R., and Ring, S.G. 2000. Effect of molecular structure and water content on the dielectric relaxation behavior of amorphous low molecular weight carbohydrates above and below their glass transition. *Carbohydr. Res.* 329, 839-845.

Ottenhof, M., MacNaughtan, W., and Farhat, I.A. 2003. FTIR study of state and phase transitions of low moisture sucrose and lactose. *Carbohydr. Res.* 338, 2195-2202.

Parker, C.A. 1968. *Photoluminescence of Solutions*. Elsevier Pub. Co., Amsterdam.

Peleg, M. 1996. On modeling changes in food and biosolids at and around the glass transition temperature range. *Crit. Rev. Food Sci. Nutr.* 36, 49-67.

Pravinata, L.C., You, Y. and Ludescher, R.D. 2005. Erythrosin B phosphorescence monitors molecularmobility and dynamic site heterogeneity in amorphous sucrose. *Biophysical J.* 88(May): 3551-3561

Richert, R. 2000. Triplet state salvation dynamics: basics and applications. *J. Chem. Phys.* 113: 8404-8429.

Richert, R. 2001. Spectral selectivity in the slow β-relaxation of a molecular glass. *Europhys. Lett.*, 54(6), 767-773.

Roos, Y. 1995. *Phase transitions in foods*. Academic Press, San Diego, CA.

Roudaut, G., Maglione, M., Dusschoten, D. van, and Le Meste, M. 1999a. Molecular mobility in glassy bread: a multispectroscopy approach. *Cereal Chem.* 76, 70-77.

Roudaut, G., Maglione, M., and Le Meste, M. 1999b. Relaxations below glass transition temperature in bread and its components. *Cereal Chem.* 76, 78-81.

Roudaut, G.; Simatos, D., Champion, D., Contreras-Lopez, E., and Le Meste, M. 2004. Molecular mobility around the glass transition temperature: a mini review. *Innovative Food Sci. Emerging Technol.* 5, 127-134.

Saleki-Gerhardt, A. and Zografi, G. 1994. Non-isothermal and isothermal crystallization of sucrose from the amorphous state. *Pharma. Res.* 11, 1166-1173.

Schartel, B. and Wendorff, J.H. 1995. Dielectric investigations on secondary relaxation of polyarylates: comparison of low molecular models and polymeric compounds. *Polymer.* 36(5), 899-904.

Schebor, C., Burin, L., Buera, M.P., Aguilera, J.M. & Chirife, J. 1997. Glassy state and thermal inactivation of invertase and lactase in dried amorphous matrices. *Biotech. Prog.* 13, 857-863.

Scandola, M., Ceccorulli, G., and Pizzoli, M. 1991. Molecular motions of polysaccharides in the solid state: dextran, pullulan, and amylose. *Intl. J. Biol. Macromol.* 13, 254-260.

Shah, N.K. & Ludescher, R.D. 1992. Hydration and the internal dynamics of Hen Egg white lysozyme. Time-Resolved Laser Spectroscopy in Biochemistry III (J.R. Lakowicz, Ed.), Proceedings of SPIE, Vol.1640, 174-179.

Shah, N.K. & Ludescher, R.D. 1993. Influence of hydration on the internal dynamics of hen egg white lysozyme in the dry state. *Photochemistry and Photobiology* 58, 169-174.

Shah, N.K. 1994. Spectroscopic Probes of Protein Hydration and Glass Transitions. Ph.D. Dissertation, Rutgers University

Shah, N.K. and Ludescher, R.D. 1995. Phosphorescence probes of the glassy state in amorphous sucrose. *Biotechnol. Prog.* 11, 540-544.

Shalaev, E.Y. and Zografi, G. 1996. How does residual water affect the solid-state degradation of drugs in the amorphous state? *J. Pharm. Sci*. 85(11), 1137-1141.

Shamblin, S.L. and Zografi, G. 1998. Enthaply relaxation in binary amorphous mixtures containing sucrose. *Pharm. Res.* 15, 1828-1834

Shamblin, S.L., Tang, X.L., Chang, L.Q., Hancock, B.C. and Pikal, M.J. 1999. Characterization of the time scales of molecular motion in pharmaceutically important glasses. *J. Phys. Chem. B.* 103: 4113-4121.

Shirke, S. 2005. Molecular mobility of sugars and sugar alcohols as detected by phosphorescence of erythrosin B; M.S. Thesis, Rutgers University, New Brunswick, NJ.

Shirke, S., Takhistov, P., and Ludescher, R.D. 2005. Molecular mobility in amorphous maltose and maltitol from phosphorescence of erythrosin B. *J. Phys. Chem. B.* 109, 16119-16126.

Shirke, S. and Ludescher, R.D. 2005a. Molecular mobility and the glass transition in amorphous glucose, maltose, and maltotriose. *Carbohydr. Res.* 340, 2654-2660.

Shirke, S. and Ludescher, R.D. 2005b. Dynamic site heterogeneity in amorphous maltose and maltitol from spectral heterogeneity in erythrosin B phosphorescence. *Carbohydr. Res.* 340, 2661-2669.

Simon-Lukasik, K.V. and Ludescher, R.D. 2004. Erythrosin B phosphorescence as a probe of oxygen diffusion in amorphous gelatin films. *Food Hydrocolloids.* 18, 621-630.

Slade, L., Levine, H., and Finley, J. 1989. Protein-water interactions: water as a plasticizer of gluten and other proteins. In *Protein Quality and the Effects of Processing* (D.C. Phillios & J. Finley, editors), pp9-124. Marcel Dekker, Inc.

Slade, L. and Levine, H. 1991. A food polymer science approach to structure-property relationships in aqueous food systems: non-equilibrium behavior of carbohydrate-water systems. *Adv. Exp. Med. Biol.* 302, 29-101.

Slade, L. and Levine, H. 1995. Glass transitions and water-food structure interactions. *Adv. Food Nutr. Res.* 38, 103-269.

Slavik, J. 1994. *Fluorescent Probes in Cellular and Molecular Biology*. CRC Press, Boca Raton, FL.

Strasburg, G. and Ludescher, R.D. 1995. Theory and applications of fluorescence spectroscopy in food research. *Trends food Sci. Technol.* 6(3), 69-75.

Streefland, L., Auffret, A.D., and Franks, F. 1998. Bond cleavage reactions in solid aqueous carbohydrate solutions. *Pharm. Res.* 15, 843-849.

Strickley, R.G. & Anderson, B.D. 1996. Solid-state stability of human insulin. I. Mechanism and the effect of water on the kinetics of degradation in lyophiles from pH 2-5 solutions. *Pharm. Res.* 13, 1142-1153.

Strickley, R.G. & Anderson, B.D. 1997. Solid-state stability of human insulin. I. Effect of water on reactive intermediate partitioning in lyophiles from pH2-5 solutions: stabilization against covalent dimmer formation. *J. Pharm. Sci.* 86, 645-653.

Suihko, E.J., Forbes, R.T., and Apperley, D.C. 2005. A solid-state NMR study of molecular mobility and phase separation in co-spray-dried protein-sugar particles. *Euro. J. Pharm. Sci.* 25, 105-112.

Sun, W.Q. and Davidson, P. 1998. Protein inactivation in amorphous sucrose and trehalose matrices: effects of phase separation and crystallization. *Biochim. Biophys. Acta.* 1425, 235-244.

Towns, J.K. 1995. Moisture content in proteins: its effects and measurement. *J. Chromatog. A.* 705, 115-127.

Tsujimi, Y., Kobayashi, M., and Yagi, T. 1999. Frequency and time-resolved spectroscopic study of liquid-glass transition in D-sorbitol. *Physica. B.* 263-264, 310-312.

Turro, N. 1991. Modern Molecular Photochemistry. University Science Books, Sausalito, CA.

Van den Dries, I.J., van Dusschoten, D., and Hemminga, M.A. 1998. Mobility in maltose-water glasses studied with ^{1}H NMR. *J. Phys. Chem. B.* 102, 10483-10489.

Van den Dries, I.J., Besseling, N.A.M., van Dusschoten, D., Hemminga, M.A., and van der linden, E. 2000. Relation between a transition in molecular mobility and collapse phynomena in glucose-water systems. *J. Phys. Chem. B.* 104, 9260-9266.

Walters, C. 2004. Temperature dependency of molecular mobility in preserved seeds. *Biophys. J.* 86, 1253-1258.

Wehry, E.L β-relaxation. 1990. Effects of molecular environment on fluorescence and phosphorescence. In *Practical Fluorescence*, 2nd Ed. (G.G.Guilbault, Editor). Marcel Dekker, Inc., NY.

Wolkers, W.F., Oldenhof, H., Alberda, M., Hoekstra, F.A. 1998. A Fourier transform infrared microspectroscopy study of sugar glasses: application to anhydrobiotic higher plant cells. *Biochim. Biophys. Acta.* 1379, 83-96.

Yoshioka, M., Hancock, B.C., and Zografi, G. 1994. Crystallization of indomethacin from the amorphous state below and above its glass transition temperature. *J. Pharm. Sci.* 83, 1700-1705.

Zallen, R. 1998. *The Physics of Amorphous Solids*. John Wiley & Sons, Inc. NY.

Zhou, D., Zhang, G.G.Z., Law, D., Grant, D.J.W. and Schmitt, E.A. 2002. Physical stability of amorphous pharmaceuticals: importance of configurational thermodynamic quantities and molecular mobility. *J. Pharm. Sci.* 91 (8), 1863-1872.

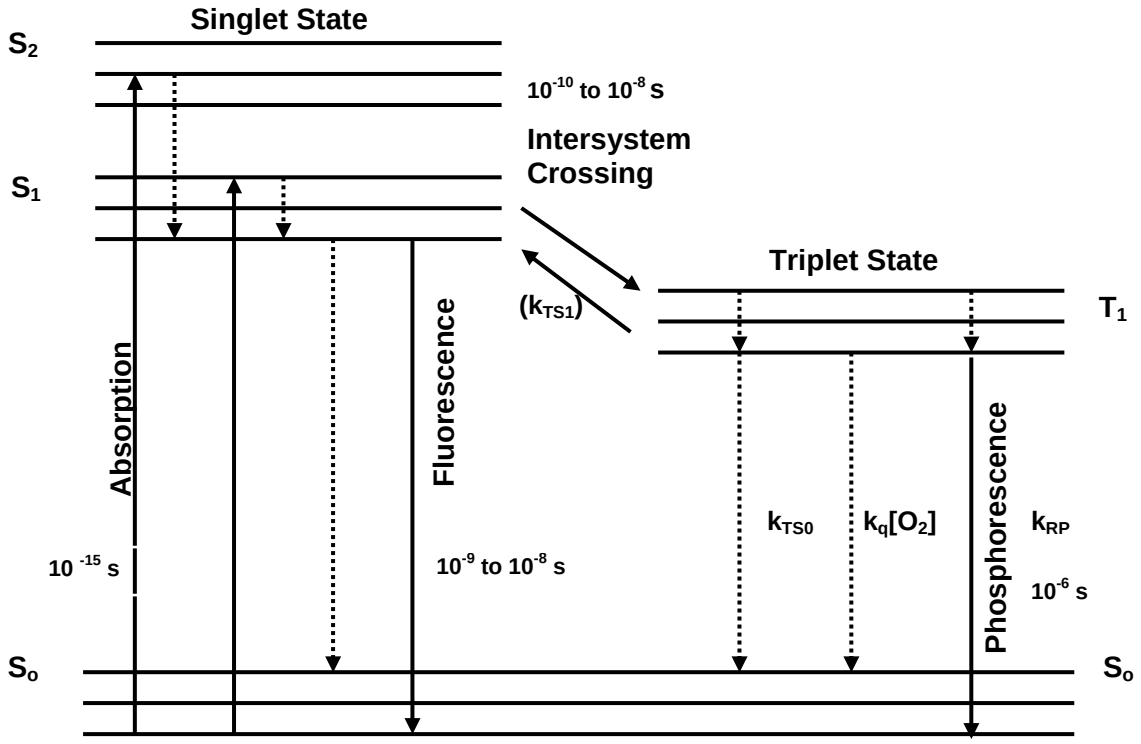

Figure 1 Jabłoński Energy Level Diagram

Chapter 1 Molecular mobility in amorphous sucrose film detected using phosphorescence of erythrosin B

Introduction

Molecular mobility in amorphous food materials plays a key role in controlling physical and chemical properties that correlate with food stability and shelf life. Luminescence is a noninvasive and sensitive tool to allow mapping the motion of probes in matrix. The information of motions dependent on temperature as well as matrix is obtained based on the physical properties of the probe in the ground and excited states, and their sensitivity to the physical and chemical nature of the local environment (Lakowicz, 1999).

This technique has been used to monitor the temperature dependence of molecular mobility in amorphous proteins and sugars. Phosphorescence of tryptophan was used to monitor the effect of hydration on the molecular mobility of lysozyme (Shah and Ludescher, 1992, 1993). Triplet probe erythrosin B incorporated in amorphous gelatin films provided information about oxygen diffusion and molecular mobility on the millisecond time scale (Simon-Lukasik and Ludescher, 2004); plasticizer effect on molecular mobility (Lukasik and Ludescher, 2006a); and plasticizer effect on dynamic site heterogeneity (Lukasik and Ludescher, 2006b). The correlation between molecular mobility and oxygen permeability was also explored using phosphorescence of erythrosin B in bovine serum albumin (BSA) (Nack and Ludescher, 2006) and β-lactoglobulin (Sundaresan and Ludescher, 2007).

Parts of this section have been published in Biophysical Journal and are included here verbatim.

Tryptophan and four halogenated tryptophan analogs used in freeze-dried sucrose showed three phosphorescence lifetimes ranging from about 10ms to over 1s in glass sucrose at 20°C, demonstrating the presence of local environments with 100-fold difference in mobility (McCaul and Ludescher, 1999). N-acetyltryptophanamide (NATA) was used to monitor the molecular mobility in freeze-dried sucrose (Shah and Ludescher, 1995). NATA was found to be sensitive to molecular changes near the glass transition and exhibited multiexponential phosphorescence intensity decays, indicating heterogeneous environments with different matrix mobility. Erythrosin B was applied to monitor the molecular mobility as well as dynamic heterogeneity in both freeze-dried sucrose (Shah and Ludescher, 1995) and amorphous sucrose thin film (Pravinata et al., 2005). Another xanthene dye Eosin Y incorporated in sucrose thin film provided the similar information about molecular mobility and site heterogeneity (Pravinata, 2003).

This technique has also been used to differentiate and compare molecular mobility of different sugars. In a study of molecular mobility of amorphous disaccharides by tryptophan luminescence, sucrose was found to be the least mobile followed by maltose and trehalose although their T_gs increased in the order of sucrose< maltose< trehalose (Zunic, 2004). Comparison among glucose, maltose and maltotriose demonstrated that the average molecular mobility in matrix and the distribution of matrix mobility rates increase with an increase in the molecular weight of the sugars (Shirke and Ludescher, 2005a). With respect to sugars and sugar alcohols, erythrosin B phosphorescence was also very effective in detecting dipolar relaxation and dynamic site heterogeneity (Shirke, 2005). A study of maltose and maltitol showed detectable dipolar relaxation in the glassy state about 50°C below individual T_g, with relaxation rate slower

than literature values for the β relaxation; while dipolar relaxation rate in the melt was comparable to values for the α relaxation determined from dielectric relaxation. in maltose, maltitol and their mixtures, collisional quenching rate k_{TS0} showed different trends over the temperature range: in maltose, k_{TS0} kept constant in the glass and increased sharply in the melt; in maltitol, k_{TS0} increased moderately in the glass even at 50°C below T_g and enhanced dramatically in the melt at 20°C above T_g; k_{TS0} of maltose-maltitol mixtures were significantly smaller than that of individual pure component, indicating the presence of specific interactions between sugar and sugar alcohol (Shirke et al., 2005). Both maltose and maltitol in both the glass and the melt state were also found to be site heterogeneous based on the results of time-resolved emission spectra and intensity decays with wavelength (Shirke and Ludescher, 2005b).

This chapter reported the basic information of molecular mobility in amorphous sucrose film using phosphorescence of erythrosin B, which builds up a solid database and provides interpretation for the sucrose-based binary systems.

Materials and Methods

1. Sample Preparation

About 50 g of sucrose (99.5% pure; Sigma Chemical Co., St. Louis, MO) were dissolved in about 30 g of deionized water containing 0.77 g of activated charcoal to remove luminescent impurities. After stirring overnight, the mixture was vacuum-filtered through ashless filter paper (Whatman No. 40); 0.7 g of activated charcoal was added to the filtrate and the process was repeated. The final concentration of purified sucrose solution was adjusted to 65-67 wt. %, confirmed using a refractometer (NSG Precision

Cells, Inc., Farmingdale, NY). Before preparing samples the sucrose solution was filtered through a membrane with 0.2 μm pores to remove particles.

Erythrosin B (Ery B; Sigma Chemical Co., St. Louis, MO) in a free acid form was dissolved in spectrophotometric grade dimethylformamide (DMF; Aldrich Chemical Co., Milwankee, WI) to prepare a 10 mM stock solution; an aliquot from this solution was added to the concentrated sucrose to obtain a dye/sucrose mole ratio of $1:10^4$.

We prepared glassy sucrose films by using a slightly modified version of our previous method (Pravinata et al., 2005). In order to improve the surface activity for spreading sucrose solutions, quartz slides were washed overnight with Alconox soap, washed with deionized water, activated for 30 minutes with concentrated nitric acid, rinsed with deionized water, cleaned with 95% ethanol for 2 hours, and finally rinsed again with deionized water. To make amorphous sucrose films with Ery B, 15 μL of the sucrose solution containing Ery B was placed on a quartz slide (30×13.5×0.6 mm, custom made by NSG Precision Cells, Farmingdale, NY). Another slide was placed on top of the solution and the slides were drawn horizontally past one another to form a thin film. The solution on the slides was then heated under a heat gun (Vidal Sassoon) for 5 minutes to a maximum temperature of 86-88°C (measured using a thermocouple probe). The thickness of amorphous sucrose film prepared by this procedure ranged from 10 to 40 μm. The slides were stored against P_2O_5 and Drie-Rite for at least 7 days. All slides were assayed for crystals under crossed polarizers in a dissecting microscope (Nikon Type 102); only slides without crystals were used for phosphorescence measurements.

The moisture content of glassy sucrose films was determined by gravimetric methods to be less than 1 wt %; this low value was presumably due to the extensive

equilibration time and the thinness of the films. We thus estimated that the T_g of these films was ~63°C using the equation for the dependence of on moisture content developed by Crowe and colleagues (Sun et al., 1996).

2. Luminescence measurements and analysis

Luminescence measurements were made using a Cary Eclipse fluorescence spectrophotometer (Varian Instruments, Walnut Creek, CA). Prior to any phosphorescence measurements, all samples were flushed for at least 15 minutes with nitrogen gas which contained less than 1 ppm oxygen to eliminate oxygen quenching. All the measurements were made in triplicate at least. The temperature of the sample holder was controlled using a thermo-electric temperature controller (Varian Instruments, Walnut Creek, CA). Samples were equilibrated at each target temperature for 1 min/1°C increase in temperature.

2.1. Delayed fluorescence and phosphorescence emission spectra

2.1.1. Delayed emission as a function of temperature (ν_P (T), Γ (T))

Delayed fluorescence and phosphorescence emission spectra were collected from 520 nm to 750 nm (10 nm bandwidth) at 1 nm intervals using excitation at 500 nm (20 nm bandwidth) over a temperature range from 5 to 100°C with an observation window of 5.0 ms and an initial delay time of 0.2 ms to suppress fluorescence coincident with the lamp pulse. An emission spectrum from sucrose film without probe was subtracted from each spectrum although the signal from background was very low.

The energy of the emission maximum (ν_p) and the FWHM of the emission band were determined by using a log-normal line shape function (Maroncelli and Fleming, 1987) to fit both delayed fluorescence and phosphorescence.

$$I(\nu) = I_0 \exp\left\{ - \ln(2)\left(\frac{\ln[1 + 2b(\nu - \nu_p)/\Delta]}{b} \right)^2 \right\} \quad (1)$$

Where I_0 is the maximum emission intensity, ν_p is the peak frequency (cm^{-1}), Δ is a linewidth parameter and b is an asymmetry parameter. The bandwidth Γ (= FWHM) is calculated according to the following equation:

$$\Gamma = \Delta\left(\frac{\sinh(b)}{b} \right) \quad (2)$$

For delayed luminescence spectra collected from 520-750 nm, a sum of log-normal functions for delayed fluorescence ($I_{DF}(\nu)$) and phosphorescence ($I_P(\nu)$) were used to fit the spectra. Each emission band was analyzed for independent fit parameters using a sum of two functions as described in Eq. 1.

The ratio of the emission intensity for delayed fluorescence (I_{DF}) and phosphorescence (I_P) is related to the rate constant for reverse intersystem crossing k_{TS1}, the rate of radiative emission k_{RP} and the quantum yield for fluorescence (ϕ_F) (Duchowicz et al., 1998):

$$I_{DF}/I_P = \phi_F k_{TS1}/k_{RP} \quad (3)$$

Since k_{TS1} is an Arrhenius process (Eq. 8), a plot of $\ln(I_{DF}/I_P)$ versus 1/T has slope of $-\Delta E_{TS}/R$.

2.1.2. Dipolar relaxation rate as a function of temperature ($\frac{1}{\varphi}(T)$)

The dipolar relaxation time φ was calculated from the temperature dependence of the phosphorescence emission peak ν(T) by analyzing the relaxation function:

$$\frac{\Delta\nu}{\Delta\nu_r} = \frac{\nu(T) - \nu_{\max}}{\nu_{\min} - \nu_{\max}} \quad (4)$$

Where ν(T) is the emission peak energy at temperature T, and ν_{min} and ν_{max} are the emission peak energy at the lowest temperature and the highest temperature, respectively. By using a stretched exponential function to approximate the phosphorescence intensity decay, the matrix dipolar relaxation time (φ) can be estimated from the following equation (Shirke et al., 2005):

$$\frac{\Delta\nu}{\Delta\nu_r} = \frac{\nu(T)-\nu_{\max}}{\nu_{\min}-\nu_{\max}} = \frac{1}{\Gamma(\frac{1}{\beta_l})}\frac{1}{1+\frac{\beta_e}{\beta_l}\frac{\tau}{\varphi}} \quad (5)$$

Where τ and β_l are the temperature-dependent stretched exponential (Kohlrausch-Williams-Watts) lifetime and stretching exponent (from Eq. 6) describing the phosphorescence intensity decay and Γ(x) in this case is the Gamma function; β_e is assumed to have a value of 0.5.

2.2. Emission spectra as a function of delay time (ν_P (t), Γ (t))

Phosphorescence emission spectra of erythrosin B in sucrose film measured as a function of the delay time after excitation used an excitation wavelength of 530 nm and emission spectra were collected from 620 to 750nm. Each spectrum was collected over a 0.5-ms observation window using time delays of 0.1, 0.6, 1.1, 1.6, 2.1, and 2.6 ms after the lamp flash. Emission energy ν_P and full width at half maximum Γ of the emission band are determined by fitting phosphorescence emission to a log-normal line-shape function (Eq. 1 and Eq. 2).

2.3. Red-edge effect measurement

Red-edge effect measurements over the temperature range from 5 to 85°C used excitation wavelengths at 530 nm and 560 nm, respectively. Phosphorescence emission was collected from 640 nm to 760 nm using an observation window of 5.0 ms and 0.1 ms

delay. Phosphorescence spectra were converted to intensity versus frequency (cm^{-1}) and analyzed to obtain the peak frequency (ν_p) and spectral bandwidth (Γ) using a lognormal function ($I(\nu)$) (Eq. 1).

2.4. Lifetime measurement (τ (T), β (T), k_{TS0} (T))

For lifetime measurements, samples were excited at 530 nm (20 nm bandwidth) and emission transients were collected at 680 nm (20 nm bandwidth) over the temperature range from 5 to 100°C. Phosphorescence intensity decays were collected over a window of 4 ms with an initial delay of 0.1 ms and increments of 0.04 ms. Because intensity decays were non-exponential, a stretched exponential function was selected to analyze the intensity decays (Richert, 2000; Lee et al., 2001; Pravinata et al., 2005).

$$I(t) = I(0) \exp[-(t/\tau)^{\beta}] + \text{constant} \quad (6)$$

Where $I(0)$ is the initial intensity, τ is the stretched exponential lifetime, and β is an exponent varying from 0 to 1 that characterizes the lifetime distribution (Lindsey and Patterson, 1980). The use of a stretched exponential model provides an analysis in terms of a continuous distribution of lifetimes, which is appropriate for describing a complex glass possessing a distribution of relaxation times for the dynamic molecular processes. The smaller the β value, the more non-exponential the intensity decays and the broader the distribution of lifetimes. The program NFIT (Galveston, TX) was used to fit the decays; goodness of fit was evaluated by examining χ^2 and R^2. Plots of modified residuals (defined as the difference between the intensity from the fit decay curve and the measured intensity divided by the square root of the measured intensity) was also used as

an indicator of the goodness of fit. R^2 for all fits ranged from 0.99 to 1.00 and modified residuals plots fluctuated randomly around zero amplitude.

The phosphorescence lifetime is directly related to the sum of the de-excitation rates for the excited triplet state (Duchowicz et al., 1998).

$$\tau = (k_{RP} + k_{TS1} + k_{TS0} + k_Q[O_2])^{-1} \quad (7)$$

Here k_{RP} is the rate of radiative emission to S_0 (equal to 41 s^{-1} for Ery B; Duchowicz et al., 1998; Lettinga et al., 2000), k_{TS1} is the rate of reverse intersystem crossing to S_1, k_{TS0} is the rate of intersystem crossing to S_0, and $k_Q[O_2]$ is the oxygen quenching rate (which is assumed negligible for this study due to the elimination of oxygen). The rate constant for reverse intersystem crossing is a thermally activated process that follows Arrhenius kinetics (Parker, 1968):

$$k_{TS1}(T) = k_{TS1}^{o} \exp(-\Delta E_{TS}/RT) \quad (8)$$

where k_{TS1}^{0} is the maximum reverse intersystem crossing rate at high temperature and ΔE_{TS} is the energy gap between T_1 and S_1. The term k_{TS0} reflects the rate at which the probe can dissipate the energy of the excited T_1 state as heat into the surrounding matrix (Papp and Vanderkooi, 1989). The phosphorescence lifetime thus varies with temperature due to changes in the magnitude of k_{TS1} and k_{TS0}. Since k_{TS1} can be calculated using measurements of ΔE_{TS}, and k_{TS1}^{o} can be estimated as described elsewhere (Pravinata et al., 2005; Shirke et al., 2005), the magnitude of k_{TS0} can be calculated by difference from Eq. 7.

2.5. Lifetime as a function of excitation and emission wavelength

Phosphorescence lifetimes of Ery B as a function of emission wavelength were measured with excitation wavelength at 530 nm (20 nm bandwidth) and emission

wavelength from 640 nm to 720 nm (20 nm bandwidth). Phosphorescence emission lifetimes as a function of excitation wavelength were measured with emission wavelength at 680 nm (20 nm bandwidth) and excitation wavelength from 490 nm to 560 nm (20 nm bandwidth). These experiments were performed at 25°C.

Results

1. Delayed fluorescence and phosphorescence emission spectra

The delayed emission spectra of erythrosin B in optically clear amorphous sucrose films at a 10^{-4} erythrosin/sucrose mole ratio exhibited maxima at ~555 and 675 nm (Figure 2). Both the delayed fluorescence and phosphorescence bands shifted to longer wavelength (lower energy) at higher temperature. The spectra collected from 5 to 100°C showed an increase in delayed fluorescence and decrease in phosphorescence intensity with increasing temperature, a result from a thermally stimulated process (Parker, 1968). The emission energy (Figure 3) decreased linearly in the glass at low temperature and the slope became more negative above T_g of sucrose, indicating an increase in the average extent of matrix dipolar relaxation around the excited triplet state prior to emission and the rate of dipolar relaxation above T_g. The phosphorescence bandwidth (Figure 3) increased gradually with temperature in the glass and much more dramatically in the melt, reflecting a large increase in the range of energetically distinct matrix environments in amorphous sucrose above T_g.

The intensity ratio when plotted as a van't Hoff plot of $\ln(I_{DF}/I_P)$ versus 1/T was linear over the entire temperature range without systematic deviations (Figure 4). The slope provides an estimate of the energy gap between the lowest triplet (T_1) and singlet (S_1) states. The value of 31.6±0.4 kJ/mol for ΔE_{TS} in amorphous sucrose was

significantly smaller than that measured in water (36.9±0.6 kJ/mol) and 66 wt. % sucrose solution (36.9±1.0 kJ/mol). The value of ΔE_{TS} for erythrosin in ethanol and polyvinyl alcohol was reported as 28.5±2.5 kJ/mol (Duchowicz et al., 1998) and 41.2±0.4 kJ/mol (Lettinga et al., 2000), respectively, suggesting that solvent/matrix properties modulate the single-triplet energy gap.

2. Red-edge excitation

Measurements of the red-edge effect as a function of temperature in both amorphous sucrose and in 66 wt % aqueous sucrose are plotted in Figure 5 as the energy difference ($\Delta\nu_p$) with 530 and 560 nm excitation. The magnitude of $\Delta\nu_p$ for erythrosin B in amorphous sucrose decreased at higher temperatures. The slope was more negative at high than low temperatures whereas the curve exhibited a break at ~60°C, suggesting the rate of matrix relaxation increased significantly in the sucrose melt above T_g. The red-edge effect for erythrosin B in aqueous sucrose was essentially low due to more rapid solvent relaxation within the viscous solution.

3. Phosphorescence intensity decay

Time-resolved phosphorescence intensity decays of erythrosin B in amorphous sucrose films were measured over the temperature range from 5 to 100°C during heating as well as cooling cycles. The phosphorescence intensity decays are plotted in Figure 6 along with fits using a stretched exponential function. All intensity decays at all temperatures were satisfactorily fit using a stretched exponential decay model in which the lifetime τ and the stretching exponent β were the physically meaningful parameters. The modified residuals varied randomly around zero and R^2 values were 0.9998 for the 5°C data and 0.9989 for the 85°C data. The stretched exponential lifetimes and exponent

β during heating are plotted as a function of temperature (Figure 7); lifetimes and β were identical within error during cooling cycle (data now shown here). The lifetimes decreased biphasically with increasing temperature, reflecting an increase in the rate of non-radiative decay of the excited triplet state T_1 due to an increase in both the rate of reverse intersystem crossing to S_1 (k_{TS1}) and the rate of non-radiative decay to the ground state S_0 (k_{TS0}). An estimate of the lower limit of k_{TS0}, based on the maximum physically reasonable value of k_{TS1}, is also plotted in Figure 8. The non-radiative quenching rate was approximately constant at 1600 s^{-1} in glassy sucrose. This value is larger than in water (3200 s^{-1}) (Duchowicz et al., 1998), and essentially the same as that in solid polyvinyl alcohol (1460 s^{-1}) (Lettinga et al., 2000). However k_{TS0} increased dramatically in the sucrose melt, indicating that the non-radiative quenching rate can sense the large scale molecular mobility activated at the glass transition.

The stretching exponent β showed the similar trend as lifetime with temperature: remaining constant at ~0.92 up to ~50°C and decreasing at higher temperatures to 0.80 at 100°C. A small decrease in β reflects a large increase in the width of the distribution of phosphorescence decay times (Lindsey and Patterson, 1980) and a corresponding distribution of dynamically distinct probe environments with different values of k_{TS0}. The decrease in β thus indicated that the range of dynamically distinct probe environments increased above T_g.

4. Spectral heterogeneity

The phosphorescence emission of erythrosin in amorphous sucrose exhibited a blue shift to higher energy as a function of time after excitation below and above the T_g

(Figure 9), which was unexpected and cannot explain the homogeneous relaxation model for spectral shifts (Lakowicz, 1999; Richert, 2000; Demchenko, 2002).

Phosphorescence intensity decays were measured as a function of excitation and emission wavelength at temperatures from 5 to 85°C. Lifetimes are plotted versus excitation and emission wavelength in Figure 10a. At low temperature up to 55°C, the lifetimes decreased systematically with increasing wavelength across the emission band. Near and above the sucrose T_g (>65°C), however, another trend became apparent as the lifetimes began to increase at intermediate wavelengths (near 660 nm); and this trend was more distinct at higher temperatures. Lifetimes also varied across the excitation band, being higher near the absorption maximum of 530 nm at all temperatures.

The stretching exponent also varied as a function of both excitation and emission wavelength: slightly smaller at the blue and red edges of both bands (Figure 10b). This trend increased at higher temperatures. At 5°C β varied from 0.910 at 490 nm to 0.932 at 530 nm while at 85°C β varied from 0.811 at 560 nm to 0.908 at 540 nm.

Discussion

Phosphorescence emission energy and intensity from Ery B is sensitive to two distinct modes of molecular mobility in amorphous biomaterials (Pravinata et al., 2005; Simon-Lukasik and Ludescher, 2004; Shirke et al., 2005): matrix dipolar relaxation around the excited T_1 triplet state prior to emission that decreases the energy of the triplet state and thus lowers the emission energy; and matrix collisions that promote intersystem crossing from the excited T_1 triplet state to the ground S_0 singlet state that increase k_{TS0} and thus lower the lifetime. This study of matrix mobility in amorphous sucrose using

Ery B phosphorescence provides insight into the solid-state biophysics of amorphous sugars.

1. Dipolar relaxation

The phosphorescence emission energy (peak frequency) reports the average S_0-T_1 energy gap which is primarily modulated by the T_1 energy and thus by the relaxation of dipolar hydroxyl groups around T_1 (Richert, 2000). Temperature has a small effect on the emission energy in the sucrose glass and a much larger effect in the sucrose melt. The relaxation rate thus increased significantly at temperature above T_g due to activation of translational motions at T_g (that is, α-relaxation). The dipolar relaxation curve (Figure 11) also showed upward curvature at higher temperatures, indicating that the activated translational motions facilitate dipolar relaxation mechanisms involving motions ranging from rotation of –OH groups to the rotation of entire molecules.

Temperature had a similar influence on the magnitude of the red-edge effect. The emission energy difference with excitation at the peak and at the red edge decreased gradually in the glass below T_g and more steeply in the melt above the T_g. Since this energy difference reflects the persistence of low-energy sited photoselected by low-energy excitation (Demchenko, 2002), the decay of the energy difference above T_g reflects an increase in the rate of matrix relaxation that equilibrates the energy of all site on the lifetime of the triplet state.

The proposal that dipolar relaxation within the sucrose matrix modulates the phosphorescence emission energy of erythrosin is hardly controversial for either phosphorescence (Richert, 2000) or fluorescence (Ware et al., 1971; Stratt and Maroncelli, 1996). For erythrosin B in sucrose, however, emission spectra did not relax

to lower energy as a function of time after excitation but rather blue-shifted to higher energy. Such anomalous behavior requires a more complicated photophysical model that correlates emission spectra with triplet state lifetime.

2. Collisional quenching

Our analysis of the effect of temperature on lifetime indicates that the nonradiative quenching rate increased dramatically in the melt above T_g. The exact mechanism of this additional quenching is uncertain, either the increase of an existing quenching pathway or the activation of a novel quenching pathway. Either mechanism involves an increase in the ability of the excited erythrosin to dissipate vibrational energy into the matrix. It is clear from the decrease of the lifetime with temperature that such dissipation is facilitated by the α-relaxations activated at T_g, that is, there is effective coupling between matrix α-relaxations and vibrational motions of the probe.

The variation of lifetime with emission wavelength reflects variation in one or more of the rate constants for deexcitation of the triplet state. We can evaluate the possible contributions of these rate constants using qualitative arguments. The intrinsic emission rate, k_{RP}, which varies with the third power of the emission energy (Cantor and Schimmel, 1980), is expected to decrease with decreasing emission energy; this would cause an increase in the lifetime with increasing wavelength rather than decrease observed. The reverse intersystem crossing rate is sensitive to the S_1 to T_1 energy gap (ΔE_{TS}), an increase in ΔE_{TS} would thus decrease this rate constant. Probes emitting at longer wavelength would be expected to have larger energy gaps S_1-T_1 due to lower T_1 energy and thus lower values of k_{TS1}; this would cause an increase in lifetime with increasing wavelength rather than the decrease seen. The decrease in lifetime with

emission wavelength thus must reflect a variation in the nonradiative quenching rate k_{TS0} with wavelength. Thus there is a correlation between emission energy and matrix quenching rate among probes within the amorphous solids: probes with high emission energy have lower matrix quenching rate and probes with lower emission energy have higher matrix quenching rate.

The wavelength dependence of the apparent activation energies (E_A) for matrix quenching in the glass below and the melt above T_g can be calculated from Arrhenius plots at temperature below and above T_g (Figure 12). In both the glass and in the melt, the values of Ea were higher for probes with blue-shifted emission and red-shifted absorption. The activation energy also exhibited spectral heterogeneity in amorphous sucrose: probes in high energy sites with lower matrix quenching rates also had higher activation energies for the motions that quench the triplet state.

3. Dynamic site heterogeneity

Our results appear to reflect the behavior of a heterogeneous population of probes distributed among dynamically distinct sites within the sucrose matrix that vary in both emission energy and matrix quenching rate. The success of stretched exponential function with $\beta \approx 0.8\text{-}0.9$ to describe the phosphorescence decay suggests that a continuum of sites, rather than that a limited set of distinct sites, gives rise to the heterogeneity. A physical model for the origin of this site heterogeneity invokes local differences in packing interactions among molecules within the amorphous sucrose. Local environments with more constrained packing would have lower overall molecular mobility; probes in such lower mobility environments would have higher emission energy due to slower/less extensive dipolar relaxation around the excited triplet state, longer lifetimes due to

slower/fewer molecular collisions quenching the triplet state, and higher activation energies for nonradiative decay due to more constraints within the sucrose matrix. Local environments with less constrained/looser packing would have higher overall molecular mobility; probes in such higher mobility environments would have lower emission energy due to faster/more extensive dipolar relaxation around the excited triplet state, shorter lifetimes due to faster/more molecular collisions quenching the triplet state, and lower activation energies for nonradiative decay due to less constraints within the sucrose matrix.

The magnitude of the variation in lifetime with wavelength decreased at higher temperature, but the emission blue shift with time persisted even at 75°C (Figure 10b), suggesting that spectral heterogeneity may have decreased but did not disappear altogether in the melt. In addition, above T_g, the emission bandwidth increased (Figure 3), indicating that the distribution of site energies broadened, and the stretching exponent β decreased (Figure 7), indicating that the distribution of matrix quenching rates broadened; there was thus a significant broadening in the distribution of dynamic environments in the sugar melt. The decrease in the spectral heterogeneity above T_g may reflect an actual decrease in site heterogeneity within the amorphous sucrose or it may merely reflect the loss of the probe's ability to report site heterogeneity.

Conclusion

This study used steady-state and time-resolved phosphorescence of erythrosin B to monitor mobility in thin films of amorphous solid sucrose as a function of temperature. The phosphorescence emission energy, intensity (lifetime), and red-edge excitation effect

were all sensitive to localized molecular mobility on the microsecond timescale in the glass and to more global modes of mobility activated at the glass transition. Blue shifts in the emission spectrum with time after excitation and systematic variations in the phosphorescence lifetime with wavelength indicated that emission originates from multiple sites ranging from short lifetime species with red-shifted emission spectrum to long lifetime species with blue-shifted emission spectrum; the activation energy for nonradiative decay of the triplet state was considerably larger for the blue-emitting species in both the glass and the melt. This study illustrates that phosphorescence from erythrosin B is sensitive both to local dipolar relaxations in the glass as well as more global relaxations in the sucrose melt and provides evidence of the value of phosphorescence as a probe of dynamic site heterogeneity as well as overall molecular mobility in amorphous biomaterials.

References

Cantor, C.R., and Schimmel, P.R. 1980. *Biophysical Chemistry*. Part II: Techniques of the study of biological structure and function. W.H. Freeman & Co., San Francisco, CA.

Demchenko, A.P. 2002. The red-edge effect: 30 years of exploration. *Luminescence. 1*7, 19-42.

Duchowicz, R., Ferrer, M.L. and Acuna, A.U. 1998. Kinetic spectroscopy of erythrosin phosphorescence and delayed fluorescence in aqueous solution at room temperature. *Photochem. Photobiol.* 68, 494-501.

Lakowicz, J.R. 1999. *Principles of Fluorescence Spectroscopy.* Plenum Press, NY.

Lee, K.C.B., Siegel, J., Webb, S.E.D., Leveque-Fort, S., Cole, M.J., Jones, R., Dowling, K., Lever, M.J., and French, P.M.W. 2001. Application of the stretched exponential function to fluorescence lifetime imaging. *Biophys. J.* 81, 1265-1274.

Lettinga, M.P., Zuilhof, H. and van Zandvoort, A.M.J. 2000. Phosphorescence and fluorescence characterization of fluorescein derivatives immobilized in various polymer matrices. *Phys. Chem. Chem. Phys.* 2, 3697-3707.

Lindsey, C.P. and Patterson, G.D. 1980. Detailed comparison of the Williams-Watts and Cole-Davidson functions. *J. Chem. Phys.* 73, 3348-3357.

Lukasik, K.V. and Ludescher, R.D. 2006a. Molecular mobility in water and glycerol plasticized cold and hot-cast gelatin films. *Food Hydrocoll.* 20, 96-105.

Lukasik, K.V. and Ludescher, R.D. 2006b. Effect of plasticizer on dynamic site heterogeneity in cold-cast gelatin films. *Food Hydrocoll.* 20, 88-95.

Maroncelli, M. and Fleming, G.R. 1987. Picosecond salvation dynamics of coumarin 153: the importance of molecular aspects of salvation. *J. Chem. Phys.* 86, 6221-6239.

McCaul, C.P. and Ludescher, R.D. 1999. Room temperature phosphorescence from tryptophan and halogenated tryptophan analogs in amorphous sucrose. *Photochem. Photobiol.* 70, 166-171.

Nack, T.J, and Ludescher, R.D. 2006. Molecular mobility and oxygen permeability in amorphous bovine serum albumin films. *Food Biophys.* 1, 151-162.

Papp, S. and Vanderkooi, J.M. 1989. Tryptophan phosphorescence at room temperature as a tool to study protein structure and dynamics. *Photochem. Photobiol.* 49, 775-784.

Parker, C.A. 1968. *Photoluminescence of Solutions.* Elsevier, Amsterdam.

Pravinata, L.C. 2003. Molecular mobility of amorphous sucrose detected by phosphorescence of erythrosin B and eosin Y. *Master Thesis*. Rutgers University, New Brunswick, NJ

Pravinata, L.C., You, Y. and Ludescher, R.D. 2005. Erythrosin B phosphorescence monitors molecularmobility and dynamic site heterogeneity in amorphous sucrose. *Biophysical J.* 88(May), 3551-3561.

Richert, R. 2000. Triplet state salvation dynamics: basics and applications. *J. Chem. Phys.* 113, 8404-8429.

Shah, N.K., and Ludescher, R.D. 1992. Hydration and the internal dynamics of Hen Egg white lysozyme. Time-Resolved Laser Spectroscopy in *Biochemistry III* (J.R. Lakowicz, Ed.), Proceedings of SPIE, Vol.1640, 174-179.

Shah, N.K., and Ludescher, R.D. 1993. Influence of hydration on the internal dynamics of hen egg white lysozyme in the dry state. *Photochem. Photobiol.* 58, 169-174.

Shirke, S. 2005. Molecular mobility of sugars and sugar alcohols as detected by phosphorescence of erythrosin B; *M.S. Thesis*, Rutgers University, New Brunswick, NJ.

Shirke, S., Takhistov, P., and Ludescher, R.D. 2005. Molecular mobility in amorphous maltose and maltitol from phosphorescence of erythrosin B. *J. Phys. Chem. B.* 109, 16119-16126.

Shirke, S., and Ludescher, R.D. 2005a. Molecular mobility and the glass transition in amorphous glucose, maltose, and maltotriose. *Carbohydr. Res.* 340, 2654-2660.

Shirke, S., and Ludescher, R.D. 2005b. Dynamic site heterogeneity in amorphous maltose and maltitol from spectral heterogeneity in erythrosin B phosphorescence. *Carbohydr. Res.* 340, 2661-2669.

Simon-Lukasik, K.V., and Ludescher, R.D. 2004. Erythrosin B phosphorescence as a probe of oxygen diffusion in amorphous gelatin films. *Food Hydrocoll.* 18, 621-630.

Shah, N.K., and Ludescher, R.D. 1995. Phosphorescence probes of the glassy state in amorphous sucrose. *Biotechnol. Prog.* 11, 540-544.

Stratt, R.M., and Maroncelli, M. 1996. Nonreactive dynamics in solution: the emerging molecular view of solvation dynamics and vibrational relaxation. *J. Phys. Chem.* 100, 12981-12996.

Sun, W.Q., Leopold, A.C., Crowe, L.M., and Crowe, J.H. 1996. Stability of dry leptosomes in sugar glasses. *Biophys. J.* 70, 1769-1776.

Sundaresan, K.V., and R.D. Ludescher. 2007. Molecular mobility and oxygen permeability in amorphous β-lactoglobulin films. *Food Hydrocolloids.* (In press)

Ware, W.R., Lee, S.K., Brant, G.J., and Chow, P.P. 1971. Nanosecond time-resolved emission spectroscopy: spectral shifts due to solvent-excited solution relaxation. *J. Chem. Phys.* 54, 4729-4737.

Zunic, A. 2004. Molecular mobility of amorphous disaccharides studied by tryptophan luminescence. *Master thesis*. Rutgers University, New Brunswick, NJ.

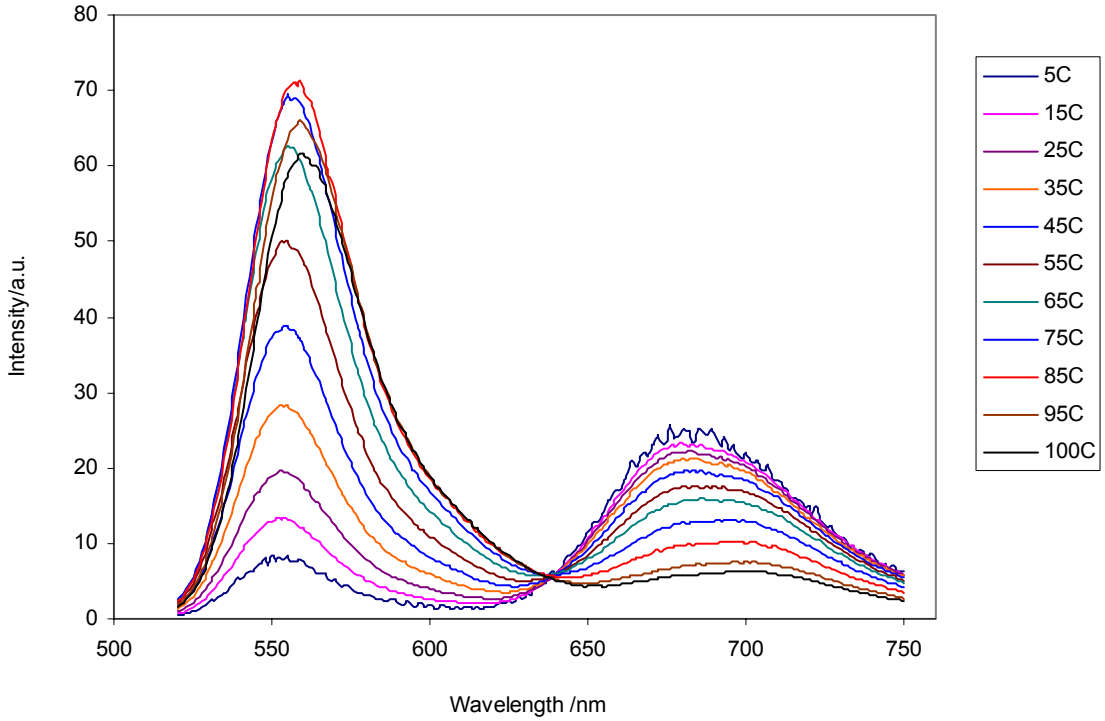

Figure 2 Delayed emission spectra of erythrosin B in amorphous sucrose films as a function of temperature (Ex=500 nm). The spectra were collected from 5 to 100°C.

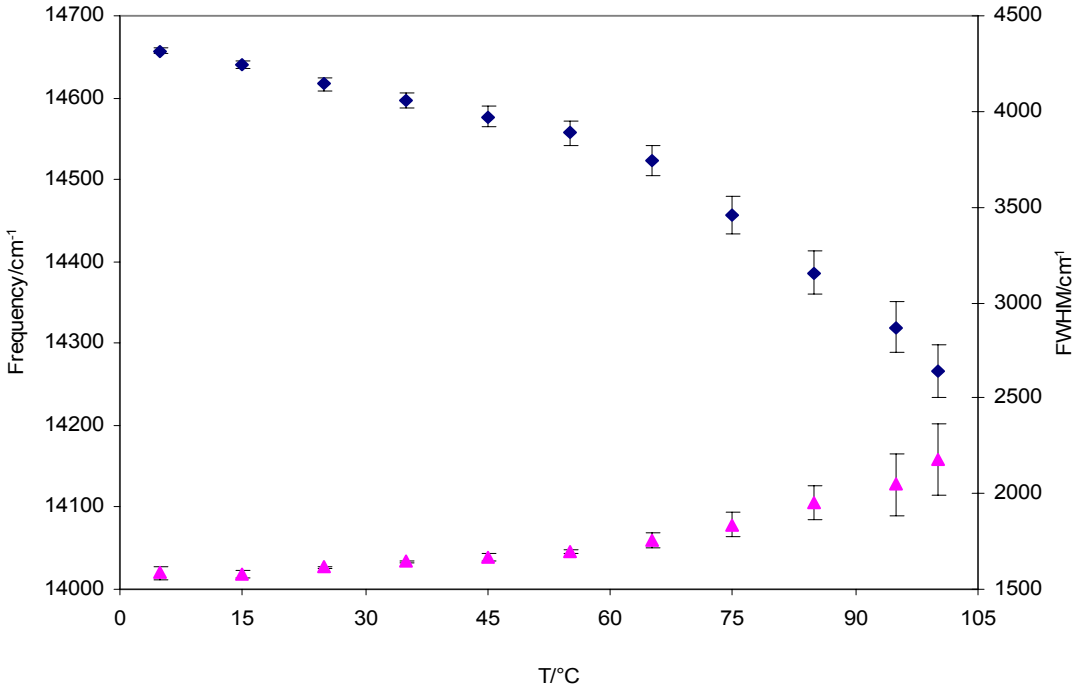

Figure 3 Peak frequency ν_p (♦, left scale) and bandwidth (full-width half maximum) (▲, right scale) for phosphorescence emission from erythrosin B in amorphous sucrose film as a function of temperature.

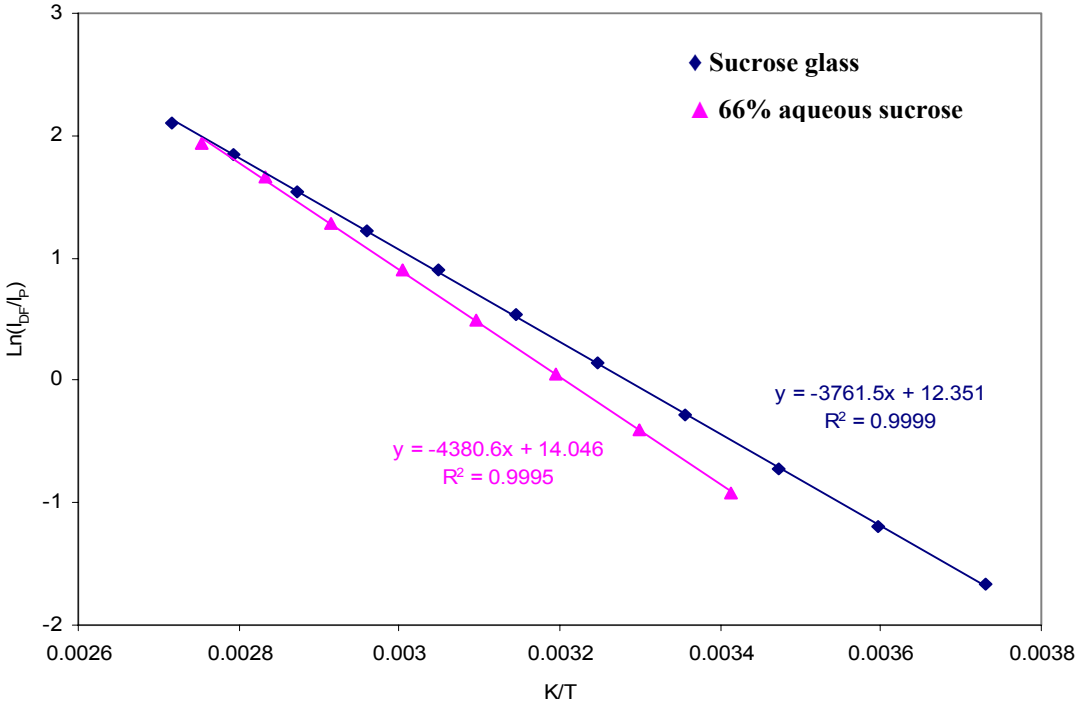

Figure 4 Plot of natural log of the intensity ratio between delayed fluorescence and phosphorescence in sucrose glass and concentrated solution as a function of inverse temperature.

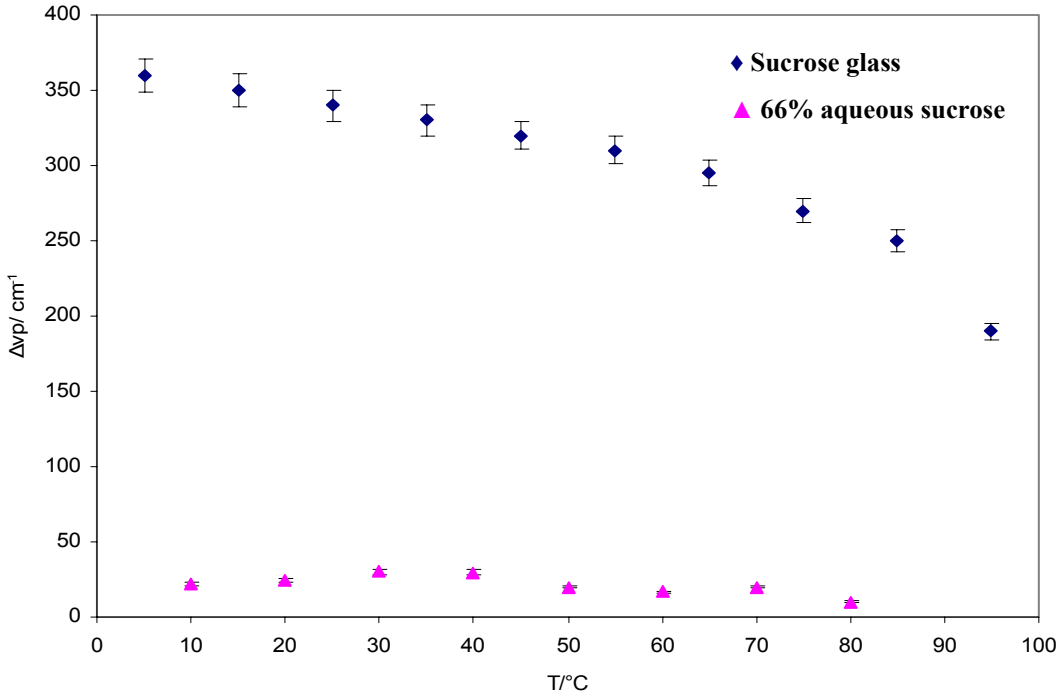

Figure 5 The red-edge effect of the phosphorescence emission of erythrosin B plotted as a function of temperature in amorphous sucrose film (♦) and 66 wt % aqueous sucrose (▲). The emission energy difference $\Delta\nu_p$ with 530 and 560 nm excitation is plotted versus temperature.

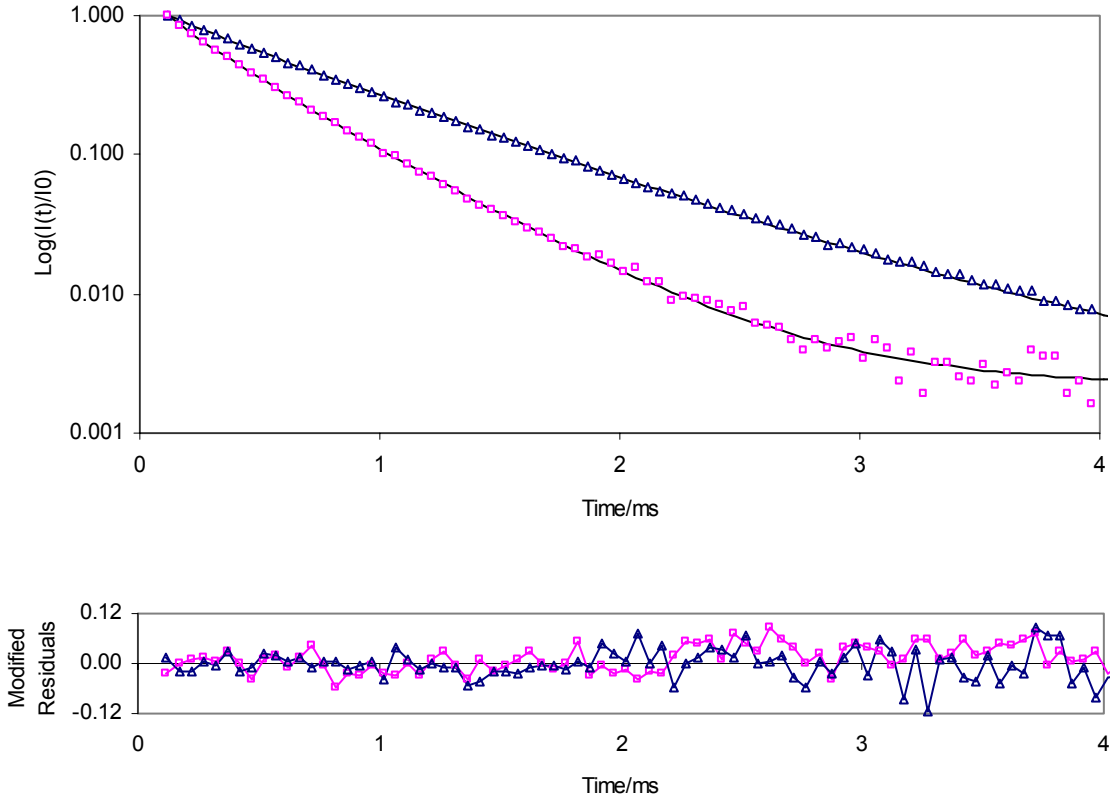

Figure 6 Normalized intensity decays (*I(t)/I(0)*) of erythrosin B in amorphous sucrose film at 5°C(Δ) and at 85°C (□). The smooth curves through the data points are fits using a stretched exponential function with τ =0.62 ms and β=0.921 (5°C data) and τ =0.32 ms and β=0.857 (85°C data). The lower figure is a plot of the modified residuals for these fits.

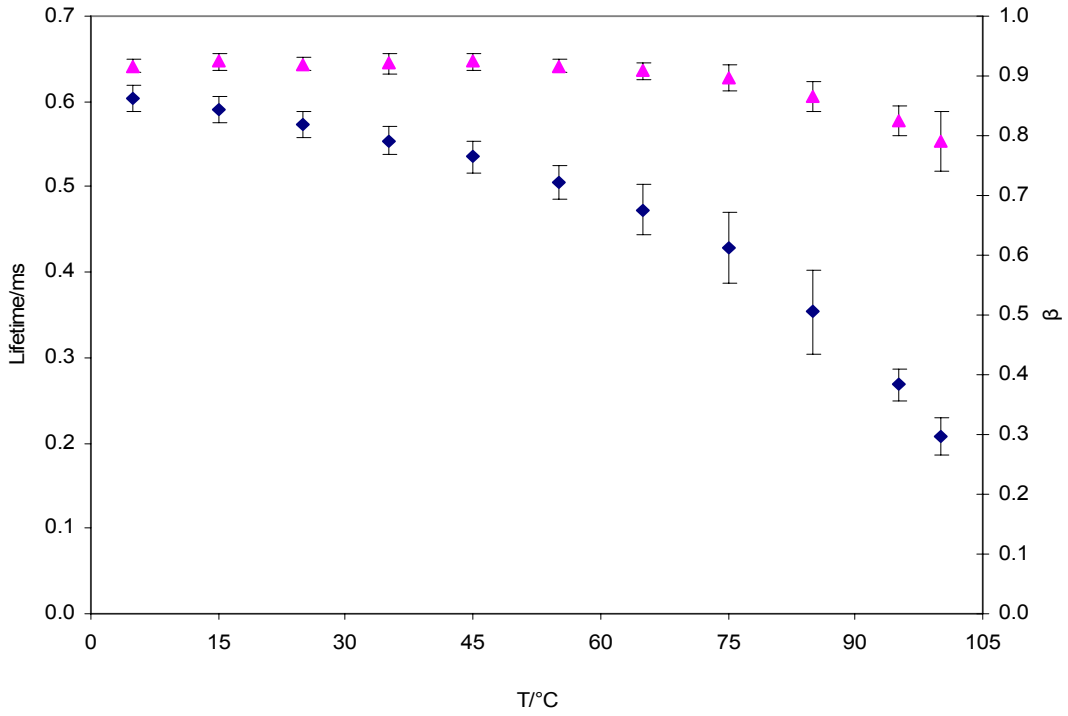

Figure 7 Temperature dependence of lifetime τ (♦, left scale) and stretching exponents β (▲, right scale) from fits to a stretched exponential model of the intensity decay of erythrosin B in amorphous sucrose.

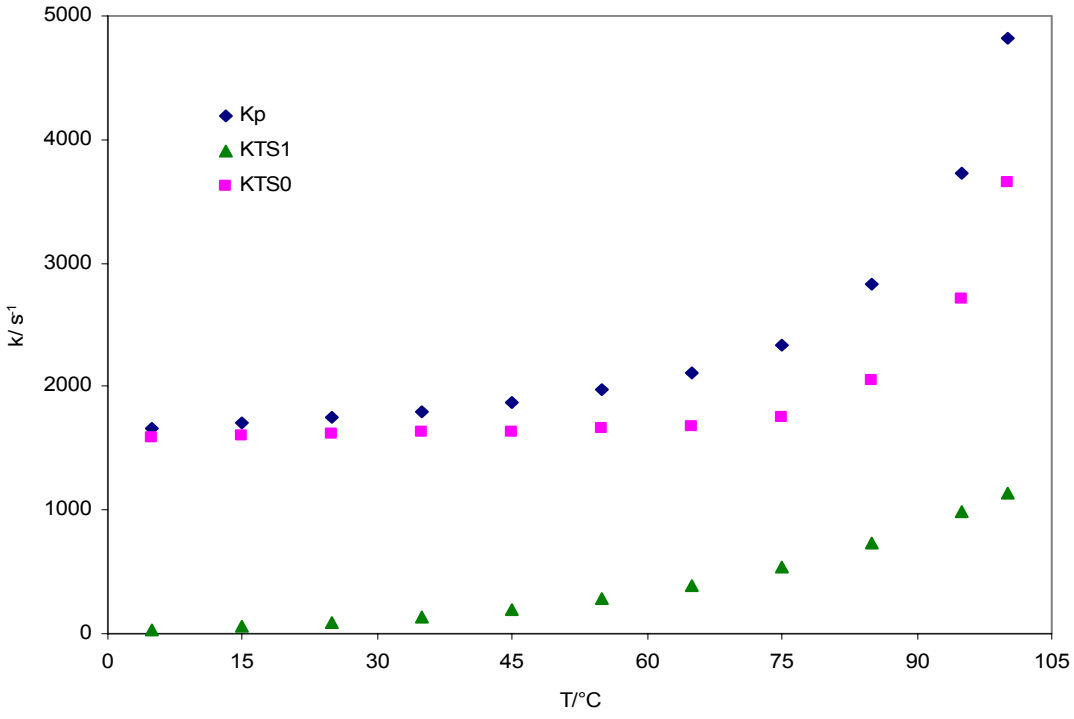

Figure 8 Temperature dependence of the total rate constant for nonradiative decay of the triplet state ($k=k_{RP}+k_{TS0}+k_{TS1}$, ♦), the rate of reverse intersystem crossing to S_1 (k_{TS1}, ▲), and the rate of nonradiative decay to S_0 (k_{TS0}, ■) of erythrosin B in amorphous sucrose over the temperature range from 5 to 100°C; values were calculated from the lifetime data in Figure 6.

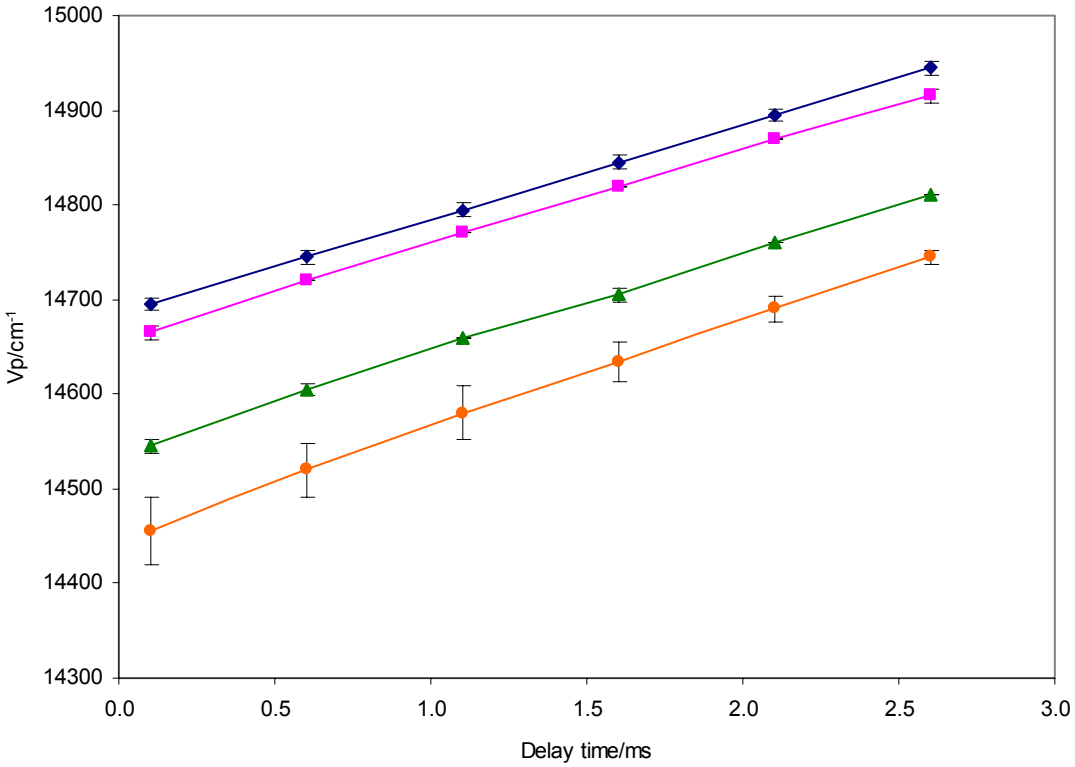

Figure 9 Blue shift of the phosphorescence emission spectrum of erythrosin B as a function of time after excitation in amorphous sucrose films at below and above T_g. The emission energy collected over a 0.5-ms window is plotted versus the time delay in films at 5°C (♦), 25°C (■), 55°C (▲), and 75°C (●).

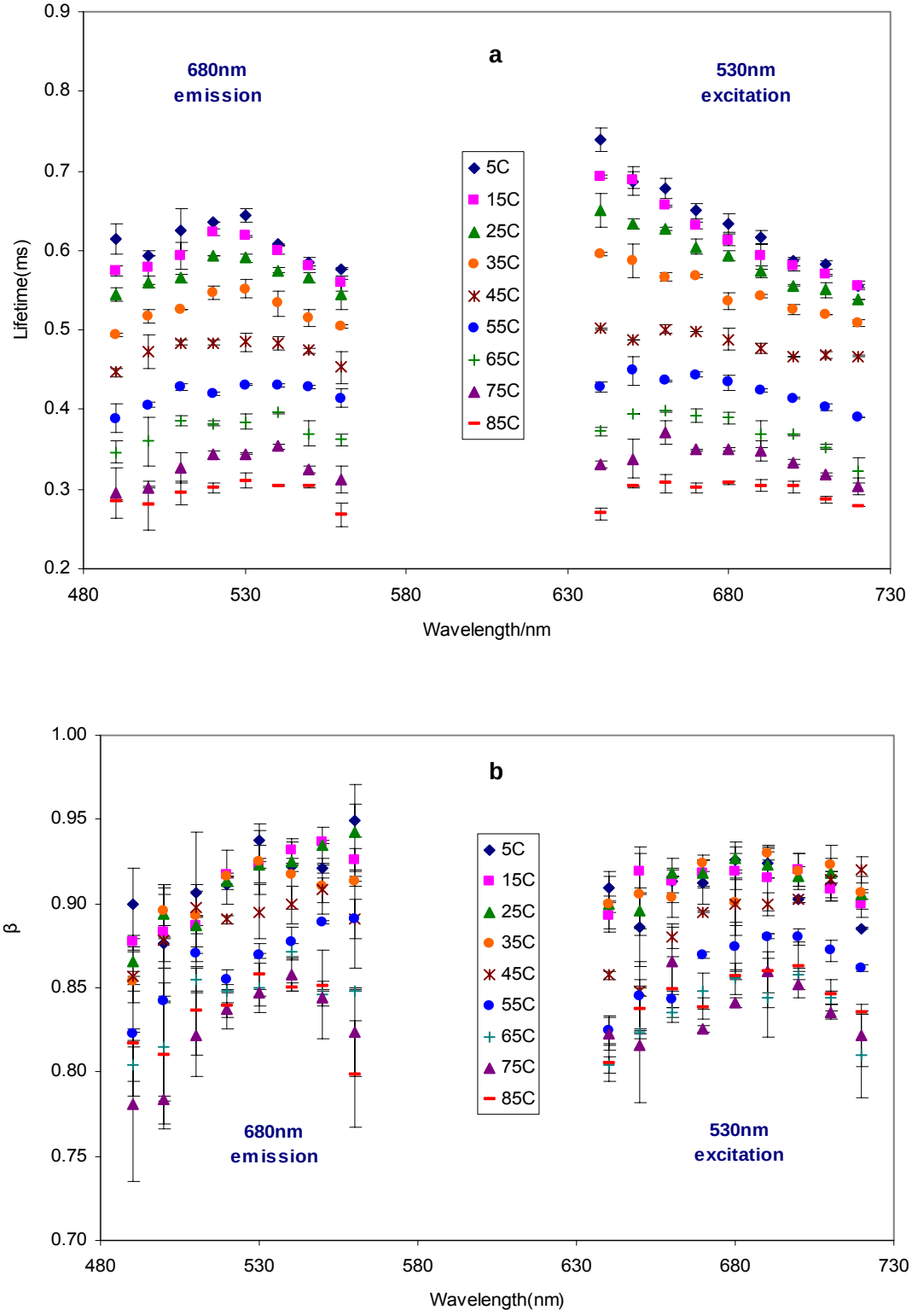

Figure 10 Lifetimes (a, upper) and stretching exponents β (b, lower) from fits to the stretched exponential model of intensity decays of erythrosin B in amorphous sucrose film collected as a function of excitation wavelength (with 680 nm emission) or emission wavelength (with 530 nm excitation).

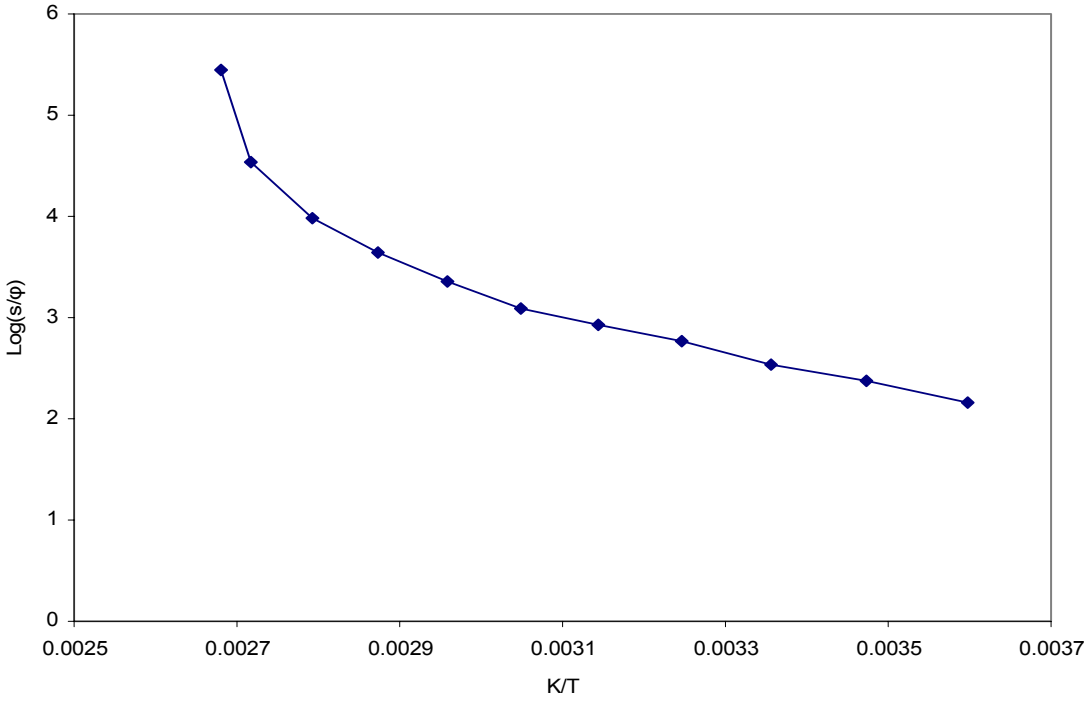

Figure 11 Arrhenius plot of the rate for dipolar relaxation (1/φ) in amorphous sucrose film as a function of inverse temperature.

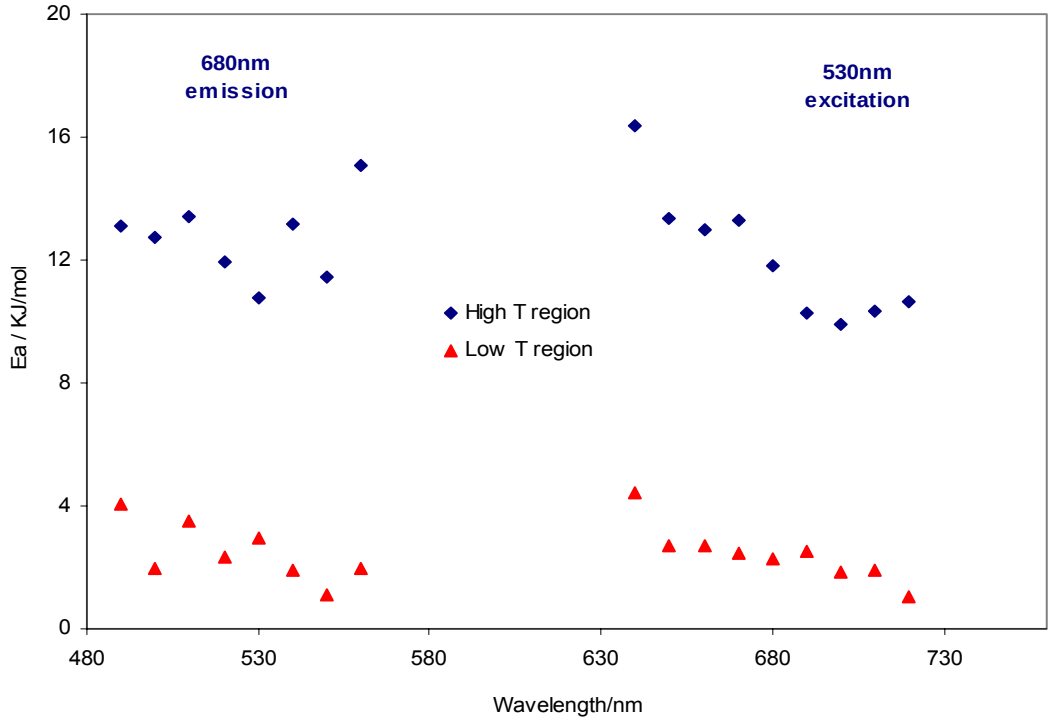

Figure 12 Apparent activation energy (E_A) for nonradiative decay rate of erythrosin B in the sucrose glass (♦) below and melt (▲) above Tg as a function of excitation and emission wavelength (calculated from an Arrhenius analysis of the data in Figure 9a sing the three lowest and highest temperatures, respectively).

Chapter 2 Factors affecting phosphorescence measurement

Introduction

Sucrose is one of the most widely used disaccharides in foods, biomaterials and pharmaceuticals for long-term storage (Noel et al., 2000) because of its propensity to form into an amorphous, non-crystalline solid upon rapid drying from aqueous solution or cooling from the melt and because, as a non-reducing sugar, it does not react with amino groups. Amorphous sucrose also acts as a natural protectant in biological materials (Crowe et al., 1998) as well as forming the basis for the worldwide confection industry. Because amorphous sucrose is thermodynamically unstable, it is also one of the major compounds in foods responsible for physical degradation reactions that include crystallization, caking/lumping, structural collapse, and stickiness (Roos, 1995; Fennema, 1996; Goff and Sahagian, 1996; Labuza et al., 2004).

Through the glass transition characteristic of amorphous materials many discontinuous changes occur in macroscopic properties such as viscosity, mechanical modulus and thermal properties (specifically, heat capacity C_p) (Angell, 1995). The dynamical glass transition is associated with molecular motions within the amorphous solid: above the glass transition temperature T_g the activated translational motion facilitates flow in melts and rubbery solids, while below T_g glassy solids are in a rigid state because the matrix molecules can only undergo limited vibrational and rotational motions (Zallen, 1998; Ludescher et al., 2001; Pravinata et al., 2005). The temperature-dependent molecular mobility thus controls physical and chemical properties by

---

Parts of this section have been published in Applied Spectroscopy and are included here verbatim.

modulating the nature and kinetics of reactions that occur during processing and storage of biomaterials.

The measurement of mobility in sucrose and other amorphous solid carbohydrates and proteins is of fundamental interest because it relates to questions of stability of the biological materials as well as degradation phenomena in amorphous foods (Roos, 1995; Fennema, 1996; Hancock and Zografi, 1997; Pikal, 2002; Buitink and Leprince, 2004). The connection between matrix mobility and stability is straightforward: the rates of chemical reaction and physical change in highly viscous amorphous solids are diffusion controlled and matrix molecular mobility controls the rates of molecular diffusion (Roos, 1995). The specific mechanisms by which molecular mobility controls diffusion remain, however, uncertain. A number of techniques have been used to characterize the properties and mobility of amorphous materials including Fourier transform infrared spectroscopy (FTIR), differential scanning calorimetry (DSC), nuclear magnetic resonance spectroscopy (NMR), and dynamic mechanical thermal analysis (DMTA). Recently, phosphorescence spectroscopy has been used to monitor the rate of dielectric relaxation around the excited triplet state of luminescent probes doped within supercooled liquids and amorphous solids (Richert, 2000). Optical techniques such as phosphorescence are rapid, sensitive, versatile, and use inexpensive instrumentation; however, they also require the use of specific chromophores as molecular probes, molecules that must often be introduced into the matrix.

Erythrosin B (tetra-iodofluorescein) is perhaps the most commonly used phosphorescence triplet probe because of its high signal-to-noise, sensitivity to molecular environment, site selectivity and experimental versatility. Based on phosphorescence

quenching by oxygen, erythrosin B (Ery B) is well suited for sensing both gaseous and dissolved oxygen when embedded in optical fibers (Vanderkooi et al., 1987; Diaz-Garcia et al., 1995; Lam et al., 1998, 2001; Chan et al., 2000, 2002; Gillanders et al., 2004a, 2004b) or for probing oxygen diffusion when dispersed in amorphous films (Simon-Lukasik and Ludescher, 2004). Due to its high phosphorescence quantum yield at room temperature in aqueous solution (Garland et al., 1979; Duchowicz, 1998), Ery B, along with the related xanthene probe eosin, has been widely used to study protein rotational dynamics on the micro- to millisecond time scale in both water-soluble and membrane-bound proteins (Cherry et al., 1976; Moore et al., 1979; Lettinga et al., 1999; Zidovetski et al., 1986; Ludescher and Thomas, 1988; Stein et al., 1990; Prochniewicz et al., 1996). Recent studies have shown that erythrosin phosphorescence can provide insight into the slow molecular mobility and dynamic site heterogeneity in amorphous solid proteins (Simon and Ludescher, 2004; Lukasik and Ludescher, 2006a, 2006b) and sugars (Pravinata et al., 2005; Shirke et al., 2005; Shirke and Ludescher, 2005a, 2005b) both below and above the glass transition temperature.

These studies of amorphous sugars have used the free acid of Ery B to avoid potential complications due to charges on the probe modulating the local structure and mobility of the amorphous solid matrix. The free acid of Ery B, however, is poorly soluble in water and thus must be introduced via an organic solvent. Owing to its aprotic and dipolar nature, N, N-dimethyl formamide (DMF) is selected for probe stability during long term storage. However, DMF may not be removed completely from the matrix during the sample preparation and may affect the matrix mobility. It is also possible that the aromatic ring system of Ery B may lead to probe aggregation within a polar

biomaterial matrix (Pant et al., 1971). The question of whether the presence of DMF and the local concentration of probe in the matrix may influence the spectra thus becomes a concern. Shah and Ludescher (1995) found that dispersion of small amount of Ery B did not perturb the glass transition temperature T_g of the matrix. This chapter reported a detailed investigation of how variations in the local concentration of probe as well as the presence of the dispersing solvent affects the emission energy, bandwidth (full-width at half-maximum, FWHM), and lifetime of Ery B in amorphous sucrose.

Materials and Methods

1. Sample Preparation

We prepared glassy sucrose films by using a slightly modified version of our published method (Pravinata et al., 2005; see details in Materials and Methods in Chapter 1).

The moisture content of glassy sucrose films was determined by gravimetric methods to be less than 1 wt %; this low value was presumably due to the extensive equilibration time and the thinness of the films. We thus estimated that the T_g of these films was ~63°C using the equation for the dependence of T_g on moisture content developed by Crowe and colleagues (Sun et al., 1996).

Films with Ery B at mole ratios ranging from $0.5x10^{-4}$ to $10x10^{-4}$ Ery B/sucrose were prepared. In order to avoid complications due to differences in concentration of the residual dispersing solvent DMF, two concentrations of Ery B/DMF stock solution were used to prepare film-forming solutions. Aliquots from a 10 mM Ery B stock solution were mixed with sucrose to prepare solutions with a mole ratio of 0.5 and $1x10^{-4}$ while

aliquots from a 100 mM Ery B stock solution were mixed with sucrose to form-film forming solutions with a mole ratio of 5 and $10x10^{-4}$. Films with mole ratio of 0.5 and $5x10^{-4}$ were thus prepared from film-forming solutions with the same concentration of DMF (around 1.2 % v/v DMF) and the same was true of films with mole ratios of 1 and $10x10^{-4}$ (around 2.5 % v/v DMF).

To make sucrose thin films with a mole ratio of $1x10^{-4}$ Ery B/sucrose but different concentrations of DMF, aliquots from Ery B stock solutions with concentrations of 1 mM, 10 mM and 100 mM were added to different sucrose solutions giving volume concentrations of DMF in the solution mixture of 25%, 2.5% and 0.25%, respectively. After thin films were prepared, spectra were collected and spectrophotometric properties were compared among the three kinds of films.

2. Luminescence measurements and analysis

Luminescence measurements were made using a Cary Eclipse fluorescence spectrophotometer (Varian Instruments, Walnut Creek, CA). Prior to any phosphorescence measurements, all samples were flushed for at least 15 minutes with nitrogen gas which contained less than 1 ppm oxygen to eliminate oxygen quenching. All the measurements were made in triplicate at least. The temperature of the sample holder was controlled using a thermo-electric temperature controller (Varian Instruments, Walnut Creek, CA). Samples were equilibrated at each target temperature for 1 min/°C increase in temperature.

Delayed fluorescence and phosphorescence emission spectra were collected from 520 nm to 750 nm (10 nm bandwidth) at 1 nm intervals using excitation at 500 nm (20 nm bandwidth) over a temperature range from 5 to 100°C with an observation window of

5.0 ms and an initial delay time of 0.1 ms to suppress fluorescence coincident with the lamp pulse. An emission spectrum from sucrose film without probe was subtracted from each spectrum although the signal from background was very low.

For lifetime measurements, samples were excited at 530 nm (20 nm bandwidth) and emission transients were collected at 680 nm (20 nm bandwidth) over the temperature range from 5 to 100°C. Phosphorescence intensity decays were collected over a window of 4 ms with an initial delay of 0.1 ms and increments of 0.04 ms. Because intensity decays were non-exponential, a stretched exponential function was selected to analyze the intensity decays (Richert, 2000; Lee et al. 2001; Pravinata et al., 2005).

$$I(t) = I(0) \exp[-(t/\tau)^{\beta}] + \text{constant} \quad (1)$$

Where I(0) is the initial intensity, τ is the stretched exponential lifetime, and β is an exponent varying from 0 to 1 that characterizes the lifetime distribution (Lindsey and Patterson, 1980). The use of a stretched exponential model provides an analysis in terms of a continuous distribution of lifetimes, which is appropriate for describing a complex glass possessing a distribution of relaxation times for the dynamic molecular processes. The smaller the β value, the more non-exponential the intensity decays and the broader the distribution of lifetimes. The program NFIT (Galveston, TX) was used to fit the decays; goodness of fit was evaluated by examining χ^2 and R^2. Plots of modified residuals (defined as the difference between the intensity from the fit decay curve and the measured intensity divided by the square root of the measured intensity) was also used as an indicator of the goodness of fit. R^2 for all fits ranged from 0.99 to 1.00 and modified residuals plots fluctuated randomly around zero amplitude.

The energy of the emission maximum (ν_p) and the FWHM of the emission band were determined by using a log-normal line shape function (Maroncelli and Fleming, 1987) to fit both delayed fluorescence and phosphorescence.

$$I(\nu) = I_0 \exp\left\{-\ln(2)\left(\frac{\ln[1+2b(\nu-\nu_p)/\Delta]}{b}\right)^2\right\} \quad (2)$$

Where I_0 is the maximum emission intensity, ν_p is the peak frequency (cm^{-1}), Δ is a linewidth parameter and b is an asymmetry parameter. The bandwidth Γ (= FWHM) is calculated according to the following equation:

$$\Gamma = \Delta\left(\frac{\sinh(b)}{b}\right) \quad (3)$$

For delayed luminescence spectra collected from 520-750 nm, a sum of log-normal functions for delayed fluorescence ($I_{DF}(\nu)$) and phosphorescence ($I_P(\nu)$) were used to fit the spectra. Each emission band was analyzed for independent fit parameters using a sum of two functions as described in Eq. 2.

The phosphorescence lifetime is directly related to the sum of the de-excitation rates for the excited triplet state (Duchowicz et al., 1998).

$$\tau = (k_{RP} + k_{TS1} + k_{TS0} + k_Q[O_2])^{-1} \quad (4)$$

Here k_{RP} is the rate of radiative emission to S_0 (equal to 41 s^{-1} for Ery B; Duchowicz et al., 1998; Lettinga et al., 2000), k_{TS1} is the rate of reverse intersystem crossing to S_1, k_{TS0} is the rate of intersystem crossing to S_0, and $k_Q[O_2]$ is the oxygen quenching rate (which is assumed negligible for this study due to the elimination of oxygen). The rate constant for reverse intersystem crossing is a thermally activated process that follows Arrhenius kinetics (Parker, 1968):

$$k_{TS1}(T) = k_{TS1}^{o} \exp(-\Delta E_{TS}/RT) \quad (5)$$

where k_{TS1}^0 is the maximum reverse intersystem crossing rate at high temperature and ΔE_{TS} is the energy gap between T_1 and S_1. The term k_{TS0} reflects the rate at which the probe can dissipate the energy of the excited T_1 state as heat into the surrounding matrix (Papp and Vanderkooi, 1989). The phosphorescence lifetime thus varies with temperature due to changes in the magnitude of k_{TS1} and k_{TS0}. Since k_{TS1} can be calculated using measurements of ΔE_{TS}, and k_{TS1}^o can be estimated as described elsewhere (Pravinata et al., 2005; Shirke et al., 2005), the magnitude of k_{TS0} can be calculated by difference from Eq. 4.

The ratio of the emission intensity for delayed fluorescence (I_{DF}) and phosphorescence (I_P) is related to k_{TS1}, k_{RP} and the quantum yield for fluorescence (ϕ_F) (Duchowicz et al., 1998):

$$I_{DF}/I_P = \phi_F k_{TS1}/k_{RP} \quad (6)$$

Since k_{TS1} is an Arrhenius process (Eq. 5), a plot of $\ln(I_{DF}/I_P)$ versus 1/T has slope of $-\Delta E_{TS}/R$.

Results

1. Delayed emission spectra

Delayed emission spectra of Ery B at 25°C in amorphous sucrose films with Ery B/sucrose mole ratios of 0.5 and $5x10^{-4}$ are plotted in Figures 13a, as relative intensity normalized to the emission maximum. As each pair of samples was prepared from sucrose solutions containing different concentrations of Ery B but the same volume % DMF, and thus the final films presumably contain the same amounts of residual DMF solvent, the spectral properties measured for each pair reflect the influence of erythrosin

concentration only. These emission spectra of samples at 25°C with 10-fold different probe concentrations were essentially identical in shape and in position (wavelength). Emission spectra were collected over the temperature range from 5 to 100 °C (data not shown here) and the peak energy and bandwidth for both delayed fluorescence and phosphorescence emission were determined by fitting to a log-normal line shape function (Eq. 2). The delayed fluorescence exhibited similar behavior in peak frequency for both pairs of concentrations while the bandwidth was almost constant for all concentrations over the entire temperature range (data not shown). The effect of temperature on the phosphorescence emission energy (peak frequency, ν_p) and bandwidth (FWHM) for films with 0.5 and $5x10^{-4}$ Ery B/sucrose ratios are shown in Figures 13b and 13c, respectively; plots from samples with a 10-fold difference in mole ratio were essentially identical in both emission energy and bandwidth. Similar behavior was seen in the emission spectra of films with Ery B/sucrose ratios of 1 and $10x10^{-4}$ (Figures 14a, 14b, and 14c).

Delayed emission spectra of Ery B in sucrose films with mole ratio of $1x10^{-4}$ prepared from 1 mM, 10 mM and 100 mM stock solution were also collected as a function of temperature. The delayed emission spectra of these samples at 25°C are plotted in Figure 15a. It is obvious that samples made from the 10 mM and 100 mM stock solutions (that is, samples with lower initial and thus residual DMF concentration) displayed identical spectra while the spectrum of the sample made from the 1 mM stock solution (that is, the sample with higher residual DMF concentration) was shifted to longer wavelength. Emission energy and bandwidth obtained from fitting are plotted versus temperature in Figures 15b and 15c. There were no noticeable differences in the peak frequency or bandwidth in sucrose films made from 10 mM and 100 mM Ery B

stock solutions, while these parameters were significantly different in samples made from the 1 mM stock solution. In the samples made from 1 mM stock solution, the peak frequency was shifted to lower values over the entire temperature range while the bandwidth was significantly smaller at higher temperatures.

2. Phosphorescence decay

Phosphorescence intensity decay transients were measured from 5 to 100°C for all samples; all decays were satisfactorily fit using a stretched exponential decay model (Pravinata et al., 2005). The lifetime τ and the stretching exponent β are the physical parameters used to describe the decay rates and the dynamic heterogeneity, respectively, within the decay processes.

The stretched exponential lifetimes for pairs of different probe concentrations are plotted versus temperature in Figure 16. The plots of lifetime versus temperature from samples with a 10-fold difference in probe concentration were nearly identical at both lower (0.5 and $5x10^{-4}$; Figure 16a) and higher (1 and $10x10^{-4}$; Figure 16b) Ery B/sucrose mole ratios; comparable plots of β versus temperature were also nearly identical at both lower and higher ratios (Figure 17a and Figure 17b).

The lifetimes of Ery B in sucrose films prepared with probe stock solutions of different concentration are plotted versus temperature in Figure 18a. Films made with 10 mM and 100 mM Ery B stock solutions, and thus lower residual DMF concentrations, exhibited similar lifetimes over the entire temperature range. However, in films made from 1 mM Ery B solution, where the concentration of residual DMF was larger, the stretched lifetimes exhibited a different trend, being comparable to or slightly longer in the glass below and significantly shorter in the melt above the sucrose T_g (around 63°C).

The values of β were identical within error in films made from 10 mM and 100 mM stock solutions (Figure 18b). In films prepared from 1 mM stock solution, the β values were slightly higher at low temperature and slightly lower around the sucrose T_g; however, this effect may not be significant.

Discussion

We have recently shown that phosphorescence from the triplet state of the xanthene chromophore of the free acid of Ery B is sensitive to dipolar relaxation and collisional quenching on the micro- to millisecond time scale in amorphous solid sugars (Pravinata et al., 2005; Shirke et al., 2005; Shirke and Ludescher, 2005a, 2005b) and gelatin (Simon-Lukasik and Ludescher, 2004; Lukasik and Ludescher, 2006a, 2006b). Here we demonstrate that the probe emission energy and lifetime, the spectroscopic observables used to monitor dipolar relaxation and collisional quenching, are not influenced by aggregation of the probe within the dehydrated solid matrix or by the effects of residual DMF solvent. This study thus confirms that the spectroscopic behavior of the probe solely reflects the properties of the amorphous matrix in which it is embedded and demonstrates that the technique is sufficiently robust to be used to probe the mobility of amorphous solids under a variety of conditions.

1. Probe concentration

Ery B molecules may aggregate to form dimers, trimers or larger clusters at sufficiently high probe concentrations or as a result of dehydration induced changes within the amorphous solid. The emission spectra of probe clusters differ in emission energy and band shape from those of monomers. Pant et al. (1971) observed the xanthene

probes Ery B and Eosin Y in a concentrated glycerol-water glass at 80K and found that at higher concentrations the phosphorescence intensity was dramatically enhanced while both the delayed fluorescence and phosphorescence emission bands shifted to longer wavelengths; the delayed fluorescence band also split into two bands due to exciton interactions between adjacent chromophores. Stomphorst et al. (2001) investigated the effect of concentration on the spectra of Ery B embedded in polyvinyl alcohol films. They observed broadening and spectral shifts at higher concentrations in this non-polar matrix and postulated that this behavior reflected the formation of small clusters through the interaction of carboxyl and hydroxyl groups.

Comparison of the normalized phosphorescence intensity (I_P) for sucrose films with Ery B/sucrose mole ratios of 0.5 versus $5x10^{-4}$ (and 1 versus $10x10^{-4}$) clearly indicated that there was no change in the emission peak wavelengths over a 10-fold increase in concentration. While there was a slight (~7%) increase in the ratio of phosphorescence to delayed fluorescence, this increase was dramatically less than that seen in the study of Pant et al. (1971); there was also no detectable splitting or generation of a shoulder in the delayed fluorescence band indicative of exciton splitting. These results indicate that a 20-fold increase in the concentration of Ery B did not induce appreciable formation of aggregates in the sucrose films. The spectral bandwidth, a measure of the inhomogeneous broadening of the emission band (Pravinata et al., 2005), was not affected by concentration over the whole temperature range, implying that the measured distribution of energetically distinct matrix environments in the amorphous sucrose films was identical at the different probe concentrations.

The absence of any observable effect of probe concentration on delayed luminescence properties is further supported by an analysis of the S_1-T_1 energy gap ΔE_{TS} obtained from a van't Hoff plot of $\ln(I_{DF}/I_P)$ versus 1/T using the maximum emission intensity values determined from fitting spectra to a log normal function. Plots at mole ratios of 0.5, 1, 5 and $10x10^{-4}$ Ery B/sucrose mole ratios were all linear with correlation coefficients ≥ 0.998 (data not shown); the energy gaps calculated from these plots were identical within error with values of 31.84 ± 0.84, 31.60 ± 0.38, 31.37 ± 0.33, and 31.60 ± 0.13 kJ mol^{-1}, respectively, indicating that dipolar interactions between probe molecules and the sucrose matrix were similar at all concentrations studied.

The phosphorescence lifetime provides information about the triplet state non-radiative quenching rates (Duchowicz et al., 1998; Lettinga et al., 2000) (see Materials and Methods). The decrease in phosphorescence lifetime with increase in temperature seen in amorphous sucrose reflects increases in both the rate of reverse intersystem crossing to T_1, k_{TS1}, and the rate of intersystem crossing to S_0, k_{TS0} (Pravinata et al., 2005). The essentially identical Ery B lifetimes seen at mole ratios of 0.5 and $5x10^{-4}$ and 1 and $10x10^{-4}$ thus indicate that the probes sample matrix environments with essentially identical values for the total rate of non-radiative quenching ($k_{TS1} + k_{TS0}$) at all temperatures. Since films with different probe concentrations had identical values of ΔE_{TS}, the effect of temperature on k_{TS1} in the different films was identical and thus the similarity in lifetimes implies a similarity in the rates of k_{TS0} in the films with different probe concentrations (Pravinata et al., 2005; Shirke et al., 2005).

The magnitude of k_{TS0} reflects internal processes that determine the extent of vibrational coupling between the excited T_1 state and the ground S_0 state as well as

external processes due to interactions between the probe molecule and its environment that affect how probe vibrational energy is dissipated into the surrounding matrix (Papp and Vanderkooi, 1989). Since the latter process is related to the molecular mobility of the matrix (Pravinata et al., 2005; Strambini and Gonnelli, 1985; Gonnelli and Strambini, 1995; Fischer et al., 2002) the magnitude of k_{TS0} provides a measure of matrix mobility. Similarity in lifetime thus implies similarity in the dynamic environment of the Ery B probe in the different sucrose films (Figure 19a and Figure 19b).

We thus conclude that over the concentration range from 0.5 to $10x10^{-4}$ mole ratio of probe to sugar, Ery B luminescence reports the behavior of individual probe molecules dispersed randomly throughout the sugar matrix. Ery B molecules in films with probe/sucrose ratios of 0.5, 1, 5, and $10x10^{-4}$ are thus separated on average by approximately 27, 22, 13, and 10 sucrose molecules, respectively.

2. Solvent effect

DMF acts as a dispersing solvent for Ery B in sucrose solutions and can be used to introduce the probe into an amorphous solid matrix under study. The sucrose solutions used to make sucrose films contained 25, 2.5 and 0.25 % (v/v) DMF when made with 1 mM, 10 mM and 100 mM Ery B stock solutions, respectively. Owing to its high boiling point (around 153°C), DMF most likely will not be completely removed during drying. The residual polar DMF may not only influence the emission energy of the triplet excited state T_1 but may also influence k_{TS0} and, perhaps, k_{TS1}. Dipolar relaxation around the triplet excited state of the probe should red-shift the emission spectrum. The magnitude of the red-shift should increase with an increase in concentration of residual solvent and

with the mobility of the matrix; the lifetime will also decrease if the mobility of the matrix increases (Pravinata et al., 2005).

Based on the similarity in emission energy of samples made from 10 mM and 100 mM stock solutions, the residual DMF concentration in these samples was too low to influence the spectroscopic properties of Ery B. The effect of temperature on the emission spectra (Figure 15) and lifetimes (Figure 18a) in these two samples was identical within error. However, the emission spectra of Ery B in the films produced from 1 mM stock solution were shifted to lower energy over the whole temperature range; the red-shift was approximately constant at low temperature and increased above ~45°C.

The lifetime in films made from 1 mM stock solution was also significantly lower at high temperature than the lifetime in films made with higher concentrations of DMF. DMF, as a small molecule diluent within the glassy matrix, will decrease the sucrose T_g. At all temperatures above the new sucrose T_g, the matrix will be a melt rather than a glass and consequently have higher molecular mobility and thus a lower probe lifetime. Arrhenius analysis of the effect of temperature on k_{TS0} clearly indicates that the matrix softens at a lower temperature in films made from 1 mM than in those from 10 and 100 mM DMF stock solutions (Figure 19c); the softening temperature, determined from extrapolation of the $\ln(k_{TS0})$ curves at high and low temperature, was 48, 71 and 74°C, respectively, in the films made from 1, 10, and 100 mM stock solutions. The former is significantly below while the latter are above the estimated T_g of these sucrose films.

The significant emission red shift seen in the films made from 1 mM DMF stock appears to reflect both direct dipolar interactions between DMF and Ery B and an indirect effect of DMF on the mobility of the sucrose matrix. Polar DMF molecules partitioned

near the probe will lower the Ery B emission energy by direct dipolar interactions with the excited triplet state; this appears to be the dominate effect at low temperature where the Arrhenius plots in Fig. 19c indicate that the matrix mobility is largely unaffected by the presence of DMF. On the other hand, the plasticizing effect of DMF on the sucrose T_g appears to increase the rate of matrix dipolar relaxation around the excited triplet state (and thus the extent of red-shift) at higher temperature in a manner similar to the increase in k_{TS0}. This qualitative argument would be significantly enhanced by studies in which the spectroscopic properties of Ery B are directly correlated with the concentration of DMF in the amorphous solid sucrose matrix, studies similar to those on the effect of residual water on probe phosphorescence in glucose glasses (Mendonsa and Hurtubise, 2001).

Conclusion

The phosphorescence of erythrosin B is sensitive to local dipolar relaxation and collisional quenching in the sucrose glass as well as in the melt. Measurements of probe phosphorescence in amorphous sucrose provide valuable information about the molecular events associated with matrix properties and storage stability. The concentration of Ery B and the presence of residual dispersing solvent (DMF) are two potentially important factors that may affect phosphorescence measurements. Our results show that variations in probe concentration over the range from 0.5 to $10x10^{-4}$ (probe/sucrose mole ratio) and 10-fold variations in the amount of DMF used to disperse the probe, did not affect the shape of the emission spectra, the emission energy, or the measured lifetimes of Ery B in amorphous sucrose. The spectroscopic properties of Ery B in amorphous sucrose

prepared over a broad range of conditions thus reflect the behavior of individual probe molecules dispersed in the sucrose matrix, demonstrating the feasibility of using exogenous spectroscopic probes to monitor molecular mobility and dynamic site heterogeneity in a variety of amorphous biomaterials including dried and frozen foods, food ingredients, pharmaceuticals, seeds, spores, and even whole organisms.

References

Angell, C.A. 1995. Formation of glasses from liquids and biopolymers. *Science*, 267, 1924-1935.

Buitink, J. and Leprince, O. 2004. Glass formation in plant anhydrobioties: survival in the dry state. *Cryobiol.* 48, 215-228.

Chan, M.A., Lawless, J.L., Lam, S.K. and Lo, D. 2000. Fiber optic oxygen sensor based on phosphorescence quenching by erythrosin B trapped in silica-gel glasses. *Anal. Chim. Acta.* 408, 33-37.

Chan, M.A., Lam, S.K. and Lo, D. 2002. Characterization of Erythrosin B-Doped Sol-Gel Materials for Oxygen Sensing in Aqueous Solutions. *J. Fluoresc.* 12, 327-332.

Cherry, R.J., Cogoli, A., Oppliger, M., Schneider, G. and Semenza, G. 1976. A spectroscopic technique for measuring slow rotational diffusion of macromolecules. 1: Preparation and properties of a triplet probe. *Biochem.* 15, 3653-3656.

Crowe, J.H., Carpenter, J.F. and Crowe, L.M. 1998. The role of vitrification in anhydrobiosis. *Ann. Rev. Physiol.* 60, 73-103.

Diaz-Garcia, M.E., Pereiro-Garcia, R. and Velasco-Garcia, N. 1995. Optical oxygen sensing materials based on the room temperature phosphorescence intensity quenching of the immobilized erythrosin B. *Analyst* (Cambridge, UK) 120, 457-461.

Duchowicz, R., Ferrer, M.L. and Acuna, A.U. 1998. Kinetic spectroscopy of erythrosin phosphorescence and delayed fluorescence in aqueous solution at room temperature. *Photochem. Photobiol.* 68, 494-501.

Fennema, O. 1996. Water and Ice. In *Food Chemistry*, 3rd Edition. Marcel Dekker, Inc. N.Y.

Fischer, C.J., Gafni, A., Steele, D.G., and Schauerte, J.A. 2002. The triplet state lifetime of indole in aqueous and viscous environments: Significance of the interpretation of room temperature phosphorescence in proteins. *J. Am. Chem. Soc.* 124, 10359-10366.

Garland, P.B. and.Moore, C.H. 1979. Phosphorescence of protein-bound eosin and erythrosine. A possible probe for measurements of slow rotational mobility. *Biochem. J.* Dec 1; 18(3), 561-572.

Gillanders, R.N., Tedford, M.C., Crilly, P.J. and Bailey, R.T. 2004a. Erythrosin B encapsulated in a fluoropolymer matrix for dissolved oxygen optical sensing in aggressive aqueous environments. *J. Photochem. Photobiol. A: Chem.* 162, 531-535.

Gillanders, R.N., Tedford, M.C., Crilly, P.J. and Bailey, R.T. 2004b. A composite sol-gel/fluoropolymer matrix for dissolved oxygen optical sensing. *J. Photochem. Photobiol. A: Chem*. 163, 193-199.

Goff, H.D. and Sahagian, M.E. 1996. Glass transitions in aqueous carbohydrate solutions and their relevance to frozen food stability. *Thermochim. Acta.* 280/281, 449-464.

Gonnelli, M. and Strambini, G.B. 1995. Phosphorescence lifetime of tryptophan in proteins. *Biochem.* 34, 13847-13857.

Hancock, B.C. and Zografi, G. 1997. Characteristics and significance of the amorphous state in pharmaceutical systems. *J. Pharm. Sci.* 86, 1-12.

Labuza, T., Roe, K., Payne, C., Panda, F., Labuza, T.J., Labuza, P.S. and Krusch, L. 2004. Storage stability of dry food systems: influence of state changes during drying and storage. *Proceedings of the 14th international drying symposium* (IDS 2004) Sao Paulo Brazil. 22-25 August. Vol A. pp. 48-68.

Lam, S.K., Namdas, E. and Lo, D. 1998. Effects of oxygen and temperature on phosphorescence and delayed fluorescence of erythrosin B trapped in sol-gel silica. *J. Photochem. Photobiol. A: Chem.* 118, 25-30.

Lam, S.K., Chan, M.A., and Lo, D. 2001. Characterization of phosphorescence oxygen sensor based on erythrosin B in sol-gel silica in wide pressure and temperature ranges. *Sens. Actuators B.* 73, 135-141.

Lee, K.C.B., Siegel, J., Webb, S.E.D., Leveque-Fort, S., Cole, M.J., Jones, R., Dowling, K., Lever, M.J., and French, P.M.W. 2001. Application of the stretched exponential function to fluorescence lifetime imaging. *Biophys. J.* 81, 1265-1274.

Lettinga, M.P., Klarenbeek, E.M., Zuihof, H., and van Zandvoort, M.A.M.J. 1999. The orientation of the phosphorescence dipole moment of erythrosine B within its molecular frame. *J. Fluoresc.* 9, 265-279.

Lettinga, M.P., Zuilhof, H. and van Zandvoort, A.M.J. 2000. Phosphorescence and fluorescence characterization of fluorescein derivatives immobilized in various polymer matrices. *Phys. Chem. Chem. Phys.* 2, 3697-3707.

Lindsey, C.P. and Patterson, G.D. 1980. Detailed comparison of the Williams-Watts and Cole-Davidson functions. *J. Chem. Phys.* 73, 3348-3357.

Ludescher, R.D., Shah, N.K., McCaul, C.P. and Simon, K.V. 2001. Beyond T_g: optical luminescence measurements of molecular mobility in amorphous solid foods. *Food Hydrocolloids.* 15, 331-339.

Ludescher, R.D. and Thomas, D.D. 1988. Microsecond rotational dynamics of phosphorescent-labeled in muscle cross-bridge. *Biochem.* 27, 3343-3351.

Lukasik, K.V. and Ludescher, R.D. 2006a. Molecular mobility in water and glycerol plasticized cold and hot-cast gelatin films. *Food Hydrocoll.* 20, 96-105.

Lukasik, K.V. and Ludescher, R.D. 2006b. Effect of plasticizer on dynamic site heterogeneity in cold-cast gelatin films. *Food Hydrocoll.* 20, 88-95.

Maroncelli, M. and Fleming, G.R. 1987. Picosecond salvation dynamics of coumarin 153: the importance of molecular aspects of salvation. *J. Chem. Phys.* 86, 6221-6239.

Mendonsa, S.D. and Hurtubise, R.J. 2001. Interactions of phosphors in glucose glasses for solid-matrix phosphorescence. *Appl. Spectrosc.* 55, 1385-1393.

Moore, C., Boxer, D. and Garland, P. 1979. Phosphorescence depolarization and the measurement of rotational motion of proteins in membranes. *FEBS Lett.* 108, 161-166.

Noel, T.R., Parker R. and Ring, S.G. 2000. Effect of molecular structure and water content on the dielectric relaxation behaviour of amorphous low molecular weight carbohydrates above and below their glass transition. *Carbohydr. Res.* 329, 839-845.

Pant, D.D., Bhagchandani, C.L., Pant, K.C. and Verma, S.P. 1971. Aggregation of xanthene dyes: exciton emission and phosphorescence enhancement. *Chem. Phys. Lett.* 9, 546-547.

Papp, S. and Vanderkooi, J.M. 1989. Tryptophan phosphorescence at room temperature as a tool to study protein structure and dynamics. *Photochem. Photobiol.* 49, 775-784.

Parker, C.A. 1968. *Photoluminescence of Solutions.* Elsevier, Amsterdam. Netherlands.

Pikal, M.J. 2002. "Chemistry in Solid Amorphous Matrices: Implication for Biostabilization", in *Amorphous Food and Pharmaceutical Systems*, H. Levine, Ed. (The Royal Society of Chemistry), Chap. 6, p.257.

Pravinata L.C., You, Y. and Ludescher, R.D. 2005. Erythrosin B phosphorescence monitors molecularmobility and dynamic site heterogeneity in amorphous sucrose. *Biophysical J.* 88(May), 3551-3561.

Prochniewicz, E., Zhang, Q., Howard, E.C. and Thomas, D.D. 1996. Microsecond rotational dynamics of actin: spectroscopic detection and theoretical simulation. *J. Mol. Biol.* 255(3), 446–457.

Richert, R. 2000. Triplet state salvation dynamics: basics and applications. *J. Chem. Phys.* 113, 8404-8429.

Roos, Y. 1995. *Phase Transitions in Foods*. Academic Press, San Diego, CA.

Shah, N.K. and Ludescher, R.D. 1995. Phosphorescence probes of the glassy state in amorphous sucrose. *Biotechnol. Prog.* 11, 540-544.

Shirke, S., Takhistov, P. and Ludescher, R.D. 2005. Molecular mobility in amorphous maltose and maltitol from phosphorescence of erythrosin B. *J. Phys. Chem.* B. 109, 16119-16126.

Shirke, S. and Ludescher, R.D. 2005a. Molecular mobility and the glass transition in amorphous glucose, maltose, and maltotriose. *Carbohydr. Res.* 340, 2654-2660.

Shirke, S. and Ludescher, R.D. 2005b. Dynamic site heterogeneity in amorphous maltose and maltitol from spectral heterogeneity in erythrosin B phosphorescence. *Carbohydr. Res.* 340, 2661-2669.

Simon-Lukasik, K.V. and Ludescher, R.D. 2004. Erythrosin B phosphorescence as a probe of oxygen diffusion in amorphous gelatin films. *Food Hydrocolloids.* 18, 621-630.

Stein, R.A., Ludescher, R.D., Dahlberg, S., Fajer, P.G., Bennet, L.H., and Thomas, D.D. 1990. Time-resolved rotational dynamics of phosphorescence-labeled myosin heads in contracting muscle fibers. *Biochem.* 29, 10023-10031.

Stomphorst, R.G., van der Zwan, G., van Zandvoort, M.A.M.J., Sieval, A.B., Zuihof, H., Vergeldt, F.J., and Schaafsma, T.J. 2001. Spectroscopic study of erythrosin B in PVB films. *J. Phys. Chem. A.* 105, 4235-4240.

Strambini, G.B. and Gonnelli, M. 1985. The indole nucleus triplet-state lifetime and its dependence on solvent microviscosity. *Chem. Phys. Lett.* 115, 196-200.

Sun, W.Q., Leopold, A.C., Crowe, L.M. and Crowe, J.H. 1996. Stability of dry liposomes in sugar glasses. *Biophys. J.* 70, 1769-1776.

Vanderkooi, J.M., Maniara, G., Green, T.J., Wilson, D.F. 1987. An optical method for measurement of dioxygen concentration based upon quenching of phosphorescence. *J. Biol. Chem.* 262, 5476-5482.

Zallen, R. 1998. *The physics of amorphours solids*, New York: John Wiley & Sons, Inc.

Zidovetski, R., Bartholdi, M., Arndt-Jovin, D. and Jovin, T.M. 1986. Rotational dynamics of the Fc receptor for immunoglobulin E on histamine- releasing rat basophilic leukemia cells. *Biochem.* 25, 4397-4401.

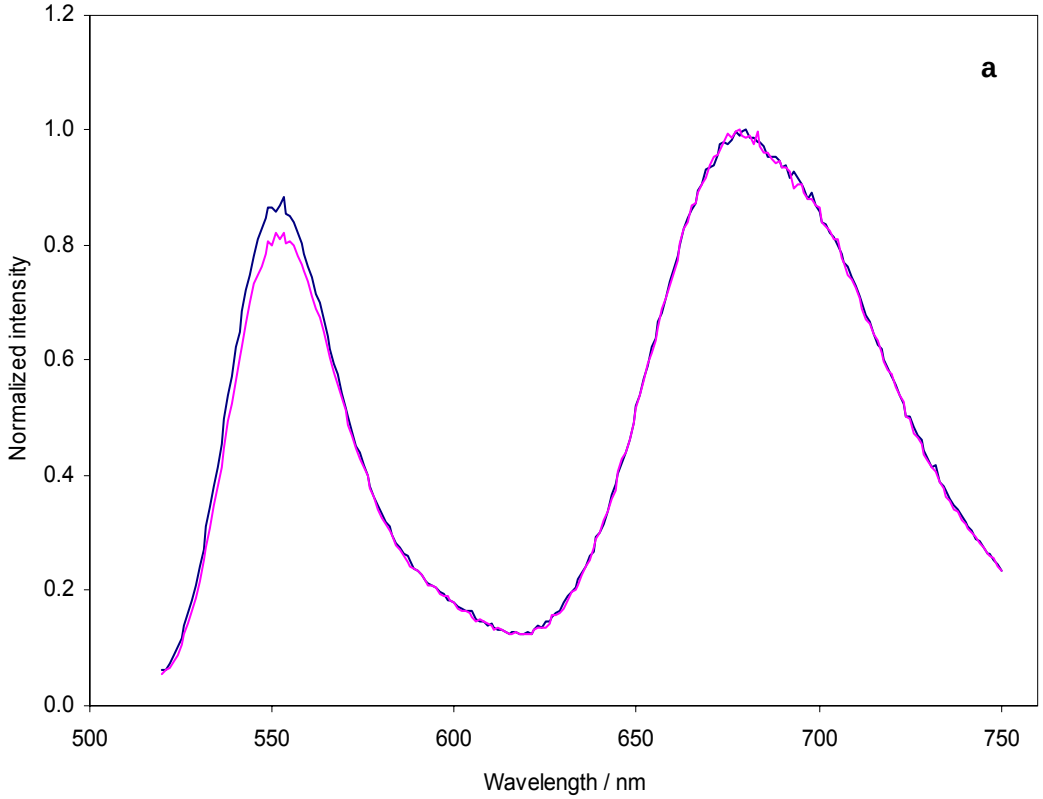
a
Normalized intensity
1.2
1.0
0.8
0.6
0.4
0.2
0.0
500
550
600
650
700
750
Wavelength / nm

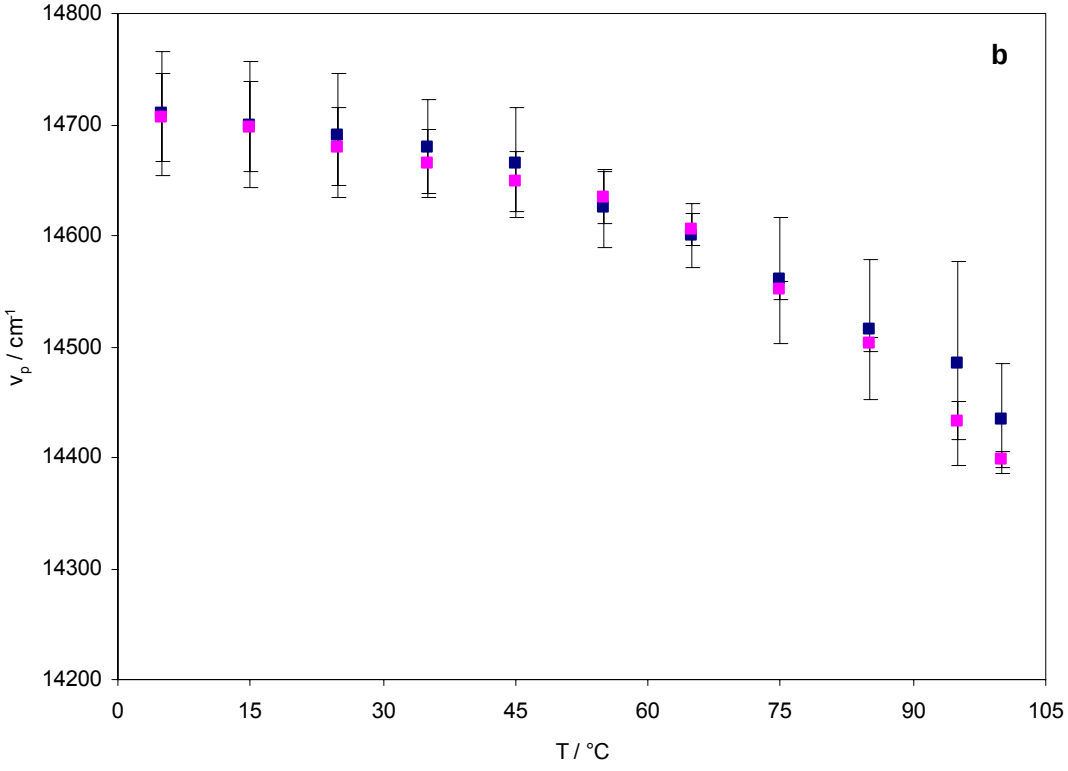
b
ν_p / cm^{-1}
14800
14700
14600
14500
14400
14300
14200
0
15
30
45
60
75
90
105
T / °C

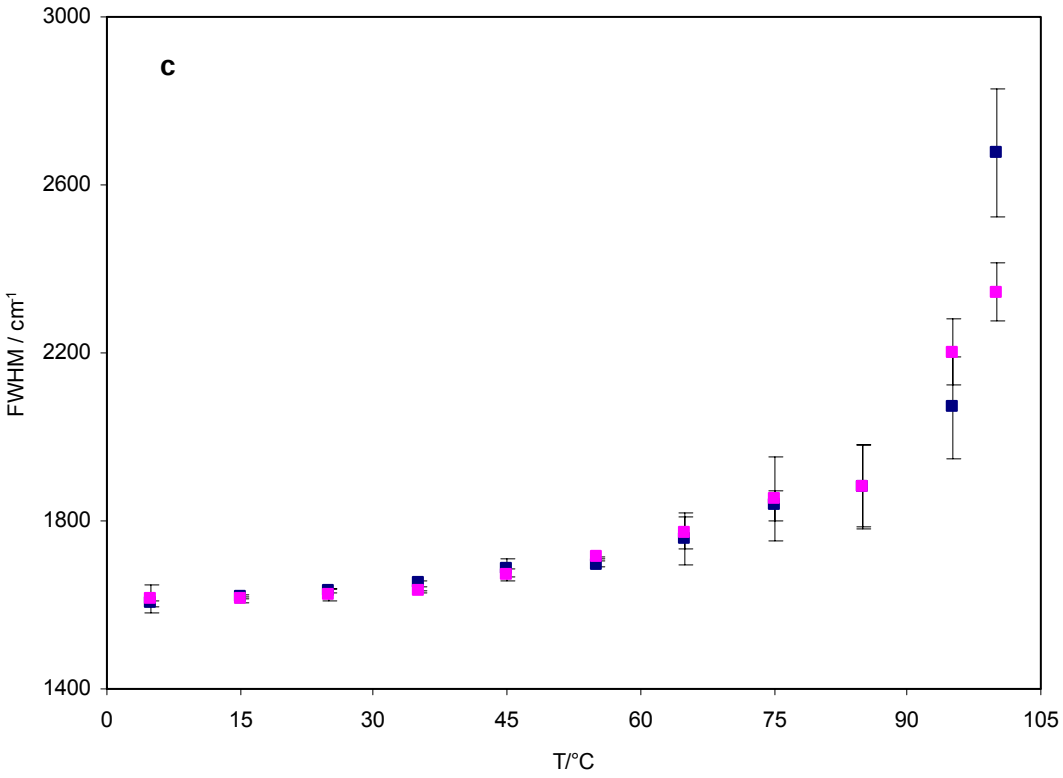

Figure 13 (a) Delayed emission spectra of erythrosin B in amorphous sucrose film at 25°C with Ery B/sucrose mole ratios of $0.5x10^{-4}$ (—) and $5x10^{-4}$ (—). (b) Peak frequency ν_P and (c) bandwidth (FWHM) for phosphorescence emission from Ery B in amorphous sucrose film as a function of temperature. The delayed emission spectra collected as a function of temperature were analyzed using log-normal line shape function. Samples are erythrosin B in sucrose films with mole ratios of $0.5x10^{-4}$ (■) and $5x10^{-4}$ (■), respectively.

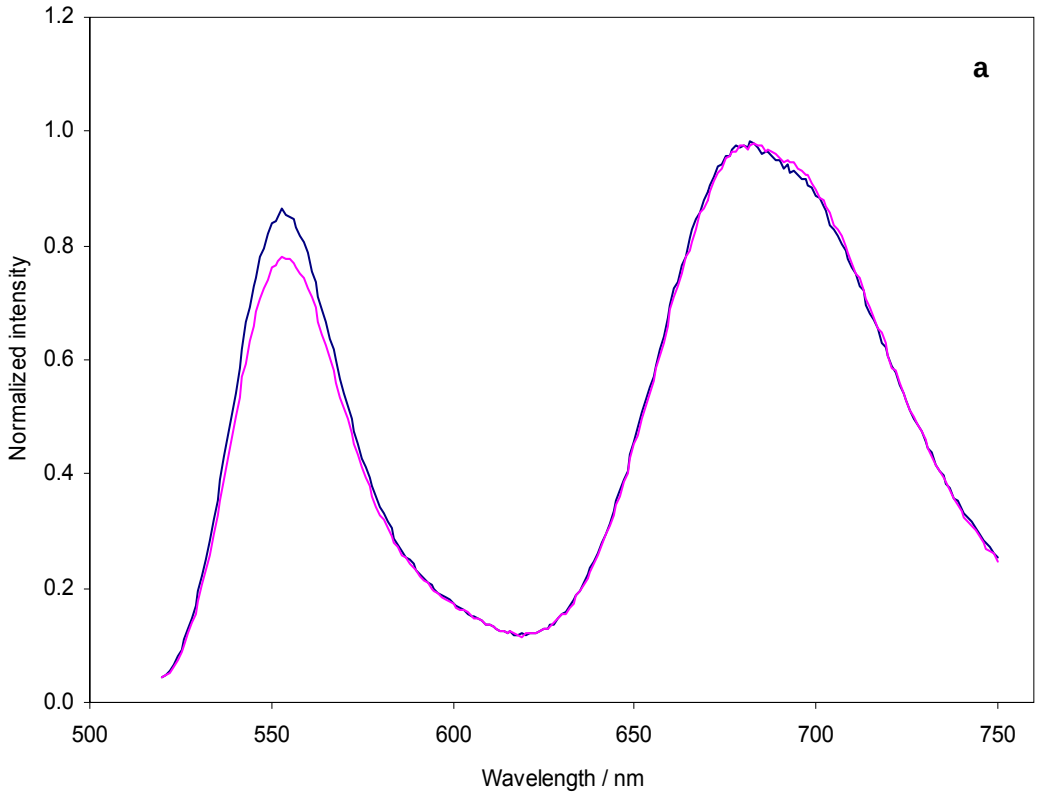
a
Normalized intensity
Wavelength / nm
1.2
1.0
0.8
0.6
0.4
0.2
0.0
500
550
600
650
700
750

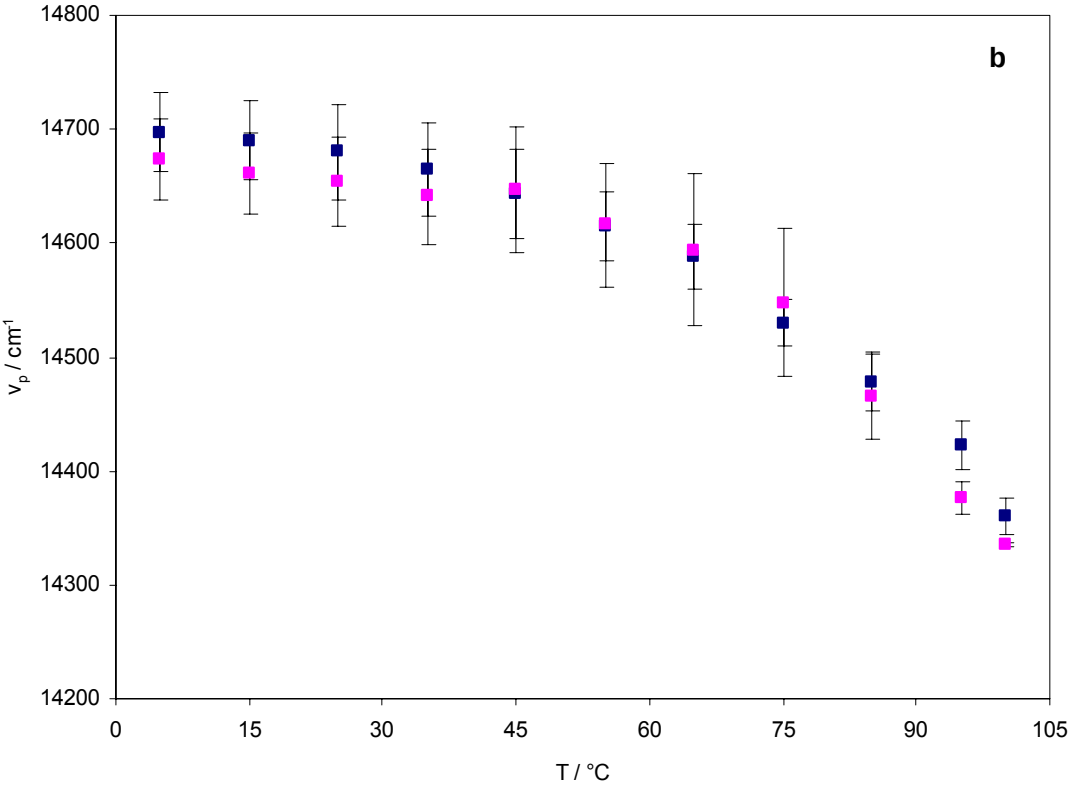
b
ν_p / cm^{-1}
T / °C
14800
14700
14600
14500
14400
14300
14200
0
15
30
45
60
75
90
105

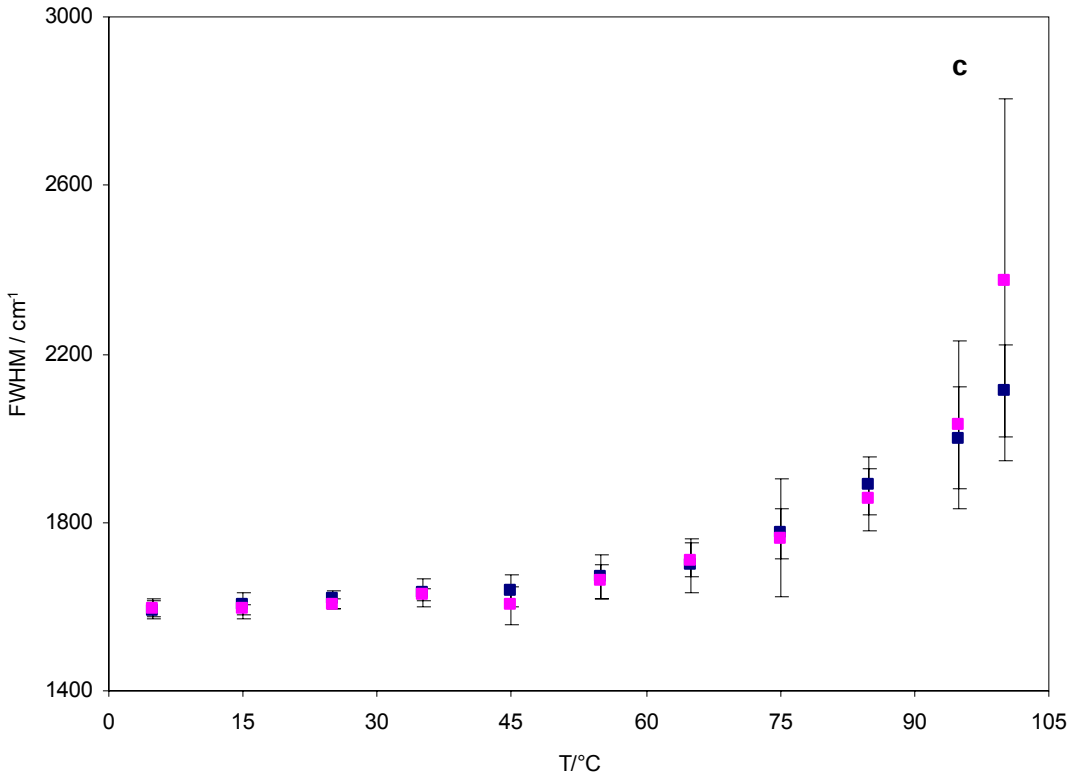

Figure 14 (a) Delayed emission spectra of erythrosin B in amorphous sucrose film at 25°C with Ery B/sucrose mole ratios of $1x10^{-4}$ (—) and $10x10^{-4}$ (—). (b) Peak frequency ν_P and (c) bandwidth (FWHM) for phosphorescence emission from Ery B in amorphous sucrose film as a function of temperature. The delayed emission spectra collected as a function of temperature were analyzed using log-normal line shape function. Samples are erythrosin B in sucrose films with mole ratios of $1x10^{-4}$ (■) and $10x10^{-4}$ (■), respectively.

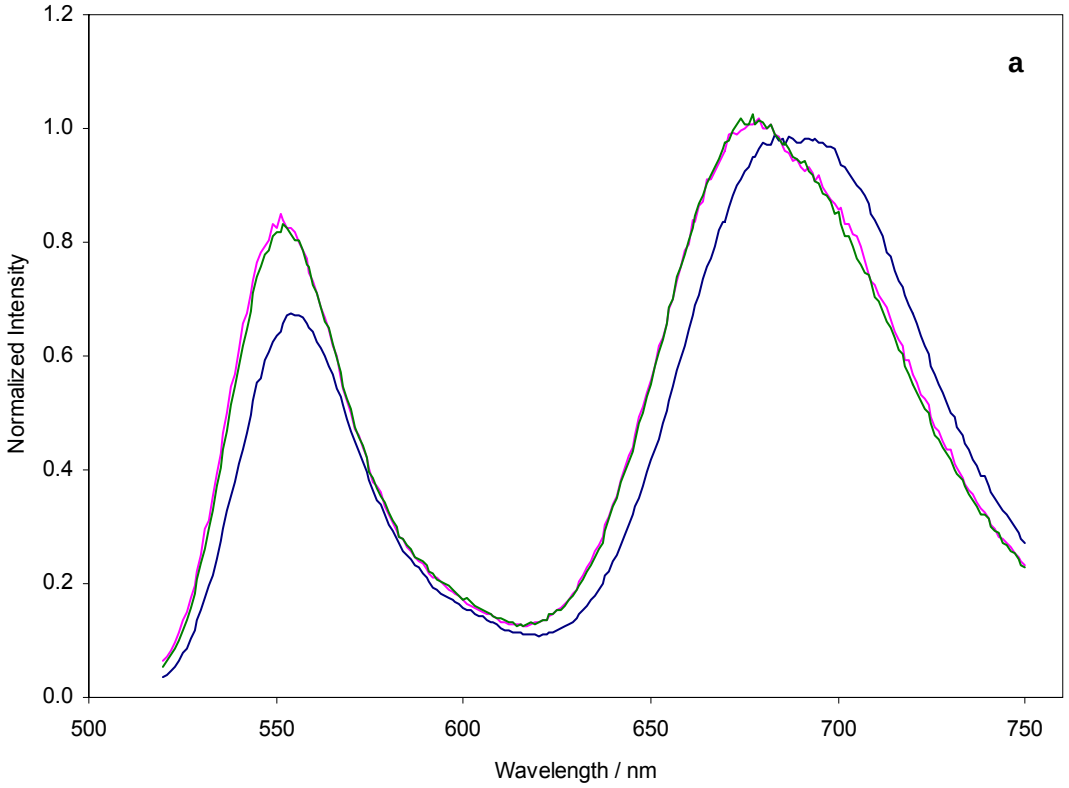
a
Normalized Intensity
Wavelength / nm
1.2
1.0
0.8
0.6
0.4
0.2
0.0
500
550
600
650
700
750

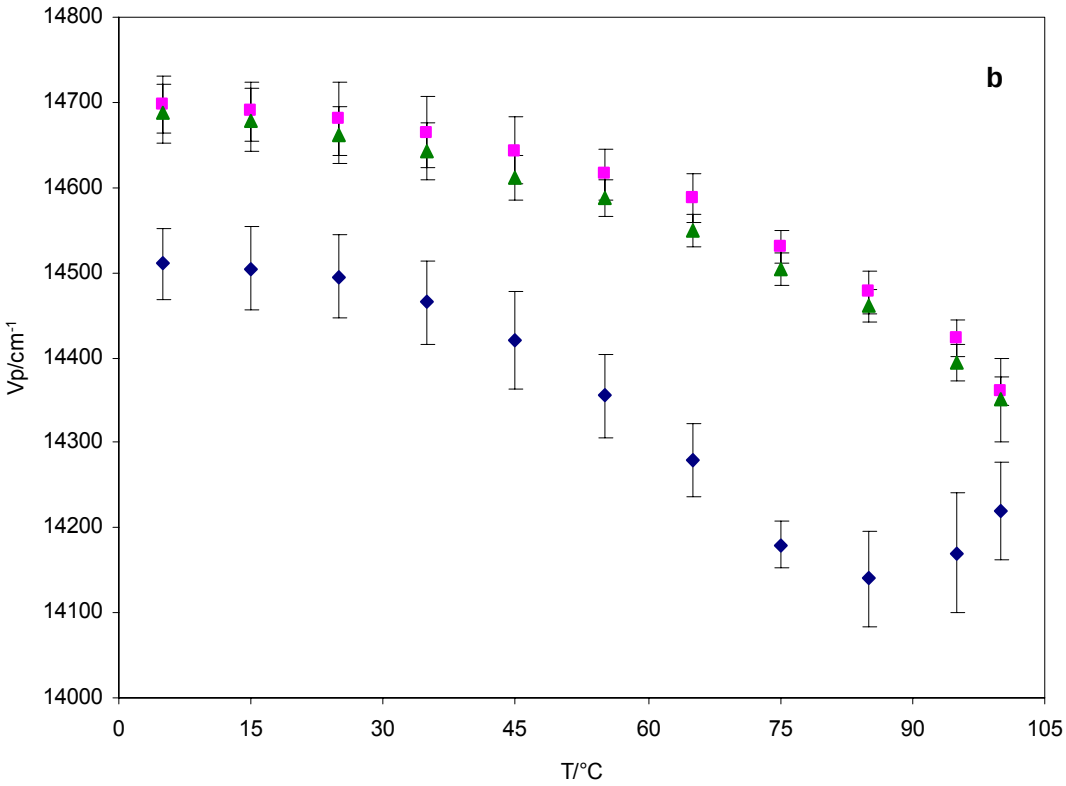
b
Vp/cm-1
T/°C
14800
14700
14600
14500
14400
14300
14200
14100
14000
0
15
30
45
60
75
90
105

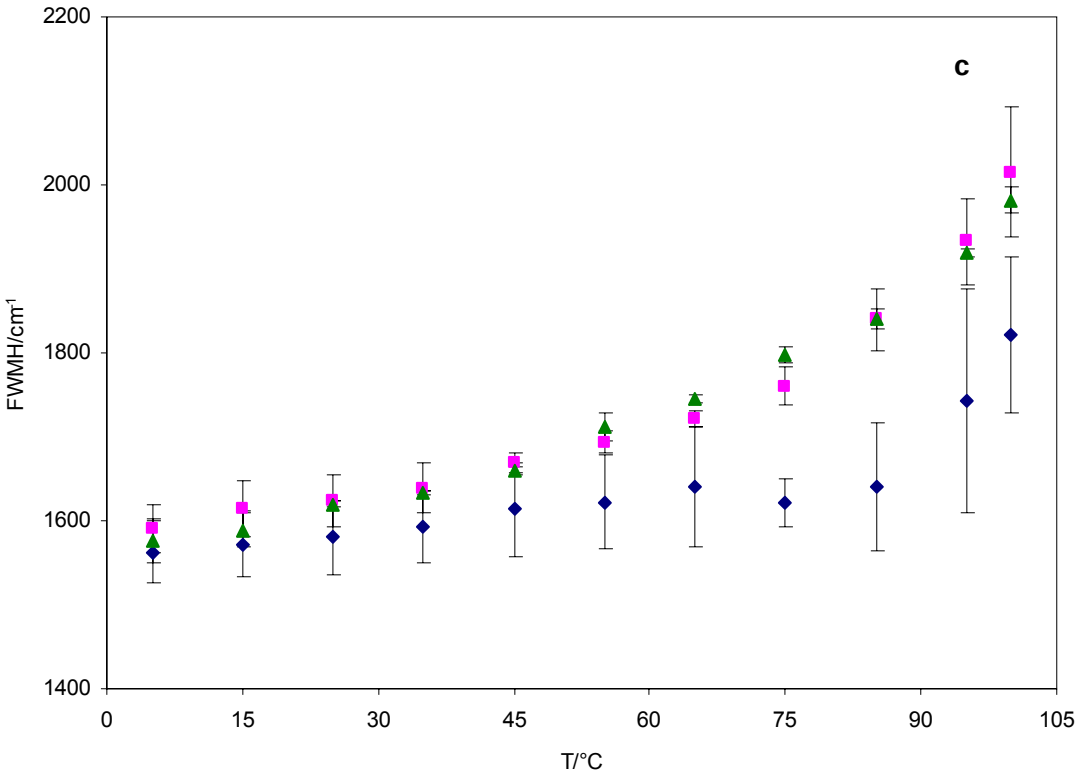

Figure 15 (a) Delayed emission spectra of erythrosin B in amorphous sucrose film at 25°C with $1x10^{-4}$ mole ratio of Ery B/sucrose prepared from stock solutions of DMF at 1 mM (—), 10mM (—), and 100 mM (—). (b) Peak frequency ν_P and (c) bandwidth (FWHM) for phosphorescence emission from Ery B in amorphous sucrose film as a function of temperature. The delayed emission spectra collected as a function of temperature were analyzed using log-normal line shape function for sucrose films with $1x0^{-4}$ mole ratio of Ery B/sucrose prepared from stock solutions of Ery B in DMF at concentration of 1 mM(♦), 10 mM (■), and 100 mM (▲).

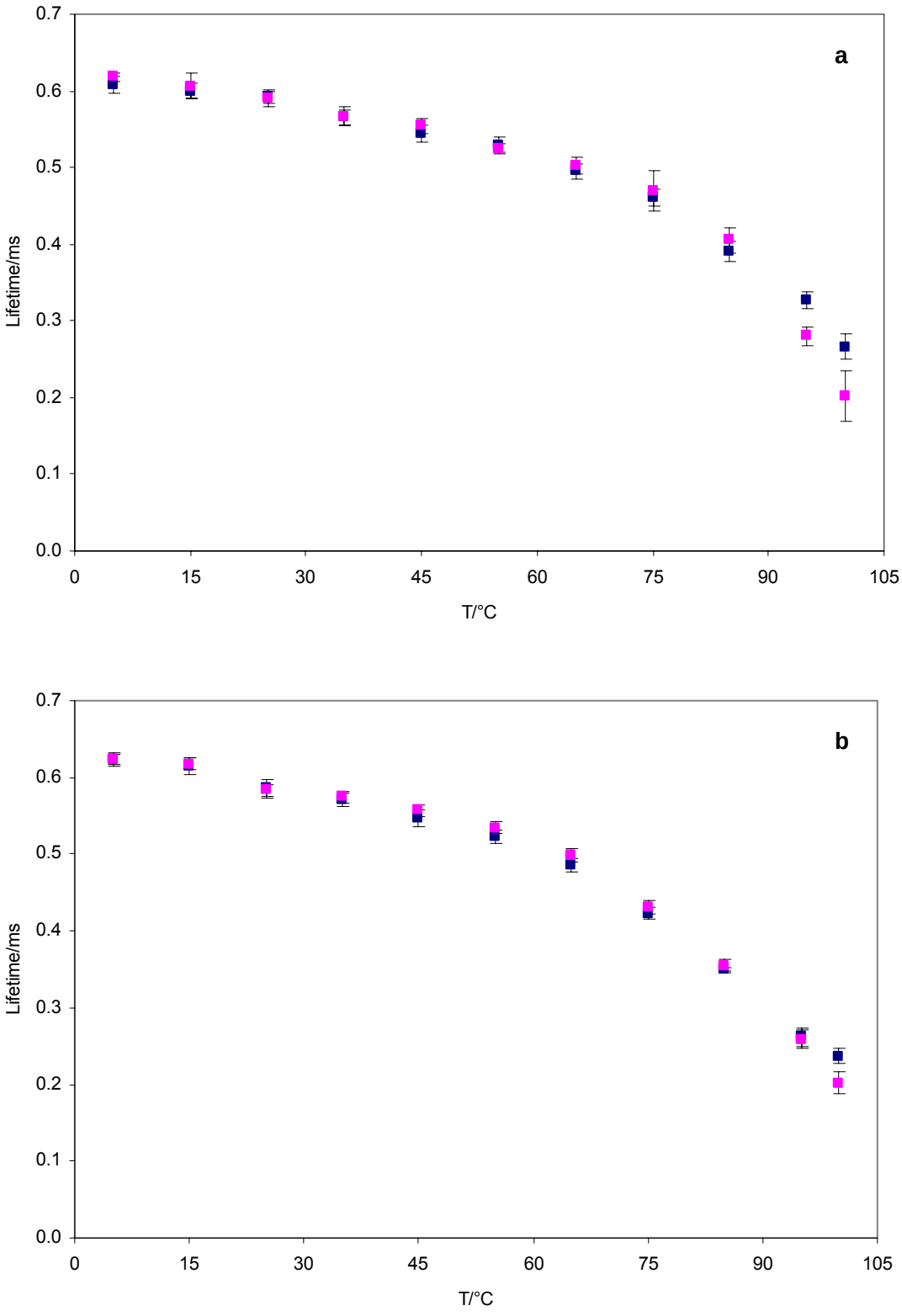

Figure 16 Temperature dependence of lifetimes obtained from fits to a stretched exponential function of the intensity decay of erythrosin B in amorphous sucrose. (a) Ery B in sucrose films with mole ratio of $0.5x10^{-4}$ (■) and $5x10^{-4}$ (■); (b) Ery B in sucrose films with mole ratio of $1x10^{-4}$ (■) and $10x10^{-4}$ (■).

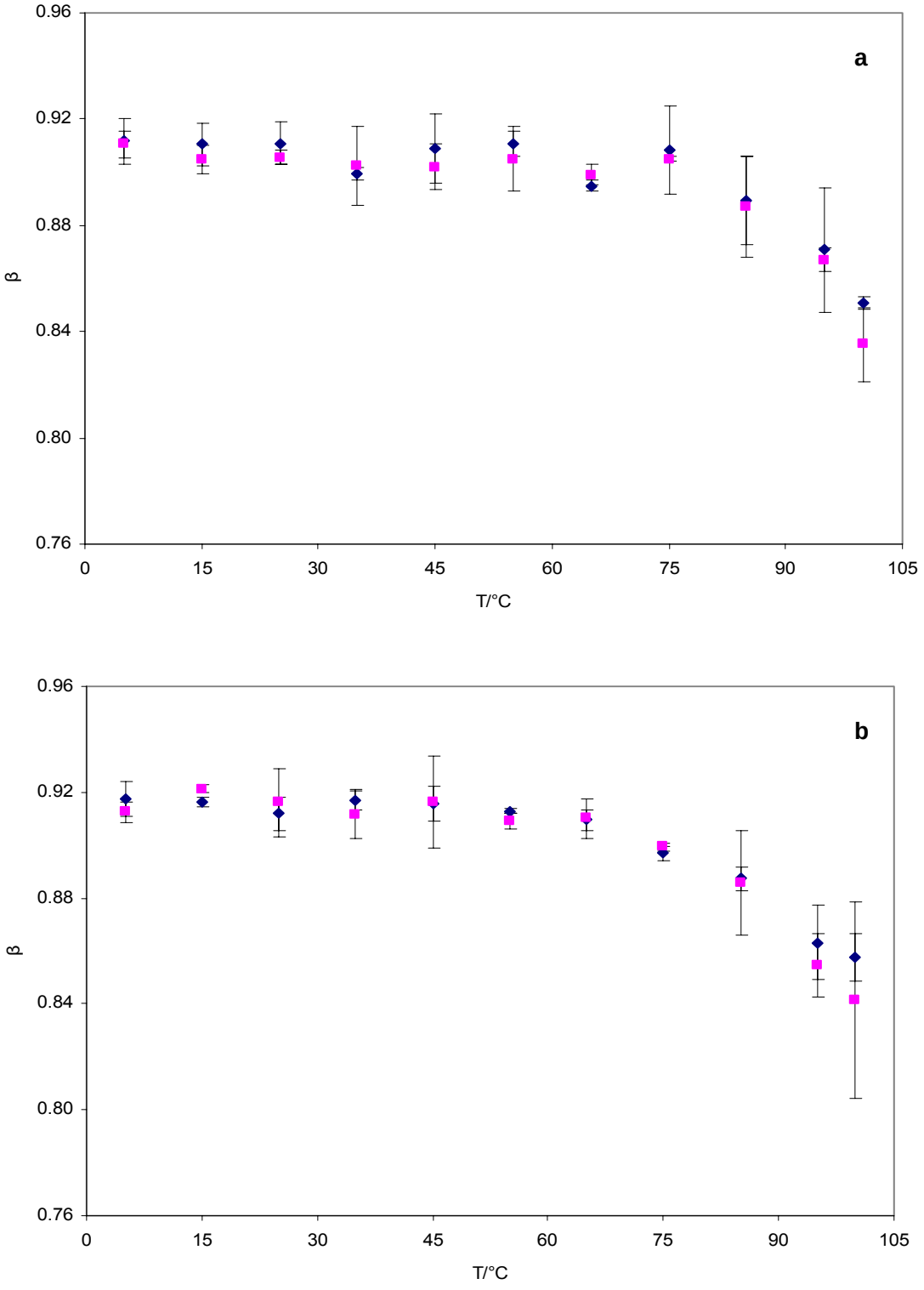

Figure 17 Temperature dependence of stretching exponents β obtained from fits to a stretched exponential function of the intensity decay of erythrosin B in amorphous sucrose. (a) Ery B in sucrose films with mole ratio of $0.5x10^{-4}$ (■) and $5x10^{-4}$ (■); (b) Ery B in sucrose films with mole ratio of $1x10^{-4}$ (■) and $10x10^{-4}$ (■).

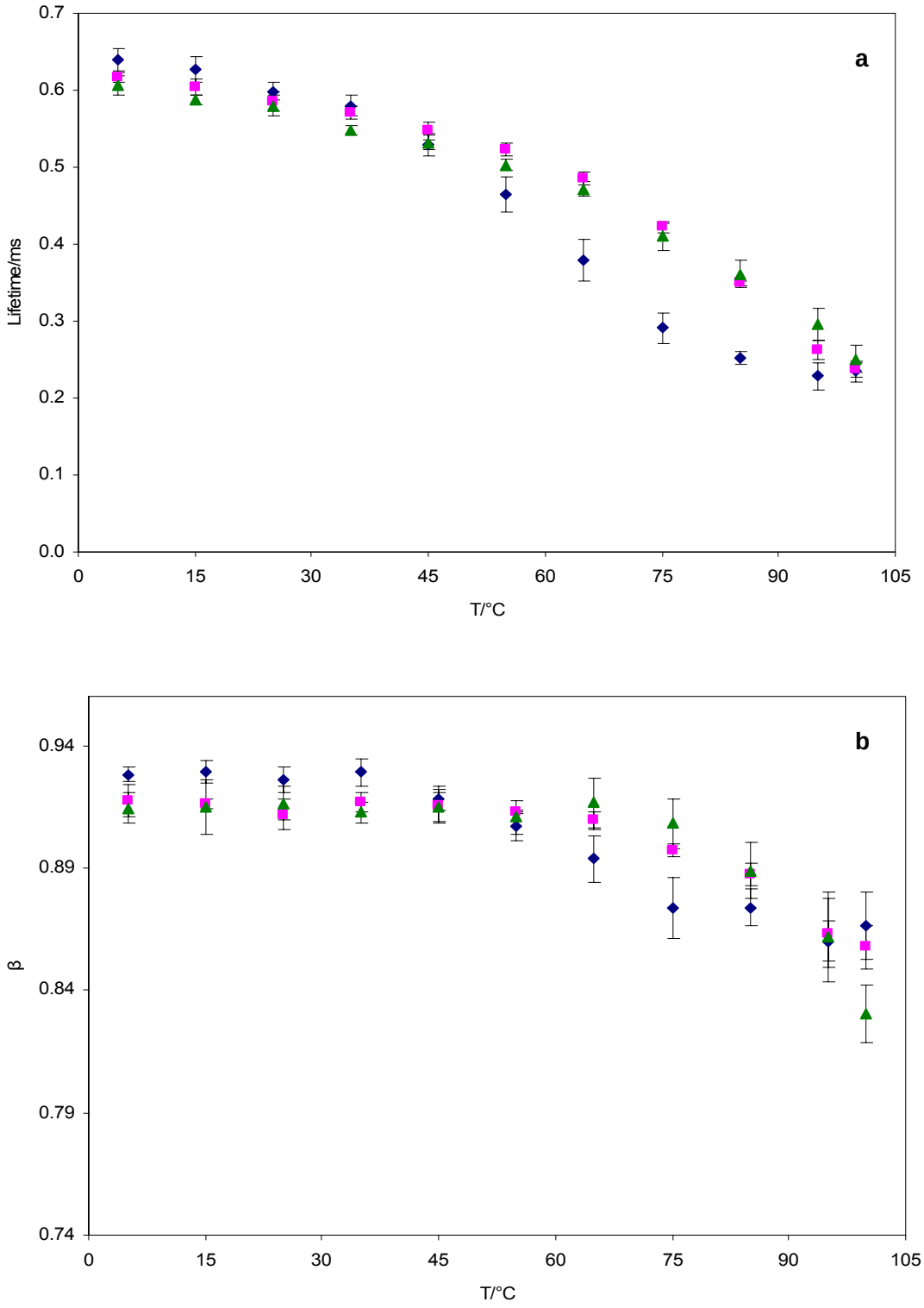

Figure 18 Temperature dependence of (a) lifetimes and (b) stretching exponents β obtained form fits to stretched exponential function of the intensity decay of erythrosin B in amorphous sucrose. Samples containing Ery B in sucrose films with mole ratio of $1x10^{-4}$ were prepared from 1 mM(♦), 10 mM (■), and 100 mM (▲).

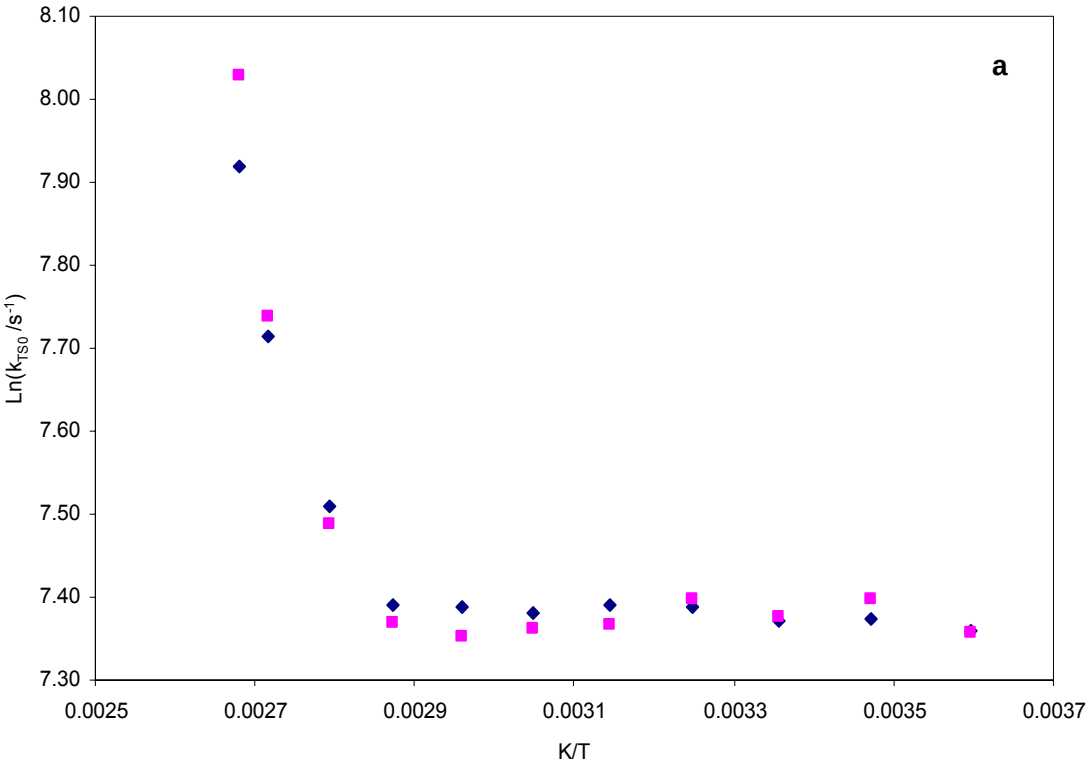
a
8.10
8.00
7.90
7.80
7.70
7.60
7.50
7.40
7.30
Ln(k_TS0 /s^-1)
0.0025
0.0027
0.0029
0.0031
0.0033
0.0035
0.0037
K/T

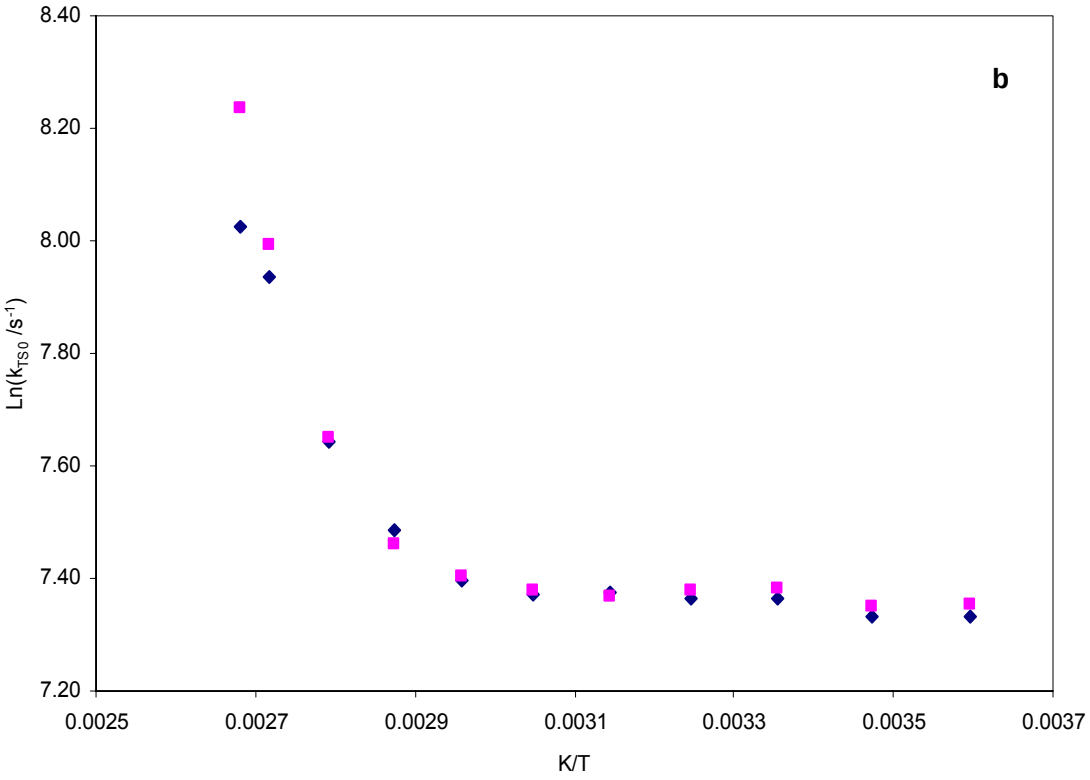
b
8.40
8.20
8.00
7.80
7.60
7.40
7.20
Ln(k_TS0 /s^-1)
0.0025
0.0027
0.0029
0.0031
0.0033
0.0035
0.0037
K/T

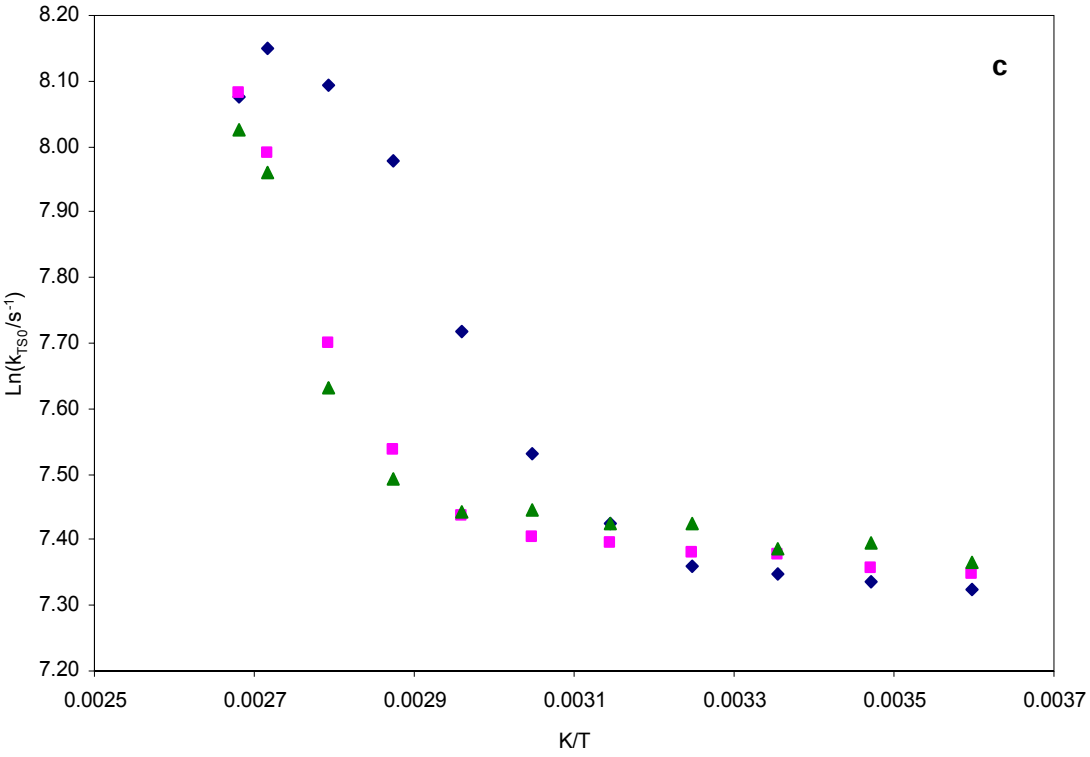

Figure 19 Arrhenius analysis of the temperature effect on the collisional quenching rate (k_{TS0}) calculated from the lifetimes. (a) Ery B in sucrose films with mole ratio of $0.5x10^{-4}$ (■) and $5x10^{-4}$ (■); (b) Ery B in sucrose films with mole ratio of $1x10^{-4}$ (■) and $10x10^{-4}$ (■); (c) Films containing erythrosin B at a mole ratio of $1x10^{-4}$ Ery B/sucrose were prepared from DMF stock solution containing Ery B concentrations of 1 mM (♦), 10 mM (■), and 100 mM (▲).

Chapter 3 The effect of glycerol on molecular mobility in amorphous sucrose detected by phosphorescence of erythrosin B

Introduction

Sucrose is one of the most widely used disaccharides in foods, biomaterials and pharmaceuticals to facilitate long-term storage (Noel et al., 2000) as well as one of the major compounds responsible for such degradation processes as crystallization, caking/lumping, structural collapse, and stickiness (Roos, 1995; Fennema, 1996; Goff and Sahagian, 1996; Labuza et al., 2004). In most low moisture and frozen foods, sucrose exists in an amorphous or partially amorphous state. By forming amorphous, that is, non-crystalline solids, sucrose acts as an effective protectant for biological materials; this property also provides the basis for the use of sucrose in the confection industry (Crowe et al., 1998). The stability and properties of amorphous biomaterials are modulated by specific physical processes and chemical reactions that are associated with the molecular mobility of amorphous solids (Ludescher et al., 2001).

Measurements of mobility of amorphous sucrose are thus of fundamental interest since it relates to questions of stabilization in the biological materials as well as degradation phenomena in amorphous foods. A number of techniques have been applied in characterizing the properties and mobility of amorphous materials including NMR and DSC. Recently phosphorescence of erythrosin B has been used to investigate the overall molecular mobility as well as the variations in molecular mobility within amorphous solid sucrose (Pravinata et al., 2005).

Parts of this section have been published in Food Biophysics and are included here verbatim.

The molecular mobility and dynamic heterogeneity of amorphous sucrose are always influenced by the presence of other compounds such as water and polyols. The effect of water on the properties of carbohydrates and other compounds has been widely studied by NMR (Partanen et al., 2004; Van den Dries et al., 1998; Yoshioka et al., 1999), DSC (Roos et al., 1996; Levine and Slade, 1988), dielectric relaxation (Noel et al., 2000; Huang et al., 1996; Kumagai et al., 2000) and other techniques (Soderholm et al., 1998; Surana et al., 2003; Wolkers et al., 1998). Among polyols, glycerol is widely used in model systems to study the properties of supercooled liquid and glassy substances because of its propensity of forming a low temperature glass (Ryabov et al., 2003). In this paper the molecular mobility of solid sucrose-glycerol mixtures was monitored by measuring the phosphorescence of erythrosin B as a function temperature. The data on mobility as a function of composition as well as temperature were used to generate mobility maps to provide both mechanistic insight into the physics of the amorphous state as well as practical guidance for predicting and controlling matrix stability.

Glycerol is used as a cryoprotectant and a humectant as well as a softener or texture modifier to improve the properties of many foods, confections, and pharmaceutical preparations. It is common knowledge that addition of glycerol and other low molecular weight compounds (water, sugars, etc) enhances the flexibility and ductility of polymer materials, an effect termed plasticization. Many studies have reported on the use of glycerol as a plasticizer of hydrocolloid films and its role in increasing extensibility, flexibility, cohesion, elasticity and mechanical resistance and decreasing rigidity (Cuq et al., 1997). Soy protein films, for example, are difficult to handle during preparation if they contain less than 17g glycerol/100g dry matter (Stuchell

and Krochta, 1994). The T_g of the polymer-plasticizer mixture also decreases due to increased free volume and segmental mobility (Seow et al., 1999).

However, recent research shows an opposite effect when certain plasticizers are present at low concentrations. Lourdin et al. (1997) reported that a starch film at 25°C with glycerol content of 12 wt % exhibited a minimum elongation at break although T_g was found to progressively decrease as the glycerol content increased from 0 to 25%, without any evidence of crystallization. When the amount of glycerol exceeded 12%, however, the elongation behavior was controlled by the glass transition. This phenomenon seems to indicate that the same compound can exhibit two different effects, either antiplasticization or plasticization, depending on concentration. Lourdin et al. (1998) also found that local mobility (specifically, β relaxations) for amorphous maltose and amylose were strongly affected by the addition of small amounts of glycerol. In the glycerol concentration range from 0% to approximately 30% (w/w), the addition of glycerol shifted the primary (α) relaxation to lower temperature and the secondary (β) relaxation to higher temperature. This effect is comparable with antiplasticization observed in synthetic polymers such as PC-dibutylethylenedibenzoate (Jackson and Caldwell, 1967a, b) and polycarbonate (BPA-PC)-dibutyl phthalate (Roy et al, 1987). The antiplasticization effect in polymer science was originally associated with an increase in both modulus and T_g of polymer materials. Lately, however, this term has been borrowed to describe the phenomena in which the glassy polymer increases modulus due to the presence of very small amounts of plasticizer that actually decrease T_g.

There are extensive studies about the effect of glycerol polymer materials; however, the effect of glycerol on small compounds is seldom reported. Here we report studies of the effect of glycerol on the molecular mobility of amorphous sucrose obtained from analysis of the phosphorescence from erythrosin B embedded in the matrix. Glycerol content was varied from 0 to 0.79 (mole ratio of glycerol/sucrose) by addition of glycerol to the concentrated sucrose solution prior to film formation. The temperature-dependence of mobility was measured and analyzed at different glycerol contents, generating families of mobility versus temperature curves. Comparisons provided information about the mechanisms by which glycerol increased or decreased mobility of the amorphous sucrose matrix.

Materials and Methods

1. Sample Preparation

We prepared glassy sucrose films by using a slightly modified version of our published method (Pravinata et al., 2005; see details in Materials and Methods in Chapter 1).

Sucrose-glycerol mixtures were prepared from solutions of sucrose containing dye. Glycerol (99% GC pure; Sigma Chemical Co., St. Louis, MO) was added to the purified sucrose solutions to obtain a series of mixtures with glycerol/sucrose mole ratios of 0.17, 0.27, 0.36, 0.47, 0.63, 0.69 and 0.79. Prior to preparing glassy films, sucrose-glycerol solutions were filtered through a membrane with 0.2 μm pores. The procedure to make a glassy sucrose-glycerol film was the same as the procedure to make a pure sucrose film.

Water content in amorphous films was determined by weighing samples before and after drying for 24 h at 70°C in an Ephortee vacuum oven (Haake Buchler, Inc.) at 1 kPa. Sample films were scrapped from quartz slides and ground into powders in a glove box containing P_2O_5 and Drie-Rite with a relative humidity less than 10%. Pure sucrose film contained 0.56±0.13 wt. % water, while the sucrose-glycerol films contained 1.20±0.49, 2.17±0.29, 2.85±0.35, 3.85±0.43, 4.49±0.35, 4.84±0.37, and 4.20±0.23 wt. % water for glycerol/sucrose mole ratios of 0.17, 0.27, 0.36, 0.47, 0.63, 0.69 and 0.79, respectively.

2. Glass transition temperatures of sucrose-glycerol films

It was not possible to directly measure the glass transition temperature (T_g) of films due to the small mass of material deposited on a slide (2-4 mg); T_g values were thus calculated based on composition. The T_g of a ternary mixture depends on the mass fraction (x_1, x_2, and x_3), change in heat capacity at T_g (ΔC_{p1}, ΔC_{p2}, and ΔC_{p3}), and glass transition temperatures (T_{g1}, T_{g2}, and T_{g3}) of the individual components. This relation is given by the modified Couchman and Karasz equation (Roos, 1995):

$$T_{gm} = \frac{w_1 \Delta C_{p1} T_{g1} + w_2 \Delta C_{p2} T_{g2} + w_3 \Delta C_{p3} T_{g3}}{w_1 \Delta C_{p1} + w_2 \Delta C_{p2} + w_3 \Delta C_{p3}} \qquad (1)$$

The ΔC_p's of glycerol and sucrose are 1.05 J/g °C (Simon, 1997) and 0.60 J/g °C (Roos, 1995), respectively. The T_g's of glycerol and sucrose are 185K (Ramos, 2003) and 335K (Roos, 1995), respectively. The ΔC_p's for pure water vary from 0.11 to 1.94 J/g °C, and the T_g's vary between 123 to 148K (Roos, 1995). The average values, 1.02 J/g °C and 136K were taken as ΔC_p and T_g for pure water in this study.

3. Luminescence measurements

Luminescence measurements were made using a Cary Eclipse fluorescence spectrophotometer (Varian Instruments, Walnut Creek, CA). Prior to any phosphorescence measurements, all samples were flushed for at least 15 minutes with nitrogen gas containing less than 1 ppm oxygen to eliminate oxygen quenching. At each target temperature samples were equilibrated for 1 min/°C increase in temperature. The temperature was controlled using a thermo-electric temperature controller (Varian Instruments, Walnut Creek, CA). To eliminate moisture condensation during the measurements below room temperature, dry air was used to flush the chamber surrounding the cuvette holder. All the measurements were made at least in triplicate.

Delayed fluorescence and phosphorescence emission spectra were collected from 520 nm to 750 nm (10 nm bandwidth) at 1 nm intervals using excitation of 500 nm (20 nm bandwidth) over temperature range from 5 to 100°C with an observation window of 5.0 ms and an initial delay time of 0.2 ms which suppresses fluorescence coincident with the lamp pulse. Emission spectra from sucrose or sucrose-glycerol films without probe were subtracted from each spectrum although the signal of background was very low.

The energy of emission maximum (ν_p) and the full width at half maximum (FWHM) of the emission bands were determined by using a log-normal line shape function (Maroncelli and Fleming, 1987) to fit both delayed fluorescence and phosphorescence.

$$I(\nu) = I_0 \exp\left\{-\ln(2)\left(\frac{\ln[1+2b(\nu-\nu_p)/\Delta]}{b}\right)^2\right\} \qquad (2)$$

Where I_0 is the maximum emission intensity, ν_p is the peak frequency (cm^{-1}), Δ is a linewidth parameter, and b is an asymmetry parameter. This equation reduces to a

Gaussian line width when b = 0. The bandwidth (FWHM; Γ) is calculated according to the following equation:

$$\Gamma = \Delta\left(\frac{\sinh(b)}{b}\right) \tag{3}$$

For delayed luminescence spectra collected from 520-750 nm, a sum of log-normal functions for delayed fluorescence ($I_{DF}(\nu)$) and phosphorescence ($I_P(\nu)$) was used to fit the spectra. Each emission band was fit to independent fit parameters.

The dipolar relaxation time φ was calculated from the temperature dependence of the phosphorescence emission peak ν(T) by analyzing the relaxation function:

$$\frac{\Delta\nu}{\Delta\nu_r} = \frac{\nu(T) - \nu_{\max}}{\nu_{\min} - \nu_{\max}} \tag{4}$$

Where ν(T) is the emission peak energy at temperature T, and ν_{min} and ν_{max} are the emission peak energy at the lowest temperature and the highest temperature, respectively. By using a stretched exponential function to approximate the phosphorescence intensity decay, the matrix dipolar relaxation time (φ) can be estimated from the following equation (Shirke et al., 2005):

$$\frac{\Delta\nu}{\Delta\nu_r} = \frac{\nu(T) - \nu_{\max}}{\nu_{\min} - \nu_{\max}} = \frac{1}{\Gamma(\frac{1}{\beta_l})} \frac{1}{1 + \frac{\beta_e}{\beta_l}\frac{\tau}{\varphi}} \tag{5}$$

Where τ and β_l are the temperature-dependent stretched exponential (Kohlrausch-Williams-Watts) lifetime and stretching exponent (from Eq. 6) describing the phosphorescence intensity decay and Γ(x) in this case is the Gamma function; β_e is assumed to have a value of 0.5.

Red-edge effect measurements over the temperature range from 5 to 85°C used excitation wavelengths at 530 nm and 560 nm, respectively. Phosphorescence emission

was collected from 640 nm to 760 nm using an observation window of 5.0 ms and 0.1 ms delay. Phosphorescence spectra were converted to intensity versus frequency (cm^{-1}) and analyzed to obtain the peak frequency (ν_p) and spectral bandwidth (Γ) using a lognormal function ($I(\nu)$) (Eq. 2).

For lifetime measurements, samples were excited at 530 nm (20 nm bandwidth) and emission transients collected at 680 nm (20 nm bandwidth) over the temperature range from 5 to 100°C. Phosphorescence intensity decays were collected over a window of 4 ms with an initial delay of 0.1 ms and increments of 0.04 ms. Each decay was the average of 20 cycles. A stretched exponential or Kohlrausch-Williams-Watts decay function was used to analyze the intensity decay (Richert, 2000; Lee, et al., 2001; Pravinata et al., 2005).

$$I(t) = I_0 \exp(-(t/\tau)^{\beta}) + \text{constant} \quad (6)$$

Where I_0 is the initial amplitude at time zero, τ is the stretched exponential lifetime, and β is an exponent varying from 0-1 characterizing the distribution of lifetimes. The use of a stretched exponential model provides a direct measurement of a continuous distribution of lifetimes, which is appropriate for describing a complex glass possessing a distribution of relaxation times for the dynamic molecular processes. The smaller the β value, the more non-exponential is the intensity decay and the broader the distribution of lifetimes. The program NFIT (Island Products, Galveston, TX) was used to fit the decay; goodness of fit was evaluated by examining χ^2 and R^2. Plots of modified residuals (the difference between the intensity from the fit decay curve and the measured intensity divided by the square root of the measured intensity) was also an indicator of the goodness of fit. R^2 for

all fits ranged from 0.99 to 1.00 and modified residuals plots fluctuated randomly around zero amplitude.

Phosphorescence lifetimes of Ery B as a function of emission wavelength were measured with excitation wavelength at 530 nm (20 nm bandwidth) and emission wavelength from 640 nm to 720 nm (20 nm bandwidth). Phosphorescence emission lifetimes as a function of excitation wavelength were measured with emission wavelength at 680 nm (20 nm bandwidth) and excitation wavelength from 490 nm to 560 nm (20 nm bandwidth). These experiments were performed at 25°C.

4. Photophysical Scheme

Our analysis of the delayed emission is similar to the photophysical scheme for Ery B outlined by Duchowicz et al. (1998). The measured emission rate for phosphorescence (k_P) is the sum of all possible deexcitation rates for the triplet state T_1:

$$\tau^{-1} = k_P = k_{RP} + k_{TS1} + k_{TS0} + k_Q[Q] \quad (7)$$

In this equation, k_{RP} is the rate of radiative emission to the ground state S_0; for Ery B, k_{RP} is 41 s^{-1} and constant with temperature (Duchowicz et al., 1998). The term k_{TS1} is the rate of thermally activated reverse intersystem crossing from the triplet state T_1 to the singlet state S_1; the value varies with temperature in an Arrhenius fashion:

$$k_{TS1}(T) = k^0_{TS1} \exp(-\Delta E_{TS}/RT) \quad (8)$$

Where k^0_{TS1} is the maximum rate of intersystem crossing from T_1 to S_1 at high temperature, ΔE_{TS} is the energy gap between T_1 and S_1, R = 8.314 J K^{-1} mol^{-1}, and T is the temperature in Kelvin. The value of ΔE_{TS} is calculated from the slope of a Van't Hoff plot of the natural logarithm of the ratio of intensity of delayed fluorescence (I_{DF}) to phosphorescence (I_P) (Duchowicz et al., 1998):

$$d[\ln(I_{DF}/I_P)]/d(1/T) = -\Delta E_{TS}/R \quad (9)$$

where I_{DF} and I_P are the maximum intensity values determined from analysis of the emission band using Eq. (2). The value of k_{TS1} at 25°C was estimated as 88 s^{-1} using k^0_{TS1} = 3.0x10^7 s^{-1} and ΔE_{TS} = 31.56 kJ mol^{-1} (Pravinata et al., 2005).

In the presence of oxygen, the quenching rate $k_Q[Q]$ is the product of the bimolecular collisional quenching constant k_Q and the oxygen concentration $[O_2]$. Since samples were flushed continuous with nitrogen throughout the measurements, we assume that oxygen quenching was negligible. One of the non-radiative decay routes is through internal conversion from T_1 to S_0 with decay rate k_{TS0}; this term reflects the rate of collisional quenching of the probe due to both internal and external factors (Papp and Vanderkooi, 1989). We assume that changes in k_{TS0} primarily reflect collisions with the external matrix environment since collisional self quenching among probe molecules can be neglected within the extremely viscous amorphous solid. In this study, the temperature-dependent term k_{TS0} can be calculated from the measured phosphorescence lifetime by rewriting Eq. 7.

$$k_{TS0}(T) = \frac{1}{\tau(T)} - k_{RP} - k_{TS1}(T) \quad (10)$$

Results

1. T_g of sucrose-glycerol films

As a plasticizer, glycerol is added to change the properties of a material, primarily through depressing its glass transition temperature T_g. The T_g's of the sucrose-glycerol films at the moisture contents determined by gravimetry were estimated using Eq. 1 (Materials and Methods); the calculated T_g's (listed in Table 1) ranged from a high of

60°C for pure sucrose containing 0.56 wt. % water to a low of 11°C for films with glycerol/sucrose at mole ratio 0.79 which contained 4.2 wt. % water.

Table 1 The calculated T_gs of sucrose-glycerol mixtures at different glycerol/sucrose mole ratios and average peak frequencies (ν_P) at T_g of individual mixture

glycerol : sucrose Mole ratio	Calculated T_g (K)	Average peak frequency at T_g (cm^{-1})
0 : 1	333.1 (60.1°C)	14601
0.17:1	320.4 (47.4°C)	14655
0.27:1	311.2 (38.2°C)	14674
0.36:1	305.1 (32.1°C)	14636
0.47:1	297.9 (24.9°C)	14605
0.63:1	289.7 (16.7°C)	14561
0.69:1	286.6 (13.6°C)	14560
0.79:1	284.0 (11.0°C)	14559

2. Delayed emission spectra

Delayed emission spectra of Ery B dispersed in amorphous sucrose films with various mole ratios of glycerol/sucrose were collected over the temperature range from 5 to 100°C. All spectra (data not shown) showed the expected decrease in phosphorescence and increase in delayed fluorescence intensity with increasing temperature seen in xanthene dyes (Parker, 1968). Both the delayed fluorescence and phosphorescence bands shifted to longer wavelength at higher temperature; the peak frequency (ν_p) and bandwidth (Γ) were determined by fitting to a log-normal lineshape function (Eq. 2 and 3). The frequency and bandwidth for phosphorescence emission are plotted in Figure 20

versus $T-T_g$ to emphasize their dependence on the physical state of the films. The peak frequency for delayed fluorescence exhibited similar thermal behavior (data not shown).

The phosphorescence peak frequency provides a measure of the average energy of emission; a decrease in emission energy reflects an increase in the average extent of dipolar relaxation around the excited triplet state prior to emission (Lakowicz, 1999; Pravinata et al., 2005; Shirke et al., 2006). The peak frequency decreased gradually and approximately linearly with temperature below T_g and much more steeply at T_g and above in all films. All $\nu_p(T-T_g)$ curves were similar in shape; however, those curves for films with low glycerol content ($\leq$ 0.36 mole ratio) were above, those with high glycerol content ($\geq$ 0.63 mole ratio) were below, and that with 0.47 mole ratio was identical with the curve for pure sucrose. The emission peak frequency decreased to ~14,200 cm^{-1} at temperatures well above T_g.

The phosphorescence bandwidth, on the other hand, provides a measure of the range of energetically distinct matrix environments seen by the Ery B probe within the amorphous matrix (Lakowicz, 1999). The bandwidth was essentially constant at ~1600 cm^{-1} at low temperature and increased gradually with temperature in the glass and more dramatically in the melt above T_g in all films. The temperature above T_g at which the bandwidth began to rise steeply increased significantly with increasing glycerol content. This increase in inhomogeneous broadening indicates there was a corresponding increase in the breadth of the distribution of energetically distinct matrix environments at temperatures above T_g.

The effect of glycerol on these spectroscopic parameters is illustrated in plots of the relative peak frequency and bandwidth normalized to the values in the pure sucrose

film at temperatures from 5 to 75°C (Figure 21). The overall trend was that the peak frequency and bandwidth at each temperature decreased with an increase in glycerol content, indicating that, in general, glycerol increased the extent of dipolar relaxation and decreased the environmental energetic heterogeneity. The effect of glycerol appeared to level off at glycerol/sucrose mole ratios ~0.6 for the emission frequency and ~0.4 for the bandwidth. However, there was a systematic increase in the peak frequency in the presence of small amounts of glycerol (at mole ratios of 0.17 and 0.27) at 45°C and below; the absolute increase in the peak frequency was ~50 cm^{-1}.

The dipolar relaxation rates for the sucrose and sucrose-glycerol films were estimated from the peak frequency data of Figure 20a as described in Materials and Methods (Eq. 5, using the lifetime data of Figure 24a); these rates are plotted in an Arrhenius fashion in Figure 3a. The relaxation rate increased over four orders of magnitude over the temperature range from 5 to 100°C; all curves exhibited upward curvature indicative of an increase in the activation energy with increasing temperature. The overall trend at each temperature was an increase in the relaxation rate with an increase in glycerol content; however, at low temperature, the relaxation rate remained constant or even slightly decreased from that in pure sucrose at mole ratios of glycerol/sucrose ranging from 0.17 to 0.47. When plotted versus temperature normalized to the glass transition temperature T_g/T (Figure 22b), however, the glycerol-containing films had slower relaxation rates than pure sucrose at all equivalent temperatures; at each value of T_g/T the rate of dipolar relaxation decreased with increasing glycerol content.

3. Red-edge effect

The emission energy of an optical probe dispersed within a condensed phase is dependent upon the energy of excitation under conditions where the matrix relaxation rate is comparable to or longer than the excited state lifetime (Prukey and Galley, 1978); the effect is most easily observed by comparing emission with excitation at the maximum and at the red edge of the absorption spectrum (Demchenko, 2002). The red-edge effect for Ery B was measured as a function of temperature in sucrose and sucrose-glycerol films at selected mole ratios; these data are plotted in Figure 23 as the energy difference ($\Delta\nu_p$) with 530 nm and 560 nm excitation versus T-T_g. This normalization appears to generate a single curve reflecting the effect of temperature on $\Delta\nu_p$. The magnitude of $\Delta\nu_p$ was significant and approximately constant (~320 cm^{-1}) at temperatures well below T_g, indicating that matrix dipolar relaxation rates were slow compared to the excited state lifetime, and decreased gradually with an increase in temperature in the glass and more steeply as the temperature exceeded T_g. At high temperature, in the melt, the energy difference approached zero, indicating that the matrix dipolar reorientation time was significantly faster than the probe triplet state lifetime in the viscous liquid far above T_g.

4. Phosphorescence decay kinetics

The phosphorescence intensity decay of Ery B in sucrose glass with different glycerol contents was measured over the temperature range from 5 to 100ºC. All decays were well fit using the stretched exponential decay model (Eq. 6) used to fit comparable data for Ery B in a variety of amorphous sugar (Pravinata et al., 2005; Shirke et al., 2005) and protein (Simon-Lukasik and Ludescher, 2004; Nack and Ludescher, 2006) matrixes. The stretched exponential lifetimes and stretching exponents (β) are plotted in Figures 24a and 24b, respectively, as a function of T-T_g; these decay parameters displayed similar

thermal response in all films. The lifetime decreased biphasically with increasing temperature, exhibiting a gradual linear decrease below and a more dramatic decrease above T_g. The lifetime was greater in the presence of glycerol at each normalized temperature. The stretching exponents β remained constant at ~0.92 below and slightly above T_g and decreased dramatically to a low of ~0.55 at temperatures significantly above T_g.

The decrease in lifetime with temperature reflects an increase in the rate of non-radiative decay of the excited T_1 triplet state due, in the case of Ery B, to an increase in both the rate of non-radiative decay to the ground state S_0 (k_{TS0}) and the rate of reverse intersystem crossing to S_1 (k_{TS1}) (Pravinata et al., 2005; Vanderkooi and Berger, 1989; Parker, 1968). The value of k_{TS0} was calculated using Eq. 10 and an estimate of the maximum physically reasonable value for k_{TS1} (Pravinata et al., 2005); these values, which provide an estimate of the lower limit of k_{TS0}, are plotted in a modified Arrhenius fashion versus T_g/T in Figure 25. The quenching rate k_{TS0} was approximately constant with T_g/T at low temperature and increased above T_g, indicating that this rate is sensitive to the molecular mobility (α relaxations) activated at the glass transition. The family of curves displayed continuous upward curvature at increasing temperature, suggesting that the activation energy also increased continuously with increasing temperature and glycerol content.

Log(k_{TS0}) is plotted versus glycerol concentration in Figure 26a. In general, the quenching rate increased dramatically with an increase in glycerol content at all temperatures; the effect of glycerol increased with an increase in temperature. At low temperature, however, the quenching rate decreased in the presence of small amounts of

glycerol; this trend is illustrated by a plot of the relative rate, normalized to the value in the pure sucrose film, versus glycerol content (Figure 26b). In the temperature range from 5 to 45°C, the rate constant k_{TS0} decreased ~5% over the range from 0.17 to 0.27 mole ratio glycerol/sucrose; at 55°C and above, however, the rate increased at all glycerol contents.

The values of β increased slightly below T_g with addition of glycerol. Since β reflects the distribution of lifetimes, and thus the corresponding distribution of dynamically distinct probe environments with different values of k_{TS0} (Pravinata et al., 2005), the small increase in β with addition of glycerol indicated a significant decrease in the range of dynamically distinct probe environments in the glass.

5. Spectral heterogeneity

The phosphorescence intensity decays of Ery B in sucrose films with different glycerol content were measured as a function of excitation and emission wavelength at 25°C. All decays were well analyzed using a stretched exponential model; the lifetimes are plotted versus excitation and emission wavelength in Figure 27a. All films showed a similar decrease in lifetime with increasing emission wavelength. In pure sucrose, the lifetimes varied from a high of 0.65 ms at 640 nm to a low of 0.52 ms at 720 nm; lifetimes showed a similar monotonic decrease with increasing wavelength in sucrose-glycerol films. Lifetimes were enhanced slightly in the presence of small amounts of glycerol, ranging from 0.65-0.70 ms at 640 nm to 0.53-0.55 ms at 720 nm. However, higher amounts of glycerol decreased the lifetime as well as the total variation in lifetime across the emission band; at a mole ratio of 0.79, the lifetime only varied from 0.49 ms at 640 nm to 0.45 ms at 720 nm. Lifetimes varied similarly across the excitation band in all

films, increasing with increasing wavelength to a maximum at ~530 nm (the excitation peak) and then decreasing at higher wavelengths.

The stretching exponent β also varied as a function of both excitation and emission wavelength (Figure 27b). The values of β were slightly higher in the presence of glycerol at all concentrations. The β values were lower at the blue edge in both the excitation and emission bands in all films; β increased to a maximum at 680-690 nm across the emission band and then decreased at the red edge but increased monotonically with increasing wavelength across the excitation band. The variation of β across the emission band was slightly smaller in the presence of glycerol.

The calculated quenching rate k_{TS0} also varied with emission and excitation wavelength (Figure 28). The rate generally increased with increasing emission wavelength. At a mole ratio ≤ 0.47, k_{TS0} increased monotonically over the range from 640 to 720 nm; at higher glycerol concentrations k_{TS0} was approximately constant at short wavelength (~640-660 nm) and then increased with increasing wavelength. At low glycerol content (≤ 0.27) k_{TS0} was below, and at high glycerol content (≥ 0.47) k_{TS0} was above that seen in pure sucrose; the variation of k_{TS0} across the emission band decreased at higher glycerol content. The quenching rate exhibited a minimum value around 530 nm in the excitation band with higher values at both the blue and the red edge in all films; the quenching rate compared to pure sucrose decreased at low and increased at high glycerol contents.

Discussion

Phosphorescence emission energy and intensity from Ery B is sensitive to two distinct modes of molecular mobility in amorphous biomaterials (Pravinata et al., 2005; Simon-Lukasik and Ludescher, 2004; Shirke et al., 2005): matrix dipolar relaxation around the excited T_1 triplet state prior to emission that decreases the energy of the triplet state and thus lowers the emission energy; and matrix collisions that promote intersystem crossing from the excited T_1 triplet state to the ground S_0 singlet state that increase k_{TS0} and thus lower the lifetime. This study of matrix mobility in amorphous sucrose using Ery B phosphorescence indicates that both of these modes of molecular mobility are modulated in a complex concentration-dependent manner by glycerol.

This study actually observed two distinct effects of glycerol on the sucrose matrix mobility. Under most conditions of temperature and concentration glycerol caused a systematic and in some cases dramatic increase in the rate and extent of both modes of matrix molecular mobility; this appears to be the molecular correlate of the well-known plasticization of biomolecules by glycerol. At low temperature and low concentration, however, glycerol caused a slight but significant decrease in the rates of both modes matrix molecular mobility; this effect may be related to the so-called antiplasticization of synthetic polymers by small molecules (Jackson and Caldwell, 1967a, 1967b). (Although, strictly speaking, plasticization and antiplasticization refer to the macroscopic mechanical properties of a polymer-diluent blend, we use them here to describe the molecular mobility of amorphous sucrose-glycerol films.)

1. Plasticization of sucrose molecular mobility by glycerol

Our estimate of the extent to which glycerol plasticizes different modes of matrix mobility is based on the behavior of spectroscopic parameters plotted versus temperature

normalized to T_g. If glycerol modulates matrix mobility solely by decreasing the matrix T_g (that is, by plasticizing the matrix) then mobility curves at different glycerol content would be identical on a plot of $T-T_g$ or, where appropriate, T_g/T. If, however, glycerol affects matrix mobility in other, more specific ways, then these curves need not be identical; more germane to this analysis, if such curves are systematically displaced from one another, then glycerol must be modulating mobility in ways beyond a mere change in T_g.

The phosphorescence emission energy, monitored here as maximum emission frequency, reflects the average $T_1 \leftarrow S_0$ energy gap; it is primarily modulated by the T_1 energy and thus by the average extent of relaxation of dipolar hydroxyl groups around the excited T_1 state prior to emission. Plots of the Ery B emission energy versus $T-T_g$ for the various sucrose-glycerol mixtures were nearly superimposable (Figure 20a). Since the normalized curves are similar, it appears that glycerol affects the extent of dipolar relaxation in the sucrose matrix primarily by reducing T_g, that is, through a typical plasticization effect. Since the curves are not identical, however, other, secondary, effects may also be operating.

Temperature normalization to $T-T_g$ also generated a single master curve for the red-edge effect (Figure 23), another measure of the average extent of matrix dipolar relaxation during the probe excited state lifetime. The emission energy difference with excitation at 530 nm (absorption peak) and 560 nm (red edge) decreased gradually in the glass below T_g and more sharply in the melt above T_g in both glycerol-containing and pure sucrose films. This energy difference reflects the persistence of matrix sites which have Ery B probes with low energy T_1 states that are photo-selected by low energy (red-

edge) excitation; the decrease of the energy difference above T_g reflects an increase in the average rate of matrix relaxation that acts to equilibrate the energy of all matrix sites on the lifetime of the triplet state (Pravinata, et al., 2005; Demchenko, 2002). The presence of a single master curve for films with 0, 0.28, 0.63, and 0.79 mole ratio of glycerol/sucrose indicates that this measure of the extent of dipolar relaxation also indicates that glycerol primarily acts by plasticizing, the matrix.

Modified Arrhenius analysis of the actual rate of dipolar relaxation calculated from these peak frequency data, when normalized to T_g (that is, plotted versus T_g/T), generated a set of parallel but non-superimposable curves in all films (Figure 22b). These parallel curves support the claim that glycerol primarily affects the rate of dipolar relaxation by modulating T_g. The curves, however, were also systematically displaced to lower relaxation rate with increasing glycerol concentration. This displacement, equivalent to a ~ 7-fold reduction in rate in films with 0.79 mole ratio glycerol/sucrose, provides evidence that glycerol also has an additional, secondary effect on the matrix dipolar relaxation rate.

The excited T_1 state is quenched by collisions with surrounding molecules that activate the dissipation of vibrational energy from the probe into the matrix and thus increase the rate of intersystem crossing, k_{TS0}, to the ground S_0 state (Fischer et al., 2002; Vanderkooi and Berger, 1989). Arrhenius plots of k_{TS0} were essentially identical when plotted versus T_g/T, providing strong evidence that the rate k_{TS0} also scaled with T_g and thus was effectively plasticized by glycerol. Such behavior is consistent with our on-going interpretation of this rate as directly reflective of the α-relaxations activated at T_g (Pravinata et al., 2005; Shirke et al., 2005; Shirke and Ludescher, 2005a). This

plasticization is also clearly illustrated in the plot of log(k_{TS0}) versus glycerol content (Figure 26a).

These results thus indicate that both dipolar relaxation and collisional quenching in amorphous sucrose primarily reflect the effect of glycerol on T_g, providing direct evidence that these modes of molecular mobility are directly plasticized by glycerol. Some of the spectroscopic measures, however, indicate that glycerol also has a secondary effect on the rate of dipolar relaxation, an effect that may correspond to the macroscopic phenomenon referred to as antiplasticization (Jackson and Caldwell, 1967a, 1967b).

2. Antiplasticization of sucrose molecular mobility by glycerol

Several spectroscopic measures indicated that the rate and extent of dipolar relaxation and the rate of collisional quenching decreased at low glycerol content and low temperature. At 45°C and below, the emission energy of Ery B increased about 5% at glycerol/sucrose mole ratios of 0.17 and 0.27, corresponding to 4.3 and 6.8 wt %, respectively (Figure 21a), indicating that the extent of dipolar relaxation was lower in the presence of small amounts of glycerol. Given the polarity of glycerol and its ability to decrease the emission energy at high concentration, and that at fixed temperature these low concentrations of glycerol actually increase the phosphorescence lifetime, this increase in emission energy at low glycerol/sucrose mole ratio reflects a decrease in the rate of dipolar relaxation. Glycerol also decreased k_{TS0} about 5% under the same conditions, at mole ratios of 0.17 and 0.27 and temperatures ≤ 45°C.

The estimated T_g's for films with glycerol/sucrose mole ratios of 0.17 and 0.27 were 47 and 38°C, respectively; the T_g was ≤ 32°C for all other films. Given the highly hygroscopic nature of sucrose-glycerol films, we feel that the moisture content was

perhaps overestimated by our measurement protocol. Since this would result in an underestimation of T_g, it is likely that mobility decreased only in glassy films below T_g. Amorphous sucrose-glycerol films were stored at 0~3 % RH for at least 7 days and flushed with dry nitrogen during measurements; given the small amount of residual moisture, antiplasticization by water is not considered to be a major factor. Since only transparent films without crystals, as assayed through crossed polarizers, were used for measurements, antiplasticization is also not attributable to increased crystallinity. It thus appears that small amounts of glycerol perturb the glassy sucrose matrix in an opposite manner to the conventional plasticization effect of glycerol. Is this phenomenon the molecular correlate of antiplasticization?

Jackson and Caldwell (1967a) reported that small, polymer-compatible compounds containing polar atoms and non-bridged ring structures and having T_gs greater than -50°C produced a relatively high degree of stiffness and rigidity in synthetic polymers; they called this phenomenon antiplasticization. As reported by Seow et al. (1999), Sears and Darby found that antiplasticization may also occur with addition of some plasticizers when present below a "plasticization threshold" that is the lowest limit of concentration for the conventional external plasticizing effects on the polymers. Glycerol and other water-compatible diluents (xylose, sorbitol, etc.) generally plasticize the mechanical properties of glassy materials (Biliaderis et al., 1999; Cuq et al., 1997; Gontard et al., 1993). At high relative humidity, glycerol may work synergistically with water, further plasticizing gelatin films (Lim et al., 1999). However, Chang et al. (2006) found that glycerol may also show an antiplasticization effect in tapioca starch film, but only if the system is relatively dry ($a_w < 0.22$). Reports that small amounts of a low-T_g

diluent can suppress local, fast dynamics in a carbohydrate glass have been mostly confined to polymer systems such as starch-glycerol and starch-sorbitol films that contain low molecular weight plasticizers (Lourdin et al., 1997; Lourdin et al., 2003; Gaudin et al., 2000). A decrease in mobility also appears to occur in mixtures of molecules of similar sizes or structures, including maltose-glycerol (Lourdin et al., 1998), glucose-maltose-water (Noel et al., 1996), trehalose-glycerol (Cicerone and Soles, 2004), maltose-maltitol (Shirke et al., 2005), and lactose-lactitol (Shirke et al., 2006). The stability of proteins lyophilized in sugar, sugar alcohol, and polymer glasses at room temperature have also been attributed to antiplasticization effects (Cicerone et al., 2003).

The mechanism of antiplasticization is controversial. Published hypotheses include reduction in matrix free volume (Vrentas et al., 1988; Benczedi, 1999), suppression of local chain motions due to specific interactions between polymer and diluent (Liu et al., 1990; Roy et al., 1987), matrix stiffening due to the presence of thin, stiff, polar antiplasticizers (Jackson and Caldwell, 1967b), increasing modulus due to an increase in the number of cross-links (crystallites) in the matrix (Guerrero, 1989), and a suppression of secondary relaxations (Ngai et al., 1991). Based on an analysis using free volume theory, phase compatibility/miscibility, molecular weight and T_g of the diluent have recently been proposed to play an important role in antiplasticization (Vilics et al., 1996; Cicerone et al., 2003).

A decrease in free volume caused by a small amount of glycerol seems inconsistent with the overall decrease in T_g. Also, free volume theory becomes problematic when applied to systems, like sucrose-glycerol mixtures, with specific interactions. A random network of hydrogen bonds primarily holds the amorphous sugar

matrix together. The presence of polar glycerol molecules may provide more, and perhaps stronger, hydrogen bonding sites, with the hydrogen bonding sites located on glycerol molecules that have fewer internal constraints on their interactions with other molecules. The presence of a few such glycerol-sugar interactions may constrain the local motions of a sugar matrix dominated by sugar-sugar interactions. At higher glycerol content, however, where glycerol-glycerol interactions become more important, an increase in matrix mobility becomes the dominant effect.

3. Modulation of sucrose matrix heterogeneity by glycerol

Ery B phosphorescence emission bandwidth Γ, variations in lifetime (due to variations in k_{TS0}) across the excitation and emission bands, and the emission decay stretching exponent β, among other indicators not investigated in this study, all provide information about matrix heterogeneity. These indictors have provided evidence for extensive matrix heterogeneity in amorphous solids composed of pure sugars and sugar alcohols (Pravinata et al., 2005; Shirke and Ludescher, 2005b; Shirke et al., 2006) and proteins (Nack and Ludescher, 2006; Lukasik and Ludescher, 2006), suggesting that such heterogeneity is a common feature of amorphous solid foods and other biomaterials. Although matrix heterogeneity can arise from compositional heterogeneity, recent research using a variety of spectroscopic and other physical techniques indicates that even pure supercooled liquids and amorphous polymers are dynamically heterogeneous on both spatial and temporal scales due to fluctuations in matrix mobility through space at any given instant and through time at any given spatial location (Ediger, 2000; Richert, 2002). Matrix heterogeneity thus appears to be an intrinsic property of the amorphous solid state whose implications require investigation.

The emission bandwidth Γ, the FWHM of the emission band, decreased at constant T-T_g with increasing glycerol content in sucrose films (Figure 20b). Although Γ increased continuously with increasing temperature in pure sucrose, at glycerol/sucrose mole ratios of 0.63 and higher, Γ was essentially constant over a broad temperature range and only began to increase ~ 50-60°C above T_g. Since the emission bandwidth provides a direct measure of the width of the distribution of energetically distinct matrix sites, glycerol causes a concentration-dependent decrease in the energetic heterogeneity of the sucrose matrix.

The variation in lifetime (and thus k_{TS0}) across the excitation and emission bands provides an indicator of dynamic, as opposed to energetic, heterogeneity. Pravinata et al. (2005) have proposed a physical model to explain the coupling of lifetime and wavelength in which probes in local matrix environments with weaker molecular interactions (due to less constrained packing or weaker hydrogen bonding networks) have higher overall molecular mobility, and thus both shorter lifetimes due to higher rates of k_{TS0} and lower emission energies due to faster rates of dipolar relaxation.

The wavelength variation of k_{TS0} increased slightly over that in pure sucrose in sucrose films with glycerol/sucrose ratios of 0.17 and 0.27. At higher glycerol contents, however, the wavelength variation decreased. The variation in k_{TS0} with wavelength also decreased at higher temperature (data not shown) suggesting that spectral heterogeneity also decreased in the melt. Since the variation of k_{TS0} with wavelength reflects the presence of a broad continuum of local matrix sites that vary in terms of their overall molecular mobility, glycerol appears to decrease the variation across this continuum.

The stretching exponent β provides a nonlinear measure of the width of the lifetime distribution required to fit an emission decay transient (Lindsey and Patterson, 1980), a value of 1 indicating an infinitely narrow distribution (a single lifetime) and lower values indicating significantly broader lifetime distributions. Since the lifetime distribution varies due to variations in k_{TS0}, the magnitude of β thus provides another indicator of dynamic matrix heterogeneity. The stretching exponent β in all glycerol-containing films was comparable to or higher than that in pure sucrose at 25°C (Figure 27b), indicating that glycerol decreased the matrix dynamic heterogeneity. At sufficiently high temperature, however, ≥ 50°C above T_g, β decreased dramatically (Figure 24b), indicating a high degree of dynamic heterogeneity within the melt, whatever the glycerol content, a result seen in all amorphous sugars and sugar alcohols investigated to date (Pravinata et al., 2005; Shirke et al., 2005; Shirke et al., 2006; Shirke and Ludescher, 2005b).

Note that phase separation in the sucrose-glycerol binary system may influence the matrix heterogeneity. At high glycerol/sucrose mole ratios (above 0.63), the sucrose content in the mixed solution was very close to the upper limit of sucrose solubility (Segur and Miner, 1953). Thus, when preparing amorphous films through air-drying the concentrated solutions, it is possible that sucrose-rich and glycerol-rich phases may co-exist on the local microdomain level. Although there is no exact definition of the size frontier of microdomains between nanoheterogeneity or phase separation (Lourdin, 1998), those phase-separated domains or aggregates/clusters may influence the spectral heterogeneity. In order to reduce this possibility, the solutions with high glycerol concentration were heated around 40°C before spreading on the quartz slides.

Conclusion

The molecular mobility of amorphous solids is strongly influenced by composition and temperature. We have used phosphorescence from Ery B embedded in amorphous sucrose films to generate detailed maps of the matrix molecular mobility as a function of temperature at glycerol/sucrose mole ratios from 0 to 0.79. The primary effect of glycerol is to plasticize the sucrose matrix by increasing both the extent of dipolar relaxation around the excited state probe and the rate of matrix collisions with the excited state probe. However, at ≤ 45°C and at ≤ 0.27 mole ratio glycerol/sucrose, glycerol slightly decreased both the rate and extent of dipolar relaxation and the rate of matrix collisions; this phenomenon appears to be the molecular correlate of the so-called antiplasticization effect seen in polymers.

Spectral heterogeneity in Ery B phosphorescence in amorphous sucrose-glycerol films provides direct evidence to support a physical model of dynamic site heterogeneities within supercooled liquids and amorphous solids both above and below the glass transition temperature (Ediger, 2000; Richert, 2002). The addition of glycerol reduces both the energetic and the dynamic heterogeneity within the amorphous sucrose matrix. The ability to report dynamic heterogeneity using Ery B phosphorescence provides additional insights into the complex dynamic properties of amorphous sugars and sugar mixtures.

References:

Biliaderis, C.G., Lazaridou A., and Arvanitoyannis, I. 1999. Glass transition and physical properties of polyol-plasticized pullulan-starch blends at low moisture. *Carbohydr. Polym.* 4, 29-47.

Benczedi, D. 1999. Estimation of the free volume of starch-water barriers. *Trends Food Sci. Technol.* 10, 21-24.

Chang, Y.P., Abd Karim, A., and Seow, C.C. 2006. Interactive plasticizing-antiplasticizing effects of water and glycerol on the tensile properties of tapioca starch fims. *Food Hydrocoll.* 20, 1-8.

Cicerone, M.T., and Soles, C.L. 2004. Fast dynamics and stabilization of proteins: binary glasses of trehalose and glycerol. *Biophys. J.* 86, 3836-3845.

Cicerone, M.T., Tellington, A., Trost, L., and Sokolov, A. 2003. Substantially improved stability of biological agents in dried form: the role of glassy dynamics in preservation of biopharmaceuticals. *BioProcess Intl.* January, 36-47.

Crowe, J.H., Carpenter, J.F. and Crowe, L.M. 1998. The role of vitrification in anhydrobiosis. *Ann. Rev. Physiol.* 60, 73-103.

Cuq, B., Gontard, N., Cuq, J., and Guilbert, S. 1997. Selected functional properties of fish myofibrillar protein-based films as affected by hydrophilic plasticizers. *J. Agric. Food Chem.* 45, 622-626.

Demchenko, A.P. 2002. The red-edge effect: 30 years of exploration. *Luminescence. 1*7, 19-42.

Duchowicz, R., Ferrer, M.L. and Acuna, A.U. 1998. Kinetic spectroscopy of erythrosin phosphorescence and delayed fluorescence in aqueous solution at room temperature. *Photochem. Photobiol.* 68, 494-501.

Ediger, M.D. 2000. Spatially heterogenous dynamics in supercooled liquids. *Annu. Rev. Phys. Chem.* 51, 99-128.

Fennema, O. 1996. Water and Ice. In *Food Chemistry*, 3rd Edition. Marcel Dekker, Inc. N.Y.

Fischer, C.J., Gafni, A., Steele, D.G., and Schauerte, J.A. 2002. The triplet state lifetime of indole in aqueous and viscous environments: Significance of the interpretation of room temperature phosphorescence in proteins. *J. Am. Chem. Soc.* 124, 10359-10366.

Gaudin, S., Lourdin, D., Forssell, P.M., and Colonna, P. 2000. Antiplasticization and oxygen permeability of starch-sorbitol films. *Carbohydr. Polym.* 43, 33-37.

Goff, H.D., and Sahagian, M.E. 1996. Glass transitions in aqueous carbohydrate solutions and their relevance to frozen food stability. *Thermochim. Acta.* 280/281, 449-464.

Gontard. N., Guilbert, S., and Cuq, J.L. 1993. Water and glycerol as plasticizers affect mechanical and water vapor barrier properties of an edible wheat gluten film. *J. Food Sci.* 58, 206-211.

Guerrero, S.J. 1989. Antiplasticization and crystallinity in poly(vinyl chloride). *Macromol.* 22, 3480-3485.

Huang, V.T., Haynes, L., Levine, H., and Slade, L. 1996. Glass transitions in starch, gluten and bread as measured. Dielectric spectroscopy and TMA methods. *J. Therm. Anal.* 47(5), 1289-1298.

Jackson, W.J. JR., and Caldwell, J.R. 1967a. Antiplasticization. II. Characteristics of antiplasticizers. *J. Appl. Polym. Sci.* 11, 211-226.

Jackson, W.J. JR., and Caldwell, J.R. 1967b. Antiplasticization. III. Characteristics and properties of antiplasticizable polymers. *J. Appl. Polym. Sci.* 11, 227-244.

Kumagai, H., Sugiyama, T., and Iwamoto, S. 2000. Effect of water content on dielectric relaxation of gelatin in a glassy state. *J. Agric. Food Chem.* 48(6), 2260-2265.

Labuza, T., Roe, K., Payne, C., Panda, F., Labuza, T.J., Labuza, P.S. and Krusch, L. 2004. Storage stability of dry food systems: influence of state changes during drying and storage. *Proceedings of the 14th international drying symposium* (IDS 2004) Sao Paulo Brazil. 22-25 August. Vol A. pp. 48-68.

Lakowicz, J.R. 1999. *Principles of fluorescence spectroscopy*. Plenum Press,NY

Lee, K.C.B., Siegel, J., Webb, S.E.D., Leveque-Fort, S., Cole, M.J., Jones, R., Dowling, K., Lever, M.J., and French, P.M.W. 2001. Application of the stretched exponential function to fluorescence lifetime imaging. *Biophys. J.* 81, 1265-1274.

Levine, H., and Slade, L. 1988. Thermomechanical properties of small-carbohydrate–water glasses and 'rubbers'. Kinetically metastable systems at sub-zero temperatures. *J Chem. Soc. Faraday Trans.* 1 84(8), 2619 – 2633**.**

Lim, L.T., Mine, Y., and Tung, M.A. 1999. Barrier and tensile properties of transglutaminase cross-linked gelatin films as affected by relative humidity, temperature, and glycerol content. *J. Food Sci.* 64, 616-622.

Lindsey, C.P. and Patterson, G.D. 1980. Detailed comparison of the Williams-Watts and Cole-Davidson functions. *J. Chem. Phys.* 73, 3348-3357.

Liu, Y., Roy, A.K., Jones, A.A., Inglefield, P.T., and Ogden, P. 1990. An NMR study of plasticization and antiplasticization of a polymeric glass. *Macromol.* 23, 968-977.

Lourdin, D., Bizot, H., and Colonna, P. 1997. “Antiplasticization” in starch-glycerol films? *J. Appl. Polym. Sci.* 63, 1047-1053.

Lourdin, D., Ring, S.G., and Colonna, P. 1998. Study of plasticizer-oligomer and plasticizer-polymer interactions by dielectric analysis: maltose-glycerol and amylase-glycerol-water systems. *Carbohydr. Res.* 306, 551-558.

Lourdin, D., Colonna, P., and Ring, S.G. 2003. Volumetric behavior of maltose-water, maltose-glycerol, and starch-sorbitol-water systems mixtures in relation to structural relaxation. *Carbohydr. Res.* 338, 2883-2887.

Ludescher, R.D., Shah, N.K., McCaul, C.P. and Simon, K.V. 2001. Beyond Tg: optical luminescence measurements of molecular mobility in amorphous solid foods. *Food Hydrocolloids* 15, 331-339.

Lukasik, K.V., and Ludescher, R.D. 2006. Effect of plasticizer on dynamic site heterogeneity in cold-cast gelatin films. *Food Hydrocoll.* 20, 88-95.

Maroncelli, M. and Fleming, G.R. 1987. Picosecond salvation dynamics of coumarin 153: the importance of molecular aspects of salvation. *J. Chem. Phys.* 86, 6221-6239.

Milton, J.G., Purkey, R.M., and Galley, W.C. 1978. The kinetics of solvent reorientation in hydroxylated solvents from the exciting-wavelength dependence of chromophore emission spectra. *J. Chem. Phys.* 68, 5396-5404.

Nack, T.J, and Ludescher, R.D. 2006. Molecular mobility and oxygen permeability in amorphous bovine serum albumin films. *Food Biophys.* 1, 151-162.

Ngai, K.L., Rendell, R.W., Yee, A.F., and Plazek, D.J. 1991. Antiplasticization effects on a secondary relaxation in plasticized glassy polycarbonates. *Macromol.* 24, 61-67.

Noel, T.R., Parker, R., and Ring, S.G. 1996. A comparative study of the dielectric relaxation behaviour of glucose, maltose, and their mixtures with water in the liquid and glassy states. *Carbohydr. Res.* 282, 193-206.

Noel, T.R., Parker, R., and Ring, S.G. 2000. Effect of molecular structure and water content on the dielectric relaxation behaviour of amorphous low molecular weight carbohydrates above and below their glass transition. *Carbohydr. Res.* 329, 839-845.

Papp, S. and Vanderkooi, J.M. 1989. Tryptophan phosphorescence at room temperature as a tool to study protein structure and dynamics. *Photochem. Photobiol.* 49, 775-784.

Parker, C.A. 1968. *Photoluminescence of Solutions.* Elsevier, Amsterdam.

Partanen, R., Marie, V., MacNaughtan, W., Forssell, P., and Farhat, I. 2004. ^{1}H NMR study of amylose films plasticized by glycerol and water. *Carbohydr. Polym.* 56(2), 147-155.

Pravinata L.C., You, Y. and Ludescher, R.D. 2005. Erythrosin B phosphorescence monitors molecularmobility and dynamic site heterogeneity in amorphous sucrose. *Biophysical J.* 88(May), 3551-3561.

Ramos, M.A., Talon, C., Jimenez-Rioboo, R.J., and Sieira, S. 2003. Low-temperature specific heat of structural and orientational glasses of simple alcohols. *J. Phys.: Condens. Matter* 15, S1007-S1018.

Richert, R. 2000. Triplet state salvation dynamics: basics and applications. *J. Chem. Phys.* 113, 8404-8429.

Richert, R. 2002. Heterogeneous dynamics in liquids: fluctuations in space and time. *J. Phys. Condens. Matter.* 14, R703-R738.

Roos, Y. 1995. *Phase Transitions in Foods*. Academic Press, San Diego, CA.

Roos, Y.H., Juppila, K., and Zielasko, B. 1996. Non-enzymic browning-induced water plasticization. Glass transition temperature depression and reaction kinetics determination using DSC. *J. Therm. Anal.* 47(5), 1437-1450.

Roy, A.K., Inglefield, P.T., Shibata, J.H., and Jones, A.A. 1987. Local intermolecular structure in an antiplasticized glassy solid-state NMR. *Macromol.* 20, 1434-1437.

Ryabov, Ya.E., Hayashi, Y., Gutina, A., and Feldman, Y. 2003. Features of supercooled glycerol dynamics. *Phys. Rev.* B. 67, 132-202.

Segur, J.B., and Miner, C.S. 1953. Sugar solubility: sucrose and dextrose in aqueous glycerol. *Agric. Food Chem.* 1 (8), 567-569.

Seow, C.C., Cheah, P.B., and Chang, Y.P. 1999. Antiplasticization by water in reduced-moisture food systems. *J. Food Sci.* 64(4), 576-581.

Simon, S.L., and Mckenna, G.B. 1997. Interpretation of the dynamic heat capacity observed in glass-forming liquids. *J. Chem. Phys.* 107 (20), 8678-8685.

Shirke, S., and Ludescher, R.D. 2005a. Molecular mobility and the glass transition in amorphous glucose, maltose, and maltotriose. *Carbohydr. Res.* 340, 2654-2660.

Shirke, S., and Ludescher, R.D. 2005b. Dynamic site heterogeneity in amorphous maltose and maltitol from spectral heterogeneity in erythrosin B phosphorescence. *Carbohydr. Res.* 340, 2661-2669.

Shirke, S., Takhistov, P. and Ludescher, R.D. 2005. Molecular mobility in amorphous maltose and maltitol from phosphorescence of erythrosin B. *J. Phys. Chem. B.* 109, 16119-16126.

Shirke, S., You, Y., and Ludescher, R.D. 2006. Molecular mobility and dynamic site heterogeneity in amorphous lactose and lactitol from erythrosin B phosphorescence. *Biophys. Chem.* 123, 122-133.

Simon-Lukasik, K.V., and Ludescher, R.D. 2004. Erythrosin B phosphorescence as a probe of oxygen diffusion in amorphous gelatin films. *Food Hydrocoll.* 18, 621-630.

Soderholm, S., Roos, Y.H., Meinander, N., and Hotokka, M. 1998. Characterization of biomaterials using FT-Raman spectroscopy. *AIP Conference Proceedings* 430*(Fourier Transform Spectroscopy)*, 316-319.

Stuchell, Y.M. and Krochta, J.M. 1994. Enzymatic treatments and thermal effects on edible soy protein films. *J. Food Sci.* 59, 1332-1337.

Surana, R., Randall, L., Pyne, A., Vemuri, N.M., and Suryanarayanan, R. 2003. Determination of glass transition temperature and in situ study of the plasticizing effect of water by inverse gas chromatography. *Pharm. Res.* 20(10), 1647-1654.

Van den Dries, I.J., Van Dusschoten, D., and Hemminga, M.A. 1998. Mobility in maltose-water glasses studied with ^{1}H NMR. *J. Phys. Chem.* B 102(51), 10483-10489.

Vanderkooi, J.M., and Berger, J.W. 1989. Excited triplet states used to study biological macromolecules at room temperature. *Biochim. Biophys. Acta, Bioenergetics* 976, 1-27.

Vilics, T., Schneider, H.A., Manoviciu, V., and Manoviciu, I. 1996. A DMA study of the suppression of the β transition in slightly plasticized PVC blends. *J. Thermal. Anal. Cal.* 47, 1141-1153.

Vrentas, J.S., Duda, J.L., and Ling, H.C. 1988. Antiplasticization and volumetric behavior in glassy polymers. *Macromol.* 21, 1470-1475.

Yoshioka, S., Aso, Y., and Kojima, S. 1999. The effect of excipients on the molecular mobility of lyophilized formulations as measured by glass transition temperature and NMR relaxation-based critical mobility temperature. *Pharm. Res.* 16(1), 135-140.

Wolkers, W.F., Oldenhof, H., Alberda, M., Hoekstra, F.A. 1998. A Fourier transform infrared microspectroscopy study of sugar glasses: application to anhydrobiotic higher plant cells. *Biochim. Biophys. Acta.* 1379, 83-96.

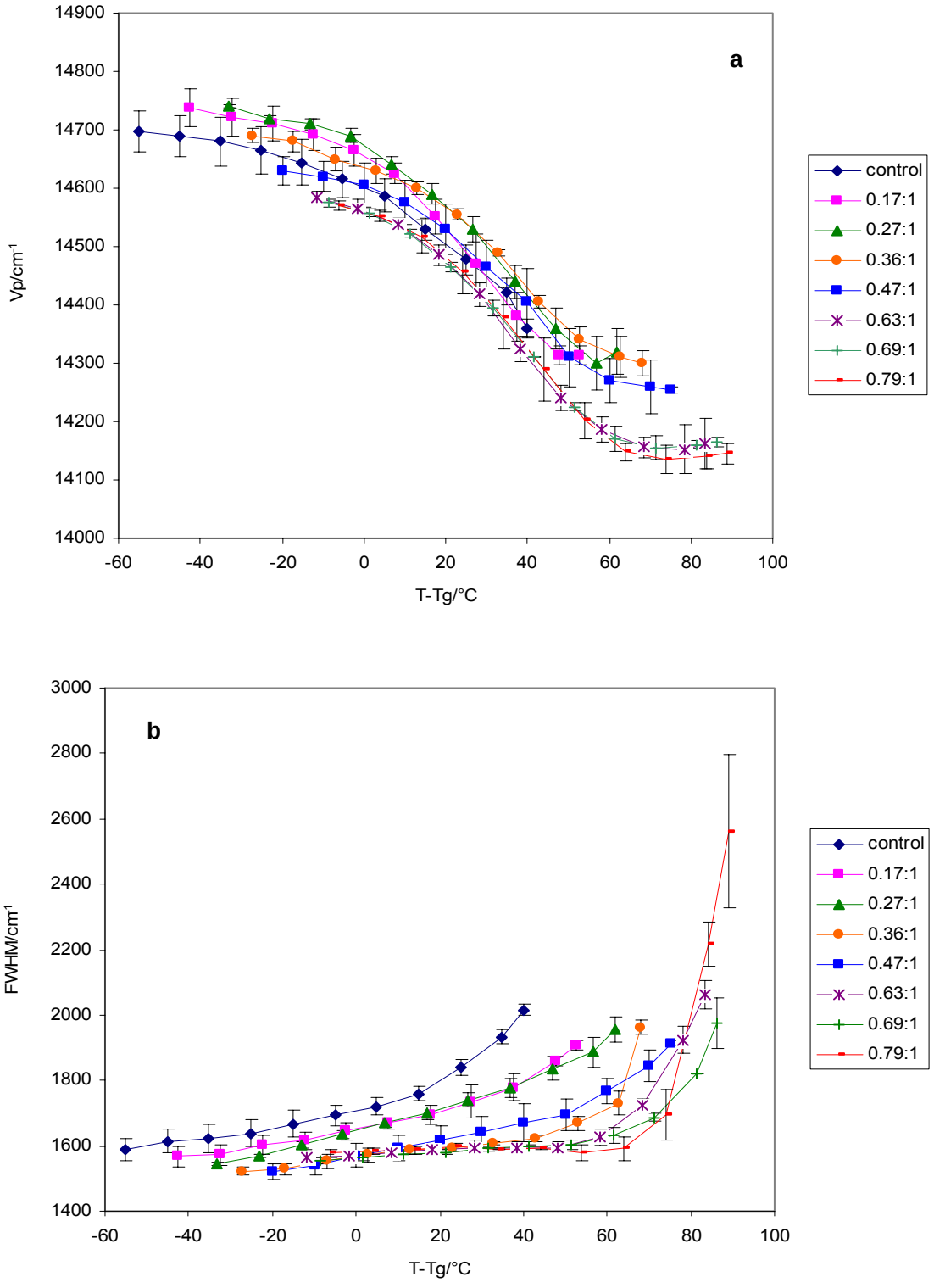

Figure 20: (a) Peak frequency (ν_p) and (b) bandwidth (full width at half maximum, FWHM) for phosphorescence emission from erythrosin B in amorphous sucrose-glycerol films plotted as a function of $T-T_g$. Delayed emission spectra collected as a function of temperature were analyzed using lognormal line shape function.

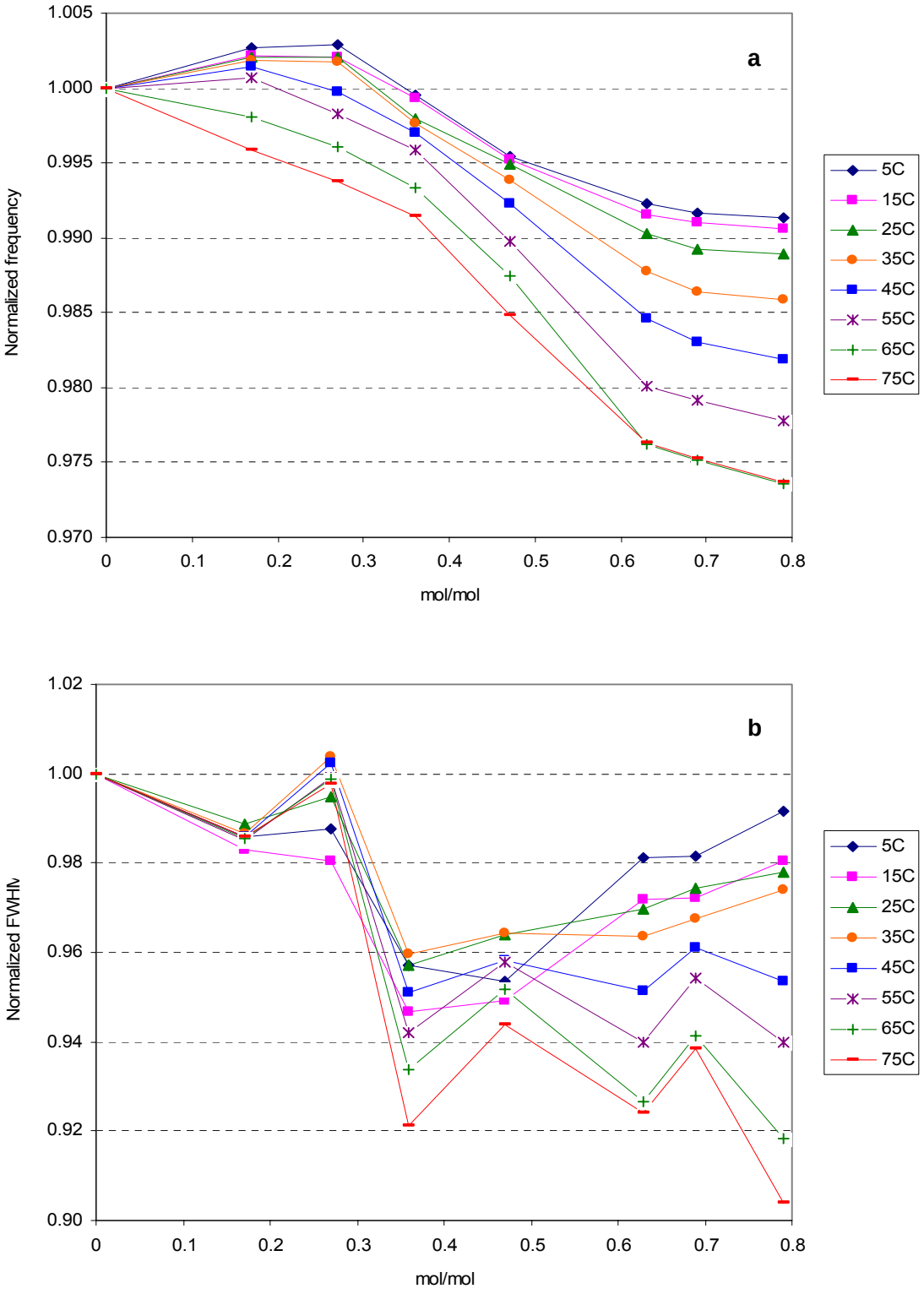

Figure 21: (a) Peak frequency and (b) bandwidth (FWHM), normalized at each temperature to the value in pure sucrose, for erythrosin B phosphorescence in amorphous sucrose-glycerol films plotted as a function of mole ratio of glycerol/sucrose. Delayed emission spectra collected as a function of temperature were analyzed using a log-normal line shape function.

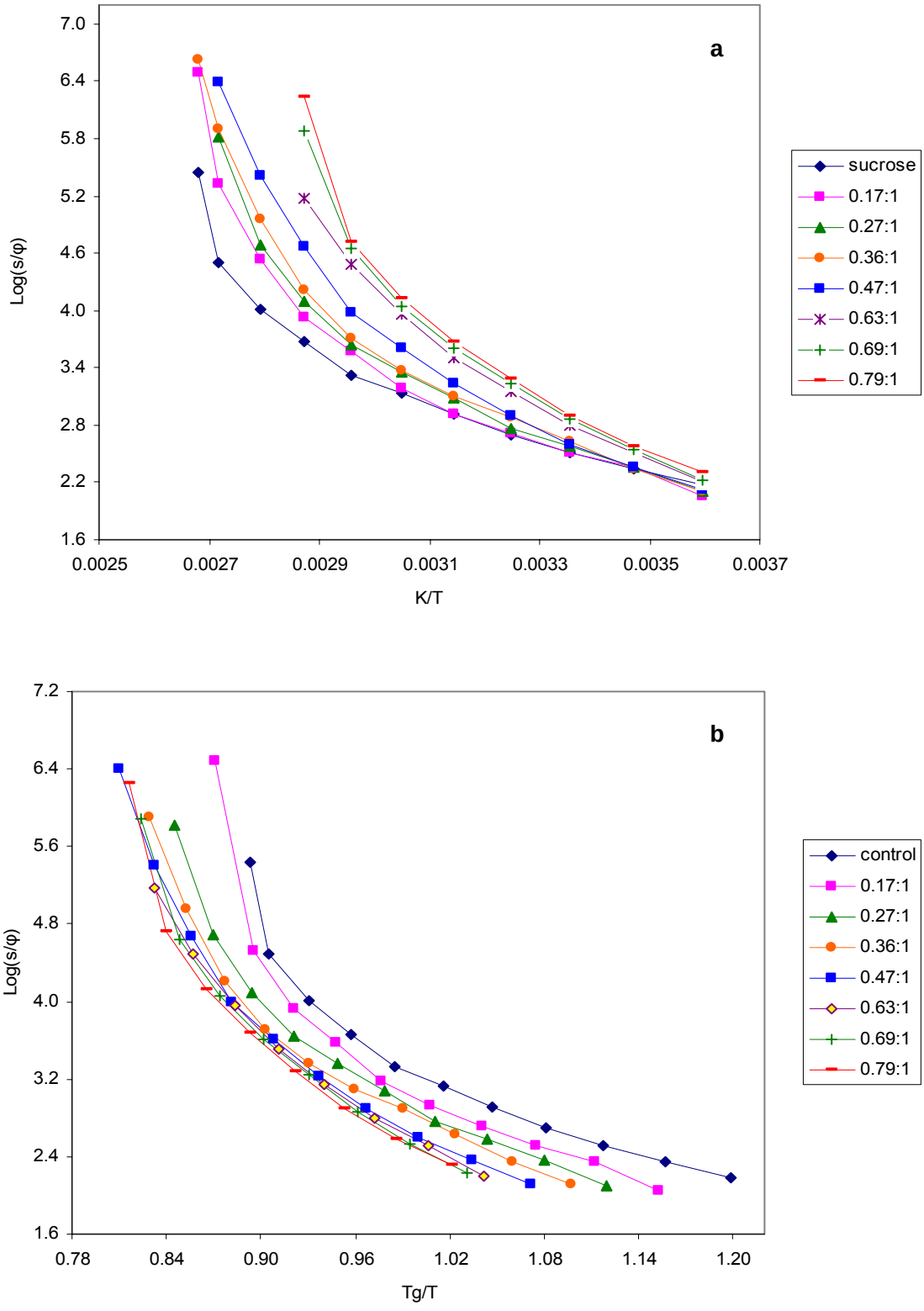

Figure 22: (a) Arrhenius plot of the effect of temperature on the rate of matrix dipolar relaxation around the excited erythrosin B triplet state in sucrose films at various glycerol contents; (b) modified Arrhenius plot of the dipolar relaxation rate versus T_g/T in sucrose with various glycerol/sucrose mole ratios.

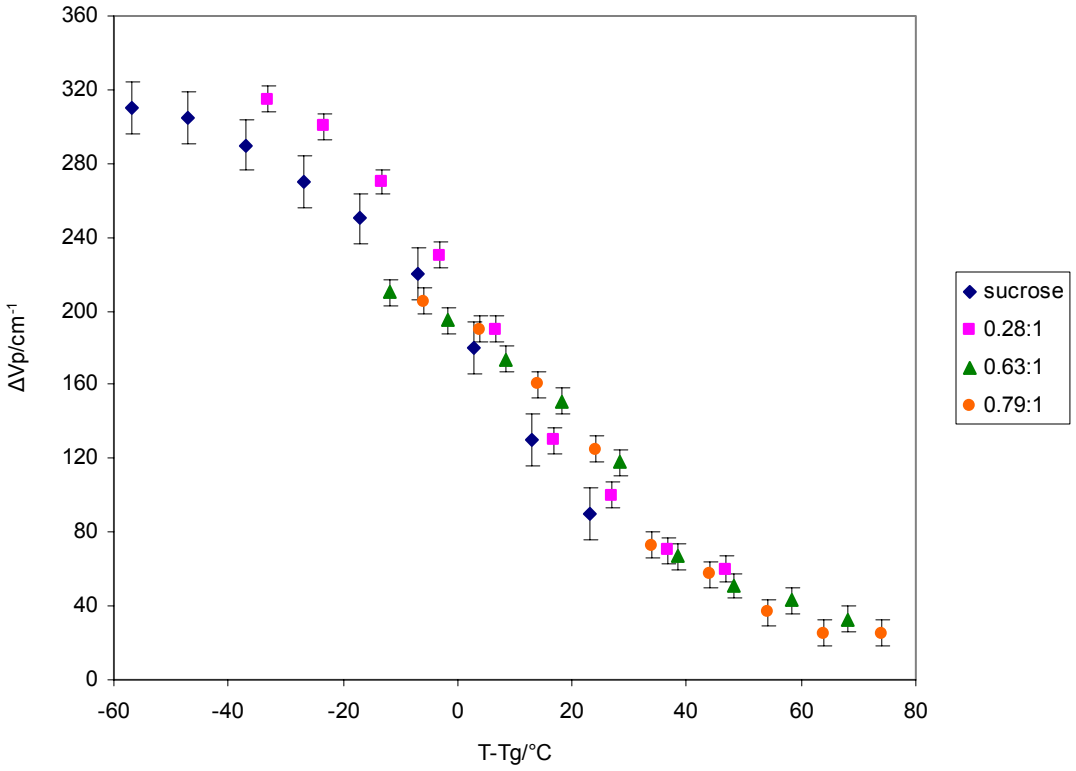

Figure 23. The phosphorescence red-edge effect for erythrosin B in amorphous sucrose films with glycerol/sucrose mole ratios of 0 (♦), 0.28 (■), 0.63 (▲) and 0.79 (●). The difference in energy ($\Delta\nu_p$) of the emission with excitation at 530 and 560 nm is plotted versus T-T_g.

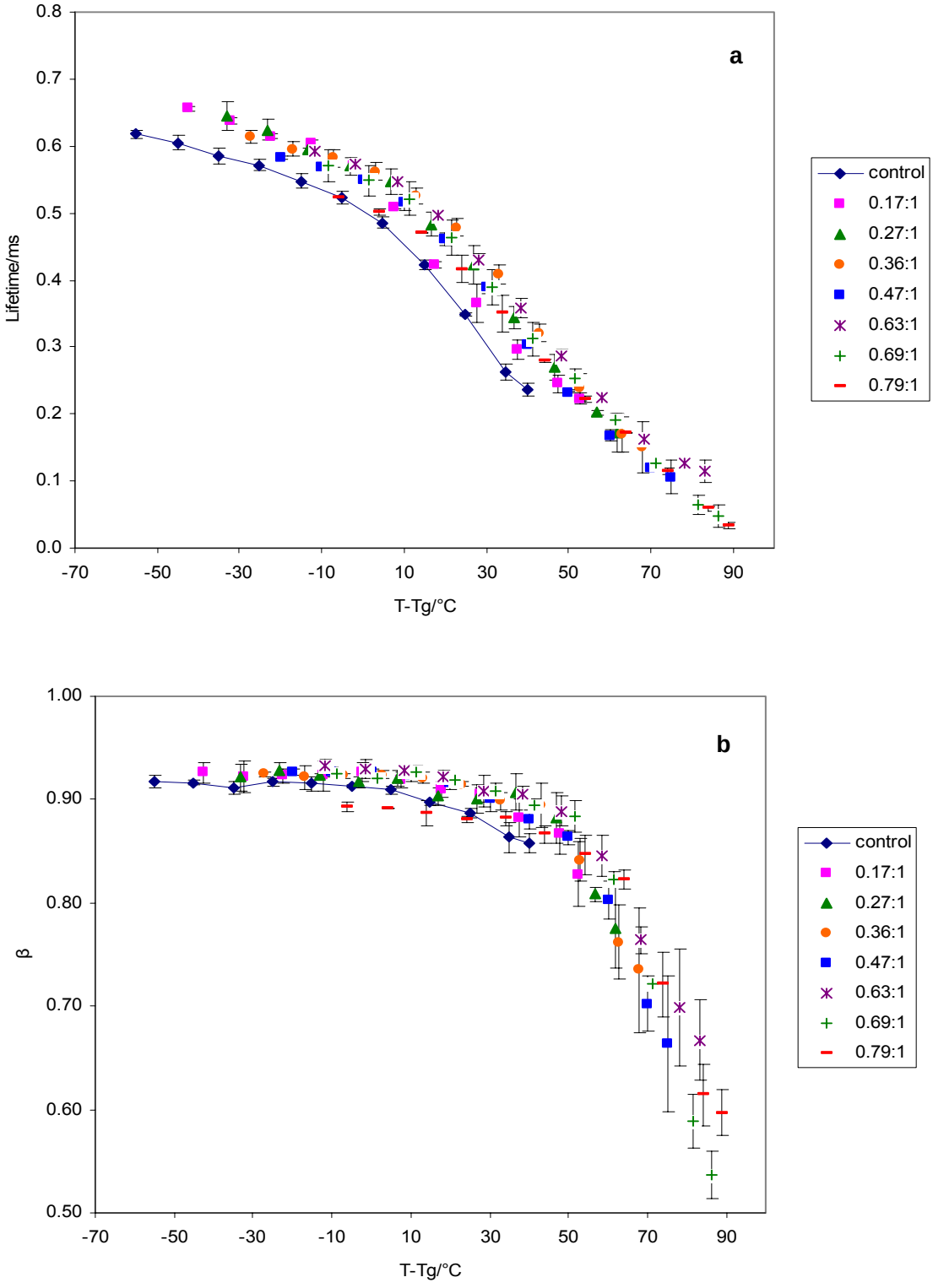

Figure 24: Temperature dependence of (a) lifetime and (b) stretching exponent β obtained from fits to a stretched exponential decay model of the intensity decay of erythrosin B in amorphous sucrose films with various glycerol/sucrose mole ratios.

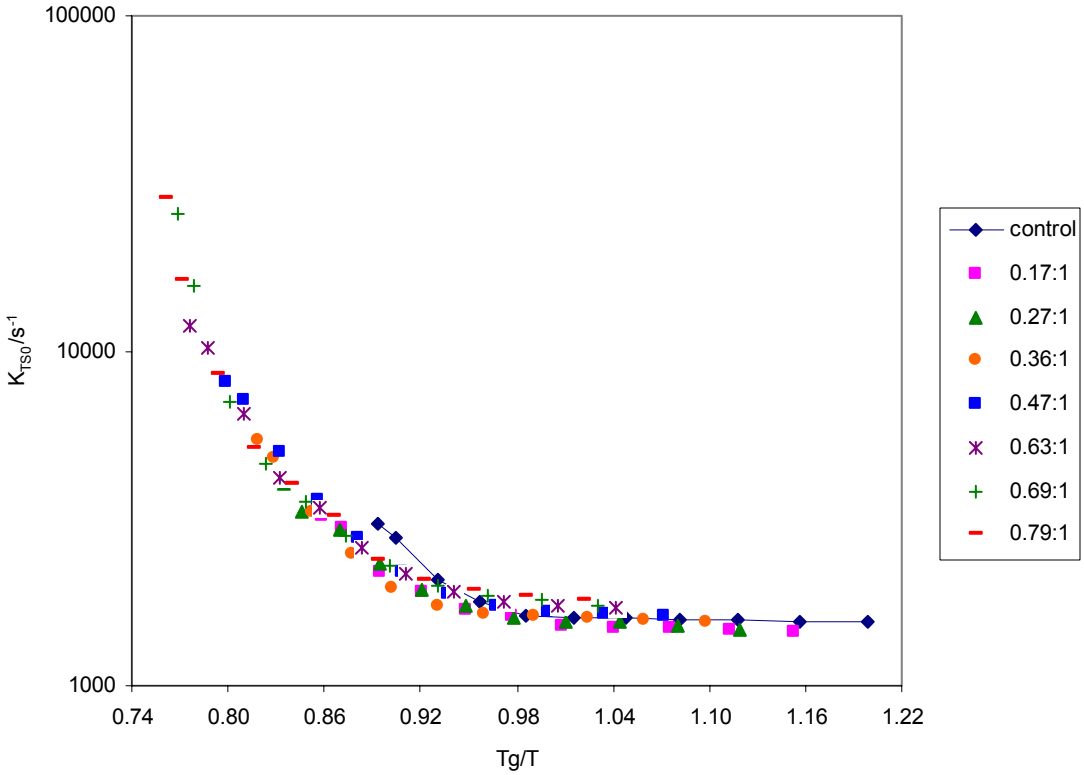

Figure 25: Temperature dependence of the rate constant for non-radiative decay of the triplet T_1 state to S_0 (k_{TS0}), calculated from the lifetime data of Figure 24a; see text for additional details. Erythrosin B in amorphous sucrose films with various glycerol/sucrose mole ratios.

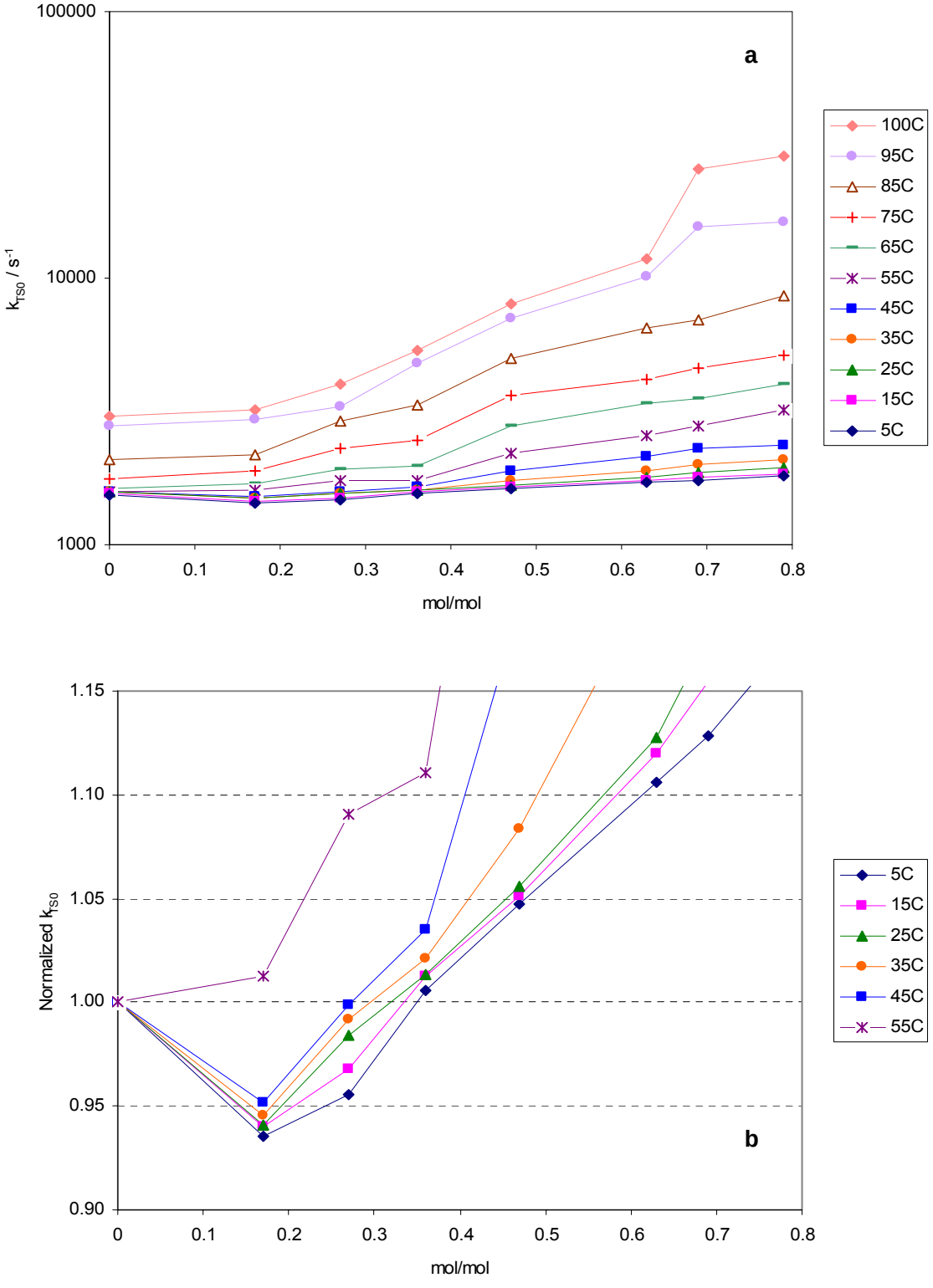

Figure 26: (a) The effect of glycerol on the rate constant for non-radiative decay of the triplet state to S_0 (k_{TS0}); data of Figure 6 were replotted as log(k_{TS0}) versus glycerol/sucrose mole ratio. (b) Normalized rate constant for non-radiative decay of the triplet state to S_0 (k_{TS0}) as a function of glycerol/sucrose mole ratio.

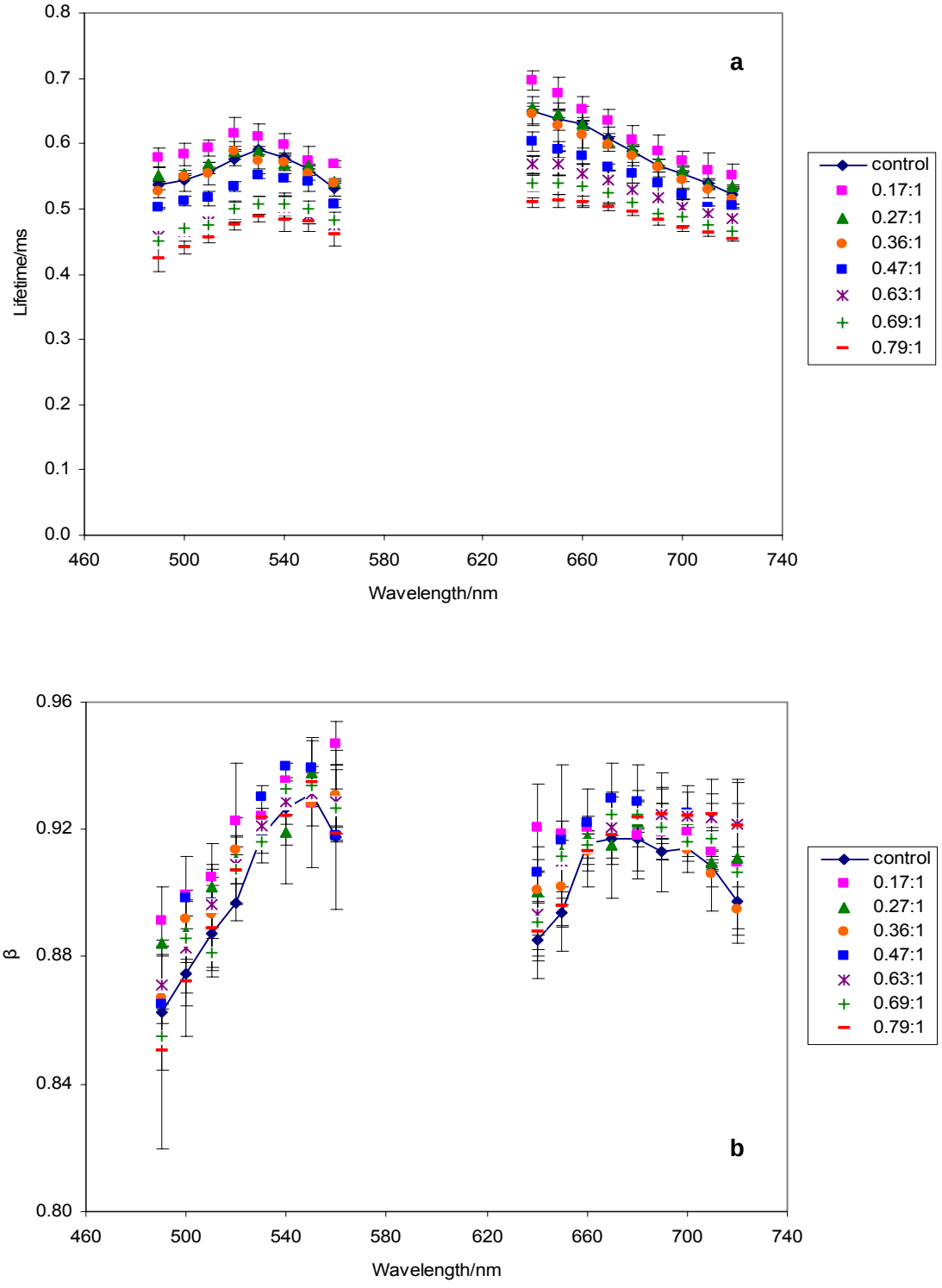

Figure 27: The effect of excitation wavelength (with 680 nm emission) and emission wavelength (with 530 nm excitation) on the lifetimes (a) and stretching exponents β (b) from fits of erythrosin B phosphorescence intensity decays to the stretched exponential decay model. Data collected in sucrose films with various glycerol/sucrose mole ratios.

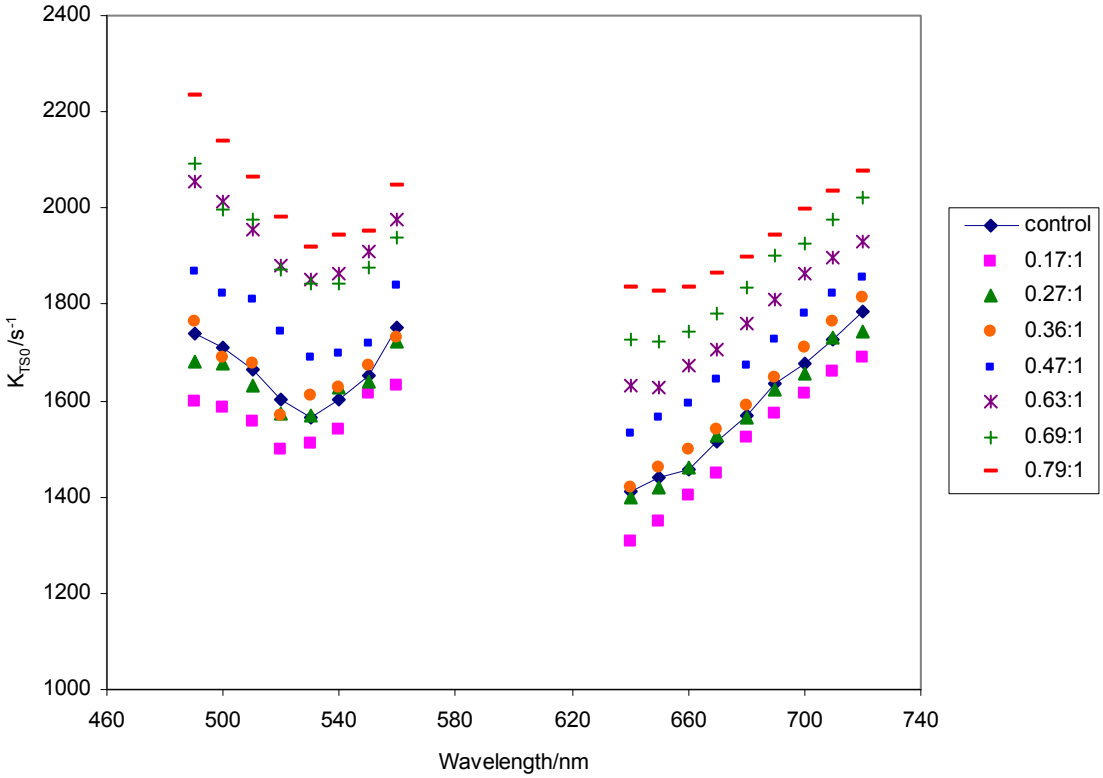

Figure 28: The rate constant for non-radiative decay of the triplet state to S_0 (k_{TS0}) plotted as a function of excitation wavelength (with 680 nm emission) and emission wavelength (with 530 nm excitation). Data collected from erythrosin B in sucrose films with various glycerol/sucrose mole ratios.

Chapter 4 Sodium chloride effect on amorphous sucrose matrix detected by triplet phosphorescence probe erythrosin B

Introduction

Recent years have seen growing interests in vitreous sugar systems since they are found to be involved in the preservation of seeds, spores and living organisms under extreme conditions (Crowe et al., 1998, 2002; Buitink et al., 2004). Vitrification (glass formation) is a vital strategy to protect sensitive materials at a kinetic level. By forming into amorphous, non-crystalline solids upon rapid drying from aqueous solution or cooling from the melt, sugars change from soft, pliable and flexible at high temperature to hard, brittle and rigid at low temperature with an extreme increase in viscosity due to the decrease in the rate of translational as well as rotational and vibrational mobility motions (Zallen, 1983). The physical properties of amorphous sugars play a key role in modulating the long-term viability of seeds and spores, and also modulating the stability and shelf life of foods and pharmaceuticals (Fennema, 1996; Roos, 1995; Slade and Levine, 1995).

Sucrose glasses have been an object of research for many years since it was found to be one of the earliest cyroprotective agents during anhydrobiosis. Its ability to protect biomaterials from freeze-thaw damage and provide long-term storage stability has attracted researchers to investigate the mechanism and develop the solid state formulations through drying or freeze-drying for the labile compounds in foods, such as vitamins and flavor compounds, and for the labile biomolecules in pharmaceuticals, such as enzymes, proteins, and antibodies. Since anhydrous glasses often consist of a variety

of compounds, such as buffers and tonicity adjusters in pharmaceuticals, complex molecules in food systems, effects of interaction with co-existing molecules can not be ignored.

Salts, universally present in biological systems and food products, always exist as impurities or minor ingredients during refinery and manufacture of sugar containing products. Salts have major influence on water structure and possible interactions with biomolecules, which may have an impact on the properties of foods and biomaterial systems. Eggleston et al. (1995) found that salts affect the thermal degradation of concentrated sucrose solutions through a manipulation of the water structure around a sucrose molecule. Although playing a vital role in many cases, salt effects on sugar glasses have received little attention. Among the limited research literature, most of them focused on the possible mechanism of crystallization inhibition effect from salts in supercooled or freeze-dried sugar systems. Inorganic salts are believed to increase the stability of the sugar systems due to their ability to inhibit crystallization. Izutsu and Aoyagi (2005) studied the effect of different inorganic salts on crystallization of poly(ethylene glycol) in frozen solutions. They found that salts prevent the crystallization by altering the molecular interactions and reducing the molecular mobility. The inhibition effect depends on the type of salt and salt concentration. Water structure-breaking salts (or salting-in salts) and water structure-enhancing salts (or salting-out salts) are defined based on their influence on the water structure. NaCl as one of the salting-in salts increases the viscosity of the mixture solutions, promotes the formation of amorphous, glassy systems, and prevents crystallization (Longinotti et al., 2002). A further study of effect of salts on sugar crystallization rate showed that the observed delayed

crystallization of sugar in aqueous solutions in the presence of salt may result from the effect on the nucleation mechanism of ion-induced microheterogeneities in the supercooled solutions (Longinotti et al., 2002).

A few studies tried to explore the salt effect on the stability of sugar glasses through modifying the glass transition temperature. Shalaev et al. (2002) studied the properties of pharmaceutically compatible buffers at sub-zero temperatures in lyophilized formulations and found that T_g' of a freeze-dried system results from a competition between two opposite actions: increased viscosity due to an increase in the electrostatic interaction and decreased viscosity due to an increased amount of unfrozen water. In a study of the effect of salts on water sorption behavior and ice crystallization in aqueous sugar systems, Mazzobre et al. (2001) reported that salts can modify the properties of concentrated sugar solutions without altering their T_g's and these effects are related to the charge/size ratio of the cations present. Kets et al. (2004) used modified DSC method to determine T_g of freeze-dried sucrose-citrate mixture. They found that when residual water was removed from the mixture, T_g increased with citrate concentration and exceeded the T_g of pure sucrose although citrate is supposed to lower the T_g of sucrose (Lu and Zografi, 1997; Wang, 2000).

Here we make no attempt to prove mechanism. Our purpose is to investigate salt's effect on the stability of amorphous sugar solids through measuring the molecular mobility in the presence of the salt sodium chloride. It is now generally recognized that molecular mobility is associated with the properties of amorphous biomaterials. Molecular mobility within amorphous solids is usually manifested by relaxation processes. The amorphous solids exhibit the primary α or glass transition at T_g, which

reflects the activation of large-scale molecular motions (α-relaxations) that underlie the onset of translational and large scale rotational motions, and the secondary β transition within the glass at T_β which reflects the activation of localized molecular motions (β-relaxations) linked to vibrational motion and local side-chain motions. The temperature-dependent molecular mobility thus controls physical and chemical properties by modulating the nature and kinetics of reactions that occur during processing and storage of biomaterials.

The measurement of molecular mobility in amorphous sugars is of fundamental interest because it provides a straightforward way to evaluate stability. A number of techniques have been used to characterize the properties and mobility of amorphous materials including Fourier transform infrared (FT-IR) spectroscopy (Wolkers et al., 1998; Ottenhof et al., 2003), dielectric relaxation (Chan et al., 1986; Gangasharan and Murthy, 1995; Richert, 2001), differential scanning calorimetry, nuclear magnetic resonance spectroscopy (van den Dries et al., 2000), electron spin resonance (Contreras-Lopez et al., 2000; Buitink et al., 2000), and phosphorescence spectroscopy (Richert, 2000).

Due to its high phosphorescence quantum yield, long lifetime, site selectivity and high sensitivity, Ery B phosphorescence has been widely used to monitor the molecular mobility as well as dynamic site heterogeneity in amorphous solid sugars (Pravinata et al., 2005; Shirke and Ludescher, 2005; Shirke et al., 2005, 2006) and proteins (Simon-Lukasik and Ludescher, 2004; Lukasik and Ludescher, 2006a, 2006b; Nack and Ludescher, 2006; Sundaresan and Ludescher, 2007). In the present study, phosphorescence of erythrosin B was used to measure the matrix mobility in thin films of

amorphous sucrose-NaCl mixtures. NaCl content was varied from 0.04 to 0.87 (mole ratio of NaCl/sucrose) by addition of NaCl to the concentrated sucrose solution prior to film formation. The temperature-dependence of mobility was measured and analyzed at different NaCl contents, generating families of mobility versus temperature curves. Comparisons thus provided information about the mechanisms by which NaCl influences mobility.

Materials and Methods

1. Sample Preparation

We prepared glassy sucrose films by using a slightly modified version of our published method (Pravinata et al., 2005; see details in Materials and Methods in Chapter 1).

Sucrose-NaCl mixtures were prepared from sucrose solution containing dye. Sodium chloride (99.5% pure; Sigma Chemical Co., St. Louis, MO) was added to the purified sucrose solutions to obtain a series of mixtures with NaCl/sucrose anhydrous mole ratios of 0.04, 0.065, 0.09, 0.20, 0.36, 0.46, 0.56, 0.73 and 0.87. Prior to preparing glassy films, sucrose-NaCl blended solutions were filtered through a membrane with 0.2μm pores. The procedure to make a glassy film was the same as the procedure to make a pure sucrose film.

Water content in amorphous sucrose and sucrose-NaCl films was determined gravimetrically (by difference of mass before and after drying for 24h at 70°C in an Ephortee (Haake Buchler, Inc.) vacuum oven at 1 kPa). Sample films were scratched from quartz slides and ground into powders in a glove box containing P_2O_5 and Drie-Rite

with a relative humidity less than 5%. Pure sucrose sample contained 0.56±0.13 wt. % water, while the NaCl/sucrose mixture samples contained 1.04±0.04, 0.81±0.21, 1.06±0.26, 1.04±0.01, 1.18±0.27, 0.54±0.29, 2.17±0.11, 2.32±0.26, and 2.34±0.25 wt. % water, respectively.

2. Luminescence measurements

Luminescence measurements were made using a Cary Eclipse Fluorescence spectrophotometer (Varian Instruments, Walnut Creek, CA). Prior to any phosphorescence measurements, all samples were flushed for at least 15 minutes with nitrogen gas which contained less than 1ppm oxygen to eliminate oxygen quenching. At each target temperature samples were equilibrated for 1min/°C increase in temperature. The temperature was controlled using a thermo-electric temperature controller (Varian Instruments, Walnut Creek, CA). To eliminate moisture condensation during the measurements below room temperature, dry air was used to flush the chamber surrounding the cuvette holder. All the measurements were made at least in triplicate.

Delayed fluorescence and phosphorescence emission spectra were collected from 520 to 750 nm (10 nm bandwidth) at 1 nm intervals using excitation of 500 nm (20 nm bandwidth) over a temperature range from 5 to 100°C with an observation window of 5.0 ms and an initial delay time of 0.2 ms which suppresses fluorescence coincident with the lamp pulse. Emission spectra from sucrose or sucrose-NaCl films without probe were subtracted from each spectrum although the signal of background was very low.

The energy of emission maximum (ν_p) and the full width at half maximum (FWHM) of the emission bands were determined by using log-normal lineshape function (Maroncelli and Fleming, 1987) to fit both delayed fluorescence and phosphorescence.

$$I(\nu) = I_0 \exp\left\{ - \ln(2)\left(\frac{\ln[1 + 2b(\nu - \nu_p)/\Delta]}{b} \right)^2 \right\} \quad (1)$$

Where I_0 is the maximum emission intensity, ν_p is the peak frequency (cm^{-1}), Δ is a linewidth parameter and b is an asymmetry parameter. This equation reduces to a Gaussian line width when b=0. The bandwidth (FWHM; Γ) was calculated according to the following equation:

$$\Gamma = \Delta\left(\frac{\sinh(b)}{b} \right) \quad (2)$$

For delayed luminescence spectra collected from 520-750 nm, a sum of log-normal functions for delayed fluorescence ($I_{df}(\nu)$) and phosphorescence ($I_p(\nu)$) was used to fit the spectra. Each emission band was fit to independent fit parameters.

Red-edge effect measurements over the temperature range from 5 to 85°C used excitation wavelength at 530 nm and 560 nm, respectively. Phosphorescence emission was collected from 640 to 760 nm using an observation window of 5.0 ms and 0.1 ms delay. Phosphorescence spectra were converted to intensity versus frequency (cm^{-1}) and analyzed to obtain the peak frequency (ν_p) and spectral bandwidth (Γ) using a log-normal function ($I(\nu)$) (Eq. 1).

For lifetime measurements, samples were excited at 530 nm (20 nm bandwidth) and emission transients collected at 680 nm (20 nm bandwidth) over the temperature range from 5 to 100°C. Phosphorescence intensity decays were collected over a window of 5 ms with an initial delay of 0.1 ms and increments of 0.04 ms. Each decay was the average of 20 cycles. Because intensity decays were non-exponential, a stretched exponential, or Kohlrausch-Williams-Watts' decay function was selected to analyze the intensity decay (Richert, 2000; Lee, et al., 2001; Pravinata et al., 2005).

$$I(t) = I_0 \exp(-(t/\tau)^{\beta}) + \text{constant} \quad (3)$$

Where I_0 is the initial amplitude, τ is the stretched exponential lifetime, and β is an exponent varying from 0-1 and characterizing the distribution of lifetimes. The use of a stretched exponential model provides a direct measurement of continuous distribution of lifetimes, which is appropriate for describing a complex glass possessing a distribution of relaxation times for the dynamic molecular processes. The smaller the β value, the more non-exponential the intensity decays and the broader the distribution of lifetimes. Program NFIT (Galveston, TX) was used to fit the decay; goodness of fit was evaluated by examining the χ^2 and R^2. Plots of modified residuals (defined as the difference between the intensity from the fit decay curve and the measured intensity divided by the square root of the measured intensity) was also an indicator of the goodness of fit. R^2 for all fits ranged from 0.99 to 1.00 and modified residuals plots fluctuated randomly around zero amplitude.

Phosphorescence emission lifetimes of Ery B as a function of emission wavelength were measured with excitation wavelength at 530 nm (20 nm bandwidth); emission wavelength varied from 640 to 720 nm (20 nm bandwidth). Phosphorescence emission lifetimes as a function of excitation wavelength were measured with emission wavelength at 680 nm (20 nm bandwidth); excitation wavelength ranged from 490 to 560 nm (20 nm bandwidth). The experiments were performed at 25°C.

3. Photophysical scheme

Our analysis of the delayed emission is similar to the photophysical scheme for erythrosin B outlined by Duchowicz et al. (1998). The measured emission rate for phosphorescence (k_P) is the sum of all possible deexcitation rates for the triplet state T_1:

$$\tau^{-1} = k_P = k_{RP} + k_{TS1} + k_{TS0} + k_Q[Q] \quad (4)$$

In this equation, k_{RP} is the rate of radiative emission to the ground state S_0. For erythrosin B, k_{RP} is 41 s^{-1} and constant with temperature (Duchowicz et al., 1998).

k_{TS1} is the rate of thermally activated reverse intersystem crossing from the triplet state T_1 to the singlet state S_1, and the value can be estimated from the Arrhenius equation:

$$k_{TS1}(T) = k^0_{TS1} \exp(-\Delta E_{TS}/RT) \quad (5)$$

where k^0_{TS1} is the maximum rate of intersystem crossing from T_1 to S_1 at high temperature, ΔE_{TS} is the energy gap between T_1 and S_1, R=8.314 J K^{-1} mol^{-1}, and T is the temperature in Kelvin. The value of ΔE_{TS} is calculated from the slope of a Van't Hoff plot of the natural logarithm of the ratio of intensity of delayed fluorescence (I_{DF}) to phosphorescence (I_P):

$$d[\ln(I_{DF}/I_P)]/d(1/T) = -\Delta E_{TS}/R \quad (6)$$

where I_{DF} and I_P are the maximum intensity values determined from analysis of the emission band using Eq. (1). The value of k_{TS1} at 25°C was estimated as 88 s^{-1} using k^0_{TS1}=3.0 x 10^7 s^{-1} and ΔE_{TS} = 31.56 kJ/mol (Pravinata et al., 2005).

In the presence of oxygen, the quenching rate $k_Q[Q]$ is the product of rate constant k_Q and the oxygen concentration [Q]. By flushing nitrogen throughout the measurements we assume that no oxygen quenching occurred. One of the non-radiative decay routes is through intersystem crossing to the ground state S_0. The decay rate is expressed by k_{TS0}, which reflects the rate of collisional quenching of the probe due to both internal and external factors (Papp and Vanderkooi, 1989). We assume that the term k_{TS0} primarily reflects the external environmental factors since the self collisional quenching among

probe molecules can be neglected within the extremely viscous amorphous solid. In this study, temperature-dependent term k_{TS0} can be calculated by difference from Eq. 4.

Results

At a probe/sucrose mole ratio of $1:10^4$, each probe is on average surrounded by a matrix shell around 10-11 sucrose molecules thick. At this concentration Ery B dispersed within the sucrose matrix does not aggregate and thus reports the physical properties of the unperturbed sucrose matrix (You and Ludescher, 2006).

1. Delayed emission spectra

The delayed emission spectra of erythrosin B in amorphous sucrose and sucrose-NaCl films at a dye/sucrose mole ratio of $1:10^4$ exhibited two emission bands: the long wavelength phosphorescence band (maximum ~680 nm) from the triplet state T_1 and the short delayed fluorescence band (maximum ~555 nm) from the singlet state S_1 that has been repopulated by reverse intersystem crossing from the triplet state (Parker, 1968). Delayed emission spectra of amorphous sucrose and sucrose-NaCl films with various molar fractions collected over the temperature range form 5 to 100 °C showed the expected trends: decrease in phosphorescence and increase in delayed fluorescence intensity with raising temperature; both the delayed fluorescence and phosphorescence bands shifted to longer wavelength at high temperature (graphs not shown here). The intensity ratio ($\ln (I_{df}/I_p)$) was plotted as a van't Hoff plot versus 1/T and the slope obtained from the linear plot can be used to estimate the energy gap between the triplet and singlet states (Eq. 6 in Materials and Methods). In amorphous sucrose the value of ΔE_{TS} is 31.56±0.56 kJ mol^{-1}; in the presence of NaCl with mole ratios from 0.04 to 0.87,

the values of ΔE_{TS} were 30.77±0.67, 31.12±0.58, 31.21±0.18, 30.80±0.52, 30.65±0.48, 30.15±0.32, 30.85±0.50, 30.44±0.26, and 29.93±0.37 kJ mol^{-1}, respectively, indicating that addition of NaCl did not significantly modulates the singlet-triplet energy gap.

The peak frequency (ν_p) and bandwidth (Γ) for both delayed fluorescence and phosphorescence emission were determined by fitting to a log-normal lineshape function (Eq.1 and Eq.2). ν_p and Γ for phosphorescence are plotted in Figure 29 and Figure 31. The peak frequency and bandwidth for delayed fluorescence displayed similar behavior (data not shown). The phosphorescence peak frequency in both pure sucrose and sucrose-NaCl mixtures decreased biphasically as a function of temperature: ν_p decreased gradually and linearly at low temperature, and then more steeply at high temperature. The decrease in emission energy reflects an increase in the average extent of dipolar relaxation around the excited triplet state prior to emission (Lakowicz, 1999).

The spectra of erythrosin B in amorphous sucrose were blue-shifted, that is, ν_p increased, in the presence of NaCl. When NaCl was added at mole ratios from 0.04 to 0.46, the peak frequency increased over the whole temperature range (shown in Figure 30a). The peak frequency at 5 °C increased from 14700 cm^{-1} in pure sucrose to 14990 cm^{-1} in sucrose-NaCl at a ratio of 0.46 (the spectrum blue-shifted by 13 nm). The shape of the curves was also similar to that of the pure sucrose. Above a mole ratio of 0.46, the peak frequency decreased with increase in NaCl concentration, but with values higher than those in pure sucrose (e.g., ν_p was 14923 cm^{-1} in NaCl/sucrose at a ratio of 0.87). Compared with pure sucrose, the shape of the curves in the presence of large amounts of NaCl changed at higher temperature, exhibiting more negative slopes with lower onset temperature that initiated the matrix melting (shown in Figure 30b).

The phosphorescence bandwidth (Figure 31) increased gradually with temperature in the glass and more dramatically in the melt above T_g. Amorphous sucrose films with different NaCl contents showed similar trends over the whole temperature range. Compared with pure sucrose, the bandwidth increased with increase in the concentration of NaCl (shown in Figure 32a). When the NaCl/sucrose mole ratio was above 0.46, the bandwidth decreased. At mole ratio of 0.87, the bandwidth was similar to that of pure sucrose (shown in Figure 32b). The increase in bandwidth with addition of NaCl was much smaller in the glass than that in the melt. This increase in inhomogeneous broadening indicates that there is a corresponding increase in the range of energetically distinct matrix environments in amorphous sucrose-NaCl mixtures.

Peak frequency over the temperature range from 5 to 100ºC is plotted versus concentration of NaCl in the sucrose film in Figure 33a. In a salt concentration range from 0 to 0.09 mole fraction, the peak frequency increased steeply with an increase in the NaCl content, showing an increment of 200 cm^{-1} at low temperatures and 100 cm^{-1} at high temperatures. When the NaCl/sucrose mole ratio increased from 0.09 to 0.46, ν_p increased gradually with a growth of 100 cm^{-1} at low temperatures and 70 cm^{-1} at high temperatures. When the amount of NaCl was added from 0.46 to 0.87 mole ratio, the peak frequency decreased slightly, showing a decline of 70 cm^{-1} at low temperatures and 120 cm^{-1} at high temperatures. Figure 34a shows a plot of relative peak frequency normalized to the values in the pure sucrose as a function of NaCl content. Clearly, NaCl has a significant influence on the emission energy (peak frequency) at lower temperature in the whole concentration range; however, this effect became smaller at higher

temperature and at higher NaCl content. The maximum peak frequencies were observable over the whole temperature range around a NaCl/sucrose mole ratio of 0.46.

Bandwidth is plotted as a function of NaCl content in the sucrose film over the temperature range from 5 to 100ºC in Figure 33b. The bandwidth increased with increasing NaCl content up to a mole ratio around 0.46, and then slightly decreased at ratios above 0.46.

The effect of NaCl on the spectroscopic parameters is illustrated in plots of the relative peak frequency and bandwidth normalized to the values in the pure sucrose film at temperatures from 5 to 100°C (Figure 34). The overall trend was that peak frequency and bandwidth at each temperature increased with an increase in NaCl content, indicating that, NaCl decreased the extent of dipolar relaxation and increased the environmental energetic heterogeneity.

2. Red-edge effect

Measurements of the red-edge effect as a function of temperature in both sucrose and sucrose-NaCl films are plotted in Figure 35 as the energy difference ($\Delta\nu_p$) with 530nm and 560nm excitation of the emission band maximum. The magnitude of $\Delta\nu_p$ for erythrosin in all films decreased gradually at low and more steeply at high temperature; suggesting that the rate of matrix relaxation increased with temperature in the sucrose and sucrose-NaCl melt. Compared with pure sucrose, the energy difference in the sucrose-NaCl film was larger and the magnitude tended to increase with increasing NaCl concentration (at least up to a mole ratio of 0.53). At higher temperatures the slope of the sucrose-NaCl curve became less negative than that of sucrose curve. All the curves exhibited a break point, in sucrose at ~58°C, in NaCl/sucrose with mole ratios of 0.06,

0.44 and 0.53 at 60, 61, and 63°C, respectively. Addition of NaCl thus reduced the matrix relaxation within the sucrose glass and more significantly in the sucrose melt.

3. Phosphorescence decay kinetics

The phosphorescence intensity decays in sucrose-NaCl glasses were measured over the temperature range from 5-100ºC. The stretched exponential lifetimes and stretching exponent β are plotted as a function of temperature in Figures 36 and 38, respectively. The lifetimes decreased biphasically with increasing temperature, exhibiting a gradual linear decrease at low and a more dramatic decrease at high temperature. The decrease in lifetime with temperature reflects an increase in the rate of non-radiative decay of the excited triplet state T_1 due to an increase in both the rate of intersystem crossing to the ground state S_0 (k_{TS0}) and the rate of reverse intersystem crossing to S_1 (k_{TS1}). The lifetimes increased with addition of NaCl over the range from 0-0.46 mole ratio, from 0.61 ms in sucrose at 5°C to 0.71 ms at NaCl/sucrose mole ratio of 0.46. With further increase in NaCl concentration, the lifetimes were almost constant over the temperature range from 5-35°C; however, at 45°C and above, the lifetimes in sucrose-NaCl with mole ratio of 0.73 and 0.87 were lower than those in sucrose-NaCl at 0.46 but still higher than those in sucrose. The curves exhibited break points, determined from extrapolation of the $\ln(k_{TS0})$ curves at high and low temperature, sensitive to NaCl content: NaCl/sucrose with mole ratio of 0.46, 0.56, 0.73 and 0.87 exhibited break points at around 62, 57, 51, and 46°C, respectively, suggesting that the fast total de-excitation rate k_p ($=1/\tau$) was initiated at lower temperature when NaCl concentration was above 0.46. In Figure 37, the data of Figure 36 are replotted as lifetime as a function of NaCl content from 5 to 100ºC. Lifetimes apparently increased with increasing NaCl amount

and reached the maxima around a ratio of 0.46; above that ratio the lifetime kept constant in the glass but decreased in the melt.

The stretching exponent β in sucrose films with NaCl at mole ratio from 0.04 to 0.87 is plotted as a function of temperature from 5-100ºC in Figure 38. At low temperature, the value of β in all sucrose-NaCl films was slightly smaller than that in pure sucrose while above 60°C (close to the glass transition temperature of pure sucrose) the value was larger than the value in sucrose. Since β reflects the distribution of lifetimes and thus the corresponding distribution of dynamically distinct probe environments with different values of k_{TS0} (Pravinata et al., 2005), the small decrease in β with addition of NaCl indicated a large increase in the range of dynamically distinct probe environments in the glass and the large increase in β indicated a very large decrease in the range of dynamically distinct probe environments in the melt.

Based on the maximum physically reasonable value of k_{TS1} (Pravinata et al., 2005), an estimate of the lower limit of k_{TS0} was calculated from Eq. 7 (Materials and Methods); these data are plotted as $\ln(k_{TS0})$ versus 1/T in Figure 39. The variation in the non-radiative quenching rate k_{TS0} was linear at low temperature and increased dramatically at high temperature, which indicated that this rate is sensitive to the molecular mobility activated at high temperature. Addition of NaCl decreased the quenching rate in both the glass and the melt, and enhanced the temperature at which the additional mobility was activated. This effect was very significant at high temperature. At a ratio of 0.46, for instance, the value of k_{TS0} decreased by 14% at 5ºC but almost 45% at 100ºC. Note that at mole ratios of 0.73 and 0.87, the quenching rate began to increase at a

temperature lower than the glass transition temperature of sucrose, however the value of k_{TS0} did not increase with temperature as much as that in other films.

Figure 40a is a plot of the quenching rate k_{TS0} as a function of mole ratio NaCl/sucrose. To obtain a clear relationship between k_{TS0} and NaCl content, the quenching rate is also plotted as the relative rate normalized to the value in pure sucrose (Figure 40b). It is obvious that temperature has a small effect on the quenching rate in the glass but a greater influence in the melt over the whole NaCl concentration range. In the temperature range from 5 to 55°C, the rate constant k_{TS0} in pure sucrose slightly increased, from 1% at 15ºC to 5% at 55ºC compared to the value of k_{TS0} at 5°C. In the presence of NaCl the rate increased 1~2% in the same temperature range (except at mole ratio of 0.87 the value increased by 6% at 55ºC). Above 65ºC, the rate changed significantly with temperature and showed different behavior at different NaCl contents. In pure sucrose, the rate increased dramatically in the melt, from 8% at 65ºC to 97% at 100ºC compared to the rate at 5°C. In the presence of NaCl, the temperature influence on the quenching rate was restricted and this inhibition effect became more noticeable at higher NaCl content. For instance, the rate k_{TS0} at a mole ratio of 0.46 increased from 1% at 65ºC to 27% at 100ºC in comparison with that at 5°C. It is worth noting that the rate in sucrose-NaCl film at a mole ratio of 0.87 increased by 10% at 65°C which was higher than that in sucrose (8%), however, it only increased by 30% at 100°C which was much lower than that in sucrose and similar as the value at a mole ratio of 0.46.

4. Spectral heterogeneity

Phosphorescence intensity decays of Ery B in sucrose films with different NaCl content were measured as a function of excitation and emission wavelength at 25°C. The

stretched exponential lifetimes are plotted versus excitation and emission wavelength in Figure 41a. All lifetimes showed a similar trend: decreasing with increasing wavelength across the emission band. In sucrose, the lifetimes varied from a high of 0.65 ms at 640 nm to a low of 0.52 ms at 720 nm; lifetimes also decreased monotonically with increasing wavelength in sucrose-NaCl films. In the presence of small amounts of NaCl (mole ratio <0.09), lifetimes were enhanced considerably, ranging from a high of 0.74 ms at 640 nm to a low of 0.53 ms at 720 nm. At a mole ratio of 0.87, the lifetime varied from a high of 0.83 ms at 640 nm to a low of 0.64 ms at 720 nm. The lifetimes as well as the variation in lifetimes increased in the presence of NaCl. Lifetimes also varied across the excitation band: increasing with increasing wavelength to a maximum at 520-540 nm and then decreasing at higher wavelengths.

The stretching exponent β also varied as a function of both excitation and emission wavelength (Figure 41b). The values of β were slightly lower in the presence of NaCl. In sucrose and sucrose-NaCl films β values were lower at the blue edge of the emission band, increased with increasing wavelength to a maximum at 680-690 nm and then decreased slightly at the red edge. The variation of β across the excitation band in sucrose-NaCl films was similar to that in the sucrose film.

The calculated non-radiative quenching rate k_{TS0} is plotted versus emission and excitation wavelength at various NaCl contents in Figure 42. The quenching rate k_{TS0} increased with increasing emission wavelength in both sucrose and sucrose-NaCl films. Compared with pure sucrose, the quenching rate was reduced dramatically in the presence of NaCl. The quenching rate decreased steeply at low NaCl concentrations until it reached a minimum value at a mole ratio around 0.56, above which the rate decreased

gradually. For instance, the rate at a mole ratio of 0.46 varied from a low of 1151 s^{-1} at 640 nm to a high of 1554 s^{-1} at 720 nm, much lower than those values in pure sucrose film (1409 s^{-1} at 640 nm and 1783 s^{-1} at 720 nm). Across the excitation band, k_{TS0} curves all showed minimum values around 530 nm with higher values at both the blue and the red edge of the excitation band in all sucrose and sucrose-NaCl films. The addition of NaCl reduced the collisional quenching dramatically at all excitation wavelengths.

Discussion

The spectroscopic data indicate that phosphorescence of erythrosin B is sensitive to the physical properties of the amorphous solid sucrose and sucrose-NaCl mixtures. Measurement of the temperature dependence of the emission energy and lifetime of the probe dispersed in the amorphous sucrose at different NaCl contents provides insight into the solid-state biophysics of amorphous sucrose in the presence of an inorganic salt.

1. Rigidification effect of NaCl on sucrose matrix

Addition of electrolyte sodium chloride increased the rigidity of sucrose matrix shown by increasing the emission energy (peak frequency, ν_P) and lifetime (τ), and decreasing the rate for both dipolar relaxation ($1/\varphi$) and collisional quenching (k_{TS0}). The rigidity effect increased with increasing mole ratio of NaCl/sucrose from 0-0.5; and kept constant at mole ratios above 0.5.

As an electrolyte, sodium chloride has a strong ability to bind water. There is competition between sucrose and NaCl for the water molecules when NaCl is added to aqueous sucrose solution, resulting in a redistribution of interactions in the sucrose-salt matrix. Electrostatic interactions from salt ions strengthen the interactions in sucrose

matrix, supported by evidence of increased viscosity upon addition of salt in the sugar solutions (Miller et al., 1999). However, the rigidification effect cannot be explained solely on the basis of charge effects since sodium chloride is an "intermediate" salt and has a less effect compared with other salt-in salts or multivalent salts.

We propose that the formation of chemical complex between sucrose and NaCl plays an important role in stabilizing sucrose matrix (rigidification effect) including increasing T_g. Similar results have been found in the other sugar-salt systems. Miller et al. (1999) studied the glass transition temperature and viscosity of aqueous mixtures of trehalose with NaCl and $Na_2B_4O_7$ (borax), and they found that addition of salts increased the viscosity as well as the T_g' of aqueous trehalose. They considered that both the ionic charges and the complex formed between the ionic solute and trehalose contributed to the effect; and the latter exhibited a greater influence on the T_g'.

The exact mechanism of sugar-salt complex formation is, however, still under investigation. The ion-ion and ion-solvent interactions in solutions are considered to contribute to the salt effect. Laudt (1936) suggested that ions cause dehydration of the sugar accompanied by a deformation of the sugar molecules by electrostatic powers, which may result in the formation of a sugar ion complex. Robinson (1970) found that at low molalities of sucrose and NaCl salting-out of sucrose by NaCl occurs due to a repulsive interaction; while at high molalities of both components salting-in of sucrose by NaCl occurs due to an attractive interaction. This may partly explained the formation of sucrose-NaCl complex.

There are a number of studies of the properties of sugar solution in the presence of inorganic salts, focusing on the measurement of osmotic coefficients, activity of

solvents, excess free energy of mixture or transference and activity coefficient in aqueous solutions (Hernandez-Luis et al., 2003; Zhuo et al., 2000; Wang et al., 1993; Robinson et al., 1970; Conner and Bulgrin, 1967). Most of them reported the existence of 1:1 salt-sugar complex (Shalaev and Franks, 1995; Schoorl, 1923; Accorsi et al., 1989; Conner and Bulgrin, 1967; Vavrinecz, 1958). Only a few researchers mentioned the presence of 1:2 salt-sugar complexes (Conner and Bulgrin, 1967; Miller et al., 1999) and the effect of this kind of complex should not be ignored (Miller et al., 1999).

In our study, the highest rigidity occurring at a NaCl/sucrose mole ratio of 0.5 may be explained by two possible mechanisms. Firstly, the $NaCl \cdot 2C_{12}H_{22}O_{11}$ complex is the most stable form in the matrix and its formation is favored by the strong sucrose-sucrose interactions originated from the concentrated sucrose solution. In concentrated sucrose solutions (higher than 50% w/w), extended sucrose clusters were found due to formation of the sucrose hydrogen bonding network, and water formed scattered clusters with star-like and chain-like portions (Molinero et al., 2003). Addition of NaCl thus changes the hydration of sucrose cluster rather than individual sucrose molecule; the formed complex probably involved more than one sucrose molecule. Secondly, a 1:1 sucrose-NaCl complex was formed but showed greatest effect at a mole ratio around 0.5. According to the solubility isotherms for the water-NaCl-sucrose system (Shalaev and Franks, 1995), sucrose has a strong propensity to form a ternary compound $NaCl \cdot C_{12}H_{22}O_{11} \cdot 2H_2O$. When NaCl is added above 0.5 mole ratio (that is, 8 wt %), the ternary compound is easily formed even at 298.15K. The decline trend in rigidification effect at mole ratios above 0.5 may be due to the complications of residual moisture (around 2.3%) in the sucrose-NaCl mixture. Water plays a plasticization effect by depressing the

T_g and increasing the mobility. The negative effect became pronounced at high NaCl content, resulting in a slight decrease in the rigidification effect. The results of transition temperature may also support this explanation. The transition temperatures, calculated from the intersection of the trendlines at high and low temperature, was 76.5°C in sucrose, and were 75.4, 77.2, 77.0, 76.8, 78.9, 80.6, 79.2, 50.4 and 47.1°C, respectively, in the films made with sucrose/NaCl mole ratios of 0.04, 0.065, 0.09, 0.20, 0.36, 0.46, 0.56, 0.73, and 0.87. The last two values are significantly below the transition temperature of the sucrose film, suggesting that other mechanisms (plasticization) probably get involved in the NaCl effect on the mobility of sucrose matrix.

The spectroscopic data showed the constrained molecular mobility mainly due to the formation of complex mechanism: higher emission energy due to the slower dipolar relaxation around the excited triplet state, and shorter lifetime due to the lower collisional quenching rate in the matrix with severely restricted molecular mobility. The knowledge of the equilibrium composition of the mixture is needed to differentiate the effects due to charges from the effects due to the complexation.

2. NaCl increases the dynamic site heterogeneity

Recent research using a variety of spectroscopic techniques indicates that supercooled liquids and amorphous polymers are dynamically heterogeneous spatially as well as temporally (Ediger, 2000; Richert, 2002). This physical model is supported by evidence from erythrosin B phosphorescence. Spectral heterogeneity in Ery B phosphorescence is observed in amorphous sugars and sugar alcohols (Pravinata, et al., 2005; Shirke et al., 2005, 2006), and proteins (Nack and Ludescher, 2006; Lukasik and Ludescher, 2006a; Sundaresan and Ludescher, 2007), indicating that the existence of

dynamic site heterogeneity may be a characteristic feature of amorphous food materials and biomaterials.

The variation of lifetime with emission energy reflects variation in one or more of the rate constants for deexcitation of the triplet state. In the amorphous sucrose matrix, the population of probes is distributed among dynamically distinct sites with varied emission energy and matrix quenching rate (Pravinata et al., 2005). Pravinata et al. proposed a physical model for the origin of this site heterogeneity on the basis of emission energy and matrix quenching rate in which probes in local environments with less constrained packing having higher overall molecular mobility and thus shorter lifetime as well as lower emission energy due to fast dipolar relaxation. When sucrose is mixed with NaCl, whether NaCl will change the local environments and further influence the site heterogeneity becomes one of our interests.

The magnitude of the variation in lifetime with wavelength decreased at high temperature (data not shown) suggesting that spectral heterogeneity may decrease in the melt. Compared with sucrose film, variations in Ery B lifetime with emission wavelength at 25°C in sucrose films containing NaCl were slightly larger (Figure 41a). The difference of lifetime with emission wavelength reflects a broad continuum of local matrix sites that vary in terms of their overall molecular mobility. Probes in the blue-shifted sites have longer lifetimes, smaller values of collisional quenching rate k_{TS0} and thus less mobile; but probes in the red-shifted sites have shorter lifetimes, larger values of quenching rate and thus more mobile. In all the sucrose-NaCl films the values of the stretching exponent β (Figure 41b) are lower than those in the sucrose film, indicating a

decreased ability within the sites to dynamically average out spectroscopic differences in the presence of NaCl.

The temperature-dependence of the stretching exponent β (Figure 38) shows that the values of β in the sucrose-NaCl films were lower than the value in pure sucrose at lower temperatures but higher at temperature above 85°C, suggesting an increased matrix heterogeneity in the glass but decreased heterogeneity in the melt in the presence of NaCl.

The emission bandwidth (Γ, FWHM) increased with NaCl content in sucrose-NaCl films (Figure 33). This effect became remarkable at higher temperatures. The increase in bandwidth indicated that the distribution of site energies was significantly broadened.

All the above shows strong evidence of increased dynamic site heterogeneity in sugar-NaCl matrix. Salts interact preferentially with water through ion-water interactions, resulting in preferential solvation around ions, and increased supersaturation and thus nucleation rate in the sugar-rich regions. Some salts may form salt-sugar complexes that can be separated from the solution in a solid or crystalline form (Mazzobre and Buera, 1999). Those local compound-rich regions or sugar-salt complexes probably exert an effect on the spectral heterogeneity.

3. Does NaCl change T_g of sucrose?

NaCl may influence the properties of sucrose glasses by perturbing the glass transition temperature. So far there are limited reports about the T_g of sucrose-NaCl mixtures. Mazzobre et al. (2001) measured the glass transition temperature of the maximally concentrated matrix (T_g') in freeze-dried trehalose and sucrose glassy systems

in the presence of different salts. They found that the apparent T_g' was decreased but the actual T_g values of the systems were not modified when small amounts of salts were added (mass fraction below 0.05). The reduction in T_g was an overall result from both the residual water in the sugar systems and salt effect (Kets et al., 2004). Salts were reported to increase the viscosity of sugar solutions containing polar solvents and may increase T_g through specific interactions such as hydrogen bonding (Miller et al., 1999; Wu et al., 2005). The apparent T_g (with moisture effect) and the actual T_g (without moisture effect) can be measured using DSC in close and open systems, respectively (Kets et al., 2004). Generally sugar-salt matrixes retain more water than sugar single matrix, leading to lower values of T_g.

In the present work, in contrast to sucrose, both emission energy and lifetime (or collisional quenching rate constant k_{TS0}) curves showed similar shape over the entire temperature range from 5 to 100°C at NaCl concentrations varying from 0.04 to 0.56, exhibiting similar transition temperatures calculated from slopes of curves at high and low temperatures. In sucrose-NaCl mixtures with mole ratio of 0.73 and 0.87, the curves changed shape and showing transition temperatures lower than pure sucrose. NaCl as an electrolyte has the ability to retain water in the matrix. Water is well known as a strong plasticizer to reduce the glass transition temperature significantly. The water content in sucrose matrix was less than 1% and varied from 1 to 2.3% in sucrose-NaCl mixtures, depending on the salt content. At low concentration, NaCl influences the transition temperature insignificantly due to the trivial change in water content. With increase in the salt content, increased remaining moisture may contribute to the decreased transition temperature.

Conclusion

The composition of amorphous solid (such as salt) and its environment (temperature) are two important factors affecting molecular mobility. Phosphorescence of erythrosin B can report a detailed mobility map within amorphous sucrose film blended with NaCl ranging from 0.04 to 0.87. Based on the emission energy and lifetime of erythrosin B in sucrose and sucrose-NaCl films over the temperature range from 5°C to 100°C, we came to a conclusion that NaCl exerts a strong rigidification effect on amorphous sucrose: increasing emission energy, increasing lifetime and reducing mobility in the glassy state. NaCl is universally present in foods and biological systems, and also widely used in solid pharmaceutical formulations. It is worthy of mapping out the relationship between the NaCl concentration and the characteristics of the matrix since the matrix properties have implications for the processing and subsequent storage stability of biological materials and foods.

Spectral heterogeneity in Ery B phosphorescence in amorphous sucrose-NaCl films provides direct evidence to support a physical model of dynamic site heterogeneities within supercooled liquids and amorphous solids above and below the glass transition temperature (Ediger, 2000; Richert, 2002). Addition of NaCl influences the dynamic heterogeneity of amorphous sucrose matrix and this effect is depended on the NaCl content and temperature. Our data indicate that there are sites of different mobility within amorphous solid sucrose and this dynamic heterogeneity is enhanced by small molecules such as NaCl. Undoubtedly the ability to report dynamic heterogeneity using Ery B phosphorescence provides an insight into the complex dynamic properties of amorphous biomaterials.

References:

Accorsi, C.A., Bellucci, F., Bertolasi, V., Ferretti, V., and Gilli, G. 1989. Structural aspects of inorganic salt-carbohydrate interactions. Part II. Redetermination of the crystal structure of sodium bromide. sucrose. 2 water. *Carbohydr. Res.* 191 (1), 105-16.

Buitink, J., van der Dries, I.J., Hoekstra, F.A., Alberda, M., and Hemminga, M.A. 2000. High Critical Temperature above T_g May Contribute to the Stability of Biological Systems. *Biophys. J.* 79, 1119-1128.

Buitink, J., and Leprince, O. 2004. Glass formation in plant anhydrobiotes: survival in the dry state. *Cryobiology.* 48, 215-228.

Chan, R.K., Pathmanthan, K., and Johari, G.P. 1986. Dielectric relaxations in the liquid and glassy states of glucose and its water mixtures. *J. Phys. Chem.* 90, 6358-6362.

Conner, J.M., and Bulgrin, V.C. 1967. Equilibria between borate ion and some polyols in aqueous solution. *J. Inorg. Nuc. Chem.* 29, 1953-1961.

Contreras-Lopez, E., Champion, D., Hervet, H., Blond, G., and Le Meste, M. 2000. Rotational and translational mobility of small molecules in sucrose plus polysaccharide solutions. *J. Agric. Food Chem.* 48, 1009-1015.

Crowe, J.H., Carpenter, J.F., and Crowe, L.M. 1998. The role of vitrification in anhydrobiosis. *Ann. Rev. Physiol.* 60, 73-103.

Crowe, J.H., Oliver, A.E., and Tablin, F. 2002. Is there a single biochemical adaptation to anhydrobiosis? *Integrat. and Comp. Biol.* 42, 497-503.

Duchowicz, R., Ferrer, M.L. and Acuna, A.U. 1998. Kinetic spectroscopy of erythrosin phosphorescence and delayed fluorescence in aqueous solution at room temperature. *Photochem. Photobiol.* 68, 494-501.

Ediger, M.D. 2000. Spatially heterogenous dynamics in supercooled liquids. *Annu. Rev. Phys. Chem.* 51, 99-128.

Eggleston, G., Vercellotti, J.R., Edye, L., and Clarke, M.A. 1995. Behavior of water structure-breaking and structure-enhancing solutes on the thermal degradation of concentrated solutions of sucrose. *J. Carbohydr. Chem.* 14(7), 1035-1042.

Fennema, O. 1996. Water and Ice. *In* Food Chemistry, 3rd Ed. O.R. Fennema, editor. Marcel Dekker, Inc., N.Y.

Gangasharan and Murthy, S.S.N. 1995. Nature of relaxation processes in the supercooled liquid and glassy states of some carbohydrates. *J. Phys. Chem.* 99, 12349-12354.

Hernandez-Luis, F., Amado-Gonzalez, E., and Esteso, M.A. 2003. Activity coefficients of NaCl in trehalose-water and maltose-water mixtures at 298.15K. *Carbohydr. Res.* 338, 1415-1424.

Izutsu K., and Aoyagi, N. 2005. Effect of inorganic salts on crystallization of polyethylene glycol in frozen solutions. *Intl. J. Pharm.* 288, 101-108.

Kets, E.P.W., IJpelaar, P.J., Hoekstra, F.A., and Vromans, H. 2004. Citrate increases glass transition temperature of vitrified sucrose preparations. *Cryobiology*. 48, 46-54.

Lakowicz, J.R. 1999. *Principles of fluorescence spectroscopy*. Plenum Press, NY

Laudt, E. 1936. The rotational influence of inorganic salts on sucrose solutions. *Deutsche Zuckerindustrie.* 61, 377-378. (English abstract)

Lee, K.C.B., Siegel, J., Webb, S.E.D., Leveque-Fort, S., Cole, M.J., Jones, R., Dowling, K., Lever, M.J., and French, P.M.W. 2001. Application of the stretched exponential function to fluorescence lifetime imaging. *Biophys. J.* 81, 1265-1274.

Longinotti, M.P., Mazzobre, M.F., Buera, M.P., and Corti, H.R. 2002. Effect of salts on the properties of aqueous sugar systems in relation to biomaterial stabilization. Part 2. Sugar crystallization rate and electrical conductivity behavior. *Phys. Chem. Chem. Phys.* 4, 533-540.

Lu, Q., and Zografi, G. 1997. Properties of citric acid at the glass transition. *J. Pharm. Sci.* 86, 1374-1378.

Lukasik, K.V. and Ludescher, R.D. 2006a. Effect of plasticizer on dynamic site heterogeneity in cold-cast gelatin films. *Food Hydrocoll.* 20, 88-95.

Lukasik, K.V., and Ludescher, R.D. 2006b. Molecular mobility in water and glycerol plasticized cold and hot-cast gelatin films. *Food Hydrocoll.* 20, 96-105.

Maroncelli, M. and Fleming, G.R. 1987. Picosecond salvation dynamics of coumarin 153: the importance of molecular aspects of salvation. *J. Chem. Phys.* 86, 6221-6239.

Mazzobre, M.F., and Buera, M.P. 1999. Combined effects of trehalose and cations on the thermal resistance of β-galactosidase in freeze-dried systems. *Biochim. Biophys. Acta*. 1473, 337-344.

Mazzobre, M.F., Longinotti, M.P., Corti, H.R., and Buera, M.P. 2001. Effect of salts on the properties of aqueous sugar systems, in relation to biomaterial stabilization. 1. Water sorption behavior and ice crystallization/melting. *Cryobiology.* 43, 199-210.

Miller, D.P., de Pablo, J.J., and Corti, H.R. 1999. Viscosity and glass transition temperature of aqueous mixtures of trehalose with borax and sodium chloride. *J. Phys. Chem.* 103, 10243-10249.

Molinero, V., Cagin, T., and Goddard III, W.A. 2003. Sugar, water and free volume networks in concentrated sucrose solution. *Chem. Phys. Lett.* 377, 469-474.

Nack, T.J, and Ludescher, R.D. 2006. Molecular mobility and oxygen permeability in amorphous bovine serum albumin films. *Food Biophys.* 1, 151-162.

Ottenhof, M., MacNaughtan, W., and Farhat, I.A. 2003. FTIR study of state and phase transitions of low moisture sucrose and lactose. *Carbohydr. Res.* 338, 2195-2202.

Papp, S. and Vanderkooi, J.M. 1989. Tryptophan phosphorescence at room temperature as a tool to study protein structure and dynamics. *Photochem. Photobiol.* 49, 775-784.

Parker, C.A. 1968. *Photoluminescence of Solutions.* Elsevier, Amsterdam. Netherlands.

Pravinata, L.C., You, Y. and Ludescher, R.D. 2005. Erythrosin B phosphorescence monitors molecularmobility and dynamic site heterogeneity in amorphous sucrose. *Biophys. J.* 88(May), 3551-3561.

Richert, R. 2000. Triplet state salvation dynamics: basics and applications. *J. Chem. Phys.* 113, 8404-8429.

Richert, R. 2001. Spectral selectivity in the slow β-relaxation of a molecular glass. *Europhys. Lett.* 54(6), 767-773.

Richert, R. 2002. Heterogeneous dynamics in liquids: fluctuations in space and time. *J. Phys. Condens. Matter.* 14, R738-R803.

Robinson, R.A., Stokes, R.H., and Marsh, K.N. 1970. Activity coefficients in the ternary system: water+sucrose+sodium chloride. *J. Chem. Thermodyn*. 2, 745-750.

Roos, Y. 1995. *Phase Transitions in Foods.* Academic Press, San Diego, CA.

Schoorl, N. 1923. The system sucrose-sodium chloride-water and the combination of these constituents. *Recueil des Travaux Chimiques des Pays-Bas et de la Belgique*. 42, 790-799. (English abstract)

Shalaev, E.Y., and Franks, F. 1995. Equilibrium phase diagram of the water-sucrose-NaCl system. *Thermochim. Acta.* 255, 49-61.

Shalaev, E.Y., Johnson-Elton, T.D., Chang, L., and Pikal, M.J. 2002. Thermophysical properties of pharmaceutically compatible buffers at sub-zero temperatures: implications for freeze-drying. *Pharm. Res.* 19(2), 195-201.

Shirke, S., and Ludescher, R.D. 2005. Dynamic site heterogeneity in amorphous maltose and maltitol from spectral heterogeneity in erythrosin B phosphorescence. *Carbohydr. Res.* 340, 2661-2669.

Shirke, S., Takhistov, P., and Ludescher, R.D. 2005. Molecular mobility in amorphous maltose and maltitol from phosphorescence of erythrosin B. *J. Phys. Chem. B.* 109, 16119-16126.

Shirke, S., You, Y., and Ludescher, R.D. 2006. Molecular mobility and dynamic site heterogeneity in amorphous lactose and lactitol from erythrosin B phosphorescence. *Biophys. Chem.* 123, 122-133.

Simon-Lukasik, K.V., and Ludescher, R.D. 2004. Erythrosin B phosphorescence as a probe of oxygen diffusion in amorphous gelatin films. *Food Hydrocoll.* 18, 621-630.

Slade, L., and Levine, H. 1995. Glass transition and water-food structure interactions. *Adv. Food Nutr. Res.* 38, 103-269.

Sundaresan, K.V., and R.D. Ludescher. 2007. Molecular mobility and oxygen permeability in amorphous β-lactoglobulin films. *Food Hydrocolloids.* (In press)

Van den Dries, I.J., Besseling, N.A.M., van Dusschoten, D., Hemminga, M.A., and van der Linden, E. 2000. Relation between a transition in molecular mobility and collapse phynomena in glucose-water systems. *J. Phys. Chem. B*. 104, 9260-9266.

Vavrinecz, G. 1958. Physical chemistry of sucrose. IV. Additional double compounds of sucrose and inorganic salts. *Elelmezesi lpar.* 12, 114-16. (English abstract)

Wang, J., Liu, W., Bai, T., and Lu, J. 1993. Standard Gibbs energies of transfer of some electrolytes from water to aqueous sucrose solutions at 298.15K. *J. Chem. Soc. Faraday Trans.* 89(11), 1741-1744.

Wang, W. 2000. Lyophilization and development of solid protein pharmaceuticals. *Int. J. Pharm.* 203, 1-60.

Wolkers, W.F., Oldenhof, H., Alberda, M., and Hoekstra, F.A. 1998. A Fourier transform infrared microspectroscopy study of sugar glasses: application to anhydrobiotic higher plant cells. *Biochim. Biophys. Acta.* 1379, 83-96.

Wu, Y., L. Li, J. Liu, and G. Zhu. 2005. The enhancement effect of CaCl2 on solid substrate room temperature phosphorescence of polyhalogenated derivatives of fluorescein and application in immunoassay. *Anal. Chim. Acta.* 539, 271-275.

You, Y., and Ludescher, R.D. 2006. Phosphorescence of erythrosin B as a robust probe of molecular mobility in amorphous solid sucrose. *Appl. Spectrosc.* 60, 813-819.

Zallen, R. 1983. *The physics of amorphous solids;* John Wiley & Sons: New York.

Zhuo, K., Wang, J., and Wang, H. 2000. Activity coefficients for NaCl-monosaccharide (D-glucose, D-galactose, D-xylose, D-arabinose) – water systems at 298.15K. *Carbohydr. Res.* 325, 46-55.

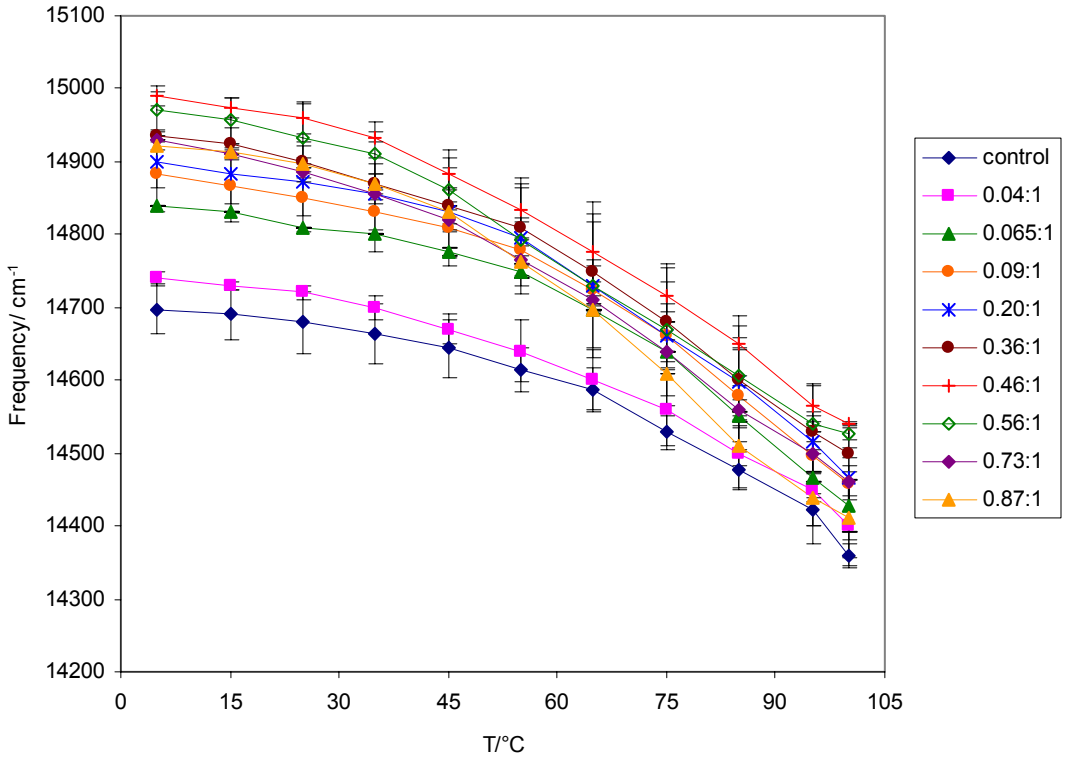

Figure 29: Peak frequency (ν_p) for phosphorescence emission from erythrosin B in amorphous sucrose-NaCl films with various NaCl concentrations over temperature range from 5 to 100°C. Delayed emission spectra collected as a function of temperature were analyzed using log-normal line shape function.

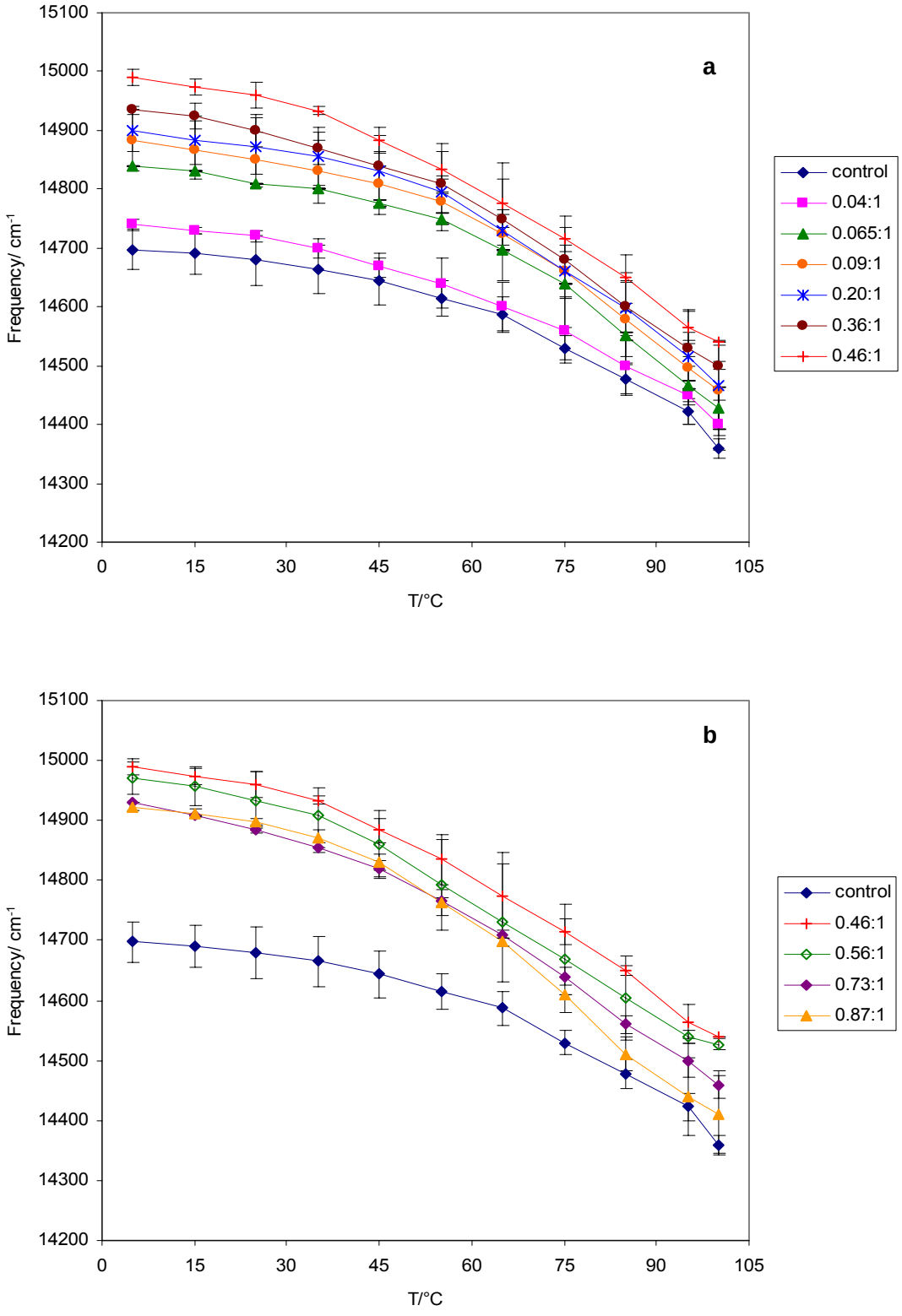

Figure 30: Peak frequency of Ery B in sucrose-NaCl films at NaCl/sucrose mole ratio from 0.04 to 0.46 (a) and from 0.46 to 0.87 (b). Delayed emission spectra collected as a function of temperature were analyzed using log-normal line shape function.

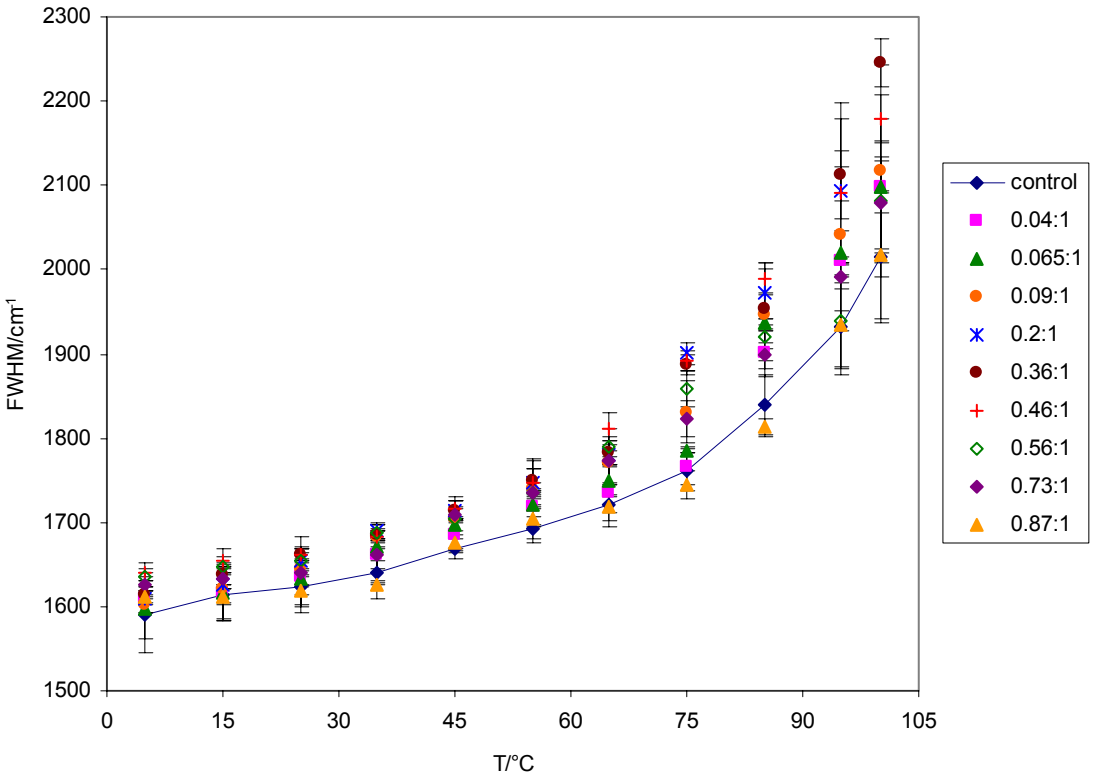

Figure 31: Bandwidth (full width at half maximum, FWHM) for phosphorescence emission from erythrosin B in amorphous sucrose-NaCl films with various NaCl concentrations over temperature range from 5 to 100°C. Delayed emission spectra collected as a function of temperature were analyzed using log-normal line shape function.

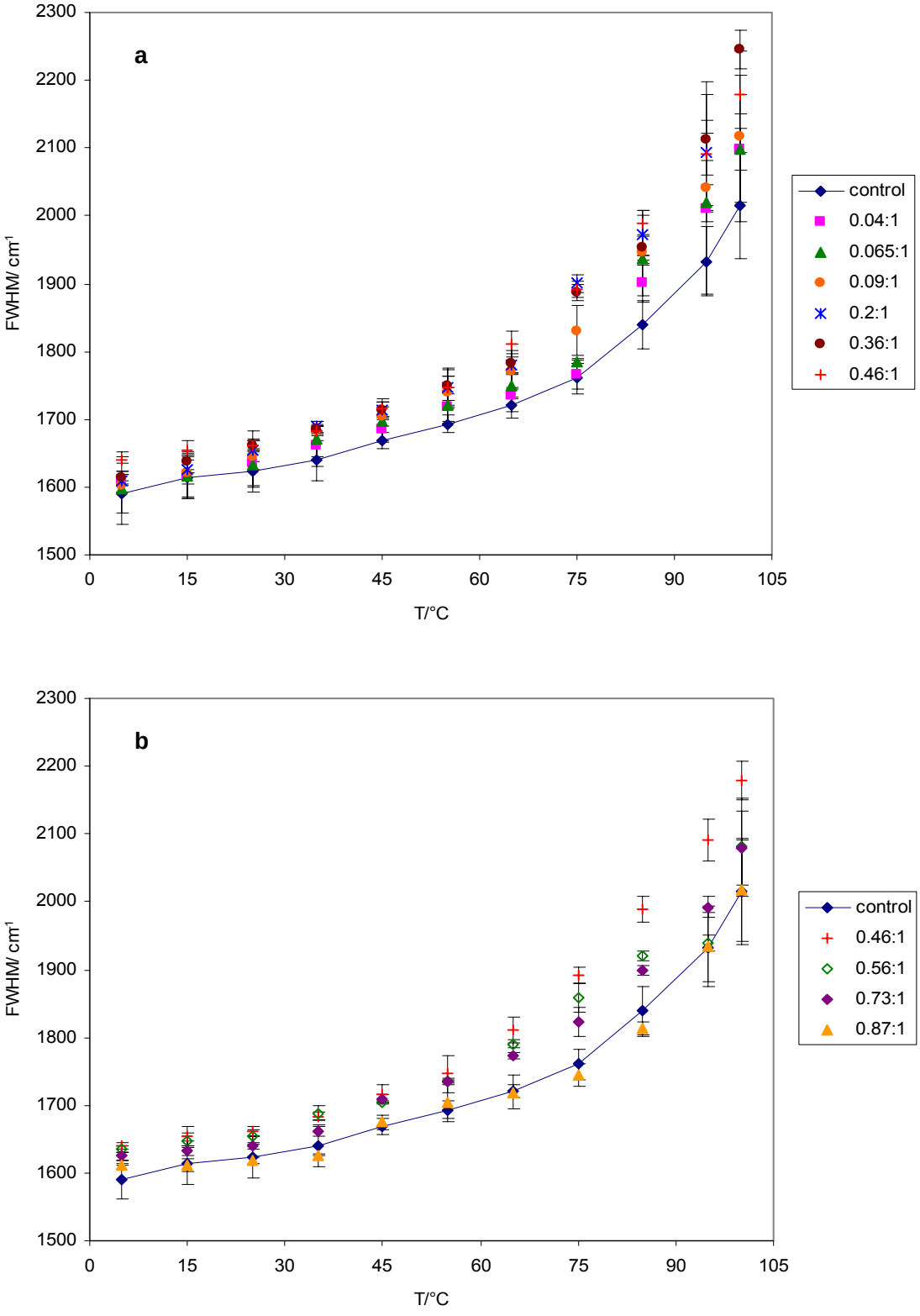

Figure 32: Bandwidth of Ery B in sucrose-NaCl films at NaCl/sucrose mole ratio from 0.04 to 0.46 (a) and from 0.46 to 0.87 (b). Delayed emission spectra collected as a function of temperature were analyzed using log-normal line shape function.

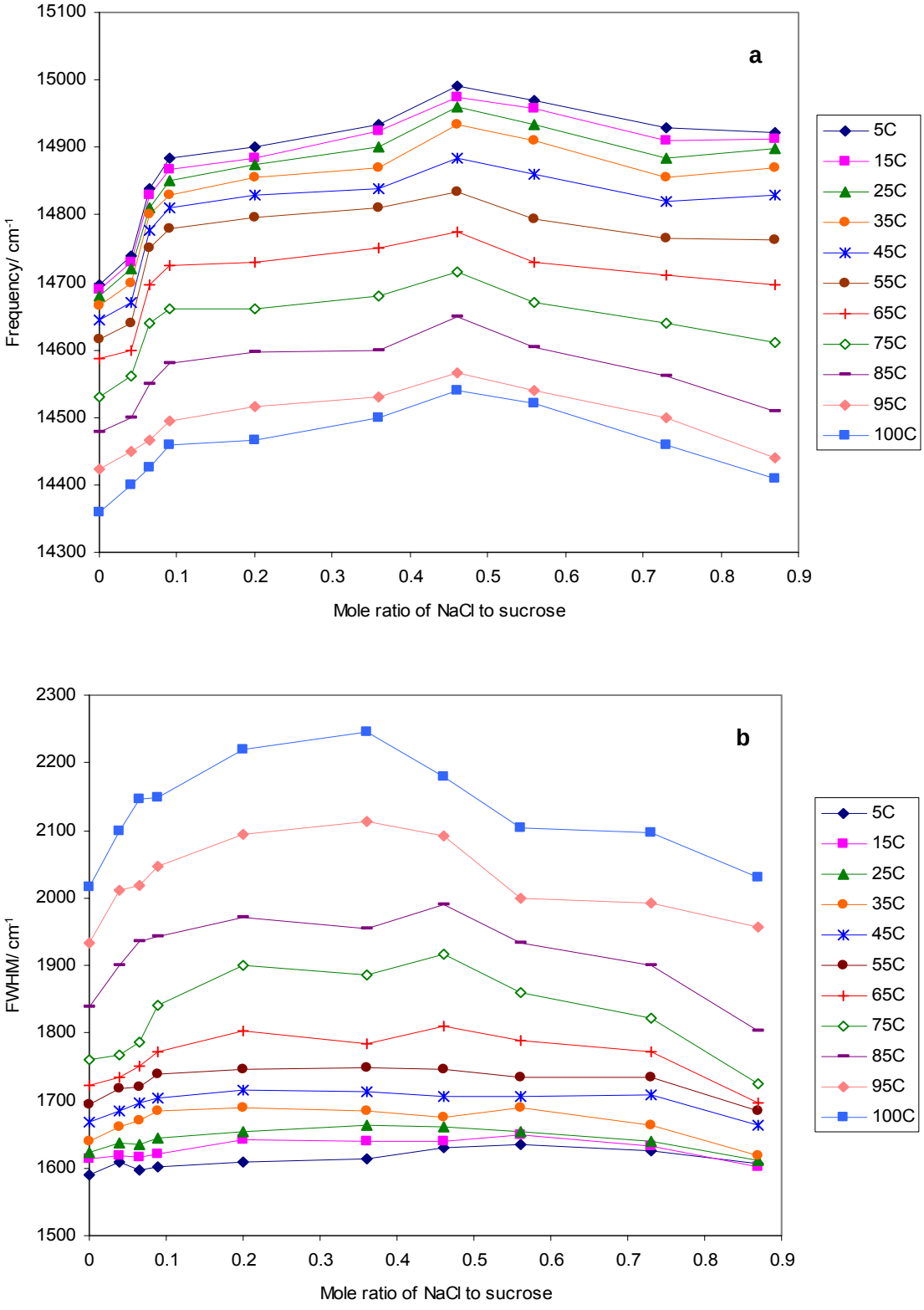

Figure 33: Peak frequency (a) and bandwidth (b) for phosphorescence emission from erythrosin B in amorphous sucrose-NaCl films as a function of NaCl content (mole ratio of NaCl to sucrose). Delayed emission spectra collected as a function of temperature were analyzed using log-normal line shape function.

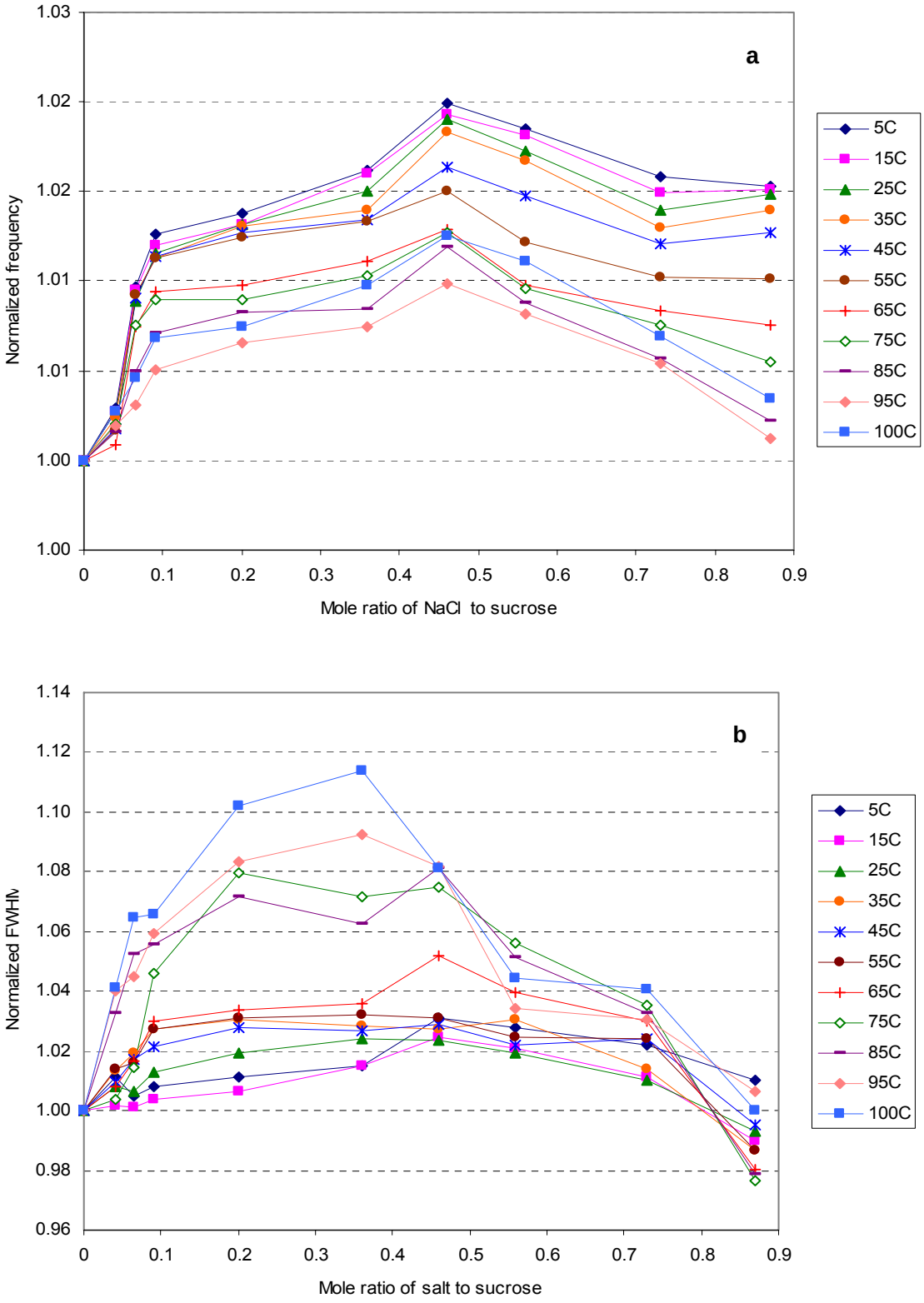

Figure 34: Normalized peak frequency (a) and bandwidth (b) for phosphorescence emission from erythrosin B in amorphous sucrose-NaCl films as a function of NaCl content (mole ratio of NaCl to sucrose). Delayed emission spectra collected as a function of temperature were analyzed using log-normal line shape function.

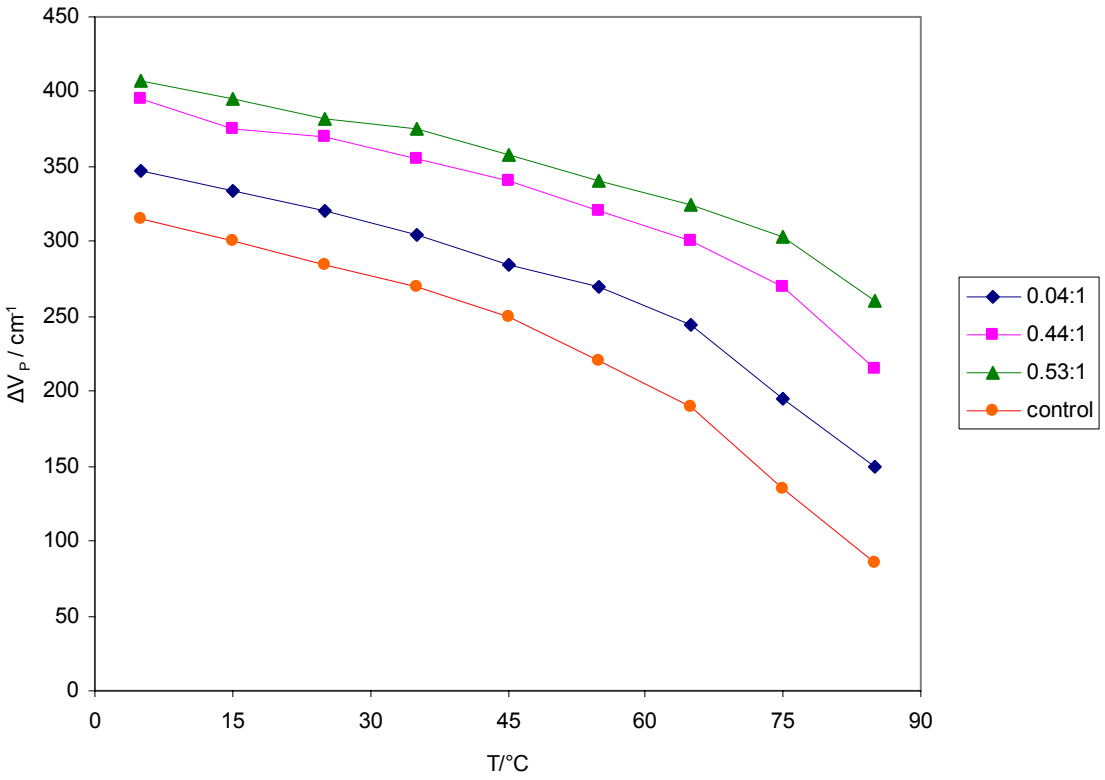

Figure 35: The red-edge effect of the phosphorescence emission of erythrosin B plotted as a function of temperature in amorphous sucrose (♦) and sucrose-NaCl films with NaCl/sucrose mole ratio of 0:04 (■), 0.44 (▲), and 0.53 (●). The difference in the peak frequency ($\Delta\nu_P$) with excitation at 530 and 560 nm is plotted versus temperature.

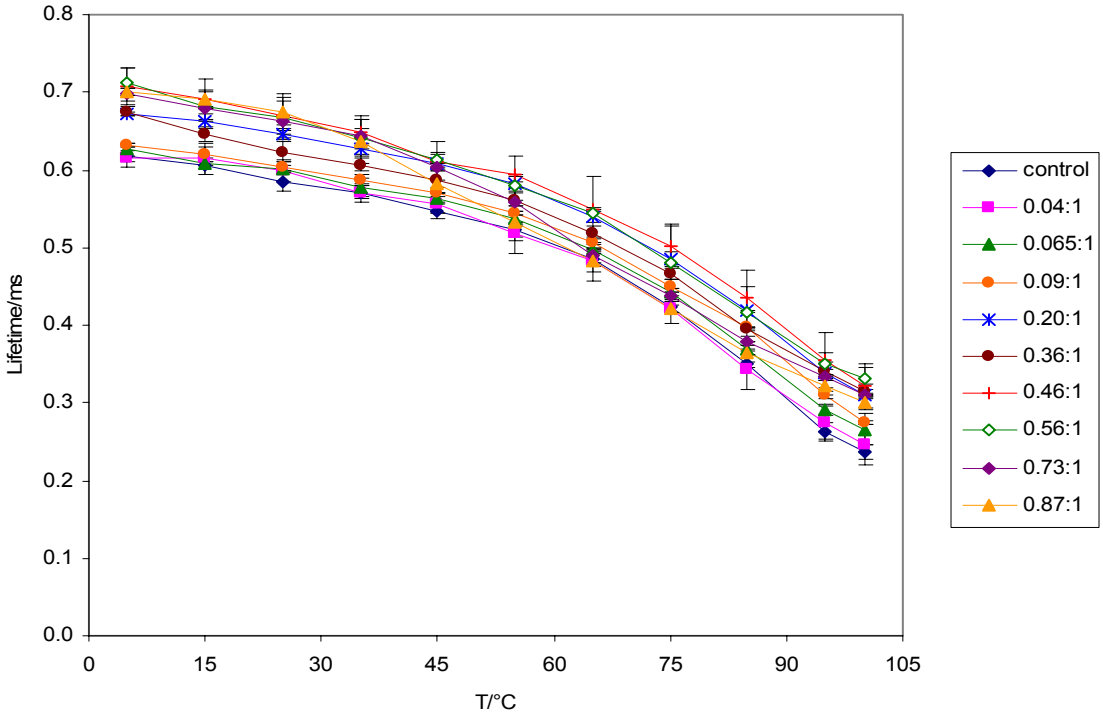

Figure 36: Temperature dependence of lifetime obtained from fits to a stretched exponential function of the intensity decay of erythrosin B in amorphous sucrose with various NaCl contents.

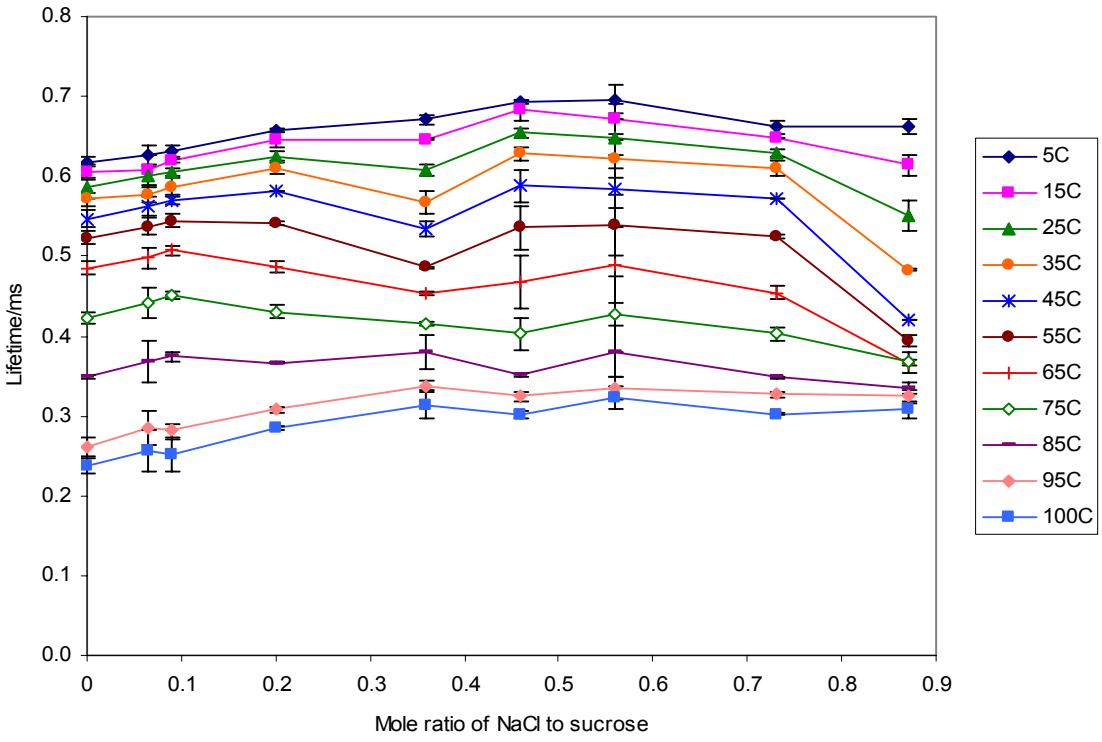

Figure 37: Lifetime of erythrosin B in amorphous sucrose-NaCl films as a function of NaCl content. Data collected from 5 to 100°C.

b

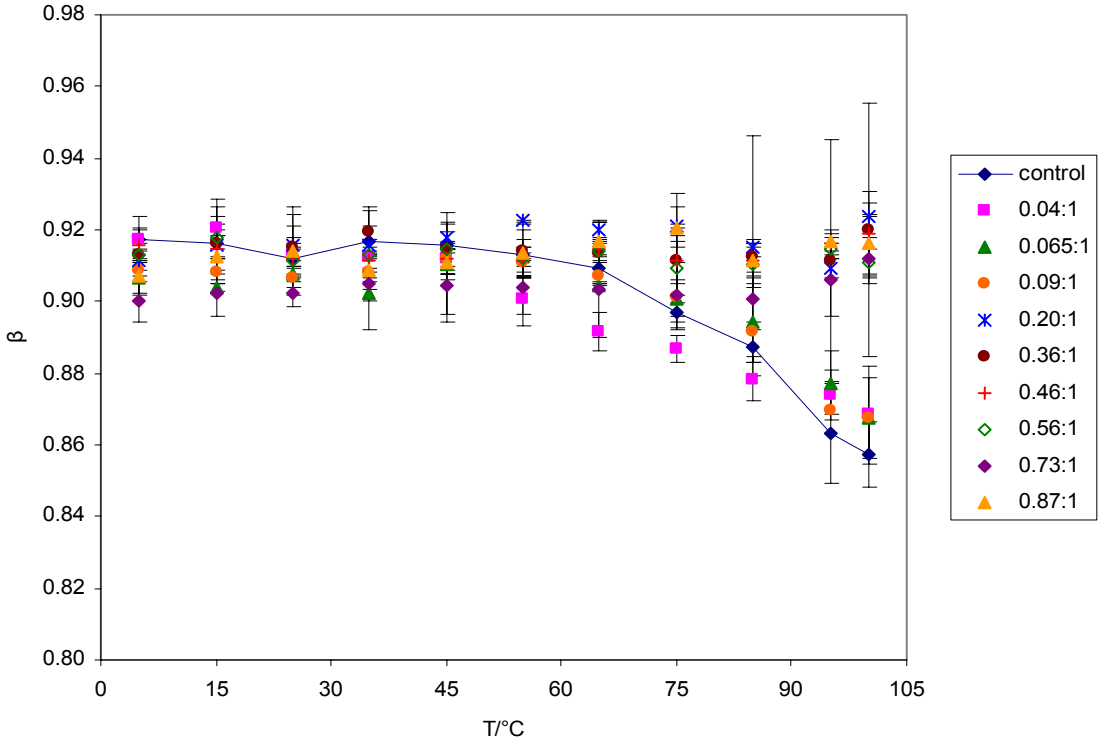

Figure 38: Temperature dependence of stretching exponents β from fits to the stretched exponential model of intensity decays of erythrosin B in amorphous sucrose film with various NaCl contents.

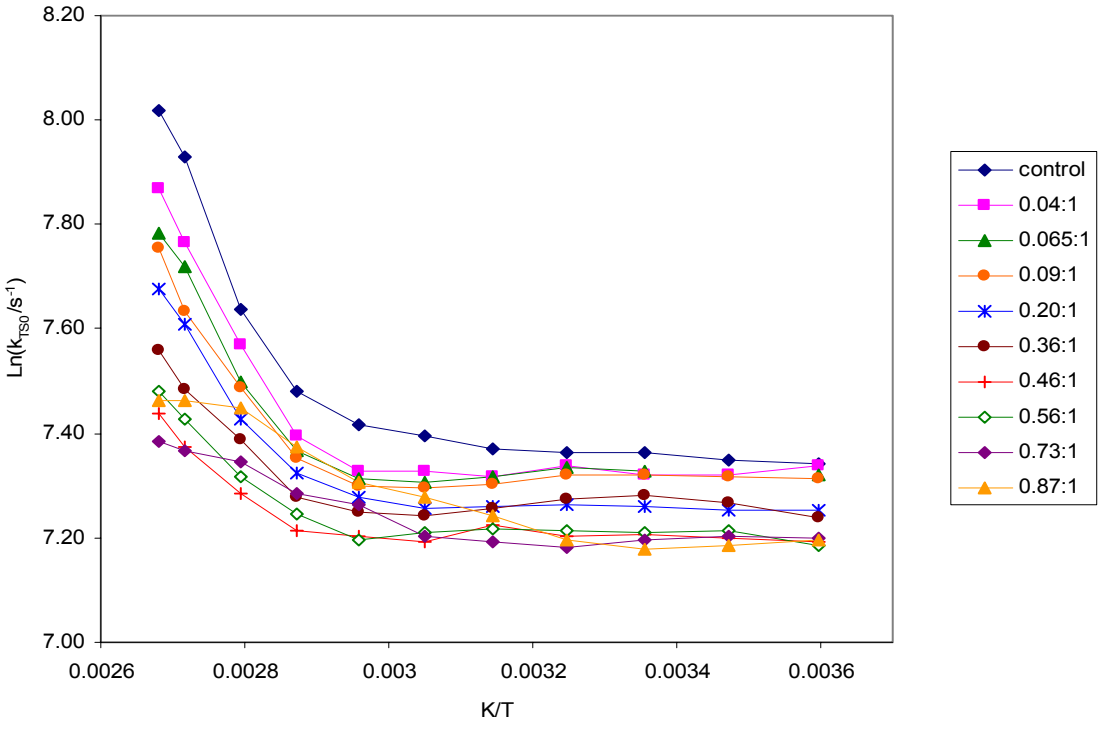

Figure 39: Arrhenius plot of the non-radiative decay rate (k_{TS0}) for the triplet state of Ery B in amorphous sucrose-NaCl films as a function of inverse temperature.

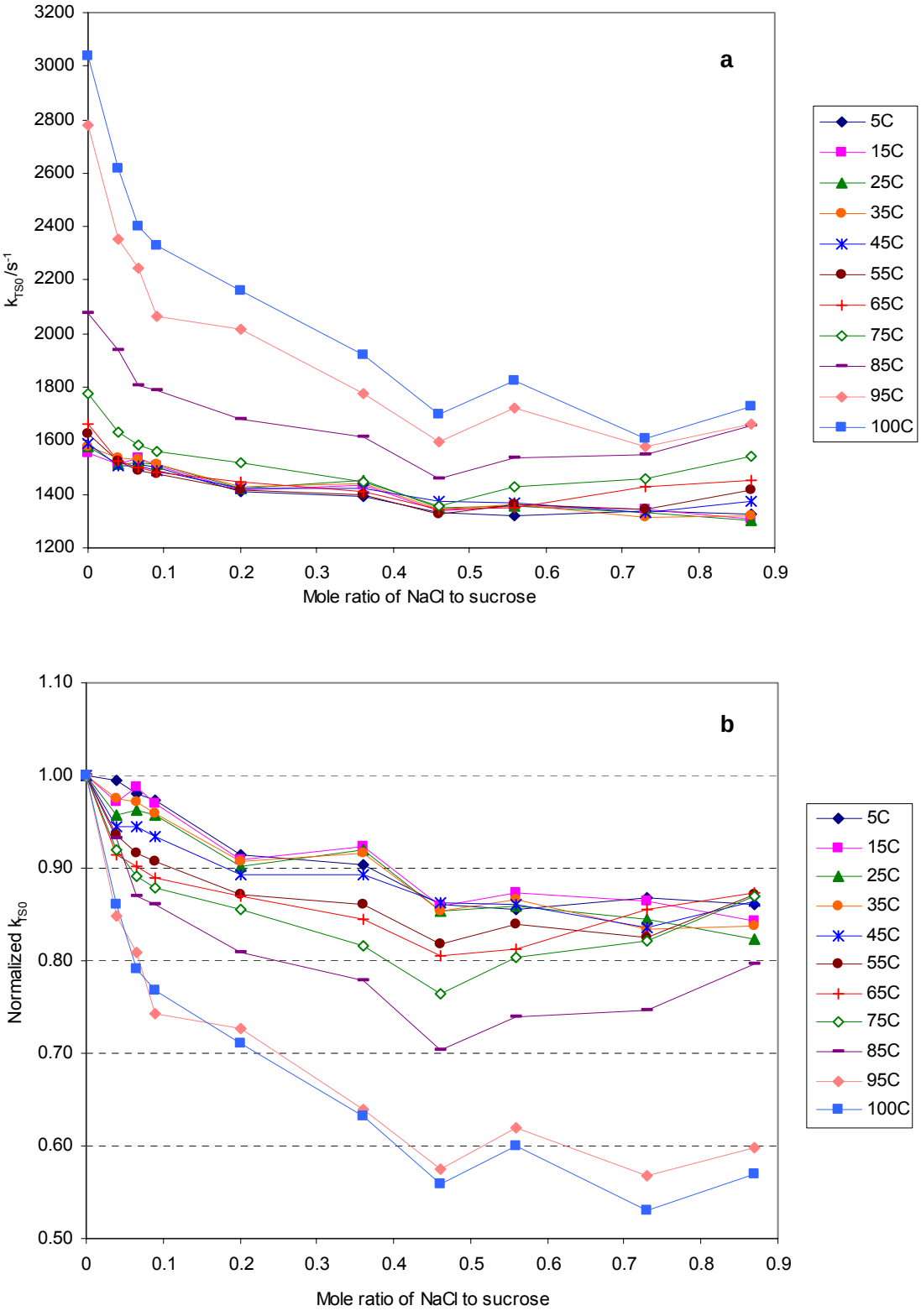

Figure 40: The rate constant for non-radiative decay of the triplet state to S_0 (k_{TS0}) (a) and normalized rate constant k_{TS0} (b) as a function of NaCl content; see text for additional details.

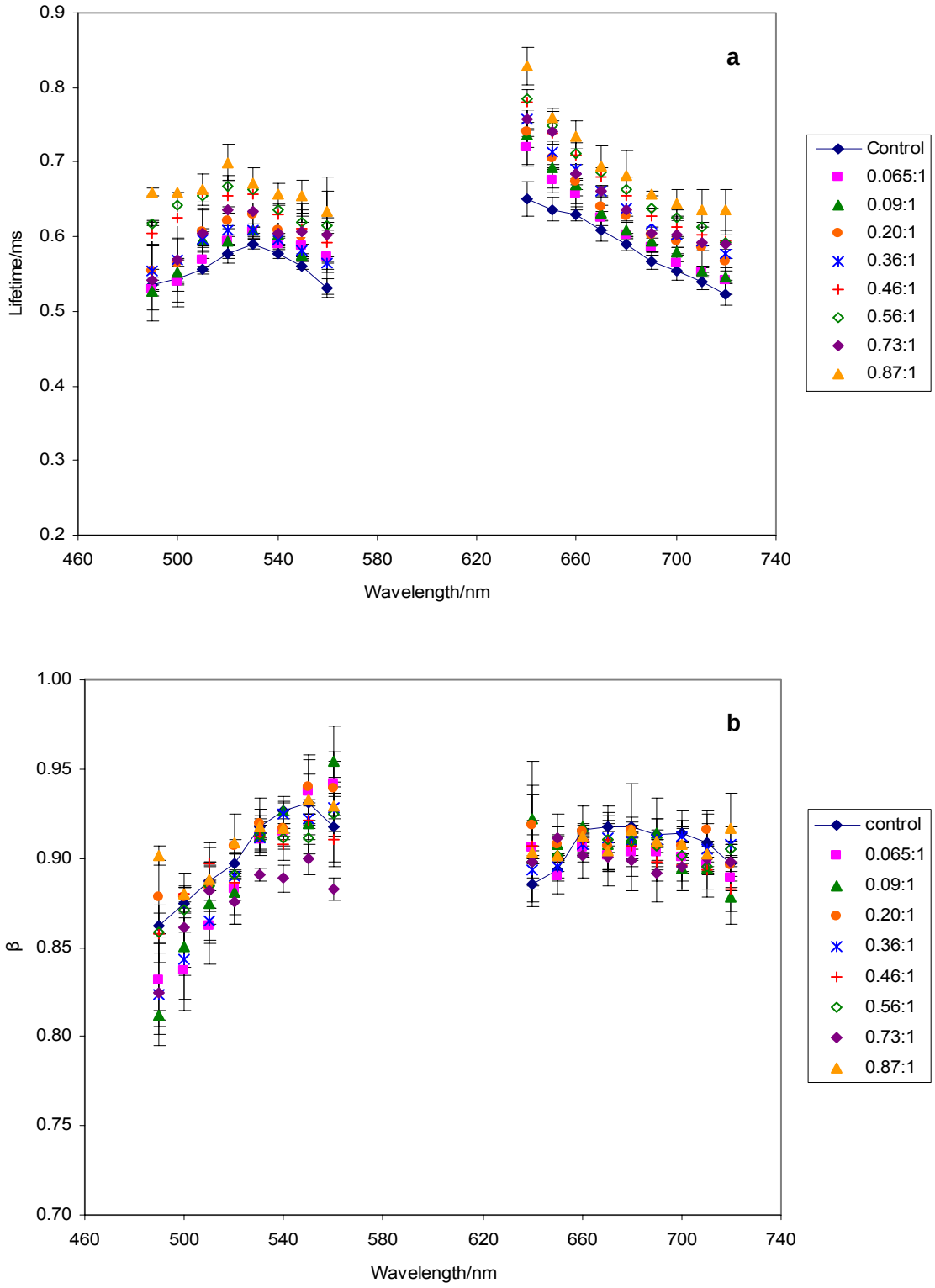

Figure 41: Lifetimes (a) and stretching exponents β (b) from fits to the stretched exponential model of intensity decays of erythrosin B in amorphous sucrose film with various NaCl contents collected as a function of excitation wavelength (with 680 nm emission) and emission wavelength (with 530 nm excitation) at 25°C.

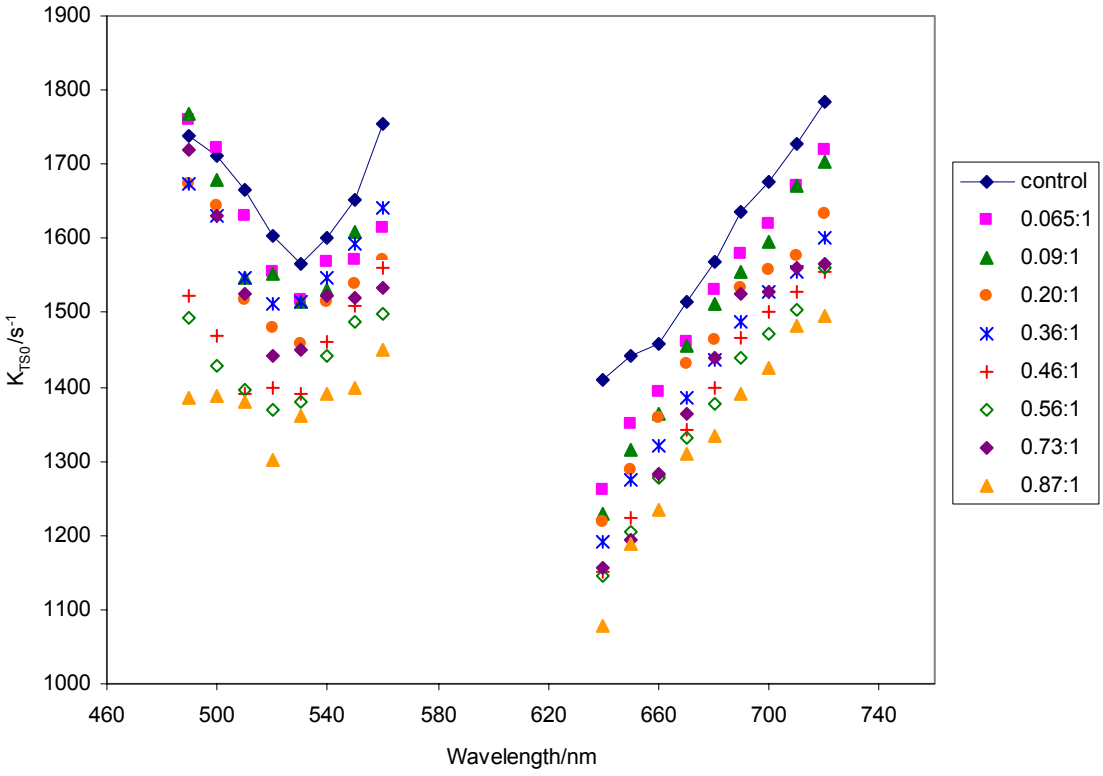

Figure 42. The rate constant for non-radiative decay of the triplet state to S_0 (k_{TS0}) as a function of excitation wavelength (with 680 nm emission) and emission wavelength (with 530 nm excitation). Data collected from Ery B in sucrose films with various NaCl contents at 25°C.

Chapter 5 Effect of salts on molecular mobility in amorphous sucrose from erythrosin B phosphorescence

Introduction

Molecular mobility is recognized to play an important role in modulating the physical properties of amorphous solids and thus in modulating the stability and the shelf life of foods, pharmaceuticals and biomaterials (Fennema, 1996; Roos, 1995; Slade and Levine, 1995). Molecular mobility is normally manifested as relaxation processes. The amorphous solids exhibit the primary α or glass transition at T_g which reflects the activation of large scale molecular motions (α-relaxations) that underlie the onset of translational and large-scale rotational motions; and the secondary β transition within the glass at T_β which reflects the activation of localized molecular motions (β-relaxations) linked to vibrational motion and local side-chain motion. The temperature-dependent molecular mobility thus controls physical and chemical properties by modulating the nature and kinetics of reactions that occur during processing and storage of biomaterials.

The measurement of molecular mobility in amorphous sugars is of fundamental interest because it provides a straightforward way to evaluate stability. A number of techniques have been used to characterize the properties and mobility of amorphous materials (Wolkers et al., 1998; Ottenhof, et al., 2003; Chan et al., 1986; Gangasharan and Murthy, 1995; Richert, 2001; van den Dries, et al., 2000; Contreras-Lopez et al., 2000; Buitink et al., 2000; and Richert, 2000). We have recently demonstrated that phosphorescence of erythrosin B (Ery B) provides a sensitive indicator of molecular mobility as well as dynamic site heterogeneity in amorphous sugars (Pravinata et al., 2005; Shirke and Ludescher, 2005; Shirke et al., 2005, 2006) and proteins (Lukasik and

Ludescher, 2006a, 2006b; Simon-Lukasik and Ludescher, 2004; Nack and Ludescher, 2006; Sundaresan and Ludescher, 2007).

Amorphous sucrose is the major sugar involved in the protection of living organisms, seeds, and spores under extreme conditions (Crowe et al., 1998, 2002; Buitink et al., 2004) and also the major component responsible for the stability of dried and frozen foods. Its ability to protect biomaterials from freeze-thaw damage and provide long-term storage stability has attracted researchers to investigate the mechanism and develop the solid state formulations through drying or freeze-drying for the labile compounds in foods, such as vitamins and flavor compounds, and for the labile biomolecules in pharmaceuticals, such as enzymes, proteins, and antibodies.

Since anhydrous glasses often consist of a variety of compounds, such as buffers and tonicity adjusters in pharmaceuticals and complex molecules in food systems, interactions with co-existing molecules may contribute to the molecular mobility of the matrix and further influence the physical properties of amorphous sucrose.

A few studies tried to explore the salt effect on the stability of sugar glasses through modifying the glass transition temperature T_g and molecule mobility. Izutsu and Aoyagi (2005) studied the effect of different inorganic salts on crystallization of poly (ethylene glycol) in frozen solutions. They found that salts prevented the crystallization by altering the molecular interactions and reducing the molecular mobility. The inhibition effect depended on the type of salt and salt concentration. Shalaev et al. (2002) studied the properties of pharmaceutically compatible buffers at sub-zero temperatures in lyophilized formulations and found that T_g' of a freeze-dried system resulted from a competition between two opposite actions: increased viscosity due to an increase in the

electrostatic interaction and decreased viscosity due to an increased amount of unfrozen water. Mazzobre et al. (1999) found that combination of trehalose and divalent cations exerted a stabilization effect on the protein in freeze-dried systems superior to sugar alone.

In the present study, phosphorescence of erythrosin B was used to measure the matrix mobility in thin films of amorphous sucrose-salt mixtures. A fixed amount of salts was added to the concentrated sucrose solution prior to film formation. The temperature-dependence of mobility was measured in different sucrose-salt matrixes, and comparisons were made to investigate the effect of salts on the molecular mobility of sugar matrix involved in the stabilization of biomaterials.

Materials and Methods

1. Preparation of pure sucrose film

We prepared glassy sucrose films by using a slightly modified version of our published method (Pravinata et al., 2005; see details in Materials and Methods in Chapter 1).

2. Preparation of sucrose-salt mixture films

Sucrose-salt mixtures were prepared from sucrose solution containing dye ($1{:}10^4$ dye/sucrose mole ratio). Seven salts (sodium chloride, NaCl; calcium chloride dihydrate, $CaCl_2 \cdot 2H_2O$; Magnesium chloride hexahydrate, $MgCl_2 \cdot 6H_2O$; acetic acid sodium salt trihydrate, $CH_3CO_2Na \cdot 3H_2O$; Na citrate dehydrate, $C_6H_5Na_3O_7 \cdot 2H_2O$; anhydrous monobasic sodium phosphate, NaH_2PO_4; and sodium phosphate dibasic heptahydrate, $Na_2HPO_4 \cdot 7H_2O$; all Sigma Chemical Co., St. Louis, MO) were added individually to the

purified sucrose solutions to obtain a mixture solution with a fixed salt/sucrose anhydrous mole ratio of 0.2. This concentration was selected to make sure that salts have observable effects on sucrose matrix without phase separation in the sucrose-salt mixtures. Prior to prepare glassy films, sucrose-salt solutions were filtered through a membrane with 0.2 μm pores. The following procedure to make a glassy film was the same as the procedure to make a pure sucrose film.

Water content in amorphous sucrose and sucrose-salt films was determined gravimetrically (by difference of mass before and after drying for 24h at 70°C in an Ephortee (Haake Buchler, Inc.) vacuum oven at 1 kPa). Sample films were scratched from quartz slides and ground into powders in a glove box containing P_2O_5 and Drie-Rite with a relative humidity less than 5%. Pure sucrose sample contained 0.56±0.13 wt. % water, while sucrose-NaCl, sucrose-$CaCl_2$, sucrose-$MgCl_2$, sucrose-acetate, sucrose-citrate, sucrose-NaH_2PO_4, and sucrose-Na_2HPO_4 mixture samples contained 1.04±0.01, 3.12±0.42, 3.81±0.98, 3.50±0.08, 4.08±0.36, 2.81±0.17, 4.26±0.18, wt. % water, respectively.

3. Luminescence measurements

Luminescence measurements were made using a Cary Eclipse Fluorescence spectrophotometer (Varian Instruments, Walnut Creek, CA). Prior to any phosphorescence measurements, all samples were flushed for at least 15 minutes with nitrogen gas which contained less than 1ppm oxygen to eliminate oxygen quenching. The temperature was controlled using a thermo-electric temperature controller (Varian Instruments, Walnut Creek, CA). To eliminate moisture condensation during the

measurements below room temperature, dry air was used to flush the chamber surrounding the cuvette holder. All the measurements were made at least in triplicate.

To obtain intensity decays of erythrosin B in sucrose and sucrose-salt mixtures, samples were excited at 530 nm (20 nm bandwidth) and emission transients collected at 680 nm (20 nm bandwidth) over the temperature range from 5 to 100°C (heating cycle). At each target temperature samples were equilibrated for 1min/°C increase in temperature. Phosphorescence intensity decays were collected over a window of 5 ms with an initial delay of 0.1 ms and increments of 0.04 ms. Each decay was the average of 20 cycles. Because intensity decays were non-exponential, a stretched exponential, or Kohlrausch-Williams-Watts' decay function was selected to analyze the intensity decay (Richert, 2000; Lee, et al., 2001; Pravinata et al., 2005).

$$I(t) = I_0 \exp\left(-(t/\tau)^{\beta}\right) + \text{constant} \quad (1)$$

Where I_0 is the initial amplitude, τ is the stretched exponential lifetime, and β is an exponent varying from 0-1 and characterizing the distribution of lifetimes. The use of a stretched exponential model provides a direct measurement of continuous distribution of lifetimes, which is appropriate for describing a complex glass possessing a distribution of relaxation times for the dynamic molecular processes. The smaller the β value, the more non-exponential the intensity decays and the broader the distribution of lifetimes. Program NFIT (Galveston, TX) was used to fit the decay; goodness of fit was evaluated by examining the χ^2 and R^2. Plots of modified residuals (defined as the difference between the intensity from the fit decay curve and the measured intensity divided by the square root of the measured intensity) was also an indicator of the goodness of fit. R^2 for

all fits ranged from 0.99 to 1.00 and modified residuals plots fluctuated randomly around zero amplitude.

Phosphorescence intensity decays of Ery B in sucrose and sucrose-salt mixtures were continuously collected from 100 to 5°C (cooling cycle) after heating cycle was done. The waiting time between the end of heating cycle and the beginning of cooling cycle was 10 min.

Phosphorescence emission lifetimes of Ery B as a function of emission wavelength were measured with excitation wavelength at 530 nm (20 nm bandwidth); emission wavelength varied from 640 to 720 nm (20 nm bandwidth). Phosphorescence emission lifetimes as a function of excitation wavelength were measured with emission wavelength at 680 nm (20 nm bandwidth); excitation wavelength ranged from 490 to 560 nm (20 nm bandwidth). The experiments were performed at 25°C.

4. Photophysical scheme

Our analysis of the delayed emission is similar to the photophysical scheme for erythrosin B outlined by Duchowicz et al. (1998). The measured emission rate for phosphorescence (k_P) is the sum of all possible deexcitation rates for the triplet state T_1:

$$\tau^{-1} = k_P = k_{RP} + k_{TS1} + k_{TS0} + k_Q[Q] \quad (2)$$

In this equation, k_{RP} is the rate of radiative emission to the ground state S_0. For erythrosin B, k_{RP} is 41 s^{-1} and constant with temperature (Duchowicz et al., 1998).

k_{TS1} is the rate of thermally activated reverse intersystem crossing from the triplet state T_1 to the singlet state S_1, and the value can be estimated from the Arrhenius equation:

$$k_{TS1}(T) = k^0_{TS1} \exp(-\Delta E_{TS}/RT) \quad (3)$$

where k^0_{TS1} is the maximum rate of intersystem crossing from T_1 to S_1 at high temperature, ΔE_{TS} is the energy gap between T_1 and S_1, R=8.314 J K^{-1} mol^{-1}, and T is the temperature in Kelvin. The value of ΔE_{TS} is calculated from the slope of a Van't Hoff plot of the natural logarithm of the ratio of intensity of delayed fluorescence (I_{DF}) to phosphorescence (I_P):

$$d[\ln (I_{DF}/I_P)]/d(1/T) = -\Delta E_{TS}/R \quad (4)$$

where I_{DF} and I_P are the maximum intensity values determined from analysis of the emission band using Eq. (1). The value of k_{TS1} at 25°C was estimated as 88 s^{-1} using k^0_{TS1}=3.0 x 10^7 s^{-1} and ΔE_{TS} = 31.56 kJ/mol (Pravinata et al., 2005).

In the presence of oxygen, the quenching rate $k_Q[Q]$ is the product of rate constant k_Q and the oxygen concentration [Q]. By flushing nitrogen throughout the measurements we assume that no oxygen quenching occurred. One of the non-radiative decay routes is through intersystem crossing to the ground state S_0. The decay rate is expressed by $k_{TS0,}$ which reflects the rate of collisional quenching of the probe due to both internal and external factors (Papp and Vanderkooi, 1989). We assume that the term k_{TS0} primarily reflects the external environmental factors since the self collisional quenching among probe molecules can be neglected within the extremely viscous amorphous solid. In this study, temperature-dependent term k_{TS0} can be calculated from phosphorescence lifetime by rewriting equation (2).

$$k_{TS0}(T) = \frac{1}{\tau(T)} - k_{RP} - k_{TS1}(T) \quad (5)$$

Results

At a probe/sucrose molar ratio of $1:10^4$, each probe is on average surrounded by a matrix shell around 10-11 sucrose molecules thick. At this concentration Ery B dispersed within the sucrose matrix does not aggregate and thus reports the physical properties of the unperturbed sucrose matrix (You and Ludescher, 2006).

In the present work, we investigated the effect of different salts on the molecular mobility of amorphous solid sucrose. A fixed amount of different cation salts with Cl^{-1} (NaCl, $CaCl_2$ and $MgCl_2$) and anion salts with Na^+ (Na_3citrate, Na acetate, NaH_2PO_4, Na_2HPO_4 and NaCl) were dispersed in sucrose matrix and the salt effect was analyzed separately based on the molecular mobility in sucrose-salt mixtures measured with Ery B phosphorescence. The NaCl data used here were measured in Chapter 4.

1. Phosphorescence decay kinetics

The phosphorescence intensity decays in sucrose and sucrose-salt glasses were measured over the temperature range from 5 to 100ºC. The stretched exponential lifetimes and exponent β obtained from fits of the intensity decay to a stretched exponential function are plotted as a function of temperature. The lifetimes during heating in sucrose-cation salt and sucrose-anion salt mixtures are shown in Figure 43a and Figure 44a and the exponents β are shown in Figure 43b and Figure 44b, respectively. The lifetimes in all films decreased biphasically with increasing temperature, exhibiting a gradual linear decrease at low and a more dramatic decrease at high temperature. The decrease in lifetime with temperature reflects an increase in the rate of non-radiative decay of the excited triplet state T_1 due to an increase in both the rate of non-radiative decay to the ground state S_0 (k_{TS0}) and reverse intersystem crossing to S_1 (k_{TS1}). The sucrose-NaCl curve of lifetime was seen above the sucrose curve over the

whole temperature range. However, both $CaCl_2$ and $MgCl_2$ salts showed different behavior: lifetimes increased slightly at low temperature (<35°C) but decreased at temperatures above 35°C over those in sucrose and $MgCl_2$ displayed a more negative effect on lifetime at high temperature. For instance, the lifetime was 0.61, 0.67, 0.64 and 0.64 ms at 5°C but 0.52, 0.58, 0.47 and 0.41 ms at 55°C in sucrose, sucrose-NaCl, sucrose-$CaCl_2$ and sucrose-$MgCl_2$, respectively. The curves exhibited different break points (obtained from the intersection of two trendlines with lifetime in low temperature and high temperature region): sucrose and sucrose-NaCl showed similar break temperature around 62°C and sucrose-$CaCl_2$ and sucrose-$MgCl_2$ at 39 and 32°C, respectively, suggesting that the fast total de-excitation rate k_p ($=1/\tau$) was initiated at lower temperature in the presence of $CaCl_2$ and $MgCl_2$.

Exponent β in sucrose and sucrose-cation salt films showed similar behavior over the temperature range from 5 to 100ºC (Figure 43b). The values of β decreased gradually and slightly at low temperature and decreased dramatically at high temperature. The values of β in sucrose-NaCl films were the same as those in sucrose at low temperature (<45°C) but became larger at 55°C and above. In sucrose-$CaCl_2$ and sucrose-$MgCl_2$ films the values of β were smaller than those in sucrose over the whole temperature range, especially in the high temperature region. Since β reflects the distribution of lifetimes and thus the corresponding distribution of dynamically distinct probe environments with different values of k_{TS0} (Pravinata et al., 2005), the change in β with addition of Ca and Mg chloride indicated an increase in the range of dynamically distinct probe environments in the glass and a larger increase in the melt; NaCl did not change the distribution significantly until the temperature reached 55°C and above.

Figures 44a and 44b show the lifetime and β in sucrose and sucrose-anion salts as a function of temperature. Addition of all anion salts except NaH_2PO_4 increased the lifetimes significantly at temperature <35°C (Figure 44a). Lifetimes began to decrease when the temperature increased from 55 to 85°C. Above 85°C, lifetimes did not change significantly and had values higher than those in sucrose. In the presence of NaH_2PO_4 the lifetimes did not change at very low temperature, and then decreased dramatically at T>25°C. Compared with sucrose (0.61 ms at 5°C and 0.52 ms at 55°C), for instance, the lifetime was 0.71, 0.76, 0.62 and 0.70 ms at 5°C, but 0.49, 0.51, 0.31 and 0.44 ms at 55°C in sucrose-citrate, sucrose-Na acetate, sucrose-NaH_2PO_4 and sucrose-Na_2HPO_4, respectively. Similarly, the curves displayed various break points: ~30°C in both sucrose-Na_3citrate and sucrose-Na acetate and ~48 and 24°C in sucrose-NaH_2PO_4 and sucrose-Na_2HPO_4, respectively, which were all lower than the T_g of 62°C in sucrose.

Exponent β are plotted versus temperature in sucrose and sucrose-anion salts (Figure 44b). All anion salts other than NaH_2PO_4 increased β values in sucrose matrix in the whole temperature range. NaH_2PO_4 increased β at low temperature but decreased β at high temperature.

As described in Materials and Methods, the non-radiative quenching rate k_{TS0} was calculated from Eq. 5 based on the maximum physically reasonable value of k_{TS1} (Pravinata et al. 2005). We assumed that ΔE_{TS}, the energy gap between T_1 and S_1, does not change significantly in the presence of small amounts of salt. The value of ΔE_{TS} in sucrose matrix (= 31.56 kJ/mol) was used to calculate k_{TS0} in all the sucrose-salt matrixes. The non-radiative quenching rate k_{TS0} is plotted versus T in Figure 43c (sucrose-cation salts) and Figure 44c (sucrose-anion salts). Apparently k_{TS0} in sucrose matrix varied

linearly at low temperature and shot up at high temperature, which indicated that this rate is sensitive to the molecular mobility activated with temperature. Addition of salts changed the temperature-dependent quenching rate in both the sucrose glass and the sucrose melt. Figure 43c clearly showed that NaCl reduced the collisional quenching rate over the whole temperature range. Ca and Mg chloride decreased k_{TS0} at T <25°C, increased it in the temperature range from 35 to 85°C, and then decreased it at T above 85°C. Anion salts showed a similar effect on k_{TS0} in Figure 44c. All the anion salts except NaH_2PO_4 decreased the quenching rate at low temperature (<45°C), then increased it from 45 to 85°C. Above 85°C the quenching rate decreased again and almost kept constant with temperature. It seemed that addition of salts made sucrose matrix more rigid (reducing k_{TS0}) at low and high temperature but more flexible in the intermediate temperature range (35-85°C). In this region higher molecular mobility seemed to be activated at a temperature lower than the glass transition temperature of sucrose (62°C).

Phosphorescence intensity decays were also measured in sucrose and sucrose-salts from 100 to 5°C (cooling cycle). Sample films were checked using crossing polarizer at each target temperature to make sure that no crystallization occurred during the cooling cycle experiment. The stretched exponential lifetimes and exponents β are plotted as a function of temperature in sucrose-cation salts (Figure 45a and Figure 45b) and sucrose-anion salts (Figure 46a and Figure 46b). Lifetimes in sucrose-salts increased over the whole temperature range, and the curves were almost parallel with the sucrose curve. All the sucrose-salt curves of lifetime displayed biphasic behavior: a gradual linear decrease at low but a more sharp decrease at high temperature. The curves exhibited similar break points around the T_g of sucrose. In the cation salts group, salts increased the

lifetime in the order of NaCl>$CaCl_2$>$MgCl_2$. $MgCl_2$ did not influence lifetime at low temperature until 65ºC but increased lifetime at 65ºC and above. Both Na and Ca salts increased lifetime but showed different effects: the lifetimes in sucrose-NaCl were slightly longer at low but shorter at high temperature than those in sucrose-$CaCl_2$. In the anion salts group, salts increased lifetime in the order of acetate>citrate/Na_2HPO_4>NaCl>NaH_2PO_4. Citrate had similar effect on lifetime as the phosphate dibasic salt. Phosphate monobasic salt had no observable influence on lifetime in sucrose matrix. The values of β in sucrose-salts did not change significantly with temperature in the cooling cycle. The β values increased in the order of acetate>citrate/Na_2HPO_4>NaCl> NaH_2PO_4>sucrose>$CaCl_2$>$MgCl_2$, suggesting that sodium salts increased homogeneity while calcium and magnesium salts increased heterogeneity in the sucrose matrix.

Figure 45c and Figure 46c are plots of the non-radiative quenching rate k_{TS0} vs. temperature calculated from lifetimes in the cooling curves. The collisional quenching rate k_{TS0} increased systematically with temperature in all sucrose-salt mixtures. In sucrose-cation salts, the Mg salt did not affect k_{TS0} in sucrose until 65ºC, then k_{TS0} decreased by 4% at 65ºC and 30% at 100ºC. Ca and Na salt showed similar effects on the sucrose glass (T<65ºC): k_{TS0} decreased from 7% at 5ºC to 13% at 65ºC. In sucrose melt k_{TS0} decreased in sucrose-NaCl less than in sucrose-$CaCl_2$ (e.g. at 95ºC, k_{TS0} decreased by ~23 and 33% in sucrose-NaCl and sucrose-$CaCl_2$, respectively). Comparably, anion salts except NaH_2PO_4 have more significant effect on the collisional quenching rate in sucrose matrix, especially at low temperature. In the presence of Na acetate, Na citrate and

Na_2HPO_4, for instance, k_{TS0} decreased by ~14% at 5ºC, and 21% at 65ºC, respectively. NaH_2PO_4 had no effect on sucrose mobility.

By comparing lifetime in heating and cooling curve, hysteresis was exhibited in some sucrose-salt mixtures (Figure 47a to Figure 47h). In sucrose film no hysteresis was observed: the lifetime in heating curve was identical with the lifetime in cooling curve. Addition of salts except NaCl exhibited hysteresis from 95ºC to 35ºC; the lifetime in cooling curve was higher than the lifetime in heating curve in that temperature range. The shape of the hysteresis loop varied depending on the type of salt. NaH_2PO_4 had an indistinct hysteresis loop from 75ºC to 55ºC.

Stretching exponents β of erythrosin B in sucrose and sucrose-salt films as a function of temperature during heating and cooling cycles are plotted in Figure 48a to Figure 48h. Similar to lifetime data, no hysteresis was observed in sucrose and sucrose-NaCl films: β in heating and cooling curves were almost superimposable. However, addition of other salts exhibited hysteresis and the shape and size of the hystersis loop varied with the salt type.

2. Spectral heterogeneity

Phosphorescence intensity decays of Ery B in sucrose-salt films with different salts were measured as a function of excitation and emission wavelength at 25°C during the heating cycle. After analysis using a stretched exponential model, lifetimes are plotted versus excitation and emission wavelength in Figures 49a and 50a. All lifetime curves showed the similar trend of decreasing with increasing wavelength across the emission band. In sucrose, the lifetimes varied from a high of 0.65 ms at 640 nm to a low of 0.52 ms at 720 nm; lifetimes also decreased monotonically with increasing wavelength in

sucrose-salt films. The cation salts appeared to have an effect on the variation of lifetime with emission wavelength greater than the anion salts. Among the cation salts, Ca and Mg salts seemed to increased heterogeneity more significantly than Na salt. Anion salts except NaH_2PO_4 increased the lifetime remarkably; however, the lifetime variation was different in different sucrose-anion salt matrixes. The variation in lifetime was smaller in most sucrose-anion salts than in sucrose while was similar in sucrose-NaH_2PO_4 and larger in sucrose-NaCl. This indicated that cations (Ca, Mg, and Na) tended to increase while anions (HPO_4^{2-}, citrate and acetate) tended to decrease dynamic site heterogeneity. NaH_2PO_4 did not influence either the value of lifetime or the variation of lifetime. Lifetimes also varied across the excitation band, increasing with increasing wavelength to a maximum at 520-540 nm and then decreasing at higher wavelengths. The variation of lifetime across the excitation band exhibited similar behavior in the presence of all salts.

The stretching exponent β also varied as a function of both excitation and emission wavelength (Figures 49b and 50b). Compared with sucrose, the values of β were slightly lower in the presence of cation salts while higher in the presence of anion salts. In sucrose and sucrose-salt films β values were lower at the blue edges of the emission bands, increased with increasing wavelength to a maximum at 680-690 nm and then decreased slightly at the red edges. At 25°C the variation of β across the emission band was somewhat eliminated in all the sucrose salts.

The calculated quenching rate k_{TS0} is plotted versus emission and excitation wavelength in sucrose-salts in Figure 51. The collisional quenching rate k_{TS0} increased with increasing emission wavelength in sucrose and sucrose-salts films. Compared with pure sucrose, the quenching rate was reduced in the presence of most salts. The

quenching rate k_{TS0} decreased the least in sucrose-$MgCl_2$, and the reduction followed the order of $MgCl_2$<$CaCl_2$<NaCl<Na_2HPO_4<Na-citrate<Na-acetate. NaH_2PO_4 appeared to have no influence on the quenching rate. Across the excitation band, k_{TS0} curves showed minimum values around 530 nm and higher values at both the blue and the red edge of the excitation band in sucrose and sucrose-salt films.

Discussion

The spectroscopic data indicated that phosphorescence of erythrosin B is sensitive to the physical properties of the amorphous solid sucrose and sucrose-salt mixtures. Measurement of temperature-dependence of the lifetime of the probe dispersed in the amorphous sucrose mixed with different salts may provide insights into the solid-state biophysics of amorphous sucrose in the presence of salt, thus further explore the salt influence (different interactions) on the properties of sucrose.

1. Rigidification effect

The phosphorescence lifetime provides information about the triplet state non-radiative quenching rates (Duchowicz et al., 1998; Lettinga et al., 2000; also see Materials and Methods). The decrease in phosphorescence lifetime with increase in temperature seen in amorphous sucrose reflects increases in both the rate of reverse intersystem crossing to T_1, k_{TS1}, and the rate of intersystem crossing to S_0, k_{TS0} (Pravinata et al., 2005). The various lifetimes in sucrose-salt matrixes indicate that the probes sample matrix environments with various values for the total rate of non-radiative quenching ($k_{TS1} + k_{TS0}$) at all temperatures. Since sucrose-salt films with a low concentration of salts (molar ratio of 0.2:1) had slightly different values of ΔE_{TS}, the

value of ΔE_{TS} of sucrose was used to calculate the temperature-dependent k_{TS1} in the different films and thus the dissimilarity in lifetimes implies a dissimilarity in the rates of k_{TS0} in the films with different salts (Pravinata et al., 2005; Shirke et al., 2005).

The magnitude of k_{TS0} reflects internal processes that determine the extent of vibrational coupling between the excited T_1 state and the ground S_0 state as well as external processes due to interactions between the probe molecule and its environment that affect how probe vibrational energy is dissipated into the surrounding matrix (Papp and Vanderkooi, 1989). Since the latter process is related to the molecular mobility of the matrix (Pravinata et al., 2005; Strambini and Gonnelli, 1985; Gonnelli and Strambini, 1995; Fischer et al., 2002), the magnitude of k_{TS0} provides a measure of matrix mobility. Dissimilarity in lifetime thus implies dissimilarity in the dynamic environment of the Ery B probe in the different sucrose-salt films.

The analysis of the effect of temperature on lifetime indicates that the nonradiative quenching rate k_{TS0} increased gradually in the glass but dramatically in the melt above T_g in sucrose. Addition of salts decreased the nonradiative quenching rate over the whole temperature range; and the effect varied with different kind of salt. Two kinds of salt were selected to investigate the possible interaction between salt and sucrose molecules, and their possible impact on the physical property of the sucrose matrix.

At a certain amount (mole ratio of 0.2:1), all salts showed a stronger suppression effect on the nonradiative quenching rate k_{TS0} except NaH_2PO_4 (Figures 45c and 46c). This suppression may be explained by increased matrix rigidity and decreased mobility due to the strengthened interactions induced by salts. All Na salts except NaH_2PO_4 showed a stronger suppression effect on k_{TS0} than Ca and Mg salts, which may be a result

of the different interactions existing in the matrix. Ca and Mg salts strengthened the matrix by inducing electrostatic interaction and/or forming complexes with sucrose molecules (Cook and Bugg, 1973). Most Na salts (except Cl salt), however, formed hydrogen bonds in addition to the ion effects, resulting in a more significant influence on the sucrose matrix. The enhanced transition temperatures also provided strong evidence of the rigidification effect of salts on the matrix mobility. In sucrose-salts matrixes, the transition occurred at temperature significantly above the glass transition of sucrose (~62°C). The transition temperatures, calculated from the intersection of the trendlines of Arrhenius plot of k_{TS0} at high and low temperature, was 76°C in sucrose, and were 77, 81, 79, 80, 85, 79 and 78°C in sucrose-NaCl, sucrose-citrate, sucrose-acetate, sucrose-Na_2HPO_4, sucrose-$CaCl_2$, sucrose-$MgCl_2$ and sucrose-NaH_2PO_4, respectively. The increase in the transition temperature indicated that larger mobility motions (α relaxations) were activated at higher temperatures due to the increased rigidity of the matrix in the presence of salts.

Also note that salts showed different behavior as shown in Figures 43 and 44. Lifetime curves in sucrose-salts showed a dramatic decrease over the temperature range from ~35 to 85°C. The sharp decrease in lifetime reflected the activation of non-radiative quenching in the matrix that involved cooperative units and large side groups. The increased mobility may be a result of the effect of salt itself or the presence of residual water. Most sucrose-salt mixtures contained residual water content higher than sucrose (<1%). NaCl matrix contained 1% and other salt matrixes 3~5% moisture. The rigidification effect of salts was weakened in the presence of moisture, especially at temperatures near the T_g.

2. Mobility hysteresis

It is interesting to note that hysteresis occurred from 95 to 35°C in some sucrose-salt matrixes: the lifetime in cooling cycle was higher than the lifetime in heating cycle at the same temperature. This behavior resembled the sorption hysteresis, a phenomenon exhibited in a moisture sorption isotherm of polymers and glasses of low-molecular-weight compounds: the water content is greater during desorption than during resorption at the same aw (Fennema, 1996). Molecular mobility is strongly temperature-dependent but it is also influenced by other factors such as matrix nature and composition. For a certain matrix at a fix temperature, it is hard to formulate an explanation of "mobility hysteresis".

There was no observable mobility hysteresis in pure sucrose matrix: lifetimes (thus the nonradiative quenching rate k_{TS0}) measured in heating cycle were identical with those measured in cooling cycle (Figure 47a). At each temperature the matrix mobility was same regardless the thermal history, indicating that the molecular interactions and conformation may not be significantly affected by the heating and cooling cycles. Similar result was found in sucrose-NaCl matrix (Figure 47b). Other sucrose-salt matrixes, however, showed mobility hysteresis and the shape of the curves, the inception and termination points of the hysteresis loop, and loop size varied depending on different type of salt (Figure 47c to Figure 47h). The hysteresis loop in the presence of Ca salt exhibited from 95 to 25°C, while in Mg salt from 85 to 35°C. The lifetime difference at 65°C in sucrose-$CaCl_2$ and sucrose-$MgCl_2$ was 0.132 and 0.167 ms, respectively. Among sucrose-anion salts, Na_2HPO_4 had the greatest while NaH_2PO_4 had the least effect. The hysteresis loop started at 95°C and ended at 25°C in sucrose-Na_2HPO_4, with lifetime variation of

0.176 ms at 65°C. In sucrose-NaH_2PO_4 a less distinct hysteresis loop was observed from 75 to 55°C, and the lifetime difference was 0.041 ms. Citrate and acetate affected the lifetime to the similar extent: hysteresis was displayed from 85-95 to 35°C and lifetime difference was around 0.15 ms.

Both sucrose and sucrose-NaCl films contained moisture content no higher than 1% while others contained moisture between 3 to 5%. Salts are able to absorb water that manipulates the physical property by inducing plasticization effect. We thus assumed that the residual moisture contributed to the mobility hysteresis.

The hysteresis loop range and magnitude probably reflected the residual water content in the matrixes. Under the same conditions for sample preparation, sucrose-salt films contained more moisture than sucrose due to the strong interaction between salt and water. Water, as a strong plasticizer, increased matrix mobility and quenching rate and then reduced the lifetime. Heating cycle followed by cooling process with equilibrium at each target temperature was in fact an annealing treatment, which facilitated the residual water inside the film to migrate to the film surface and then to be removed by dry nitrogen flow. The lifetime measured in cooling process was higher, indicating low mobility in matrix due to the exclusion of water plasticization. After heating/cooling cycle, the lifetime was measured in the same sample film (sucrose-Na citrate) for the second time from low to high temperature. The lifetimes measured in the second heating cycle were identical with the lifetimes in the first cooling cycle (data not shown).

All the lifetime curves in cooling cycle were parallel, suggesting a similar transition temperature. However, the lifetime curves in heating cycle exhibited different transition temperatures, which were in accordance with the residual moisture determined

in sucrose-salt films. This may be evidence that the residual water in mixture films led to the mobility hysteresis through plasticization.

In heating cycle, cation salts showed strong moisture effect in the order of NaCl (no effect) <$CaCl_2$<$MgCl_2$, which was consistent with the ability of these salts to bind water. The residual water content depends on the charge/size ratio of salts, varying in the same order as above. The transition temperature calculated from Arrehenius plot of k_p in the presence of Na, Ca and Mg salt was 68.2, 38.1 and 35.5°C, respectively, lower than the T_g of sucrose.

Similar effect due to moisture was observed in all anion salts except NaCl. The lifetime curves in the presence of other salts exhibited a transition (decreased steeply) at a lower temperature than the T_g of sucrose. This effect was in agreement with the nature of the different salts. For instance, disodium phosphate and sodium citrate are hygroscopic and retain more water than other salts; the corresponding transition temperatures were calculated as 31.9 and 33.8°C, respectively. Monosodium phosphate is less hygroscopic than other salts and the transition temperature was around 54°C.

Based on the transition temperature calculated from lifetimes in cooling cycle, salts themselves appeared to increase matrix rigidity and decrease molecular mobility in the sucrose matrix without modifying T_g too much (slightly increased). The presence of residual moisture in the matrix led to the depression of T_g, and may decrease the strength or the extent of molecular interactions within the matrix. The overall influence of salts was determined both by the residual moisture and by the salt effect.

3. Interactions in sucrose-salt matrixes

Ionic salts bind water through water-ion bonds, which are stronger than water-water hydrogen bonds. Compared with sucrose matrix, sucrose-salt matrixes may keep more water under the same experiment conditions. The strength of water-ion bonds, which depended on the salt type and salt concentration, increased in the order of $NaCl<CaCl_2<MgCl_2$, in agreement with the order of charge/size ratio of the cations. The residual water content increased in the same order and the T_g of the mixture was reduced correspondingly. During cooling cycle, lifetimes increased in sucrose-cation salts to some extent, but with a slight difference in their behaviors. The rigidification effect (increase in lifetime and decrease in quenching rate) may be due to the strengthened sucrose-sucrose hydrogen bonds induced by salts. The values of lifetime in Ca salt were larger than those in Na salt at temperatures above 65°C although the former were somewhat smaller than those in Na salt at temperatures below 65°C. The lifetime slightly increased in the sucrose-$MgCl_2$ glass; and above 65°C this influence became significant. Compared with univalent cations, divalent cations tend to form complex through chelation. Cook and Bugg (1973) found that hydroxyl groups at the O2 and O3 position in hexose molecules served as effective Ca-chelation sites, but this interaction was weak due to the constraints from steric arrangement. Morel-Desrosiers et al. (1991) reported that Ca^{2+} has stronger interactions with sugar than Mg^{2+}, resulting in a denser or more tightly packed matrix. At concentration of 0.2:1, Na has similar effect as Ca on the lifetime in the sucrose glass, and Mg does not show apparent influence at low temperature; while above 65°C Ca affected the lifetime to the greatest extent, followed by Na and Mg salts.

As for anion salts, more specific interactions besides water-ion interaction were involved and influenced the mobility of matrix. Regardless of moisture influence, we

discuss the results based on the data in the cooling process. In cooling cycle, lifetime increased significantly in the order of NaCl<Na_2HPO_4<Na-citrate<Na-acetate. NaH_2PO_4 has little effect on the matrix mobility. The effect was basically dependent on the concentration of cation in the salts without ability to form specific interactions such as hydrogen bonding. More cations can bind more water and strengthen the interactions among sugar molecules. At a fixed concentration of Na ion (0.2:1), lifetime increased in the order of NaH_2PO_4<NaCl<Na acetate (Figure 52a). In comparison to the effect from Na_2HPO_4 /sucrose (0.2:1) and acetate/sucrose (0.4:1), lifetime was enhanced more significantly in acetate than in phosphate at the same Na concentration of 0.4:1 (Figure 52b). All the above results showed strong evidence that hydrogen bonding plays an important role in increasing lifetime and reducing mobility. Citrate and acetate are two typical salts in remarkably decreasing mobility through forming hydrogen bonds among the matrix molecules. At a fixed amount of 0.2:1, citrate showed the rigidification effect similar to acetate although it contained more hydrogen bonding sites and more Na ions. This was perhaps due to less steric hindrance, carboxyl groups in low-molecular-weight acetate participate in forming hydrogen bonds effectively among alike molecules (sucrose-sucrose, acetate-acetate) or non-alike molecules (sucrose-acetate), making matrix more rigid and less mobile.

4. T_g of sucrose-salt mixtures

Until now not much research has focused on the glass transition temperature in sugar-salt systems. Among the limited published results, different values of T_g were reported, depending on the measurement techniques used. Mazzobre et al. (2001) measured the glass transition temperature of the maximally concentrated matrix (T_g') in

freeze-dried trehalose and sucrose glassy systems in the presence of different salts. They found that the T_g' was decreased but the actual T_g values of the systems were not modified when small amounts of salts were added (mass fraction below 0.05). Kets et al. (2004) used a modified DSC method to determine T_g of freeze-dried sucrose-citrate mixture. They found that when residual water was removed from the mixture, T_g increased with citrate concentration and exceeded the T_g of pure sucrose although citrate is supposed to lower T_g of sucrose (Lu and Zografi, 1997; Wang, 2000). The apparent T_g (with moisture effect) and the actual T_g (without moisture effect) can be measured using DSC in close and open systems, respectively (Kets et al., 2004). Salts were reported to increase the viscosity of sugar solutions containing polar solvents and may increase T_g through specific interactions such as hydrogen bonding (Miller et al., 1999; Wu et al., 2005). Generally sugar-salt matrixes retain more water than sugar single matrix, leading to lower values of T_g.

In the present work, some salts (NaCl and $MgCl_2$) may not affect the T_g values through water-ion interactions while salts such as citrate, acetate and phosphate may increase the T_g values through specific interactions like hydrogen bonding in the matrix. In the meanwhile salts as electrolytes retain higher water content in the sucrose matrix than sucrose alone, leading to depression of T_g. Therefore, the overall effect should be considered from the above two aspects. We assume that phosphorescence technique can report information about the transition. On the basis of the lifetimes measured from phosphorescence of Ery B dispersed in sucrose and sucrose-salt matrixes, we found that lifetime (or collisional quenching rate constant k_{TS0}) curves showed different shape over the entire temperature range from 5 to 100°C (heating cycle) in sucrose-salts, exhibiting

various transition temperatures calculated from slopes of curves at high and low temperatures. The mobility transition temperature may act as an indicator of the apparent T_g (with moisture effect) and thus reflect the overall effect. Lifetime was also measured in sucrose-salts from 100 to 5°C (cooling cycle). The lifetime or k_{TS0} curves of sucrose-salts showed similar shape as that of sucrose, indicating similar transition temperatures which may act as a marker for the actual T_g (without moisture effect) and reflect the salt effect. Regarding the transition temperature obtained from lifetime curve in cooling cycle, salts are found to increase the actual T_g to some extent, depending on the type of salt. However, the apparent T_gs decrease due to the residual moisture in the matrixes. The mobility transition temperatures calculated from lifetime curves, Arrhenius plots of k_p and k_{TS0} in sucrose-salt films are listed in Table 2.

Table 2 Transition temperatures (°C) calculated from lifetime, k_p and k_{TS0} in heating and cooling cycles

	Heating cycle from τ	Heating cycle from k_P	Cooling cycle from τ	Cooling cycle from k_P	Cooling cycle from k_{TS0}
sucrose	62.6	70.1	62.5	70.2	75.8
Sucrose-NaCl	62.2	68.2	61.8	68.8	76.9
Sucrose-$CaCl_2$	39.5	38.1	71.7	73.7	85.3
Sucrose-$MgCl_2$	32.0	35.5	60.8	68.3	79.0
Sucrose-citrate	29.5	33.8	65.5	71.2	81.1
Sucrose-acetate	30.3	35.1	64.2	71.1	79.1
Sucrose-Na_2HPO_4	24.1	31.9	63.3	67.5	80.0
Sucrose-NaH_2PO_4	45.5	45.5	69.9	69.9	78.7

5. *Dynamic site heterogeneity*

Dynamic site heterogeneity is perhaps a common characteristic feature of amorphous solids and supercooled liquids below and above the T_g (Ediger, 2000; Richert, 2002). Extensive research applying different physical techniques reveal the presence of dynamically distinct regions in amorphous synthetic polymers (Schmidt-Rohr and Spiess, 1991; Ediger and Skinner, 2001; Deschenes and Vanden Bout, 2001a, 2001b). Basically the concept of dynamic site heterogeneity involved those regions whose boundaries and intrinsic rates of molecular mobility fluctuate through both time and space. Recently site heterogeneity has been found in amorphous small molecules such as sugars and sugar alcohols (Pravinata et al., 2005; Shirke and Ludescher, 2005; Shirke et al., 2006) and also in amorphous biomolecules including proteins (Lukasik and Ludescher, 2006; Nack and Ludescher, 2006; Sundaresan and Ludescher, 2007).

Dynamic site heterogeneity along with molecular mobility has attracted great interest because it may be pertinent to many degradation processes including physical aging (Courtney and Ediger, 2002, 2003) and chemical reactions such as the Asp-Pro bond cleavage in the peptide Physalaemin in the freeze-dried and freeze-concentrated carbohydrate solutions (Streefland et al., 1998). In the present work, we investigated spectroscopic heterogeneity in both amorphous sucrose and sucrose-salt matrixes.

Sucrose and sucrose-salt matrixes showed spectroscopic heterogeneity: the lifetime varied with both excitation and emission wavelength. In the presence of cation salts, the spectral heterogeneity considerably increased. An increase in spectral heterogeneity reflects an increase in dynamic site heterogeneity, thus an increase in the coupling between the rates for solvent relaxation and collisional quenching within the

matrix. Therefore, in sucrose-cation salts, the sites with slow dipolar relaxation rate inevitably have slow collisional rates. The difference of lifetime with emission wavelength reflects a broad continuum of local matrix sites that vary in terms of their overall molecular mobility. Probes in the blue-shifted sites have longer lifetimes, smaller values of collisional quenching rate k_{TS0} and become less mobile; but probes in the red-shifted sites have shorter lifetimes, larger values of quenching rate and become more mobile. In the sucrose-cation salt films the values of the stretching exponent β are comparable lower than those in the sucrose film, indicating a decreased ability within the sites to dynamically average out spectroscopic differences in the presence of salts. The enhanced dynamic site heterogeneity may result from a change in the distribution of local environments as a consequence of water-ion interactions introduced by cation salts. Comparably, addition of anion salts into sucrose matrix did not affect or slightly increased the dynamic site heterogeneity. Note that those matrixes which had lowered transition temperatures due to the residual moisture were in the glassy state at a temperature closer to the apparent T_g (with moisture effect). Dynamic site heterogeneity was reduced dramatically near the T_g and above. The moisture effect probably influenced the spectral heterogeneity as well.

Conclusion

Salts are commonly present in foods and biological systems, and also widely used in solid pharmaceutical formulations. It is worthy of mapping out the effect of salts on the characteristics of the matrix since the matrix properties have implications for the processing and subsequent storage stability of biological materials and foods.

Phosphorescence of erythrosin B can report a detailed mobility map within amorphous sucrose film blended with various salts at a fixed mole ratio of 0.2:1. Based on the lifetime of erythrosin B in sucrose and sucrose-salt films over the temperature range from 5 to 100°C, we came to a conclusion that salts exert a rigidification effect on amorphous sucrose: increasing lifetime and reducing matrix mobility (collisional quenching rate k_{TS0}) in the glassy state. The rigidification effect in anion salt groups (Na acetate, Na_3 citrate, disodium phosphate) is more significant that in cation salt groups (NaCl, $CaCl_2$ and $MgCl_2$). "Mobility hysteresis" was observed in most sucrose-salt mixtures, the magnitude of hysteresis was dependent on the type of salt. Salts had strong ability to bind water, a certain amount of moisture thus remained in the sucrose-salt films. The residual moisture plasticize the matrixes, resulting in an increase in matrix mobility and a depression of mobility transition temperature, which may be responsible for the mobility hysteresis. The mobility transition temperatures obtained from lifetime curves in heating and cooling cycles may work as indicators for the apparent T_g (with moisture effect) and the actual T_g (without moisture effect), and reflect the overall effect and salt effect correspondingly. The mobility map provides some hints about the possible interactions in the sucrose-salt matrixes as well.

Spectral heterogeneity in Ery B phosphorescence in amorphous sucrose-salt films also provides direct evidence to support a physical model of dynamic site heterogeneities within supercooled liquids and amorphous solids above and below the glass transition temperature (Ediger, 2000; Richert, 2002). Addition of salts influences the dynamic site heterogeneity of amorphous sucrose matrix and this effect is depended on the type of salt. Our data indicate that there are sites of different mobility within amorphous solid sucrose

and this dynamic heterogeneity is enhanced in the presence of salts, especially the cation salts. Undoubtedly the ability to report dynamic heterogeneity using Ery B phosphorescence provides an insight into the complex dynamic properties of amorphous biomaterials.

References:

Buitink, J., van der Dries, I.J., Hoekstra, F.A., Alberda, M., and Hemminga, M.A. 2000. High Critical Temperature above T_g May Contribute to the Stability of Biological Systems. *Biophys. J.* 79, 1119-1128.

Buitink, J., and Leprince, O. 2004. Glass formation in plant anhydrobiotes: survival in the dry state. *Cryobiology*. 48, 215-228.

Chan, R.K., Pathmanthan, K., and Johari, G.P. 1986. Dielectric relaxations in the liquid and glassy states of glucose and its water mixtures. *J. Phys. Chem.* 90, 6358-6362.

Contreras-Lopez, E., Champion, D., Hervet, H., Blond, G., and Le Meste, M. 2000. Rotational and translational mobility of small molecules in sucrose plus polysaccharide solutions. *J. Agric. Food Chem.* 48, 1009-1015.

Cook, W.J., and Bugg, C.E. 1973. Calcium interactions with D-glucans: crystal structure of α-α trehalose-calcium bromide monohydrate. *Carbohydr. Res. 31,* 265-275.

Courtney, T.T., and Ediger, M.D. 2002. Influence of spatially heterogeneous dynamics on physical aging of polystyrene. *J. Chem. Phys.* 116 (2), 9089-9099.

Courtney, T.T., and Ediger, M.D. 2003. Change in the temperature dependence of segmental dynamics in deeply supercooled polycarbonate. *J. Chem. Phys.* 118 (4), 1996-2004.

Crowe, J.H., Carpenter, J.F., and Crowe, L.M. 1998. The role of vitrification in anhydrobiosis. *Ann. Rev. Physiol.* 60, 73-103.

Crowe, J.H., Oliver, A.E., and Tablin, F. 2002. Is there a single biochemical adaptation to anhydrobiosis? *Integrat. and Comp. Biol.* 42, 497-503.

Deschenes, L.A., and Vanden Bout, D.A. 2001a. Single-molecule studies of heterogeneous dynamics in polymer melts near the glass transition. *Sci.* 292 (5515), 255-258.

Deschenes, L.A., and Vanden Bout, D.A. 2001b. Molecular motions in polymer films near the glass transition: A single molecule study of rotational dynamics. *J. Phys. Chem.* B., 105, 11978-11985.

Duchowicz, R., Ferrer, M.L. and Acuna, A.U. 1998. Kinetic spectroscopy of erythrosin phosphorescence and delayed fluorescence in aqueous solution at room temperature. *Photochem. Photobiol.* 68, 494-501.

Ediger, M.D. 2000. Spatially heterogenous dynamics in supercooled liquids. *Annu. Rev. Phys. Chem.* 51, 99-128.

Ediger, M.D., and Skinner, J.L. 2001. Single molecules rock and roll near the glass transition. *Sci.* 292 (5515) 233-234.

Fennema, O. 1996. Water and Ice. *In* Food Chemistry, 3rd Ed. O.R. Fennema, editor. Marcel Dekker, Inc., N.Y.

Fischer, C.J., Gafni, A., Steele, D.G., and Schauerte, J.A. 2002. The triplet state lifetime of indole in aqueous and viscous environments: Significance of the interpretation of room temperature phosphorescence in proteins. *J. Am. Chem. Soc.* 124, 10359-10366.

Gangasharan and Murthy, S.S.N. 1995. Nature of relaxation processes in the supercooled liquid and glassy states of some carbohydrates. *J. Phys. Chem.* 99, 12349-12354.

Gonnelli, M., and Strambini, G.B. 1995. Phosphorescence lifetime of tryptophan in proteins. *Biochem.* 34(42), 13847-13857.

Izutsu K., and Aoyagi, N. 2005. Effect of inorganic salts on crystallization of polyethylene glycol in frozen solutions. *Intl. J. Pharm.* 288, 101-108.

Kets, E.P.W., IJpelaar, P.J., Hoekstra, F.A., and Vromans, H. 2004. Citrate increases glass transition temperature of vitrified sucrose preparations. *Cryobiology*. 48, 46-54.

Lee, K.C.B., Siegel, J., Webb, S.E.D., Leveque-Fort, S., Cole, M.J., Jones, R., Dowling, K., Lever, M.J., and French, P.M.W. 2001. Application of the stretched exponential function to fluorescence lifetime imaging. *Biophys. J.* 81, 1265-1274.

Lettinga, M.P., Zuilhof, H., and van Zandvoort, A.M.J. 2000. Phosphorescence and fluorescence characterization of fluorescein derivatives immobilized in various polymer matrices. *Phys. Chem. Chem. Phys.* 2, 3697-3707.

Lu, Q., and Zografi, G. 1997. Properties of citric acid at the glass transition. *J. Pharm. Sci.* 86, 1374-1378.

Lukasik, K.V. and Ludescher, R.D. 2006a. Effect of plasticizer on dynamic site heterogeneity in cold-cast gelatin films. *Food Hydrocoll.* 20, 88-95.

Lukasik, K.V., and Ludescher, R.D. 2006b. Molecular mobility in water and glycerol plasticized cold and hot-cast gelatin films. *Food Hydrocoll.* 20, 96-105.

Mazzobre, M.F., and Buera, M.P. 1999. Combined effects of trehalose and cations on the thermal resistance of β-galactosidase in freeze-dried systems. *Biochim. Biophys. Acta*. 1473, 337-344.

Mazzobre, M.F., Longinotti, M.P., Corti, H.R., and Buera, M.P. 2001. Effect of salts on the properties of aqueous sugar systems, in relation to biomaterial stabilization. 1. Water sorption behavior and ice crystallization/melting. *Cryobiology.* 43, 199-210.

Miller, D.P., de Pablo, J.J., and Corti, H.R. 1999. Viscosity and glass transition temperature of aqueous mixtures of trehalose with borax and sodium chloride. *J. Phys. Chem.* 103, 10243-10249.

Morel-Desrosiers, N., Lhermet, C., and Morel, J. 1991. Interactions between cations and sugars. Part 6.-Calorimetric method for simultaneous determination of the stability constant and enthalpy change for week complexation. *J. Chem. Soc. Faraday Trans.* 87 (14), 2173-2177.

Nack, T.J, and Ludescher, R.D. 2006. Molecular mobility and oxygen permeability in amorphous bovine serum albumin films. *Food Biophys.* 1, 151-162.

Ottenhof, M., MacNaughtan, W., and Farhat, I.A. 2003. FTIR study of state and phase transitions of low moisture sucrose and lactose. *Carbohydr. Res.* 338, 2195-2202.

Papp, S. and Vanderkooi, J.M. 1989. Tryptophan phosphorescence at room temperature as a tool to study protein structure and dynamics. *Photochem. Photobiol.* 49, 775-784.

Pravinata, L.C., You, Y. and Ludescher, R.D. 2005. Erythrosin B phosphorescence monitors molecularmobility and dynamic site heterogeneity in amorphous sucrose. *Biophys. J.* 88(May), 3551-3561.

Richert, R. 2000. Triplet state salvation dynamics: basics and applications. *J. Chem. Phys.* 113, 8404-8429.

Richert, R. 2001. Spectral selectivity in the slow β-relaxation of a molecular glass. *Europhys. Lett.* 54(6), 767-773.

Richert, R. 2002. Heterogeneous dynamics in liquids: fluctuations in space and time. *J. Phys. Condens. Matter.* 14, R738-R803.

Roos, Y. 1995. *Phase Transitions in Foods.* Academic Press, San Diego, CA.

Schmidt-Rohr, K., and Spiess, H.W. 1991. Nature of nonexponential loss of correlation above the glass transition investigated by multidimensional NMR. *Phys. Rev. Lett.* 66 (23), 3020-3023.

Shalaev, E.Y., Johnson-Elton, T.D., Chang, L., and Pikal, M.J. 2002. Thermophysical properties of pharmaceutically compatible buffers at sub-zero temperatures: implications for freeze-drying. *Pharm. Res.* 19(2), 195-201.

Shirke, S., and Ludescher, R.D. 2005. Dynamic site heterogeneity in amorphous maltose and maltitol from spectral heterogeneity in erythrosin B phosphorescence. *Carbohydr. Res.* 340, 2661-2669.

Shirke, S., Takhistov, P., and Ludescher, R.D. 2005. Molecular mobility in amorphous maltose and maltitol from phosphorescence of erythrosin B. *J. Phys. Chem. B.* 109, 16119-16126.

Shirke, S., You, Y., and Ludescher, R.D. 2006. Molecular mobility and dynamic site heterogeneity in amorphous lactose and lactitol from erythrosin B phosphorescence. *Biophys. Chem.* 123, 122-133.

Simon-Lukasik, K.V., and Ludescher, R.D. 2004. Erythrosin B phosphorescence as a probe of oxygen diffusion in amorphous gelatin films. *Food Hydrocoll.* 18, 621-630.

Slade, L., and Levine, H. 1995. Glass transition and water-food structure interactions. *Adv. Food Nutr. Res.* 38, 103-269.

Strambini, G.B., and Gonnelli, M. 1985. The indole nucleus triplet-state lifetime and its dependence on solvent microviscosity. *Chem. Phys. Lett.* 115, 196-200.

Streeland, L., Auffret, A.D., and Franks, F. 1998. Bond cleavage reactions in solid aqueous carbohydrate solutions. *Pharm. Res.* 15, 843-849.

Sundaresan, K.V., and R.D. Ludescher. 2007. Molecular mobility and oxygen permeability in amorphous β-lactoglobulin films. *Food Hydrocolloids.* (In press)

Van den Dries, I.J., Besseling, N.A.M., van Dusschoten, D., Hemminga, M.A., and van der Linden, E. 2000. Relation between a transition in molecular mobility and collapse phynomena in glucose-water systems. *J. Phys. Chem. B*. 104, 9260-9266.

Wolkers, W.F., Oldenhof, H., Alberda, M., and Hoekstra, F.A. 1998. A Fourier transform infrared microspectroscopy study of sugar glasses: application to anhydrobiotic higher plant cells. *Biochim. Biophys. Acta.* 1379, 83-96.

Wu, Y., Li, L., Liu, J., and Zhu, G. 2005. The enhancement effect of CaCl2 on solid substrate room temperature phosphorescence of polyhalogenated derivatives of fluorescein and application in immunoassay. *Anal. Chim. Acta.* 539, 271-275.

Wang, W. 2000. Lyophilization and development of solid protein pharmaceuticals. *Int. J. Pharm.* 203, 1-60.

You, Y., and Ludescher, R.D. 2006. Phosphorescence of erythrosin B as a robust probe of molecular mobility in amorphous solid sucrose. *Appl. Spectrosc.* 60, 813-819.

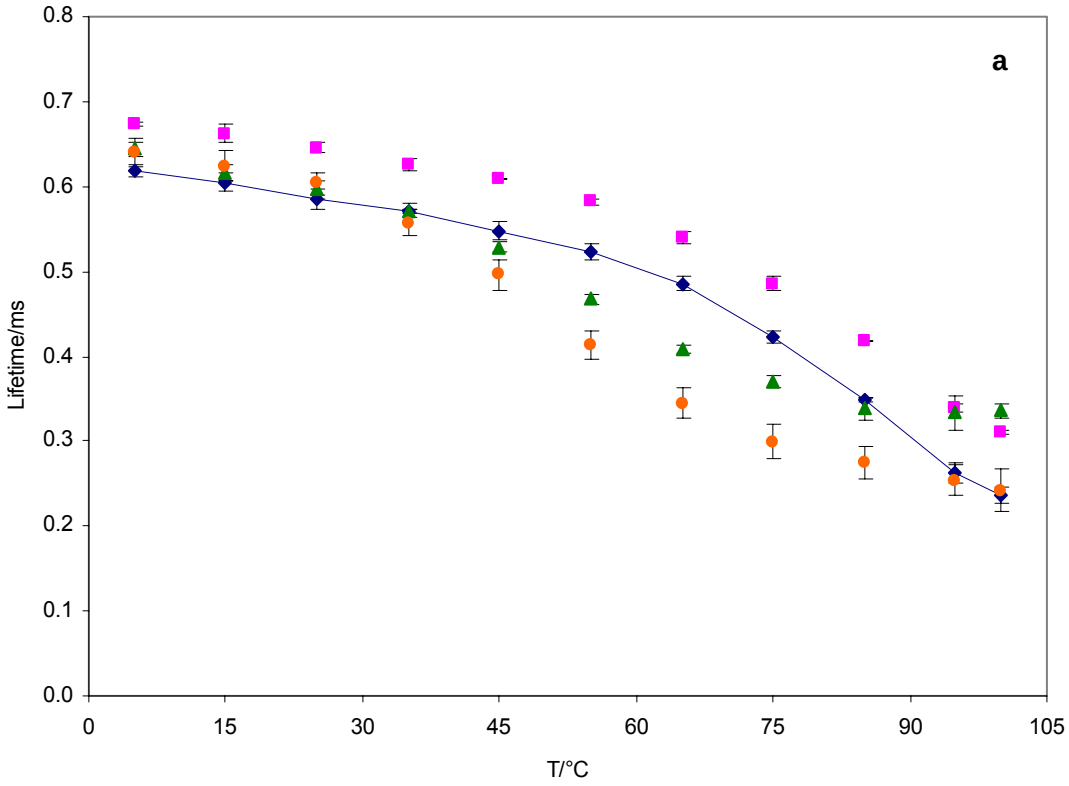
a
Lifetime/ms
0.8
0.7
0.6
0.5
0.4
0.3
0.2
0.1
0.0
0
15
30
45
60
75
90
105
T/°C

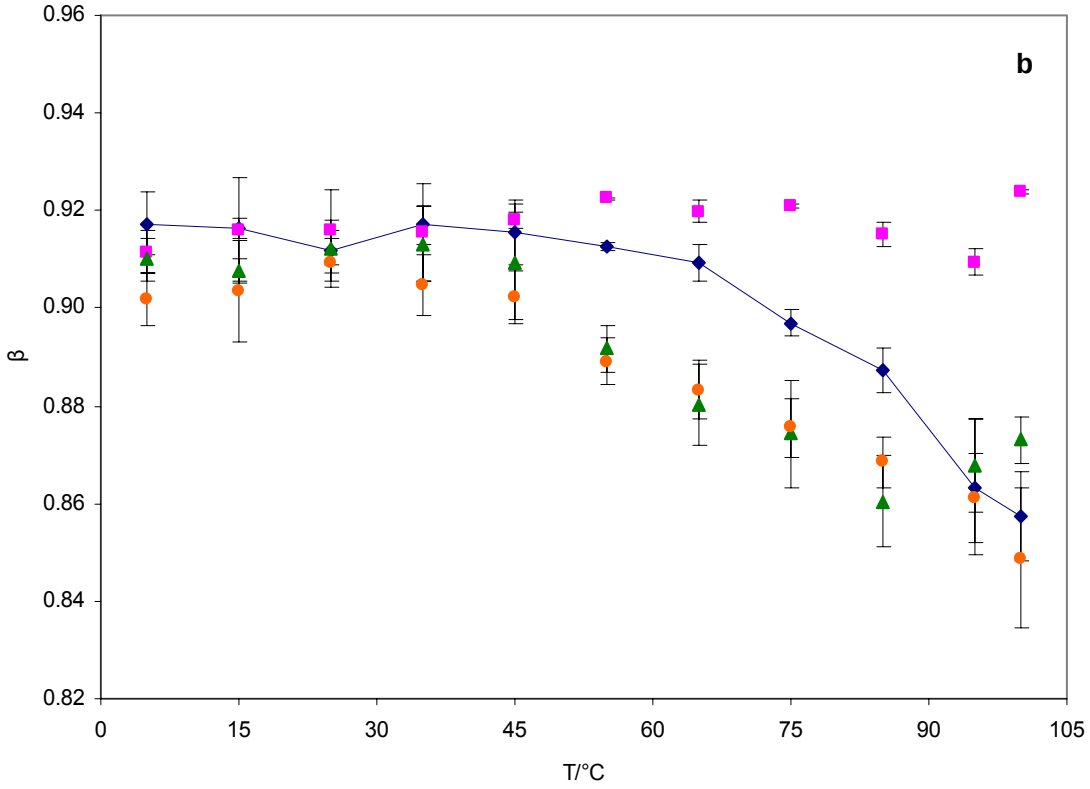
b
β
0.96
0.94
0.92
0.90
0.88
0.86
0.84
0.82
0
15
30
45
60
75
90
105
T/°C

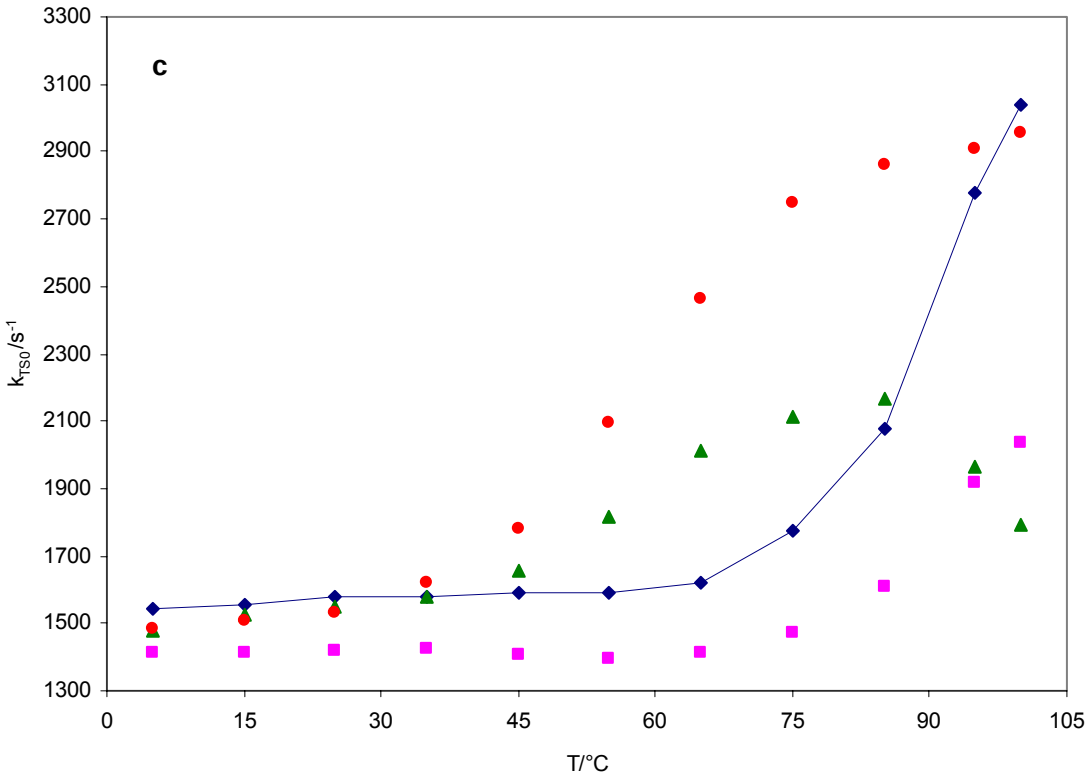

Figure 43: Temperature dependence of lifetime (a) and stretching exponents β (b) obtained from fits to a stretched exponential function of the intensity decay of erythrosin B in amorphous sucrose-salt matrixes; and the non-radiative decay rate k_{TS0} for the triplet state (c) in amorphous sucrose-salt matrixes: see text for additional details. The phosphorescence intensity data collected from 5 to 100°C (heating cycle). Samples are sucrose-salt films with a salt/sucrose molar ratio of 0.2:1 (♦, sucrose; ■, sucrose-NaCl; ▲, sucrose-$CaCl_2$; ●, sucrose-$MgCl_2$).

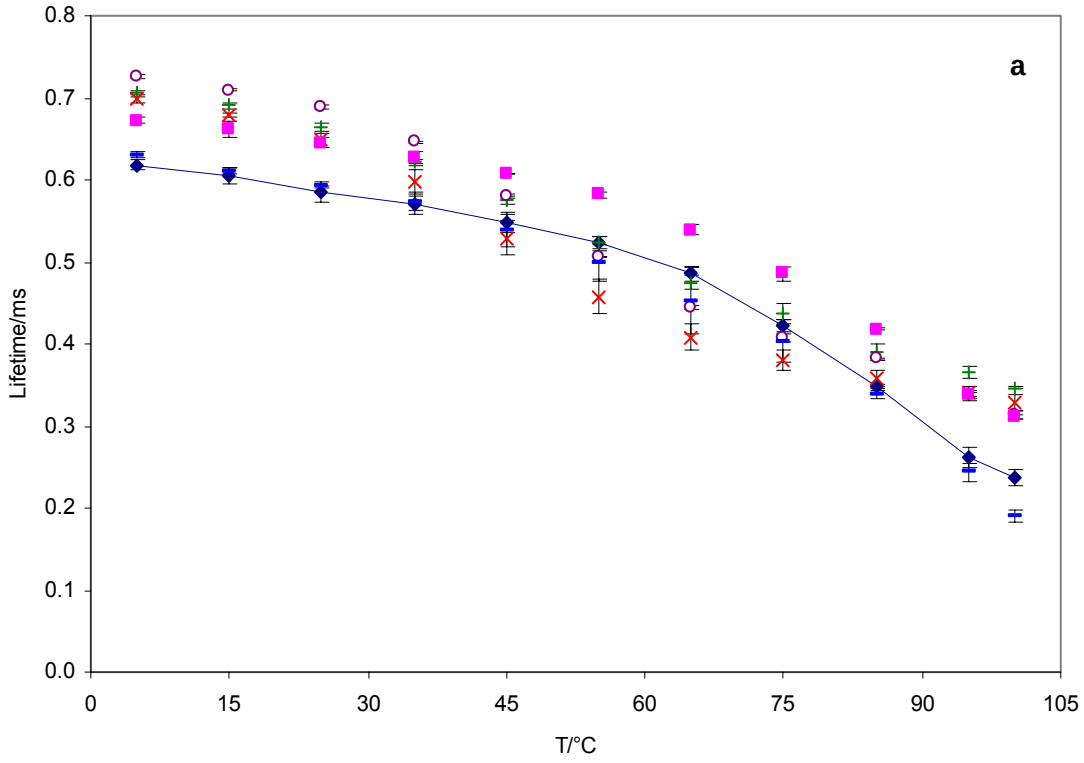
a
Lifetime/ms
0.8
0.7
0.6
0.5
0.4
0.3
0.2
0.1
0.0
0
15
30
45
60
75
90
105
T/°C

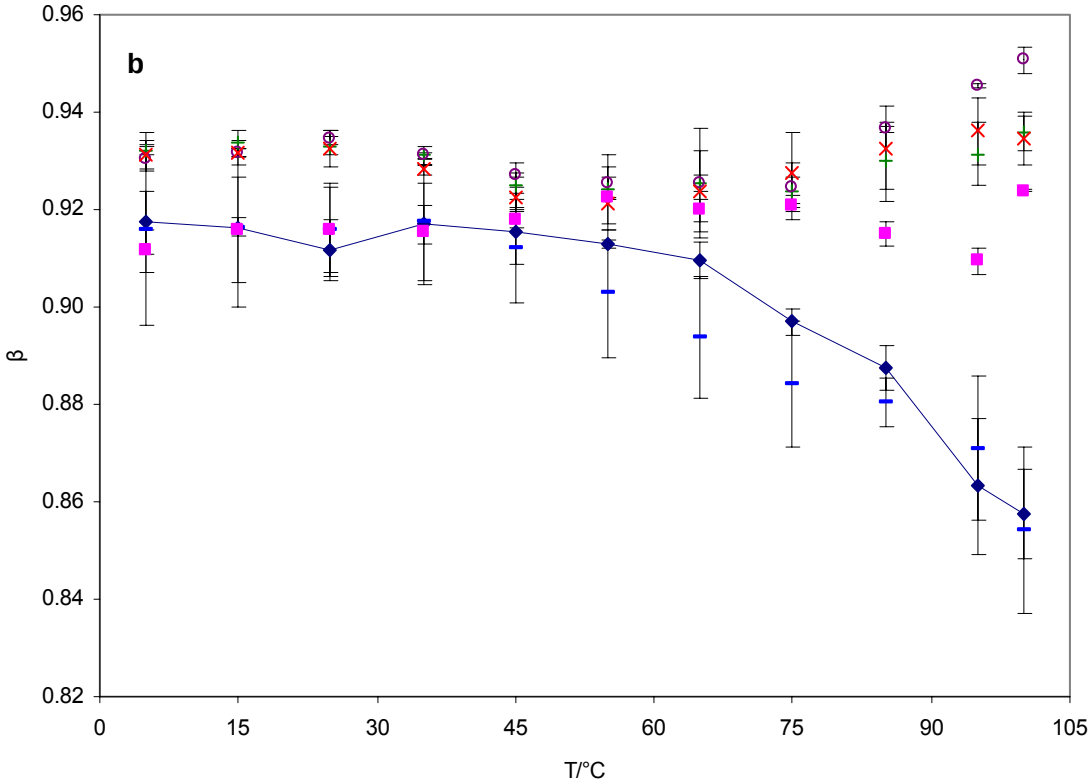
b
β
0.96
0.94
0.92
0.90
0.88
0.86
0.84
0.82
0
15
30
45
60
75
90
105
T/°C

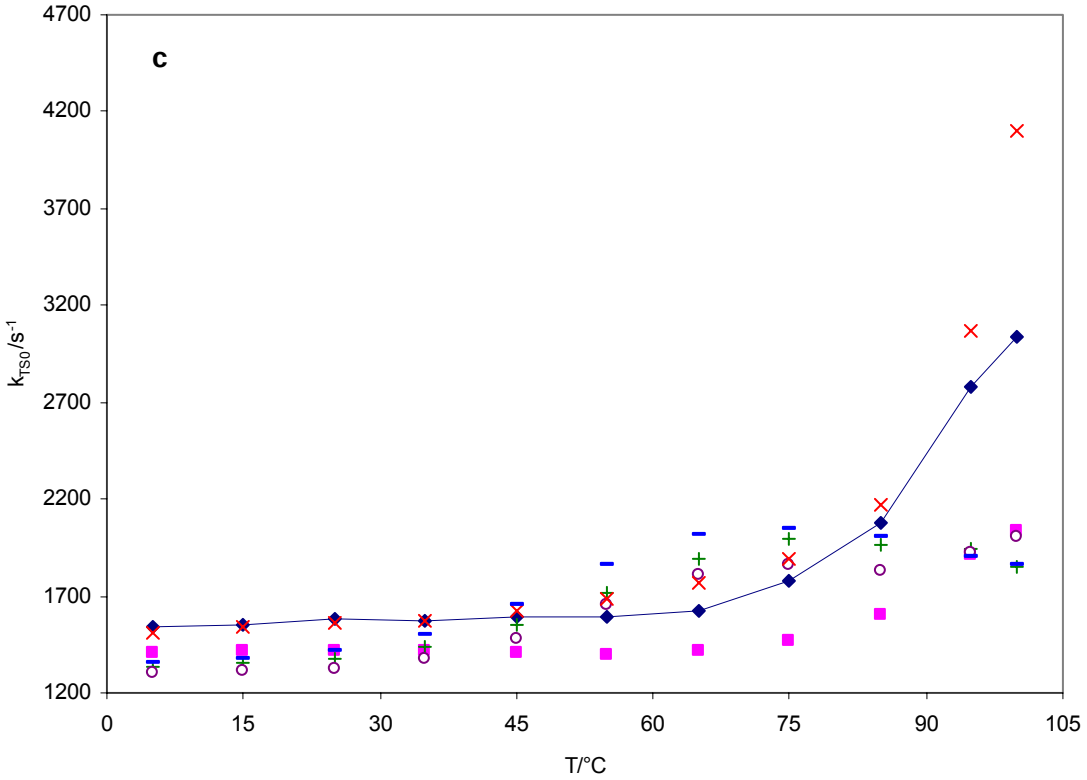

Figure 44: Temperature dependence of lifetime (a) and stretching exponents β (b) obtained from fits to a stretched exponential function of the intensity decay of erythrosin B in amorphous sucrose-salt matrixes; and the non-radiative decay rate k_{TS0} for the triplet state (c) in amorphous sucrose-salt matrixes: see text for additional details. The phosphorescence intensity data collected from 5 to 100°C (heating cycle). Samples are sucrose-salt films with a salt/sucrose molar ratio of 0.2:1 (♦, sucrose; ■, sucrose-NaCl; +, sucrose-citrate; ○, sucrose-acetate; –, sucrose-NaH_2PO_4; ×, sucrose-Na_2HPO_4).

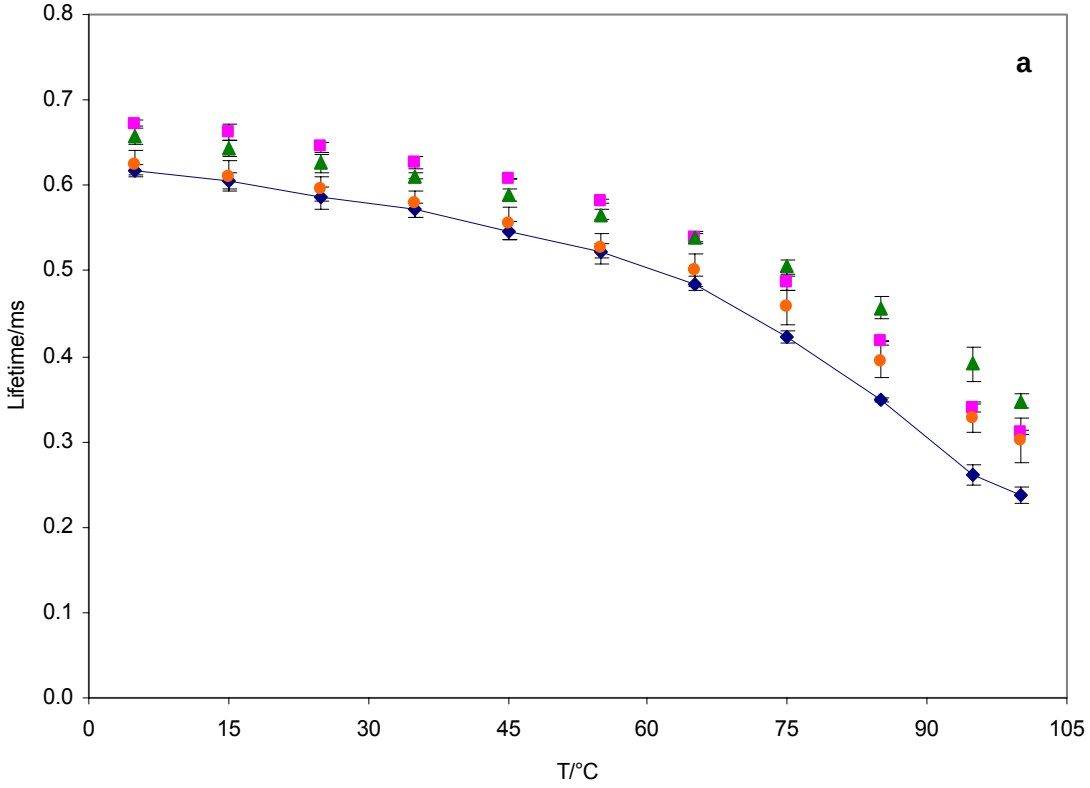
a
Lifetime/ms
0.8
0.7
0.6
0.5
0.4
0.3
0.2
0.1
0.0
0
15
30
45
60
75
90
105
T/°C

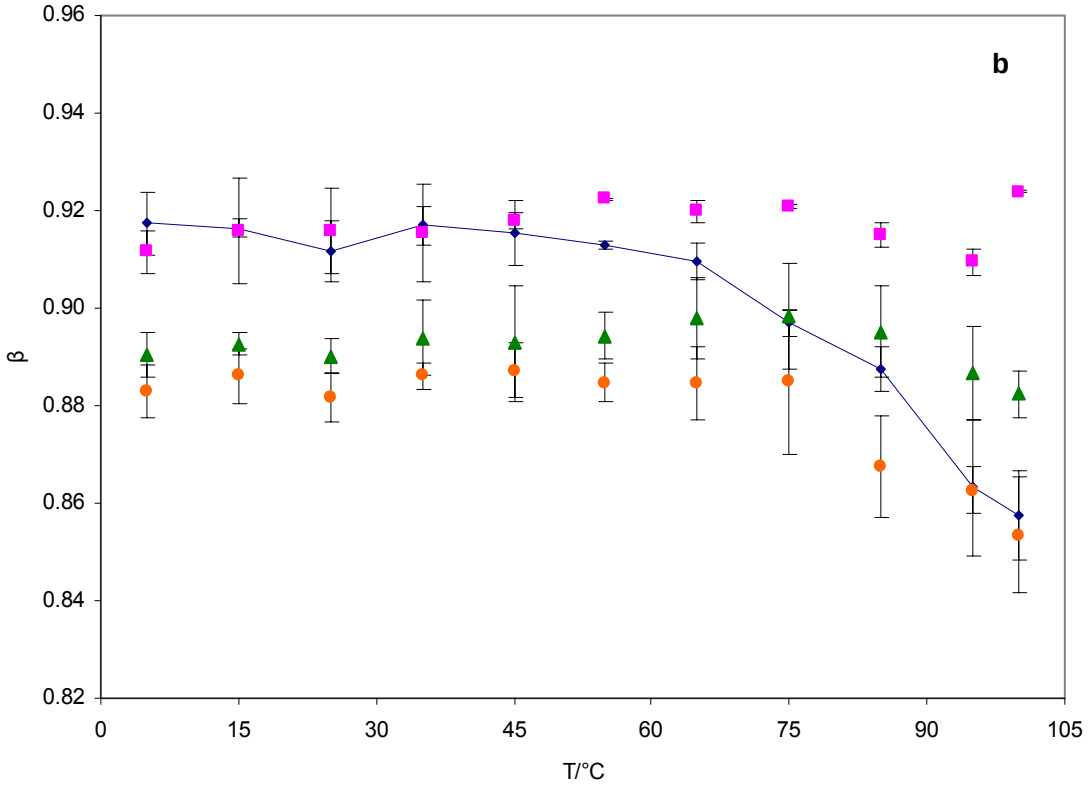
b
β
0.96
0.94
0.92
0.90
0.88
0.86
0.84
0.82
0
15
30
45
60
75
90
105
T/°C

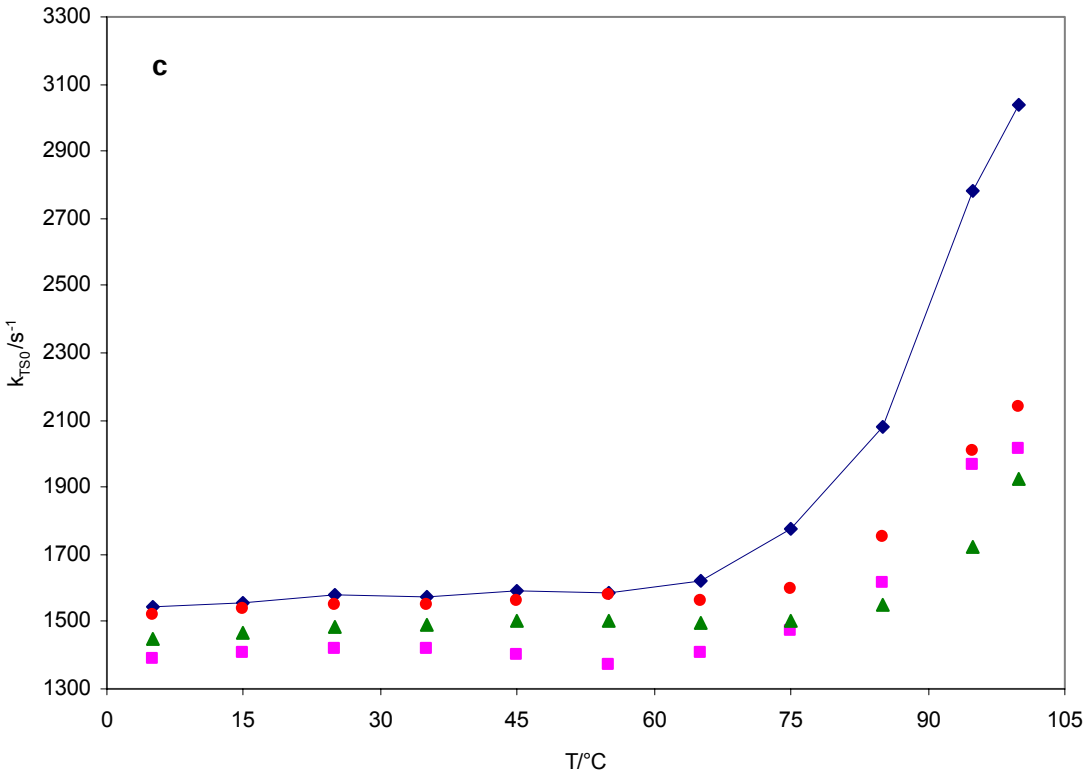

Figure 45: Temperature dependence of lifetime (a) and stretching exponents β (b) obtained from fits to a stretched exponential function of the intensity decay of erythrosin B in amorphous sucrose-salt matrixes; and the non-radiative decay rate k_{TS0} for the triplet state (c) in amorphous sucrose-salt matrixes: see text for additional details. The phosphorescence intensity data collected from 100 to 5°C (cooling cycle). Samples are sucrose-salt films with a salt/sucrose molar ratio of 0.2:1 (♦, sucrose; ■, sucrose-NaCl; ▲, sucrose-$CaCl_2$; ●, sucrose-$MgCl_2$).

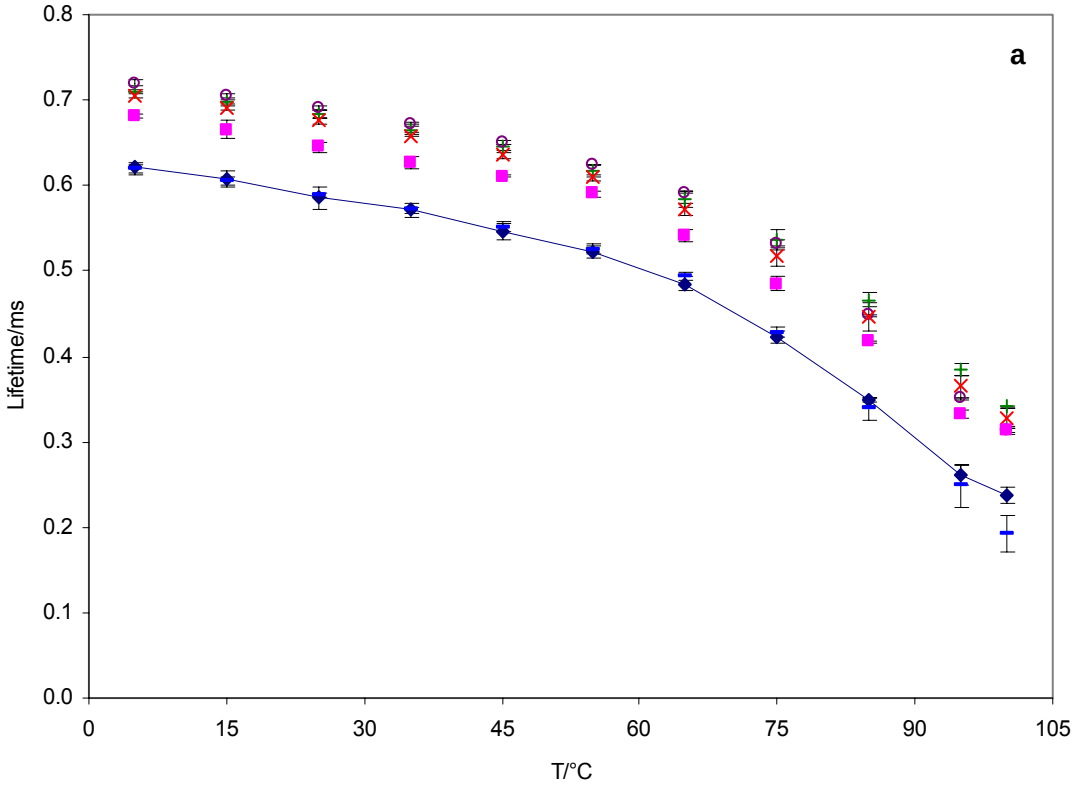
a
Lifetime/ms
T/°C
0.0
0.1
0.2
0.3
0.4
0.5
0.6
0.7
0.8
0
15
30
45
60
75
90
105

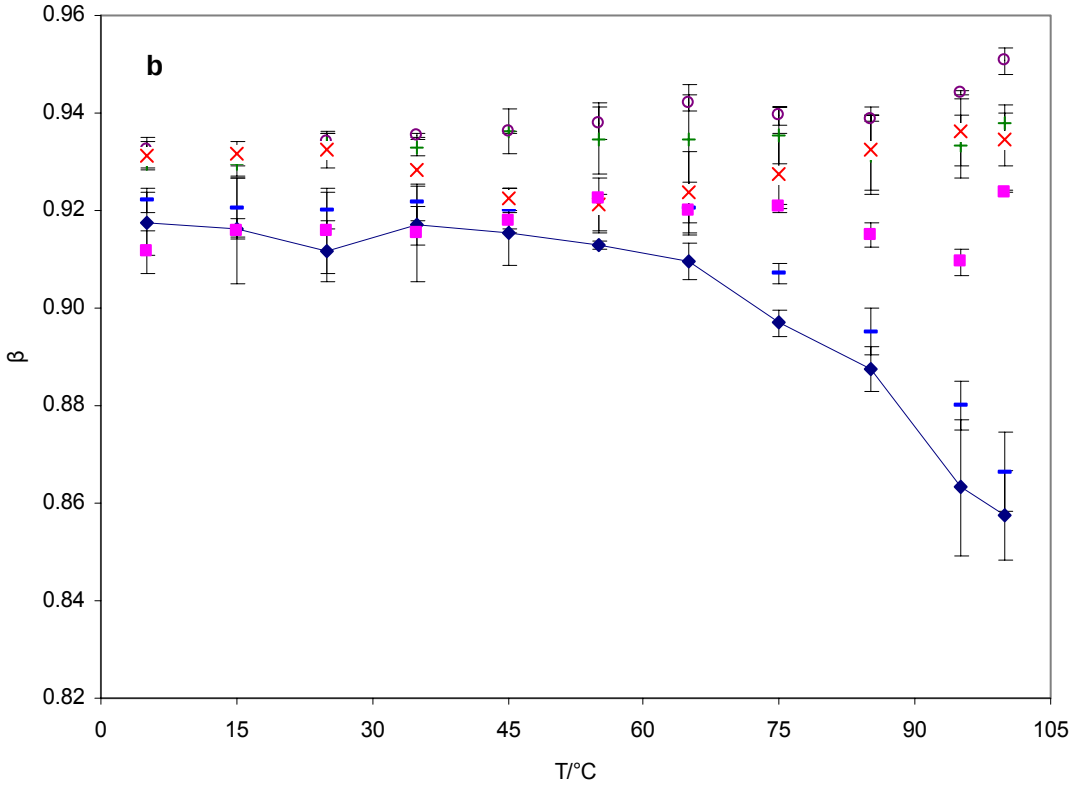
b
β
T/°C
0.82
0.84
0.86
0.88
0.90
0.92
0.94
0.96
0
15
30
45
60
75
90
105

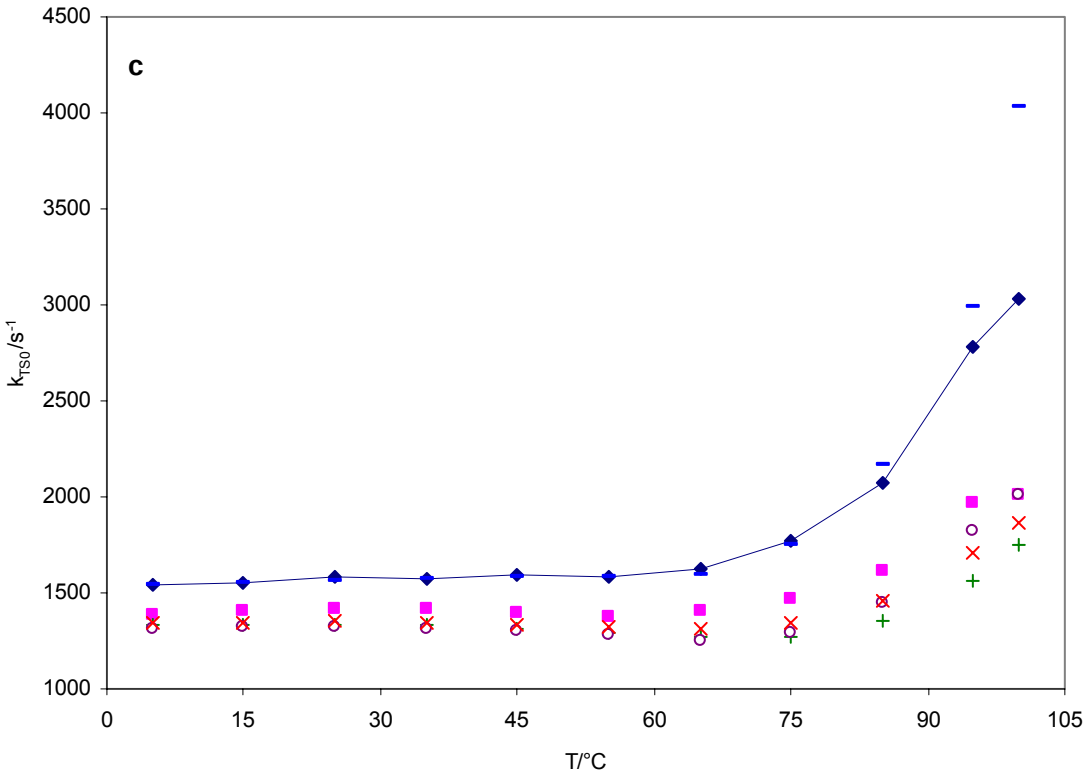

Figure 46: Temperature dependence of lifetime (a) and stretching exponents β (b) obtained from fits to a stretched exponential function of the intensity decay of erythrosin B in amorphous sucrose-salt matrixes; and the non-radiative decay rate k_{TS0} for the triplet state (c) in amorphous sucrose-salt matrixes: see text for additional details. The phosphorescence intensity data collected from 100 to 5°C (cooling cycle). Samples are sucrose-salt films with a salt/sucrose molar ratio of 0.2:1 (♦, sucrose; ■, sucrose-NaCl; +, sucrose-citrate; ○, sucrose-acetate; –, sucrose-NaH_2PO_4; ×, sucrose-Na_2HPO_4).

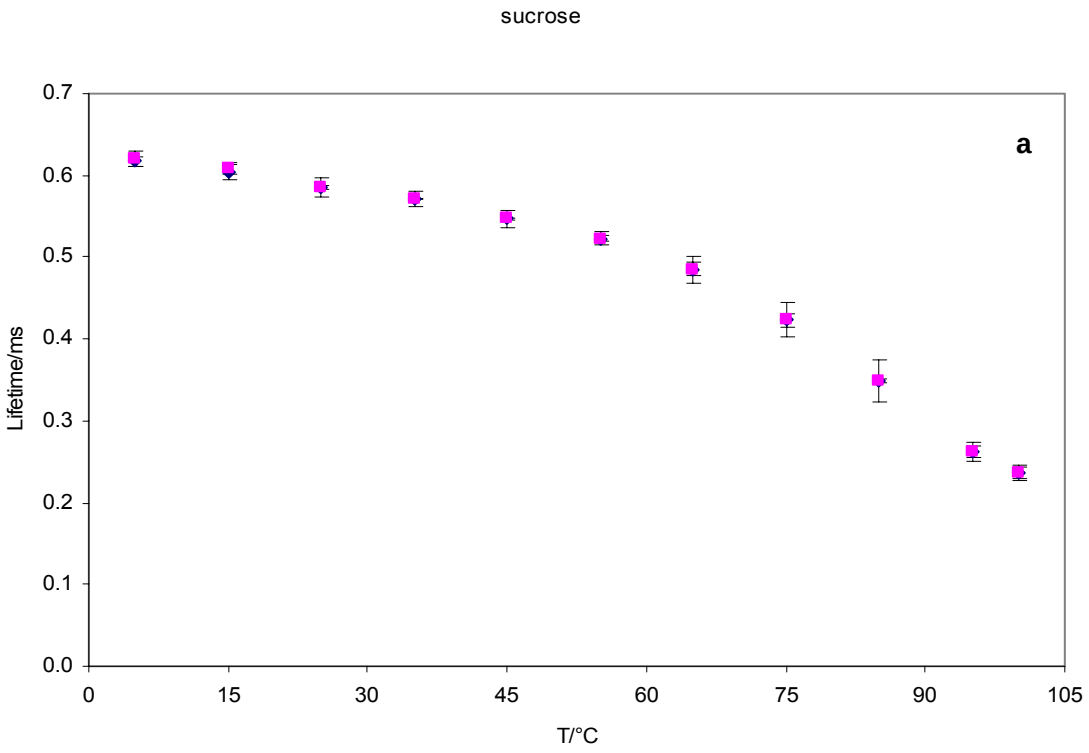
sucrose
a
Lifetime/ms
0.0
0.1
0.2
0.3
0.4
0.5
0.6
0.7
0
15
30
45
60
75
90
105
T/°C

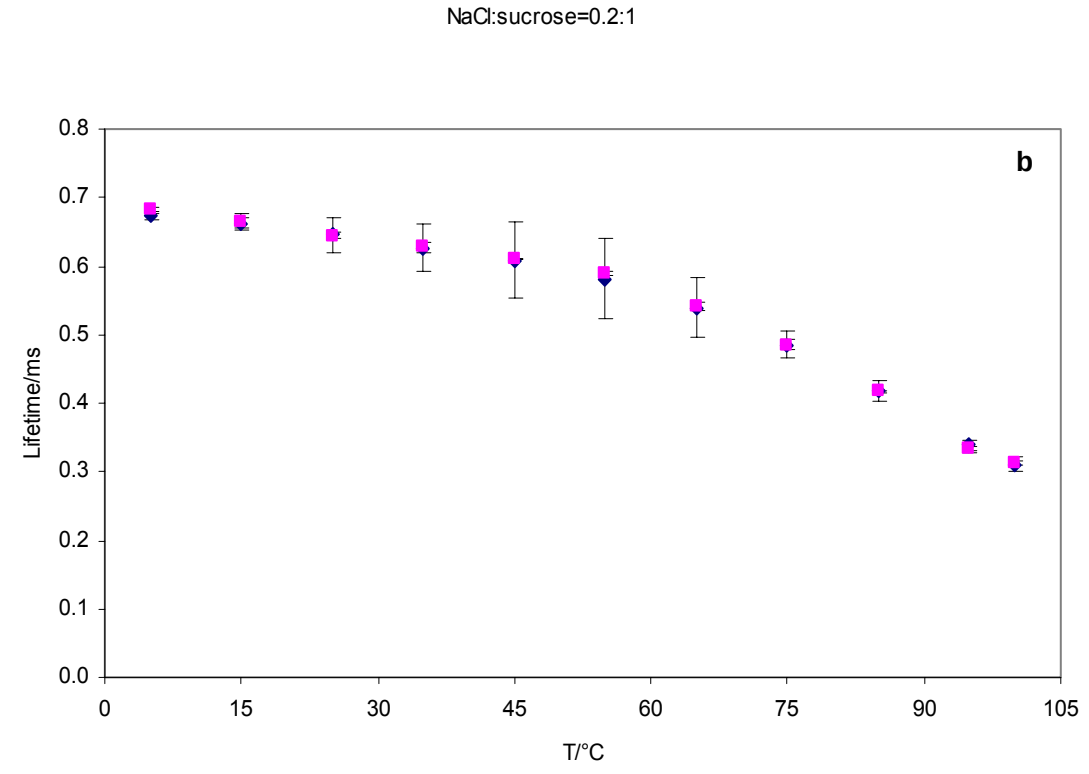
NaCl:sucrose=0.2:1
b
Lifetime/ms
0.0
0.1
0.2
0.3
0.4
0.5
0.6
0.7
0.8
0
15
30
45
60
75
90
105
T/°C

$CaCl_2$:sucrose=0.2:1

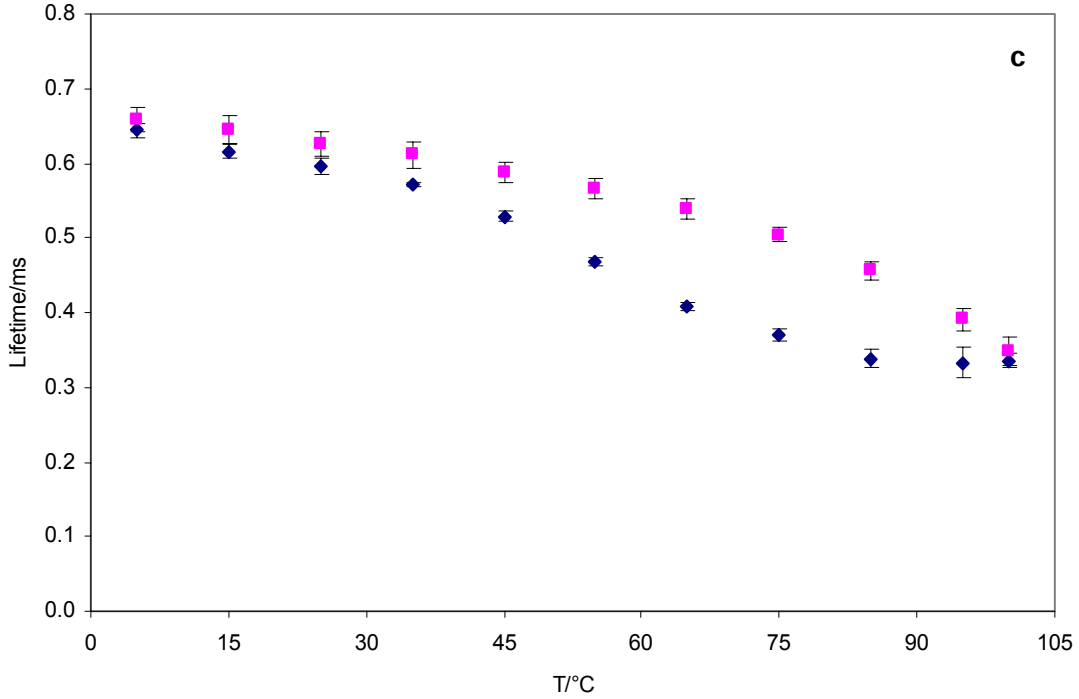

$MgCl_2$: sucrose=0.2:1

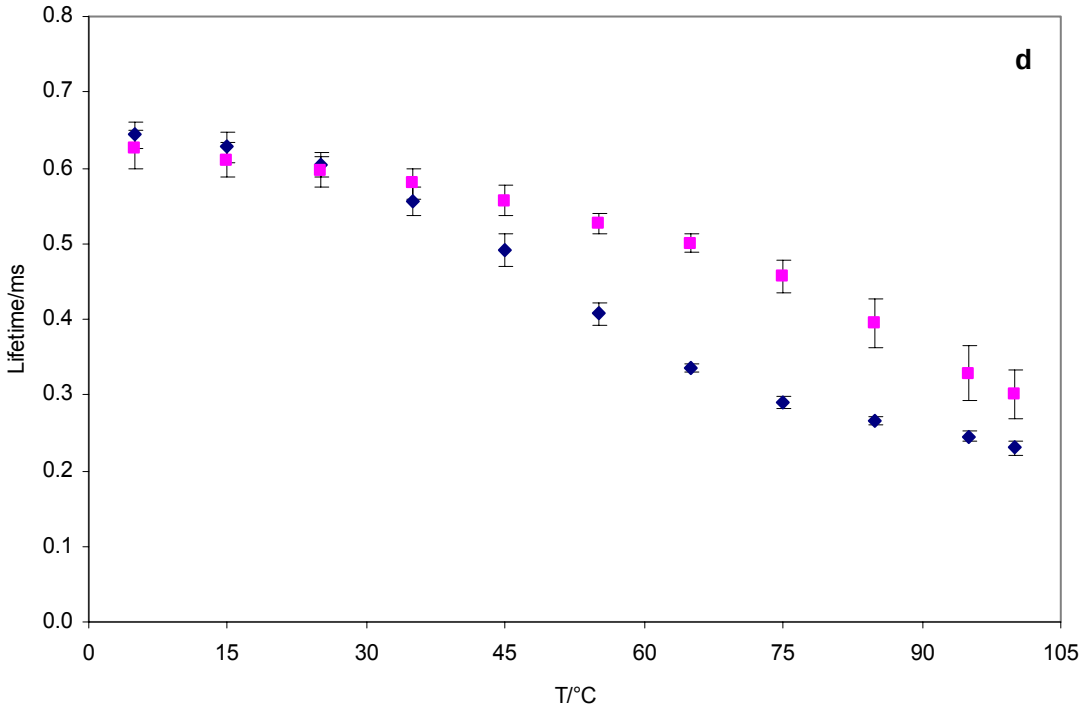

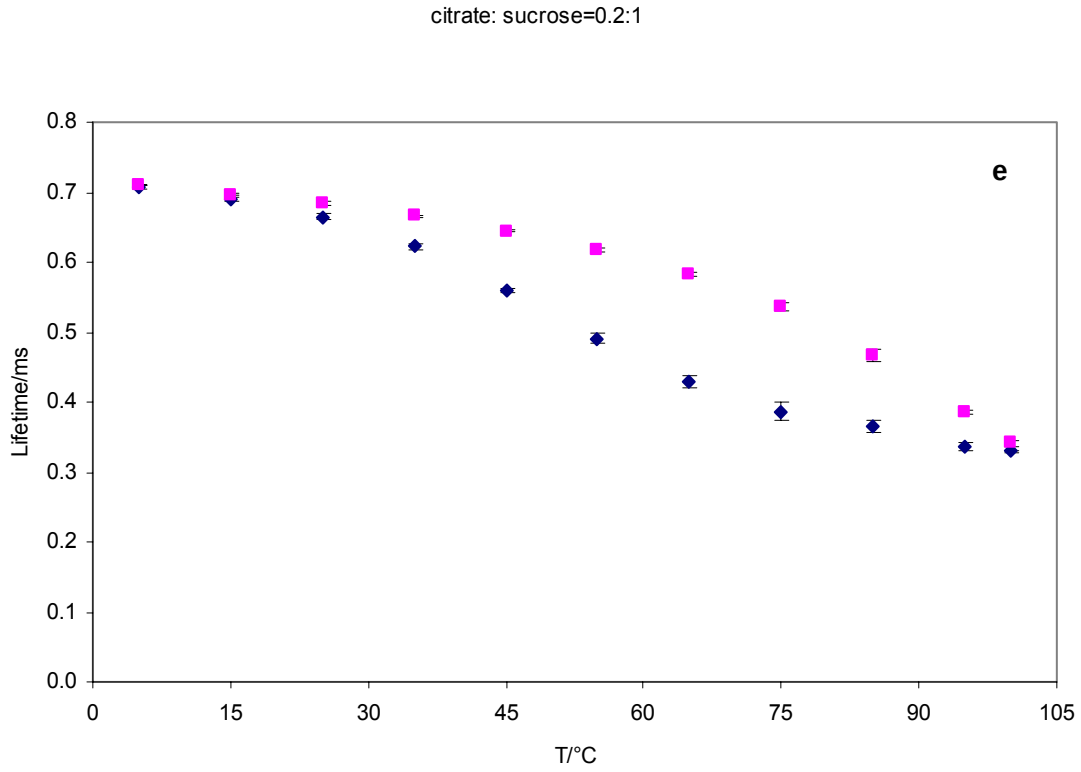
citrate: sucrose=0.2:1
e
Lifetime/ms
T/°C
0.0
0.1
0.2
0.3
0.4
0.5
0.6
0.7
0.8
0
15
30
45
60
75
90
105

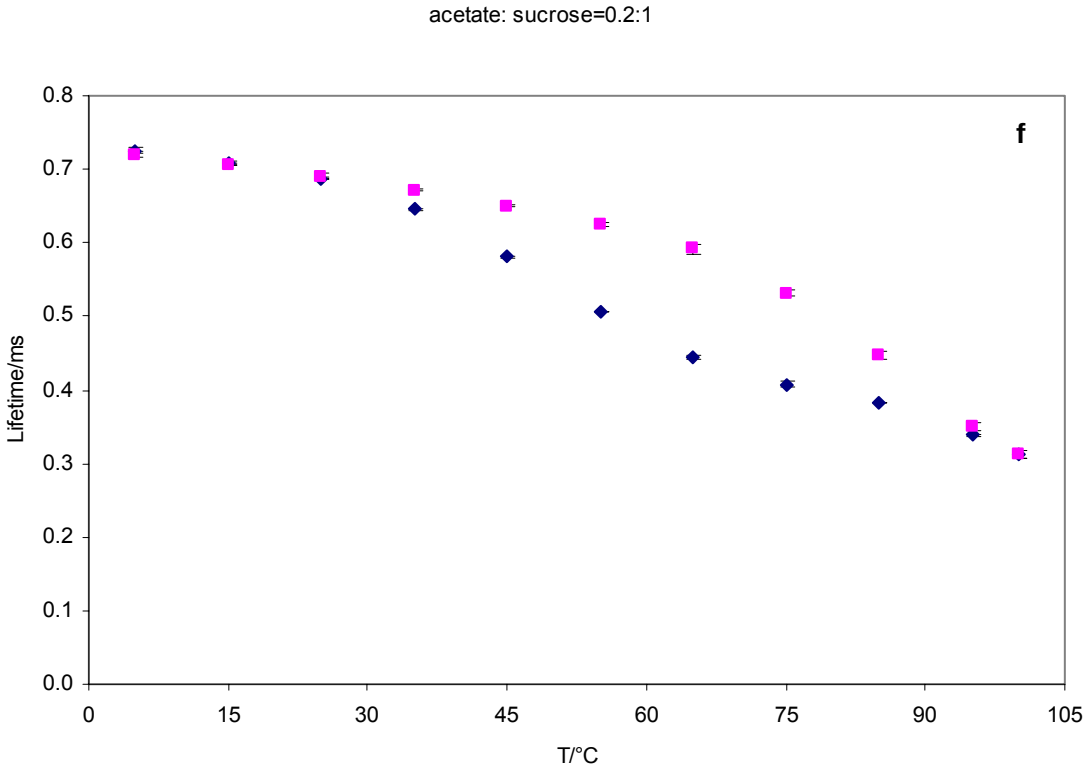
acetate: sucrose=0.2:1
f
Lifetime/ms
T/°C
0.0
0.1
0.2
0.3
0.4
0.5
0.6
0.7
0.8
0
15
30
45
60
75
90
105

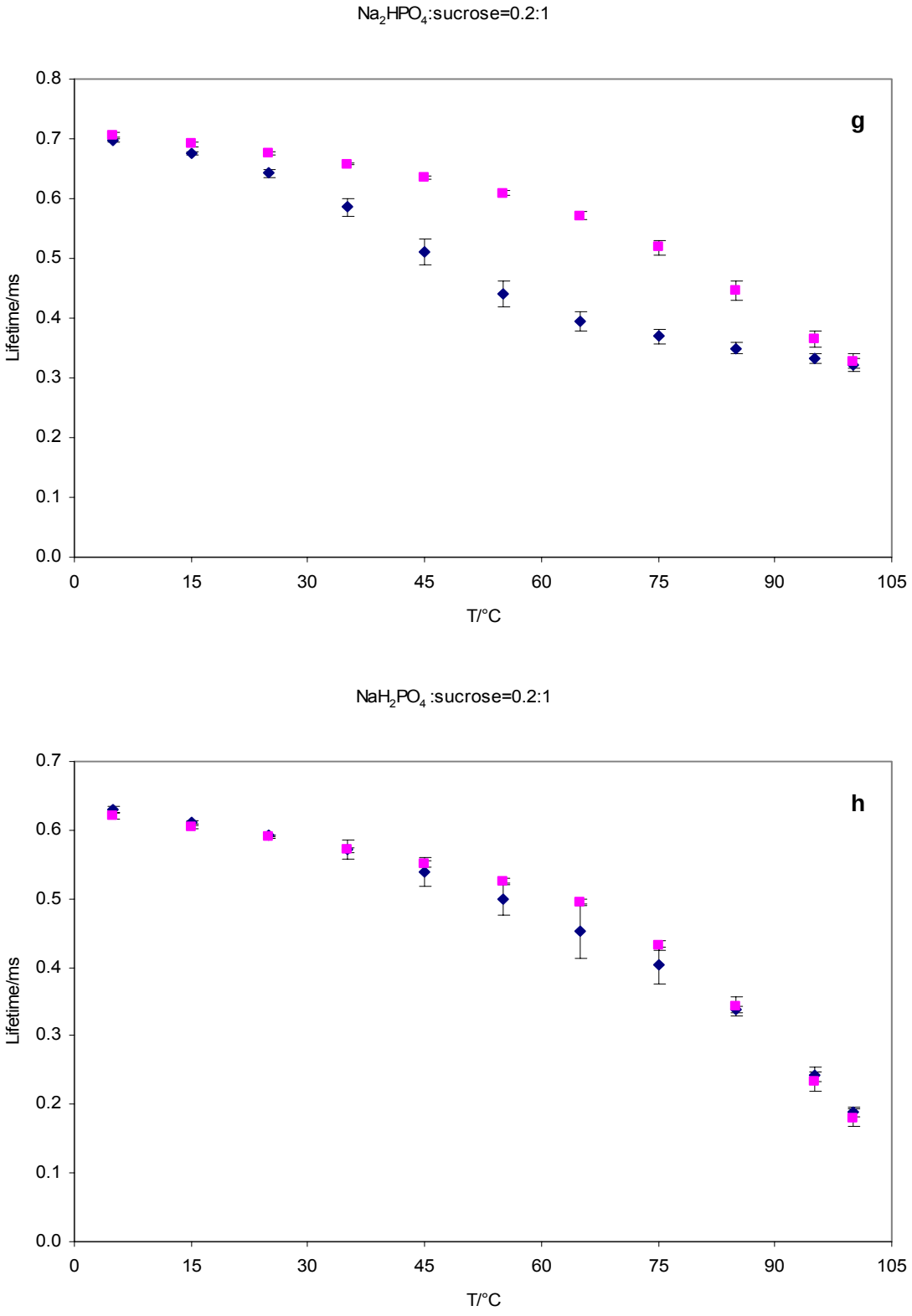

Figure 47: Phosphorescence lifetime of erythrosin B in sucrose-salt films as a function of temperature during heating (♦) and cooling cycles (■). (a) sucrose; (b) sucrose-NaCl; (c) sucrose-$CaCl_2$; (d) sucrose-$MgCl_2$; (e) sucrose-citrate; (f) sucrose-acetate; (g) sucrose-Na_2HPO_4; (h) sucrose-NaH_2PO_4.

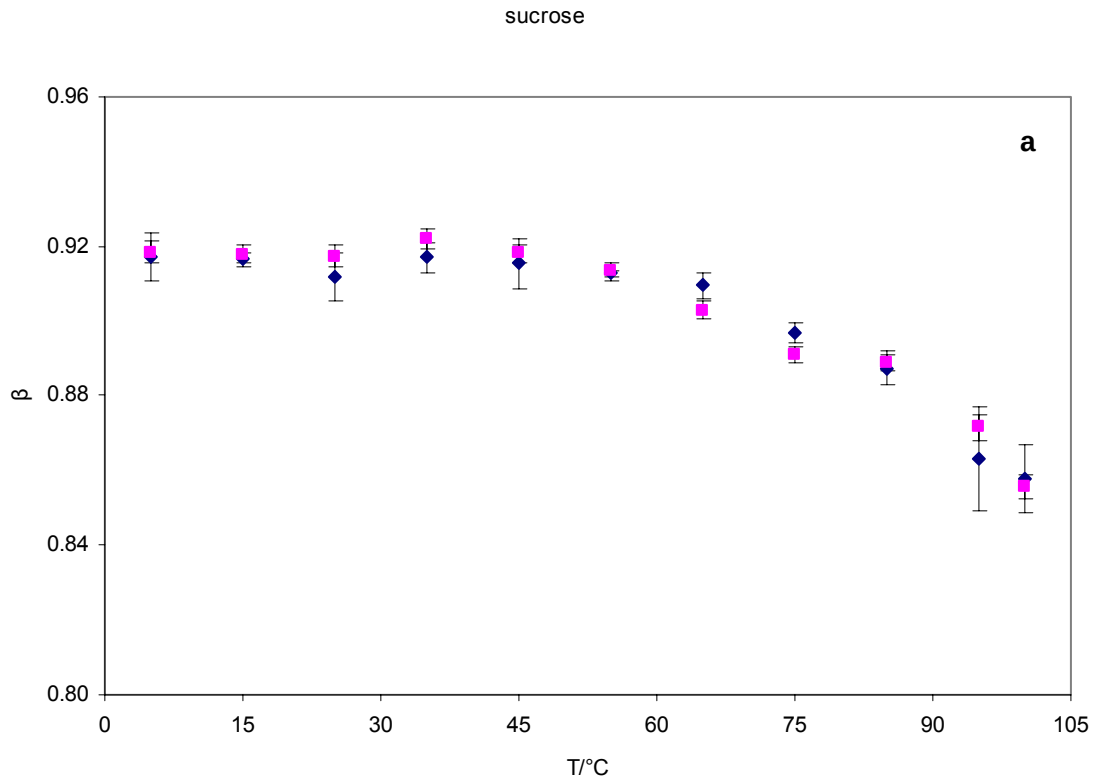
sucrose
a
0.96
0.92
0.88
0.84
0.80
β
0
15
30
45
60
75
90
105
T/°C

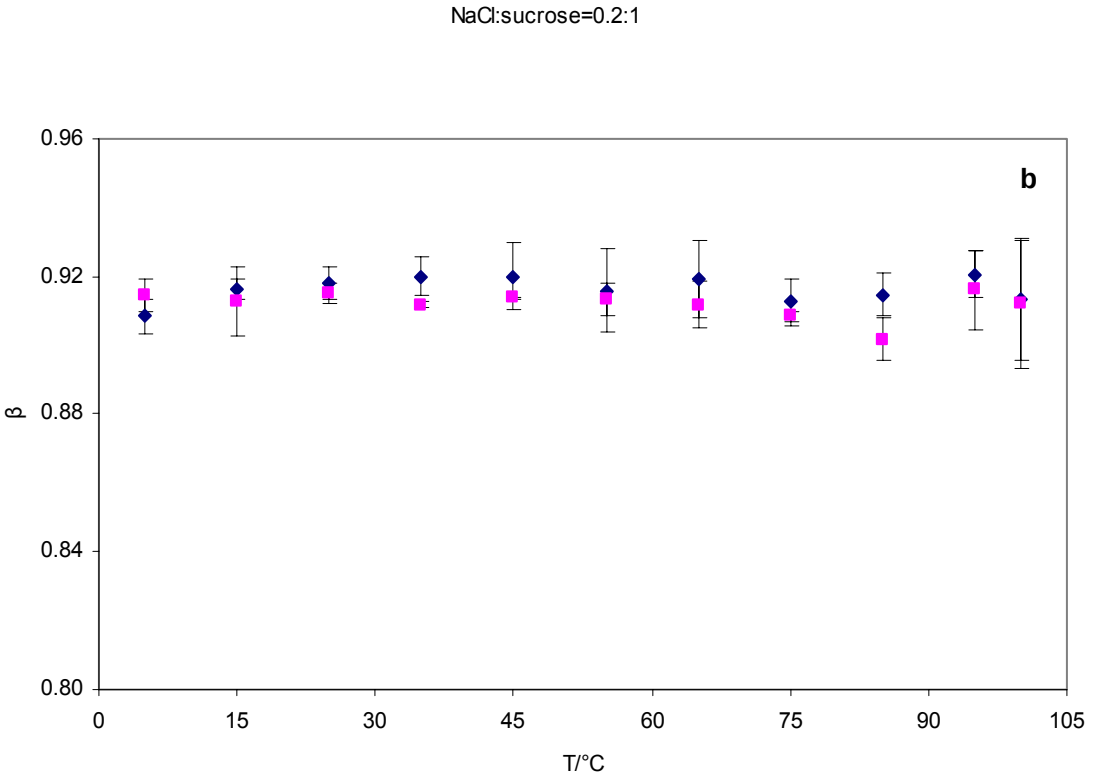
NaCl:sucrose=0.2:1
b
0.96
0.92
0.88
0.84
0.80
β
0
15
30
45
60
75
90
105
T/°C

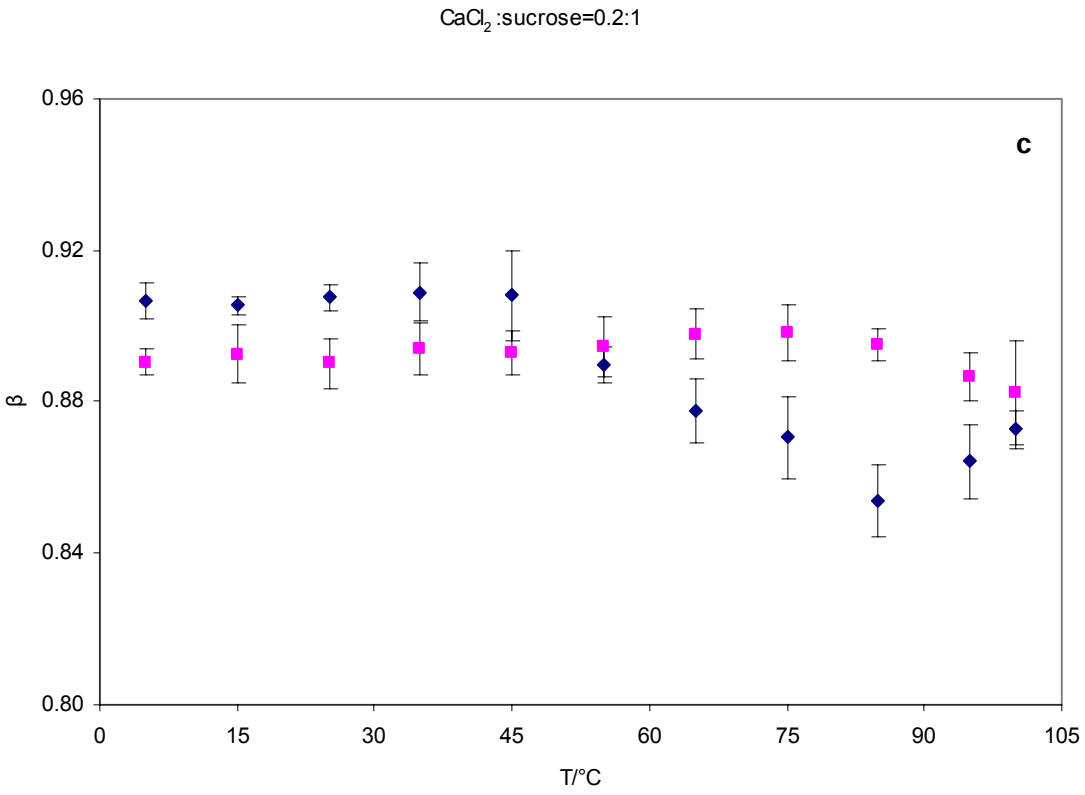
CaCl2 :sucrose=0.2:1
c
β
T/°C
0.96
0.92
0.88
0.84
0.80
0
15
30
45
60
75
90
105

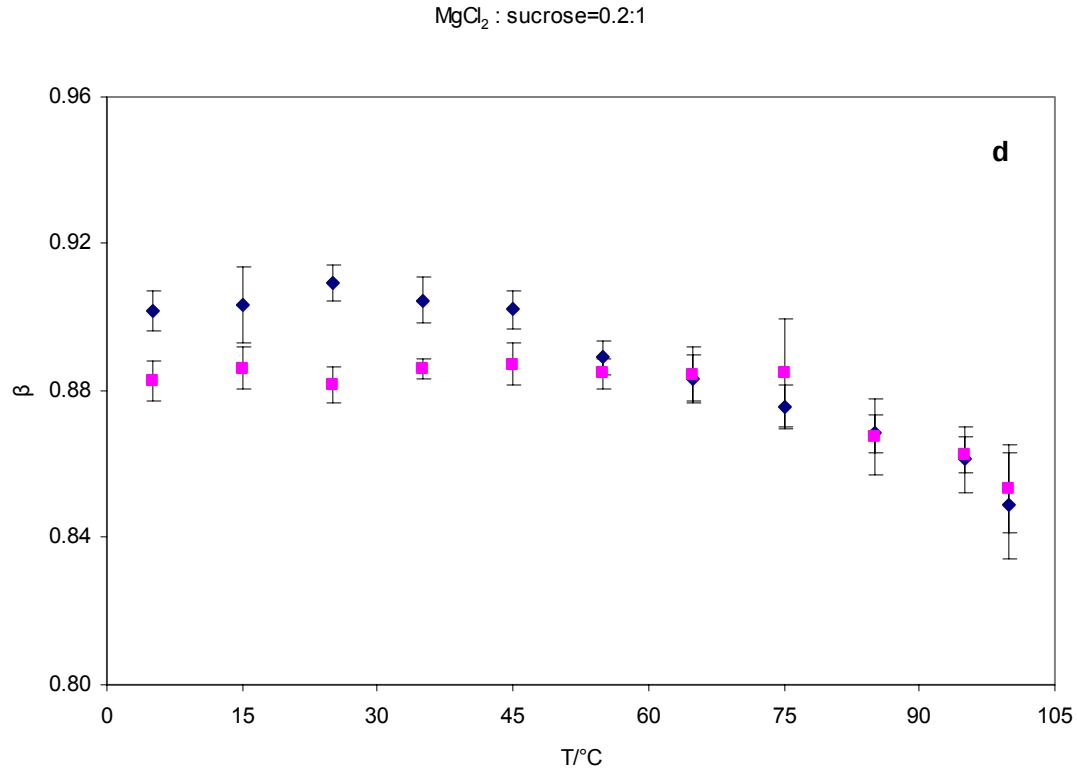
MgCl2 : sucrose=0.2:1
d
β
T/°C
0.96
0.92
0.88
0.84
0.80
0
15
30
45
60
75
90
105

citrate: sucrose=0.2:1

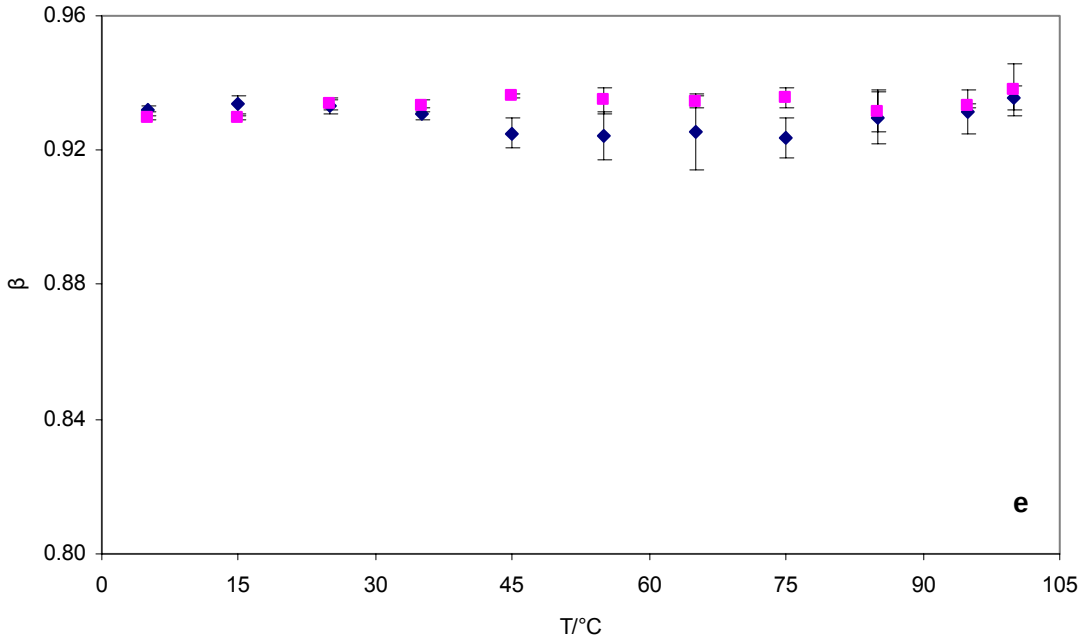

acetrate: sucrose=0.2:1

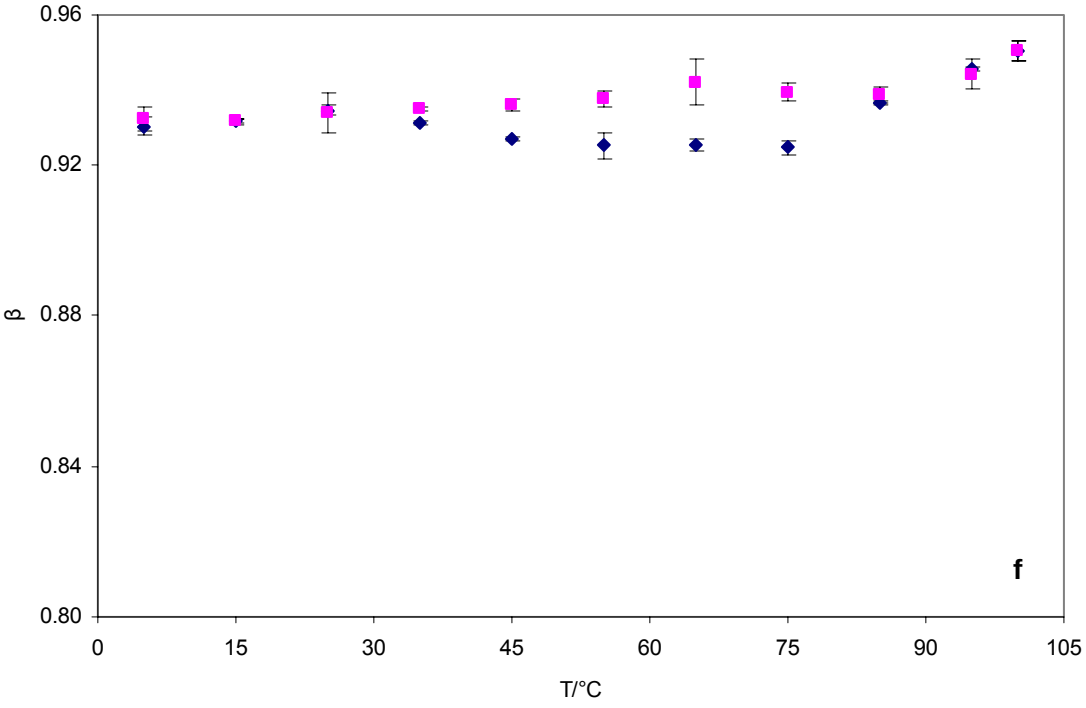

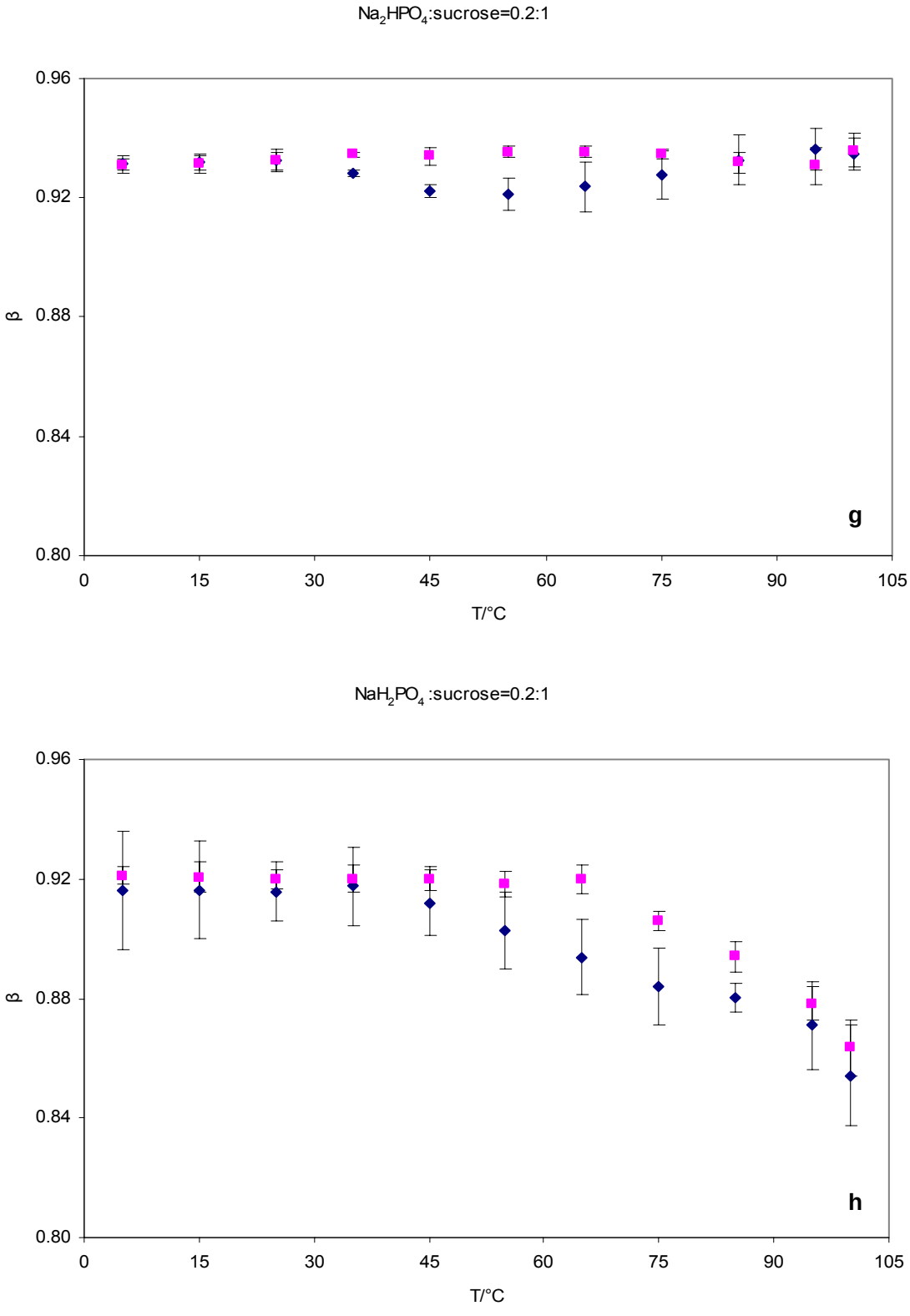

Figure 48: Stretching exponents β of erythrosin B in sucrose-salt films as a function of temperature during heating (♦) and cooling cycles (■). (a) sucrose; (b) sucrose-NaCl; (c) sucrose-$CaCl_2$; (d) sucrose-$MgCl_2$; (e) sucrose-citrate; (f) sucrose-acetate; (g) sucrose-Na_2HPO_4; (h) sucrose-NaH_2PO_4.

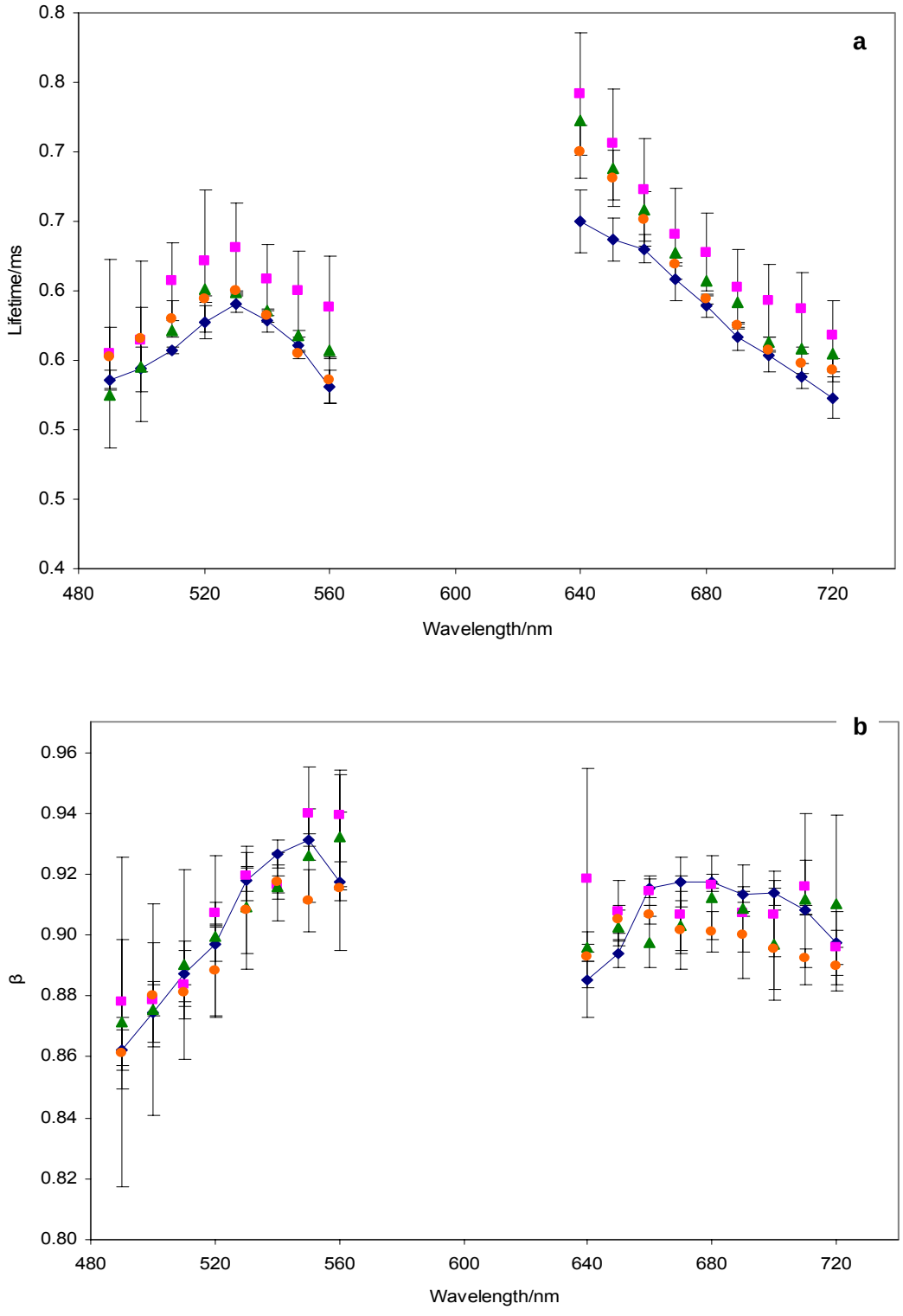

Figure 49: Lifetimes (a) and stretching exponents β (b) from fits to the stretched exponential model of intensity decays of erythrosin B in amorphous sucrose-salt films with a salt/sucrose mole ratio of 0.2:1 collected as a function of excitation wavelength (with 680 nm emission) and emission wavelength (with 530 nm excitation) at 25°C during heating cycle. Data collected from Ery B in sucrose films with various salts (♦, sucrose; ■, sucrose-NaCl; ▲, sucrose-$CaCl_2$; ●, sucrose-$MgCl_2$).

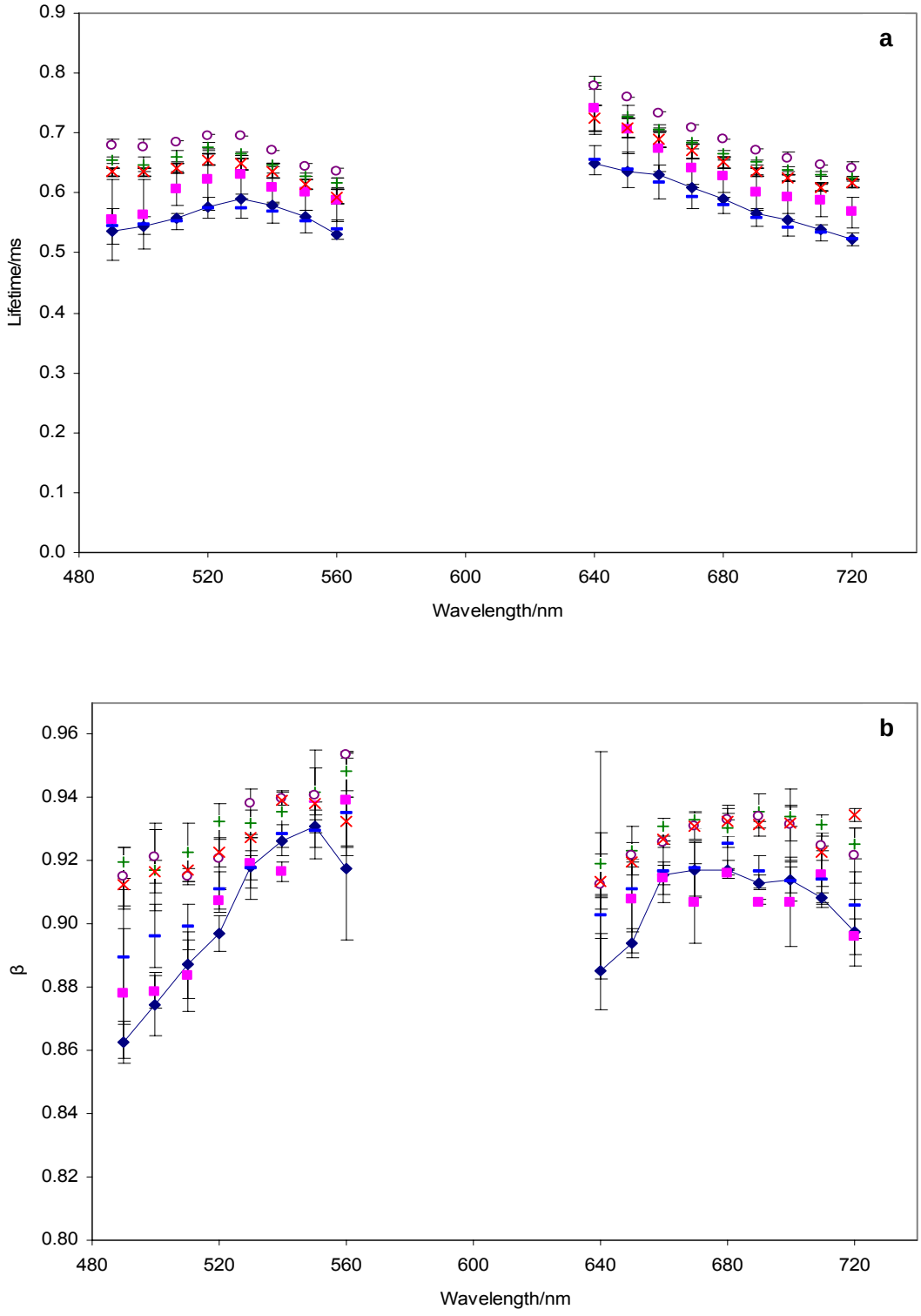

Figure 50: Lifetimes (a) and stretching exponents β (b) from fits to the stretched exponential model of intensity decays of erythrosin B in amorphous sucrose-salt films with a salt/sucrose mole ratio of 0.2:1 collected as a function of excitation wavelength (with 680 nm emission) and emission wavelength (with 530 nm excitation) at 25°C during heating cycle. Data collected from Ery B in sucrose films with various salts (♦, sucrose; ■, sucrose-NaCl; +, sucrose-citrate; ○, sucrose-acetate; –, sucrose-NaH_2PO_4; ×, sucrose-Na_2HPO_4).

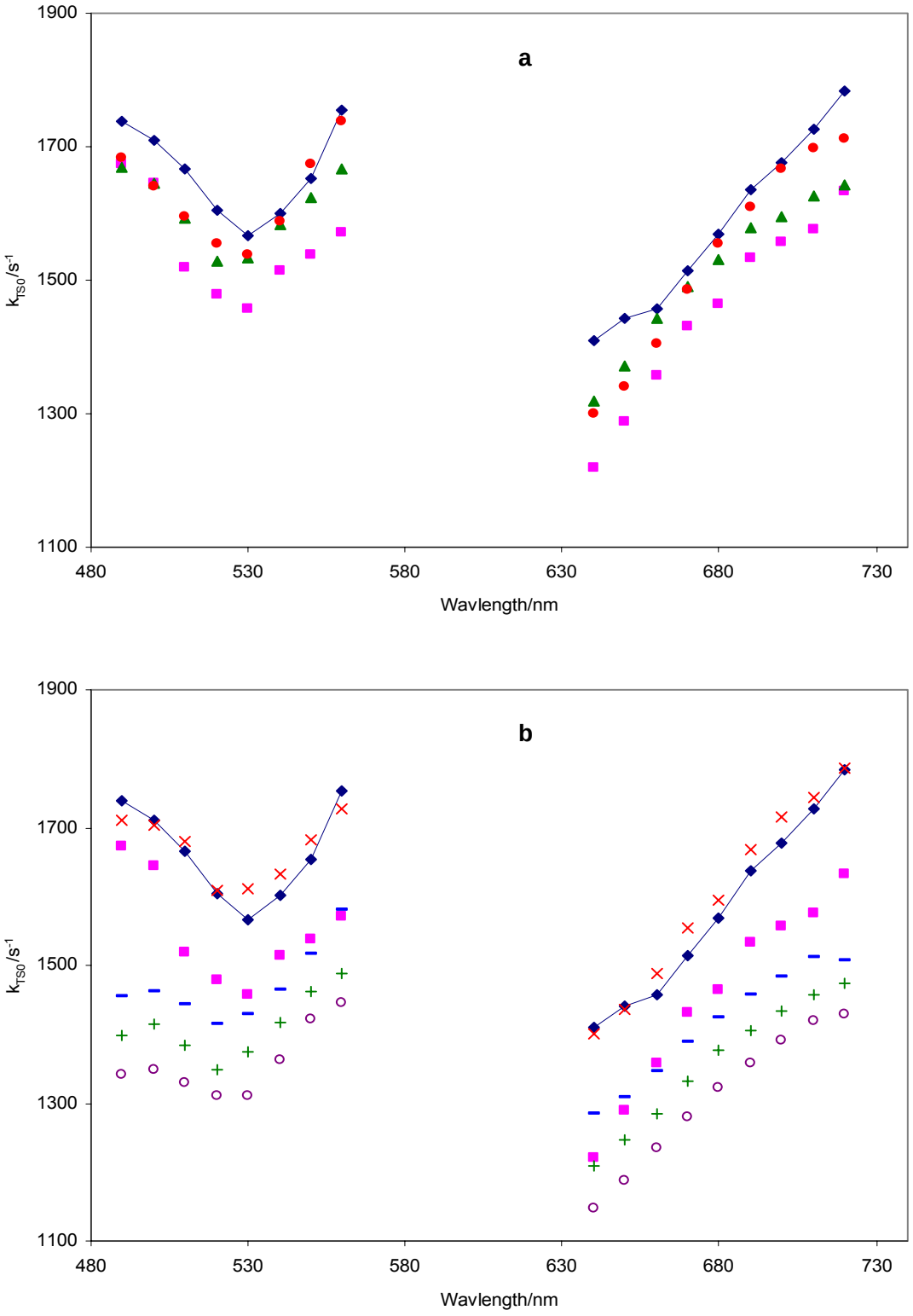

Figure 51: The non-radiative decay rate constant k_{TS0} as a function of excitation wavelength (with 680 nm emission) and emission wavelength (with 530 nm excitation) at 25°C during heating cycle. Data collected from Ery B in sucrose films with various salts ((a); ♦, sucrose; ■, sucrose-NaCl; ▲, sucrose-$CaCl_2$; ●, sucrose-$MgCl_2$; and (b); +, sucrose-citrate; ○, sucrose-acetate; –, sucrose-NaH_2PO_4; ×, sucrose-Na_2HPO_4).

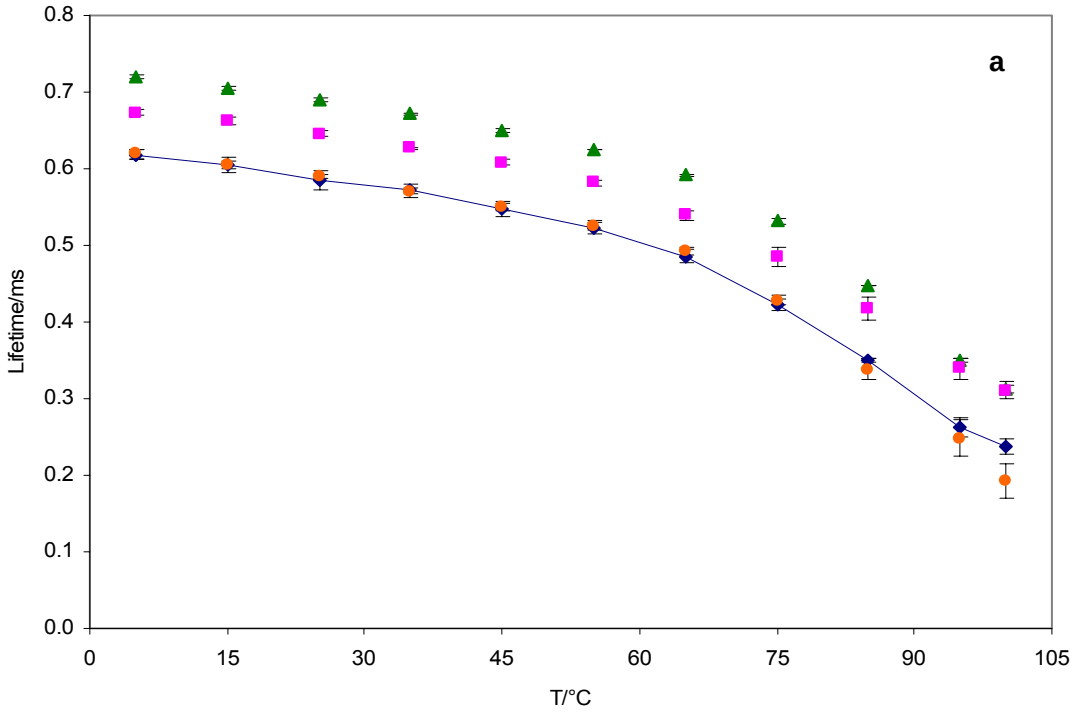

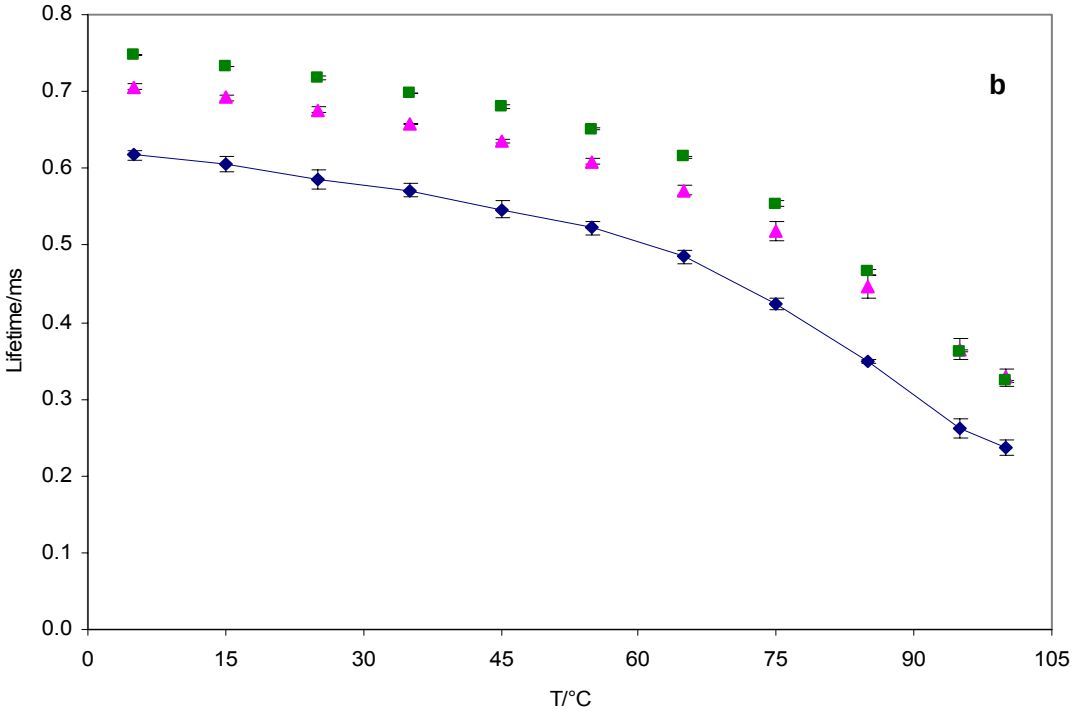

Figure 52a: Phosphorescence lifetime of erythrosin B as a function of temperature in sucrose-salt matrixes (♦, sucrose; ▲, sucrose-acetate; ●, sucrose-NaH_2PO_4; ■, sucrose-NaCl). Figure 52b: Phosphorescence lifetime of erythrosin B as a function of temperature in sucrose-salt matrixes (♦, sucrose; ▲, Na_2HPO_4-sucrose (0.2:1); ■, acetate-sucrose (0.4:1)).

Chapter 6 Maltodextrin effect on molecular mobility of amorphous sucrose from erythrosin B phosphorescence

Introduction

Sucrose glass has been the object of research for many years since it was found to be one of the earliest cryoprotective agents during anhydrobiosis. Its ability to protect biomaterials from freeze-thaw damage and provide long-term storage stability has attracted researchers to investigate the mechanism and develop solid state formulations through spray drying or freeze-drying for labile compounds in foods, such as vitamins and flavor compounds, and for labile biomolecules in pharmaceuticals, such as enzymes, proteins, and antibodies.

Two main mechanisms, glass dynamics and specific interactions, are proposed to understand the role of sucrose in stabilization of sensitive compounds during dehydration and storage (Kets et al., 2004; Chang et al., 2005). The glass dynamics mechanism (Franks et al., 1991; Slade and Levine, 1991) focuses on the rigid, inert matrix formed by vitrification (glass formation) of stabilizers such as sugars. Glass formation is a purely kinetic mechanism, and the stability is expected to correlate to molecular mobility in the rigid matrix. The specific interaction mechanism (Carpenter and Crowe, 1989; Carpenter et al., 1993; Crowe et al., 1993), commonly applied in protein stabilization, states that stabilizers form hydrogen bonds at specific sites with the target compounds, which helps maintain the native structure, keep the spatial integrity of the compound after water is removed, and consequently enhance the stability. Sucrose is an ideal matrix material since it is a good glass former as well as a good hydrogen bond former. However,

compared with other disaccharides such as trehalose, sucrose is considered to have relatively poor physical stability (lower T_g). A combination with other compounds with inherently high T_g such as polysaccharides is suggested to mix with sucrose for better functionalities (Allison et al., 2000; Imamura et al., 2002).

Maltodextrin, defined as a hydrolyzed starch product with dextrose equivalent (DE) less than 20, is a glucose polymer mixture with different polymer lengths and a wide molecular weight distribution. Due to its cold-water solubility, bland taste, and non-hygroscopic nature, commercial maltodextrins are commonly used as spray-drying aids for flavors and seasonings, carriers for synthetic sweeteners, flavor enhancers, fat replacers and bulking agents (Wang and Wang, 2000). Since the "food polymer" concept was introduced by Slade and Levine, maltodextrin has attracted attentions because of its potential applications for stability improvement. Levine and Slade (1986) studied 55 commercial starch hydrolysis products and found that low DE maltodextrins may be used to improve storage stability of frozen foods. Recently maltodextrin has been used in combination with other excipients including sugars, proteins and polysaccharides to protect enzymes (Rossi et al., 1997; Mazzobre et al., 1997; Corveleyn and Remon, 1996), microorganisms (Oldenhof et al., 2005), and encapsulated lipids (Grattard et al., 2002). Maltodextrin was selected mainly due to its high T_g and its ability to act as an osmotically inactive bulking agent (Oldenhof et al., 2005). However, some studies found no correlation between the T_g values and protection during storage. For example, maltodextrin was less effective than small molecules such as trehalose and sucrose in protecting the enzyme EcoRI from inactivation (Rossi et al., 1997) and the T_g of maltodextrin failed to control the rate of lipid oxidation in freeze-dried emulsions

(Grattard et al., 2002). This situation became even more complicated as to maltodextrin with different DE values.

To simplify the complex issue of stabilizing biomaterials, the present study only focused on the properties of the host matrix. Phosphorescence of Ery B was used to investigate how maltodextrin influenced the properties of sucrose matrix by measuring the matrix mobility in amorphous sucrose thin films containing maltodextrin with different DE values (5, 10, 15 and 18). We try to find out whether sucrose-maltodextrin mixtures could exhibit the improved stability. Two concentrations of maltodextrin (10/90 and 50/50 weight ratio of maltodextrin/sucrose) were selected by addition of maltodextrin to the concentrated sucrose solution prior to film formation. The temperature-dependence of mobility was measured and analyzed at different maltodextrin contents and DE values, generating families of mobility versus temperature curves. Comparisons provided information about the mechanisms by which maltodextrin influenced mobility of the amorphous sucrose matrix.

Materials and Methods

1. Preparation of pure sucrose film

We prepared glassy sucrose films by using a slightly modified version of our published method (Pravinata et al., 2005; see details in Materials and Methods in Chapter 1).

2. Preparation of maltodextrin-sucrose film

Corn Maltodextrin products (Maltrin M040, M100, M150 and M180) were obtained as kind gifts from the Grain Processing Corporation (Muscatine, Iowa) and used

without further treatment. The corresponding average dextrose equivalence (DE) was 5, 10, 15 and 18 and theoretical molecular weight was 3600, 1800, 1200 and 1000, respectively. Maltodextrin-sucrose solutions were prepared from sucrose solution containing dye. Maltodextrin powder with different DE values was individually dispersed into a certain amount of water and then mixed with 66% sucrose solution. The mixtures were heated with mild stirring at 60-70°C for 5 min (mixture containing M040 heated in water bath at 80°C for 10 min). The final solid content was adjusted to 65-66% and confirmed by using a refractometer (NSG Precision Cells, Inc., Farmingdale, NY). The final mixtures were checked using a microscope to ensure that maltodextrin granules were completely hydrated and dissolved. Mixture solutions with 10/90 and 50/50 weight ratio of maltodextrin/sucrose were prepared for each maltodextrin product. The procedure to make a glassy film was the same as the procedure to make a pure sucrose film.

3. Preparation of pure maltodextrin film

Maltodextrin powder was dissolved into deionized water and heated to prepare a maltodextrin solution with the final solid content of 65-66%. The procedure to make a glassy film was similar to the procedure to make a maltodextrin-sucrose film.

4. Moisture measurement

Water content in amorphous sucrose and maltodextrin-sucrose films was determined gravimetrically (by difference of mass before and after drying for 24h at 70°C in an Ephortee (Haake Buchler, Inc.) vacuum oven at 1 kPa). Sample films were scrapped from quartz slides and ground into powders in a glove box containing P_2O_5 and Drie-Rite with a relative humidity less than 5%. Pure sucrose films contained 0.56±0.13 wt. %

water. The moisture content in maltodextrin (MD) and sucrose-maltodextrin films was less than 1.5 wt. % (shown in Table 3).

Table 3 Moisture content in maltodextrin (MD) and sucrose-maltodextrin films (wt. %)

MD/S (W/W)	M040	M100	M150	M180
10/90	0.26±0.04	0.35±0.06	0.51±0.03	0.66±0.08
50/50	0.60±0.07	0.54±0.18	1.46±0.14	1.47±0.23
MD	0.93±0.15	1.01±0.07	1.23±0.10	1.35±0.10

5. Estimation of T_g of sucrose-maltodextrin mixtures.

The T_g of sucrose-maltodextrin mixtures can be estimated using equation 1:

$$T_g = \frac{w_1 T_{g1} + k w_2 T_{g2}}{w_1 + k w_2} \quad (1)$$

where T_g, T_{g1} and T_{g2} are the glass transition temperature of the mixture, maltodextrin and sucrose, respectively; w_1 and w_2 are weight fraction of maltodextrin and sucrose, and k is a constant and the average value for sucrose-maltodextrin mixtures was reported as 3 (Roos and Karel, 1991).

6. Luminescence measurements

Luminescence measurements were made using a Cary Eclipse Fluorescence spectrophotometer (Varian Instruments, Walnut Creek, CA). Prior to any phosphorescence measurements, all samples were flushed for at least 15 minutes with nitrogen gas which contained less than 1ppm oxygen to eliminate oxygen quenching. At each target temperature samples were equilibrated for 1min/°C increase in temperature. The temperature was controlled using a thermo-electric temperature controller (Varian Instruments, Walnut Creek, CA). To eliminate moisture condensation during the

measurements below room temperature, dry air was used to flush the chamber surrounding the cuvette holder. All the measurements were made at least in triplicate.

Delayed fluorescence and phosphorescence emission spectra were collected from 520 to 750 nm (10 nm bandwidth) at 1 nm intervals using excitation of 500 nm (20 nm bandwidth) over a temperature range from 5 to 100°C with an observation window of 5.0 ms and an initial delay time of 0.2 ms which suppresses fluorescence coincident with the lamp pulse. Emission spectra from sucrose or sucrose-maltodextrin films without probe were subtracted from each spectrum although the signal of background was very low.

The energy of emission maximum (ν_p) and the full width at half maximum (FWHM) of the emission bands were determined by using log-normal lineshape function (Maroncelli and Fleming, 1987) to fit both delayed fluorescence and phosphorescence.

$$I(\nu) = I_0 \exp\left\{-\ln(2)\left(\frac{\ln[1+2b(\nu-\nu_p)/\Delta]}{b}\right)^2\right\} \quad (2)$$

Where I_0 is the maximum emission intensity, ν_p is the peak frequency (cm^{-1}), Δ is a linewidth parameter and b is an asymmetry parameter. This equation reduces to a Gaussian line width when b=0. The bandwidth (FWHM; Γ) was calculated according to the following equation:

$$\Gamma = \Delta\left(\frac{\sinh(b)}{b}\right) \quad (3)$$

For delayed luminescence spectra collected from 520-750 nm, a sum of log-normal functions for delayed fluorescence ($I_{df}(\nu)$) and phosphorescence ($I_p(\nu)$) was used to fit the spectra. Each emission band was fit to independent fit parameters.

The dipolar relaxation time φ was calculated from the temperature-dependence of the phosphorescence emission peak ν (T) by analyzing the relaxation function:

$$\frac{\Delta\nu}{\Delta\nu_r} = \frac{\nu(T) - \nu_{\max}}{\nu_{\min} - \nu_{\max}} \tag{4}$$

Where ν (T) is the emission peak energy at Temperature T, ν_{min} and ν_{max} are the emission peak energy at the lowest temperature and the highest temperature, respectively. By incorporating a stretched exponential function, the relaxation time can be calculated from the following equation:

$$\frac{\Delta\nu}{\Delta\nu_r} = \frac{\nu(T) - \nu_{\max}}{\nu_{\min} - \nu_{\max}} = \frac{1}{\Gamma(\frac{1}{\beta_l})} \frac{1}{1 + \frac{\beta_e}{\beta_l}\frac{\tau}{\varphi}} \tag{5}$$

Where τ and β_l are the temperature-dependent stretched exponential (Kohlrausch-Williams-Watts) lifetime and stretching exponent (from Eq. 6) describing the phosphorescence intensity decay and Γ(x) in this case is the Gamma function; β_e is assumed to have a value of 0.5.

For lifetime measurements, samples were excited at 530 nm (20 nm bandwidth) and emission transients collected at 680 nm (20 nm bandwidth) over the temperature range from 5 to 100°C. Phosphorescence intensity decays were collected over a window of 5 ms with an initial delay of 0.1 ms and increments of 0.04 ms. Each decay was the average of 20 cycles. Because intensity decays were non-exponential, a stretched exponential, or Kohlrausch-Williams-Watts' decay function was selected to analyze the intensity decay (Richert, 2000; Lee, et al., 2001; Pravinata et al., 2005).

$$I(t) = I_0 \exp(-(t/\tau)^{\beta}) + \text{constant} \tag{6}$$

Where I_0 is the initial amplitude, τ is the stretched exponential lifetime, and β is an exponent varying from 0-1 and characterizing the distribution of lifetimes. The use of a stretched exponential model provides a direct measurement of continuous distribution of lifetimes, which is appropriate for describing a complex glass possessing a distribution of relaxation times for the dynamic molecular processes. The smaller the β value, the more non-exponential the intensity decays and the broader the distribution of lifetimes. Program NFIT (Galveston, TX) was used to fit the decay; goodness of fit was evaluated by examining the χ^2 and R^2. Plots of modified residuals (defined as the difference between the intensity from the fit decay curve and the measured intensity divided by the square root of the measured intensity) was also an indicator of the goodness of fit. R^2 for all fits ranged from 0.99 to 1.00 and modified residuals plots fluctuated randomly around zero amplitude.

Phosphorescence emission lifetimes of Ery B as a function of emission wavelength were measured with excitation wavelength at 530 nm (20 nm bandwidth); emission wavelength varied from 640 to 720 nm (20 nm bandwidth). Phosphorescence emission lifetimes as a function of excitation wavelength were measured with emission wavelength at 680 nm (20 nm bandwidth); excitation wavelength ranged from 490 to 560 nm (20 nm bandwidth). The experiments were performed at 25°C.

7. Photophysical scheme

Our analysis of the delayed emission is similar to the photophysical scheme for erythrosin B outlined by Duchowicz et al. (1998). The measured emission rate for phosphorescence (k_P) is the sum of all possible deexcitation rates for the triplet state T_1:

$$\tau^{-1} = k_P = k_{RP} + k_{TS1} + k_{TS0} + k_Q[Q] \qquad (7)$$

In this equation, k_{RP} is the rate of radiative emission to the ground state S_0. For erythrosin B, k_{RP} is 41 s^{-1} and constant with temperature (Duchowicz et al., 1998).

k_{TS1} is the rate of thermally activated reverse intersystem crossing from the triplet state T_1 to the singlet state S_1, and the value can be estimated from the Arrhenius equation:

$$k_{TS1}(T) = k^0_{TS1} \exp(-\Delta E_{TS}/RT) \quad (8)$$

where k^0_{TS1} is the maximum rate of intersystem crossing from T_1 to S_1 at high temperature, ΔE_{TS} is the energy gap between T_1 and S_1, R=8.314 J K^{-1} mol^{-1}, and T is the temperature in Kelvin. The value of ΔE_{TS} is calculated from the slope of a Van't Hoff plot of the natural logarithm of the ratio of intensity of delayed fluorescence (I_{DF}) to phosphorescence (I_P):

$$d[\ln(I_{DF}/I_P)]/d(1/T) = -\Delta E_{TS}/R \quad (9)$$

where I_{DF} and I_P are the maximum intensity values determined from analysis of the emission band using Eq. (2). The value of k_{TS1} at 25°C was estimated as 88 s^{-1} using k^0_{TS1}=3.0 x 10^7 s^{-1} and ΔE_{TS} = 31.56 kJ/mol (Pravinata et al., 2005).

In the presence of oxygen, the quenching rate $k_Q[Q]$ is the product of rate constant k_Q and the oxygen concentration [Q]. By flushing nitrogen throughout the measurements we assume that no oxygen quenching occurred. One of the non-radiative decay routes is through intersystem crossing to the ground state S_0. The decay rate is expressed by k_{TS0}, which reflects the rate of collisional quenching of the probe due to both internal and external factors (Papp and Vanderkooi, 1989). We assume that the term k_{TS0} primarily reflects the external environmental factors since the self collisional quenching among

probe molecules can be neglected within the extremely viscous amorphous solid. In this study, temperature-dependent term k_{TS0} can be calculated by difference from Eq. (7).

Results

At a probe/sucrose molar ratio of $1:10^4$, each probe is on average surrounded by a matrix shell around 10-11 sucrose molecules thick. At this concentration Ery B dispersed within the sucrose matrix does not aggregate and thus reports the physical properties of the unperturbed sucrose matrix (You and Ludescher, 2006). Similar behaviors is expected in sucrose-maltodextrin mixtures.

1. T_g of sucrose-maltodextrin films

Due to the small mass of sample deposited on a slide (2-4 mg) it was very difficult to directly measure the glass transition temperature (T_g) of films. The T_g values can be calculated based on the composition using Eq.1. Because of the small moisture content, the water influence was not considered in the calculation. The glass transition temperatures of maltodextrins and sucrose-maltodextrin mixtures are shown in Table 4. Maltodextrin itself is a mixture and the T_g of maltodextrin varies depending on its composition, DE value, average molecular weight, molecular weight distribution and moisture. Generally maltodextrin with low DE has high average molecular weight and correspondingly high T_g. Moisture depresses the T_g, shown as a plasticization effect. A molecular weight distribution usually results in a wide glass transition temperature range. Recently it was suggested to be a more accurate tool to predict the properties of maltodextrin rather than the T_g (Avaltroni et al., 2004). The calculated T_g values thus may be underestimated due to all the complications mentioned above. However, they

were useful in better understanding the properties of maltodextrin related to its physical state.

Table 4. T_gs of maltodextrins (MD) and sucrose-maltodextrin films (°C)

MD/Sucrose	MD*	10/90[c]	50/50[d]	0/100 (sucrose)
M040	188 (160)	66.5	93.5	62
M100	160 (133)	65.5	86.5	62
M150	152[a] (125)	65.2	84.5	62
M180	146[b] (120)	65.0	83.0	62

* Data from Roos and Karel (1991); the data in parentheses are estimated from the moisture dependence of the T_g and used as the T_gs of maltodextrin films in our data analysis.

[a, b] estimated from the molecular weight dependence of the T_g (Roos and Karel, 1991).

[c, d] calculated using Eq.1 with k = 3 (Roos and Karel, 1991).

2. Delayed emission spectra

The delayed emission spectra of erythrosin B dispersed in amorphous sucrose films with various maltodextrin/sucrose weight ratios were collected over the temperature range from 5 to 100°C. All spectra (data not shown) showed the expected decrease in phosphorescence and increase in delayed fluorescence intensity with increasing temperature seen in xanthene dyes (Parker, 1968). Both the delayed fluorescence and phosphorescence bands shifted to longer wavelength at higher temperature; the peak frequency (ν_p) and bandwidth (Γ) were determined by fitting to a log-normal lineshape function (Eq. 2 and 3). The temperature effect on frequency and bandwidth for phosphorescence emission are plotted in Figure 53 and Figure 54 versus T- T_g to emphasize their dependence on the physical state of the films. The peak frequency for delayed fluorescence exhibited similar thermal behavior (data not shown).

The phosphorescence peak frequency provides a measure of the average energy of emission; a decrease in emission energy reflects an increase in the average extent of

dipolar relaxation around the excited triplet state prior to emission (Lakowicz, 1999). The peak frequency decreased gradually and approximately linearly with temperature below T_g and much more steeply at T_g in the sucrose film. In pure maltodextrin films the peak frequency was much lower than that in sucrose and increased with increasing maltodextrin DE values. The peak frequency decreased more monotonically in maltodextrin than in sucrose film. The curves of the sucrose-maltodextrin mixed films were in between the pure sucrose and the pure maltodextrin curves. The peak frequency increased with increasing sucrose content and this effect was more significant in films containing low DE than high DE maltodextrin. For instance, at T- T_g = -60°C, the peak frequency occurred at 14586 cm^{-1} in the 50/50 sucrose-M040 and 14632 cm^{-1} in the 50/50 sucrose-M100 film, that is, the emission correspondingly blue shifted ~17 nm and ~10 nm, respectively, compared to pure M040 and M100 film. In films containing M150 and M180 at the same ratio, the value was 14584 cm^{-1} (blue shift 7 nm) and 14567 cm^{-1} (4 nm), respectively. With further increasing sucrose content, the value of the peak frequency became close to that in pure sucrose.

The change in peak frequency ($\Delta\nu_p$) with changing in temperature varied with maltodextrin content and maltodextrin DE value. Compared with sucrose (~340 cm^{-1}), the change in peak frequency from 5 to 100°C was much smaller in maltodextrins (~190 cm^{-1}). The $\Delta\nu_p$ was slightly smaller in 10/90 films (~320 cm^{-1}) and much smaller in 50/50 films (~190 cm^{-1}) than in sucrose. The maltodextrin DE value had less influence on the $\Delta\nu_p$ at low (10/90) but more influence at high maltodextrin content (50/50). Compared with other maltodextrins, a relatively strong effect (275 cm^{-1}) was seen in 10/90 and a relatively weak effect (210 cm^{-1}) in 50/50 sucrose-M180 film. The peak frequency

difference reflects the corresponding change in average extent of dipolar relaxation around the excited triplet state over this temperature range.

The phosphorescence bandwidth provides a measure of the range of energetically distinct matrix environments seen by the Ery B probe within the amorphous matrix (Lakowicz, 1999). The bandwidth was essentially constant at ~1600 cm^{-1} at low temperature and increased gradually with temperature in the glass and more dramatically in the melt above T_g in sucrose film. The curves of bandwidth in maltodextrin films with various DE values merged with the sucrose curve at low temperatures. The maltodextrin films did not show the obvious biphasic behavior of sucrose but tended to show upward curvature at temperatures below their T_gs (Figure 54a). Probably due to their high T_g values, maltodextrin films examined in the temperature range from 5 to ~ 80°C existed in the glassy state and the curves mainly reflected the glassy behavior. In the sucrose-maltodextrin films the bandwidth curves changed depending on the maltodextrin content. At 50/50 weight ratio, the bandwidth curves were slightly above the sucrose curve in M040 and M100 films but slightly below the sucrose curve in M150 and M180 films. However the curves in all 10/90 films were slightly below sucrose. The overall influence of DE on the bandwidth was not significant in maltodextrin and 10/90 sucrose-maltodextrin films, but in 50/50 films the bandwidth seemed to be larger at low and smaller at high DE, indicating that the environmental energetic heterogeneity increased in films containing low DE maltodextrins but insignificantly decreased in films containing high DE maltodextrins at the equivalent temperature.

The intensity ratio (ln (I_{df}/I_p)) was plotted as a van't Hoff plot versus 1/T and the slope obtained from the linear plot can be used to estimate the energy gap between the

triplet and singlet states (Eq. 9 in Materials and Methods). In amorphous sucrose the value of ΔE_{TS} is 31.56±0.56 kJ mol^{-1}. The singlet-triplet energy gap ΔE_{TS} ($S_1 \leftarrow T_1$) was slightly higher in maltodextrin films than in sucrose film, increasing by 8% in M040 and 7% in the other maltodextrins. The energy gap ΔE_{TS} does not change significantly with addition of maltodextrin in 10/90 (increase by 2~3%) and 50/50 films (increased by 4~5%). The values ΔE_{TS} in maltodextrin and sucrose-maltodextrin films are shown in Table 5.

Table 5 The energy gap between triplet and singlet state ΔE_{TS} in maltodextrin (MD) and sucrose-maltodextrin films (kJ/mol)

MD/S (W/W)	M040	M100	M150	M180
10/90	32.21±0.32	32.52±0.34	32.84±0.23	32.73±0.06
50/50	33.26±0.13	32.88±0.42	33.02±0.12	32.99±0.03
MD	34.19±0.09	33.64±0.16	33.75±0.11	33.88±0.32

The dipolar relaxation rates for the sucrose and sucrose-maltodextrin films were estimated from the peak frequency data of Figure 53 as described in Materials and Methods (Eq. 5, using the lifetime data of Figure 56); these rates are plotted in an Arrhenius fashion in Figure 55 as log(1/φ) versus inverse temperature normalized to the glass transition temperature (T_g/T). These curves showed upward curvature at high temperatures indicating the increased activation energy with increasing temperature. The overall trend at each equivalent temperature was an increase in the relaxation rate with an increase in maltodextrin content and this effect was more significant in films containing low DE maltodextrins.

Figures 62 to 64 clearly showed the maltodextrin concentration effect on the emission energy, bandwidth and dipolar relaxation rate in each sucrose-maltodextrin film.

3. Phosphorescence decay kinetics

The phosphorescence intensity decays in sucrose-maltodextrin glass with different maltodextrin DEs were measured over the temperature range from 5-100ºC. All decays were well fit using the stretched exponential decay model (Eq. 6) used to fit comparable data for Ery B in a variety of amorphous sugar and protein matrixes. The stretched exponential lifetime and exponent β are plotted in Figures 56 and 57, as a function of T-T_g. The lifetimes decreased biphasically with increasing temperature in sucrose film, exhibiting a gradual linear decrease at low and a more dramatic decrease at high temperature. The lifetime in maltodextrin films was much smaller than that in sucrose and decreased with temperature more linearly in comparison with sucrose. The lifetime increased with increasing sucrose content in the films. At 10/90 weight ratio the lifetime in sucrose-maltodextrin was similar to sucrose. The stretching exponent β in sucrose film remained constant at ~0.92 below and slightly above T_g and decreased dramatically to a low of ~0.86 at temperatures significantly above T_g. Comparably the values of β in maltodextrin films were smaller than in sucrose. β in sucrose-maltodextrin increased with increasing sucrose content: the curves were slightly below the sucrose at 50/50 but slightly above the sucrose curve at 10/90 ratio. DE had significant influence on both lifetime and β; however this effect declined with increasing sucrose content. The difference in both lifetime and β due to DE values became insignificant in 10/90 sucrose-maltodextrin films.

The decrease in lifetime with temperature reflects an increase in the rate of non-radiative decay of the excited triplet state T_1 due to an increase in both the rate of non-radiative decay to the ground state S_0 (k_{TS0}) and reverse intersystem crossing to S_1 (k_{TS1}).

Based on the maximum physically reasonable value of k_{TS1} (Pravinata et al., 2005), an estimate of the lower limit of k_{TS0} was calculated from Eq. 10 (Materials and Methods) and it is plotted as $\ln(k_{TS0})$ versus T_g/T in Figure 58. The non-radiative quenching rate k_{TS0} in sucrose increased linearly at low temperature and shot up at high temperature, which indicated that this rate is sensitive to the molecular mobility (α relaxations) activated at the sucrose glass transition. The quenching rate k_{TS0} curves in maltodextrin films also increased linearly at low temperature but with larger magnitude and more negative slope, suggesting more mobile environment in amorphous maltodextrin solids. With addition of sucrose, the quenching rate was significantly repressed in 50/50 and 10/90 films; and the quenching rate was reduced with increasing sucrose content. The quenching rate in maltodextrin films increased in an order of M180≈M150<M100<M040. The maltodextrin with low DE tended to have a greater effect on sucrose with higher contents while the maltodextrin with high DE showed relatively strong effect at lower levels.

Lifetime, β, and k_{TS0} in films containing maltodextrin with each DE value varied with maltodextrin concentration, as shown in Figures 65 to 67, respectively.

4. Spectral heterogeneity

Phosphorescence intensity decays of Ery B in sucrose films with different maltodextrin contents were measured as a function of excitation and emission wavelength at 25°C. All decays were well analyzed using a stretched exponential model; lifetimes are plotted versus excitation and emission wavelength in Figure 59. All lifetime curves showed the similar trend: lifetimes decreased with increasing wavelength across the emission band. The values of the lifetime were smaller in maltodextrin than in sucrose

and decreased in the order M180≈M150>M100>M040. The variations in lifetime in maltodextrin films, however, were slightly larger than in sucrose. The lifetime and lifetime variation in 50/50 films showed similar results to pure sucrose. However, the difference among the films with different maltodextrin DE was greatly reduced. When sucrose content increased to the ratio of 10/90, lifetime variation kept constant but lifetime showed different response depending on DE values: lifetime curves were above sucrose in the low DE and below in the high DE maltodextrin-sucrose films. Lifetimes also varied across the excitation band: lifetimes increased with increasing wavelength to a maximum at 530 nm and then decreased at higher wavelengths. The variation of lifetime within the excitation band showed similar trends as within the emission band.

The stretching exponent β also varied as a function of both excitation and emission wavelength (Figure 60). In all films β values were lower at the blue edges in both emission and excitation bands, increased with increasing wavelength to a maximum at 670-680 nm across the emission band and a maximum at 540-550 nm across the excitation band, then decreased slightly at the red edges. The variations of β across the emission band in maltodextrin and sucrose-maltodextrin films were slightly smaller or very close to those in the sucrose film while the values varied depending on the content. In maltodextrin and 50/50 sucrose-maltodextrin films β was lower than sucrose; however, β were slightly higher in 10/90 films.

The calculated quenching rate k_{TS0} is plotted versus emission and excitation wavelength at various maltodextrin contents in Figure 61. k_{TS0} increased approximately monotonically with increasing emission wavelength in all the films. k_{TS0} in maltodextrin films was greater than that seen in pure sucrose and the variation of k_{TS0} was larger than

in sucrose. The variation in 50/50 films was slightly larger than in sucrose while in 10/90 films the variation was similar to sucrose. Across the excitation band, k_{TS0} curves showed minimum values around 530 nm with higher values at both blue and red edge of the excitation band in all sucrose and sucrose-maltodextrin films. The quenching rate decreased with increasing sucrose content but was still higher than that in pure sucrose.

The maltodextrin concentration effect on lifetime, β and k_{TS0} was also clearly illustrated in Figures 68 to 70, respectively.

Discussion

Phosphorescence emission energy and intensity from Ery B is sensitive to two distinct modes of molecular mobility in amorphous biomaterials: matrix dipolar relaxation around the excited T_1 triplet state prior to emission that decreases the energy of the triplet state and thus lowers the emission energy and matrix collisions that promote intersystem crossing from the excited T_1 triplet state to the ground S_0 singlet state that increase k_{TS0} and thus lower the lifetime. This study of matrix mobility in amorphous sucrose using Ery B phosphorescence indicates that both of these modes of molecular mobility are modulated in both a complex concentration-dependent and DE-dependent manner by maltodextrin.

This study actually observed two distinct effects of maltodextrin on the sucrose matrix mobility. Under most conditions of temperature and concentration maltodextrin with different DE values caused a systematic and in some cases dramatic increase in the rate and extent of both modes of matrix molecular mobility although maltodextrins have higher T_gs. This clearly indicated that there was no clear-cut relationship between the

glass transition temperature T_g and molecular mobility; that is, higher T_g does not necessarily mean lower mobility and thus greater stability. T_g only reflects the temperature range in which the matrix remains its glassy state and cannot act as an index temperature of mobility and stability. Our results (including those from other chapters, such as sucrose-glycerol, sucrose-gelatin, etc.) suggested that more accurate parameters are needed to reflect the physical properties in the glassy matrixes. Both concentration and DE value of maltodextrin influenced the mobility of the sucrose matrix. At low concentration maltodextrin had an insignificant effect on the rates of both modes of matrix molecular mobility and on dynamic site heterogeneity; however, at high concentration, maltodextrin caused an obvious increase in the matrix mobility as well as site heterogeneity. Maltodextrins with different DE values displayed different behaviors depending on their concentrations.

1. Effect of maltodextrin on mobility of amorphous sucrose

Our estimate of the extent to which maltodextrin influences different modes of matrix mobility is based on the behavior of spectroscopic parameters plotted versus temperature normalized to T_g. If maltodextrin modulates matrix mobility solely by increasing the matrix T_g (that is, to strengthen/stabilize the glassy matrix) then mobility curves at different maltodextrin content or DE would be identical on a plot of $T-T_g$ or, where appropriate, T_g/T. If, however, maltodextrin affects matrix mobility in other, more specific ways, then these curves need not be identical; more relevant to this analysis, if such curves are systematically displaced from one another, then maltodextrin must be modulating mobility in specific ways beyond a mere change in T_g.

1.1. Effect of maltodextrin concentration on mobility of amorphous sucrose

The phosphorescence emission energy reflects the average $T_1 \leftarrow S_0$ energy gap; it is primarily modulated by the T_1 energy and thus by the average extent of relaxation of dipolar hydroxyl groups around the excited T_1 state prior to emission. Plots of the Ery B emission energy versus $T-T_g$ were nearly superimposable in the various sucrose-maltodextrin mixtures at low maltodextrin content (10/90) (Figure 53c). At high maltodextrin content (50/50) the plots shifted to lower energy to some extent but had similar shape. Since the temperature normalized curves are similar, it appears that maltodextrin affects the extent of dipolar relaxation in the sucrose matrix primarily by increasing T_g, that is, through a typical stabilizing effect. Since the curves are not identical, however, other, secondary, effects appear also to be working. The secondary effects were insignificant at low maltodextrin concentration but became more dramatic at high maltodextrin concentration.

Arrhenius analysis of the rate of dipolar relaxation calculated from these peak frequency data, when normalized to T_g (that is, plotted versus T_g/T), generated superimposable curves in films with 10/90 weight ratio and parallel but non-superimposable curves in films with 50/50 weight ratio of maltodextrin/sucrose (Figures 55b and 55c). The dipolar relaxation rate $1/\varphi$ increased in the glass below T_g and more sharply in the melt above T_g in both maltodextrin-containing and pure sucrose films. The superimposable curves for films with 10/90 weight ratio of maltodextrin/sucrose indicates that the dipolar relaxation rate measurement also provides additional evidence that maltodextrin primarily stabilizes the matrix by increasing the T_g. The parallel curves in films with 50/50 weight ratio supports the claim that maltodextrin primarily affects the rate of dipolar relaxation by modulating T_g. The curves, however, were also

systematically shifted to higher relaxation rate with increasing maltodextrin content. This ~4-fold increase in rate in films with 50/50 weight ratio of maltodextrin/sucrose provides evidence that maltodextrin also has a secondary effect on the dipolar relaxation rate at high maltodextrin level.

The emission intensity and the lifetime are directly modulated by the rate of radiative emission k_{RP}, of reverse intersystem crossing to the excited triplet state k_{TS1} and of intersystem crossing to the ground state k_{TS0}. The rate of intersystem crossing k_{TS0}, which is modulated by the physical state of the amorphous matrix, reflects both the manner in which the excited T_1 state is vibrational coupled to the S_0 ground state as well as the manner in which the ground state vibrational energy can dissipate from the excited probe into the surrounding matrix. Since the efficiency of this vibrational dissipation is related to the overall mobility of the matrix, k_{TS0} provides a direct measure of matrix mobility. Arrhenius plots of k_{TS0} in films with 10/90 weight ratio of maltodextrin/sucrose were essentially identical when plotted versus T_g/T, again providing strong evidence that the rate k_{TS0} also scaled with T_g and thus was effectively stabilized by maltodextrin. The plots of k_{TS0} in films with 50/50 weight ratio maltodextrin/sucrose were shifted to higher values, indicating that additional effects may exist at high maltodextrin content in addition to the primary effect on T_g.

These results thus indicate that both dipolar relaxation and collisional quenching in amorphous sucrose primarily reflect the effect of maltodextrin on T_g, providing direct evidence that these modes of molecular mobility are directly influenced by maltodextrin. However, data at higher maltodextrin content indicates that maltodextrin also has a secondary effect by increasing the rate of dipolar relaxation and collisional quenching.

These two effects in effect lead to opposite behaviors and are dependent on the content of maltodextrin. At low maltodextrin concentration, both effects are not significant and the overall effect is not obvious. The behavior in sucrose-maltodextrin films is thus similar to pure sucrose. The two effects become stronger with increasing maltodextrin content, especially the promoting effect on the mobility. The enhanced matrix mobility is a result of the competition between these two effects.

1.2. Effect of maltodextrin DE on mobility of amorphous sucrose

For each maltodextrin product, DE is an average value of a certain range. Within these ranges, the maltodextrin with a small shift in DE will not show significant differences in functionality and thus show insignificant effect on sucrose film. In pure maltodextrin films with DE value of 5, 10, 15 and 18 the T_g increased in the order M180<M150<M100<M040 (See Table 2). The matrix mobility, however, increased in the same order. Thus maltodextrin matrixes with higher T_g had higher mobility!

All the parameters discussed above, emission energy, dipolar relaxation and collisional quenching, were compared on a temperature scale normalized to T_g at various DE values. At low weight ratio of maltodextrin/sucrose (10/90), high DE maltodextrin had a larger influence than low DE maltodextrin: higher DE maltodextrin had lower emission energy, higher dipolar relaxation rate and higher collisional quenching rate. At low maltodextrin level, the DE effect has a minor influence on the properties of sucrose. At high maltodextrin/sucrose weight ratio (50/50), however, low DE maltodextrin had a larger influence than high DE maltodextrin. Since these normalized T_g curves are similar, it appears that maltodextrin DE affects the sucrose matrix primarily by modulating T_g,

that is, through a typical stabilization effect. Since the curves are not identical, however, other, secondary, effects appear also to be operating.

1.2. Mobility of 'pure' maltodextrin films

'Pure' maltodextrin films have higher molecular mobility than sucrose, following the rank order M040>M100>M150≥ M180>sucrose. These results appeared to be in conflict with the general viewpoint that systems with higher T_gs are supposed to have lower molecular mobility. However, our results are in agreement with the work of some researchers. Duddu et al. (1997) found that a sucrose formulation at temperatures below 12°C displayed lower mobility than trehalose which has a higher T_g. They attributed the abnormality to differences in the fragilities of glass-forming materials. Rossi et al. (1997) reported that maltodextrin (DE10) and PVP provided less effective protection for the enzyme EcoRI from inactivation during storage at 37 and 45°C than trehalose and sucrose although maltodextrin and PVP have significantly higher T_gs than trehalose and sucrose.

The variance in mobility among the maltodextrins with different DE value could be explained by variation in the packing of the matrix. Maltodextrin is a complex mixture, consisting of small molecules such as mono-, di- and oligosaccharides as well as bigger polysaccharides. The heterogeneous nature and molecular polydispersity of maltodextrin lead to a wide distribution of molecular weight. The molecular weight of the polymers is believed to control the molecular packing occurring upon vitrification (Bartos and Kristiak, 1998; Li et al., 1999). Compared with homogeneous small molecules (sucrose), maltodextrin molecules are expected to pack more loosely owing to the steric constraints from various irregular molecular structures including both linear and

branched forms. The maltodextrins with low DE and high proportion of high-Mw components are predictably packed more loosely than maltodextrins with high DE and thus a small proportion of high-Mw components due to weak dipolar interactions (Grattard et al., 2002). Samuhasaneetoo et al. (2006) also found that low DE maltodextrin had a high proportion of microvoids compared to high DE maltodextrin. Based on their compositions, four maltodextrins are expected to form a glass structure with an increased order of packing: M040<M100<M150≤ M180<sucrose. The loosely packed structures facilitate molecular motions in both the glassy and the rubbery state.

With respect to M150 and M180, no apparent difference in any parameter was observed either in the 'pure' maltodextrin films or in the sucrose-maltodextrin films. This may be due to the similar nature of these two matrixes. DE value is only an average concept to evaluate the content of reducing-end groups. It cannot reflect the real distribution of molecular weight. Based on their T_gs (see Table 2; Roos and Karel, 1991) and polydispersity information provided by the manufacture, M150 and M180 have similar properties and thus have parallel influence on amorphous sucrose.

2. Influence of maltodextrin on the dynamic site heterogeneity

The Ery B phosphorescence emission bandwidth Γ, the intensity decay stretching exponent β, and variations in lifetime (due to variations in k_{TS0}) and β across the excitation and emission bands all provide information about matrix heterogeneity. Supercooled liquids and amorphous polymers are dynamically heterogeneous both on spatial and temporal scales reported by a variety of spectroscopic techniques (Ediger, 2000; Richert, 2002). This physical model is supported by more evidence from erythrosin B phosphorescence. Spectral heterogeneity in Ery B phosphorescence is observed in

amorphous sugars and sugar alcohols (Pravinata, et al., 2005; Shirke and Ludescher, 2005; Shirke et al., 2006), and proteins (Nack and Ludescher, 2006; Lukasik and Ludescher, 2006), indicating that dynamic site heterogeneity may be a characteristic feature of amorphous food materials and biomaterials.

The variation of lifetime with emission energy reflects variation in one or more of the rate constants for deexcitation of the triplet state. In amorphous sucrose matrix, the population of probes is distributed among dynamically distinct sites with varied dipolar relaxation rate (and thus emission energy) and matrix quenching rate (Pravinata et al., 2005). Pravinata et al. proposed a physical model for the origin of this site heterogeneity on the basis of emission energy and matrix quenching rate in which probes in local environments with less constrained packing have higher overall molecular mobility and thus shorter lifetime and have lower emission energy due to fast dipolar relaxation. The site heterogeneity of sucrose-maltodextrin films reported from phosphorescence of Ery B provides another aspect of the maltodextrin influence at the molecular level.

2.1. Effect of maltodextrin concentration on site heterogeneity

The curves for bandwidth Γ (FWHM) in all films merged at temperatures well below the individual T_gs (Figures 54 and 63). The emission bandwidth Γ was almost identical at constant $T-T_g$ in films at low concentration of maltodextrin (10/90). At high maltodextrin content (50/50), these curves diverged and the magnitudes were higher than that those in sucrose when temperature increased ~ 0-20°C below T_g. Since the emission bandwidth provides a direct measure of the width of the distribution of energetically distinct matrix sites, maltodextrin causes a concentration-dependent change in the energetic heterogeneity of the sucrose matrix.

The stretching exponent β provides a nonlinear measure of the width of the lifetime distribution required to fit an emission decay transient, a value of 1 indicating an infinitely narrow distribution (a single lifetime) and lower values indicating significantly broader lifetime distributions. Since the lifetime distribution varies due to variations in k_{TS0}, the magnitude of β thus provides another indicator of dynamic matrix heterogeneity. The stretching exponent β in all maltodextrin-containing films was comparable to or lower than that in pure sucrose (Figure 66), indicating that maltodextrin increased the matrix dynamic heterogeneity at high concentration (50/50) but had no apparent influence at low concentration (10/90). β in sucrose decreased dramatically at temperature above T_g, indicating a high degree of dynamic heterogeneity within the melt. However, a smaller decrease in β was seen in films with high maltodextrin content, suggesting less temperature dependence of heterogeneity in the presence of maltodextrin.

The variation in lifetime (and thus k_{TS0}) across the excitation and emission bands provides an indicator of dynamic heterogeneity. The wavelength variation of k_{TS0} increased slightly over that in pure sucrose in sucrose films with increasing maltodextrin/sucrose ratio (Figure 70). The variation in k_{TS0} with wavelength also decreased at higher temperature (data not shown) suggesting that spectral heterogeneity also decreased in the melt. Since the variation of k_{TS0} with wavelength reflects the presence of a broad continuum of local matrix sites that vary in terms of their overall molecular mobility, maltodextrin appears to slightly increase the variation across this continuum at low temperature.

2.2. Effect of maltodextrin DE on site heterogeneity

The curves for bandwidth Γ (FWHM) in films with different DE values at low maltodextrin/sucrose weight ratio were almost superimposable and slightly below the curve in pure sucrose (Figure 54c), indicating a minor decrease in the width of the distribution of energetically distinct matrix sites. As the maltodextrin content increased to 50/50, the curves for bandwidth in films with low DE maltodextrin were above while the curves with high DE maltodextrin were slightly below the curve in pure sucrose (Figure 54b). Maltodextrins with low DE appear to influence the sucrose matrix more effectively than those with high DE. Low DE maltodextrin containing many larger molecules increased while high DE maltodextrin containing few larger molecules but more medium and/or small molecules decreased site heterogeneity in sucrose.

The stretching exponent β in films with various DE values at low maltodextrin content increased compared with sucrose (Figure 57c). At high content, however, β in films with low DE maltodextrin was smaller while β in films with high DE maltodextrin was comparable to that of sucrose, indicating that maltodextrin with low DE increased the matrix dynamic heterogeneity but high DE maltodextrin did not.

The variation in lifetime (and thus k_{TS0}) across the excitation and emission bands provides similar information about dynamic heterogeneity. The wavelength variation of k_{TS0} was similar to that in pure sucrose at 10/90 weight ratio of maltodextrin/sucrose (Figure 59c). In films with 50/50 maltodextrin/sucrose weight ratio the variation of k_{TS0} with wavelength increased slightly at high DE and more dramatically at low DE (M040 and M100) (Figure 59b).

In general, both DE value and maltodextrin concentration modulate the site heterogeneity of sucrose matrix. The influence is negligible at low maltodextrin

concentration; however, apparent changes were observable at high maltodextrin concentration. Maltodextrins with low DE increase the dynamic site heterogeneity more effectively than maltodextrins with high DE. The spectral heterogeneity affected by high DE maltodextrins is less concentration dependent than by low DE maltodextrins. This can be explained by the composition of maltodextrin. Low DE maltodextrin is more loosely packed due to its high fraction of high-molecular-weight species. At low content, small molecule sucrose can fit in the microvoids produced in maltodextrin molecules and may not significantly influence the heterogeneity of matrix. At 50/50 weight ratio, the molecular polydispersity and loose packing in low DE maltodextrins became predominant and thus decreased the homogeneity. High DE maltodextrin has smaller molecules that pack more easily to form a denser matrix. However, sucrose may not fit as well in the low DE maltodextrins. As a result, the heterogeneity does not change or even tends to increase at low concentration. With increasing high DE maltodextrin content, the heterogeneity increased but not as much as in low DE maltodextrin due to the comparably smaller molecular structure.

2.3. Dynamic site heterogeneity in 'pure' maltodextrin films

The emission bandwidth Γ increased continuously with increasing temperature in pure sucrose while in 'pure' maltodextrin films Γ was essentially constant over a broad temperature range and increased at a temperature ~ 50-60°C below T_g. The curves of all the films were nearly superimposable at very low temperature and then showed sudden increase at different temperatures.

Similar behavior was observed in the curves for the stretched exponent β versus temperature. B was nearly constant over a broad temperature range in 'pure' maltodextrin films with smaller magnitude than in pure sucrose.

The variations in collisional quenching rate constant k_{TS0} with emission wavelength at 25°C (Figure 61) showed similar results, suggesting an increased heterogeneity in 'pure' maltodextrin films. Variations in the exponent β (Figure 60b) were almost the same in high DE maltodextrin but slightly higher in low DE maltodextrin films.

All the spectroscopic characteristics seemed to show that 'pure' maltodextrin films were more dynamically heterogeneous than sucrose, perhaps resulting from composition variety as well as site heterogeneity. The low DE maltodextrin film was more heterogeneous than the high DE maltodextrin film due to its more complex composition.

3. Can maltodextrin provide stability?

Maltodextrin has a notably high T_g and significantly increases the T_g of mixed matrix at a 50/50 weight ratio of maltodextrin/sucrose. Because maltodextrin is commonly used as an encapsulation material and/or as a stability aid during processing and storage, it is not expected that maltodextrin increase the molecular mobility in amorphous sucrose film along with the T_g effect. At high usage level (50/50), maltodextrin shows an obvious destabilization effect at low temperature: increasing the rate for both dipolar relaxation and collisional quenching. This probably accounts for the lower stability of maltodextrins compared with sucrose and trehalose and may also

partially explain why the high T_g of maltodextrin cannot modulate the lipid oxidation rate.

However, maltodextrin was reported to efficiently inhibit crystallization of sugars by increasing the crystallization temperature (Shamblin et al., 1996). It was also found to have similar effects in solid-state emulsions at high level (Myers and Shively, 1993). The propensity of sugars to crystallize in freeze-dried and other dehydrated system is a major factor causing the loss of protection or stability (Kreilgaard et al, 1999; Izutsu et al., 1993). Therefore, maltodextrin is able to provide stability through thwarting the formation of sugar crystals. We found in 50/50 mixtures that the matrix mobility was obviously diminished at temperature above T_g (~35% decrease in k_{TS0} at 100°C), which may help slow down crystallization and other mobility-related activities at high temperature and/or high relative humidity.

When maltodextrin is used as a matrix material to provide protection, the stability is also dependent on the compound being protected. More research is necessary to fully understand the functions of maltodextrin as an excipient in dehydrated formulations. The results presented here support the proposal that carbohydrates with high molecular weights and/or high T_gs have higher mobility and thus less capacity to protect lyophilized biomolecules compared with small molecule sugars (Duddu and Monte, 1997; Allision et al., 2000; Prestrelski et al., 1995). This result clearly demonstrates that phosphorescence is a potential tool to investigate the physical state and molecular mobility of maltodextrin and its impact on sucrose matrix. However, other techniques including Fourier transform infrared spectroscopy are needed in order to explore the mechanism leading to stability during processing and storage.

Conclusion

Molecular mobility can be modulated by the composition of an amorphous solid and the temperature. Phosphorescence of erythrosin B can report a detailed mobility map within amorphous sucrose film doped with maltodextrin. Maltodextrin itself is a relatively mobile matrix with high T_g. Maltodextrin influences sucrose matrix through a primary effect of increasing T_g and a secondary effect of increasing mobility (both dipolar relaxation and collisional quenching). The overall effect is dependent on the maltodextrin concentration. The effect is insignificant at low concentration (10/90) but becomes apparent at high concentration (50/50). Maltodextrin DE values modulate the extent of this influence (increasing matrix mobility).

Dynamic site heterogeneities above and below the glass transition temperature may be a characteristic feature of amorphous food materials and biomaterials (Ediger, 2000; Richert, 2002), a conclusion supported by phosphorescence from Ery B along with other techniques. Addition of maltodextrin increases the dynamic heterogeneity of amorphous sucrose matrix, the extent varying with the maltodextrin content and DE values.

References:

Allison, S.D., Manning, M.C., Randolph, T.W., Middleton, K., Davis, A., and Carpenter, J.F. 2000. Optimization of storage stability of lyophilized actin using combinations of disaccharides and dextran. *J. Pharm. Sci.* 89, 199-214.

Avaltroni, F., Bouquerand, P.E., and Normand, V. 2004. Maltodextrin molecular weight distribution influence on the glass transition temperature and viscosity in aqueous solutions. *Carbohydr. Polym.* 58, 323-334.

Bartos, J. and Kristiak, J. 1998. Free volume aspects of the strong-fragile classification of polymer liquids. *J. Non-Cryst Sol.* 235, 293-295.

Carpenter, J.F., Prestrelski, S.J., and Arakawa, T. 1993. Separation of freezing- and drying-induced denaturation of lyophilized proteins using stress-specific stabilization. I. Enzyme activity and calorimetric studies. *Arch Biochem Biophys.* 303, 456-464.

Carpenter, J.F., and Crowe, J.H. 1989. An infrared spectroscopic study of the interactions of carbohydrates with dried proteins. *Biochem.* 28, 3916-3922.

Chang, L., Shepherd, D., Sun, J., Ouellette, D., Grant, K.L., Tang, X., and Pikal, M.J. 2005. Mechanisms of protein stabilization by sugars during freeze-drying and storage: native structure preservation, specific interaction, and/or immobilization in a glassy matrix? *J. Pharm. Sci.* 94(7), 1427-1444.

Corveleyn, S., and Remon, J. 1996. Maltodextrin as lyoprotectants in the lyophilization of a model protein, LDH. *Pharm. Res.* 13, 146-150.

Crowe, J.H., Crowe, L.M., and Carpenter, J.F. 1993. Preserving dry biomaterials: the water replacement hypothesis. Part 1. *BioPharm.* 6, 28-29, 32-33.

Duchowicz, R., Ferrer, M.L. and Acuna, A.U. 1998. Kinetic spectroscopy of erythrosin phosphorescence and delayed fluorescence in aqueous solution at room temperature. *Photochem. Photobiol.* 68, 494-501.

Duddu, S.P., and Monte, P.R.D. 1997. Effect of glass transition temperature on the stability of lyophilized formulations containing a chimeric therapeutic monoclonal antibody. *Pharm. Res.* 14, 591-595.

Duddu, S.P., Zhang, G., and Monte, P.R.D. 1997. The relationship between protein aggregation and molecular mobility below the glass transition temperature of lyophilized formulations containing a monoclonal antibody. *Pharm. Res.* 14, 596-600.

Ediger, M.D. 2000. Spatially heterogenous dynamics in supercooled liquids. *Annu. Rev. Phys. Chem.* 51, 99-128.

Franks, F., Hatley, R.H.M., and Mathias, S.F. 1991. Materials science and the production of shelf-stable biologicals. *BioPharm.* 4, 38, 40-42, 55.

Grattard N., Salaun, E., Champion, D., Roudaut, G., and Le Meste, M. 2002. Influence of physical state and molecular mobility of freeze-dried maltodextrin matrices on the oxidation rate of encapsulated lipids. *J. Food Sci.* 67 (8), 3002-3010.

Imamura, K., Fukushima, A., Sakaura, K., Sugita, T., Sakiyama, T., and Nakanishi, K. 2002. Water sorption and glass transition behaviors of freeze-dried sucrose-dextran mixtures. *J. Pharm. Sci.* 91, 2175-2181.

Izutsu, K., Yoshioka, S., and Terao, T. 1993. Decreased protein-stabilizing effects of cryoprotectants due to crystallization. *Pharm. Res.* 10, 1232-1237.

Kets, E.P.W., IJpelaar, P.J., Hoekstra, F.A., and Vromans, H. 2004. Citrate increases glass transition temperature of vitrified sucrose preparations. *Cryobiology*. 48, 46-54.

Kreilgaard L., Frokjaer, S., Flink, J.M., Randolph, T.W., and Carpenter, J.F. 1999. Effects of additives on the stability of Humicola lanuginosa lipase during freeze-drying and storage in the dried solid. *J. Pharm Sci.* 88 (3), 281-290.

Lakowicz, J.R. 1999. *Principles of fluorescence spectroscopy*. Plenum Press, NY

Lee, K.C.B., Siegel, J., Webb, S.E.D., Leveque-Fort, S., Cole, M.J., Jones, R., Dowling, K., Lever, M.J., and French, P.M.W. 2001. Application of the stretched exponential function to fluorescence lifetime imaging. *Biophys. J.* 81, 1265-1274.

Levine, H. and Slade, L. 1986. A polymer physico-chemical approach to the study of commercial starch hydrolysis products (SHPs). *Carbohydr. Polym.* 6(3), 213-244.

Li, H.L., Hjihira, Y., Nanaswater, C.A., and Jean, C.Y. 1999. Estimation of free volume in polystyrene-polyphenylene ether blend probed by the positron annihilation lifetime technique. *Polym.* 40, 349-355.

Lukasik, K.V. and Ludescher, R.D. 2006. Effect of plasticizer on dynamic site heterogeneity in cold-cast gelatin films. *Food Hydrocoll.* 20, 88-95.

Maroncelli, M., and Fleming, G.R. 1987. Picosecond solvation dynamics of coumarin 153: the importance of molecular aspects of solvation. *J. Chem. Phys.* 86, 6221-6239.

Mazzobre M.F., Buera, M.P., and Chirife, J. 1997. Glass transition and thermal stability of lactase in low-moisture amorphous polymeric matrices. *Biotechnol. Prog.* 13, 195-199.

Myers, S.L. and Shively, M.L. 1993. Solid-state emulsions: the effect of maltodextrin on microcrystalline aging. *Pharm. Res.* 10(9), 1389-1391.

Nack, T.J, and Ludescher, R.D. 2006. Molecular mobility and oxygen permeability in amorphous bovine serum albumin films. *Food Biophys.* 1, 151-162.

Oldenhof H., Wolkers, W.F., Fonseca, F., Passot, S., and Marin, M. 2005. Effect of sucrose and maltodextrin on the physical properties and survival of air-dried lactobacillus bulgaricus: an in situ fourier transform infrared spectroscopy study. *Biotechnol. Prog.* 21, 885-892.

Papp, S. and Vanderkooi, J.M. 1989. Tryptophan phosphorescence at room temperature as a tool to study protein structure and dynamics. *Photochem. Photobiol.* 49, 775-784.

Parker, C.A. 1968. *Photoluminescence of Solutions.* Elsevier, Amsterdam.Netherlands.

Pravinata, L.C., You, Y. and Ludescher, R.D. 2005. Erythrosin B phosphorescence monitors molecularmobility and dynamic site heterogeneity in amorphous sucrose. *Biophys. J.* 88(May), 3551-3561.

Prestrelski S.J., Pikal, K.A., and Arakawa, T. 1995. Optimization of lyophilization conditions for recombinant human interleukin-2 by dried-state conformation analysis using fourier-transform infrared spectroscopy. *Pharm. Res.* 12, 1250-1259.

Richert, R. 2000. Triplet state salvation dynamics: basics and applications. *J. Chem. Phys.* 113, 8404-8429.

Richert, R. 2002. Heterogeneous dynamics in liquids: fluctuations in space and time. *J. Phys. Condens. Matter.* 14, R738-R803.

Roos, Y. and Karel, M. 1991. Phase transition of mixtures of amorphous polysaccharides and sugars. *Biotechnol. Prog.* 7, 49-53.

Rossi S., Buera, M.P., Moreno, S., and Chirife, J. 1997. Stabilization of the restriction enzyme EcoRI dried with trehalose and other selected glass-forming solutes. *Biotechnol. Prog.* 13, 609-616.

Samuhasaneetoo, S., Chaiseri, S., Farhat, I.A., Sajjaanantakul, T., and Pongsawatmanit, R. 2006. Determination of microvoids of maltodextrin with various DE by the "dual sorption model". *Royal Society Chem*. 303, 275-283.

Shamblin, S.L., Huang, E.Y., and Zografi, G. 1996. The effects of co-lyophilized polymeric additives on the glass transition temperature and crystallization of amorphous sucrose. *J. Thermal. Anal. Cal.* 47 (5), 1567-1579.

Shirke, S., and Ludescher, R.D. 2005. Dynamic site heterogeneity in amorphous maltose and maltitol from spectral heterogeneity in erythrosin B phosphorescence. *Carbohydr. Res.* 340, 2661-2669.

Shirke, S., Takhistov, P., and Ludescher, R.D. 2005. Molecular mobility in amorphous maltose and maltitol from phosphorescence of erythrosin B. *J. Phys. Chem. B.* 109, 16119-16126.

Shirke, S., You, Y., and Ludescher, R.D. 2006. Molecular mobility and dynamic site heterogeneity in amorphous lactose and lactitol from erythrosin B phosphorescence. *Biophys. Chem.* 123, 122-133.

Slade, L., and Levine, H. 1991. Beyond water activity: recent advances based on an alternative approach to the assessment of food quality and safety. *Crit. Rev. Food Sci. Nutr*. 30, 115-360.

Wang, Y., and Wang, L. 2000. Structures and properties of commercial maltodextrins from corn, potato, and rice starches. *Starch/Starke*. 52, 296-304.

You, Y., and Ludescher, R.D. 2006. Phosphorescence of erythrosin B as a robust probe of molecular mobility in amorphous solid sucrose. *Appl. Spectrosc.* 60, 813-819.

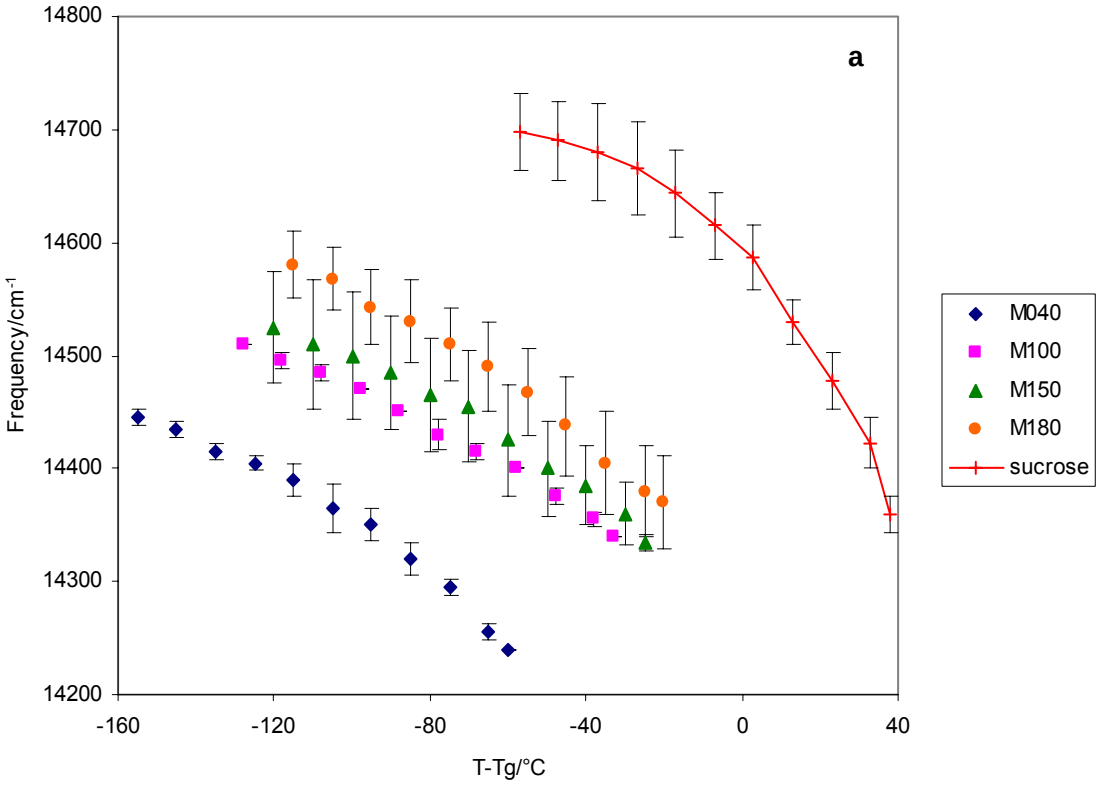
a
14800
14700
14600
14500
14400
14300
14200
Frequency/cm-1
-160
-120
-80
-40
0
40
T-Tg/°C
M040
M100
M150
M180
sucrose

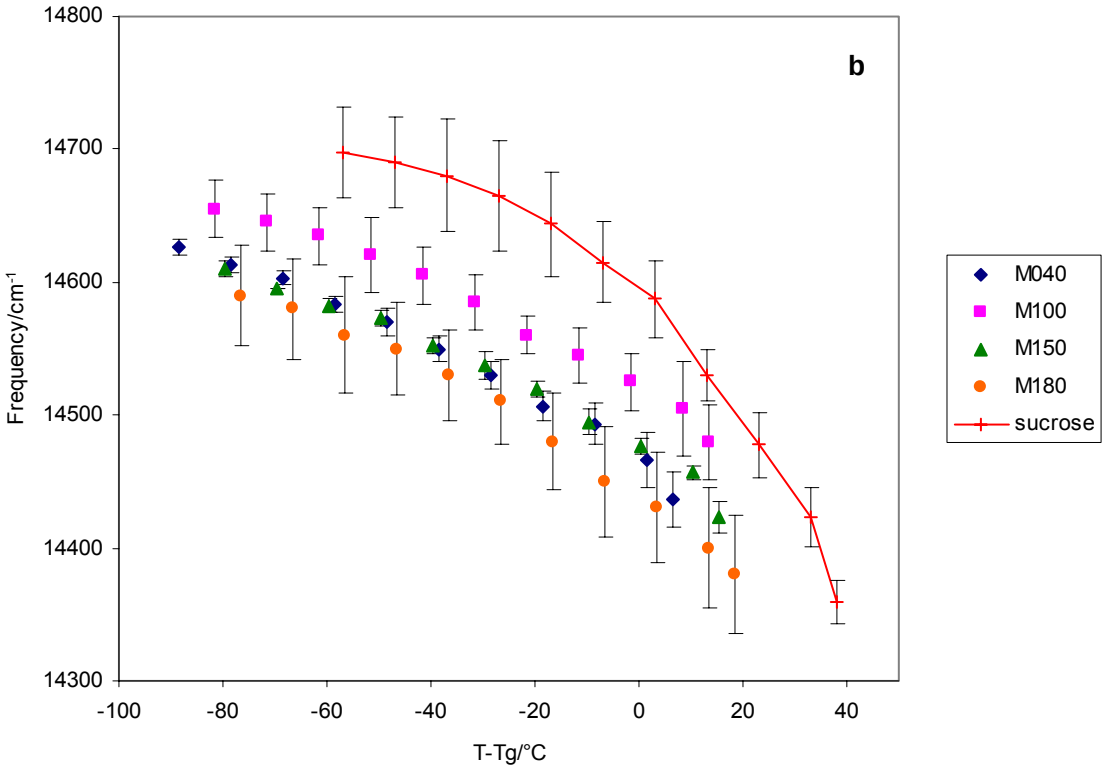
b
14800
14700
14600
14500
14400
14300
Frequency/cm-1
-100
-80
-60
-40
-20
0
20
40
T-Tg/°C
M040
M100
M150
M180
sucrose

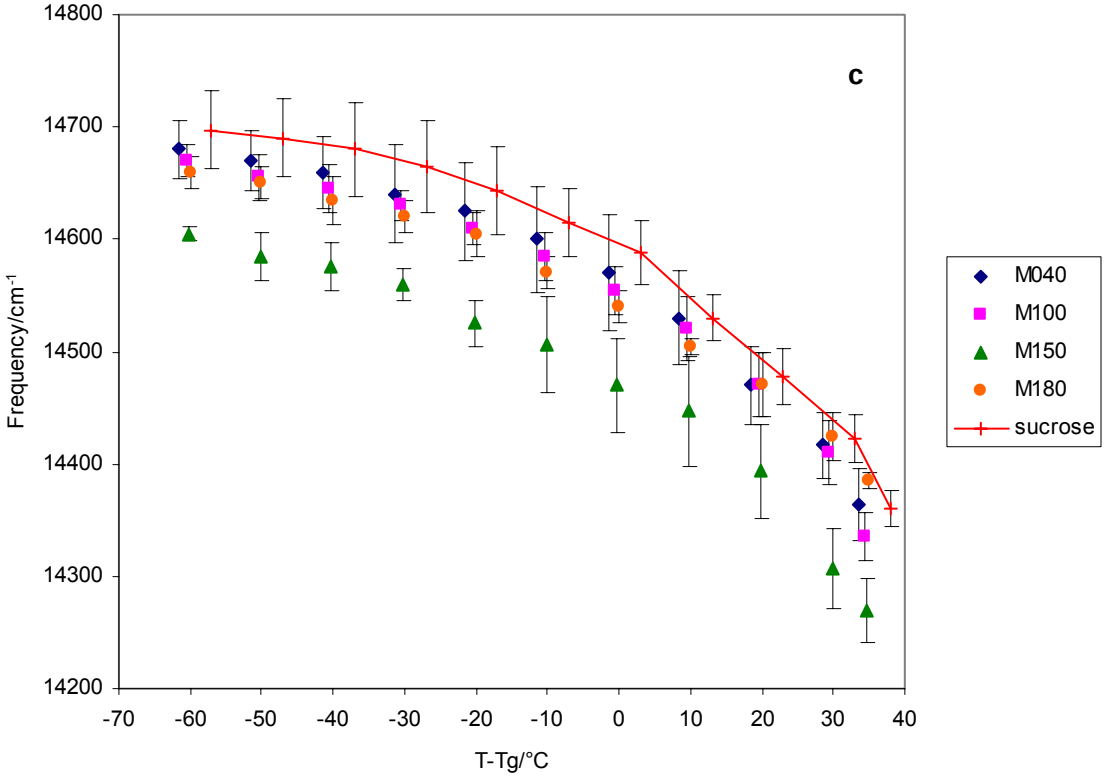

Figure 53: Peak frequency (ν_p) for phosphorescence emission from erythrosin B plotted as a function of $T-T_g$ in amorphous films with maltodextrin/sucrose weight ratio of (a) 100:0; (b) 50:50 and (c) 10:90. Delayed emission spectra collected as a function of temperature were analyzed using log-normal line shape function.

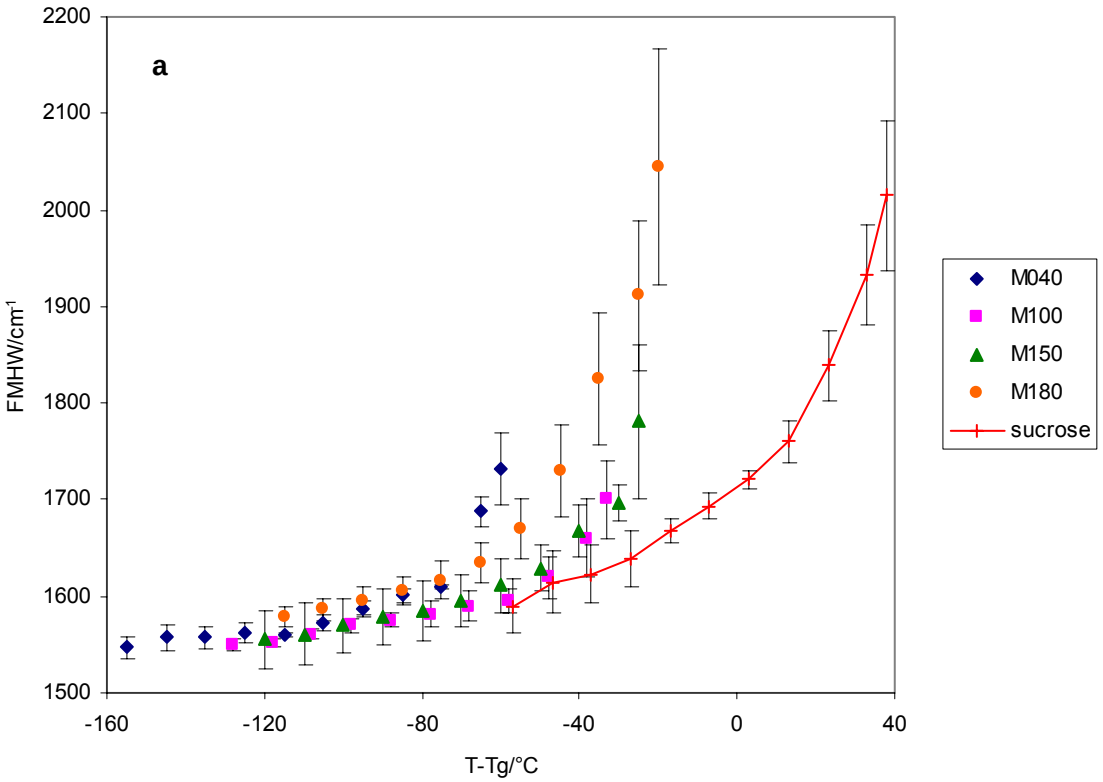
a
2200
2100
2000
1900
1800
1700
1600
1500
FMHW/cm-1
-160
-120
-80
-40
0
40
T-Tg/°C
M040
M100
M150
M180
sucrose

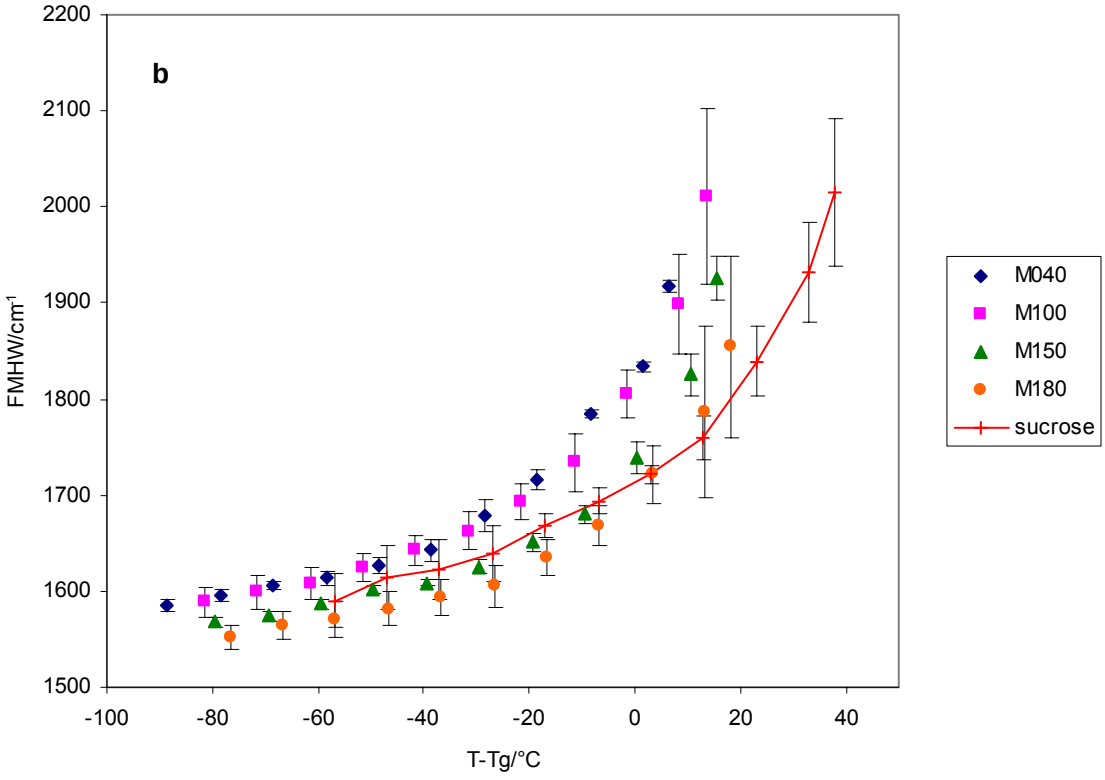
b
2200
2100
2000
1900
1800
1700
1600
1500
FMHW/cm-1
-100
-80
-60
-40
-20
0
20
40
T-Tg/°C
M040
M100
M150
M180
sucrose

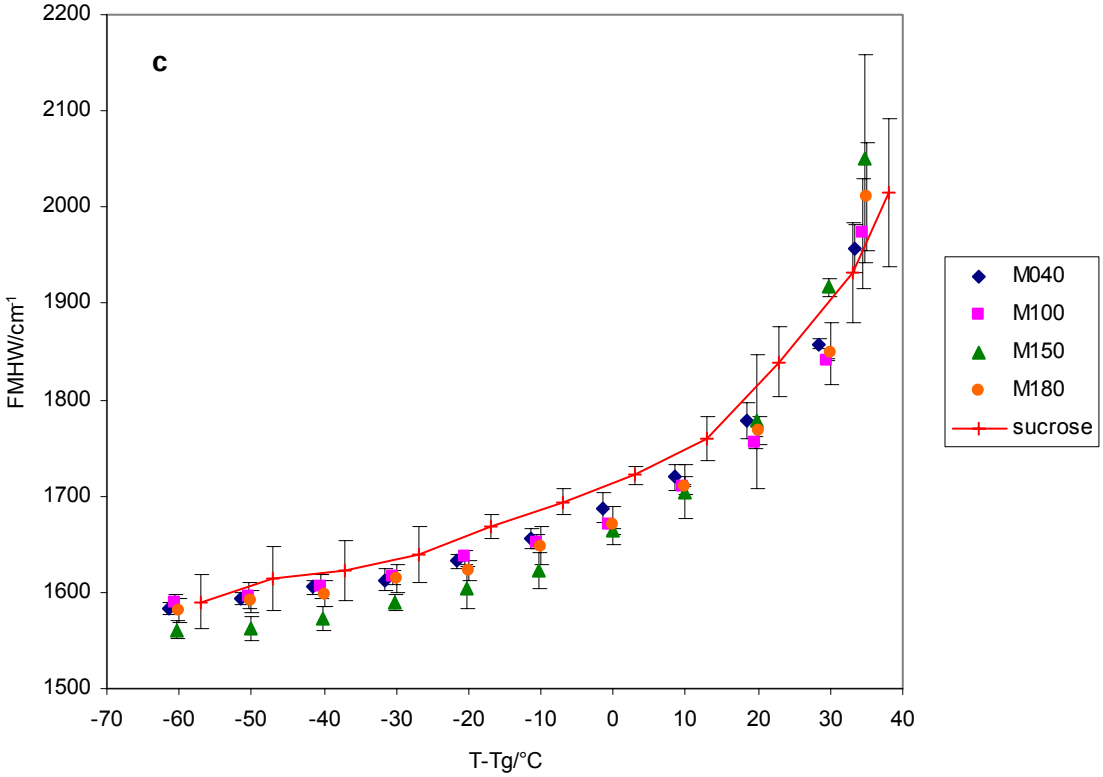

Figure 54: Bandwidth (full width at half maximum, FWHM) for phosphorescence emission from erythrosin B plotted as a function of T-T_g in amorphous films with maltodextrin/sucrose weight ratio of (a) 100:0; (b) 50:50 and (c) 10:90. Delayed emission spectra collected as a function of temperature were analyzed using log-normal line shape function.

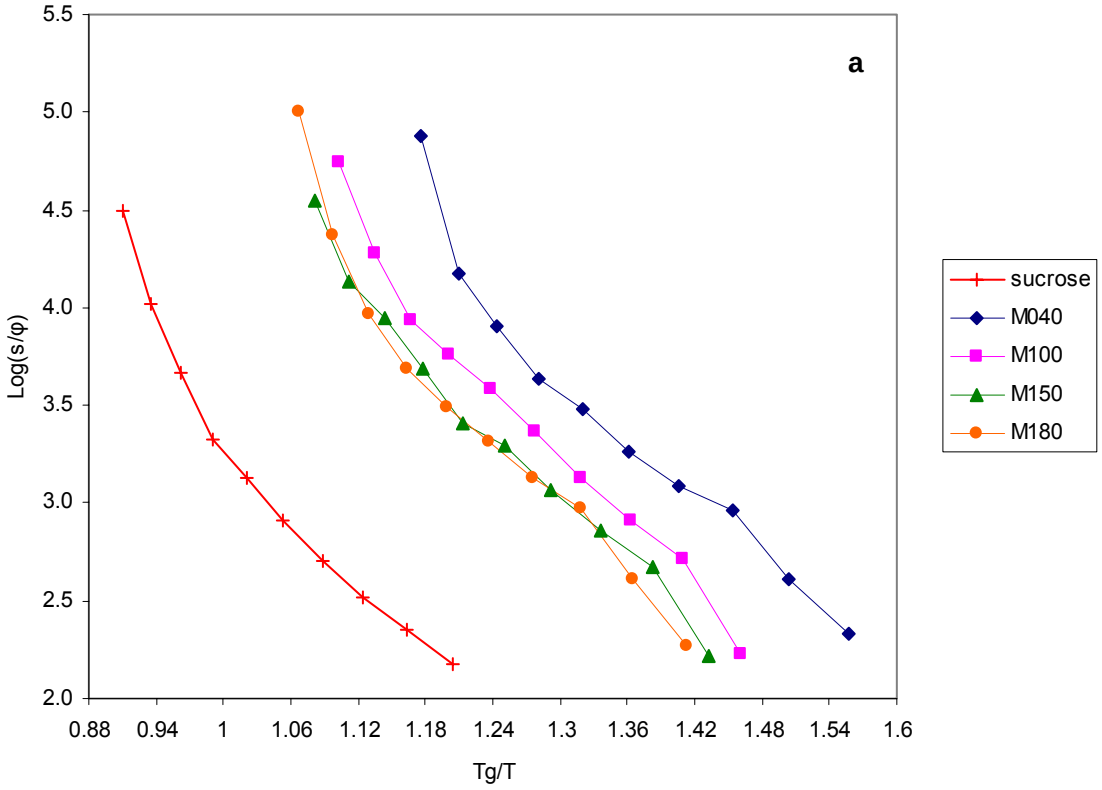
a
Log(s/φ)
Tg/T
5.5
5.0
4.5
4.0
3.5
3.0
2.5
2.0
0.88
0.94
1
1.06
1.12
1.18
1.24
1.3
1.36
1.42
1.48
1.54
1.6
sucrose
M040
M100
M150
M180

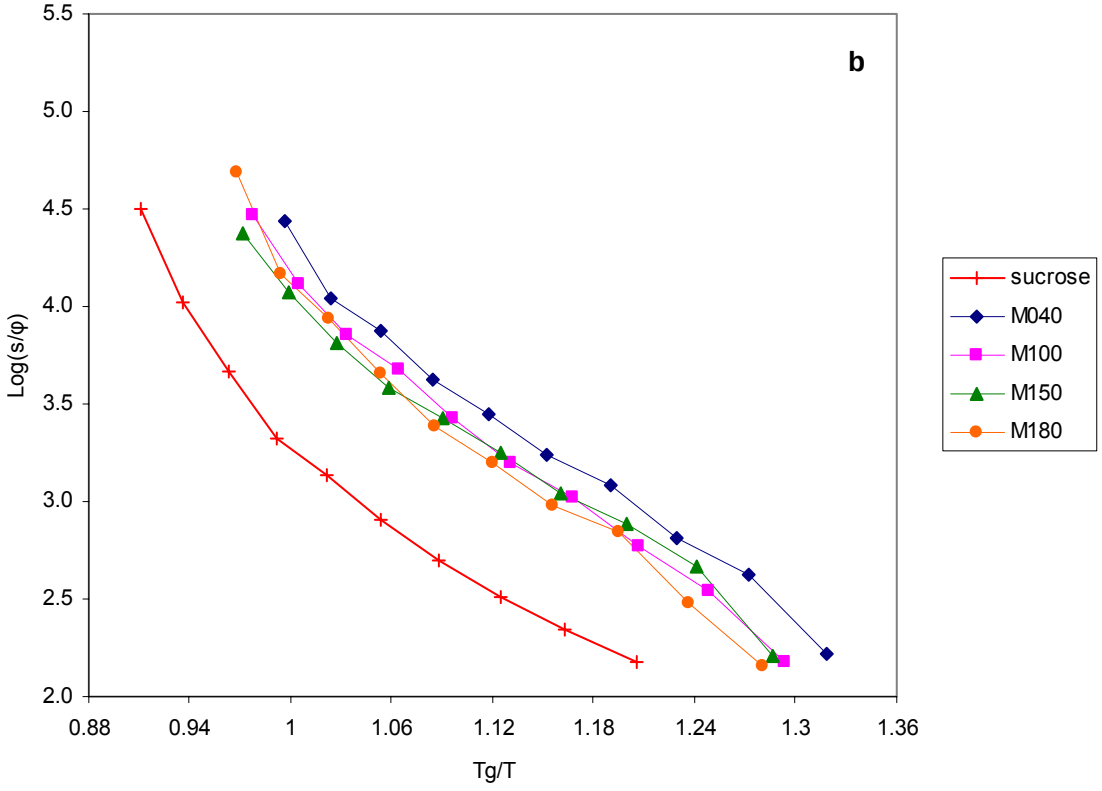
b
Log(s/φ)
Tg/T
5.5
5.0
4.5
4.0
3.5
3.0
2.5
2.0
0.88
0.94
1
1.06
1.12
1.18
1.24
1.3
1.36
sucrose
M040
M100
M150
M180

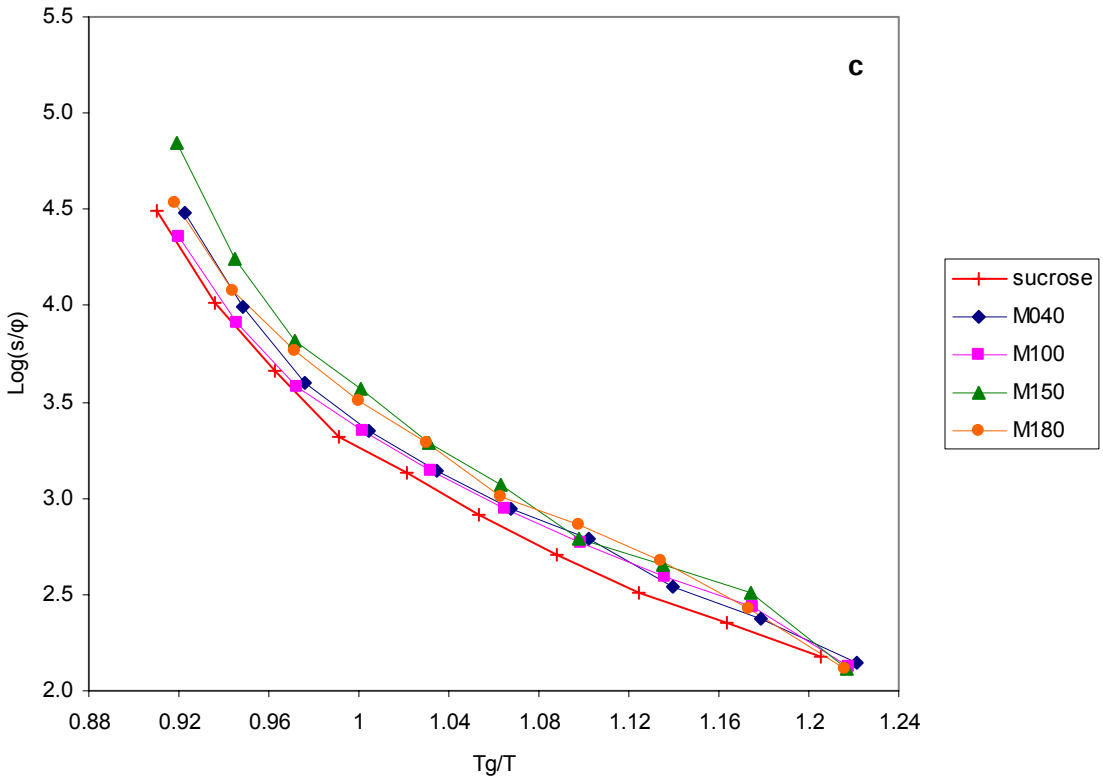

Figure 55: Modified Arrhenius plot of the dipolar relaxation rate versus T_g/T in amorphous films with maltodextrin/sucrose weight ratio of (a) 100:0; (b) 50:50 and (c) 10:90.

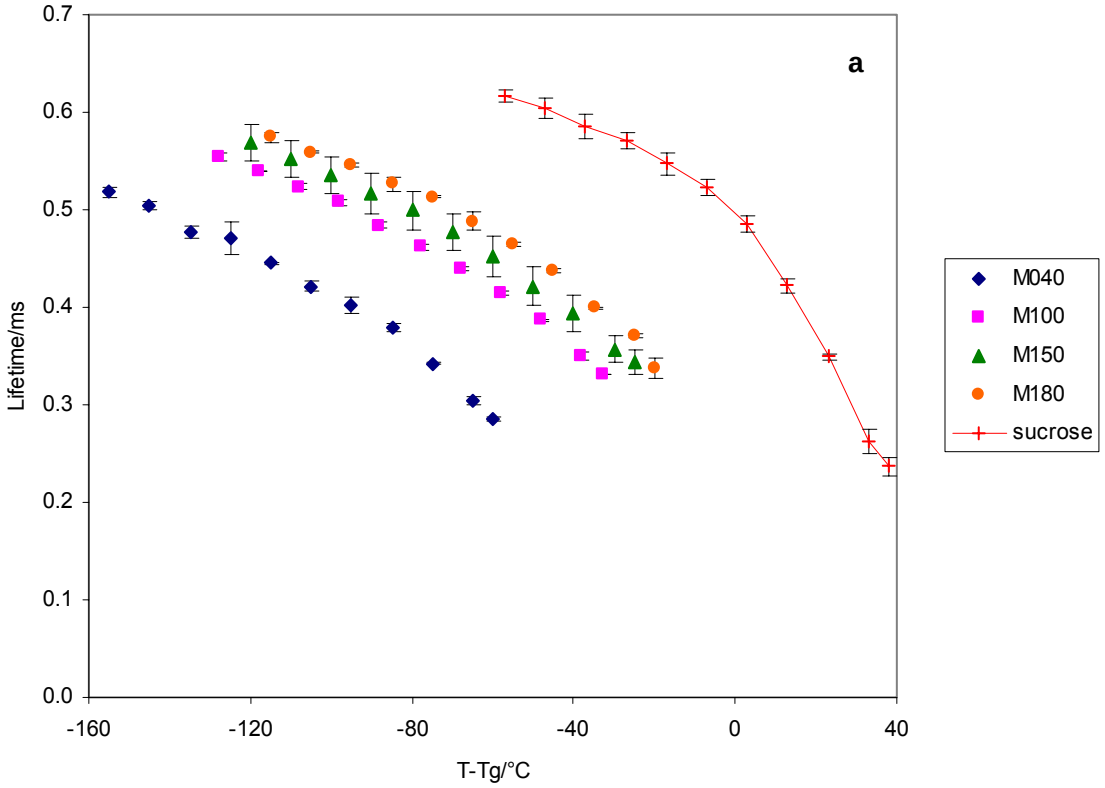
a
Lifetime/ms
T-Tg/°C
0.0
0.1
0.2
0.3
0.4
0.5
0.6
0.7
-160
-120
-80
-40
0
40
M040
M100
M150
M180
sucrose

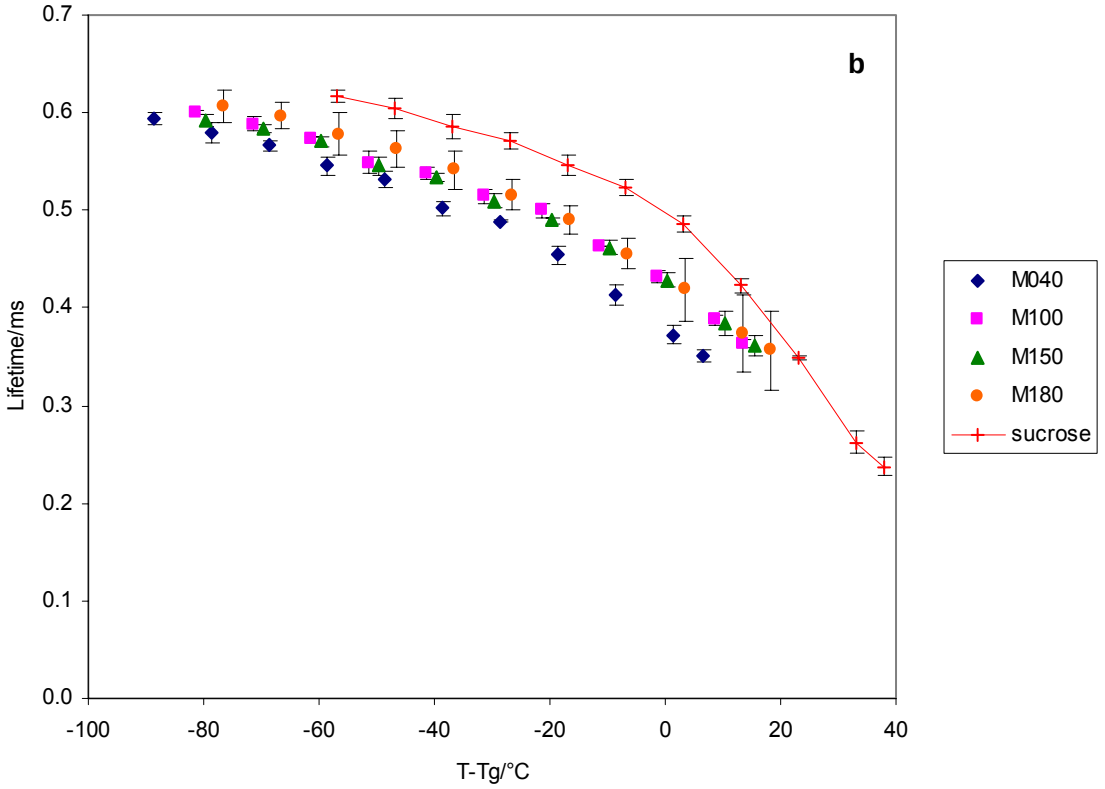
b
Lifetime/ms
T-Tg/°C
0.0
0.1
0.2
0.3
0.4
0.5
0.6
0.7
-100
-80
-60
-40
-20
0
20
40
M040
M100
M150
M180
sucrose

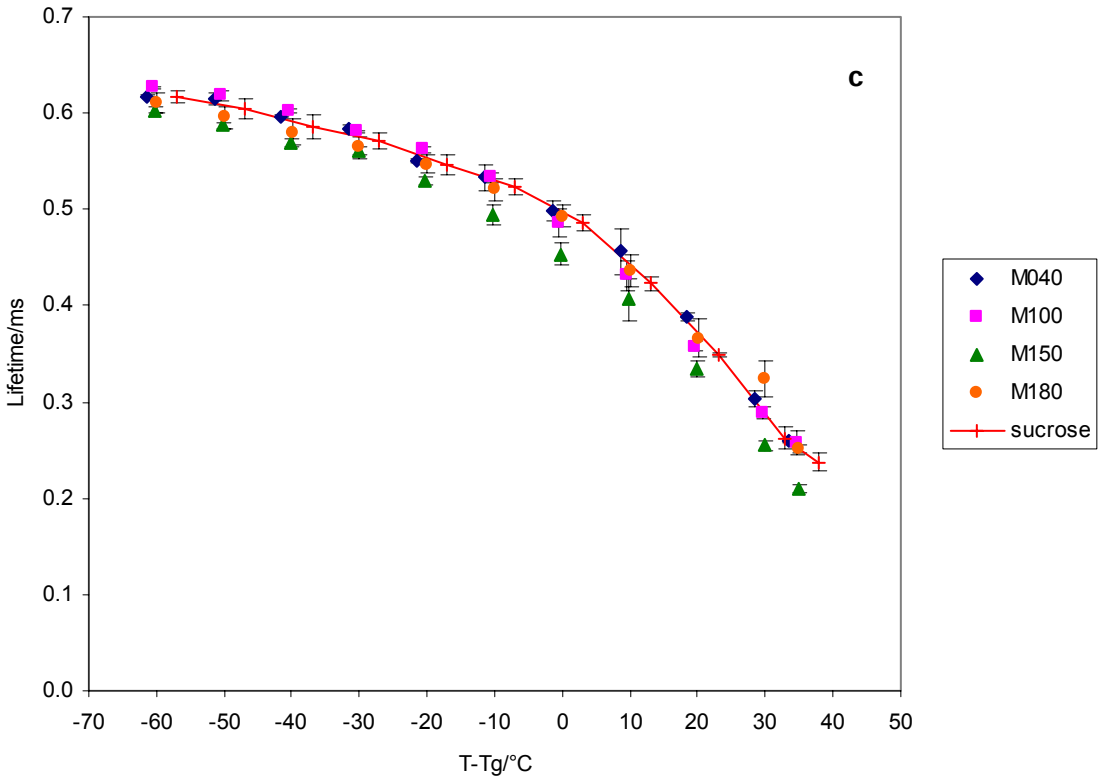

Figure 56: Plot of lifetime obtained from fits to a stretched exponential decay model of the intensity decay of erythrosin B versus T-T_g in amorphous films with maltodextrin/sucrose weight ratio of (a) 100:0; (b) 50:50 and (c) 10:90.

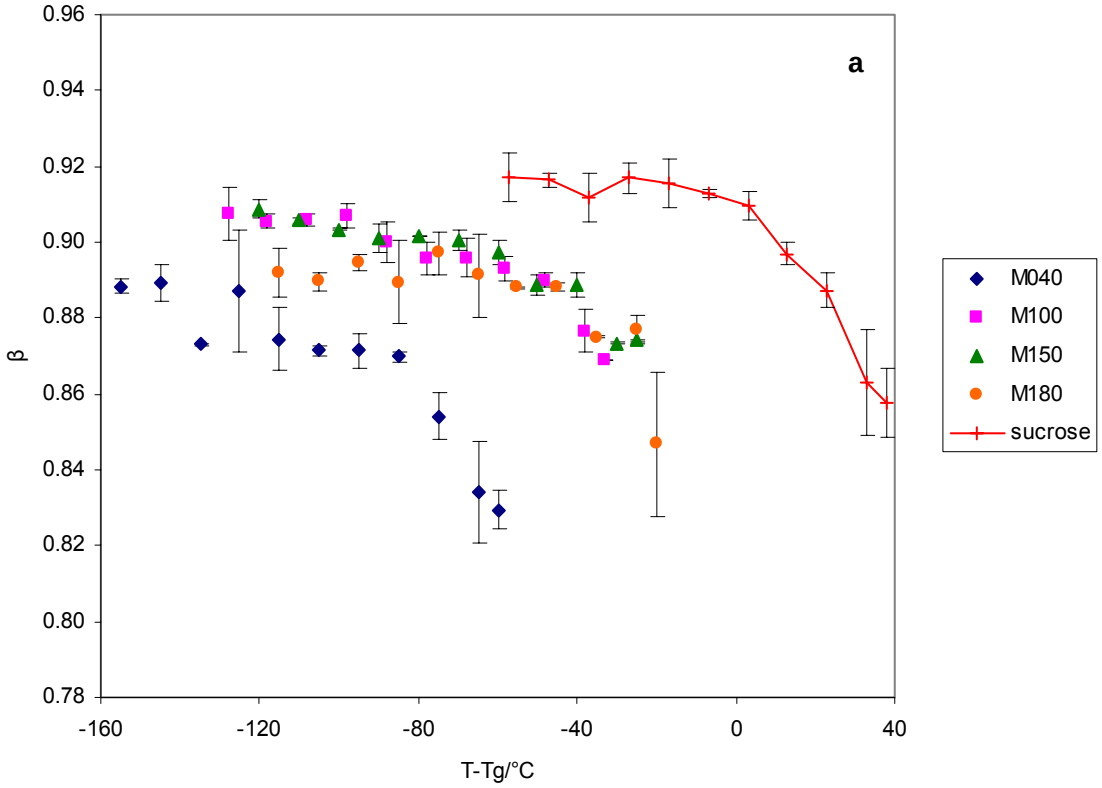
a
0.96
0.94
0.92
0.90
0.88
0.86
0.84
0.82
0.80
0.78
β
-160
-120
-80
-40
0
40
T-Tg/°C
M040
M100
M150
M180
sucrose

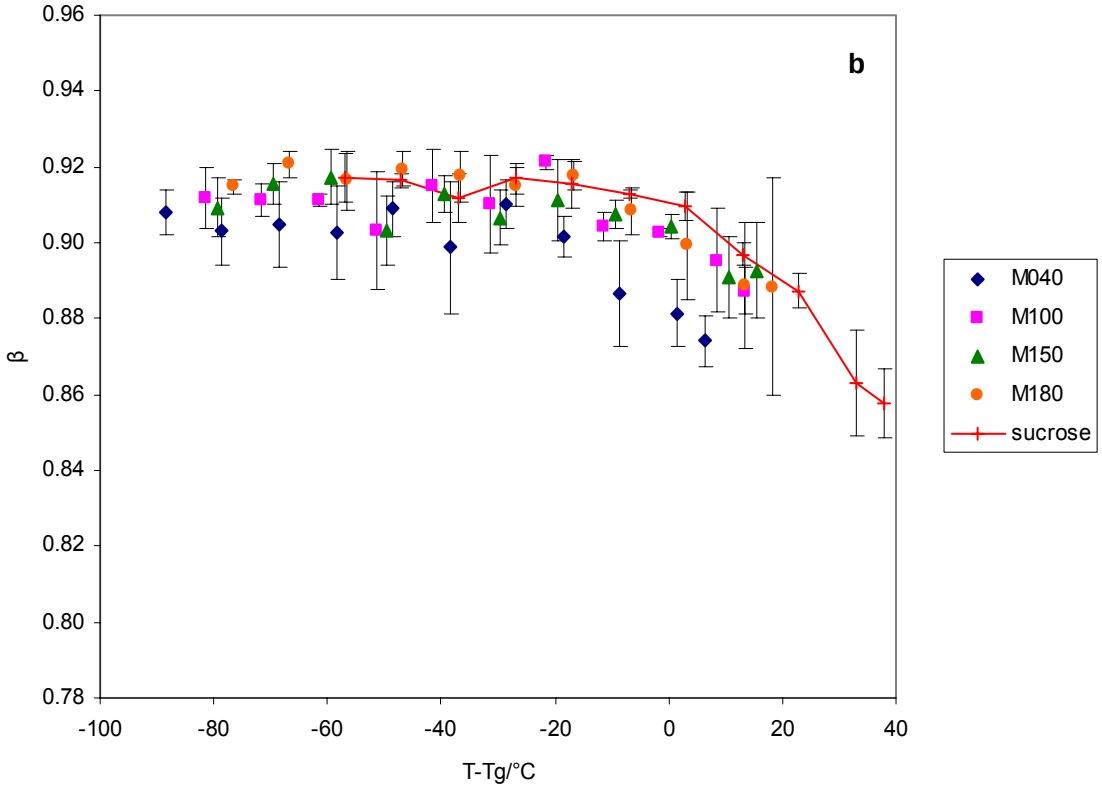
b
0.96
0.94
0.92
0.90
0.88
0.86
0.84
0.82
0.80
0.78
β
-100
-80
-60
-40
-20
0
20
40
T-Tg/°C
M040
M100
M150
M180
sucrose

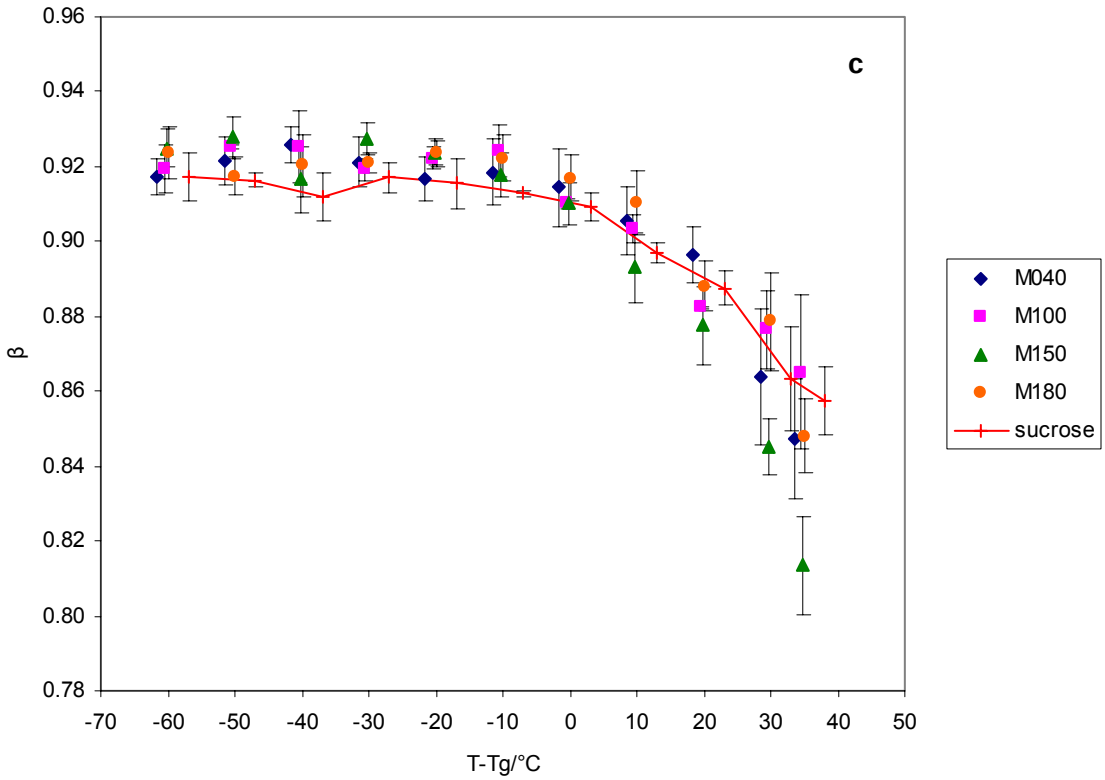

Figure 57: Stretching exponent β obtained from fits to a stretched exponential decay model of the intensity decay of erythrosin B as a function of T- T_g in amorphous films with maltodextrin/sucrose weight ratio of (a) 100:0; (b) 50:50 and (c) 10:90.

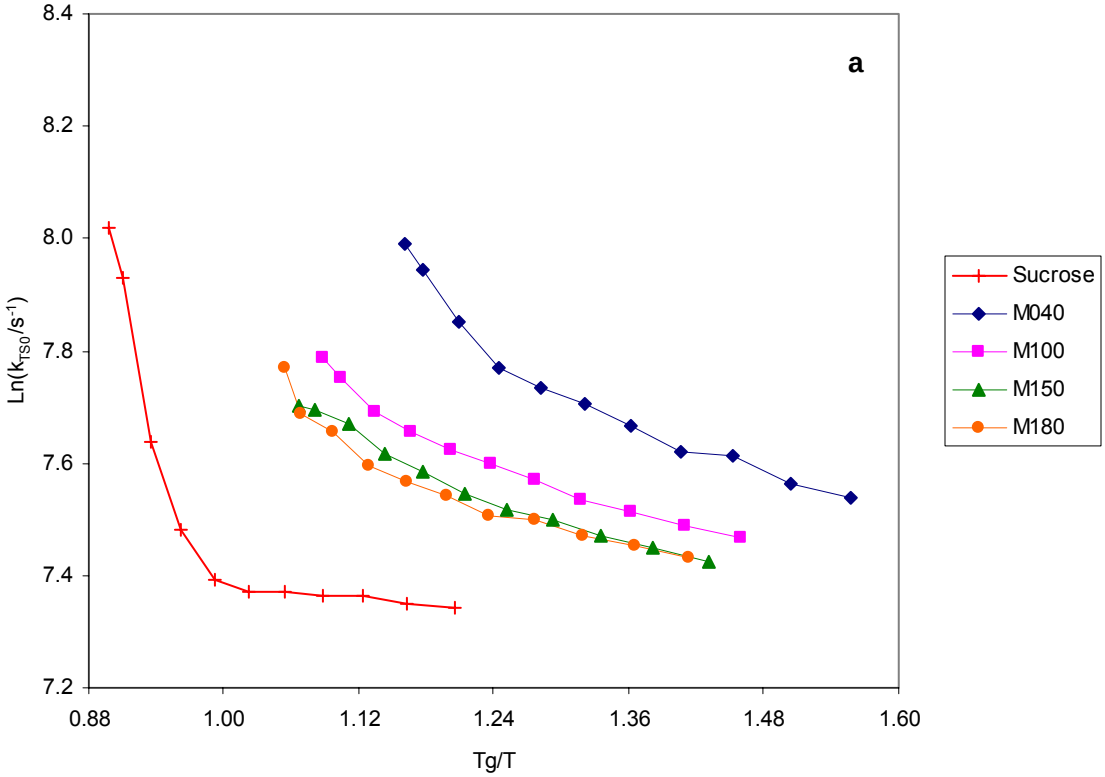
a
8.4
8.2
8.0
7.8
7.6
7.4
7.2
Ln(k_TS0/s^-1)
0.88
1.00
1.12
1.24
1.36
1.48
1.60
Tg/T
Sucrose
M040
M100
M150
M180

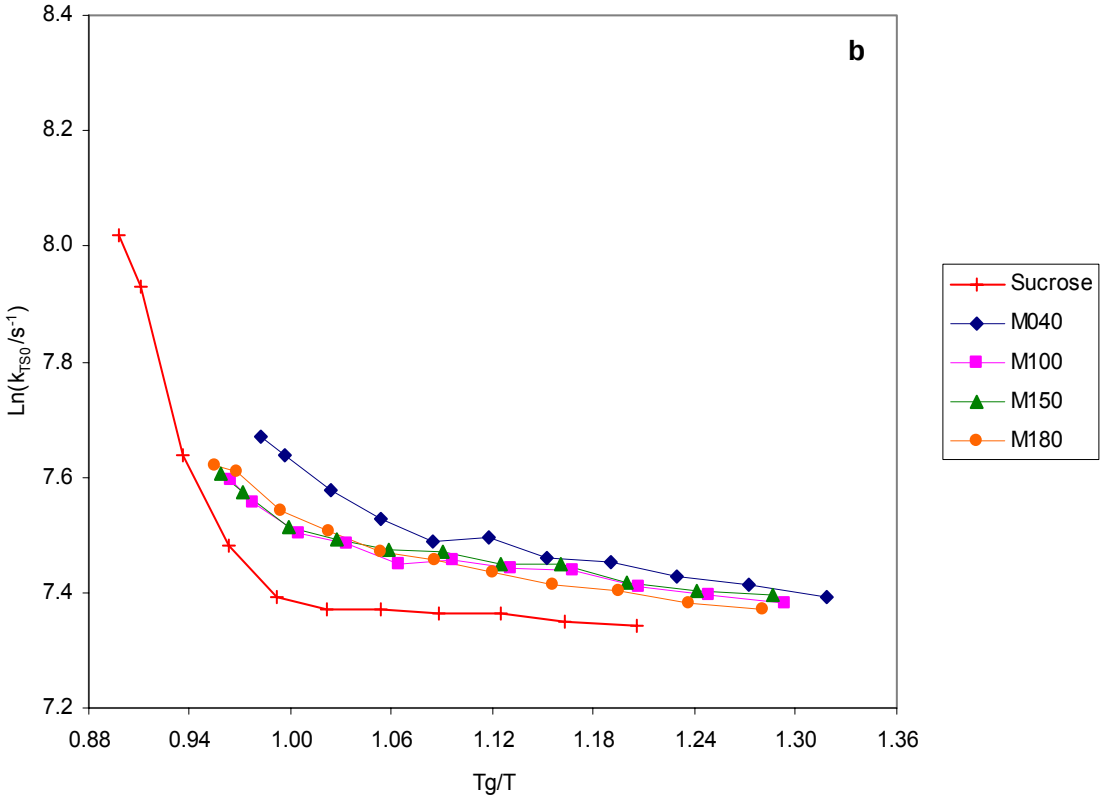
b
8.4
8.2
8.0
7.8
7.6
7.4
7.2
Ln(k_TS0/s^-1)
0.88
0.94
1.00
1.06
1.12
1.18
1.24
1.30
1.36
Tg/T
Sucrose
M040
M100
M150
M180

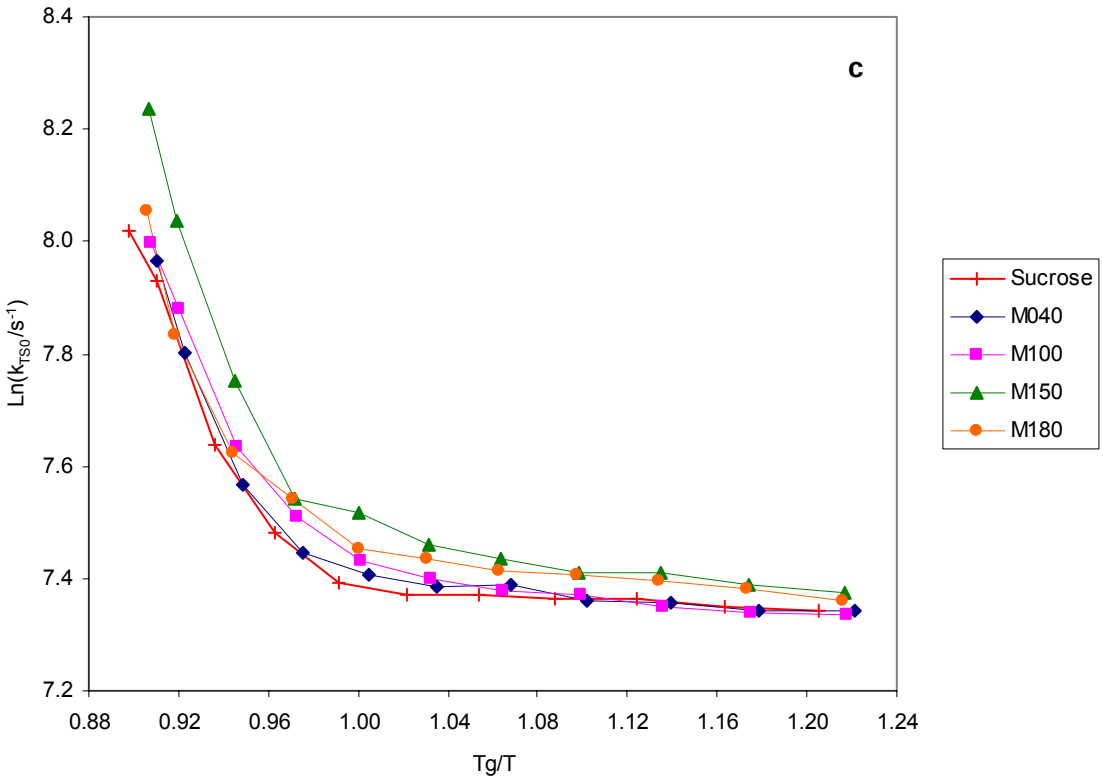

Figure 58: Arrhenius plot of the rate constant for non-radiative decay of the triplet T_1 state to S_0 (k_{TS0}) versus T_g/T, data calculated from the lifetime data of Figure 5; see text for additional details. Samples are erythrosin B in amorphous films with maltodextrin/sucrose weight ratio of (a) 100:0; (b) 50:50 and (c) 10:90.

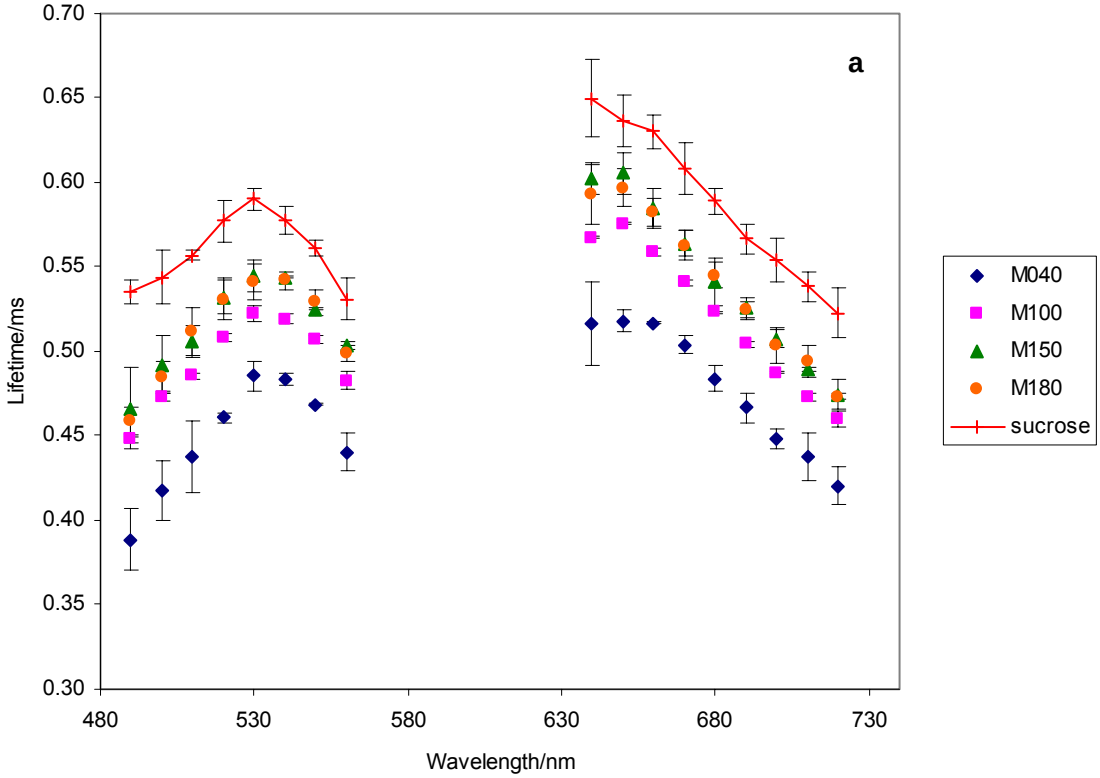
a
Lifetime/ms
Wavelength/nm
0.70
0.65
0.60
0.55
0.50
0.45
0.40
0.35
0.30
480
530
580
630
680
730
M040
M100
M150
M180
sucrose

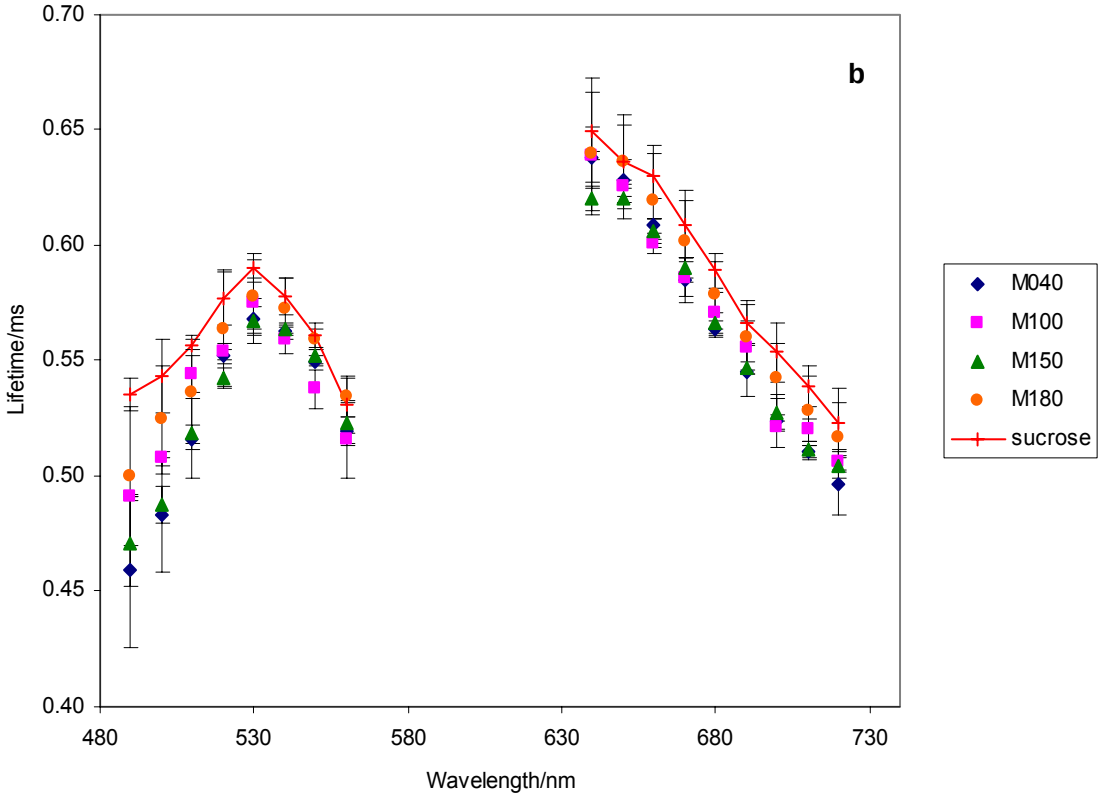
b
Lifetime/ms
Wavelength/nm
0.70
0.65
0.60
0.55
0.50
0.45
0.40
480
530
580
630
680
730
M040
M100
M150
M180
sucrose

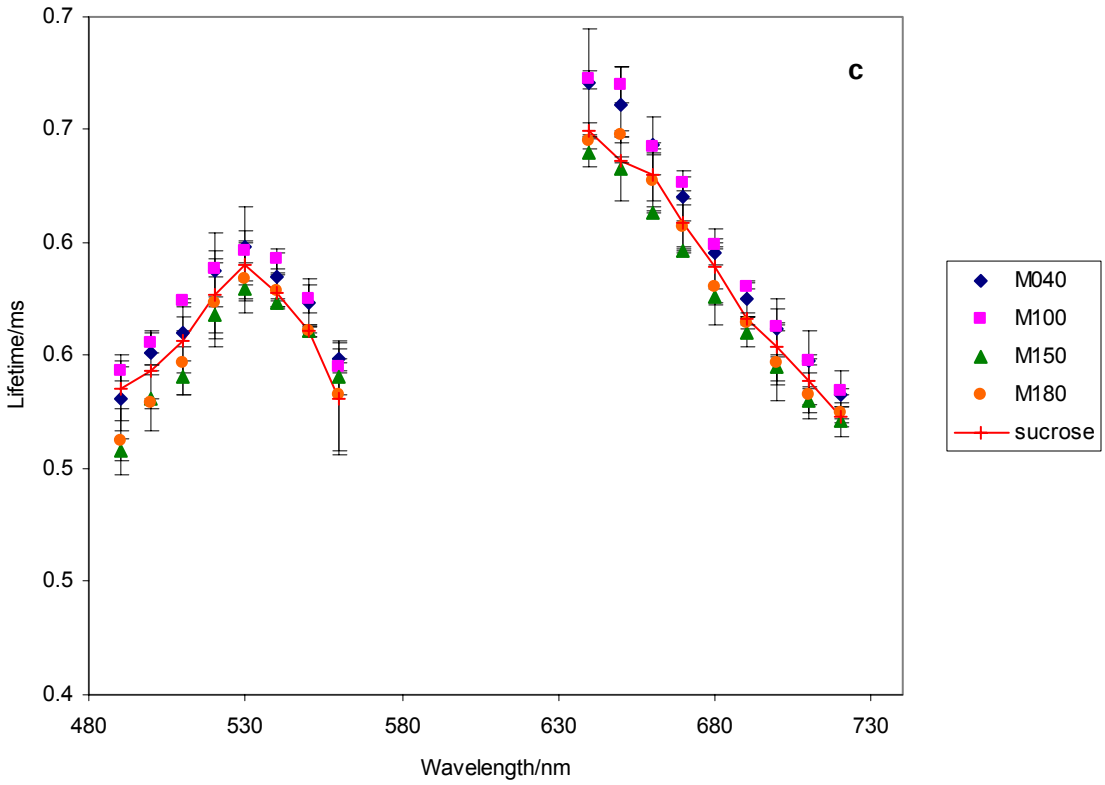

Figure 59: The effect of excitation wavelength (with 680 nm emission) and emission wavelength (with 530 nm excitation) on the lifetimes from fits of erythrosin B phosphorescence intensity decays to the stretched exponential decay model. Data collected in amorphous films with maltodextrin/sucrose weight ratio of (a) 100:0; (b) 50:50 and (c) 10:90.

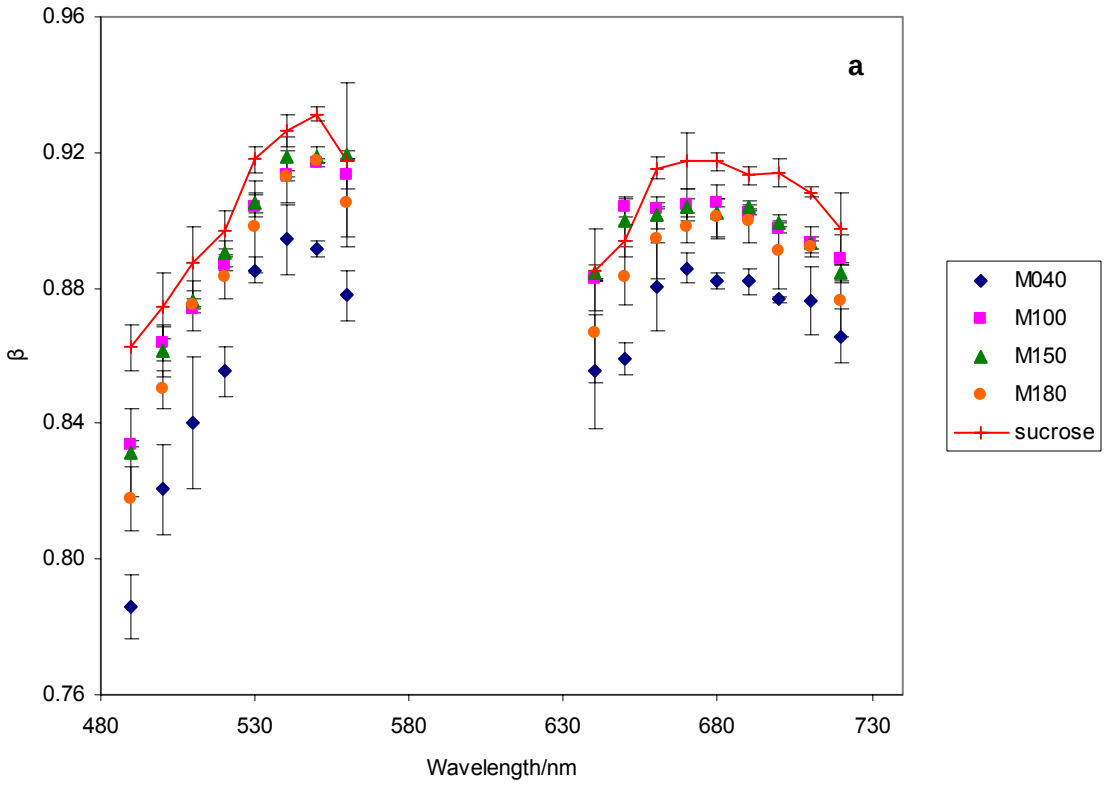
a
0.96
0.92
0.88
0.84
0.80
0.76
β
480
530
580
630
680
730
Wavelength/nm
M040
M100
M150
M180
sucrose

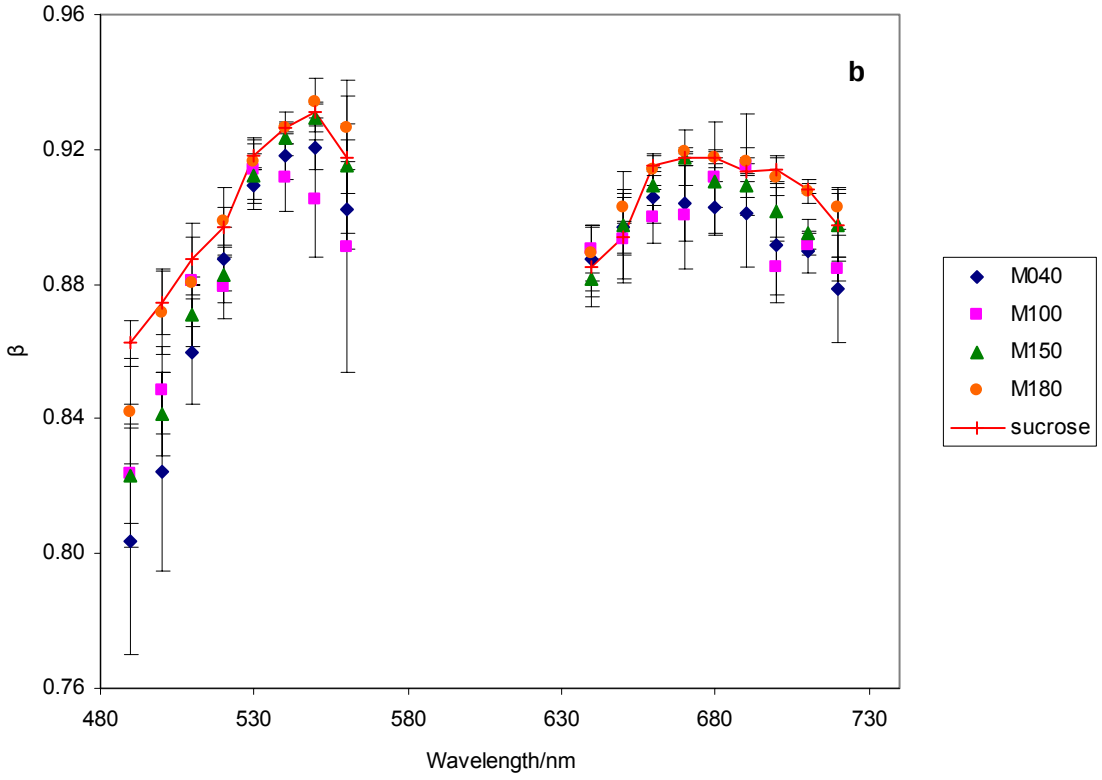
b
0.96
0.92
0.88
0.84
0.80
0.76
β
480
530
580
630
680
730
Wavelength/nm
M040
M100
M150
M180
sucrose

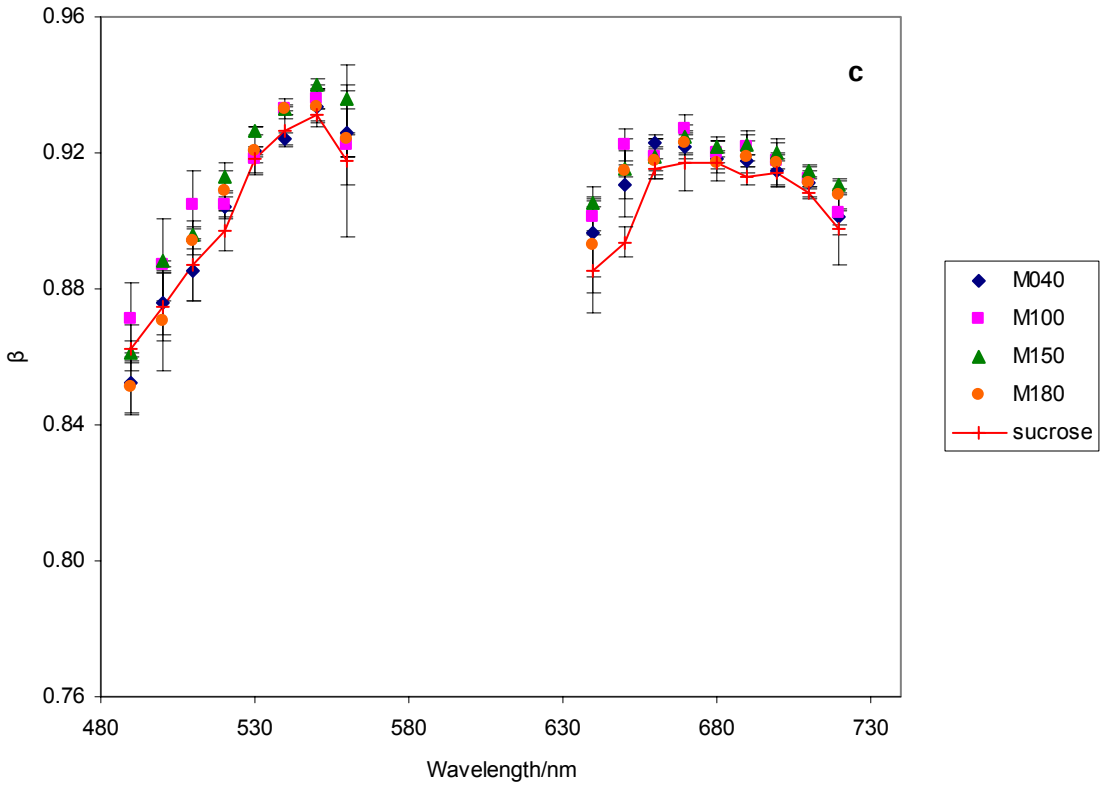

Figure 60: The effect of excitation wavelength (with 680 nm emission) and emission wavelength (with 530 nm excitation) on the stretching exponents β from fits of erythrosin B phosphorescence intensity decays to the stretched exponential decay model. Data collected in amorphous films with maltodextrin/sucrose weight ratio of (a) 100:0; (b) 50:50 and (c) 10:90.

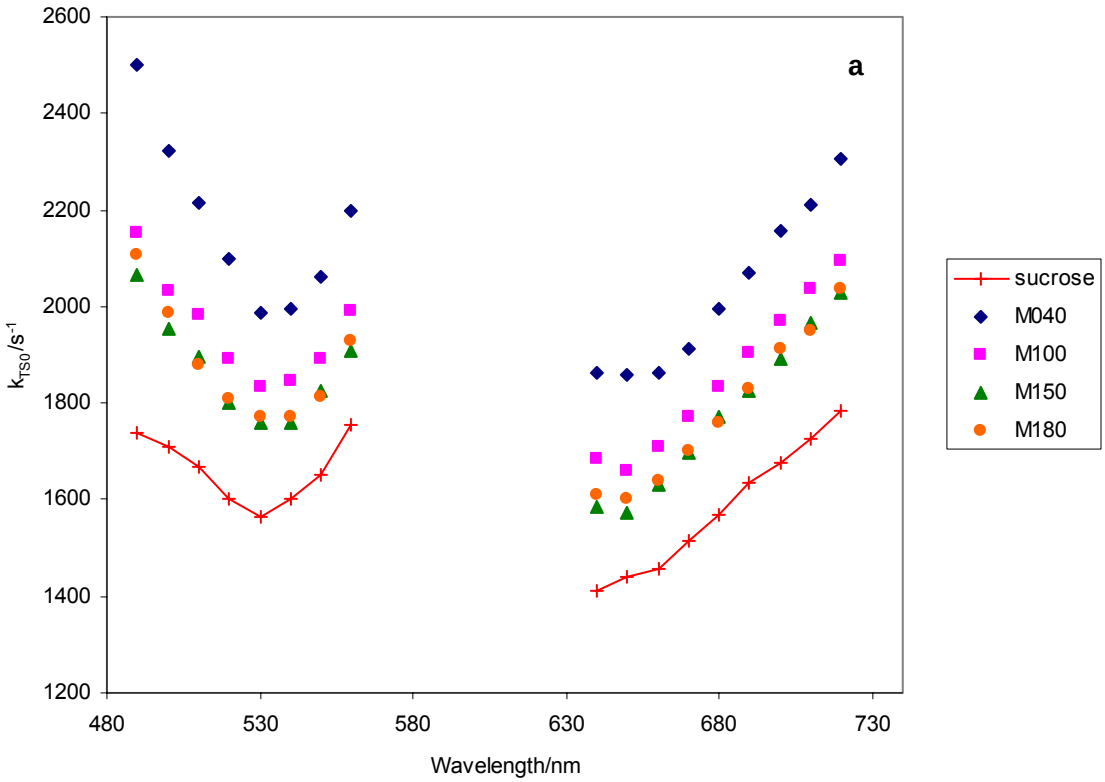
a
2600
2400
2200
2000
1800
1600
1400
1200
480
530
580
630
680
730
Wavelength/nm
k_{TS0}/s^{-1}
sucrose
M040
M100
M150
M180

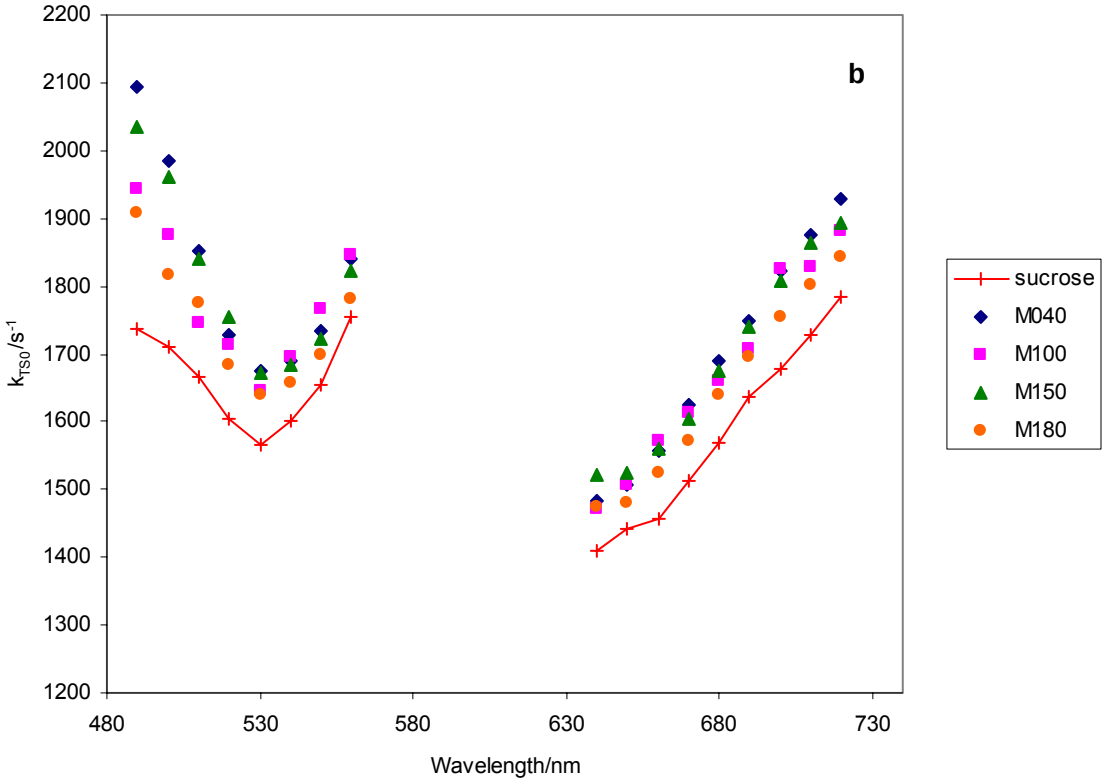
b
2200
2100
2000
1900
1800
1700
1600
1500
1400
1300
1200
480
530
580
630
680
730
Wavelength/nm
k_{TS0}/s^{-1}
sucrose
M040
M100
M150
M180

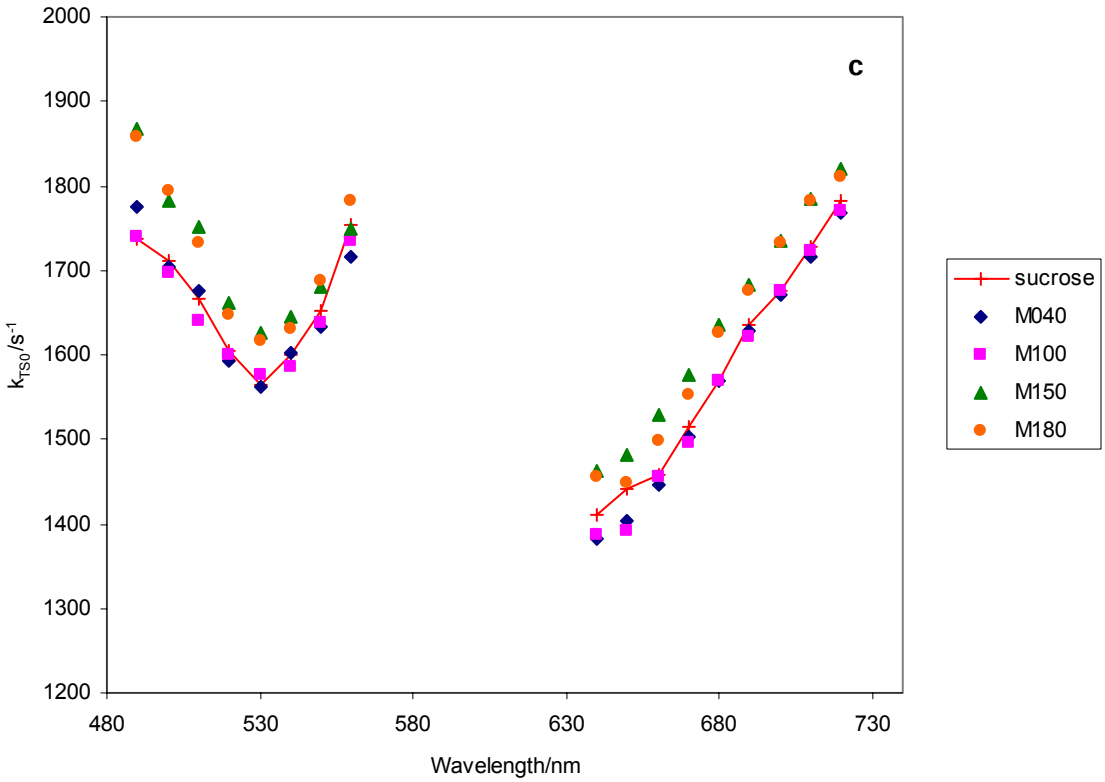

Figure 61: The rate constant for non-radiative decay of the triplet state to S_0 (k_{TS0}) plotted as a function of excitation wavelength (with 680 nm emission) and emission wavelength (with 530 nm excitation). Data collected in in amorphous films with maltodextrin/sucrose weight ratio of (a) 100:0; (b) 50:50 and (c) 10:90.

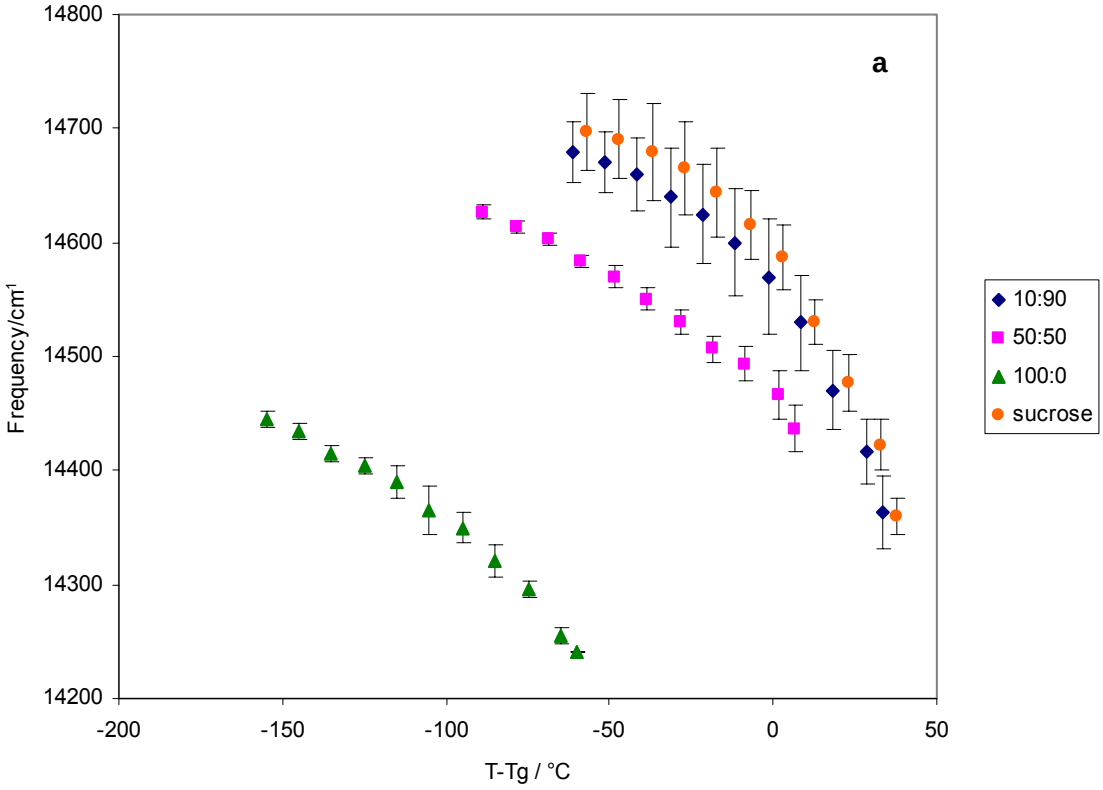
a
14800
14700
14600
14500
14400
14300
14200
Frequency/cm¹
-200
-150
-100
-50
0
50
T-Tg / °C
10:90
50:50
100:0
sucrose

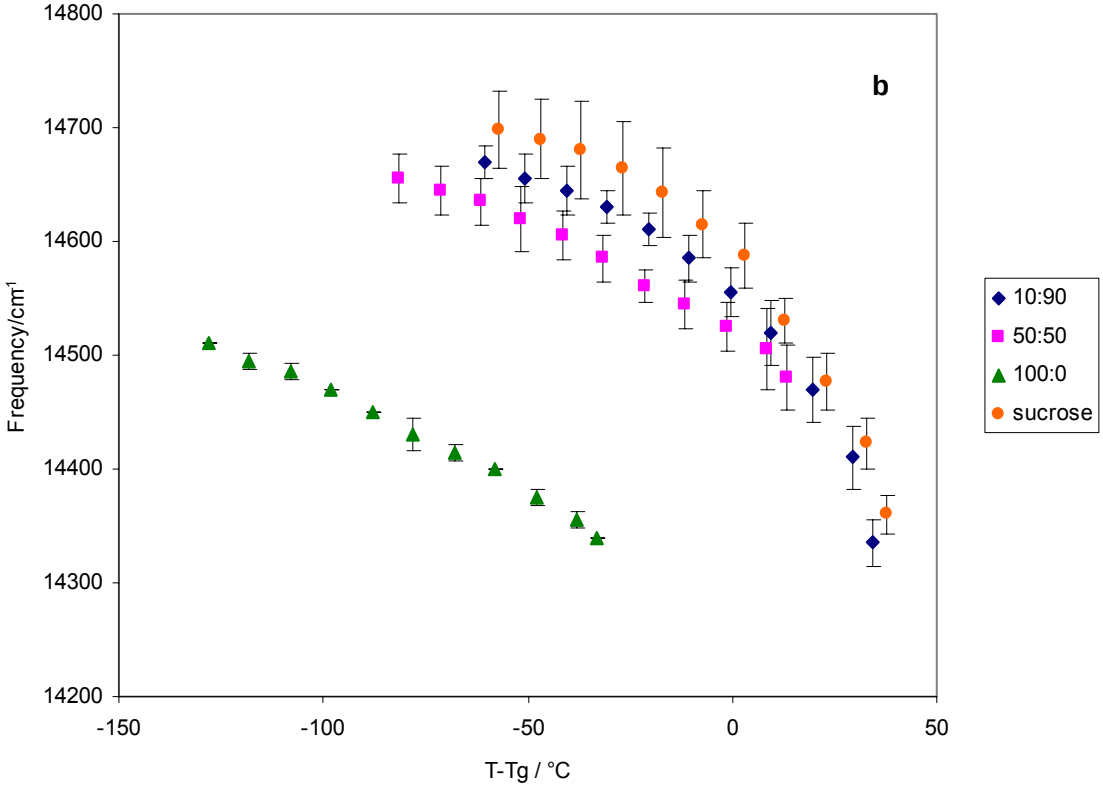
b
14800
14700
14600
14500
14400
14300
14200
Frequency/cm¹
-150
-100
-50
0
50
T-Tg / °C
10:90
50:50
100:0
sucrose

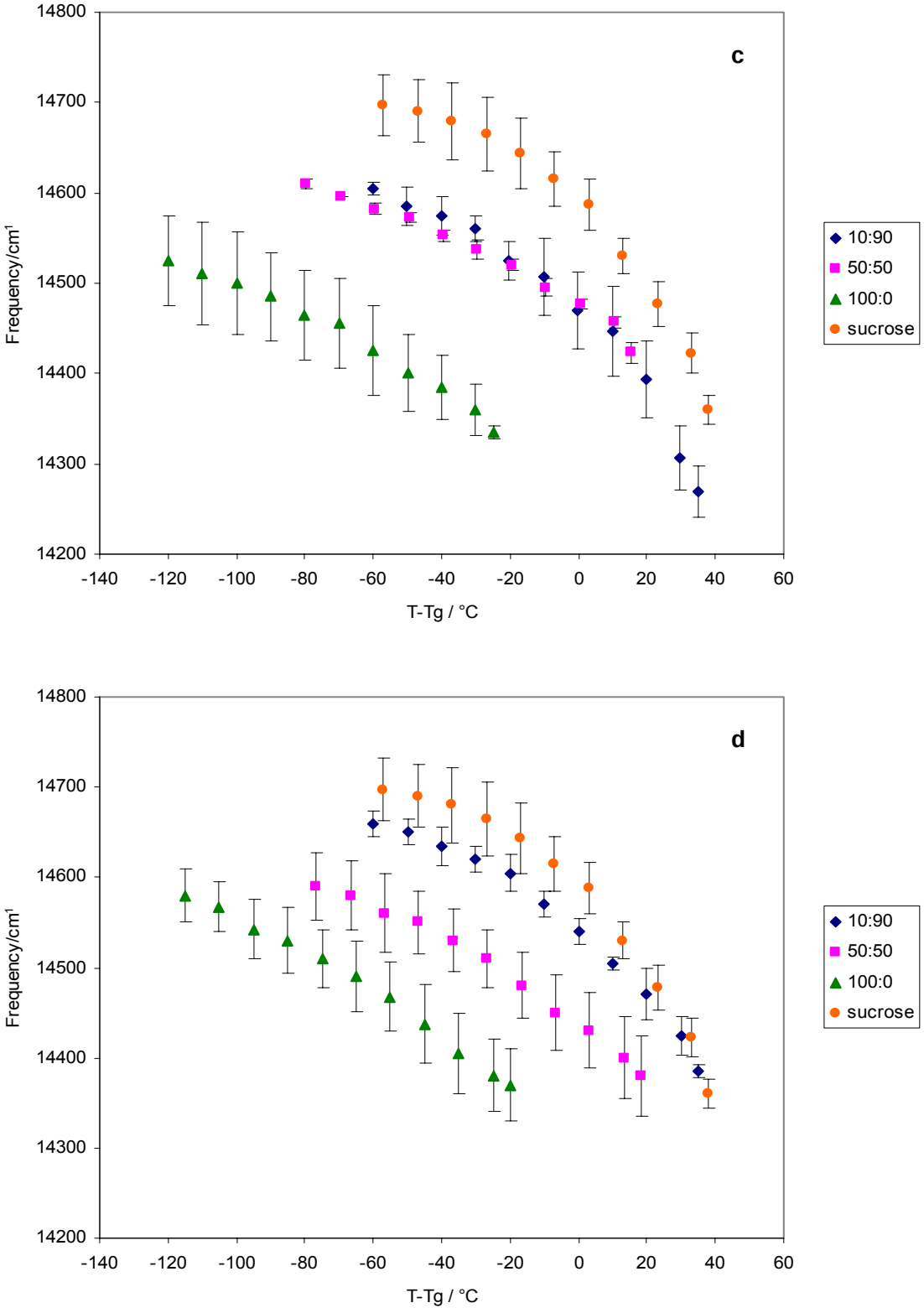

Figure 62: Peak frequency (ν_p) for phosphorescence emission from erythrosin B plotted as a function of T-T_g in amorphous sucrose films containing maltodextrin with DE5 (a); DE10 (b); DE15 (c); and DE18 (d). Delayed emission spectra collected as a function of temperature were analyzed using log-normal line shape function.

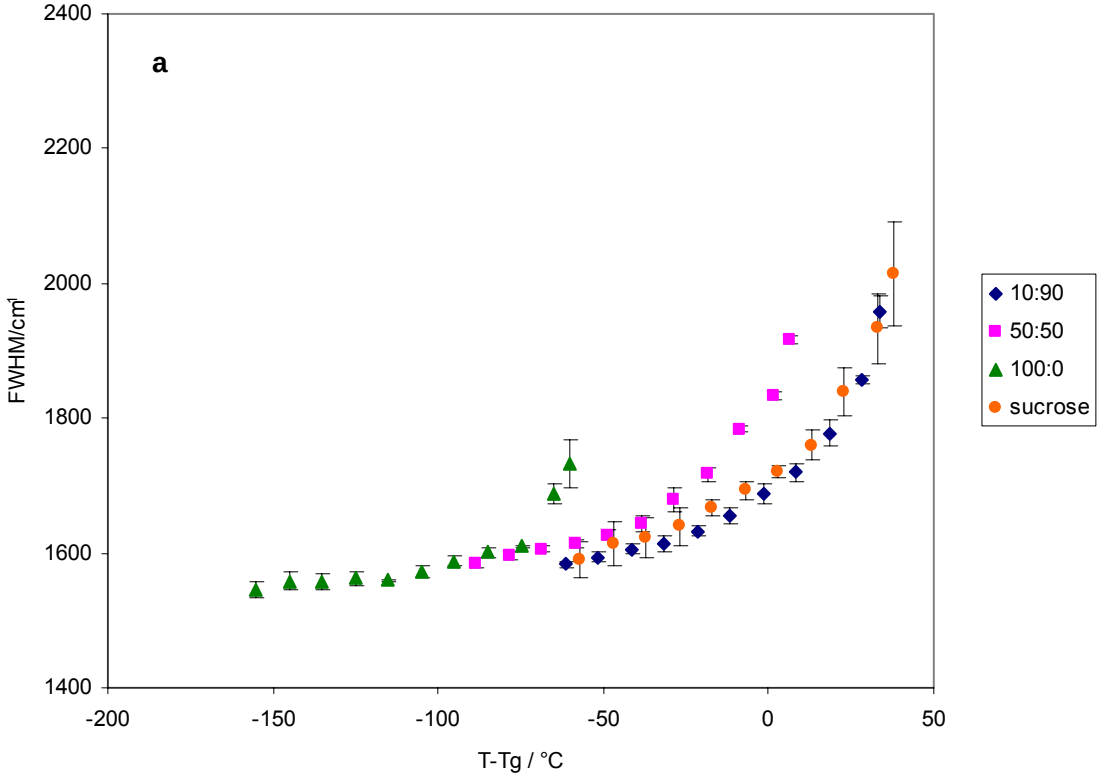
a
2400
2200
2000
1800
1600
1400
FWHM/cm-1
-200
-150
-100
-50
0
50
T-Tg / °C
10:90
50:50
100:0
sucrose

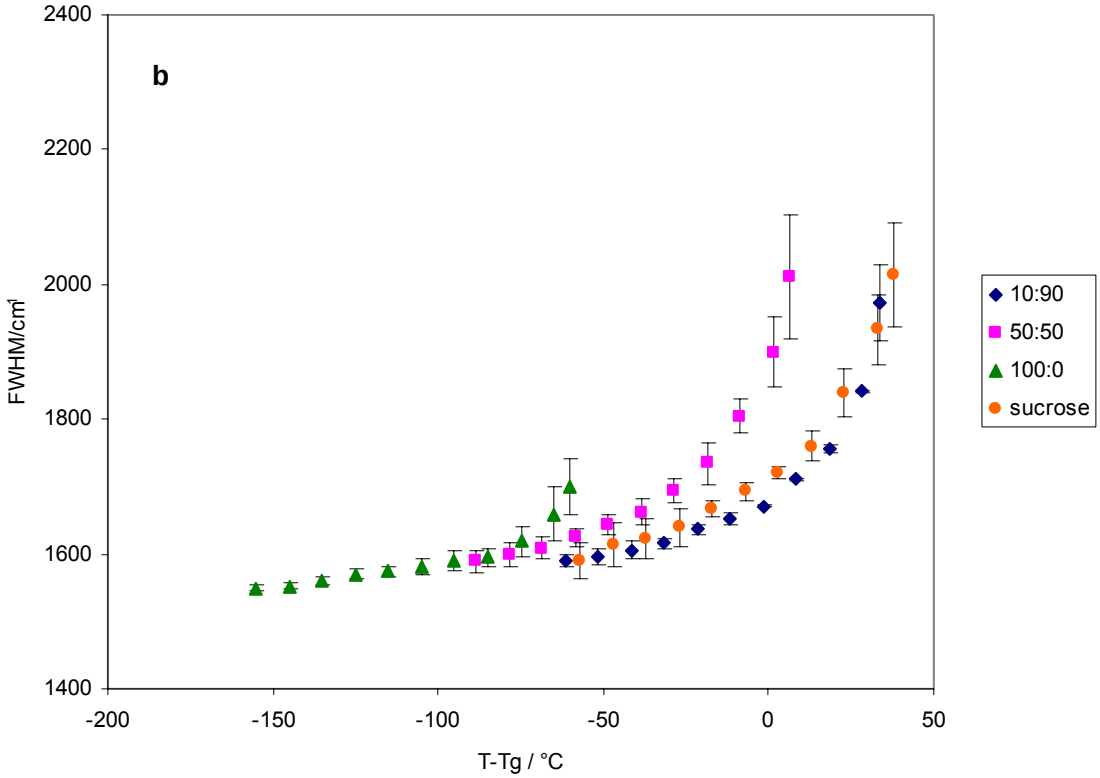
b
2400
2200
2000
1800
1600
1400
FWHM/cm-1
-200
-150
-100
-50
0
50
T-Tg / °C
10:90
50:50
100:0
sucrose

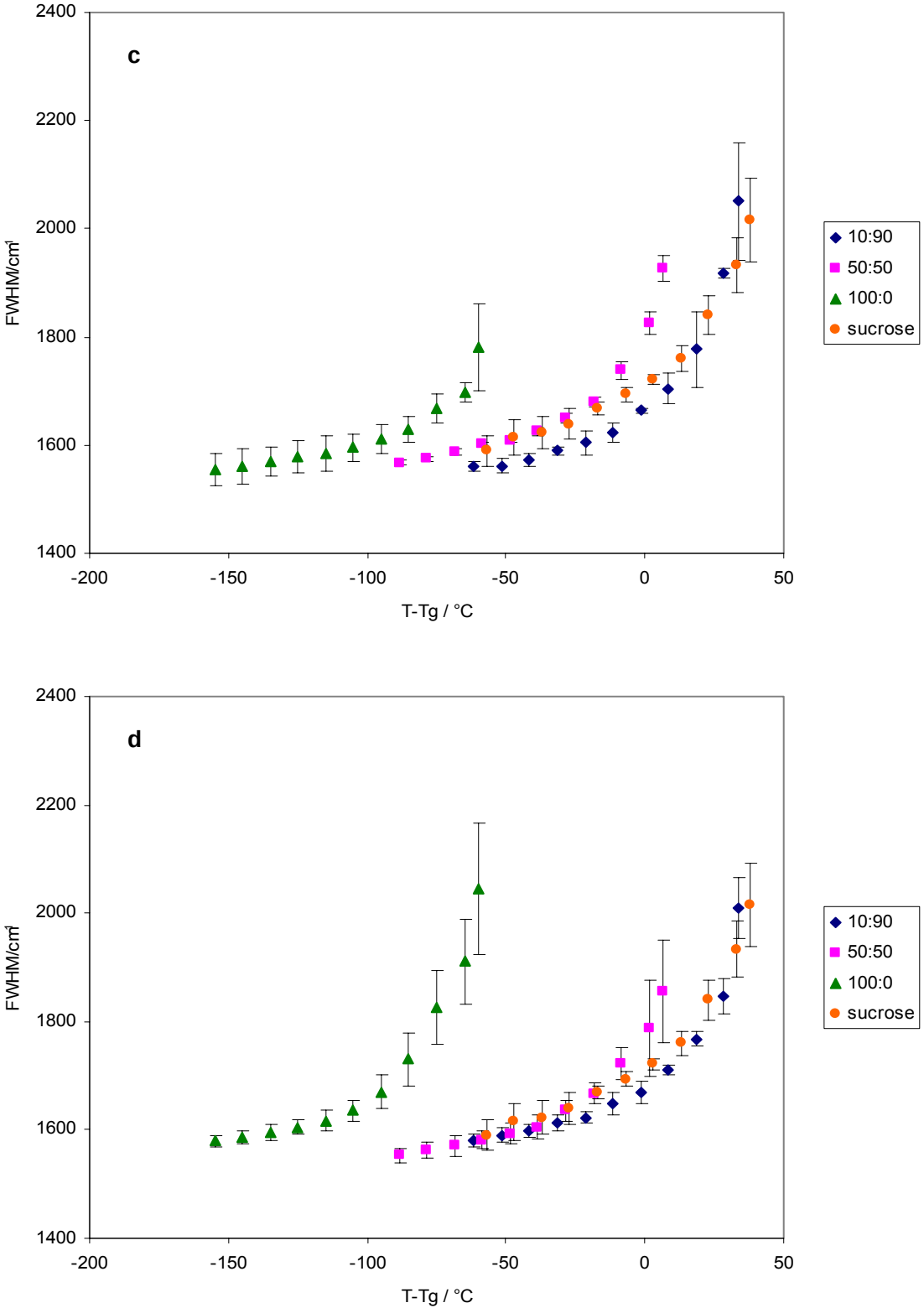

Figure 63: Bandwidth (FWHM) for phosphorescence emission from erythrosin B plotted as a function of T-T_g in amorphous sucrose films containing maltodextrin with DE5 (a); DE10 (b); DE15 (c); and DE18 (d). Delayed emission spectra collected as a function of temperature were analyzed using log-normal line shape function

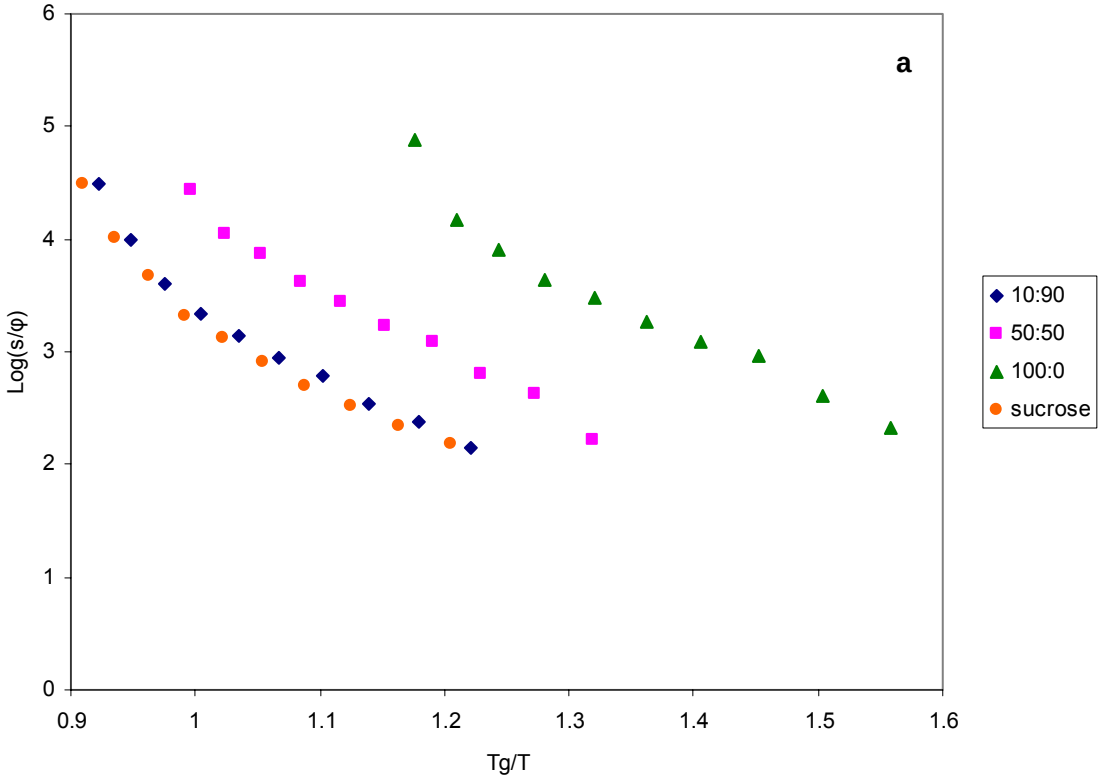
a
Log(s/φ)
Tg/T
0
1
2
3
4
5
6
0.9
1
1.1
1.2
1.3
1.4
1.5
1.6
10:90
50:50
100:0
sucrose

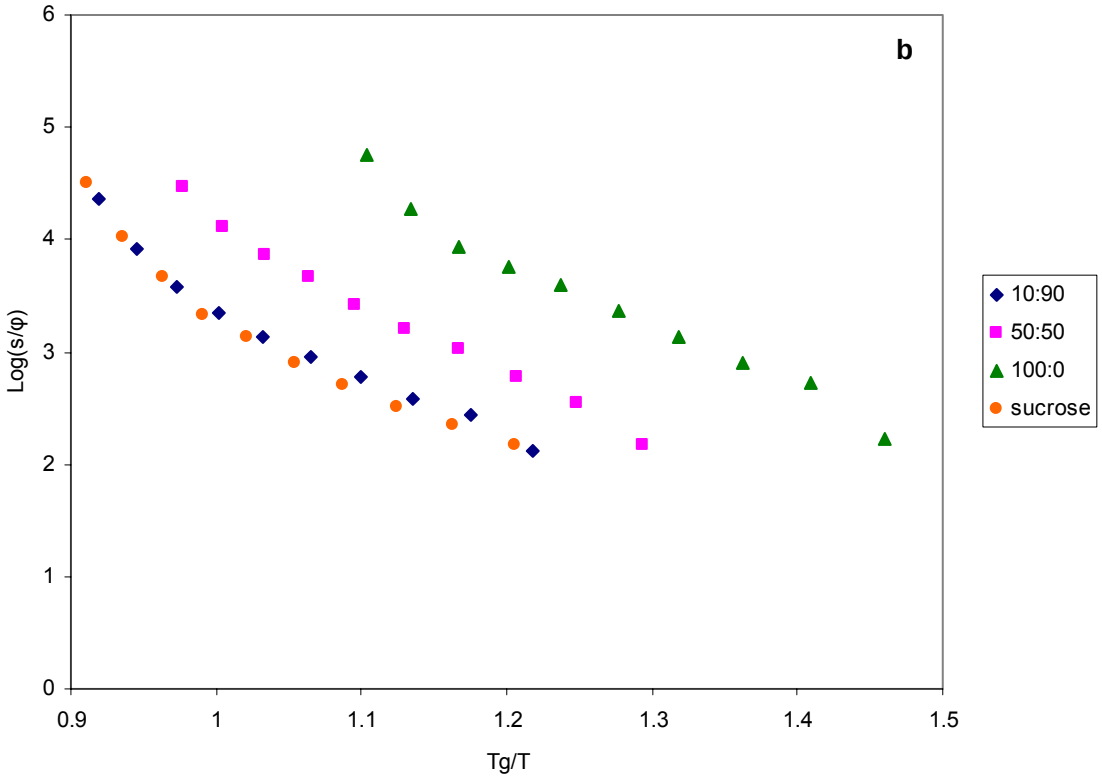
b
Log(s/φ)
Tg/T
0
1
2
3
4
5
6
0.9
1
1.1
1.2
1.3
1.4
1.5
10:90
50:50
100:0
sucrose

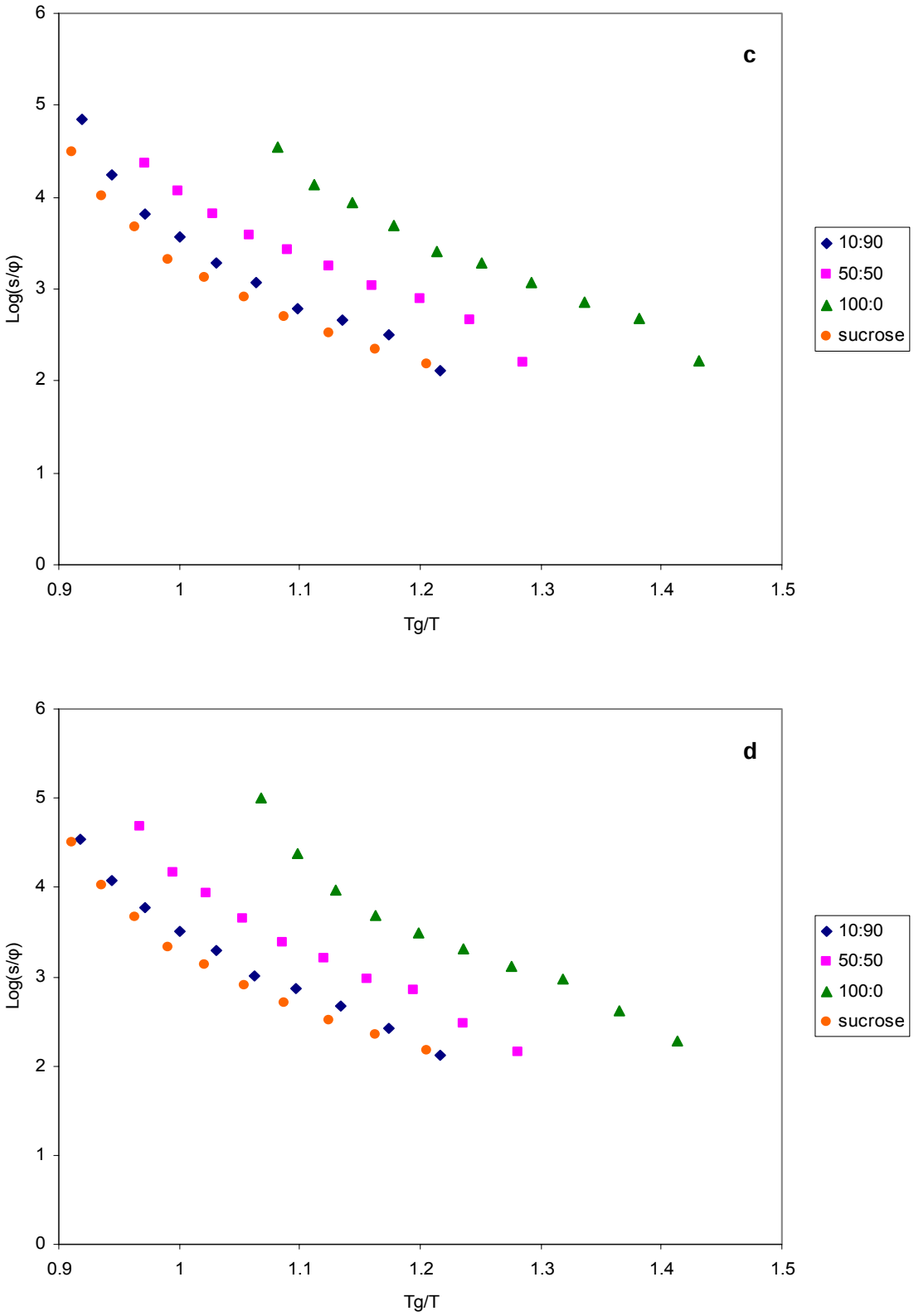

Figure 64: Modified Arrhenius plot of the dipolar relaxation rate versus T_g/T in amorphous sucrose films containing maltodextrin with DE5 (a); DE10 (b); DE15 (c); and DE18 (d).

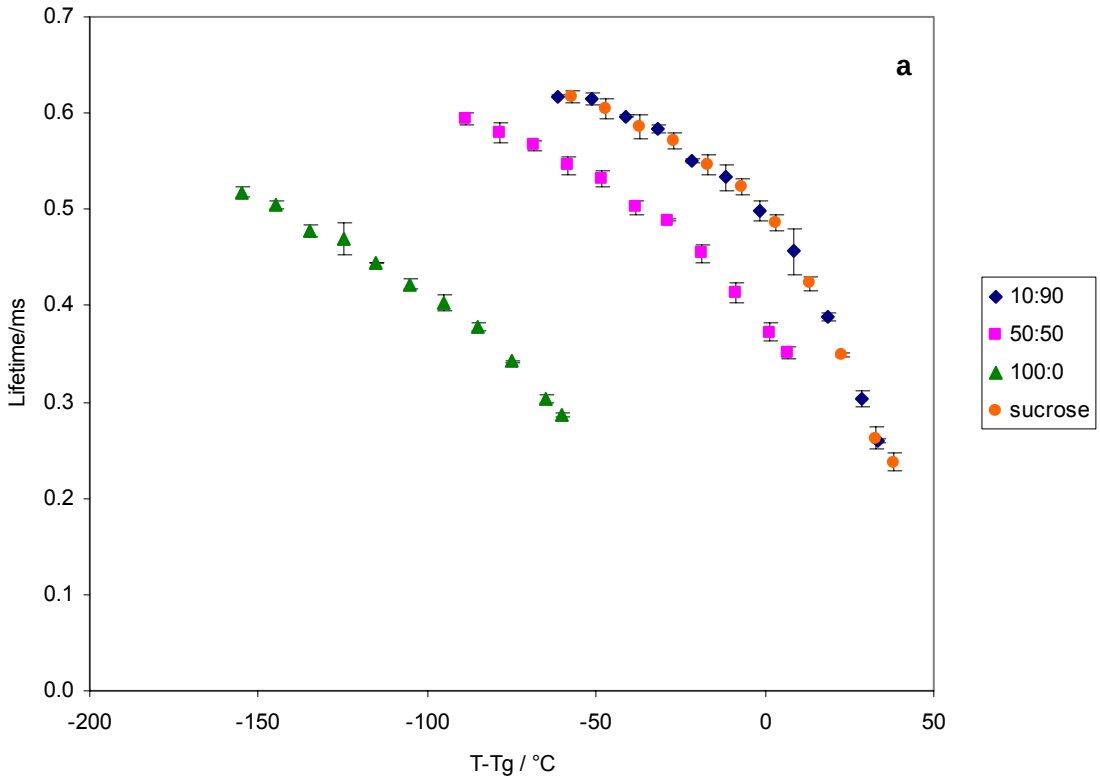
a
Lifetime/ms
T-Tg / °C
0.0
0.1
0.2
0.3
0.4
0.5
0.6
0.7
-200
-150
-100
-50
0
50
10:90
50:50
100:0
sucrose

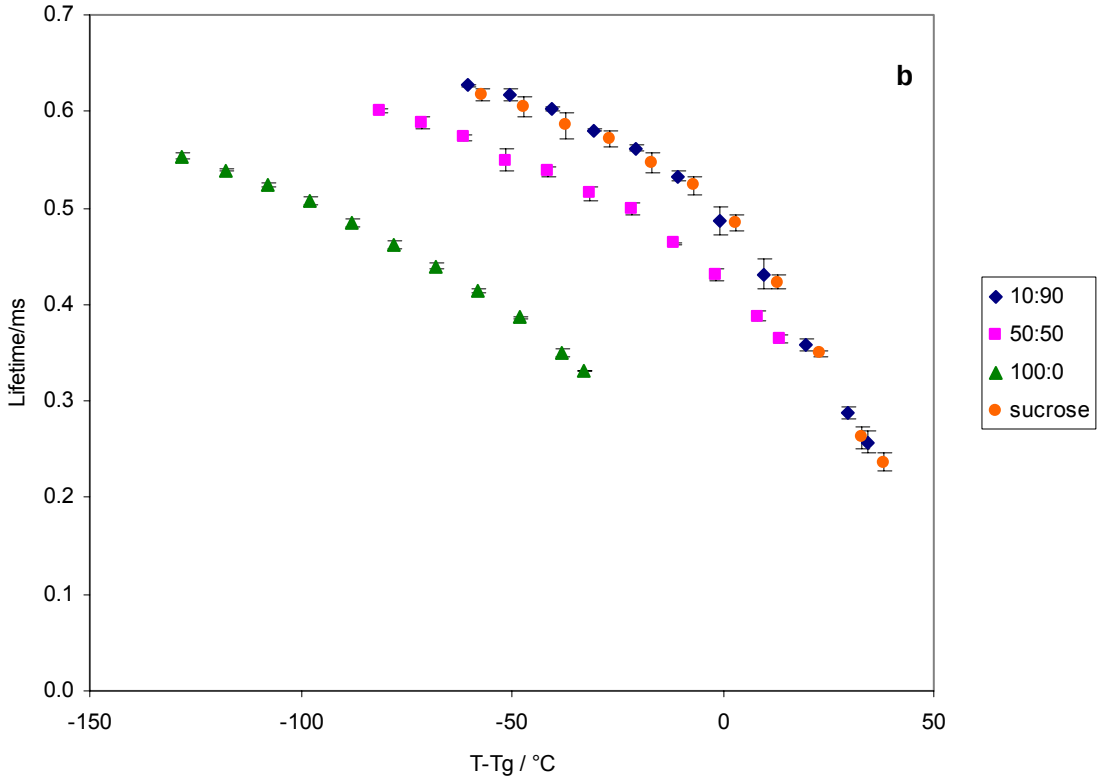
b
Lifetime/ms
T-Tg / °C
0.0
0.1
0.2
0.3
0.4
0.5
0.6
0.7
-150
-100
-50
0
50
10:90
50:50
100:0
sucrose

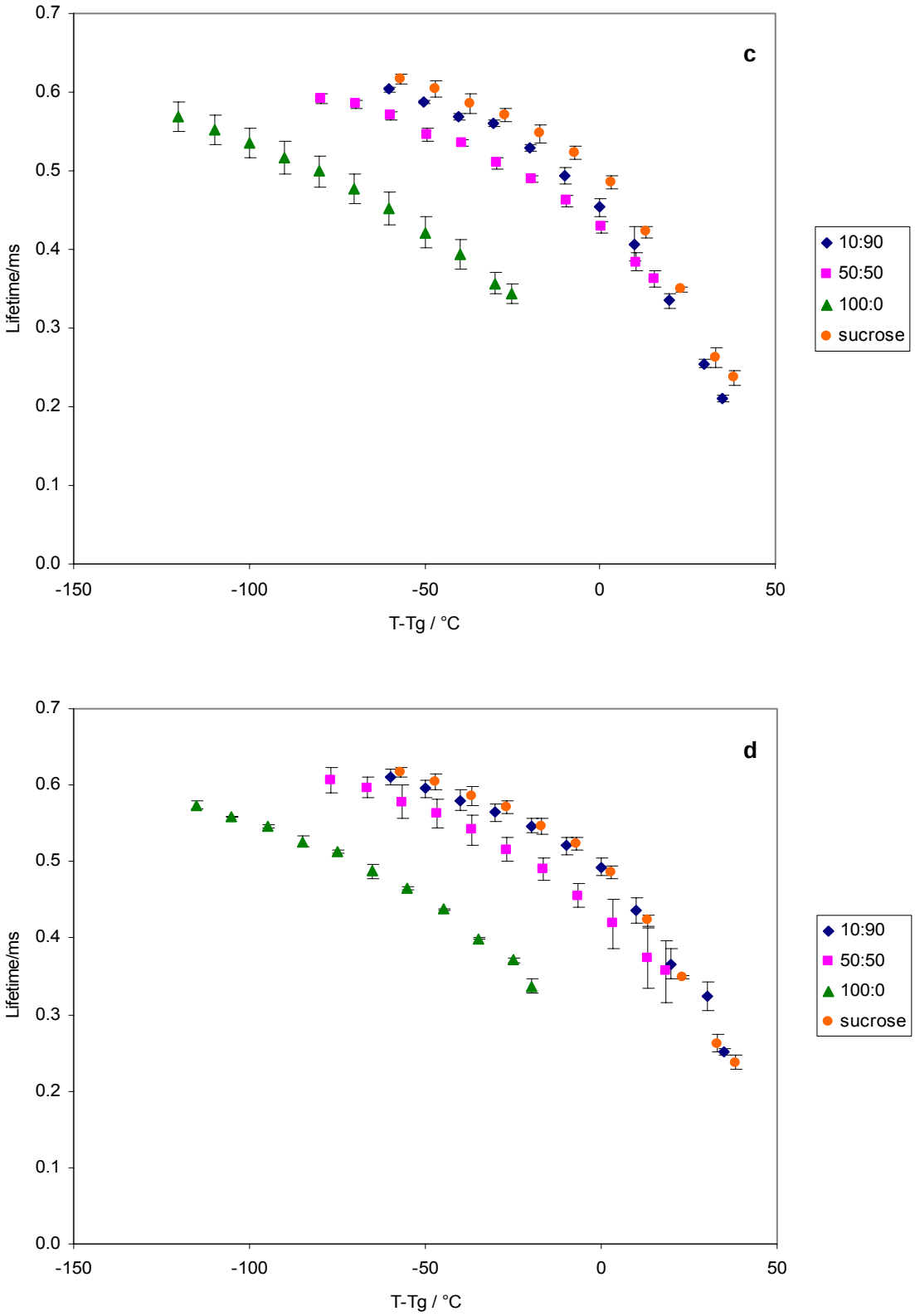

Figure 65: Plot of lifetime obtained from fits to a stretched exponential decay model of the intensity decay of erythrosin B versus T-T_g in amorphous sucrose films containing maltodextrin with DE5 (a); DE10 (b); DE15 (c); and DE18 (d).

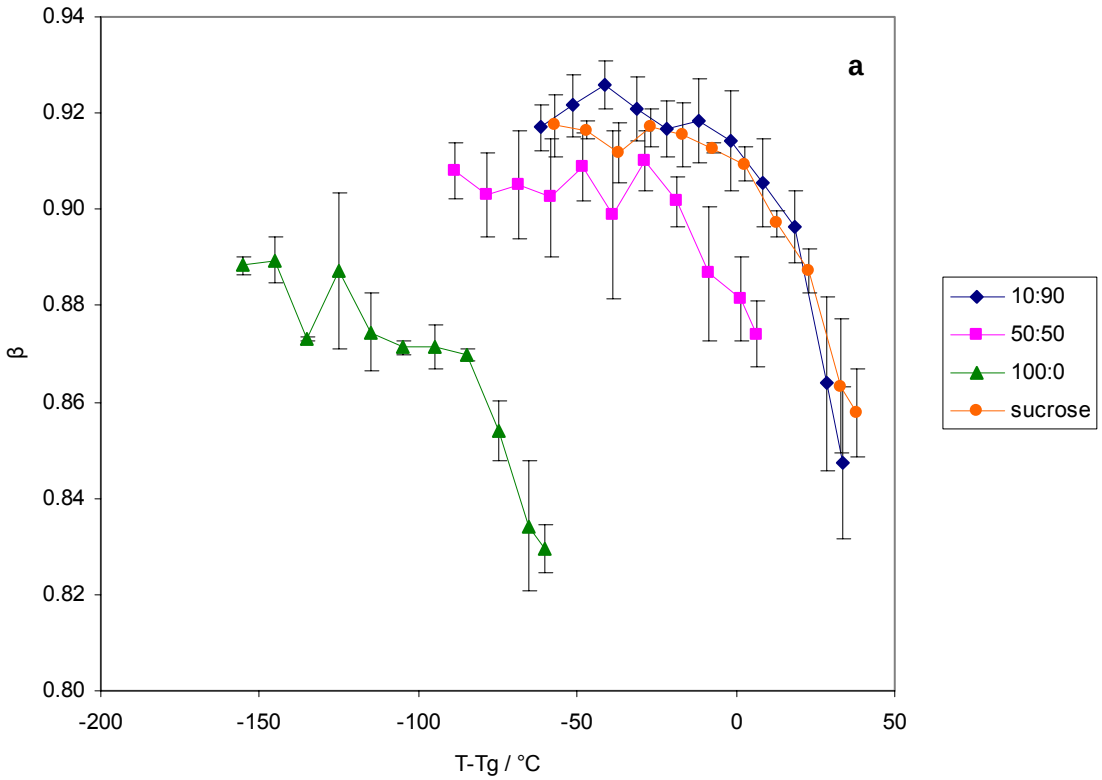
a
0.94
0.92
0.90
0.88
0.86
0.84
0.82
0.80
β
-200
-150
-100
-50
0
50
T-Tg / °C
10:90
50:50
100:0
sucrose

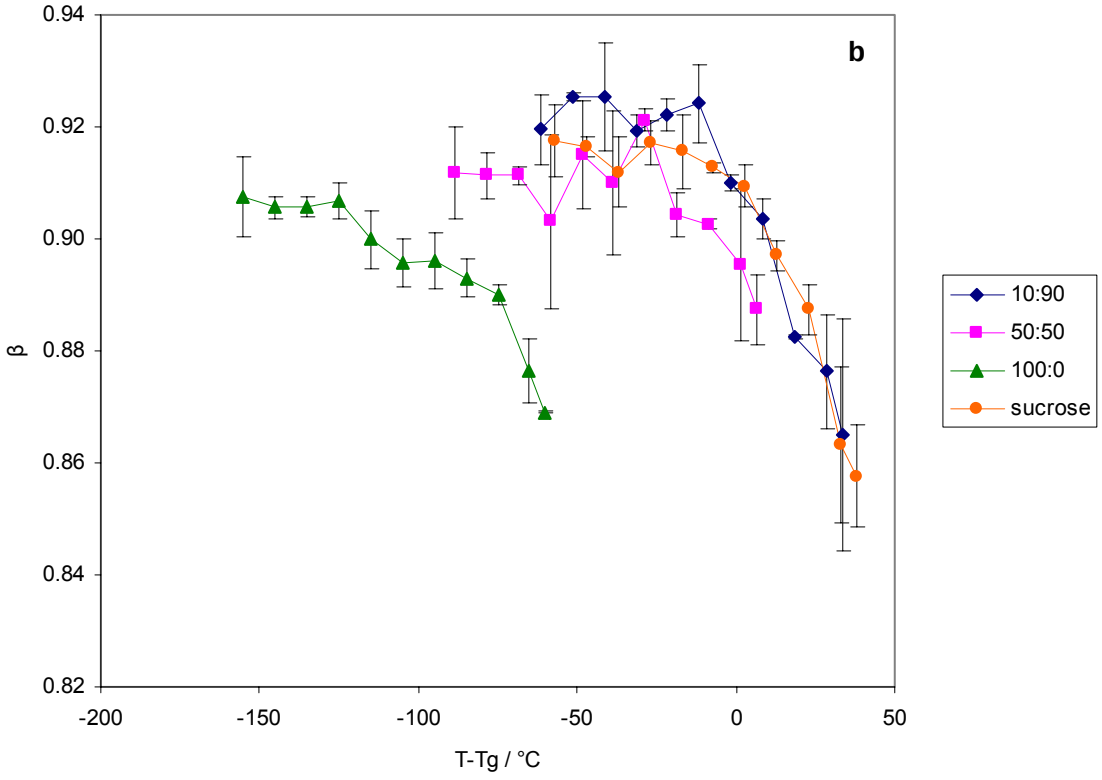
b
0.94
0.92
0.90
0.88
0.86
0.84
0.82
β
-200
-150
-100
-50
0
50
T-Tg / °C
10:90
50:50
100:0
sucrose

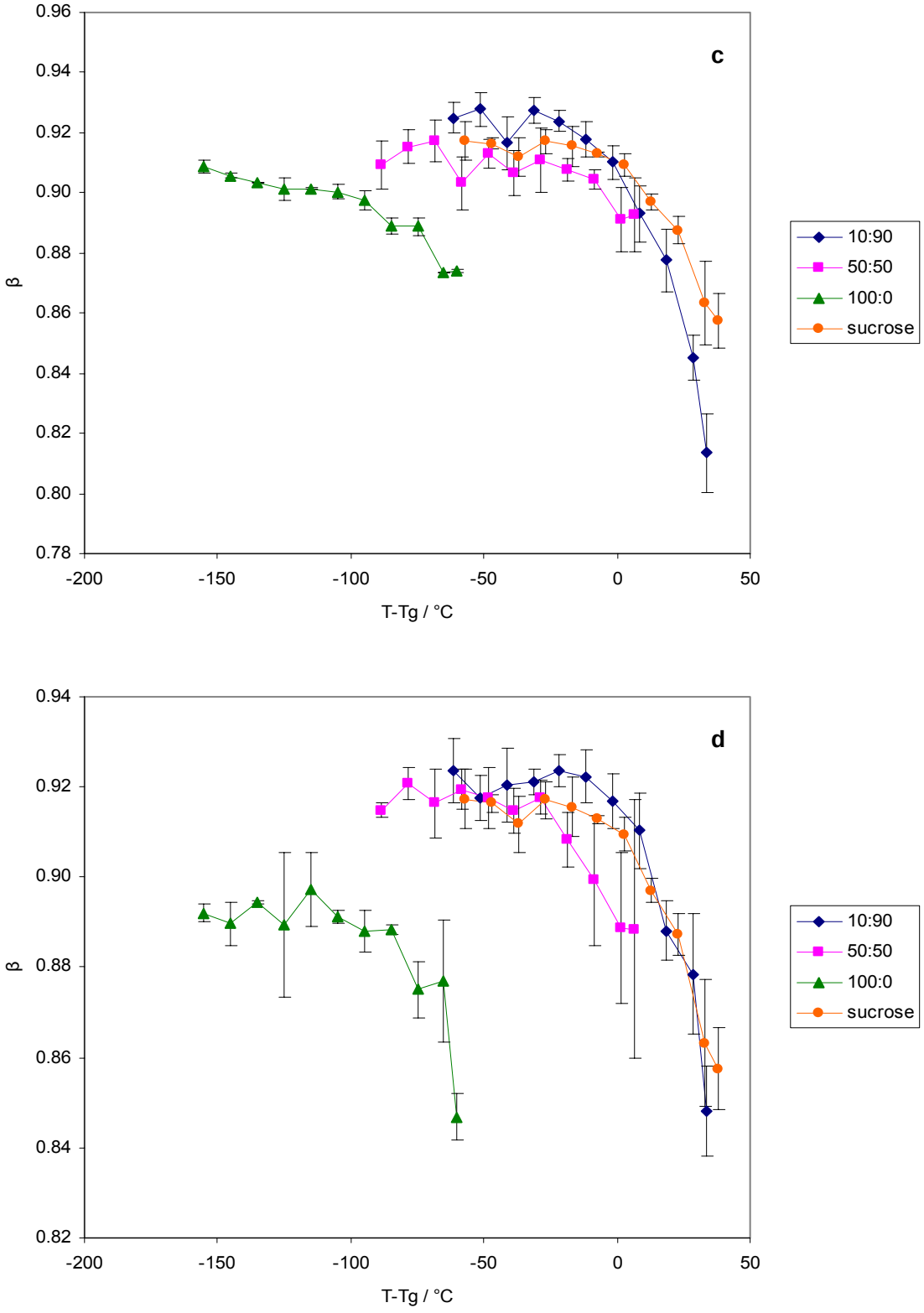

Figure 66: Stretching exponent β obtained from fits to a stretched exponential decay model of the intensity decay of erythrosin B as a function of T- T_g in amorphous sucrose films containing maltodextrin with DE5 (a); DE10 (b); DE15 (c); and DE18 (d).

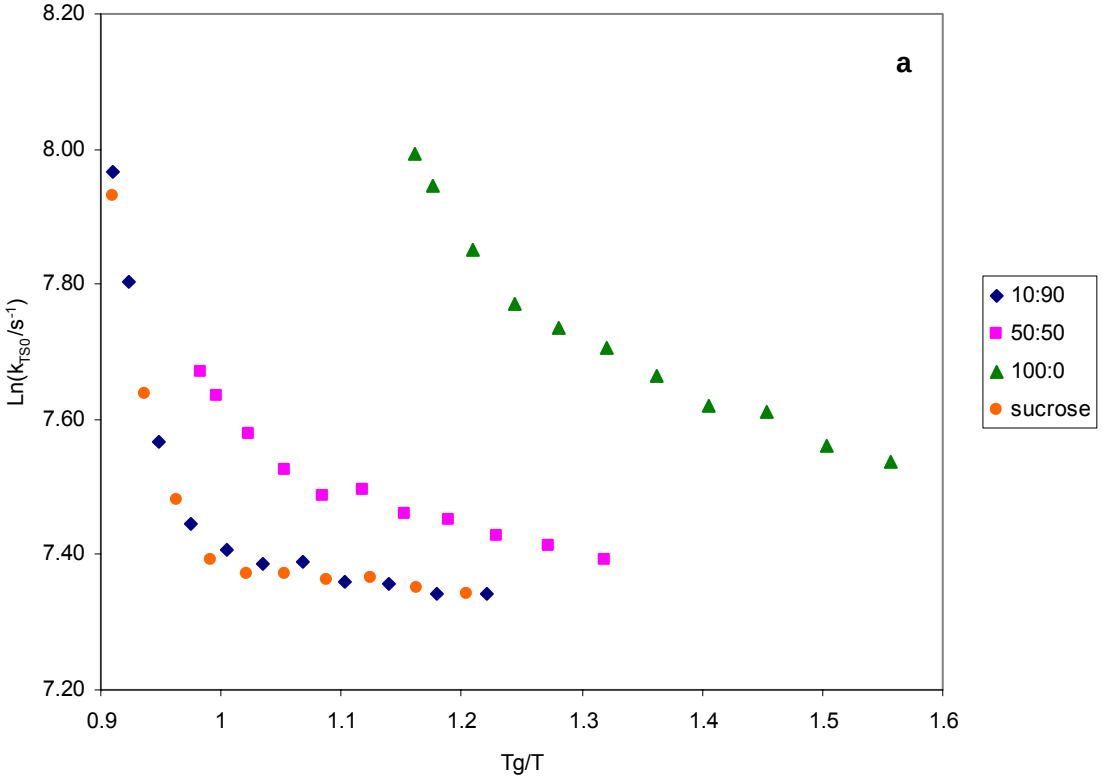
a
8.20
8.00
7.80
7.60
7.40
7.20
0.9
1
1.1
1.2
1.3
1.4
1.5
1.6
Ln(k_TS0/s^-1)
Tg/T
10:90
50:50
100:0
sucrose

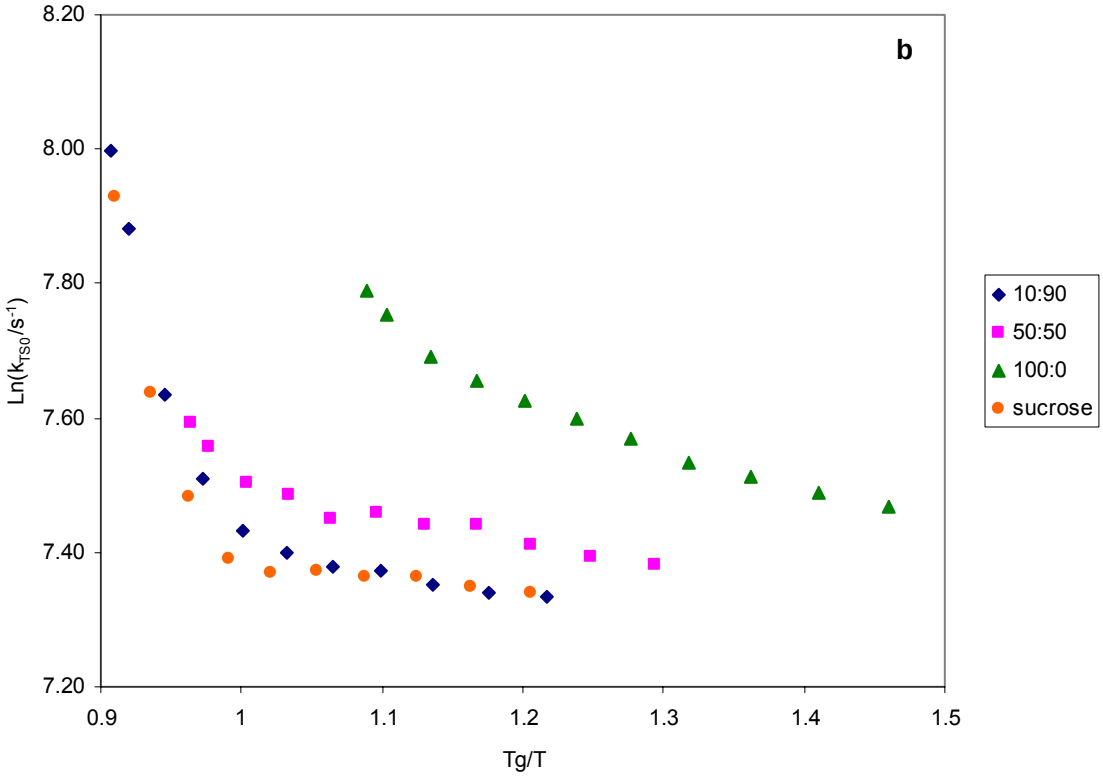
b
8.20
8.00
7.80
7.60
7.40
7.20
0.9
1
1.1
1.2
1.3
1.4
1.5
Ln(k_TS0/s^-1)
Tg/T
10:90
50:50
100:0
sucrose

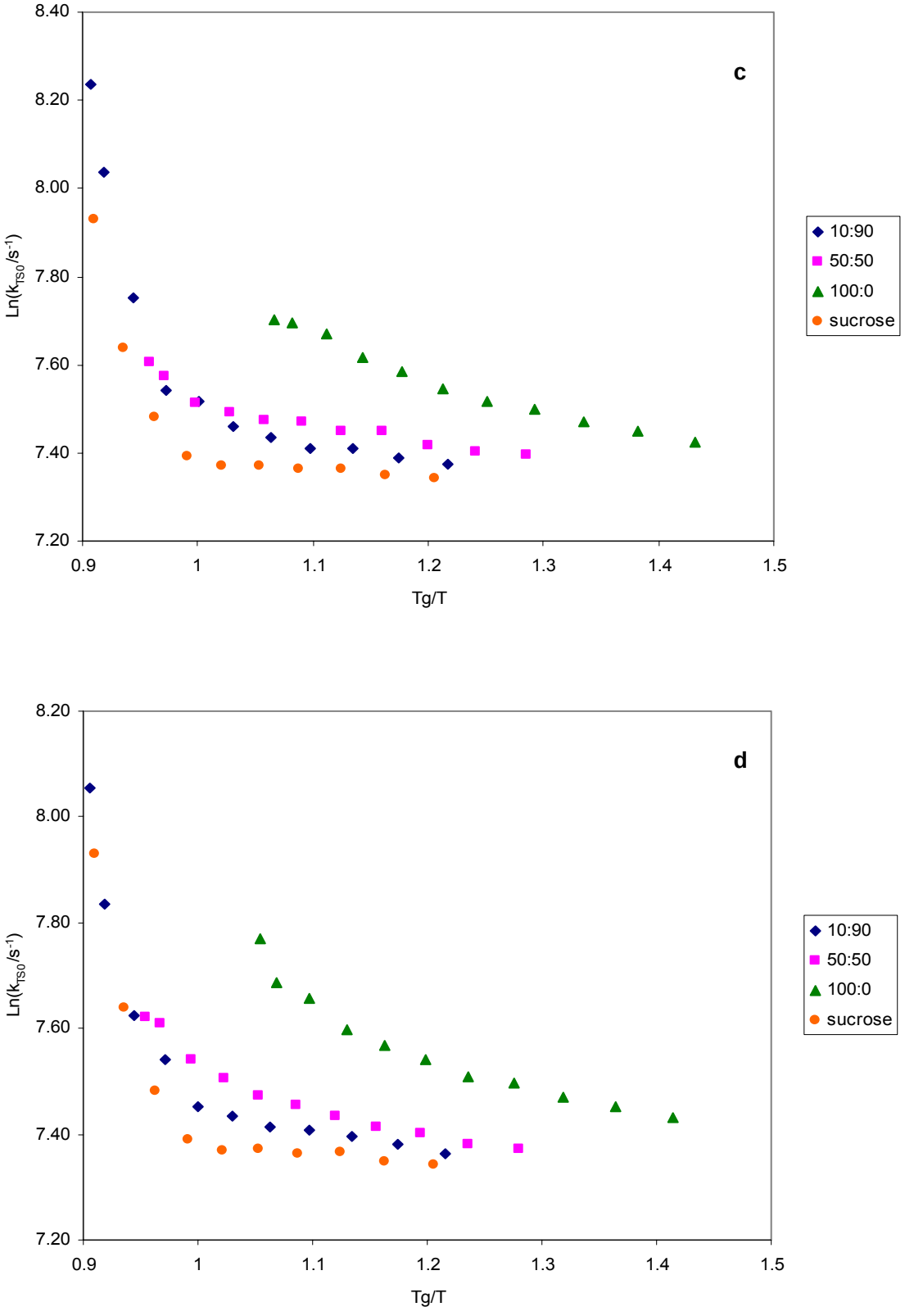

Figure 67: Arrhenius plot of the rate constant for non-radiative decay of the triplet T_1 state to S_0 (k_{TS0}) versus T_g/T in amorphous sucrose films containing maltodextrin with DE5 (a); DE10 (b); DE15 (c); and DE18 (d).

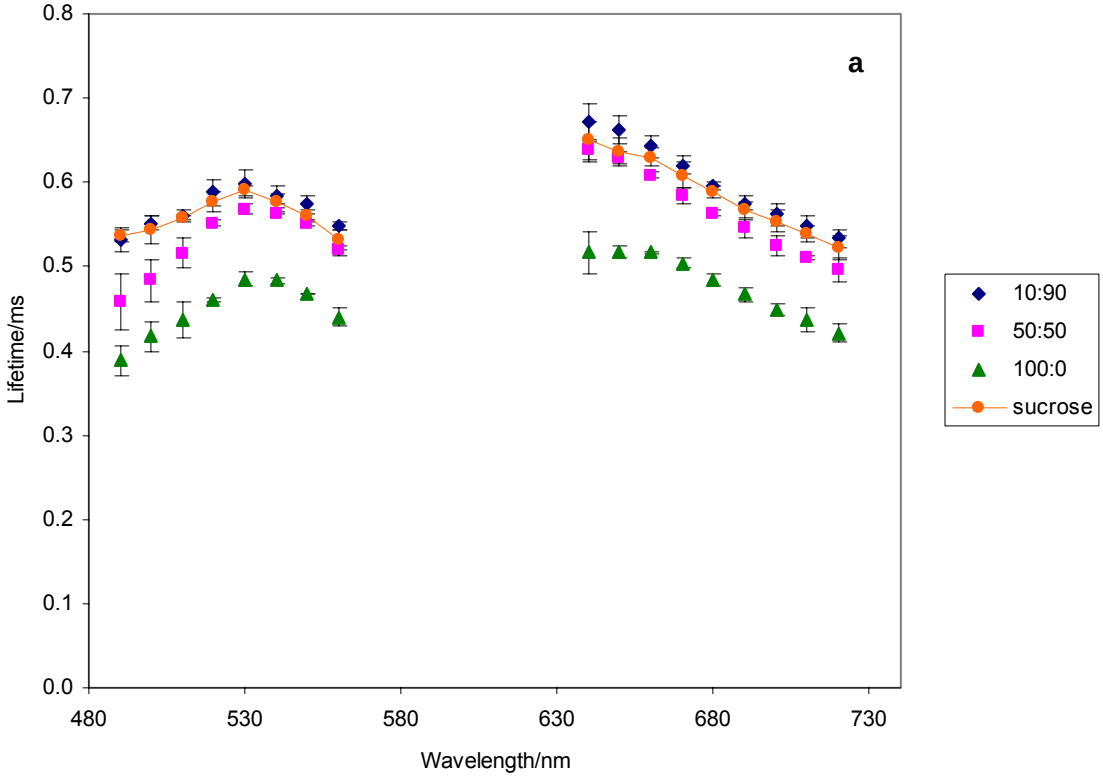
a
Lifetime/ms
Wavelength/nm
0.0
0.1
0.2
0.3
0.4
0.5
0.6
0.7
0.8
480
530
580
630
680
730
10:90
50:50
100:0
sucrose

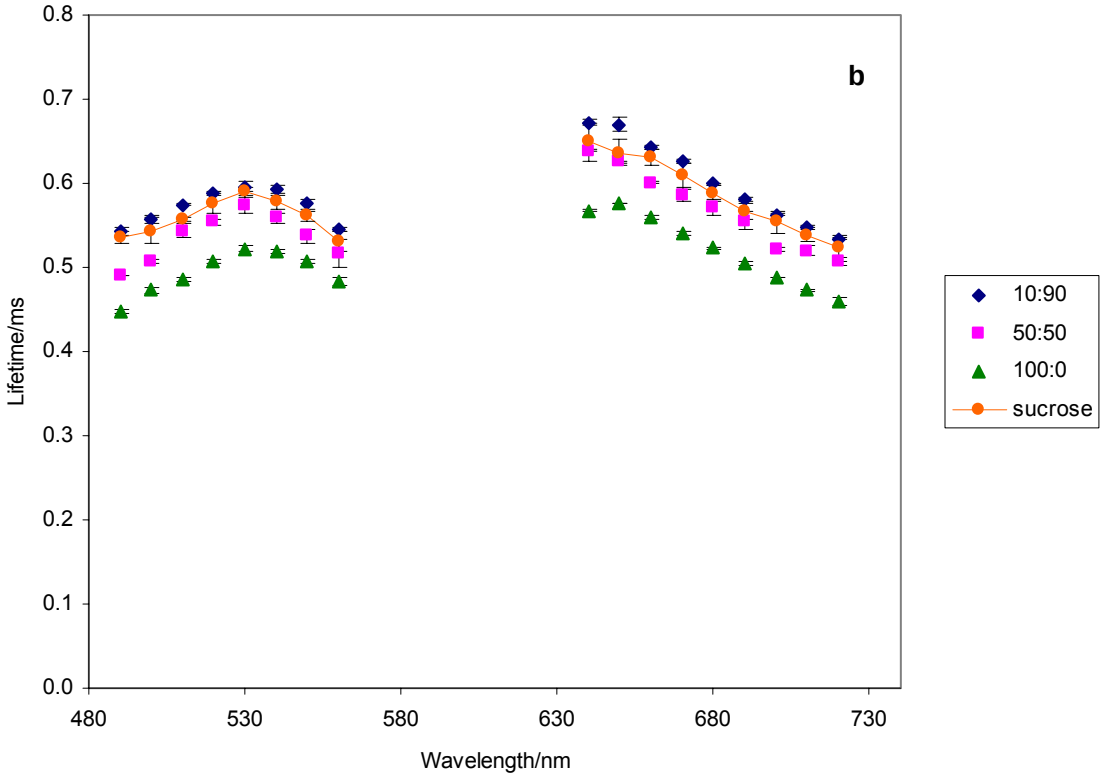
b
Lifetime/ms
Wavelength/nm
0.0
0.1
0.2
0.3
0.4
0.5
0.6
0.7
0.8
480
530
580
630
680
730
10:90
50:50
100:0
sucrose

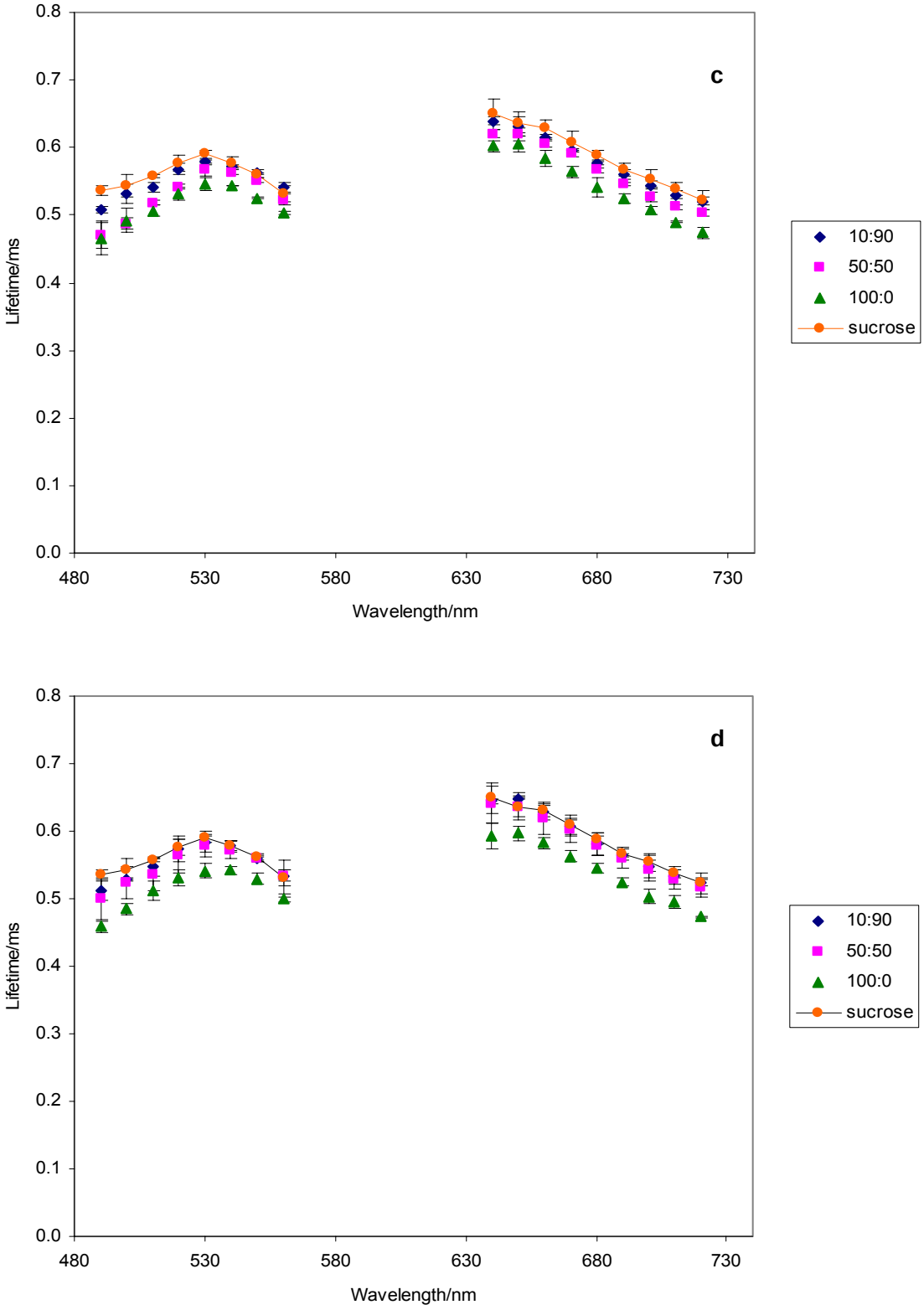

Figure 68: The effect of excitation wavelength (with 680 nm emission) and emission wavelength (with 530 nm excitation) on the lifetimes from fits of erythrosin B phosphorescence intensity decays to the stretched exponential decay model in amorphous sucrose films containing maltodextrin with DE5 (a); DE10 (b); DE15 (c); and DE18 (d).

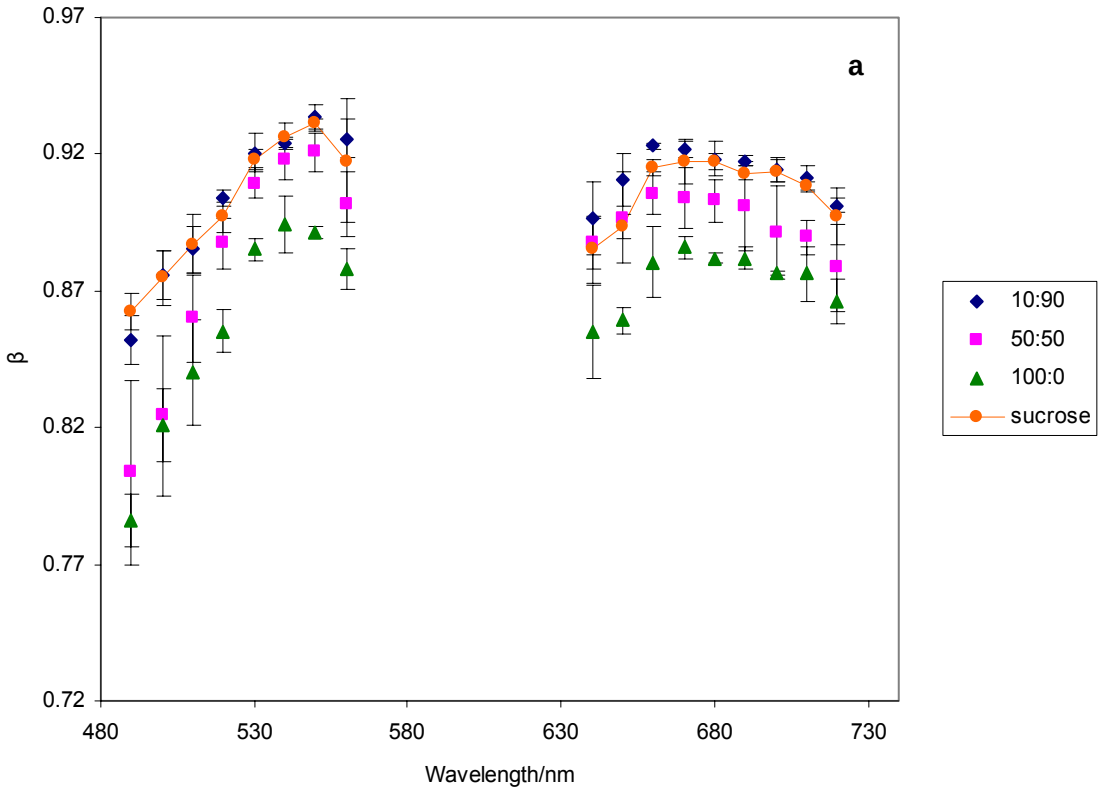
a
0.97
0.92
0.87
0.82
0.77
0.72
β
480
530
580
630
680
730
Wavelength/nm
10:90
50:50
100:0
sucrose

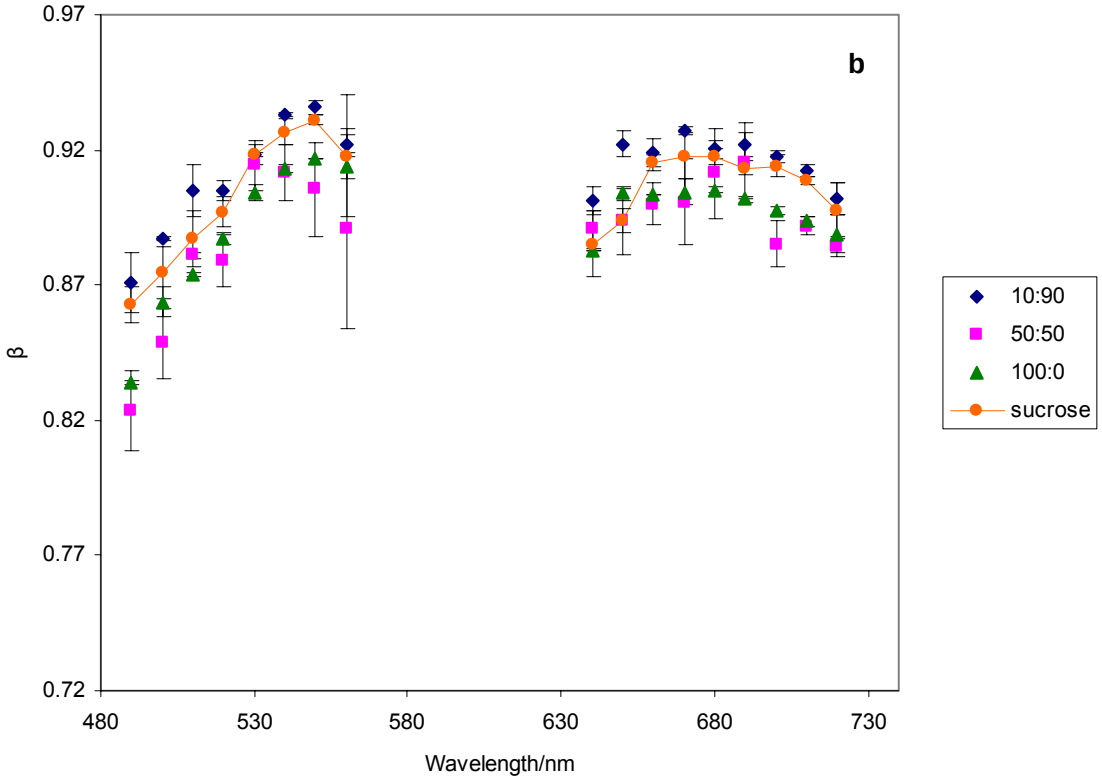
b
0.97
0.92
0.87
0.82
0.77
0.72
β
480
530
580
630
680
730
Wavelength/nm
10:90
50:50
100:0
sucrose

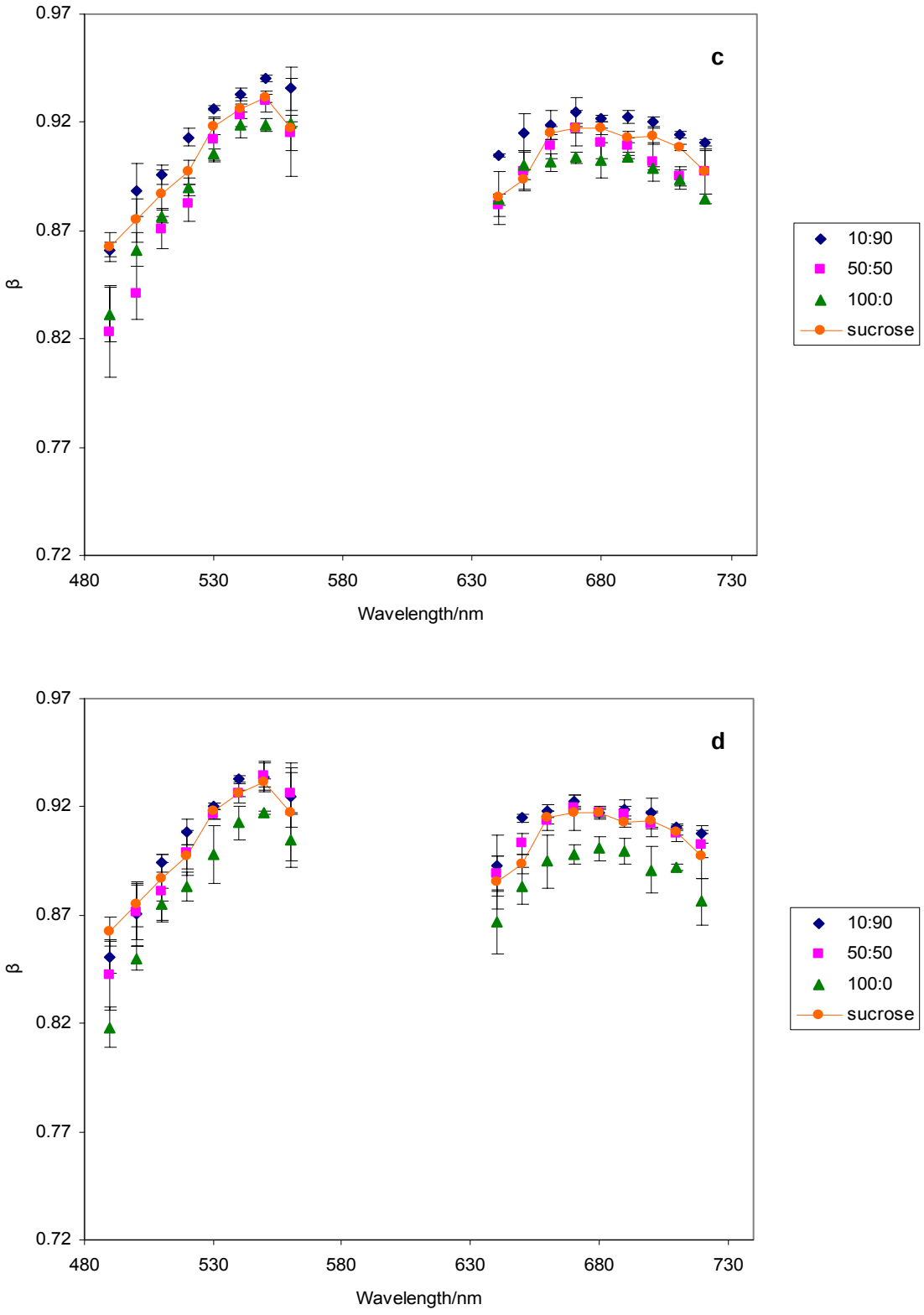

Figure 69 The effect of excitation wavelength (with 680 nm emission) and emission wavelength (with 530 nm excitation) on the stretching exponents β from fits of erythrosin B phosphorescence intensity decays to the stretched exponential decay model in amorphous sucrose films containing maltodextrin with DE5 (a); DE10 (b); DE15 (c); and DE18 (d).

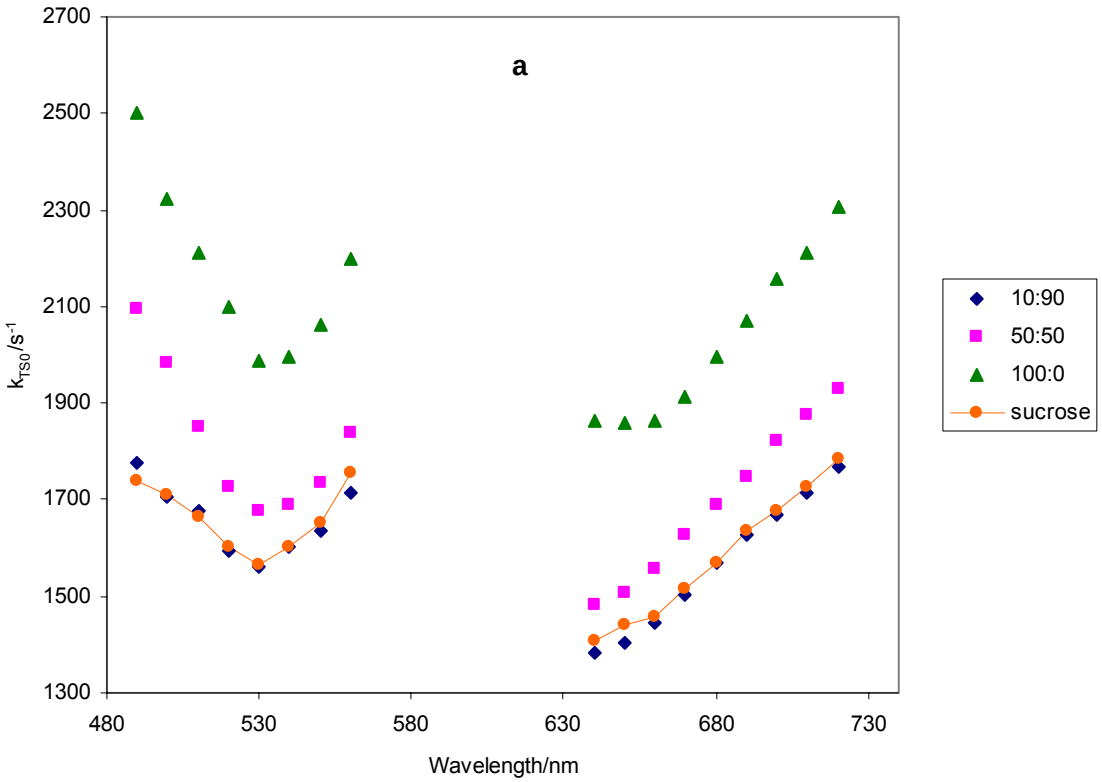
a
2700
2500
2300
2100
1900
1700
1500
1300
480
530
580
630
680
730
Wavelength/nm
k_{TS0}/s^{-1}
10:90
50:50
100:0
sucrose

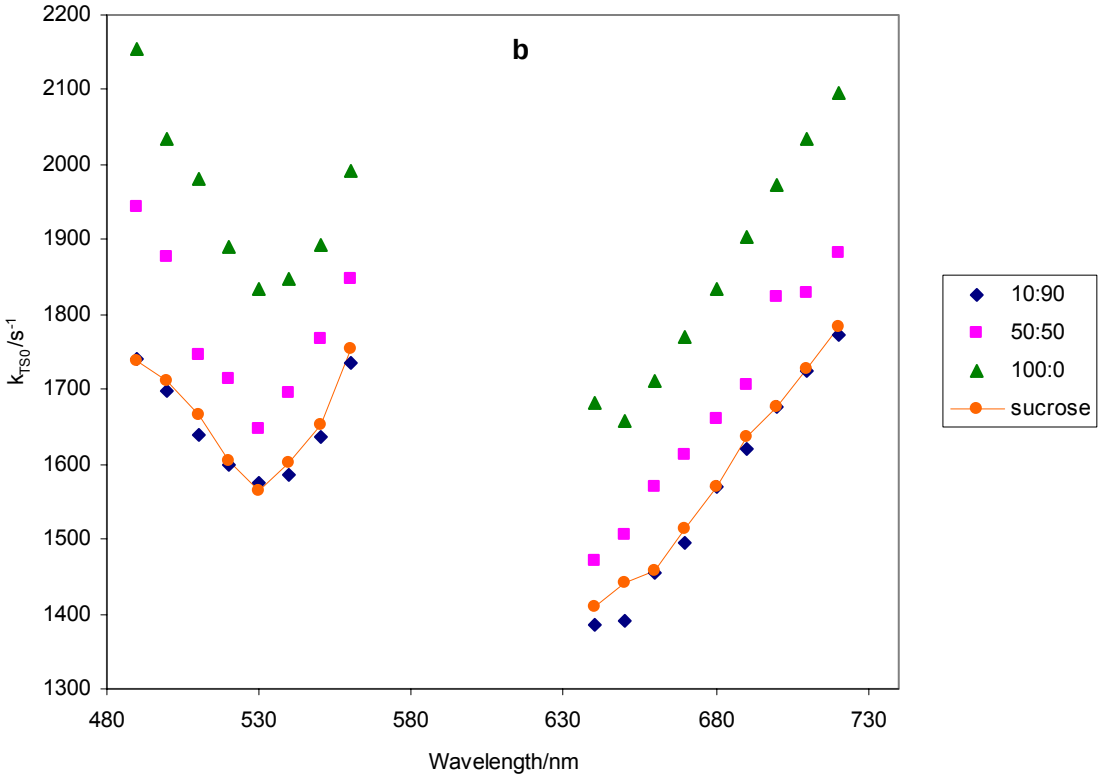
b
2200
2100
2000
1900
1800
1700
1600
1500
1400
1300
480
530
580
630
680
730
Wavelength/nm
k_{TS0}/s^{-1}
10:90
50:50
100:0
sucrose

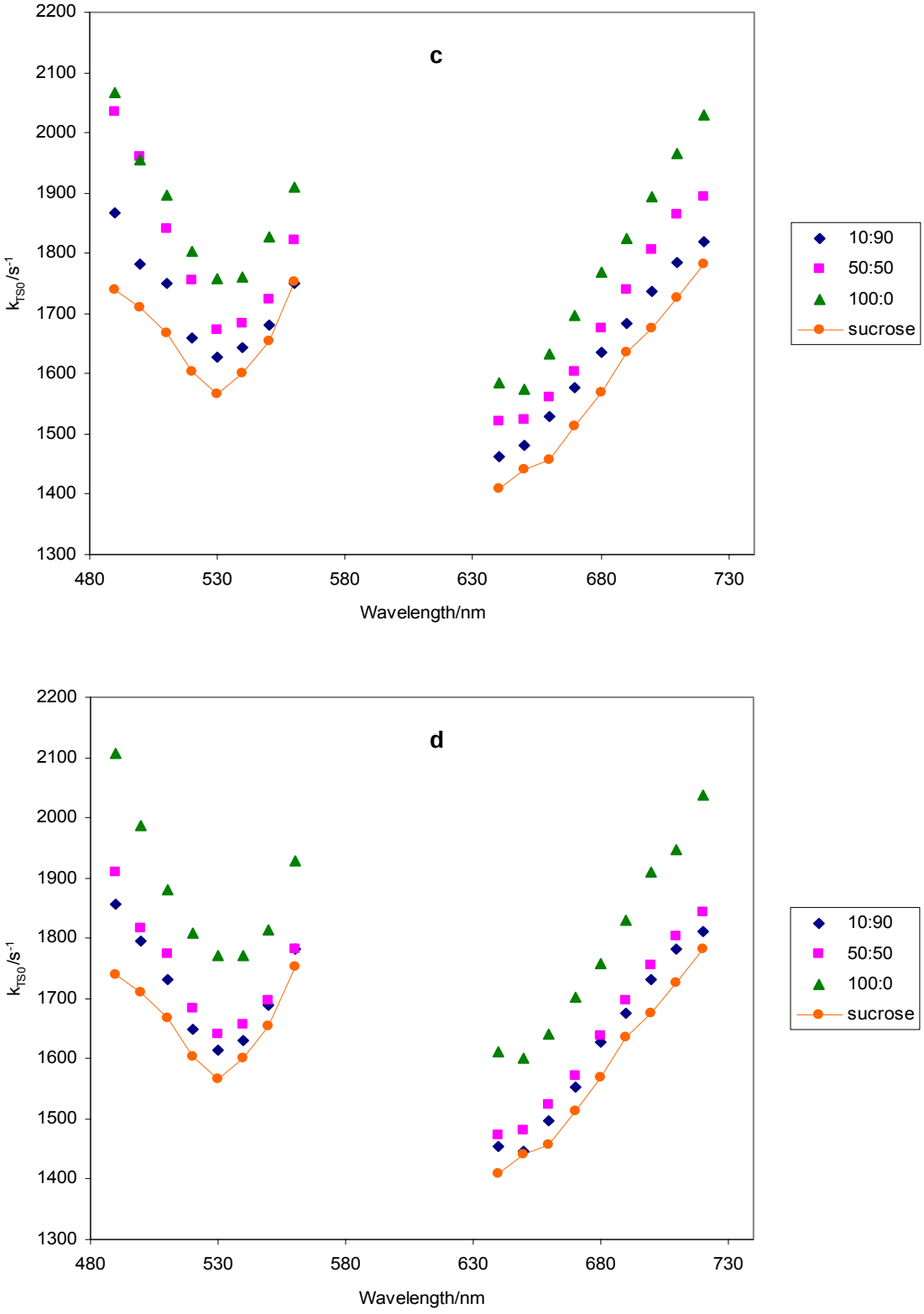

Figure 70: The rate constant for non-radiative decay of the triplet state to S_0 (k_{TS0}) plotted as a function of excitation wavelength (with 680 nm emission) and emission wavelength (with 530 nm excitation) in amorphous sucrose films containing maltodextrin with DE5 (a); DE10 (b); DE15 (c); and DE18 (d).

Chapter 7 Gelatin effect on molecular mobility of amorphous sucrose from erythrosin B phosphorescence

Introduction

Sucrose glasses have been an object of research for many years since it was found to be one of the earliest cryoprotective agents during anhydrobiosis. Its ability to protect biomaterials from freeze-thaw damage and provide long-term storage stability has attracted researchers to investigate the mechanism and develop solid state formulations through drying or freeze-drying for labile compounds in foods, such as vitamins and flavor compounds, and for labile biomolecules in pharmaceuticals, such as enzymes, proteins, and antibodies.

Two main mechanisms, glass dynamics and specific interaction, are proposed to understand the role of sucrose in stabilization of sensitive compounds during dehydration and storage (Kets et al., 2004; Chang et al., 2005). The glass dynamics mechanism (Franks et al., 1991; Slade and Levine, 1991) focuses on the rigid, inert matrix formed by vitrification (glass formation) of stabilizers such as sugars. By forming into amorphous, non-crystalline solids upon rapid drying from aqueous solution or cooling from the melt, sugars change from soft, pliable and flexible at high temperature to hard, brittle and rigid at low temperature with an extreme increase in viscosity due to the decrease in the rate of translational as well as rotational and vibrational mobility motions (Zallen, 1983). Therefore, glass formation is a purely kinetic mechanism, and the stability is expected to correlate to molecular mobility in the rigid matrix. The specific interaction mechanism (Carpenter and Crowe, 1989; Carpenter et al., 1993; Crowe et al., 1993), commonly

applied in protein stabilization, states that stabilizers form hydrogen bonds at specific sites with the target compounds, which helps maintain the native structure, keep the spatial integrity of the compound after water is removed, and consequently enhance the stability. Sucrose is an ideal matrix material since it is a good glass former as well as a good hydrogen bonding former. For better functionalities, formulation design tends to choose sucrose glasses mixed with other compounds, including small molecules such as salts and macromolecules such as hydrocolloids.

In food and pharmaceutical industries, high solids formulations have been developed in low moisture systems to govern the molecular mobility that is associated with the macroscopic properties of the materials. Molecular mobility within amorphous solids is usually manifested by relaxation processes. The amorphous solids exhibit the primary α or glass transition at T_g which reflects the activation of large-scale molecular motions (α-relaxations) that underlie the onset of translational and rotational motions and the secondary β transition within the glass at T_β which reflects the activation of localized molecular motions (β-relaxations) linked to vibrational motion and local side-chain motion. The temperature-dependent molecular mobility thus controls physical and chemical properties by modulating the nature and kinetics of reactions that occur during processing and storage of biomaterials. Hydrocolloids are normally selected to stabilize the formulations due to their tremendously high viscosities in the solutions or high T_gs far above the room temperature in the solid state.

Gelatin is one of the most frequently used hydrocolloids in food, pharmaceutical and photographic industries (Wood, 1977). As a product of the structural and chemical degradation of collagen, gelatin has a large number of quite useful features including

gelation and film-formation. Recently, edible gelatin film attracts extensive interest due to its functional properties as well as its importance as an appropriate model in studying the behavior of amorphous biopolymers in the solid state (D'Cruz and Bell, 2005). Many studies have focused on the phase transition of gelatin (Marshall and Petrie, 1980; Slade and Levine, 1987; Sobral and Habitante, 2001; Kasapis and Sablani, 2005; D'Cruz and Bell, 2005) and the thermal and mechanical properties of gelatin films under the influence of plasticizers and large molecular weight carbohydrates (Pinhas et al., 1996; Sablani et al., 2002; Sobral et al., 2001; Vanin et al., 2005; Arvanitoyannis, Nakayama, and Aiba, 1998a, 1998b; Arvanitoyannis, Psomiadou, Nakayama, Aiba and Yamamoto, 1997).

Gelatin has the capacity to form a large variety of supermolecular structures in gelatin films or layers, depending on the casting temperature and time, the initial concentration in the gelatin solution, the nature of the solvent and co-existing compounds, etc. (Kozlov and Burdygina, 1983). The variety of structures determines the physico-chemical and mechanical properties of the gelatin films. Cold-cast gelatin films, spread at room temperature and lower, have an entangled network with a variable number of physical cross-links that contribute to macroscopic stability and strength of gelatin films (Menegalli et al., 1999). Hot-cast films, spread from aqueous solutions at temperature above 35°C, are assumed to have conformation of a statistical coil without cross-links (Kozlov and Burdygina, 1983). Lukasik and Ludescher (2006b) found that the matrix mobility (both the extent of matrix relaxation and matrix collisional quenching rates) was higher in cold-cast (with cross-links) than hot-cast films (without cross-links). Since no information is available on the relationship between the triple helix formation

and matrix mobility, hot-cast gelatin films without cross-links were selected for the present study to avoid the complications.

So far as we are aware, most studies focused on the stabilization of protein affected by sugars in protein-based solid systems (Tzannis and Prestrelski, 1999; Chinachoti and Steinberg, 1988; D'Cruz and Bell, 2005) or the stability of protein entrapped in the sugar matrixes (Chang et al., 2005; Wright et al., 2003). There is scanty information in the literature on the biopolymer behavior in a high sugar environment. The measurement of molecular mobility of amorphous sugars at low levels of macromolecules thus provides insight into the mechanism of biopolymer effect on sucrose matrix mobility, which is of considerable fundamental and technological interest. In a previous study we used erythrosin B phosphorescence to monitor the molecular mobility as well as dynamic site heterogeneity in amorphous solid sucrose (Pravinata et al., 2005). In the present study, phosphorescence of Ery B was used to measure the matrix mobility in thin films of amorphous sucrose-gelatin mixtures. Gelatin content was varied from 0.00022 to 0.365 (g gelatin/g sucrose) by addition of gelatin to the concentrated sucrose solution prior to film formation. The temperature-dependence of mobility was measured and analyzed at different gelatin contents, generating families of mobility versus temperature curves.

Materials and Methods

1. Preparation of pure sucrose film

We prepared glassy sucrose films by using a slightly modified version of our published method (Pravinata et al., 2005; see details in Materials and Methods in Chapter 1).

2. Preparation of gelatin-sucrose film

We prepared gelatin stock solution by using a slightly modified version of previous method in our lab (Simon-Lukasik and Ludescher, 2004). Gelatin solution was prepared in distilled deionized water at an approximate concentration of 100 mg/ml. VEE GEE Superclear Type A 300 bloom pigskin gelatin was obtained from Vyse Gelatin Co. (Schiller Park, IL). Gelatin solution was purified using dialysis to minimize the presence of counter ions. An aqueous gelatin solution was dialyzed using a regenerated cellulose dialysis tube with a 12-14 kDa molecular weight cutoff (Spectrum, Houston, TX). The solution was dialyzed against 0.1M potassium chloride for 24 hr with frequent change of the distilled water. During dialysis, the temperature of the solution was controlled above 65°C to ensure that the protein remained unfolded and to maximize the effectiveness of the dialysis process. The gelatin solution was rapidly frozen in a Labconco shell-freezer (Kansas City, MO) then annealed in a standard freezer overnight. The frozen solution was placed in a Labconco Model 4.5 freeze drier (Kansas City, MO) for a minimum of 48 hr to remove the residual moisture. The temperature of a cool collector was -40°C and a chamber 25°C, and a pressure of 0.1kPa was used. After freeze-drying, the gelatin solid was sealed and stored in the desiccator against P_2O_5 prior to future use.

Lyophilized gelatin was dissolved in deionized water at a concentration of 100 mg/ml. An aliquot from 10 mM erythrosin B stock solution was added to the purified gelatin solution to obtain an approximated dye content of 5.6×10^{-5} mol dye/mol residues.

Calculations were made assuming an average residue molecular weight of 93 g/mol, calculated from the relative abundance of each amino acid in acid-processed porcine skin gelatin (Clark & Courts, 1977; Eastoe & Leach, 1977; Creighton, 1993). This mole ratio was selected in order to produce tractable films under established conditions; the amount of dye was sufficient to provide adequate signal/noise in spectroscopic measurements. It is assumed that at this low level of dispersing ~56 dye molecules per million residues, that the physical properties of the resultant films are unaffected. The mixture was stirred and heated above 65°C until a clear solution was obtained. The solution was pipetted in 15μL aliquots onto quartz slides. The following procedure to make a glassy gelatin film was the same as the procedure to make a pure sucrose film.

Gelatin-sucrose solutions were prepared from sucrose solution containing dye. Gelatin solution was added to the purified sucrose solutions to obtain a series of mixtures with gelatin/sucrose weight ratio of 0.00022, 0.00073, 0.0022, 0.0073, 0.022, 0.073, and 0.365, respectively. Prior to prepare glassy films, sucrose-gelatin blended solutions were filtered through a membrane with 0.2μm pores. The following procedure to make a glassy film was the same as the procedure to make a pure sucrose film.

Gelatin-sucrose films were dried using heat gun for 10 min. The films were also dehydrated using hot plate and vacuum-drying methods: the cast films were either placed on top of a heat plate, drying around 65°C for 20min, or dried under a pressure of 1 kPa for at least 24 h at 55°C.

3. Moisture measurement

Water content in amorphous sucrose and sucrose-gelatin films was determined gravimetrically (by difference of mass before and after drying for 24h at 70°C in an

Ephortee (Haake Buchler, Inc.) vacuum oven at 1 kPa). Sample films were scratched from quartz slides and ground into powders in a glove box containing P_2O_5 and Drie-Rite with a relative humidity less than 5%. Pure sucrose and pure gelatin films contained 0.56±0.13 and 4.78±0.35 wt. % water, respectively; while gelatin/sucrose mixture samples contained 0.63±0.02, 0.95±0.14, 0.78±0.20, 0.82±0.15, 0.98±0.26, 1.38±0.01, and 1.52±0.15 wt. % water, respectively.

4. Luminescence measurements

Luminescence measurements were made using a Cary Eclipse Fluorescence spectrophotometer (Varian Instruments, Walnut Creek, CA). Prior to any phosphorescence measurements, all samples were flushed for at least 15 minutes with nitrogen gas which contained less than 1ppm oxygen to eliminate oxygen quenching. At each target temperature samples were equilibrated for 1min/°C increase in temperature. The temperature was controlled using a thermo-electric temperature controller (Varian Instruments, Walnut Creek, CA). To eliminate moisture condensation during the measurements below room temperature, dry air was used to flush the chamber surrounding the cuvette holder. All the measurements were made at least in triplicate.

Delayed fluorescence and phosphorescence emission spectra were collected from 520 to 750 nm (10 nm bandwidth) at 1 nm intervals using excitation of 500 nm (20 nm bandwidth) over a temperature range from 5 to 100°C with an observation window of 5.0 ms and an initial delay time of 0.2 ms which suppresses fluorescence coincident with the lamp pulse. Emission spectra from sucrose or sucrose-gelatin films without probe were subtracted from each spectrum although the signal of background was very low.

The energy of emission maximum (ν_p) and the full width at half maximum (FWHM) of the emission bands were determined by using log-normal lineshape function (Maroncelli and Fleming, 1987) to fit both delayed fluorescence and phosphorescence.

$$I(\nu) = I_0 \exp\left\{-\ln(2)\left(\frac{\ln[1+2b(\nu-\nu_p)/\Delta]}{b}\right)^2\right\} \quad (1)$$

Where I_0 is the maximum emission intensity, ν_p is the peak frequency (cm^{-1}), Δ is a linewidth parameter and b is an asymmetry parameter. This equation reduces to a Gaussian line width when b=0. The bandwidth (FWHM; Γ) was calculated according to the following equation:

$$\Gamma = \Delta\left(\frac{\sinh(b)}{b}\right) \quad (2)$$

For delayed luminescence spectra collected from 520-750 nm, a sum of log-normal functions for delayed fluorescence ($I_{df}(\nu)$) and phosphorescence ($I_p(\nu)$) was used to fit the spectra. Each emission band was fit to independent fit parameters.

The dipolar relaxation time φ was calculated from the temperature-dependence of the phosphorescence emission peak ν (T) by analyzing the relaxation function:

$$\frac{\Delta\nu}{\Delta\nu_r} = \frac{\nu(T)-\nu_{max}}{\nu_{min}-\nu_{max}} \quad (3)$$

Where ν (T) is the emission peak energy at temperature T, and ν_{min} and ν_{max} are the emission peak energy at the lowest temperature and the highest temperature, respectively. By using a stretched exponential function to approximate the phosphorescence intensity decay, the matrix dipolar relaxation time (φ) can be estimated from the following equation (Shirke et al., 2005):

$$\frac{\Delta\nu}{\Delta\nu_r} = \frac{\nu(T) - \nu_{\max}}{\nu_{\min} - \nu_{\max}} = \frac{1}{\Gamma(\frac{1}{\beta_l})} \frac{1}{1 + \frac{\beta_e}{\beta_l}\frac{\tau}{\varphi}} \quad (4)$$

Where τ and β_l are the temperature-dependent stretched exponential (Kohlrausch-Williams-Watts) lifetime and stretching exponent (from Eq. 5) describing the phosphorescence intensity decay and $\Gamma(x)$ in this case is the Gamma function; β_e is assumed to have a value of 0.5.

For lifetime measurements, samples were excited at 530 nm (20 nm bandwidth) and emission transients collected at 680 nm (20 nm bandwidth) over the temperature range from 5 to 100°C. Phosphorescence intensity decays were collected over a window of 5 ms with an initial delay of 0.1 ms and increments of 0.04 ms. Each decay was the average of 20 cycles. Because intensity decays were non-exponential, a stretched exponential, or Kohlrausch-Williams-Watts' decay function was selected to analyze the intensity decay (Richert, 2000; Lee, et al., 2001; Pravinata et al., 2005).

$$I(t) = I_0 \exp(-(t/\tau)^{\beta}) + \text{constant} \quad (5)$$

Where I_0 is the initial amplitude, τ is the stretched exponential lifetime, and β is an exponent varying from 0-1 and characterizing the distribution of lifetimes. The use of a stretched exponential model provides a direct measurement of continuous distribution of lifetimes, which is appropriate for describing a complex glass possessing a distribution of relaxation times for the dynamic molecular processes. The smaller the β value, the more non-exponential the intensity decays and the broader the distribution of lifetimes. Program NFIT (Galveston, TX) was used to fit the decay; goodness of fit was evaluated by examining the χ^2 and R^2. Plots of modified residuals (defined as the difference between the intensity from the fit decay curve and the measured intensity divided by the

square root of the measured intensity) was also an indicator of the goodness of fit. R^2 for all fits ranged from 0.99 to 1.00 and modified residuals plots fluctuated randomly around zero amplitude.

Phosphorescence emission lifetimes of Ery B as a function of emission wavelength were measured with excitation wavelength at 530 nm (20 nm bandwidth); emission wavelength varied from 640 to 720 nm (20 nm bandwidth). Phosphorescence emission lifetimes as a function of excitation wavelength were measured with emission wavelength at 680 nm (20 nm bandwidth); excitation wavelength ranged from 490 to 560 nm (20 nm bandwidth). The experiments were performed at 25°C.

5. Photophysical scheme

Our analysis of the delayed emission is similar to the photophysical scheme for erythrosin B outlined by Duchowicz et al. (1998). The measured emission rate for phosphorescence (k_P) is the sum of all possible deexcitation rates for the triplet state T_1:

$$\tau^{-1} = k_P = k_{RP} + k_{TS1} + k_{TS0} + k_Q[Q] \quad (6)$$

In this equation, k_{RP} is the rate of radiative emission to the ground state S_0. For erythrosin B, k_{RP} is 41 s^{-1} and constant with temperature (Duchowicz et al., 1998).

k_{TS1} is the rate of thermally activated reverse intersystem crossing from the triplet state T_1 to the singlet state S_1, and the value can be estimated from the Arrhenius equation:

$$k_{TS1}(T) = k^0_{TS1} \exp(-\Delta E_{TS}/RT) \quad (7)$$

where k^0_{TS1} is the maximum rate of intersystem crossing from T_1 to S_1 at high temperature, ΔE_{TS} is the energy gap between T_1 and S_1, R=8.314 J K^{-1} mol^{-1}, and T is the temperature in Kelvin. The value of ΔE_{TS} is calculated from the slope of a Van't Hoff

plot of the natural logarithm of the ratio of intensity of delayed fluorescence (I_{DF}) to phosphorescence (I_P):

$$d[\ln (I_{DF}/I_P)]/d(1/T) = -\Delta E_{TS}/R \quad (8)$$

where I_{DF} and I_P are the maximum intensity values determined from analysis of the emission band using Eq. (1). The value of k_{TS1} at 25°C was estimated as 88 s^{-1} using k^0_{TS1}=3.0 x 10^7 s^{-1} and ΔE_{TS} = 31.56 kJ/mol (Pravinata et al., 2005).

In the presence of oxygen, the quenching rate $k_Q[Q]$ is the product of rate constant k_Q and the oxygen concentration [Q]. By flushing nitrogen throughout the measurements we assume that no oxygen quenching occurred. One of the non-radiative decay routes is through intersystem crossing to the ground state S_0. The decay rate is expressed by $k_{TS0,}$ which reflects the rate of collisional quenching of the probe due to both internal and external factors (Papp and Vanderkooi, 1989). We assume that the term k_{TS0} primarily reflects the external environmental factors since the self collisional quenching among probe molecules can be neglected within the extremely viscous amorphous solid. In this study, temperature-dependent term k_{TS0} can be calculated by the difference from Eq. (6).

Results

At a probe/sucrose molar ratio of 1:10^4, each probe is on average surrounded by a matrix shell around 10-11 sucrose molecules thick. At this concentration Ery B dispersed within the sucrose matrix does not aggregate and thus reports the physical properties of the unperturbed sucrose matrix (You and Ludescher, 2006). The phosphorescence spectra of erythrosin B in 66% sucrose solution and in gelatin solution (100mg/ml) show emission peaks at the same position, suggesting no extensive binding of probe to gelatin.

Data collected from phosphorescence measurements in sucrose-gelatin films prepared from three different drying methods (heat gun drying, hot plate drying, and freeze drying) were almost the same, indicating that the physical state and properties of films were almost identical. That also implied that those films contained the minimum residual moisture content and the remaining water could not be removed under the experimental conditions. The comparable high moisture content in pure gelatin film (~5%) was probably overestimated using gravimetric method due to the hydrophilic nature of gelatin.

1. Delayed emission spectra

The delayed emission spectra of erythrosin B in amorphous sucrose and sucrose-gelatin films at a dye/sucrose molar ratio of $1:10^4$ exhibited two emission bands: the long wavelength phosphorescence band (maximum ~680 nm) from the triplet state T_1 and the short wavelength delayed fluorescence band (maximum ~555 nm) from the singlet state S_1 that has been repopulated by reverse intersystem crossing from the triplet state (Parker, 1968). Delayed emission spectra of amorphous sucrose and sucrose-gelatin films with various weight ratios collected over the temperature range from 5 to 100 °C showed the similar trends: decrease in phosphorescence and increase in delayed fluorescence intensity with raising temperature; both the delayed fluorescence and phosphorescence bands shifted to longer wavelength at high temperature (graphs not shown here). The intensity ratio ($\ln (I_{df}/I_p)$) was plotted as a van't Hoff plot versus 1/T and the slope obtained from the linear plot can be used to estimate the energy gap between the triplet and singlet states (Eq. 6 in Materials and Methods). In amorphous sucrose and gelatin the values of ΔE_{TS} were 31.56±0.56 and 33.62±0.52 kJ mol^{-1}, respectively. In the presence of

gelatin with weight ratio of 0.00022, 0.00073, 0.0022, 0.0073, 0.022, 0.073, and 0.365, the values of ΔE_{TS} were 32.41±0.40, 32.34±0.26, 31.74±0.60, 31.54±0.21, 31.37±0.43, 31.81±0.48, and 32.40±0.31 kJ mol^{-1}, respectively, indicating that addition of gelatin slightly modulates the singlet-triplet energy gap.

The peak frequency (ν_p) and bandwidth (Γ) for both delayed fluorescence and phosphorescence emission were determined by fitting to a log-normal lineshape function (Eq.1 and Eq.2). ν_p and Γ for phosphorescence are plotted in Figure 71a and Figure 71b. The peak frequency and bandwidth for delayed fluorescence displayed similar behavior (data not shown). The phosphorescence peak frequency in sucrose decreased biphasically as a function of temperature: decreased gradually and linearly at low temperature and then more steeply at high temperature. The decrease in emission energy reflects an increase in the average extent of dipolar relaxation around the excited triplet state prior to emission (Lakowicz, 1999). The phosphorescence peak frequency in gelatin did not show obvious biphasically behavior over the whole temperature range: ν_p decreased linearly and slowly, from 14616 cm^{-1} at 5°C to 14439 cm^{-1} at 100°C. The change in frequency with temperature was much smaller than that in sucrose (from 14698 to 14360 cm^{-1}). Note that the decrease in frequency in gelatin was similar to that in sucrose at temperatures below 65°C (the reduction of frequency between 5°C and 65°C was around 110 cm^{-1}), however, the difference at high temperature was dramatically less in gelatin compared with sucrose (frequency decreased by 230 cm^{-1} from 65°C to 100°C in sucrose while it decreased by 65 cm^{-1} in gelatin). The sucrose-gelatin mixtures showed behavior in between sucrose and gelatin. With increase in gelatin content (>0.0022), the decrease in peak frequency became less at low temperature and much less at high temperature. At

temperatures below 65°C the reduction in frequency decreased maximally by 30% while 56% above 65°C at high gelatin level compared to $\Delta\nu_p$ of 110 cm^{-1} and 230 cm^{-1} in sucrose, respectively. The biphasical trend in sucrose-gelatin mixtures became less significant compared with sucrose; the slope of the curve at high temperatures became less negative. With gelatin concentration less than 0.0022, the change in frequency with temperature was slightly larger in sucrose-gelatin mixtures than in sucrose.

The spectra of erythrosin B in amorphous sucrose shifted with gelatin content. The peak frequency is plotted as a function of gelatin concentration in Figure 72a. The effect of gelatin is also illustrated in plots of the relative peak frequency normalized to the values in the pure sucrose film at temperatures from 5 to 65°C (Figure 72b). Compared to sucrose, the peak frequency (ν_p) was slightly shifted to lower values at gelatin/sucrose weight ratios below 0.0073. At gelatin/sucrose ratio of 0.00022, the peak frequency occurred at 14660 cm^{-1} at 5°C and 14277 cm^{-1} at 100°C, red-shifted 1.5 nm and 4.0 nm from pure sucrose, respectively. When gelatin content was increased by 10 fold to 0.0022, the values of the peak frequency increased and were almost the same as those of sucrose. With addition of gelatin concentration up to 0.0073, the peak frequency changed insignificantly in the glass (<65°C) but significantly in the melt (>65°C). When gelatin was increased from 0.022 to 0.365, the curves of peak frequency shifted up over the whole temperature range (shown in Figure 71a). The peak frequency at 5°C increased from 14698 cm^{-1} in pure sucrose to 14800 cm^{-1} in gelatin/sucrose matrix of 0.365 (the spectrum blue-shifted by 5 nm), and at 100°C from 14360 cm^{-1} to 14627 cm^{-1} (blue-shifted by 13 nm). Above 0.073 gelatin/sucrose ratio, the peak frequency increased insignificantly at low temperature but increased remarkably at high temperature.

The linear relationship between peak frequency and temperature indicated no obvious glass transition in gelatin from 5 to 100°C. The values of peak frequency of pure gelatin were lower than those of sucrose over the temperature range from 5 to 85°C and higher above 85°C. The lower frequency indicated that the average extent of dipolar relaxation was higher in the pure gelatin than in the sucrose.

The phosphorescence bandwidth (Figure 71b) increased gradually with temperature in the glass and more dramatically in the melt above T_g. This increase in inhomogeneous broadening indicates that there is a corresponding increase in the range of energetically distinct matrix environments in amorphous sucrose mixture. Amorphous sucrose films with different gelatin contents showed similar trends over the whole temperature range. Addition of gelatin did not change bandwidth significantly. Compared with the pure sucrose, bandwidth slightly increased at very low concentration of gelatin (<0.0073) while slightly decreased at high gelatin level. Pure gelatin exhibited smaller bandwidth in the glass but larger bandwidth in the melt. The slopes of bandwidth curve in gelatin at low and high temperature were slightly more positive than those of sucrose.

The dipolar relaxation rates for sucrose and sucrose-gelatin mixtures are plotted in an Arrhenius fashion in Figure 73. These curves show upward curvature at high temperatures indicating increased activation energy with increasing temperature. Compared with sucrose, the relaxation rate in sucrose-gelatin films slightly increased at temperature below 65°C and decreased above 65°C. Pure gelatin showed different behavior: the relaxation rate was larger than that in the mixtures over the same temperature range.

2. Phosphorescence decay kinetics

The phosphorescence intensity decays in sucrose-gelatin glass with different gelatin contents were measured over the temperature range from 5 to 100ºC. The stretched exponential lifetime and exponent β are plotted as a function of temperature (Figure 74a and Figure 74b). The lifetimes decreased biphasically with increasing temperature, exhibiting a gradual linear decrease at low and a more dramatic decrease at high temperature. The decrease in lifetime with temperature reflects an increase in the rate of non-radiative decay of the excited triplet state T_1 due to an increase in both the rate of non-radiative decay to the ground state S_0 (k_{TS0}) and reverse intersystem crossing to S_1(k_{TS1}). The lifetimes increased correspondingly with addition of gelatin, from 0.60 ms at 5°C in gelatin-sucrose film at weight ratio of 0.00022 to 0.73 ms at 0.073. With further increase in gelatin concentration, the lifetimes did not increase apparently until the temperature reached 65°C and above. Compared with sucrose, pure gelatin exhibited higher lifetime values over the same temperature range: from 0.73 ms at 5°C to 0.43 ms at 100°C (0.61 ms and 0.24 ms in sucrose at 5 and 100°C, respectively). Note that below gelatin/sucrose weight ratio of 0.0073, lifetimes were slightly lower than those of sucrose.

Exponent β in sucrose films with gelatin at weight ratio from 0.00022 to 0.022 showed similar behavior as sucrose over the temperature range from 5 to 100ºC (Figure 74b): kept constant in the glass and decreased sharply in the melt. Very small amounts of gelatin such as ratio of 0.00022 did not change β obviously. Increasing gelatin content by 10 fold from 0.00073 to 0.0073, the values of β decreased and were smaller than those in sucrose. In the presence of gelatin at ratio of 0.022, β increased a little bit and was almost

the same as that of sucrose. Above 0.022, β kept almost constant over the whole temperature range and values were slightly larger than those of sucrose at low temperature but significantly larger at high temperature. For instance, the value of β was 0.922 at 55ºC and 0.911 at 95ºC in gelatin-sucrose film with ratio of 0.073 while in sucrose β was 0.913 and 0.863 correspondingly. Since β reflects the distribution of lifetime and thus the corresponding distribution of dynamically distinct probe environments with different values of k_{TS0} (Pravinata et al., 2005), the small increase in β with addition of gelatin above ratio of 0.073 indicated a large decrease in the range of dynamically distinct probe environments in the glass and a distinctively larger decrease in the melt. At low gelatin concentration from 0.00073 to 0.0073, the small decrease in β indicated a large increase in the range of dynamically distinct probe environments both in the glass and in the melt. Pure gelatin, compared with sucrose, showed larger and smaller β values at temperatures below and above 45°C, respectively.

Based on the maximum physically reasonable value of k_{TS1} (Pravinata et al., 2005), an estimate of the lower limits of k_{TS0} was calculated from Eq. 9 (Materials and Methods) and it is plotted as $\ln(k_{TS0})$ versus 1/T in Figure 75. The non-radiative quenching rate k_{TS0} was linear at low temperature and shot up at high temperature, which indicated that this rate is sensitive to the molecular mobility activated with temperature. Addition of gelatin in sucrose above ratio of 0.0073 decreased the quenching rate k_{TS0} in both the glass and the melt. This enhancement effect was more significant with increasing gelatin content, especially at high temperature. At ratio of 0.0073, for instance, the value of k_{TS0} decreased by 5% at 5ºC and 24% at 100ºC; upon increasing the ratio to 0.365, the value of k_{TS0} decreased by 15% at 5ºC and almost 53% at 100ºC. However, at low gelatin

concentration from 0.00022 to 0.0022, the quenching rate k_{TS0} increased moderately in the glass and remarkably in the melt. For instance, k_{TS0} increased by 5% at 5ºC and 35% at 100ºC at ratio of 0.00073. k_{TS0} in pure gelatin matrix showed different behavior from sucrose: the values were much lower than those in sucrose and less sensitive to temperature than sucrose matrix.

Figure 76 is a plot of the gelatin concentration-dependence of the quenching rate k_{TS0}. Obviously gelatin increased the quenching rate at very low concentrations from 0.00022 to 0.0073, which was consistent over the whole temperature range. However, the quenching rate decreased at gelatin concentration of 0.0073 and above. The values of k_{TS0} in gelatin/sucrose mixtures of 0.073 and 0.365 were smaller than those both in pure sucrose and in pure gelatin.

By normalizing the quenching rate k_{TS0} to the value in sucrose, a clear picture of the effect of gelatin content on sucrose matrix mobility was obtained. In Figure 77a, normalized k_{TS0} is plotted as a function of gelatin concentration ranging from 0 to 0.01 at temperatures varied from 5 to 65ºC. The quenching rate k_{TS0} increased with increasing gelatin content from 0.00022 to 0.0022, and then decreased and the values became smaller than those in sucrose at ratio of 0.0073. This effect of increasing matrix mobility kept consistent in the temperature range of measurement and became more significant at higher temperatures. Figure 77b displayed the plot of relative rate in gelatin concentration range from 0.001 to 0.1. At the ratio of 0.0073 the relative rate increased with temperature, exhibiting a positive effect of temperature. When gelatin/sucrose ratio increased up to 0.022, the relative rate decreased with increasing temperature, exhibiting a negative effect of temperature although the temperature had a positive influence on the

absolute rate (Figure 76). The transition probably indicated the formation of different matrixes due to the increased gelatin amounts.

3. Spectral heterogeneity

Phosphorescence intensity decays of Ery B in sucrose films with different gelatin contents were measured as a function of excitation and emission wavelength at 25°C. After analysis using a stretched exponential model, lifetimes are plotted versus excitation and emission wavelength in Figure 78a. All lifetime curves showed a similar trend: lifetime decreased with increasing wavelength across the emission band. In sucrose, the lifetimes varied from a high of 0.65 ms at 640 nm to a low of 0.52 ms at 720 nm; lifetimes also decreased monotonically with increasing wavelength in sucrose-gelatin films. The values of lifetime gradually increased with increasing gelatin concentration. In the presence of small amounts of gelatin (<0.00073), lifetimes changed insignificantly. At ratio of 0.0073, lifetimes increased slightly and above that ratio lifetimes increased considerably. There were no evident changes in the variation of lifetime in the presence of gelatin at 25°C. Lifetimes also varied across the excitation band: lifetime increased with increasing wavelength to a maximum at 520-540 nm and then decreased at higher wavelengths. The variation of lifetime within the excitation band appeared to be smaller than that in sucrose at high gelatin level.

The stretching exponent β also varied as a function of both excitation and emission wavelength (Figure 78b). The values of β were slightly lower in the presence of gelatin. In sucrose and sucrose-gelatin films β values were lower at the blue edges of the emission bands, increased with increasing wavelength to a maximum at 680-690 nm and

then decreased slightly at the red edge. The variation of β across the emission band in sucrose-gelatin films was similar as that in sucrose film.

The calculated quenching rate k_{TS0} is plotted versus emission and excitation wavelength at various gelatin contents in Figure 79. The collisional quenching rate k_{TS0} increased with increasing emission wavelength in both sucrose and sucrose-gelatin films. The quenching rate did not changed significantly at gelatin concentrations below 0.00073. When gelatin content increased above 0.0073, the collisional quenching rate decreased with increasing gelatin amounts. For instance, the rate at ratio of 0.073 varied from a low of 1239 s^{-1} at 640 nm to a high of 1539 s^{-1} at 720 nm, much lower than those values in pure sucrose film (1409 s^{-1} at 640 nm and 1783 s^{-1} at 720 nm). Across the excitation band, k_{TS0} curves showed minimum values around 530 nm; the values were higher at both blue and red edge of excitation bands in all sucrose and sucrose-gelatin films. Similarly, addition of gelatin reduced the collisional quenching dramatically. At low gelatin concentration, the variation in the quenching rate across both emission and excitation band were similar to that in the sucrose matrix. Increasing gelatin concentration diminished the variation in the quenching rate with emission and excitation wavelength.

Discussion

The phosphorescence emission wavelength and intensity of erythrosin B in amorphous sucrose and sucrose-gelatin mixtures are influenced by two kinds of molecular mobility: dipolar relaxation and collisional quenching. Our discussion of

gelatin effect on molecular mobility in amorphous sucrose is based on the emission energy and lifetime data that are modulated by these two modes of mobility.

1. Stabilization effect at high gelatin level

Phosphorescence emission energy (peak frequency), the energy gap between T_1 and S_0, is primarily influenced by the T_1 energy and thus the dipolar relaxation of hydroxyl groups around T_1 within the matrix (Pravinata et al., 2005). The emission energy decreased 350 cm^{-1} in sucrose over a temperature range of ~100°C, and decreased much less in sucrose-gelatin mixtures. The change in emission energy decreased with an increase in gelatin content. At gelatin/sucrose ratio of 0.0022, the emission energy decreased around 300 cm^{-1}. At content of 0.365 the decrease was 177 cm^{-1}. The decrease was consistent with a dipolar relaxation mechanism around the excited triplet state. In amorphous solid sugars, dipolar relaxation reflects mobility of the hydroxyl groups of sugars due either to localized motions in the glass or to large-scale α-relaxations associated with flow activated at T_g. The total decrease in emission energy appears to be significantly larger in sucrose than in sucrose-gelatin, indicating the larger amplitude of the localized motions seen in sucrose than in sucrose-gelatin mixtures due to onset of α-relaxation above T_g in sucrose and the suppression of the motions by gelatin.

Emission energy of erythrosin B in different sucrose-gelatin mixtures showed similar trends as sucrose with temperature changes. The dramatic decrease of emission energy at high temperature reflects a significant increase in the relaxation rate in the melt. Compared with sucrose, no changes have been observed in the shape of the spectra collected from sucrose-gelatin mixtures, indicating that the probe molecules did not form probe aggregates. The emission energy increased with increasing gelatin content in

sucrose. At concentrations below 0.0073, the emission energy values were smaller than in sucrose. The decrease in emission energy suggested an increase in the dipolar relaxation rate due to the enhanced mobility motion of hydroxyl groups in the presence of small amounts of gelatin. Above 0.0073, the emission energy values were larger than in sucrose, indicating a decrease in the matrix relaxation rate at high gelatin level.

The emission intensity and the lifetime are directly modulated by the rate of radiative emission k_{RP}, of reverse intersystem crossing to the excited triplet state k_{TS1} and of intersystem crossing to the ground state k_{TS0}. The rate of intersystem crossing k_{TS0}, which is modulated by the physical state of the amorphous matrix, reflects both the manner in which the excited T_1 state is vibrational coupled to the S_0 ground state as well as the manner in which the ground state vibrational energy can dissipate from the excited probe into the surrounding matrix. Since the efficiency of this vibrational dissipate is related to the overall mobility of the matrix, provides a direct measure of matrix mobility.

Compared with sucrose, k_{TS0} in sucrose-gelatin above gelatin/sucrose ratio of 0.0073 decreased with increasing gelatin content, indicating more restricted mobility in gelatin-sucrose matrixes of these concentrations. The magnitude of k_{TS0} in sucrose was 1550 cm^{-1} at 5°C and increased gradually up to 65°C, and then dramatically at higher temperature. Similarly, the magnitude of k_{TS0} increased slowly up to a certain temperature in the presence of gelatin, and then steeply at higher temperature. This temperature reflects the activation of α relaxations at T_g and can be calculated from the intersection of the trendlines at high and low temperature in Arrhenius plots of k_{TS0}. The calculated transition temperatures were 76.5°C in sucrose, and 83.2, 84.5, 88.1, and 94.2°C in the sucrose-gelatin mixtures with gelatin/sucrose ratios of 0.0073, 0.022, 0.073

and 0.365, respectively. The significant increase in the transition temperature suggested that addition of gelatin stretched the glassy state range of sucrose, keeping the probe in a rigid environment over a wider temperature range. Gelatin itself features a rather wide temperature range of the glassy state with a T_g above 100°C.

Lower dipolar relaxation (higher emission energy), lower matrix mobility (longer lifetime and lower k_{TS0}) and enhanced mobility transition temperature clearly suggested a rigidification effect in sucrose-gelatin mixtures at high gelatin content, especially at high temperatures. When gelatin content is at 0.073 and above, a synergy effect can be observed.

2. Destabilization effect at low gelatin level

In the gelatin concentration range from 0.00022 to 0.0073, gelatin showed a different influence on the sucrose matrix. The values of the peak frequency were lower and the magnitude of dipolar relaxation (the total decrease in emission energy) larger than those in sucrose. For instance, the peak frequency at 5°C in sucrose-gelatin at a ratio of 0.00022 was 14660 cm^{-1} and the total decrease in emission energy was 385 cm^{-1}, compared with 14700 cm^{-1} and 338 cm^{-1} in sucrose. With an increase in gelatin content, the peak frequency increased and became comparable with sucrose; the decrease in emission energy was less from 65 to 100°C while the decrease from 5 to 65°C was similar to sucrose. Clearly a larger amplitude of localized mobility motions existed in the glassy matrix in the presence of very small amount of gelatin.

The magnitude of k_{TS0} in the same gelatin concentration range was larger than sucrose over the whole temperature range. At a ratio of 0.00022, k_{TS0} was 1600 s^{-1} and 4330 s^{-1} at 5 and 100°C, respectively, compared with 1550 s^{-1} and 3000 s^{-1} in sucrose.

The transition temperatures were calculated as 76.5°C in sucrose, and 77.9, 75.9, and 77.0°C in the sucrose-gelatin mixtures with ratio of 0.00022, 0.00073, and 0.0022, respectively.

Addition of very small amounts of gelatin seemed not to influence the T_g of sucrose matrix significantly, however, the level was enough to make matrix more pliant over the whole temperature range. Fast dipolar relaxation (low emission energy) and high matrix mobility (short lifetime and low k_{TS0}) indicated a comparatively flexible sucrose matrix in the presence of the macromolecule gelatin. Pure sucrose matrix has hydrogen-bonded networks that contribute to the rigidity and tightly packing environment of matrix. Small amounts of gelatin interfere with the formation of hydrogen-bonding network because gelatin is large molecule and has constrained mobility to adjust for favorable steric conformations in the extreme viscous matrix and participate in the hydrogen bond with sucrose. Therefore, sucrose-gelatin matrixes with very low gelatin concentrations have comparably loosely packing regions and higher mobility compared to pure sucrose.

Another possible reason is that sugars are known to exert excluded volume effect and show a tendency to phase separation. The formed sucrose-rich and gelatin-rich domains may influence the molecular packing and matrix density, leading to a less compact matrix with fluctuating mobility. Tzannis and Prestrelski (1999) reported destabilizing effects of sucrose on trypsinogen at high sucrose contents (>1:1 weight ratio) due to the presence of aggregate clusters. Kasapis et al. (2003) announced similar findings when they investigated the morphological behavior of gelatin in gelatin-sugar

mixtures. At high levels of sucrose, gelatin was visualized in an aggregated form thus producing a phase-separated topology with sucrose.

3. Interactions between sucrose and gelatin

Sugar-protein interaction is always of interest since protein is reported to be stabilized in the presence of sugars and polyols. Carpenter and Crowe reported (1989) that trehalose replaced the water molecules that form hydrogen bonds to the surface of the globular protein. Addition of sorbitol decreased the partial specific volume, resulting in a more compact structure of the protein (Barreto et al., 2003). Sucrose was found to increase the apparent activation energy of unfolding process of protein (Lee and Timasheff, 1981). Recently, sucrose was known to be able to inhibit the large-scale conformation changes associated with protein denaturation because sucrose molecules are preferentially excluded from the protein surface, leading to the increased chemical potential of protein and promote the protein to stay in a more compact native state (Kim et al., 2003). This finding is similar to the result reported in protein/glycerol-water mixtures (Gekko and Timasheff, 1981): the protein preferentially hydrated and glycerol was excluded from the domain of the protein, resulting in a more folded or native state. The interaction between the solvent and the protein is nonspecific and the stabilizing effect takes place only at high solvent concentrations. It seemed that the preferential exclusion from the domain of the protein is a common characteristic of protein structure stabilizing solvents such as sugars and polyols.

In the present work, films were prepared from aqueous gelatin and sucrose-gelatin solution by evaporating the solvent off at temperature above 50°C and therefore gelatin

macromolecules was assumed to have the conformation of a statistical coil with no indications of ordering (Kozlov and Burdygina, 1981). Compared to pure sucrose, coiled gelatin may have more loose structure, facilitating the dipolar relaxation process and resulting in decreased emission energy. The high residual moisture also contributed to the lowered emission energy due to the strong polarity. Addition of macromolecular gelatin may increase the free volume in the sucrose matrix as well as interactions between sucrose and gelatin, the former leading to a depression of T_g while the latter leading to an increase in T_g. The apparent gelatin effect may result from the competition of these two opposite actions. At very low concentrations of gelatin (i.e. high sucrose contents), the addition of gelatin may increase the free volume and interfere with the existed interactions within the sucrose matrix; while the possible interaction between sucrose and gelatin is not sufficient to strengthen the whole amorphous sucrose structure. Sucrose was reported to exert excluded volume effect and phase separation may also contribute to the disrupted structure in sucrose-rich matrix. Therefore, the sucrose-gelatin matrix at low gelatin level is less compact; exhibiting somewhat enhanced mobility leading to decreased emission energy and lifetime. With increasing gelatin content, the gelatin-sucrose interaction is strong enough to compete against the increase effect on the free volume in the matrix, leading to a constrained mobility that is reflected by increased emission energy and lifetime.

Gelatin has the capacity to bind water due to its hydrophilic functional groups. In sucrose solution, the interactions are altered in the presence of gelatin and the change is depended on the gelatin concentration. The sucrose-water interaction (hydrogen bonding) is initially weakened due to the preferential hydration of gelatin and formation of gelatin-

water interaction. With increase in gelatin content, sucrose molecules can participate in hydrogen bonding-mediated interactions with gelatin's polar functional groups. In Figure 72 data clearly showed that the emission energy in sucrose-gelatin was lower than in sucrose until the gelatin content increased to 0.0073, indicating that below 0.0073 the sucrose matrix structure is weakened in the presence of a small amount of gelatin. Above 0.022, the emission energy in sucrose-gelatin increased and was higher than in pure sucrose and gelatin matrix, suggesting a synergy effect in the sucrose-gelatin mixture. In Figure 77a and Figure 77b, the collisional quenching rate k_{TS0} in sucrose-gelatin was larger than in sucrose when gelatin content was below 0.0073, and increased with raising temperature. This indicated that at low concentration of gelatin interactions formed with sucrose molecules are not strong enough to strengthen sucrose matrix. At the ratio of 0.0073, the strength of sucrose-gelatin interaction can compete against the increased free volume effect, leading to decreased matrix mobility. When gelatin is added at a level of 0.022, the collisional quenching rate k_{TS0} was smaller than in sucrose and decreased with temperature. This suggests that at certain gelatin content, intermolecular interactions are facilitated by raising temperature and the increased interactions are so strong that they prevail over the increase in the thermal mobility of structural fragments. Kozlov and Burdygina (1981) reported that heating of gelatin film containing a large number of functional groups increase the material rigidity because of increased intermolecular interactions. All these suggested that some specific interactions exist in the sucrose-gelatin film and "network" structure is more likely to build up at high gelatin level, which exhibit considerably constrained mobility and a fairly wide range of heat resistance.

Therefore, the emission energy and collisional quenching rate maps may be divided into a destabilization effect region (<0.0073) and a stabilization effect region (>0.0073). At high gelatin content (≥0.073) a synergy effect is observed. The gelatin concentration range from 0.0073 to 0.022 may be considered as an interaction transition region from randomly distributed sucrose-gelatin interaction to sucrose-gelatin network.

4. Influence of gelatin on dynamic site heterogeneity

Recent research using a variety of spectroscopic techniques indicates that supercooled liquids and amorphous polymers are dynamically heterogeneous spatially as well as temporally (Ediger, 2000; Richert, 2002). This physical model is supported by more evidence from erythrosin B phosphorescence. Spectral heterogeneity in Ery B phosphorescence is observed in amorphous sugars and sugar alcohols (Pravinata, et al., 2005; Shirke et al., 2005, 2006), and proteins (Nack and Ludescher, 2006; Lukasik and Ludescher, 2006a; Sundaresan and Ludescher, 2007), indicating that dynamic site heterogeneity may be a characteristic feature of amorphous food materials and biomaterials.

The variation of lifetime with emission energy reflects variation in one or more of the rate constants for deexcitation of the triplet state. In amorphous sucrose matrix, the population of probes is distributed among the dynamically distinct sites with varied emission energy and matrix quenching rate (Pravinata et al., 2005). Pravinata et al. proposed a physical model for the origin of this site heterogeneity on the basis of emission energy and matrix quenching rate; that is, probes in local environments with less constrained packing have higher overall molecular mobility and thus shorter lifetime and have lower emission energy due to fast dipolar relaxation. When sucrose is mixed

with gelatin, whether gelatin will change the local environments and further influence the site heterogeneity becomes one of our interests.

Compared with sucrose, variations in lifetime at 25°C of erythrosin B in sucrose films containing gelatin with emission wavelength were slightly larger (Figure 78a). The difference of lifetime with emission wavelength reflects a broad continuum of local matrix sites that vary in terms of their overall molecular mobility. Probes in the blue-shifted sites have longer lifetimes, smaller values of collisional quenching rate k_{TS0} and become less mobile; but probes in the red-shifted sites have shorter lifetimes, larger values of quenching rate and become more mobile. In all the sucrose-gelatin films the values of stretching exponent β (Figure 78b) are comparably lower than those in the sucrose film, indicating a decreased ability within the sites to dynamically average out spectroscopic differences in the presence of gelatin. The variations in collisional quenching rate constant k_{TS0} with emission wavelength (Figure 79) were larger at low gelatin level while smaller at high gelatin level compared with sucrose, suggesting increased heterogeneity in sucrose-gelatin mixture at high levels of sucrose but decreased with increasing gelatin content above 0.0073.

The temperature-dependence of the stretching exponent β (Figure 74b) shows that the values of β in the sucrose-gelatin films were lower than the value in pure sucrose at lower gelatin content but higher at gelatin content above 0.073 (especially at high temperature), suggesting an increased matrix heterogeneity with addition of small amounts of gelatin but decreased heterogeneity when gelatin molecules can form specific interactions with sucrose molecules and show a synergy effect.

The emission bandwidth (Γ, FWHM) slightly increased with gelatin content in sucrose-gelatin films until at gelatin levels above 0.073 the bandwidth decreased instead (Figure 71b). The decrease in bandwidth indicated that the distribution of site energies was slightly narrowed at high gelatin level, probably a result of the formation of sucrose-gelatin network interaction with more uniform allocation of site energy.

All the above shows strong evidence of increased dynamic site heterogeneity in sugar-gelatin films when gelatin is added at low levels. Inducing rigid-chain gelatin macromolecules into a matrix made of small molecules disturbs the distribution of local regions with different packing degree or varied rigidity. Kasapis et al. (2003) reported the heterogeneity in the sugar-gelatin mixture in a high sucrose environment with sucrose promoting chain association rather than inhibiting it. At high gelatin level the formed sucrose-gelatin interactions are more uniformly distributed throughout the matrix and even a certain "network" is built up, making the matrix more homogeneous with more similar local environments. More significant increase in dynamic homogeneity at high temperature (compared with sucrose) is a result of the built-up "network" throughout the matrix.

5. Gelatin change T_g of sucrose?

Gelatin may influence the properties of sucrose glasses by changing the glass transition temperature of sucrose. Tsereteli and Smirnova (1991) reported the T_g of gelatin as 153°C and ΔCp as 0.5 J/g °C. The T_g of sucrose-gelatin mixtures can be estimated using the Couchman and Karasz equation (Roos, 1995). Because the gelatin levels used in the sucrose-gelatin films are very low, the T_gs of mixtures are not

significantly influenced except for the mixture with gelatin content of 0.365 (the calculated value is around 83°C).

An Arrhenius plot of the collisional quenching rate k_{TS0} shows biphasic behavior: the values increased linearly and gradually in the glass and more dramatically in the melt. The transition temperatures, calculated from the intersection of the linear fits to low and high temperature data, were estimated as 76.5°C for sucrose, and 77.9, 76.0, 77.0, 83.2, 84.5, 88.1, and 94.2°C in sucrose-gelatin matrixes with gelatin/sucrose weight ratio of 0.00022, 0.00073, 0.0022, 0.0073, 0.022, 0.073 and 0.365, respectively. Compared with sucrose, the transition temperature slightly increased in the presence of low gelatin content and significantly increased at high gelatin concentration. When the values of k_{TS0} were plotted on a temperature scale normalized to the individual T_g, all the curves were similar in the shape; and the curves with lower gelatin contents were slightly above and those with higher gelatin contents significantly below the sucrose curve (data not shown). This suggested that gelatin influenced the sucrose matrix essentially through modulating the T_g; however, a secondary effect existed in the sucrose-gelatin matrixes as well. At low concentration the overall mobility increased although gelatin did not influence the T_g of matrix significantly; while at higher concentrations, the overall mobility was greatly reduced beyond gelatin effect on the T_g. This provided evidence that interactions between sucrose and gelatin was a key factor determining the overall effect on the mobility.

Conclusion

The composition of an amorphous solid (such as polymers) and its environment (temperature) are two important factors affecting molecular mobility. Phosphorescence

of erythrosin B can report a detailed mobility map within amorphous sucrose film blended with gelatin ranging from 0.00022 to 0.365 (weight ratio). Based on the emission energy and lifetime of erythrosin B in sucrose and sucrose-gelatin films over the temperature range from 5°C to 100°C, we come to a conclusion that gelatin exerts a strong effect on amorphous sucrose and the effect is depended on the gelatin content. At gelatin concentration lower than 0.0073, both emission energy and lifetime decreased and k_{TS0} increased, indicating a destabilization effect; at concentration above 0.0073, gelatin exerts a stabilization effect: increasing emission energy, increasing lifetime and reducing mobility in the glassy state. When gelatin content increased by 10-fold (that is to 0.073) or even more, a synergy effect was observed, especially significant at high temperature. The interactions existing in the sucrose-gelatin matrix, along with gelatin conformation, are considered as determined factors to influence the molecular mobility of sucrose-gelatin mixtures. The interactions vary with gelatin content, leading to different influence on mobility map of sucrose matrix. It is worthy of mapping out the relationship between the gelatin concentration and the characteristics of the matrix since the matrix properties have implications for the processing and subsequent storage stability of biological materials and foods.

Spectral heterogeneity in Ery B phosphorescence in amorphous sucrose-gelatin films provides direct evidence to support a physical model of dynamic site heterogeneities within supercooled liquids and amorphous solids above and below the glass transition temperature (Ediger, 2000; Richert, 2002). Addition of gelatin influences the dynamic heterogeneity of amorphous sucrose matrix and this effect is dependent on the gelatin content and temperature. Our data indicate that there are sites of different

mobility within amorphous solid sucrose and this dynamic heterogeneity is enhanced in the presence of macromolecules such as gelatin. However, the dynamic heterogeneity can be diminished by increasing gelatin content at which a synergy effect is exhibited. Undoubtedly the ability to report dynamic heterogeneity using Ery B phosphorescence provides an insight into the complex dynamic properties of amorphous biomaterials.

References:

Arvanitoyannis, I., Nakayama, A., and Aiba, S. 1998a. Edible films made from hydroxypropyl starch and gelatin and plasticized by polyols and water. *Carbohydr. Polym.* 36, 105-119.

Arvanitoyannis, I., Nakayama, A., and Aiba, S. 1998b. Chitosan and gelatin based edible films: State diagram, mechanical and permeation properties. *Carbohydr. Polym.* 37, 371-382.

Arvanitoyannis, I., Psomiadou, E., Nakayama, A., Aiba, S., and Yamamoto, N. 1997. Edible films made from gelatin, soluble starch, and polyols. Part 3. *Food Chem.* 60, 593-604.

Barreto, P.L.M., Roeder, J., Crespo, J.S., Maciel, G.R., Terenzi, H., Pires, A.T.N., and Soldi, V. 2003. Effect of concentration, temperature, and plasticizer content on rheological properties of sodium caseinate and sodium caseinate/sorbitol solutions and glass transition of their films. *Food Chem.* 82, 425-431.

Carpenter, J.F., Prestrelski, S.J., and Arakawa, T. 1993. Separation of freezing- and drying-induced denaturation of lyophilized proteins using stress-specific stabilization. I. Enzyme activity and calorimetric studies. *Arch Biochem Biophys.* 303, 456-464.

Carpenter, J.F., and Crowe, J.H. 1989. An infrared spectroscopic study of the interactions of carbohydrates with dried proteins. *Biochem.* 28, 3916-3922.

Chang, L., Shepherd, D., Sun, J., Ouellette, D., Grant, K.L., Tang, X., and Pikal, M.J. 2005. Mechanisms of protein stabilization by sugars during freeze-drying and storage: native structure preservation, specific interaction, and/or immobilization in a glassy matrix? *J. Pharm. Sci.* 94(7), 1427-1444.

Chinachoti, P., and Steinberg, M.P. 1988. Interaction of sucrose with gelatin, egg albumin and gluten in freeze-dried mixtures as shown by water sorption. *J. Food Sci.* 53 (3), 932-934.

Clark, R.C., and Courts, A. 1977. The chemical reactivity of gelatin. In A.G. Ward, & A. Courts (Eds.), *The science and technology of gelatin* (pp. 209-247). New York: Academic Press.

Creighton, T.E., 1993. *Proteins: Structures and molecular properties*. New York: W.H. Freeman.

Crowe, J.H., Crowe, L.M., and Carpenter, J.F. 1993. Preserving dry biomaterials: the water replacement hypothesis. Part 1. *BioPharm.* 6, 28-29, 32-33.

D'Cruz, N.M., and Bell, L.N. 2005. Thermal unfolding of gelatin in solids as affected by the glass transition. *J. Food Sci.* 70, E64-E68.

Duchowicz, R., Ferrer, M.L. and Acuna, A.U. 1998. Kinetic spectroscopy of erythrosin phosphorescence and delayed fluorescence in aqueous solution at room temperature. *Photochem. Photobiol.* 68, 494-501.

Eastoe, J.E., and Leach, A.A. 1977. Chemical constitution of gelatin. In A.G. Ward, & A. Courts (Eds.), *The science and technology of gelatin* (pp. 73-107). New York: Academic Press.

Ediger, M.D. 2000. Spatially heterogenous dynamics in supercooled liquids. *Annu. Rev. Phys. Chem.* 51, 99-128.

Franks, F., Hatley, R.H.M., and Mathias, S.F. 1991. Materials science and the production of shelf-stable biologicals. *BioPharm.* 4, 38, 40-42, 55.

Gekko, K., and Timasheff, S.N. 1981. Mechanism of protein stabilization by glycerol: preferential hydration in glycerol-water mixtures. *Biochem.* 20, 4667-4676.

Kasapis, S., AI-Marhoobi, I.M., Deszczynski, M., Mitchell, J.R., and Abeysekera, R. 2003. Gelatin vs polysaccharide in mixture with sugar. *Biomacromol.* 4, 1142-1149.

Kasapis, S., and Sablani, S.S. 2005. A fundamental approach for the estimation of the mechanical glass transition temperature in gelatin. *Interl. J. Biol. Macrom.* 36, 71-78.

Kets, E.P.W., IJpelaar, P.J., Hoekstra, F.A., and Vromans, H. 2004. Citrate increases glass transition temperature of vitrified sucrose preparations. *Cryobiology*. 48, 46-54.

Kim, Y-S, Jones, L.S., Dong, A., Kendrick, B.S., Chang, B.S., Manning, M.C., Randolph, T.W., and Carpenter, J.F. 2003. Effects of sucrose on conforamtional equilibria and flucturations within the native-state ensemble of proteins. *Protein Sci.* 12, 1252-1261.

Kozlov, P.V., and Burdygina, G.I. 1983. The structure and properties of solid gelatin and the principles of their modification. *Polym.* 24 (June), 651-666.

Lakowicz, J.R. 1999. *Principles of fluorescence spectroscopy*. Plenum Press, NY

Lee, J.C., and Timasheff, S.N. 1981. The stabilization of proteins by sucrose. *J. Biol. Chem.* 256(4), 7193-7201.
Lee, K.C.B., Siegel, J., Webb, S.E.D., Leveque-Fort, S., Cole, M.J., Jones, R., Dowling, K., Lever, M.J., and French, P.M.W. 2001. Application of the stretched exponential function to fluorescence lifetime imaging. *Biophys. J.* 81, 1265-1274.

Lukasik, K.V. and Ludescher, R.D. 2006a. Effect of plasticizer on dynamic site heterogeneity in cold-cast gelatin films. *Food Hydrocoll.* 20, 88-95.

Lukasik, K.V., and Ludescher, R.D. 2006b. Molecular mobility in water and glycerol plasticized cold and hot-cast gelatin films. *Food Hydrocoll.* 20, 96-105.

Maroncelli, M. and Fleming, G.R. 1987. Picosecond salvation dynamics of coumarin 153: the importance of molecular aspects of salvation. *J. Chem. Phys.* 86, 6221-6239.

Marshall, A.S., and Petrie, S.E.B. 1980. Thermal transitions in gelatin and aqueous gelatin solutions. *J. Photogr Sci.* 28, 128-134.

Menegalli, F.C., Sobral, P.J.A., Roques, M.A., and Laurent, S. 1999. Characteristics of gelatin biofilms in relation to drying process conditions near melting. *Drying Technol.* 17, 1697-1706.

Nack, T.J, and Ludescher, R.D. 2006. Molecular mobility and oxygen permeability in amorphous bovine serum albumin films. *Food Biophys.* 1, 151-162.

Papp, S. and Vanderkooi, J.M. 1989. Tryptophan phosphorescence at room temperature as a tool to study protein structure and dynamics. *Photochem. Photobiol.* 49, 775-784.

Parker, C.A. 1968. *Photoluminescence of Solutions.* Elsevier, Amsterdam. Netherlands.

Pinhas, M.F., Blanshard, J.M.V., Derbyshire, W., and Mitchell, J.R. 1996. The effect of water on the physicochemical and mechanical properties of gelatin. *J. Therm. Anal.* 47, 1499-1511.

Pravinata, L.C., You, Y. and Ludescher, R.D. 2005. Erythrosin B phosphorescence monitors molecularmobility and dynamic site heterogeneity in amorphous sucrose. *Biophys. J.* 88(May), 3551-3561.

Richert, R. 2000. Triplet state salvation dynamics: basics and applications. *J. Chem. Phys.* 113, 8404-8429.

Richert, R. 2001. Spectral selectivity in the slow β-relaxation of a molecular glass. *Europhys. Lett.* 54(6), 767-773.

Richert, R. 2002. Heterogeneous dynamics in liquids: fluctuations in space and time. *J. Phys. Condens. Matter.* 14, R738-R803.

Roos, Y. 1995. *Phase Transitions in Foods.* Academic Press, San Diego, CA.
Sablani, S.S., Kasapis, S., Al-Rahbi, Y., and Al-Mugheiry, M. 2002. Water sorption isotherms and glass transition properties of gelatin. *Drying Technol.* 20, 2081-2092.

Shirke, S., and Ludescher, R.D. 2005. Dynamic site heterogeneity in amorphous maltose and maltitol from spectral heterogeneity in erythrosin B phosphorescence. *Carbohydr. Res.* 340, 2661-2669.

Shirke, S., Takhistov, P., and Ludescher, R.D. 2005. Molecular mobility in amorphous maltose and maltitol from phosphorescence of erythrosin B. *J. Phys. Chem. B.* 109, 16119-16126.

Shirke, S., You, Y., and Ludescher, R.D. 2006. Molecular mobility and dynamic site heterogeneity in amorphous lactose and lactitol from erythrosin B phosphorescence. *Biophys. Chem.* 123, 122-133.

Simon-Lukasik, K.V., and Ludescher, R.D. 2004. Erythrosin B phosphorescence as a probe of oxygen diffusion in amorphous gelatin films. *Food Hydrocoll.* 18, 621-630.

Slade, L. and Levine, H. 1987. Polymer-chemical properties of gelatin in foods. In A. M. Pearson, T.R. Dutson, and A.J. Bailey, editors. *Advances in meat research: collagen as a food*. New York: AV1, Vol. 4, p. 251-266.

Slade, L., and Levine, H. 1991. Beyond water activity: recent advances based on an alternative approach to the assessment of food quality and safety. *Crit. Rev. Food Sci. Nutr.* 30, 115-360.

Sobral, P.J.A., Menegalli, F.C., Hubinger, M.D., and Roques, M.A. 2001. Mechanical, water vapor barrier and thermal properties of gelatin based edible films. *Food Hydrocoll.* 15, 423-432.

Sobral, P.J.A., and Habitante, A.M.Q.B. 2001. Phase transitions of pigskin gelatin. *Food Hydrocoll.* 15, 377-382.

Tsereteli, G.I., and Smirnova, O.I. 1992. DSC study of melting and glass transition of gelatins. *J. Thermal Anal. Cal.* 38 (5), 1189-1201.

Tzannis, S.T., and Prestrelski, S.J. 1999. Moisture effects on protein-excipient interactions in spray-dried powders. Nature of destabilizing effects of sucrose. *J. Pharm. Sci.* 88(3), 360-370.

Vanin, F.M., Sobral, P.J.A., Menegalli, F.C., Carvalho, R.A., and Habitante, A.M.Q.B. 2005. Effects of plasticizers and their concentrations on thermal and functional properties of gelatin-based films. *Food Hydrocoll.* 19, 899-907.

Wood, P.D., 1977. Technical and pharmaceutical uses of gelatin. In A.G. Ward, & A. Courts (Eds.), *The science and technology of gelatin* (pp. 414-437). New York: Academic Press.

Wright W.W., Guffanti, G.T., and Vanderkooi, J.M. 2003. Protein in sugar films and in glycerol/water as examined by infrared spectroscopy and by the fluorescence and phosphorescence of Tryptophan. *Biophys. J.* 85 (September), 1980-1995.

You, Y., and Ludescher, R.D. 2006. Phosphorescence of erythrosin B as a robust probe of molecular mobility in amorphous solid sucrose. *Appl. Spectrosc.* 60, 813-819.

Zallen, R. 1983. *The physics of amorphous solids;* John Wiley & Sons: New York.

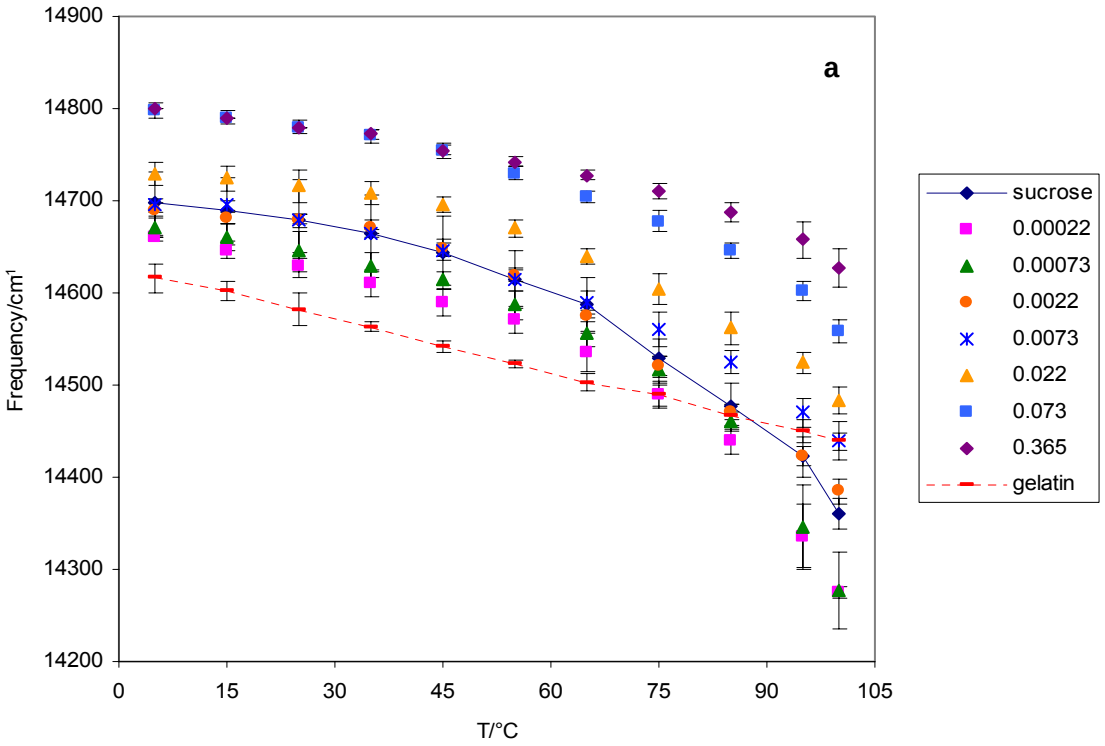
a
Frequency/cm-1
T/°C
14900
14800
14700
14600
14500
14400
14300
14200
0
15
30
45
60
75
90
105
sucrose
0.00022
0.00073
0.0022
0.0073
0.022
0.073
0.365
gelatin

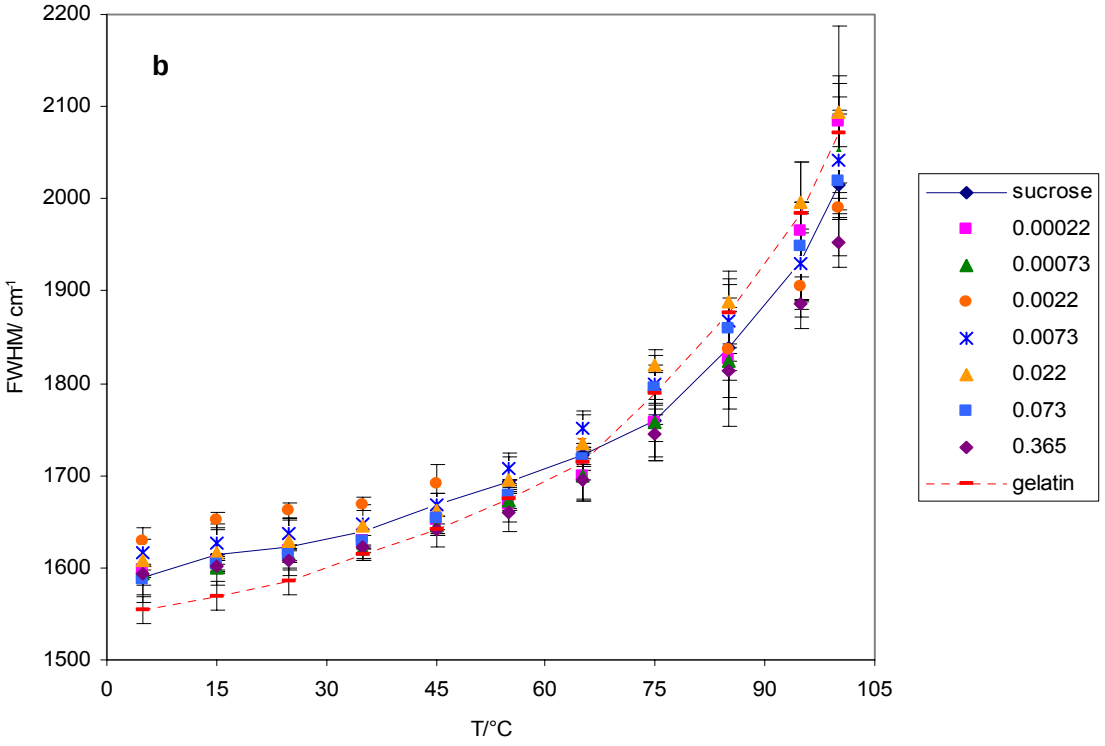
b
FWHM/ cm-1
T/°C
2200
2100
2000
1900
1800
1700
1600
1500
0
15
30
45
60
75
90
105
sucrose
0.00022
0.00073
0.0022
0.0073
0.022
0.073
0.365
gelatin

Figure 71: (a) Peak frequency (ν_p) and (b) bandwidth (full width at half maximum, FWHM) for phosphorescence emission from erythrosin B in amorphous sucrose-gelatin films plotted as a function of temperature. Delayed emission spectra collected as a function of temperature were analyzed using lognormal line shape function.

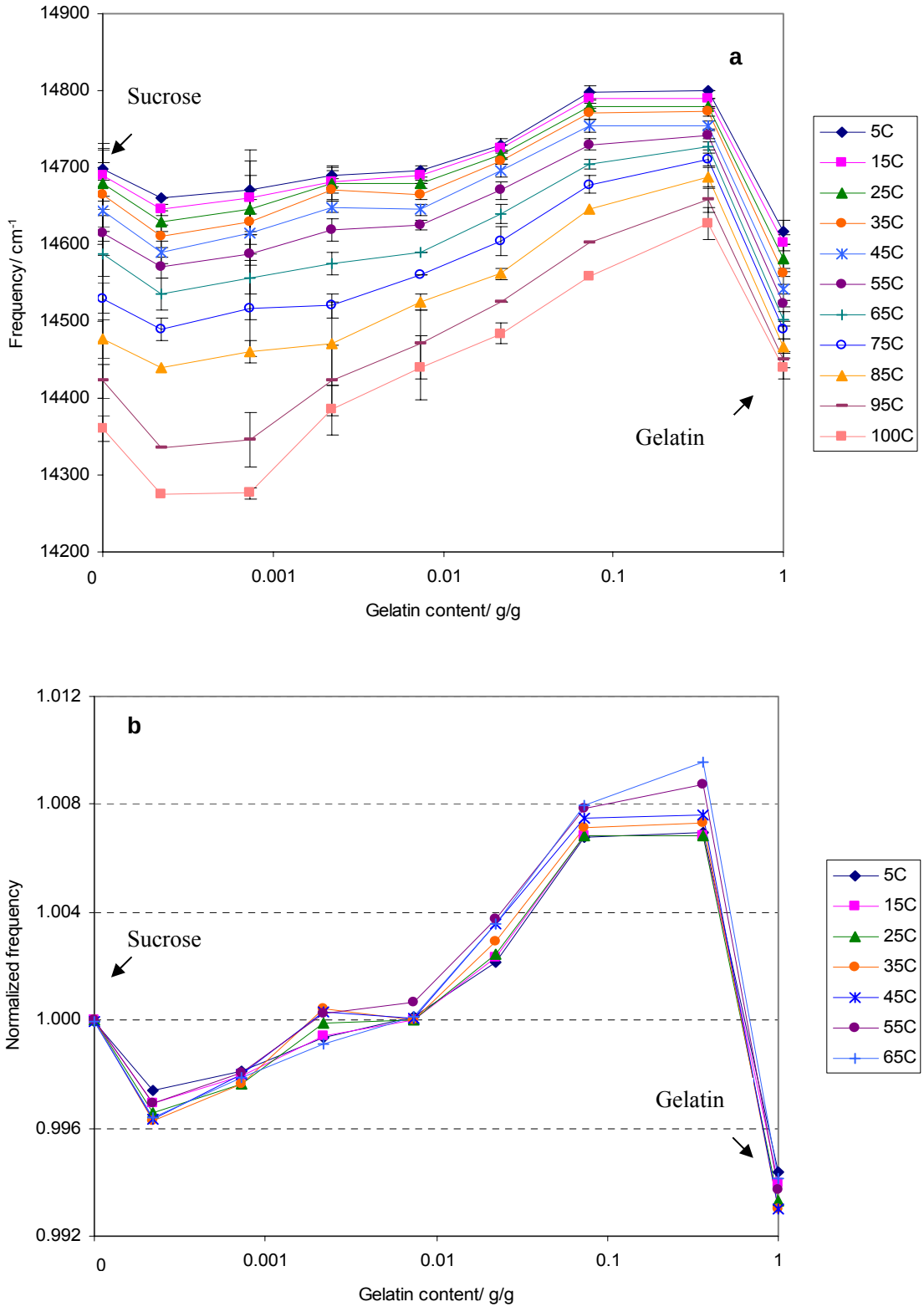

Figure 72: (a) Peak frequency (ν_p) for phosphorescence emission from erythrosin B in amorphous sucrose-gelatin films as a function of gelatin content (weight ratio of gelatin/sucrose) over the temperature range from 5 to 100°C. (b) Normalized peak frequency as a function of gelatin content from 5 to 65°C.

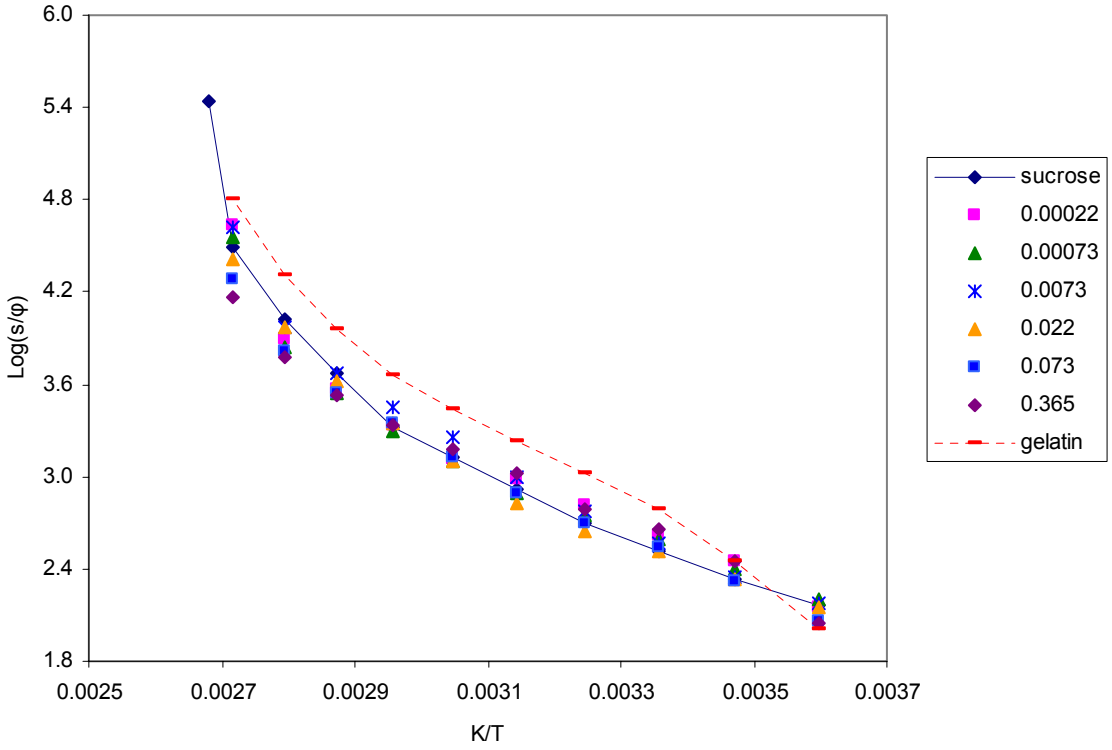

Figure 73: Arrhenius plot of the effect of temperature on the rate of matrix dipolar relaxation around the excited erythrosin B triplet state in sucrose films at various gelatin contents.

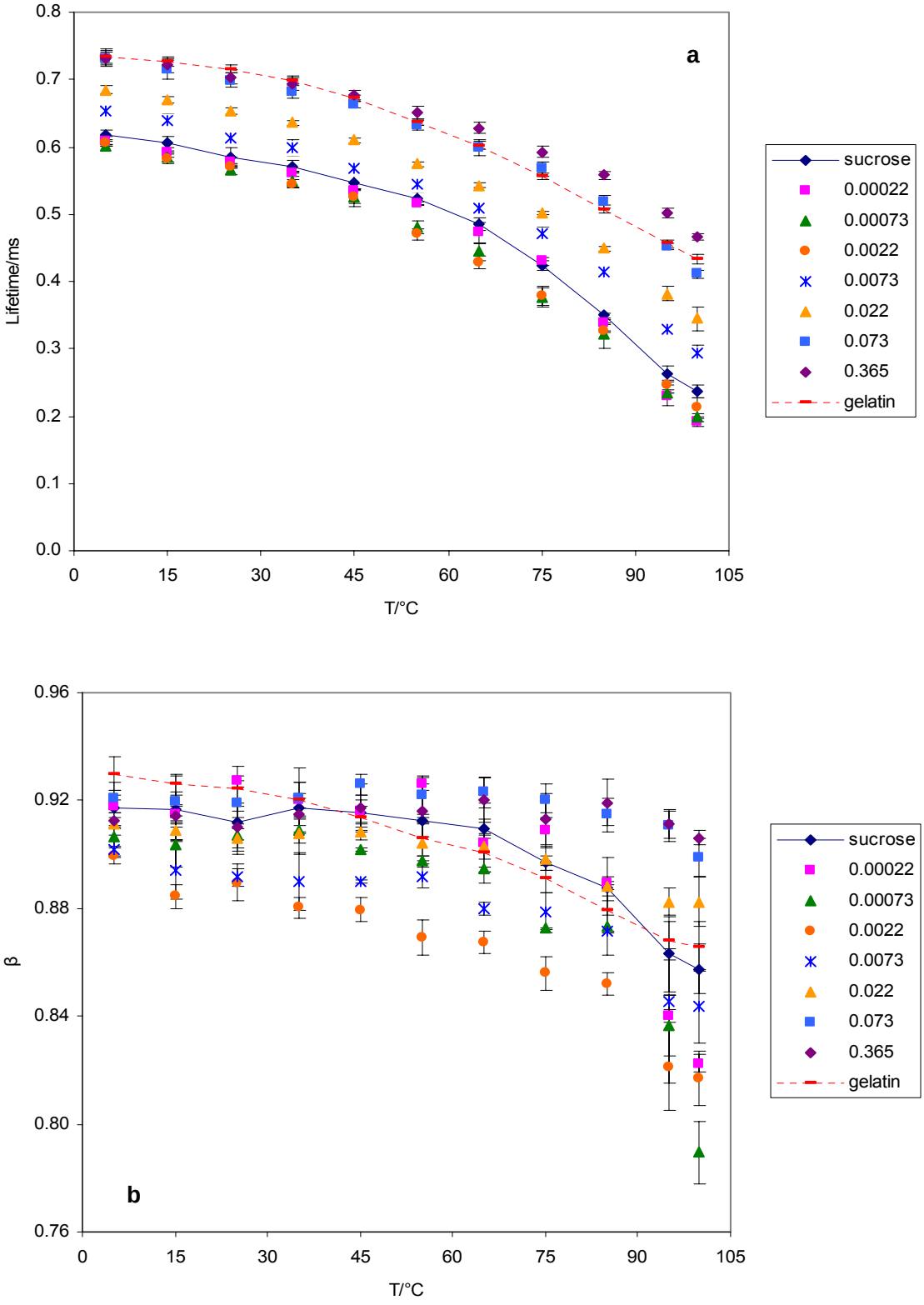

Figure 74: Temperature dependence of (a) lifetime and (b) stretching exponent β obtained from fits to a stretched exponential decay model of the intensity decay of erythrosin B in amorphous sucrose films with various gelatin/sucrose weight ratios.

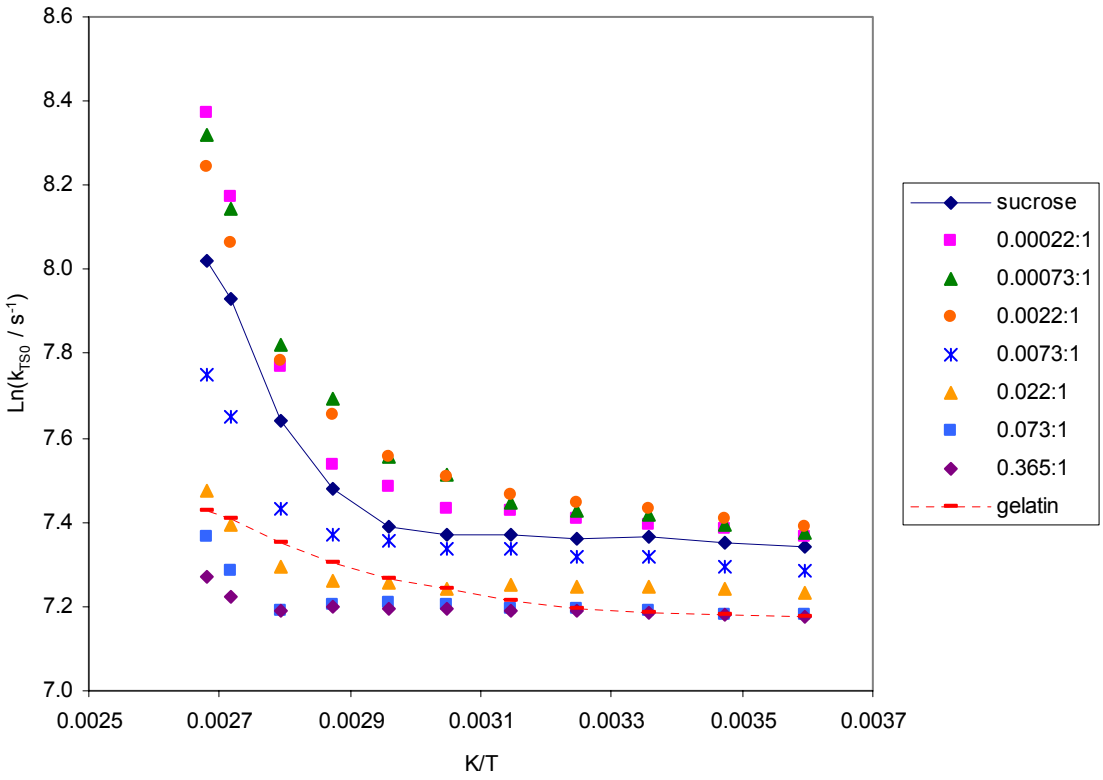

Figure 75: Arrhenius plot of the temperature effect on the rate constant for non-radiative decay of the triplet T_1 state to S_0 (k_{TS0}), data calculated from the lifetime data of Figure 74a; see text for additional details. Samples are erythrosin B in amorphous sucrose films with various gelatin/sucrose weight ratios.

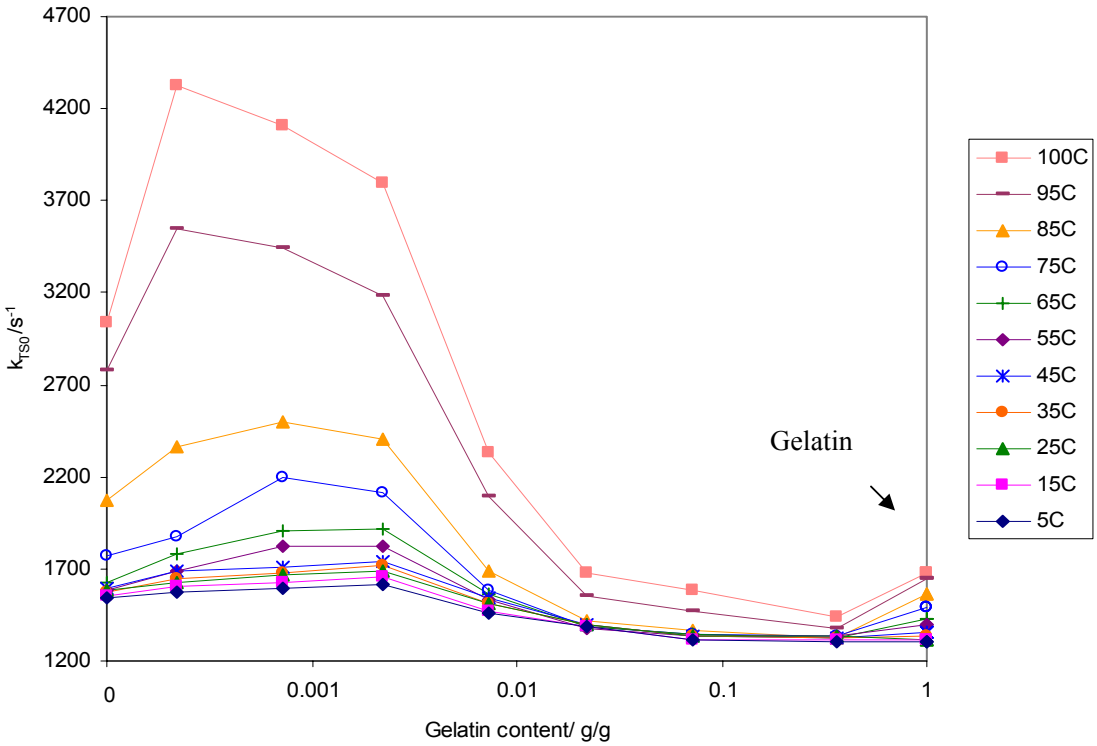

Figure 76: The effect of gelatin content on the rate constant for non-radiative decay of the triplet state to S_0 (k_{TS0}); data of Figure 75 were replotted as k_{TS0} versus gelatin/sucrose weight ratio.

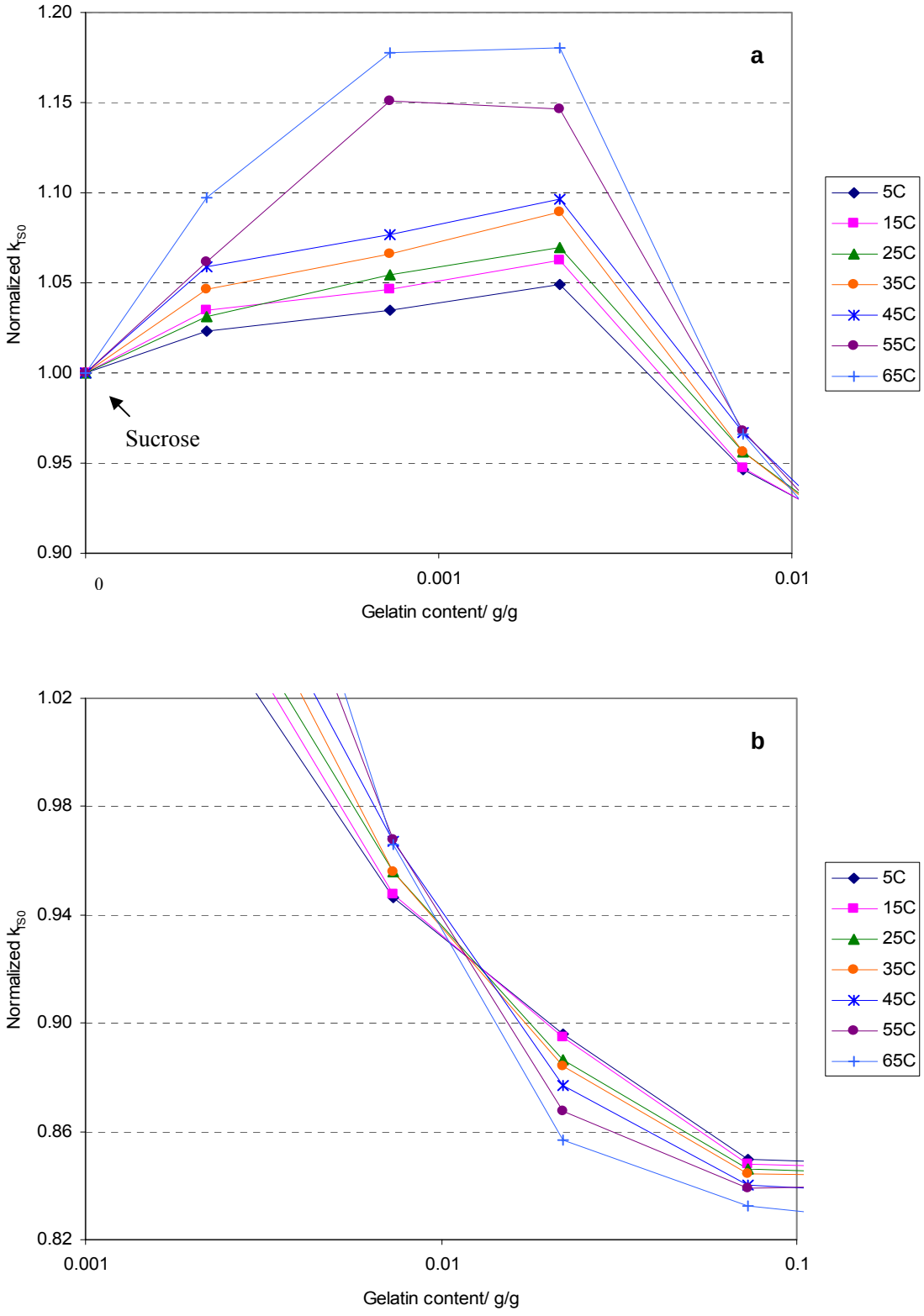

Figure 77: (a) Normalized rate constant for non-radiative decay of the triplet state to S_0 (k_{TS0}) as a function of gelatin content from 0 to 0.01 (g/g). (b) Normalized rate constant for non-radiative decay of the triplet state to S_0 (k_{TS0}) as a function of gelatin content from 0.001 to 0.1 (g/g).

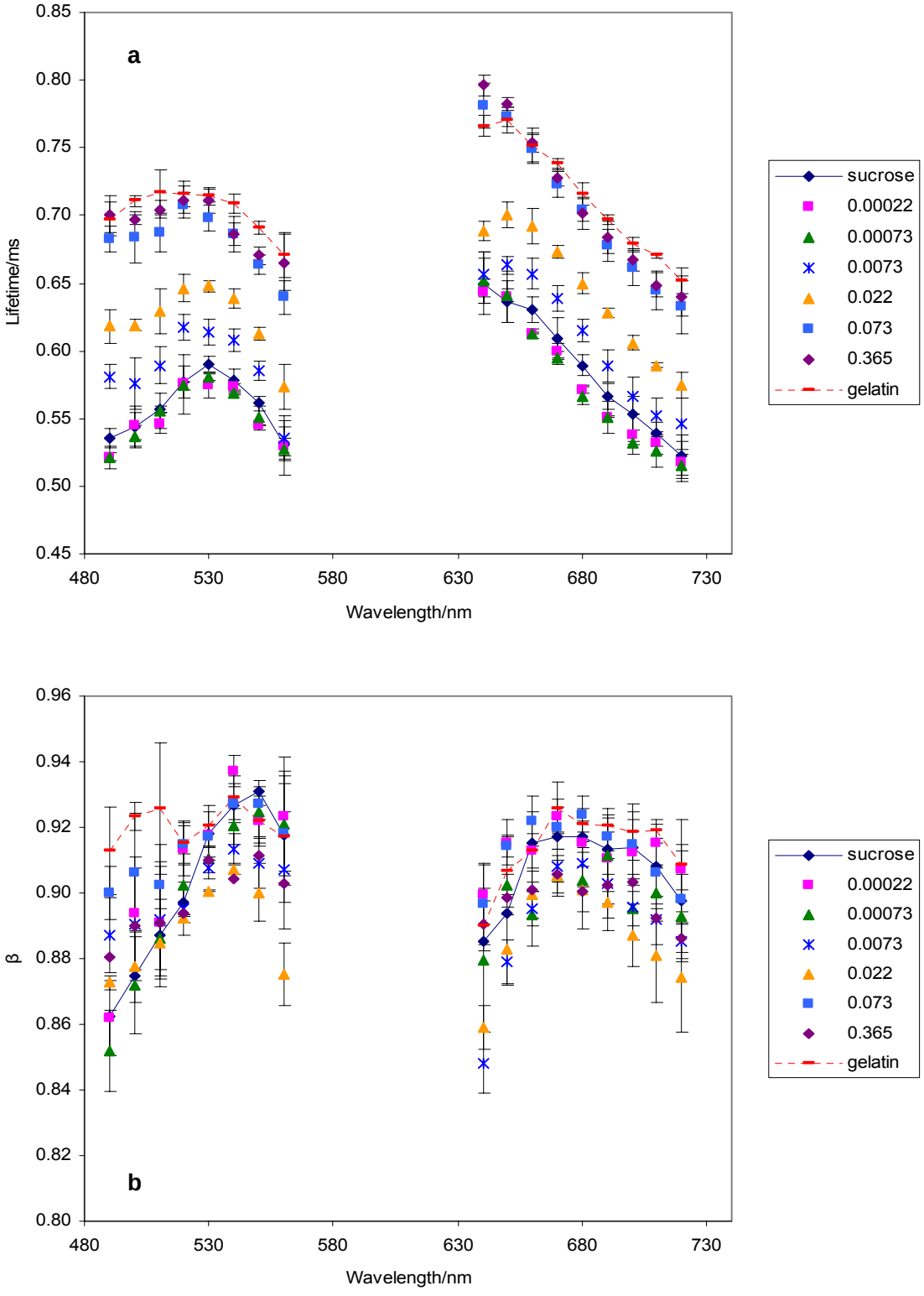

Figure 78: The effect of excitation wavelength (with 680 nm emission) and emission wavelength (with 530 nm excitation) on the lifetimes (a) and stretching exponents β (b) from fits of erythrosin B phosphorescence intensity decays to the stretched exponential decay model. Samples are erythrosin B in amorphous sucrose films with various gelatin/sucrose weight ratios.

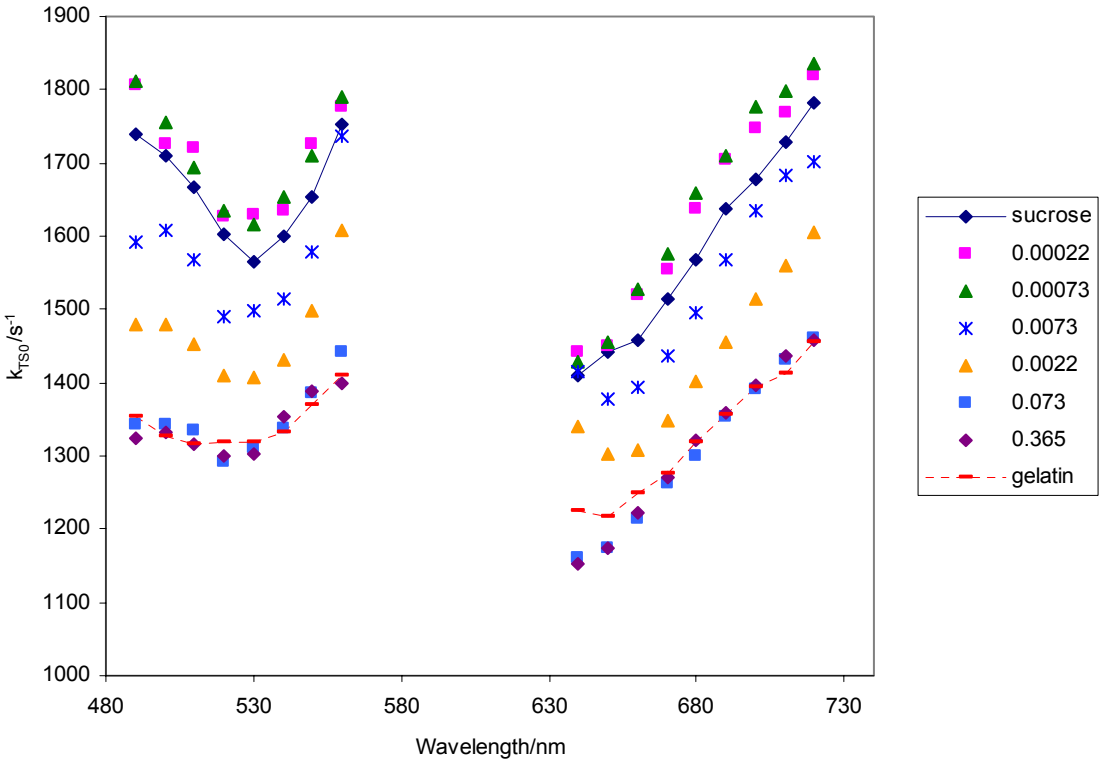

Figure 79: The rate constant for non-radiative decay of the triplet state to S_0 (k_{TS0}) plotted as a function of excitation wavelength (with 680 nm emission) and emission wavelength (with 530 nm excitation). Samples are erythrosin B in amorphous sucrose films with various gelatin/sucrose weight ratios.

Chapter 8 Starch effect on molecular mobility of amorphous sucrose from erythrosin B phosphorescence

Introduction

Sucrose glasses have been an object of research for many years since it was found to be one of the earliest cryoprotective agents during anhydrobiosis. Its ability to protect biomaterials from freeze-thaw damage and provide long-term storage stability has attracted researchers to investigate the mechanism and develop solid state formulations through drying or freeze-drying for labile compounds in foods, such as vitamins and flavor compounds, and for labile biomolecules in pharmaceuticals, such as enzymes, proteins, and antibodies.

Two main mechanisms, glass dynamics and specific interaction, are proposed to understand the role of sucrose in stabilization of sensitive compounds during dehydration and storage (Kets et al., 2004; Chang et al., 2005). The glass dynamics mechanism (Franks et al., 1991; Slade and Levine, 1991) focuses on the rigid, inert matrix formed by vitrification (glass formation) of stabilizers such as sugars. By forming into amorphous, non-crystalline solids upon rapid drying from aqueous solution or cooling from the melt, sugars change from soft, pliable and flexible at high temperature to hard, brittle and rigid at low temperature with an extreme increase in viscosity due to the decrease in the rate of translational as well as rotational and vibrational mobility motions (Zallen, 1983). Therefore, glass formation is a purely kinetic mechanism, and the stability is expected to correlate to molecular mobility in the rigid matrix. The specific interaction mechanism (Carpenter and Crowe, 1989; Carpenter et al., 1993; Crowe et al., 1993), commonly

applied in protein stabilization, states that stabilizers form hydrogen bonds at specific sites with the target compounds, which help maintain the native structure, keep the spatial integrity of the compound after water is removed, and consequently enhance the stability. Sucrose is an ideal matrix material since it is a good glass former as well as a good hydrogen bond former. However, compared with other disaccharides such as trehalose, sucrose has a relatively poor physical stability (lower T_g). A polysaccharide is suggested to mix with sucrose for better functionalities (Allison et al., 2000; Imamura et al., 2002).

Starch is a versatile food ingredient and widely used as a texturizer, thickener, gelling agent, adhesive and moisture-retainer. The starch granule is a partially crystalline particle composed of amylose and amylopectin polysaccharides. Amylose is a mainly linear polymer containing 100 to10,000 glucose units linked with 1,4-α-D-glucosidic bonds; whereas amylopectin is a highly branched polysaccharide consisting of 1,4-α-D-glucosidic bond linked main chain with a great proportion of α-1,6-linkages. Both of them contribute to the high T_g of starch molecule (above 200°C; Bizot et al., 1997). Recently much research have been carried out on the influence of small molecules on the properties of starch, such as the plasticization effect of water (Benczedi, 1998), glycerol (Lourdin et al., 1998; Myllarinen et al., 2002; Partanen et al., 2004), and sorbitol (Gaudin, 1999), the antiplasticization effect of small molecules (Lourdin et al., 1997, 2003), and the effect of sugars on glass transition (Jiang et al., 2001) and molecular mobility in starch-based systems (Poirier-Brulez et al., 2006). Few studies focused on the effect of starch on the properties of sucrose-based systems. Since starch is selected to improve the stability of sucrose, the molecular mobility of mixed starch-sucrose matrix becomes a pressing issue.

Molecular mobility within amorphous solids is usually manifested by relaxation processes. The amorphous solids exhibit the primary α or glass transition at T_g which reflects the activation of large-scale molecular motions (α-relaxations) that underlie the onset of translational and rotational motions; and the secondary β transition within the glass at T_β which reflects the activation of localized molecular motions (β-relaxations) linked to vibrational motion and local side-chain motion. Temperature-dependent molecular mobility thus controls physical and chemical properties by modulating the nature and kinetics of reactions that occur during processing and storage of biomaterials.

In a previous study we used erythrosin B phosphorescence to monitor the molecular mobility as well as dynamic site heterogeneity in amorphous solid sucrose (Pravinata et al., 2005). In the present study, phosphorescence of Ery B was used to measure the matrix mobility in thin films of amorphous sucrose-starch mixtures. High-amylose starch was selected because of its ability to form films. The measurement of molecular mobility of amorphous sugars at low levels of macromolecules thus provides insight into the mechanism of biopolymer effect on sucrose matrix mobility, which is of considerable fundamental and technological interest. Starch content was varied from 0.001 to 0.1 (g starch/g sucrose) by addition of starch to the concentrated sucrose solution prior to film formation. The temperature-dependence of mobility was measured and analyzed at different starch contents, generating families of mobility versus temperature curves.

Materials and Methods

1. Preparation of pure sucrose film

We prepared glassy sucrose films by using a slightly modified version of our published method (Pravinata et al., 2005; see details in Materials and Methods in Chapter 1).

2. Preparation of starch-sucrose

Corn starch HYLON VII (71% amylose, molecular weight 243,000~972,000) was obtained as a kind gift from National Starch (Bridgewater, NJ) and used without further treatment. Starch-sucrose solutions were prepared from sucrose solution containing dye. Starch powder and a certain amount of water were added to 64-66% sucrose solution, and the starch concentration was controlled less than 3 wt %. The mixtures were heated with vigorous stirring in water bath at 90-100°C for 30-40 min. The final mixtures were checked using microscope to ensure that starch granules were completely hydrated and gelatinized. The solutions had starch/sucrose weight ratio of 0.001, 0.0025, 0.005, 0.01, 0.025, 0.05, and 0.1. The procedure to make a glassy film was the same as the procedure to make a pure sucrose film except for drying films for 10 min instead of 5 min.

Water content in amorphous sucrose and sucrose-starch films was determined gravimetrically (by difference of mass before and after drying for 24h at 70°C in an Ephortee (Haake Buchler, Inc.) vacuum oven at 1kPa). Sample films were scrapped from quartz slides and ground into powders in a glove box containing P_2O_5 and Drie-Rite with a relative humidity less than 5%. Pure sucrose films contained 0.56±0.13 wt. % water while the starch/sucrose mixture samples contained 0.58±0.01, 0.50±0.08, 1.05±0.03, 1.28±0.27, 1.50±0.05, 1.75±0.03, and 1.78±0.09 wt. % water, respectively.

3. Luminescence measurements

Luminescence measurements were made using a Cary Eclipse Fluorescence spectrophotometer (Varian Instruments, Walnut Creek, CA). Prior to any phosphorescence measurements, all samples were flushed for at least 15 minutes with nitrogen gas which contained less than 1ppm oxygen to eliminate oxygen quenching. At each target temperature samples were equilibrated for 1min/°C increase in temperature. The temperature was controlled using a thermo-electric temperature controller (Varian Instruments, Walnut Creek, CA). To eliminate moisture condensation during the measurements below room temperature, dry air was used to flush the chamber surrounding the cuvette holder. All the measurements were made at least in triplicate.

Delayed fluorescence and phosphorescence emission spectra were collected from 520 to 750 nm (10 nm bandwidth) at 1 nm intervals using excitation of 500 nm (20 nm bandwidth) over a temperature range from 5 to 100°C with an observation window of 5.0 ms and an initial delay time of 0.2 ms which suppresses fluorescence coincident with the lamp pulse. Emission spectra from sucrose or sucrose-starch films without probe were subtracted from each spectrum although the signal of background was very low.

The energy of emission maximum (ν_p) and the full width at half maximum (FWHM) of the emission bands were determined by using log-normal lineshape function (Maroncelli and Fleming, 1987) to fit both delayed fluorescence and phosphorescence.

$$I(\nu) = I_0 \exp\left\{-\ln(2)\left(\frac{\ln[1+2b(\nu-\nu_p)/\Delta]}{b}\right)^2\right\} \quad (1)$$

Where I_0 is the maximum emission intensity, ν_p is the peak frequency (cm^{-1}), Δ is a linewidth parameter and b is an asymmetry parameter. This equation reduces to a

Gaussian line width when b=0. The bandwidth (FWHM; Γ) was calculated according to the following equation:

$$\Gamma = \Delta\left(\frac{\sinh(b)}{b}\right) \tag{2}$$

For delayed luminescence spectra collected from 520-750 nm, a sum of log-normal functions for delayed fluorescence ($I_{df}(\nu)$) and phosphorescence ($I_p(\nu)$) was used to fit the spectra. Each emission band was set to independent fit parameters.

The dipolar relaxation time φ was calculated from the temperature-dependence of the phosphorescence emission peak ν (T) by analyzing the relaxation function:

$$\frac{\Delta\nu}{\Delta\nu_r} = \frac{\nu(T) - \nu_{\max}}{\nu_{\min} - \nu_{\max}} \tag{3}$$

Where ν (T) is the emission peak energy at Temperature T, ν_{min} and ν_{max} are the emission peak energy at the lowest temperature and the highest temperature, respectively. By incorporating a stretched exponential function, the relaxation time can be calculated from the following equation:

$$\frac{\Delta\nu}{\Delta\nu_r} = \frac{\nu(T) - \nu_{\max}}{\nu_{\min} - \nu_{\max}} = \frac{1}{\Gamma(\frac{1}{\beta_l})} \frac{1}{1 + \frac{\beta_e}{\beta_l}\frac{\tau}{\varphi}} \tag{4}$$

Where τ and β_l are stretched lifetime and exponents from Eq. 5, Γ is the Gamma function, β_e is assumed as value of 0.5 (Shirke et al., 2005).

For lifetime measurements, samples were excited at 530 nm (20 nm bandwidth) and emission transients collected at 680 nm (20 nm bandwidth) over the temperature range from 5 to 100°C. Phosphorescence intensity decays were collected over a window of 5 ms with an initial delay of 0.1 ms and increments of 0.04 ms. Each decay was the average of 20 cycles. Because intensity decays were non-exponential, a stretched

exponential, or Kohlrausch-Williams-Watts' decay function was selected to analyze the intensity decay (Richert, 2000; Lee, et al., 2001; Pravinata et al., 2005).

$$I(t) = I_0 \exp(-(t/\tau)^{\beta}) + \text{constant} \quad (5)$$

Where I_0 is the initial amplitude, τ is the stretched exponential lifetime, and β is an exponent varying from 0-1 and characterizing the distribution of lifetimes. The use of a stretched exponential model provides a direct measurement of continuous distribution of lifetimes, which is appropriate for describing a complex glass possessing a distribution of relaxation times for the dynamic molecular processes. The smaller the β value, the more non-exponential the intensity decays and the broader the distribution of lifetimes. Program NFIT (Galveston, TX) was used to fit the decay; goodness of fit was evaluated by examining the χ^2 and R^2. Plots of modified residuals (defined as the difference between the intensity from the fit decay curve and the measured intensity divided by the square root of the measured intensity) was also an indicator of the goodness of fit. R^2 for all fits ranged from 0.99 to 1.00 and modified residuals plots fluctuated randomly around zero amplitude.

Phosphorescence emission lifetimes of Ery B as a function of emission wavelength were measured with excitation wavelength at 530 nm (20 nm bandwidth); emission wavelength varied from 640 to 720 nm (20 nm bandwidth). Phosphorescence emission lifetimes as a function of excitation wavelength were measured with emission wavelength at 680 nm (20 nm bandwidth); excitation wavelength ranged from 490 to 560 nm (20 nm bandwidth). The experiments were performed at 25°C.

4. Photophysical scheme

Our analysis of the delayed emission is similar to the photophysical scheme for erythrosin B outlined by Duchowicz et al. (1998). The measured emission rate for phosphorescence (k_P) is the sum of all possible deexcitation rates for the triplet state T_1:

$$\tau^{-1} = k_P = k_{RP} + k_{TS1} + k_{TS0} + k_Q[Q] \quad (6)$$

In this equation, k_{RP} is the rate of radiative emission to the ground state S_0. For erythrosin B, k_{RP} is 41 s^{-1} and constant with temperature (Duchowicz et al., 1998).

k_{TS1} is the rate of thermally activated reverse intersystem crossing from the triplet state T_1 to the singlet state S_1, and the value can be estimated from the Arrhenius equation:

$$k_{TS1}(T) = k^0_{TS1} \exp(-\Delta E_{TS}/RT) \quad (7)$$

where k^0_{TS1} is the maximum rate of intersystem crossing from T_1 to S_1 at high temperature, ΔE_{TS} is the energy gap between T_1 and S_1, R=8.314 J K^{-1} mol^{-1}, and T is the temperature in Kelvin. The value of ΔE_{TS} is calculated from the slope of a Van't Hoff plot of the natural logarithm of the ratio of intensity of delayed fluorescence (I_{DF}) to phosphorescence (I_P):

$$d[\ln(I_{DF}/I_P)]/d(1/T) = -\Delta E_{TS}/R \quad (8)$$

where I_{DF} and I_P are the maximum intensity values determined from analysis of the emission band using Eq. (1). The value of k_{TS1} at 25°C was estimated as 88 s^{-1} using k^0_{TS1}=3.0 x 10^7 s^{-1} and ΔE_{TS} = 31.56 kJ/mol (Pravinata et al., 2005).

In the presence of oxygen, the quenching rate $k_Q[Q]$ is the product of rate constant k_Q and the oxygen concentration [Q]. By flushing nitrogen throughout the measurements we assume that no oxygen quenching occurred. One of the non-radiative decay routes is through intersystem crossing to the ground state S_0. The decay rate is expressed by $k_{TS0,}$

which reflects the rate of collisional quenching of the probe due to both internal and external factors (Papp and Vanderkooi, 1989). We assume that the term k_{TS0} primarily reflects the external environmental factors since the self collisional quenching among probe molecules can be neglected within the extremely viscous amorphous solid. In this study, temperature-dependent term k_{TS0} can be calculated by difference from Eq. (6).

Results

At a probe/sucrose molar ratio of $1:10^4$, each probe is on average surrounded by a matrix shell around 10-11 sucrose molecules thick. At this concentration Ery B dispersed within the sucrose matrix does not aggregate and thus reports the physical properties of the unperturbed sucrose matrix (You and Ludescher, 2006).

1. Delayed emission spectra

The delayed emission spectra of erythrosin B dispersed in amorphous sucrose films with various starch/sucrose weight ratios were collected over the temperature range from 5 to 100°C. All spectra (data not shown) showed the expected decrease in phosphorescence and increase in delayed fluorescence intensity with increasing temperature seen in xanthene dyes (Parker, 1968). Both the delayed fluorescence and phosphorescence bands shifted to longer wavelength at higher temperature; the peak frequency (ν_p) and bandwidth (Γ) were determined by fitting to a log-normal lineshape function (Eq. 1 and 2). The temperature effect on frequency and bandwidth for phosphorescence emission are plotted versus temperature in Figure 80. The peak frequency for delayed fluorescence exhibited similar thermal behavior (data not shown).

The phosphorescence peak frequency provides a measure of the average energy of emission; a decrease in emission energy reflects an increase in the average extent of

dipolar relaxation around the excited triplet state prior to emission (Lakowicz, 1999). The peak frequency decreased gradually and approximately linearly with temperature below T_g and much more steeply at T_g and above in all films. All the curves showed similar shape; however, the curve for film with starch/sucrose weight ratio of 0.0025 was below while those with starch/sucrose weight ratio higher than 0.005 were above the curve for pure sucrose. At ratio of 0.001, the curve was almost identical with the curve for sucrose. At a ratio of 0.0025, the peak frequency was 14670 cm^{-1} at 5°C and 14285 cm^{-1} at 100°C, slightly red-shifted by 1.3 nm and 3.6 nm, respectively (compared with 14698 cm^{-1} and 14360 cm^{-1} in sucrose). When the starch content increased by 10-fold to 0.025, the values of peak frequency increased to 14834 cm^{-1} at 5°C and 14534 cm^{-1} at 100°C, the spectrum blue-shifting by 6.3 and 8.4 nm, respectively. Addition of more starch decreased the peak frequency.

The total change in peak frequency ($\Delta\nu_p$) with changing temperature from 5 to 100°C varied with starch content. Compared with sucrose (~340 cm^{-1}), the change in peak frequency in starch/sucrose films was larger at low but smaller at high starch content. The value of $\Delta\nu_p$ reached a maximum of 380 cm^{-1} at a ratio of 0.0025. With more starch added, the value began to decrease and achieved a minimum of 300 cm^{-1} at a ratio around 0.025. The peak frequency difference reflects the corresponding change in average extent of dipolar relaxation around the excited triplet state.

The phosphorescence bandwidth provides a measure of the range of energetically distinct matrix environments seen by the Ery B probe within the amorphous matrix (Lakowicz, 1999). The bandwidth was essentially constant at ~1600 cm^{-1} at low temperature and increased gradually with temperature in the glass and more dramatically

in the melt above T_g in all films. Addition of starch did not significantly influence the bandwidth over the whole temperature range, indicating that no obvious change occurred in the width of the distribution of energetically distinct matrix environments both in the glass and in the melt in the studied concentration range of starch.

The effect of starch is demonstrated in plots of peak frequency and bandwidth as a function of starch content (Figure 81). At low concentrations of starch (ratio$\leq$ 0.005), the curve of the peak frequency showed a valley with minimum values at a ratio of 0.0025. The value of peak frequency increased when starch content increased at ratio of 0.005 and above, and then slightly decreased with further increase in starch/sucrose ratio. Bandwidth curves as a function of starch content fluctuated within the error range, indicating that addition of starch had no obvious effect on the distribution of local environments with different energies. The starch effect is more clearly illustrated in plots of relative peak frequency normalized to the values in pure sucrose film at temperature from 5 to 65°C (Figure 82).

The intensity ratio (ln (I_{df}/I_p)) was plotted as a van't Hoff plot versus 1/T and the slope obtained from the linear plot used to estimate the energy gap between the triplet and singlet states (Eq. 8 in Materials and Methods). In amorphous sucrose the value of ΔE_{TS} was 31.56±0.56 kJ mol^{-1}. In the presence of starch with weight ratio of 0.001, 0.0025, 0.005, 0.01, 0.025, 0.05, and 0.1, the values of ΔE_{TS} were 31.92±0.19, 31.32±0.86, 31.64±0.16, 32.12±0.77, 31.13±0.55, 31.32±0.38, and 31.29±0.16 kJ mol^{-1}, respectively, indicating that addition of starch had insignificant influence on the singlet-triplet energy gap.

The dipolar relaxation rates for sucrose and sucrose-starch films are plotted in an Arrhenius fashion in Figure 83 (Eq. 4 in Materials and Methods). These curves show upward curvature at high temperatures indicating an increased activation energy with increasing temperature. Compared with sucrose, the relaxation rate in sucrose-starch films slightly increased at low but decreased at high starch contents.

2. Phosphorescence decay kinetics

The phosphorescence intensity decays in sucrose-starch glass with different starch contents were measured over the temperature range from 5-100ºC. The stretched exponential lifetime and exponent β are plotted as a function of temperature (Figure 84). The lifetimes decreased biphasically with increasing temperature in all films, exhibiting a gradual linear decrease at low and a more dramatic decrease at high temperature. All the curves showed a similar shape; however, the curve for film with starch/sucrose weight ratio lower than 0.005 were below, while those with starch/sucrose weight ratio higher than 0.005 were above the curve for pure sucrose. The lifetimes increased correspondingly with addition of starch, from 0.63 ms at 5°C in starch-sucrose film at weight ratio of 0.005 to 0.67 ms in the film with a ratio of 0.01. With further increase in starch concentration, the lifetimes slightly decreased.

Exponent β in sucrose film showed biphasical behavior over the temperature range from 5 to 100ºC: β kept almost constant at low temperature and decreased at high temperature. All the curves for starch-sucrose films were above the curve for sucrose at low temperature, except the curves with ratio higher than 0.05 at the low end of the temperature range (5 and 15°C). At 65°C and above, the curves for films with ratio lower than 0.005 were below while the others were above the curve for sucrose. With

increasing starch content, the decrease in exponent β with temperature became less and the biphasic behavior became vague at ratios above 0.01. Since β reflects the distribution of lifetimes, and thus the corresponding distribution of dynamically distinct probe environments with different values of k_{TS0} (Pravinata et al., 2005), the small increase in β with addition of starch indicated a significant decrease in the range of dynamically distinct probe environments both in the glass and in the melt (except at ratio≤0.005).

The decrease in lifetime with temperature reflects an increase in the rate of non-radiative decay of the excited triplet state T_1 due to an increase in both the rate of non-radiative decay to the ground state S_0 (k_{TS0}) and reverse intersystem crossing to S_1 (k_{TS1}). Based on the maximum physically reasonable value of k_{TS1} (Pravinata et al. 2005), an estimate of the lower limits of k_{TS0} was calculated from Eq. 9 (Materials and Methods) and it is plotted as $\ln(k_{TS0})$ versus 1/T in Figure 85. The non-radiative quenching rate k_{TS0} was linear at low temperature and shot up at high temperature, which indicated that this rate is sensitive to the molecular mobility activated at the glass transition. The quenching rate k_{TS0} was identical with that in sucrose with addition of starch at a ratio of 0.005. Above 0.005 the quenching rate k_{TS0} decreased significantly both in the glass and in the melt. This depression effect on mobility was more significant at high temperature. At a ratio of 0.01, for instance, the value of k_{TS0} decreased by 6% at 5ºC and 17% at 100ºC compared to pure sucrose. However, the quenching rate increased slightly in the glass and moderately in the melt at starch/sucrose ratios lower than 0.005. For instance, the value of k_{TS0} increased by 2% at 5ºC and 20% at 100ºC at a ratio of 0.001.

Figure 86a shows the starch content-dependence of the collisional quenching rate k_{TS0} in sucrose films and Figure 86b is the plot of the relative rate normalized to the

values in pure sucrose at temperatures from 5 to 65ºC. At ratios lower than 0.005 the rate constant k_{TS0} increased compared with that in sucrose and the magnitude of the increase was higher at elevated temperature. At ratios higher than 0.005 the rate decreased and the magnitude of the decrease was higher at elevated temperature. The quenching rate did not decrease further upon addition of more starch at weight ratios above 0.01.

It is clear that temperature had a positive effect on mobility (absolute rate) in all sucrose-starch films (Figure 86a). However, it showed different impact on the relative rate: at starch/sucrose ratio above 0.01, the relative rate decreased with increasing temperature, exhibiting a negative effect of temperature although the temperature had a positive influence on the absolute rate (Figure 86b).

3. Spectral heterogeneity

Phosphorescence intensity decays of Ery B in sucrose films with different starch contents were measured as a function of excitation and emission wavelength at 25°C. All decays were well analyzed using a stretched exponential model; lifetimes are plotted versus excitation and emission wavelength in Figure 87a. All lifetime curves showed a similar trend: the lifetimes decreased with increasing wavelength across the emission band. In sucrose, the lifetimes varied from a high of 0.65 ms at 640 nm to a low of 0.52 ms at 720 nm; lifetimes also decreased monotonically with increasing wavelength in sucrose-starch films. The values of the lifetime increased with increasing starch concentration (≥0.005). In the presence of small amounts of starch (ratio of 0.001 and 0.0025) lifetime and lifetime variation were almost same as those in sucrose. With increasing starch content up to 0.1, both lifetime and lifetime variation increased (i.e. 0.73 ms at 640 nm to 0.57 ms at 720 nm). Lifetimes also varied across the excitation

band: the lifetimes increased with increasing wavelength to a maximum at 530 nm and then decreased at higher wavelengths. The variation of lifetime within the excitation band showed similar trends as within the emission band.

The stretching exponent β also varied as a function of both excitation and emission wavelength (Figure 87b). In all films β values were lower at the blue edges in both emission and excitation bands, and increased with increasing wavelength to a maximum at 670-680 nm across the emission band and a maximum at 540-550 nm across the excitation band, then decreased slightly at the red edges. The values of β were higher and the variation of β across the emission as well as excitation band in sucrose films was smaller in the presence of starch. At the high end of the starch content (ratio of 0.1), the values of β were lower but variation of β was larger than sucrose.

The calculated quenching rate k_{TS0} is plotted versus emission and excitation wavelength at various starch contents in Figure 88. k_{TS0} increased monotonically with increasing emission wavelength in all of the films. At low starch content (<0.005) k_{TS0} was above, and at high starch content (≥ 0.005) k_{TS0} was below that seen in pure sucrose. The variation of k_{TS0} decreased with increasing starch content. Across the excitation band, k_{TS0} curves showed minimum values around 530 nm with higher values at both the blue and red edge of the excitation band in all sucrose and sucrose-starch films. The quenching rate increased at low and decreased at high starch contents.

Discussion

1. Sample preparation and starch conformation

The behavior of starch in solutions is complicated by its composition (amylose and amylopectin) and the physical properties are dependent on various factors, including the source of the starch, the amylose/amylopectin ratio, other components, and processing conditions (temperature, shearing, and heating/cooling rate). Sucrose is known to influence starch by inhibiting the granule swell, decreasing the maximum viscosity, reducing the amount of soluble amylose from the granule, and enhancing the gelatinization temperature through competition for water. Sucrose effect is pronounced when the concentration increases above 60% (provided by National Starch). The gelatinization temperature of 6% starch paste in the presence of 60% sucrose was reported as 100°C compared to 60-70°C in the absence of sucrose. High-amylose starch has higher gelatinization temperature compared with regular starch and jet cooking is required for granule dissolution in the food industry. In the present work, the final concentration of starch in sucrose solution was controlled at 3% and the dispersions were heated at 90-100°C for 40 min to ensure gelatinization (evaluated by the loss of birefringence) in the starch granules in all starch-sucrose mixtures. Upon gelatinization, amylose is leached out of the granules and the molecules in solution at high temperatures show conformation of a random coil (Dintzis and Tobin, 1969; Hayashi et al., 1981), whereas amylospectin stays within the granules without any crystalline order (Eliasson, 2006). Continued heating resulted in a continuous phase of solubilized amylose and amylopectin and a discontinuous phase of granule remnants (Fennema, 1996). Microfiltration with 0.2μm membrane was applied after gelatinization was finished to remove the insoluble granule remnants. We thus presumed that there were no crystalline

or highly ordered structures present in the gelatinized starch-sucrose solution or in the films cast from this solution.

Gelatinized starch molecules are not in thermodynamic equilibrium, and thus easy to change from initially amorphous state to a more ordered or crystalline state, which is referred to as retrogradation. Sucrose is reported to prevent the retrogradation of starch (Kohyama and Nishinari, 1991; Le Botlan and Desbois, 1995) and retrogradation will not occur until a certain amount of water is present in the matrix (Eliasson, 2006). During the preparation of samples, starch was added to sucrose solution before gelatinization began and sucrose is thus expected to act as a retrogradation inhibitor. Drying was applied to remove the water immediately after gelatinization was done and the films were stored in a desiccator with 0% RH for one week. We thus make the assumption that no obvious recrystallization or formation of orderly structure takes place after 7-day equilibration. In this case complications from the change in the structure or conformation can be avoided during the interpretation of the data.

A number of studies have discovered that amylose molecules in neutral aqueous solution exhibit a global random coil conformation with locally helical segments (Norisuye, 1994, 1996; Elmgren, 1987; Ebert and Elmgren, 1984; Hayashi et al., 1981; Pfannemueller et al., 1971; Rao & Foster, 1963). This conformation model seems common to amylose in a variety of solvents (Norisuye, 1994). The locally ordered structure disappears when water content increases and thermal energy is applied. Cheetham and Tao (1997) found that the helical conformation was lost with increasing temperature at water content above 33% and a complete transition from helix to coil was obtained at 66% water content. In the present study, gelatinization ($T_{gelatinization}$>63°C,

above which the amylose molecule must be in a random coil; Hayashi et al., 1983) of starch in dilute aqueous solution ensures that the conformation of starch in solution is a uniformly random coil. The starch macromolecules in the films cast from the solution should have the same conformation. Our results thus provide insight into the polymer effect (molecular weight and interactions with host molecules) on the molecular mobility of the sucrose matrix.

2. Effect of starch on mobility of amorphous sucrose

The phosphorescence emission wavelength and intensity of erythrosin B in amorphous sucrose and sucrose-starch mixtures are influenced by two kinds of molecular mobility: dipolar relaxation and collisional quenching. Our discussion of the starch effect on molecular mobility in amorphous sucrose is based on the emission energy and lifetime data that are modulated by these two mobility motions. Starch showed two different effects on the molecular mobility in amorphous sucrose solids. A destabilization influence on sucrose matrix was observed at low starch contents (<0.005), indicated by a decrease in emission energy and lifetime, and increases in the dipolar relaxation rate $1/\varphi$ and the nonradiative collisional quenching rate k_{TS0}. At contents above 0.005, starch demonstrated a stabilization influence, indicated by an increase in emission energy and lifetime, and a depression of the dipolar relaxation rate and collisional quenching rate.

Phosphorescence emission energy (peak frequency), the energy gap between T_1 and S_0, is primarily modulated by the T_1 energy and thus the dipolar relaxation of hydroxyl groups around T_1 within the matrix (Pravinata et al., 2005). The emission energy increased with increasing starch content in sucrose. The increase in emission energy suggested a decrease in the dipolar relaxation rate due to the reduced mobility

motion of polar groups around the excited probe molecules in the presence of starch. Also the lower polarity due to a lower average density of polar (-OH) groups contributed to the increased emission energy. Water and sucrose have higher densities of polar groups per molecular mass than starch, namely 1/18 and 8/342, respectively, compared to 3/162. At very low starch contents, the decrease in emission energy is the result mainly of the increased relaxation rate despite the lower polarity.

The emission intensity and the lifetime are directly modulated by the rate of radiative emission k_{RP}, of reverse intersystem crossing to the excited triplet state k_{TS1} and of intersystem crossing to the ground state k_{TS0}. The rate of intersystem crossing k_{TS0}, which is modulated by the physical state of the amorphous matrix, reflects both the manner in which the excited T_1 state is vibrational coupled to the S_0 ground state as well as the manner in which the ground state vibrational energy can dissipate from the excited probe into the surrounding matrix. Since the efficiency of this vibrational dissipation is related to the overall mobility of the matrix, k_{TS0} provides a direct measure of matrix mobility. Compared with sucrose, k_{TS0} in sucrose-starch decreased at high but increased at low starch content, indicating a more rigid matrix containing large amounts of starch but a less rigid matrix containing small amounts of starch.

In the sucrose-starch matrix two competing effects are considered: weakening of the structure due to an increased free volume with addition of a foreign macromolecule; and strengthening of the structure due to increased sucrose-starch and starch-starch interactions. Corn starch Hylon VII is rich in amylose, a linear polymer with the degree of polymerization (DP) between 100 and 10,000. Another polysaccharide amylopectin has a highly branched structure with molecular weight ranging from 10^6 to 10^9 g/mol

(Cui, 2006). When sucrose is added to water, the density of the solution increases and the free volume decreases compared to the pure water (Molinero et al., 2003). However, addition of starch macromolecules induces extra free volume into the amorphous sucrose matrix and leads to a weakened structure. In addition, the starch molecules in the amorphous films are expected to contain some void spaces that are free of inter- and intramolecular interactions due to steric hindrance. The hydroxyl groups of starch molecules thus have mobility to some extent. Small molecules like sucrose, more or less, would be integrated into these spaces and interact with the starch molecules. The strength of these interactions depends on the starch concentration.

In sucrose-starch matrix three interactions at RH 0% are taken into consideration. Sucrose-sucrose interaction is predominant in sucrose-starch matrix at very low starch contents. Sucrose-starch interaction increased with increasing starch content upon addition of starch molecules. Similar to other polysaccharides (Shamblin et al., 1996; Shamblin et al., 1998; Oliver et al., 1998; Imamura et al., 2002), addition of small amounts of starch had insignificant influence on the glass transition temperature T_g of sucrose, indicating that the sucrose-starch interaction is similar to the sucrose-sucrose interaction. When more starch molecules are added, starch-starch and starch-sucrose interactions increased and the former become predominant in the matrix. The increase in T_g at high starch levels suggested a contribution from a stronger starch-starch interactions. These interactions strengthen the structure of sucrose-starch matrix.

The total effect of adding very small amounts of starch (<0.005) seemed to increase the molecular mobility in amorphous sucrose matrix. The formed sucrose-starch interactions failed to compensate the reverse effects from the increased free volume and

from the motions of the hydroxyl and even hydroxymethyl groups in starch with fewer constraints. The sucrose-starch matrix showed higher flexibility although the T_g did not change apparently. For sucrose, the T_g is around 62°C; for sucrose-starch at ratios <0.005, the calculated T_gs are around 63°C.

When starch content increased (≥0.005), the sucrose-starch and starch-starch interactions increased and overweighed the opposite effect from the increased free volume. Sucrose was reported to strongly interact with starch molecules through G1, G6, F1 and F3 carbon atoms (Hansen et al., 1989). In addition, more starch molecules participated in forming starch-starch interactions. These interactions are much stronger than starch-sucrose interactions either due to the interaction nature or due to the high percentage of starch-starch interactions. The calculated T_g of starch-sucrose at ratio of 0.05 was around 68°C, suggesting the strengthened structure resulted from starch-starch interactions. The mobility transition temperature obtained from the intersection of the trendlines at high and low temperature in Arrhenius plots of k_{TS0} also reflected the similar phenomenon. The calculated transition temperatures was 76.5°C in sucrose, and 74.4, 74.7, 73.3, 83.0, 83.2, 84.4 and 83.7°C in the sucrose-starch mixtures with starch/sucrose ratio of 0.001, 0.0025, 0.005, 0.01, 0.025, 0.05 and 0.01, respectively. The significant increase in the emission energy and lifetime, decrease in the dipolar relaxation and collisional quenching rate, and increase in the transition temperature at high starch levels all strongly suggest that addition of starch stretched the glassy state range of sucrose, keeping the probe in a rigid environment over a wider temperature range.

The results showed a maximum effect at a ratio of 0.01 in the starch-sucrose matrix. Above that ratio, the starch seemed to have less influence on the molecular

mobility both in the melt and in the glass. At high starch content, the effect of the branched polymer amylopectin probably became important and should be considered in interpretation of the results. The steric hindrance from branched structures weakened both the starch-sucrose and the starch-starch interactions, resulting in a loosely packing matrix with less rigidity. In addition, the relatively increased mobility may be due to the complications of residual moisture. In comparison with sucrose and low-starch sucrose films with moisture less than 1%, high-starch sucrose films contained more water molecules (moisture >1%). Sucrose molecules preferably interact with water rather than starch and as a result a water plasticization effect occurred to increase the mobility.

3. Influence of starch on the dynamic site heterogeneity

Supercooled liquids and amorphous polymers are dynamically heterogeneous spatially as well as temporally as reported by a variety of spectroscopic techniques (Ediger, 2000; Richert, 2002). This physical model is supported by more evidence from erythrosin B phosphorescence. Spectral heterogeneity in Ery B phosphorescence is observed in amorphous sugars and sugar alcohols (Pravinata, et al., 2005; Shirke and Ludescher, 2005; Shirke et al., 2006), and proteins (Nack and Ludescher, 2006; Lukasik and Ludescher, 2006), indicating that the existence of dynamic site heterogeneity may be a characteristic feature of amorphous food materials and biomaterials.

The variation of lifetime with emission energy reflects variation in one or more of the rate constants for deexcitation of the triplet state. In amorphous sucrose matrix, the population of probes is distributed among dynamically distinct sites with varied emission energy and matrix quenching rate (Pravinata et al., 2005). Pravinata et al. proposed a physical model for the origin of this site heterogeneity on the basis of emission energy

and matrix quenching rate; that is, probes in local environments with less constrained packing have higher overall molecular mobility and thus shorter lifetime and have lower emission energy due to fast dipolar relaxations. When sucrose is mixed with starch, whether starch will change the local environments and further influence the site heterogeneity becomes one of our interests.

In comparison with sucrose, variations in erythrosin B lifetime at 25°C with emission wavelength were similar in sucrose films containing starch at ratios smaller than 0.005 but were larger at ratio of 0.005 and above (Figure 87a), indicating an insignificant influence at low starch content but a decreased ability within the sites to dynamically average out spectroscopic differences at higher starch content. The variations in collisional quenching rate constant k_{TS0} with emission wavelength (Figure 88) showed similar results, suggesting an increased heterogeneity in sucrose films with addition of high starch content. Variations in exponent of β (Figure 87b) were almost the same in sucrose as well as sucrose films containing starch at low ratios. At high content, the increased variations with emission and excitation wavelength showed the evidence of increased heterogeneity.

The temperature-dependence of the stretching exponent β (Figure 84b) shows that the values of β in the glassy sucrose-starch films were slightly larger at low but smaller at high starch contents, suggesting that small amounts of starch decreased the matrix heterogeneity while large amounts of starch increased heterogeneity in the glassy state. The starch effect on spectroscopic heterogeneity was sensitive to temperature. At high temperature, the presence of starch reduced heterogeneity at high but increased heterogeneity at low starch content.

The emission bandwidth (Γ, FWHM) insignificantly decreased with addition of starch (Figure 80b), indicating a possible, corresponding decrease in the width of the distribution of energetically distinct matrix environments both in the glass and in the melt. However at high starch/sucrose ratio, the bandwidth increased slightly at high temperature.

All spectroscopic characteristics seemed to show that addition of a small amount of starch did not change or slightly decreased the dynamic heterogeneity while a large amount of starch increased the heterogeneity in amorphous sucrose.

Amorphous sucrose is considered structurally heterogeneous and consists of sucrose clusters (Molinero et al., 2003). Sucrose glass is also reported to have dynamically distinct sites with varied emission energy and matrix quenching rate (Pravinata et al., 2005). Addition of the macromolecule starch was expected to increase the heterogeneity indicated by a decrease in β as well as an increase in variation of β and lifetime. However the larger value of β and smaller variation in both β and lifetime at low starch content was unexpected in the binary starch-sucrose mixtures. Poirier-Brulez et al. (2006) found similar results when they investigated the sucrose effect on mobility in starch-based glasses. The relaxation time distribution indicator β was larger in starch glass mixed with sucrose (0.56) than in pure starch (0.31) or in pure sucrose (0.32, reported by Urbani et al., 1997; or 0.51, reported by Hancock et al., 1995). They proposed that the larger value was probably a sign of an asymmetric distribution dominated by short times through a narrow peak over a wide basis at larger relaxation time values. This was possibly the same in our work.

4. Starch change T_g of sucrose?

As mentioned above in the discussion of starch effect on the molecular mobility in amorphous sucrose, addition of starch did not significantly change the T_g of sucrose matrix in the studied concentration range. In the present work, we estimated the T_gs of the starch-sucrose mixtures using an extension of the Couchman & Karasz equation (1978):

$$T_g = \frac{\sum_i w_i \Delta C_{p_i} T_{gi}}{\sum_i w_i \Delta C_{p_i}} \quad (9)$$

where W_i, ΔC_{pi} and T_{gi} refer to the weight fraction, the change in specific heat capacity and the glass transition temperature of individual components. T_g and ΔC_p for sucrose are 62°C and 0.6 J/g °C, respectively (Roos, 1995). For Hylon VII corn starch, T_g and ΔC_p are estimated based on its composition (71% amylose). The T_gs of amylose and amylopectin are generally obtained by extrapolating the plot of T_g versus water content. However calorimetric glass transition of amylose and amylopectin are not easy to detect because of the similar polymer behaviors. The values varied from 200°C for potato amylose (Partanen et al., 2004) to 332°C for pea amylose (Bizot et al., 1997). Amylopectin was reported to have a depressed T_g value of 285°C due to the branching effect (Bizot et al., 1997). ΔC_p was reported as 0.265 J/g °C for dry pea amylose (Bizot et al., 1997) and 0.54 J/g °C for potato amylose film (Partanen et al., 2004). Despite the variance in the values of T_g and ΔC_p, the calculated T_gs of starch-sucrose mixtures are not significantly influenced due to the very low starch contents. The estimated T_g for starch-sucrose mixture at ratio less than 0.025 varied between 62-63°C compared with 62°C for pure sucrose. At ratio of 0.1, the T_g value increased up to 68°C. This suggested that starch affects the sucrose matrix not only through influencing the glass transition

temperature, but also through changing the interactions and thus the molecular mobility in amorphous sucrose solids.

Conclusion

Molecular mobility can be modulated by the composition of amorphous solid (such as polymers) and its environment (temperature). Phosphorescence of erythrosin B can report a detailed mobility map within amorphous sucrose film doped with starch ranging from 0.001 to 0.1 (g starch/g sucrose). Based on the emission energy and lifetime of erythrosin B in sucrose and sucrose-starch films over the temperature range from 5°C to 100°C, we came to the conclusion that starch exerts different effects on amorphous sucrose, depending on the starch content. At starch/sucrose weight ratio below 0.005, both emission energy and lifetime decreased and dipolar relaxation rate $1/\varphi$ and collisional quenching rate k_{TS0} increased, indicating a destabilization effect. At ratio above 0.005, starch exerts a stabilization effect indicated by an increase in emission energy and lifetime, and a decrease in the mobility both in the glass and in the melt. The mobility showed a maximum value at the starch/sucrose ratio of 0.01. The interactions existing in the sucrose-starch matrix are considered as a determining factor to influence the molecular mobility of sucrose-starch mixtures. The interactions vary with starch content, leading to different influence on mobility map of sucrose matrix. It is worthy of mapping out the relationship between the starch concentration and the characteristics of the matrix since the matrix properties have implications for the processing and subsequent storage stability of biological materials and foods.

Dynamic site heterogeneities above and below the glass transition temperature may be a characteristic feature of amorphous food materials and biomaterials (Ediger, 2000; Richert, 2002), a conclusion which has been supported by a series of techniques. Direct evidence is provided by Ery B phosphorescence in amorphous sucrose-starch films. Addition of starch influences the dynamic heterogeneity of amorphous sucrose matrix and this effect is dependent on the starch content and temperature. Our data indicate that there are sites of different mobility within amorphous solid sucrose and an increased dynamic heterogeneity is seen in the presence of macromolecules such as starch at ratio above 0.05. However, the dynamic heterogeneity does not change or is slightly decreased by adding small amounts of starch.

References:

Allison, S.D., Manning, M.C., Randolph, T.W., Middleton, K., Davis, A., and Carpenter, J.F. 2000. Optimization of storage stability of lyophilized actin using combinations of disaccharides and dextran. *J. Pharm. Sci*. 89, 199-214.

Benczedi, D., Tomka, L., and Escher, F. 1998. Thermodynamics of amorphous starch-water systems. 1. Volume fluctuations. *Macromol.* 31, 3055-3061.

Bizot, H., Le Bail, P., Leroux, B., Davy, J., Roger, P., and Buleon, A. 1997. Calorimetric evaluation of the glass transition in hydrated, linear and branched polyanhydroglucose compounds. *Carbohydr. Polym.* 32, 33-50.

Carpenter, J.F., Prestrelski, S.J., and Arakawa, T. 1993. Separation of freezing- and drying-induced denaturation of lyophilized proteins using stress-specific stabilization. I. Enzyme activity and calorimetric studies. *Arch Biochem Biophys.* 303, 456-464.

Carpenter, J.F., and Crowe, J.H. 1989. An infrared spectroscopic study of the interactions of carbohydrates with dried proteins. *Biochem.* 28, 3916-3922.

Chang, L., Shepherd, D., Sun, J., Ouellette, D., Grant, K.L., Tang, X., and Pikal, M.J. 2005. Mechanisms of protein stabilization by sugars during freeze-drying and storage: native structure preservation, specific interaction, and/or immobilization in a glassy matrix? *J. Pharm. Sci.* 94(7), 1427-1444.

Cheetham, N.W.H., and Tao, L. 1997. Amylose conformational transitions in binary DMSO/water mixtures. *Starch/Staerke.* 49(10), 407-415.

Couchman, P.R., and Karasz, F.E. 1978. A classical thermodynamic discussion of the effect of composition on glass-transition temperatures. *Macromol.* 11(1), 117-119.

Crowe, J.H., Crowe, L.M., and Carpenter, J.F. 1993. Preserving dry biomaterials: the water replacement hypothesis. Part 1. *BioPharm.* 6, 28-29, 32-33.

Cui, S.W. 2005. *Food carbohydrates*: chemistry, physical properties, and applications. Taylor & Francis, New York.

Dintzis, F.R., and Tobin, R. 1969. Optical rotation of some α-1,4-linked glucopyranosides in the system H2O-DMSO and solution conformation of amylose. *Biopolym.* 7(4), 581-593.

Duchowicz, R., Ferrer, M.L. and Acuna, A.U. 1998. Kinetic spectroscopy of erythrosin phosphorescence and delayed fluorescence in aqueous solution at room temperature. *Photochem. Photobiol.* 68, 494-501.

Ediger, M.D. 2000. Spatially heterogenous dynamics in supercooled liquids. *Annu. Rev. Phys. Chem.* 51, 99-128.

Ebert, B. and Elmgren, H. 1984. Helical conformation of amylose in aqueous solution. II. Electron spin resonance, fluorescence depolarization, and sedimentation measurements. *Biopolym.* 23(11, Pt. 2), 2543-2557.

Elmgren, H. 1987. The concentration dependence of the sedimentation rate of amylose, cellulose, and dextran in aqueous solution. *Carbohydr. Res.* 160, 227-241.

Eliasson, A. 2006. *Carbohydrates in food*; 2nd Edition. Taylor & Francis, New York

Fennema, O. 1996. Water and Ice. In *Food Chemistry*, 3rd Edition. Marcel Dekker, Inc. N.Y.

Franks, F., Hatley, R.H.M., and Mathias, S.F. 1991. Materials science and the production of shelf-stable biologicals. *BioPharm.* 4, 38, 40-42, 55.

Gaudin, S., Lourdin, D., Le Botlan, D., Ilari, J.L., and Colonna, P. 1999. Plasticization and mobility in starch-sorbitol films. *J. Cereal Sci.* 29, 273-284.

Hancock, B.C., Shamblin, S.L., and Zografi, G. 1995. Molecular mobility of amorphous pharmaceutical solids below their glass transition temperatures. *Pharm. Res.* 12(6), 799-806.

Hansen, L.M., Sester, C.S., and Paukstelis, J.V. 1989. Investigation of sugar-starch interactions using carbon-13 nuclear magnetic resonance. I. Sucrose. *Cereal Chem.* 66, 411-415.

Hayashi, A., Kinoshita, K., and Miyake, Y. 1981. Conformation of amylose in solution. *Polym. J.* (Tokyo, Japan) 13(6), 537-541.

Hayashi, A., Kinoshita, K., and Kotani, Y. 1983. Phase changes in amylose-butanol complex solution. *Agric. Biol. Chem.* 47 (8), 1705-1709.

Imamura, K., Fukushima, A., Sakaura, K., Sugita, T., Sakiyama, T., and Nakanishi, K. 2002. Water sorption and glass transition behaviors of freeze-dried sucrose-dextran mixtures. *J. Pharm. Sci.* 91, 2175-2181.

Jiang, J.K., Lee, S.H., Cho, S.C., and Pyun, Y.R. 2001. Effect of sucrose on glass transition, gelatinization, and retrogradation of wheat starch. *Cereal chem.* 78(2), 186-192.

Kets, E.P.W., IJpelaar, P.J., Hoekstra, F.A., and Vromans, H. 2004. Citrate increases glass transition temperature of vitrified sucrose preparations. *Cryobiology*. 48, 46-54.

Kohyama, K. and Nishinari, K. 1991. Effect of soluble sugars on gelatinization and retrogradation of sweet potato starch. *J. Agric. Food Chem.* 39, 1406-1410.

Lakowicz, J.R. 1999. *Principles of fluorescence spectroscopy*. Plenum Press, NY

Le Botlan, D. and Desbois, P. 1995. Starch retrogradation study in presence of sucrose by low-resolution nuclear magnetic resonance. *Cereal Chem.* 72(20), 191-193.

Lee, K.C.B., Siegel, J., Webb, S.E.D., Leveque-Fort, S., Cole, M.J., Jones, R., Dowling, K., Lever, M.J., and French, P.M.W. 2001. Application of the stretched exponential function to fluorescence lifetime imaging. *Biophys. J.* 81, 1265-1274.

Lourdin, D., Bizot, H., and Colonna, P. 1997. Antiplasticization in starch-glycerol films? *J. Appl. Polym. Sci.* 63, 1047-1053.

Lourdin, D., Ring, S.G., and Colonna, P. 1998. Study of plasticizer-oligomer and plasticizer-polymer interactions by dielectric analysis: maltose-glycerol and amylose-glycerol-water systems. *Carbohydr. Res.* 306, 551-558.

Lourdin, D., Colonna, P., and Ring, S.G. 2003. Volumetric behavior of maltose-water, maltose-glycerol, and starch-sorbitol-water systems mixtures in relation to structural relaxation. *Carbohydr. Res*. 338, 2883-2887.

Lukasik, K.V. and Ludescher, R.D. 2006. Effect of plasticizer on dynamic site heterogeneity in cold-cast gelatin films. *Food Hydrocoll.* 20, 88-95.

Maroncelli, M., and Fleming, G.R. 1987. Picosecond solvation dynamics of coumarin 153: the importance of molecular aspects of solvation. *J. Chem. Phys*. 86, 6221-6239.

Molinero, V., Cagin, T., and Goddard III, W.A. 2003. Sugar, water and free volume networks in concentrated sucrose solutions. *Chem. Phys. Lett.* 377, 469-474.

Myllarinen, P., Partanen, R., Seppala, J., and Forssell, P. 2002. Effect of glycerol on behaviour of amylose and amylopectin films. *Carbohydr. Polym.* 50, 355-361.

Myllarinen, P., Buleon, A., Lahtinen, R., and Forssell, P. 2002. The crystallinity of amylose and amylopectin films. *Carbohydr. Polym.* 48, 41-48.

Nack, T.J, and Ludescher, R.D. 2006. Molecular mobility and oxygen permeability in amorphous bovine serum albumin films. *Food Biophys.* 1, 151-162.

Norisuye, T. 1994. Viscosity behavior and conformation of amylose in various solvents. *Polymer J.* (Tokyo, Japan) 26(11), 1303-1307.

Norisuye, T. 1996. Conformation and properties of amylose in dilute solution. *Food Hydrocoll.* 10(1), 109-115.

Oliver, A.E., Crowe, L.M., and Crowe, J.H. 1998. Methods for dehydration-tolerance: Depression of the glass transition temperature in dry membranes and carbohydrate vitrification. *Seed Sci. Res*. 8, 211-221.

Papp, S. and Vanderkooi, J.M. 1989. Tryptophan phosphorescence at room temperature as a tool to study protein structure and dynamics. *Photochem. Photobiol.* 49, 775-784.

Parker, C.A. 1968. *Photoluminescence of Solutions.* Elsevier, Amsterdam.Netherlands.

Partanen, R., Marie, V., MacNaughtan, W., Forssell, P., and Farhat, I. 2004. ^{1}H NMR study of amylose films plasticized by glycerol and water. *Carbohydr. Polym.* 56, 147-155.

Pfannemueller, B., Mayerhoefer, H., and Schulz, R.C. 1971. Conformation of amylose in aqueous solution: optical rotatory dispersion and circular dichroism of amylose-iodine complexes and dependence on chain length of retrogradation of amylose. *Biopolym.* 10(2), 243-261.

Poirier-Brulez, F., Roudaut, G., Champion, D., Tanguy, M., and Simatos, D. 2006. Influence of sucrose and water content on molecular mobility in starch-based glasses as assessed through structure and secondary relaxation. *Biopolym.* 81, 63-73.

Pravinata, L.C., You, Y. and Ludescher, R.D. 2005. Erythrosin B phosphorescence monitors molecularmobility and dynamic site heterogeneity in amorphous sucrose. *Biophys. J.* 88(May), 3551-3561.

Rao, V.S.R. and Foster, J.F. 1963. The conformation of amylose in solution. *Biopolym.* 1(6), 527-544.

Richert, R. 2000. Triplet state salvation dynamics: basics and applications. *J. Chem. Phys.* 113, 8404-8429.

Richert, R. 2002. Heterogeneous dynamics in liquids: fluctuations in space and time. *J. Phys. Condens. Matter.* 14, R738-R803.

Roos, Y. 1995. *Phase Transitions in Foods*. Academic Press, San Diego, CA.

Shamblin, S.L., Huang, E.Y., and Zografi, G. 1996. The effects of co-lyophilized polymeric additives on the glass transition temperature and crystallization of amorphous sucrose. *J. Thermal. Anal. Cal.* 47 (5), 1567-1579.

Shamblin, S.L., Taylor, L.S., and Zografi, G. 1998. Mixing behavior of co-lyophilized binary systems. *J. Pharm. Sci.* 87, 694-701.

Shimada, J., Kaneko, H., Takada, T., Kitamura, S., and Kajiwara, K. 2000. Conformation of amylose in aqueous solutions: small-angle X-ray scattering measurements and simulations. *J. Phys. Chem. B* 104, 2136-2147.

Shirke, S., and Ludescher, R.D. 2005. Dynamic site heterogeneity in amorphous maltose and maltitol from spectral heterogeneity in erythrosin B phosphorescence. *Carbohydr. Res.* 340, 2661-2669.

Shirke, S., Takhistov, P., and Ludescher, R.D. 2005. Molecular mobility in amorphous maltose and maltitol from phosphorescence of erythrosin B. *J. Phys. Chem. B.* 109, 16119-16126.

Shirke, S., You, Y., and Ludescher, R.D. 2006. Molecular mobility and dynamic site heterogeneity in amorphous lactose and lactitol from erythrosin B phosphorescence. *Biophys. Chem.* 123, 122-133.

Slade, L., and Levine, H. 1991. Beyond water activity: recent advances based on an alternative approach to the assessment of food quality and safety. *Crit. Rev. Food Sci. Nutr.* 30, 115-360.

Sugiyama, H., Nitta, T., Horii, M., Motohashi, K., Sakai, J., Usui, T., Hisamichi, K., and Ishiyama, J. 2000. The conformation of α-(1→4)-linked glucose oligomers from maltose to maltoheptaose and short-chain amylose in solution. *Carbohydr. Res.* 325, 177-182.

Urbani, R., Sussich, F., Prejac, S., and Cesaro, A. 1997. Enthalpy relaxation and glass transition behaviour of sucrose by static and dynamic DSC. *Thermochim Acta.* 304-305, 359-367.

You, Y., and Ludescher, R.D. 2006. Phosphorescence of erythrosin B as a robust probe of molecular mobility in amorphous solid sucrose. *Appl. Spectrosc.* 60, 813-819.

Zallen, R. 1983. *The physics of amorphous solids*; John Wiley & Sons: New York.

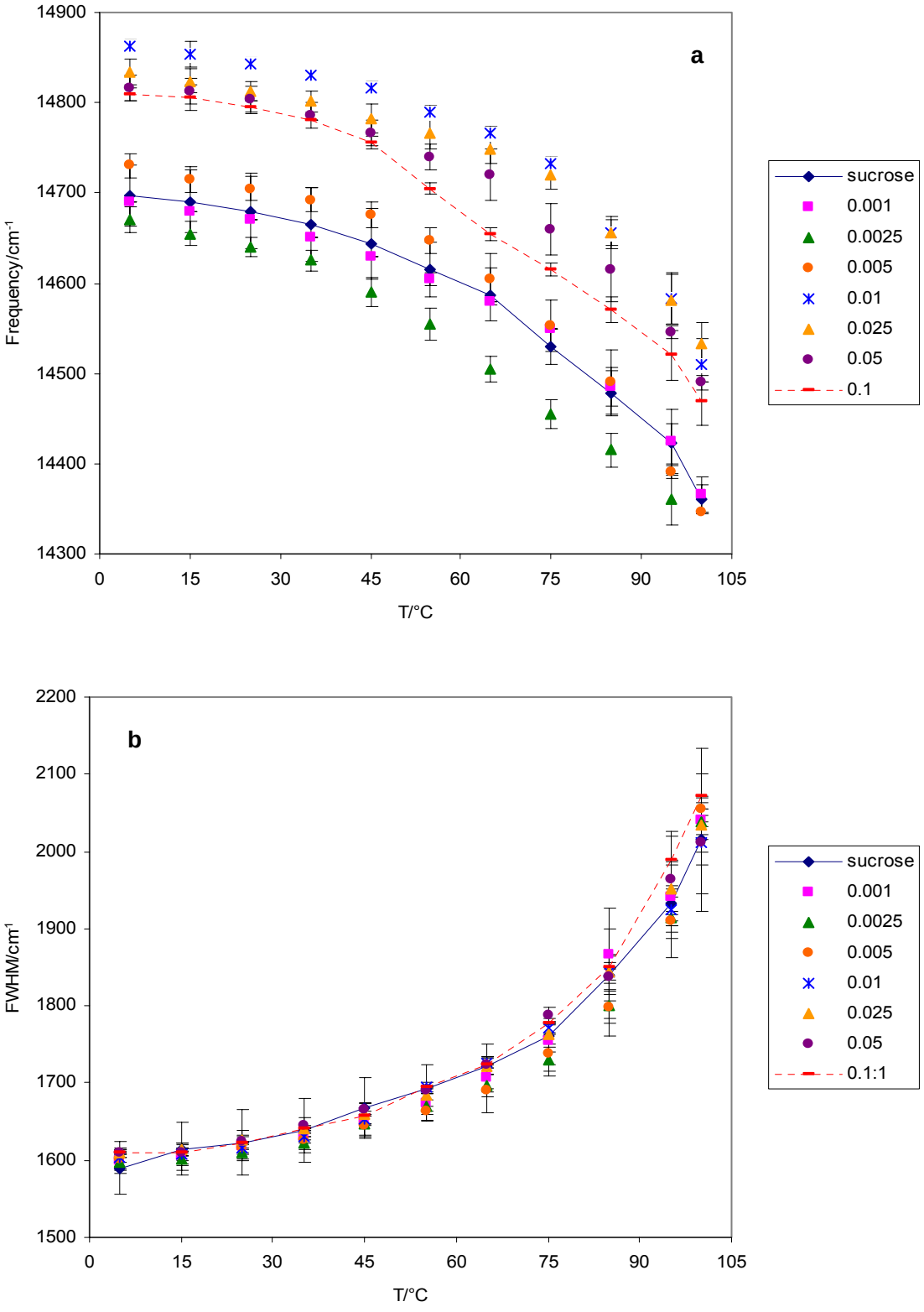

Figure 80: (a) Peak frequency (ν_p) and (b) bandwidth (full width at half maximum, FWHM) for phosphorescence emission from erythrosin B in amorphous sucrose-starch films plotted as a function of temperature. Delayed emission spectra collected as a function of temperature were analyzed using log-normal line shape function.

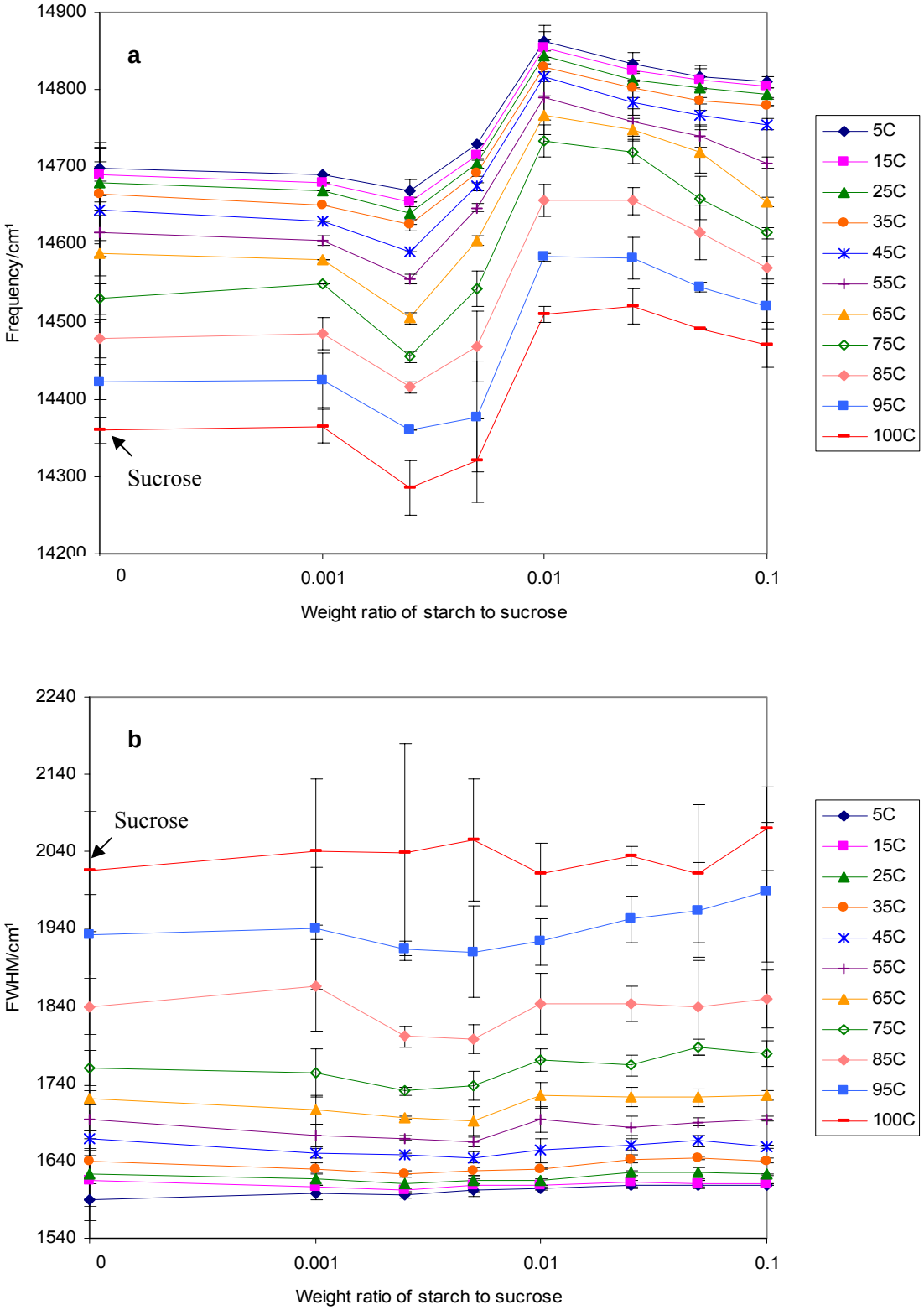

Figure 81: (a) Peak frequency (ν_p) and (b) bandwidth (full width at half maximum, FWHM) for phosphorescence emission from erythrosin B in amorphous sucrose-starch films as a function of weight ratio of starch/sucrose. Delayed emission spectra collected as a function of temperature were analyzed using log-normal line shape function.

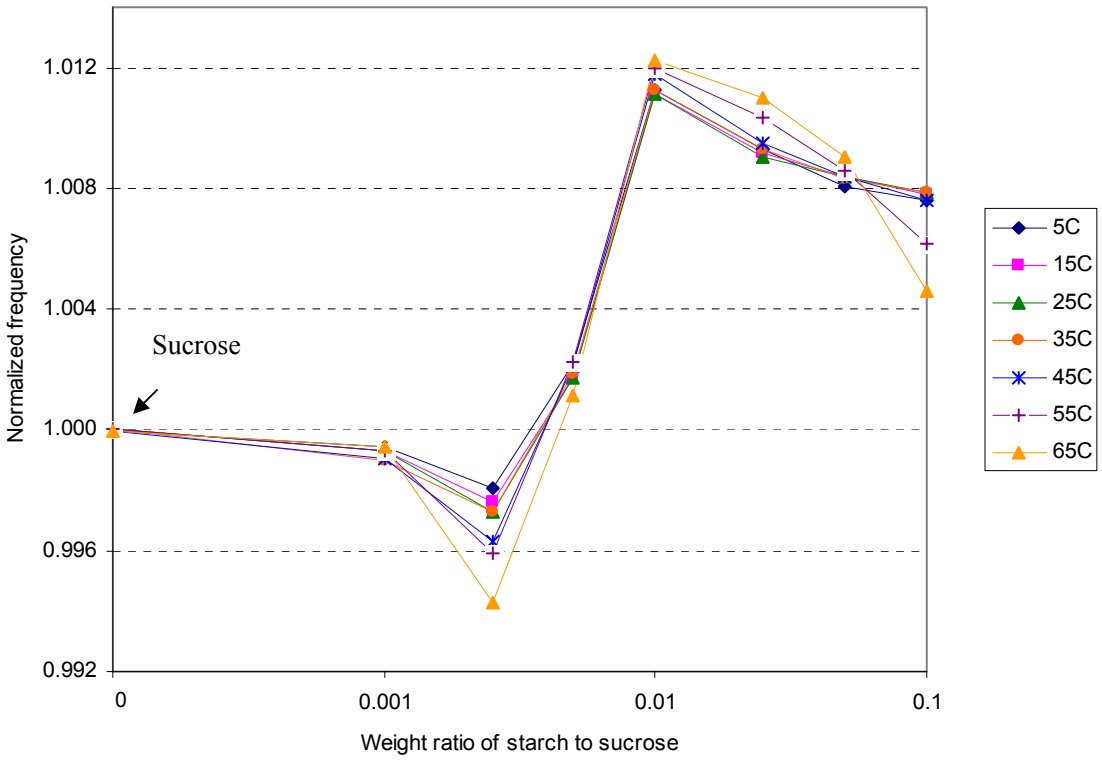

Figure 82: Peak frequency normalized at each temperature to the value in pure sucrose, for erythrosin B phosphorescence in amorphous sucrose-starch films plotted as a function of weight ratio of starch/sucrose. Delayed emission spectra collected as a function of temperature were analyzed using a log-normal line shape function.

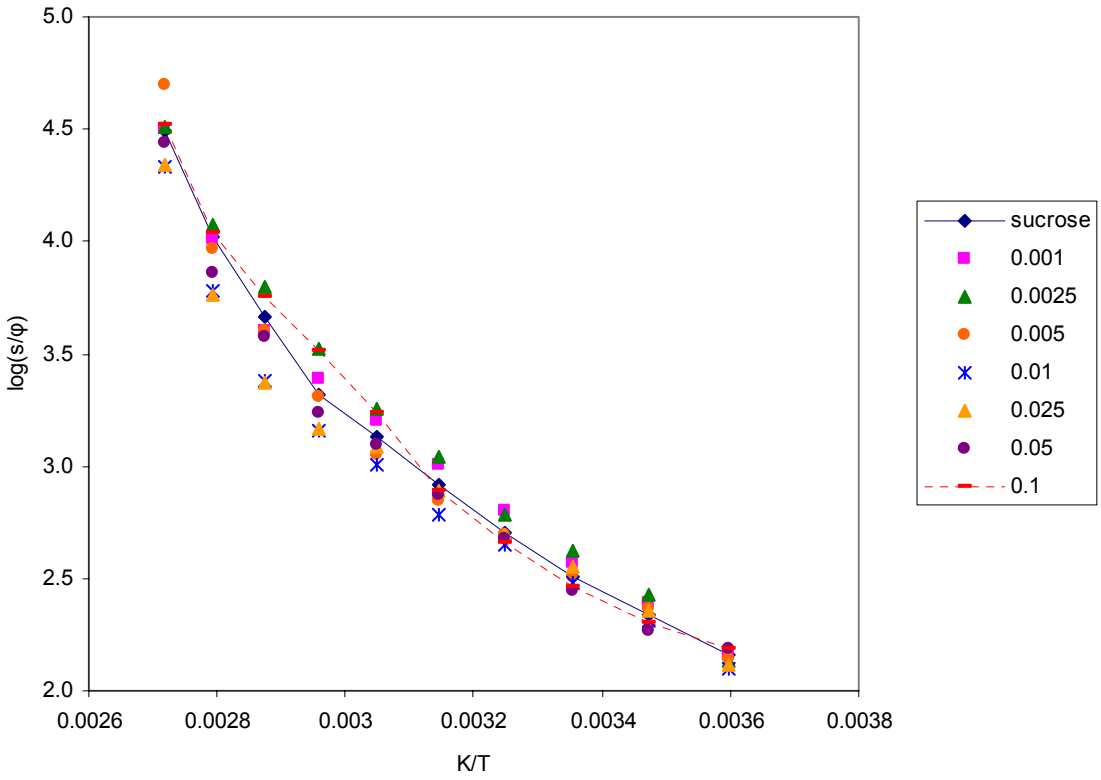

Figure 83: Arrhenius plot of the effect of temperature on the rate of matrix dipolar relaxation around the excited erythrosin B triplet state in sucrose films at various starch content.

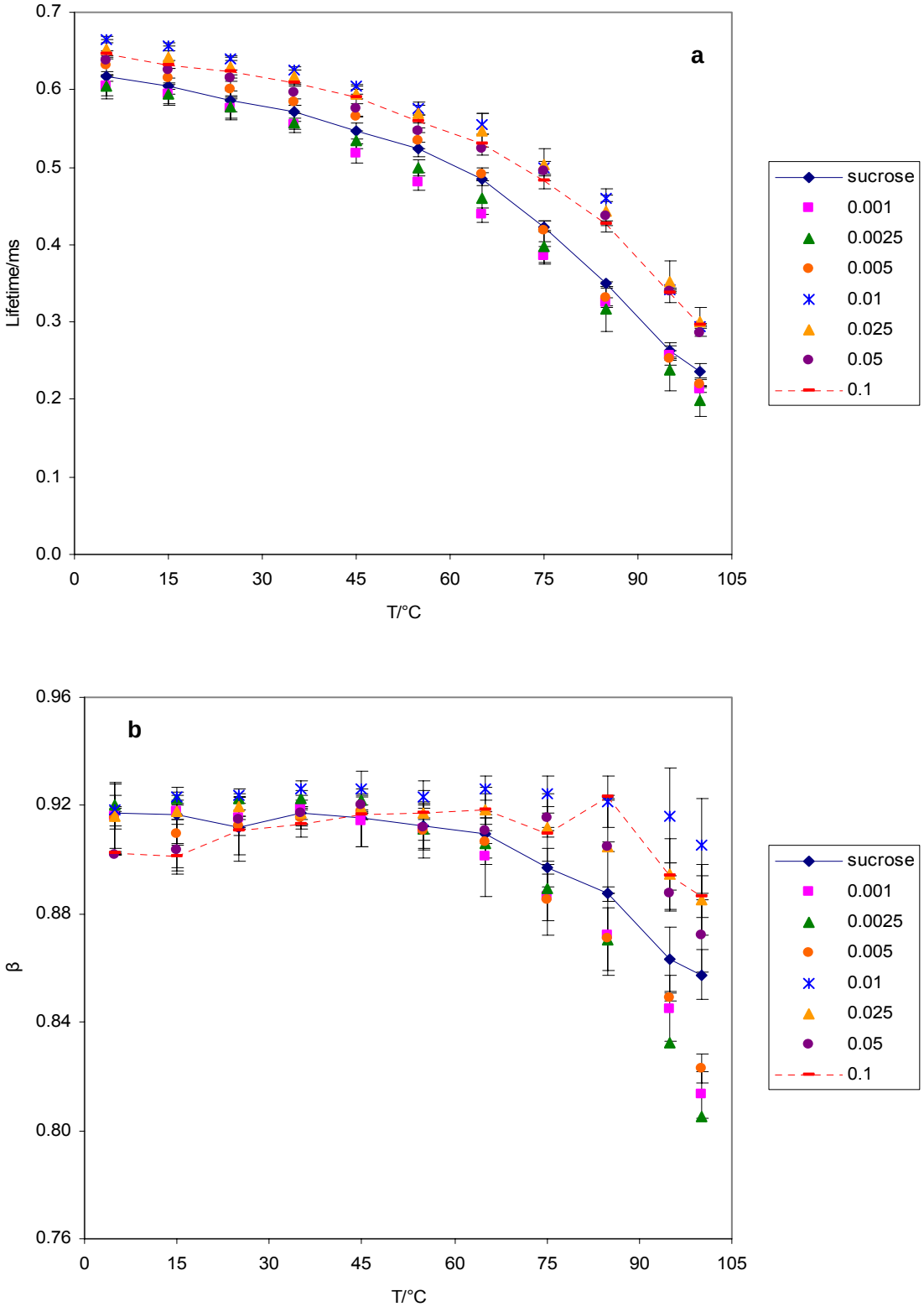

Figure 84: Temperature dependence of (a) lifetime and (b) stretching exponent β obtained from fits to a stretched exponential decay model of the intensity decay of erythrosin B in amorphous sucrose films with various starch/sucrose weight ratios.

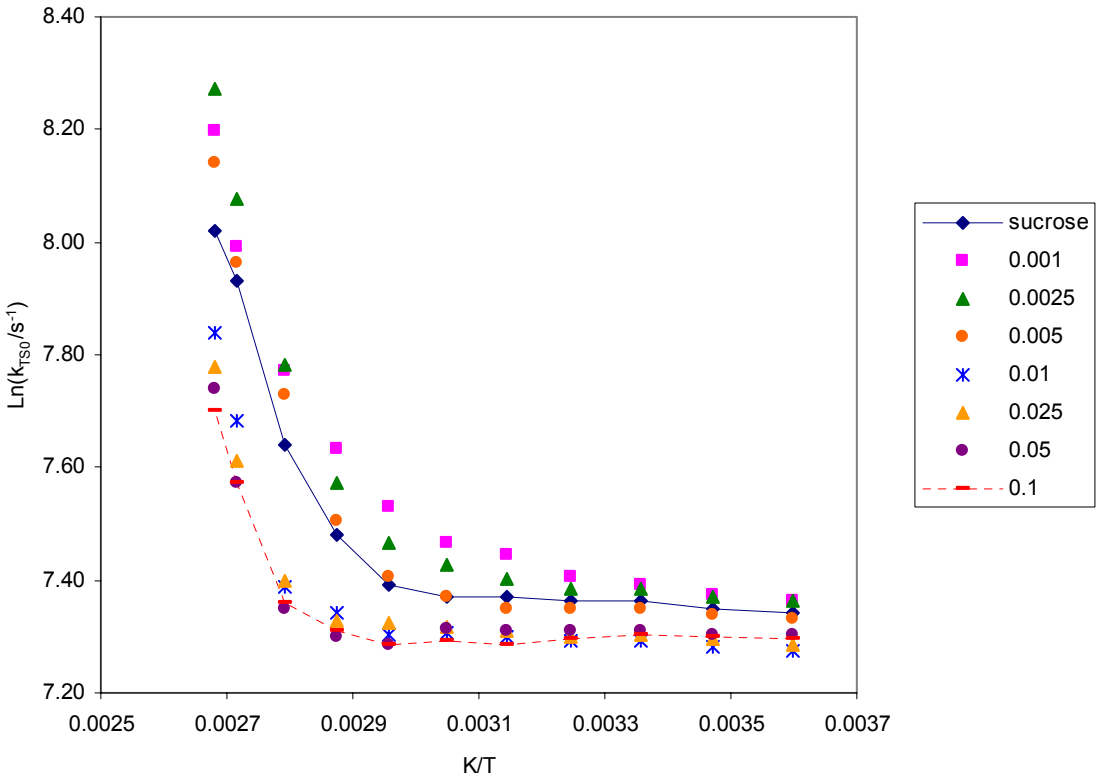

Figure 85: Arrhenius plot of the temperature effect on the rate constant for non-radiative decay of the triplet T_1 state to S_0 (k_{TS0}), data calculated from the lifetime data of Figure 5a; see text for additional details. Erythrosin B in amorphous sucrose films with various starch/sucrose weight ratios.

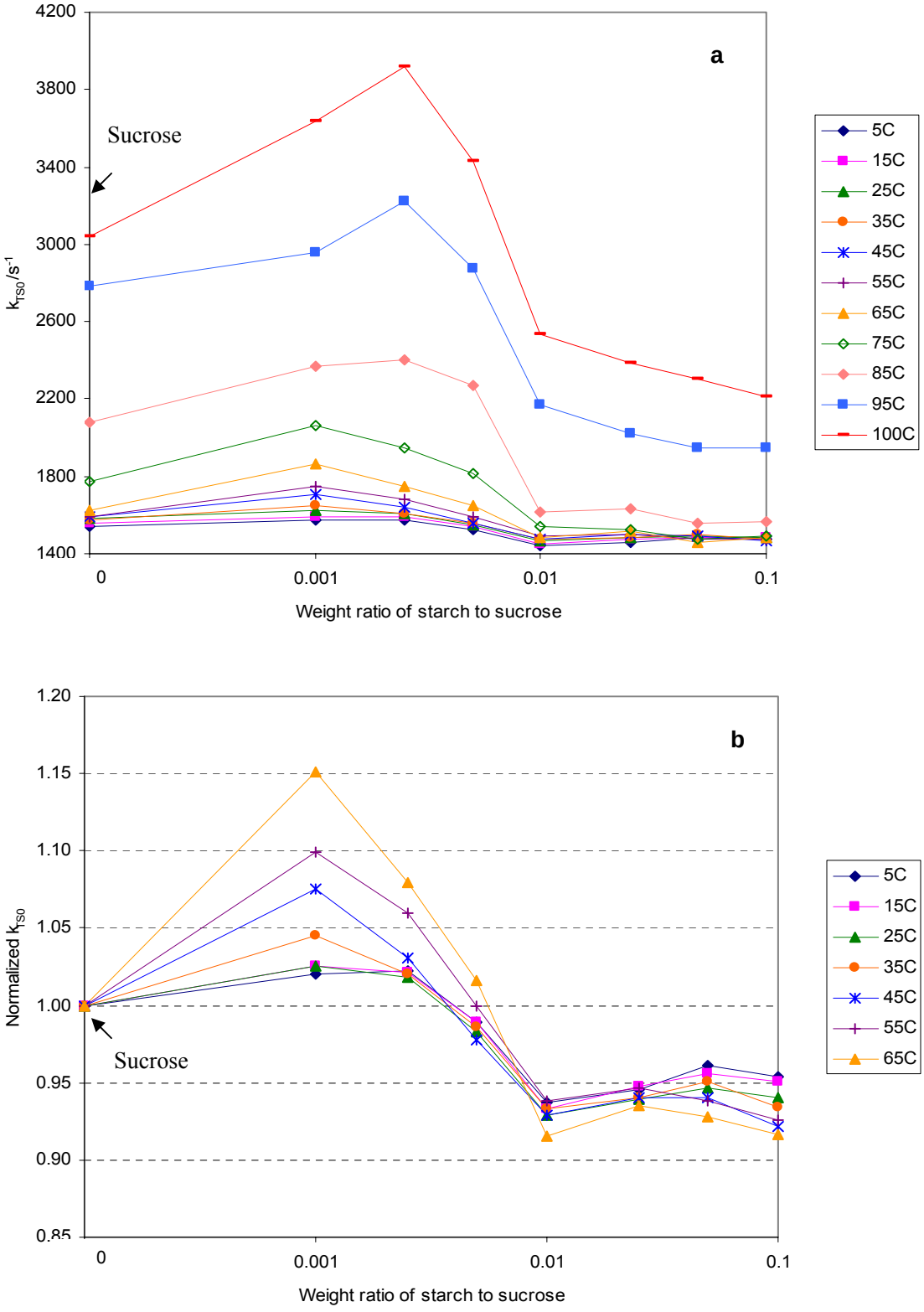

Figure 86: (a) The effect of starch on the rate constant for non-radiative decay of the triplet state to S_0 (k_{TS0}); data of Figure 6 were replotted as k_{TS0} versus starch/sucrose weight ratio. (b) Normalized rate constant for non-radiative decay of the triplet state to S_0 (k_{TS0}) as a function of starch/sucrose weight ratio at low starch contents.

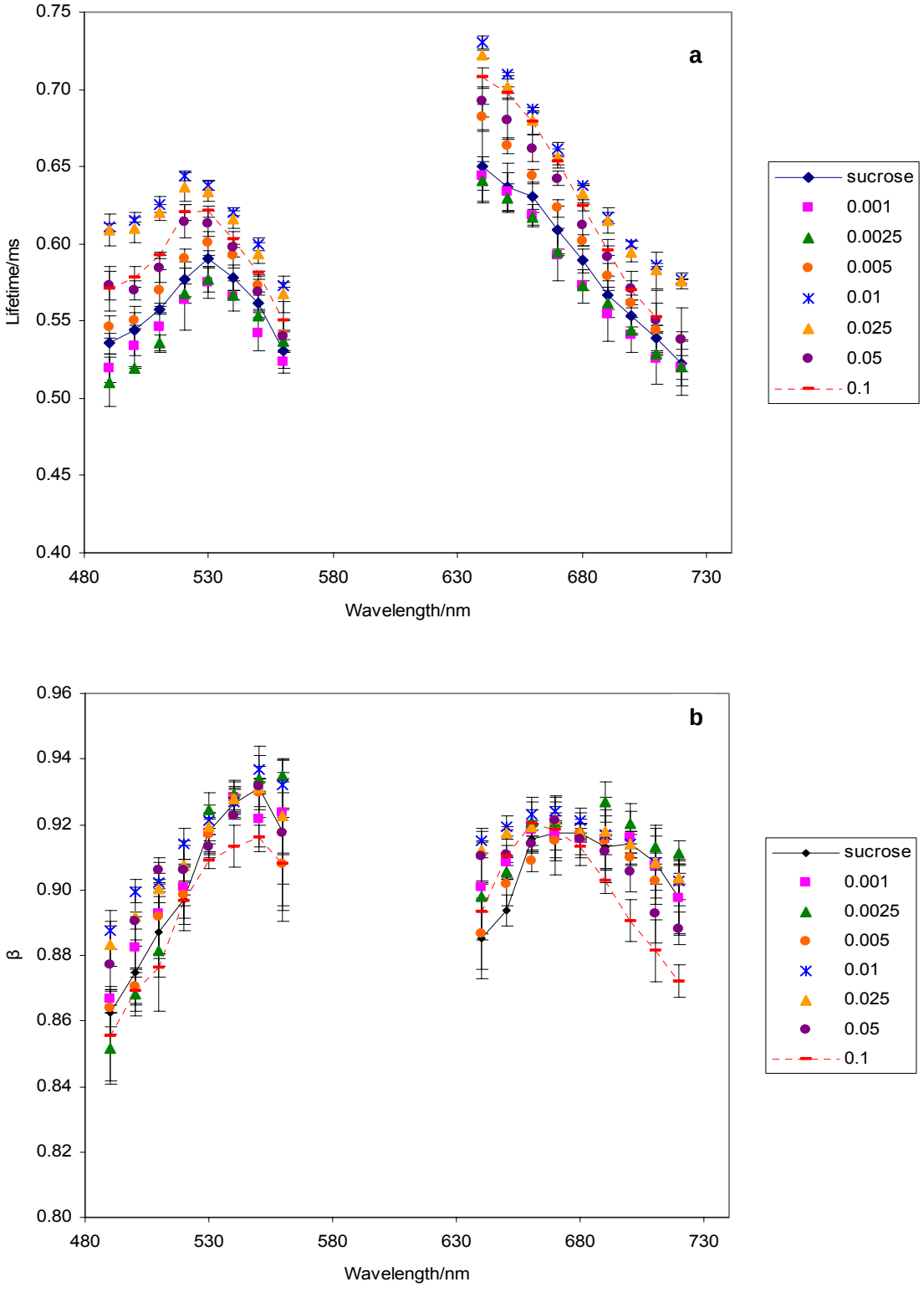

Figure 87: The effect of excitation wavelength (with 680 nm emission) and emission wavelength (with 530 nm excitation) on the lifetimes (a) and stretching exponents β (b) from fits of erythrosin B phosphorescence intensity decays to the stretched exponential decay model. Data collected in sucrose films with starch/sucrose weight ratio from 0 to 0.1 at 25°C.

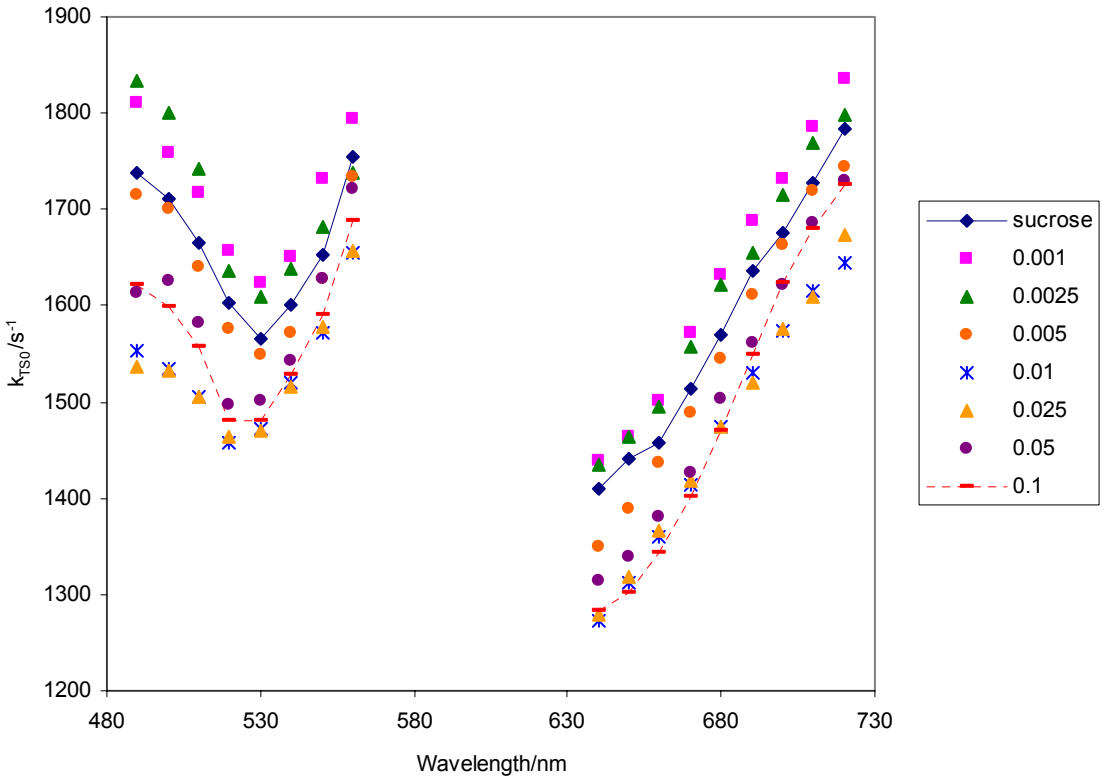

Figure 88: The rate constant for non-radiative decay of the triplet state to S_0 (k_{TS0}) plotted as a function of excitation wavelength (with 680 nm emission) and emission wavelength (with 530 nm excitation). Data collected from erythrosin B in sucrose films with starch/sucrose weight ratio from 0 to 0.1at 25°C.

Chapter 9 Xanthan effect on molecular mobility of amorphous sucrose from erythrosin B phosphorescence

Introduction

Sucrose glasses have been an object of research for many years since it was found to be one of the earliest cryoprotective agents during anhydrobiosis. Its ability to protect biomaterials from freeze-thaw damage and provide long-term storage stability has attracted researchers to investigate the mechanism and develop solid state formulations through drying or freeze-drying for labile compounds in foods, such as vitamins and flavor compounds, and for labile biomolecules in pharmaceuticals, such as enzymes, proteins, and antibodies.

Two main mechanisms, glass dynamics and specific interaction, are proposed to understand the role of sucrose in stabilization of sensitive compounds during dehydration and storage (Kets et al., 2004; Chang et al., 2005). The glass dynamics mechanism (Franks et al., 1991; Slade and Levine, 1991) focuses on the rigid, inert matrix formed by vitrification (glass formation) of stabilizers such as sugars. By forming into amorphous, non-crystalline solids upon rapid drying from aqueous solution or cooling from the melt, sugars change from soft, pliable and flexible at high temperature to hard, brittle and rigid at low temperature with an extreme increase in viscosity due to the decrease in the rate of translational as well as rotational and vibrational mobility motions (Zallen, 1983). Therefore glass formation is a purely kinetic mechanism, and stability is expected to correlate to molecular mobility in the rigid matrix. The specific interaction mechanism (Carpenter and Crowe, 1989; Carpenter et al., 1993; Crowe et al., 1993), commonly

applied in protein stabilization, states that stabilizers form hydrogen bonds at specific sites with the target compounds, which helps maintain the native structure, keep the spatial integrity of the compound after water is removed, and consequently enhance the stability. Sucrose is an ideal matrix material since it is a good glass former as well as a good hydrogen bond former. For better functionalities, formulation design tends to choose sucrose glasses mixed with other compounds, including small molecules such as salts and macromolecules such as hydrocolloids.

In food and pharmaceutical industries, the high solids formulations have been developed in low moisture systems to govern the molecular mobility that is associated with the macroscopic properties of the materials. Molecular mobility within amorphous solids is usually manifested by relaxation processes. The amorphous solids exhibit the primary α or glass transition at T_g which reflects the activation of large-scale molecular motions (α-relaxations) that underlie the onset of translational and rotational motions and the secondary β transition within the glass at T_β which reflects the activation of localized molecular motions (β-relaxations) linked to vibrational motion and local side-chain motion. The temperature-dependent molecular mobility thus controls physical and chemical properties by modulating the nature and kinetics of reactions that occur during processing and storage of biomaterials. Hydrocolloids are normally selected to stabilize the formulations due to their tremendously high viscosities in the solutions or T_gs far above room temperature in the solid state.

Hydrocolloids, an important class of food ingredients, comprise a wide range of proteins and polysaccharides. They are used in aqueous solutions as thickners and

gelling agents, in foam emulsions and dispersions as stabilizers, in low-molecular-weight carbohydrates and frozen foods as crystallization inhibitors, and in encapsulated systems as controlled releasing agents. Polysaccharides are in particular a unique group in providing desirable rheological and/or organoleptic properties in food and pharmaceutical products at a low level of approximately 1 wt% (Ptaszek et al., 2007).

Polysaccharides can be classified as gelling polysaccharides such as pectin, gellan, and carrageenan, and non-gelling polysaccharides such as agarose and locust bean gum. Kasapis et al. (2004) reported that the formed three-dimensional structure in the presence of gelling polysaccharides resulted in different values of the glass transition temperature T_g. The rheologically measured T_g values were lower than those calorimetrically determined. Addition of non-gelling polysaccharides, however, showed no significant difference between rheology and calorimetry. To avoid this complication a non-gelling polysaccharide was selected in the present work. The outcome would be expected to shed light on the relationship between the nature of biopolymers (macromolecules) and stabilization of vitrified systems.

So far as we are aware, most research has focused on the rheological properties of polysaccharides in aqueous solutions and in solid gels at low to medium sugar levels. Here we investigated the effect of polysaccharides on the stability in high sugar system. Xanthan, a β-(1→4)-D-glucopyranose glucan backbone with side chains of (3→1)-α-linked D-mannopyranose-(2→1)-β-D-glucuronic acid-(4→1)-β-D-mannopyranose on alternating residues, is an anionic polysaccharide that provides very high viscosity and is commonly used as a thickener and stabilizer. It forms very weak gel only at high concentration (~1%) (Ross-Murphy et al., 1983). Xanthan was selected as a nongelling

polysaccharide model due to its rigid-rod structure with high molecular weight of ~1,000,000 Daltons, and stable rheological properties under various conditions.

In a previous study we used erythrosin B phosphorescence to monitor the molecular mobility as well as dynamic site heterogeneity in amorphous solid sucrose (Pravinata et al., 2005). In the present study, phosphorescence of Ery B was used to measure the matrix mobility in thin films of amorphous sucrose-xanthan mixtures. The measurement of molecular mobility of amorphous sugars at low levels of macromolecules thus provides insight into the mechanism of biopolymer effect on sucrose matrix mobility, which is of considerable fundamental and technological interest. Xanthan content was varied from 0.0001 to 0.01 (g xanthan/g sucrose) by addition of xanthan to the concentrated sucrose solution prior to film formation. The temperature-dependence of mobility was measured and analyzed at different xanthan contents, generating families of mobility versus temperature curves.

Materials and Methods

1. Preparation of pure sucrose film

We prepared glassy sucrose films by using a slightly modified version of our published method (Pravinata et al., 2005; see details in Materials and Methods in Chapter 1).

2. Preparation of xanthan-sucrose film

Xanthan solution was prepared in distilled deionized water at a concentration of 1 g/100ml. Xanthan gum (XR80), a kind gift from Food Ingredient Solution, LLC (Blauvelt, NY), was used without further treatment. Xanthan-sucrose solutions were

prepared from sucrose solution containing dye. Xanthan solution was kept at 60°C for 10 min before adding to the purified sucrose solutions to obtain a series of mixtures with xanthan/sucrose weight ratio of 0.0001, 0.0005, 0.001, 0.002, 0.004, 0.005, and 0.01, respectively. Prior to preparing glassy films, sucrose-xanthan blended solutions were filtered through a membrane with 0.2μm pores (except xanthan/sucrose ratio of 0.01). The procedure to make a glassy film was the same as the procedure to make a pure sucrose film except for drying films for 10 min instead of 5 min.

Water content in amorphous sucrose and sucrose-xanthan films was determined gravimetrically (by difference of mass before and after drying for 24h at 70°C in an Ephortee (Haake Buchler, Inc.) vacuum oven at 1kPa). Sample films were scratched from quartz slides and ground into powders in a glove box containing P_2O_5 and Drie-Rite with a relative humidity less than 5%. Pure sucrose films contained 0.56±0.13 wt. % water; while xanthan/sucrose mixture samples contained 0.41±0.01, 0.47±0.09, 0.68±0.25, 0.39±0.01, 0.48±0.16, 0.66±0.06, and 0.72±0.21 wt. % water, respectively.

3. Luminescence measurements

Luminescence measurements were made using a Cary Eclipse Fluorescence spectrophotometer (Varian Instruments, Walnut Creek, CA). Prior to any phosphorescence measurements, all samples were flushed for at least 15 minutes with nitrogen gas which contained less than 1ppm oxygen to eliminate oxygen quenching. At each target temperature samples were equilibrated for 1min/°C increase in temperature. The temperature was controlled using a thermo-electric temperature controller (Varian Instruments, Walnut Creek, CA). To eliminate moisture condensation during the

measurements below room temperature, dry air was used to flush the chamber surrounding the cuvette holder. All the measurements were made at least in triplicate.

Delayed fluorescence and phosphorescence emission spectra were collected from 520 to 750 nm (10 nm bandwidth) at 1 nm intervals using excitation of 500 nm (20 nm bandwidth) over temperature range from 5 to 100°C with an observation window of 5.0 ms and an initial delay time of 0.2 ms which suppresses fluorescence coincident with the lamp pulse. Emission spectra from sucrose or sucrose-xanthan films without probe were subtracted from each spectrum although the signal of background was very low.

The energy of emission maximum (ν_p) and the full width at half maximum (FWHM) of the emission bands were determined by using log-normal lineshape function (Maroncelli and Fleming, 1987) to fit both delayed fluorescence and phosphorescence.

$$I(\nu) = I_0 \exp\left\{-\ln(2)\left(\frac{\ln[1+2b(\nu-\nu_p)/\Delta]}{b}\right)^2\right\} \quad (1)$$

Where I_0 is the maximum emission intensity, ν_p is the peak frequency (cm^{-1}), Δ is a linewidth parameter and b is an asymmetry parameter. This equation reduces to a Gaussian line width when b=0. The bandwidth (FWHM; Γ) was calculated according to the following equation:

$$\Gamma = \Delta\left(\frac{\sinh(b)}{b}\right) \quad (2)$$

For delayed luminescence spectra collected from 520-750 nm, a sum of log-normal function for delayed fluorescence ($I_{df}(\nu)$) and phosphorescence ($I_p(\nu)$) was used to fit the spectra. Each emission band was fit to independent fit parameters.

The dipolar relaxation time φ was calculated from the temperature-dependence of the phosphorescence emission peak ν (T) by analyzing the relaxation function:

$$\frac{\Delta\nu}{\Delta\nu_r} = \frac{\nu(T) - \nu_{\max}}{\nu_{\min} - \nu_{\max}} \tag{3}$$

Where ν (T) is the emission peak energy at Temperature T, ν_{min} and ν_{max} are the emission peak energy at the lowest temperature and the highest temperature, respectively. By incorporating a stretched exponential function, the relaxation time can be calculated from the following equation:

$$\frac{\Delta\nu}{\Delta\nu_r} = \frac{\nu(T) - \nu_{\max}}{\nu_{\min} - \nu_{\max}} = \frac{1}{\Gamma(\frac{1}{\beta_l})} \frac{1}{1 + \frac{\beta_e}{\beta_l}\frac{\tau}{\varphi}} \tag{4}$$

Where τ and β_l are the temperature-dependent stretched exponential (Kohlrausch-Williams-Watts) lifetime and stretching exponent (from Eq. 5) describing the phosphorescence intensity decay and Γ(x) in this case is the Gamma function; β_e is assumed to have a value of 0.5.

For lifetime measurements, samples were excited at 530 nm (20 nm bandwidth) and emission transients collected at 680 nm (20 nm bandwidth) over the temperature range from 5 to 100°C. Phosphorescence intensity decays were collected over a window of 5 ms with an initial delay of 0.1 ms and increments of 0.04 ms. Each decay was the average of 20 cycles. Because intensity decays were non-exponential, a stretched exponential, or Kohlrausch-Williams-Watts' decay function was selected to analyze the intensity decay (Richert, 2000; Lee, et al., 2001; Pravinata et al., 2005).

$$I(t) = I_0 \exp(-(t/\tau)^{\beta}) + \text{constant} \tag{5}$$

Where I_0 is the initial amplitude, τ is the stretched exponential lifetime, and β is an exponent varying from 0-1 and characterizing the distribution of lifetimes. The use of a stretched exponential model provides a direct measurement of continuous distribution of lifetimes, which is appropriate for describing a complex glass possessing a distribution of relaxation times for the dynamic molecular processes. The smaller the β value, the more non-exponential the intensity decays and the broader the distribution of lifetimes. Program NFIT (Galveston, TX) was used to fit the decay; goodness of fit was evaluated by examining the χ^2 and R^2. Plots of modified residuals (defined as the difference between the intensity from the fit decay curve and the measured intensity divided by the square root of the measured intensity) was also an indicator of the goodness of fit. R^2 for all fits ranged from 0.99 to 1.00 and modified residuals plots fluctuated randomly around zero amplitude.

Phosphorescence emission lifetimes of Ery B as a function of emission wavelength were measured with excitation wavelength at 530 nm (20 nm bandwidth); emission wavelength varied from 640 to 720 nm (20 nm bandwidth). Phosphorescence emission lifetimes as a function of excitation wavelength were measured with emission wavelength at 680 nm (20 nm bandwidth); excitation wavelength ranged from 490 to 560 nm (20 nm bandwidth). The experiments were performed at 25°C.

4. Photophysical scheme

Our analysis of the delayed emission is similar to the photophysical scheme for erythrosin B outlined by Duchowicz et al. (1998). The measured emission rate for phosphorescence (k_P) is the sum of all possible deexcitation rates for the triplet state T_1:

$$\tau^{-1} = k_P = k_{RP} + k_{TS1} + k_{TS0} + k_Q[Q] \qquad (6)$$

In this equation, k_{RP} is the rate of radiative emission to the ground state S_0. For erythrosin B, k_{RP} is 41 s^{-1} and constant with temperature (Duchowicz et al., 1998).

k_{TS1} is the rate of thermally activated reverse intersystem crossing from the triplet state T_1 to the singlet state S_1, and the value can be estimated from the Arrhenius equation:

$$k_{TS1}(T) = k^0_{TS1} \exp(-\Delta E_{TS}/RT) \quad (7)$$

where k^0_{TS1} is the maximum rate of intersystem crossing from T_1 to S_1 at high temperature, ΔE_{TS} is the energy gap between T_1 and S_1, R=8.314 J K^{-1} mol^{-1}, and T is the temperature in Kelvin. The value of ΔE_{TS} is calculated from the slope of a Van't Hoff plot of the natural logarithm of the ratio of intensity of delayed fluorescence (I_{DF}) to phosphorescence (I_P):

$$d[\ln(I_{DF}/I_P)]/d(1/T) = -\Delta E_{TS}/R \quad (8)$$

where I_{DF} and I_P are the maximum intensity values determined from analysis of the emission band using Eq. (1). The value of k_{TS1} at 25°C was estimated as 88 s^{-1} using k^0_{TS1}=3.0 x 10^7 s^{-1} and ΔE_{TS} = 31.56 kJ/mol (Pravinata et al., 2005).

In the presence of oxygen, the quenching rate $k_Q[Q]$ is the product of rate constant k_Q and the oxygen concentration [Q]. By flushing nitrogen throughout the measurements we assume that no oxygen quenching occurred. One of the non-radiative decay routes is through intersystem crossing to the ground state S_0. The decay rate is expressed by k_{TS0}, which reflects the rate of collisional quenching of the probe due to both internal and external factors (Papp and Vanderkooi, 1989). We assume that the term k_{TS0} primarily reflects the external environmental factors since the self collisional quenching among

probe molecules can be neglected within the extremely viscous amorphous solid. In this study, temperature-dependent term k_{TS0} can be calculated by the difference from Eq. (6).

Results

At a probe/sucrose molar ratio of $1:10^4$, each probe is on average surrounded by a matrix shell around 10-11 sucrose molecules thick. At this concentration Ery B dispersed within the sucrose matrix does not aggregate and thus reports the physical properties of the unperturbed sucrose matrix (You and Ludescher, 2006).

1. Delayed emission spectra

The delayed emission spectra of erythrosin B dispersed in amorphous sucrose films with various weight ratios of xanthan/sucrose were collected over the temperature range from 5 to 100°C. All spectra (data not shown) showed the expected decrease in phosphorescence and increase in delayed fluorescence intensity with increasing temperature seen in xanthene dyes (Parker, 1968). Both the delayed fluorescence and phosphorescence bands shifted to longer wavelength at higher temperature; the peak frequency (ν_p) and bandwidth (Γ) were determined by fitting to a log-normal lineshape function (Eq. 1 and 2). The frequency and bandwidth for phosphorescence emission are plotted versus temperature in Figure 89. The peak frequency for delayed fluorescence exhibited similar thermal behavior (data not shown).

The phosphorescence peak frequency provides a measure of the average energy of emission; a decrease in emission energy reflects an increase in the average extent of dipolar relaxation around the excited triplet state prior to emission (Lakowicz, 1999). The peak frequency decreased gradually and approximately linearly at low temperature and

much more steeply at higher temperature in all films. All the curves showed a similar shape; however, the curve for the film with xanthan/sucrose weight ratio of 0.0001 was below while those with xanthan/sucrose weight ratio higher than 0.0005 were above the curve for pure sucrose. At ratio of 0.0001, the peak frequency was 14600 cm^{-1} at 5°C and 14205 cm^{-1} at 100°C, that is, the emission red-shifted 5 nm and 8.0 nm, respectively, compared with 14698 cm^{-1} and 14360 cm^{-1} in pure sucrose. When the xanthan content was increased by 5 fold to 0.0005, the values of the peak frequency increased and were almost the same as those of sucrose. At a weight ratio of 0.004 the peak frequency at 5 °C increased to 14890 cm^{-1} (the spectrum blue-shifted by 8 nm), and to 14490 cm^{-1} at 100°C (blue-shifted by 6 nm). Addition of more xantan did not increase the peak frequency significantly.

The total decrease in peak frequency over the range of temperature increased with xanthan content. The total change reached the maximum at a ratio of 0.002 (~480 cm^{-1}) and then the change in peak frequency began to decrease and remained constant at a ratio above 0.005. Compared with sucrose (~340 cm^{-1}), the change in peak frequency in all xanthan/sucrose films was larger, indicating an increased average extent of dipolar relaxation around the excited triplet state in the presence of xanthan.

The phosphorescence bandwidth provides a measure of the range of energetically distinct matrix environments seen by the Ery B probe within the amorphous matrix (Lakowicz, 1999). The bandwidth increased slowly at low temperature and more dramatically at high temperature in all films. All the curves in sucrose-xanthan films were below the sucrose curve and the biggest decrease in bandwidth seemed to occur at the lowest xanthan concentration (weight ratio of 0.0001). Addition of xanthan decreased the

bandwidth over the whole temperature range, indicating a corresponding decrease in the width of the distribution of energetically distinct matrix environments over the whole temperature range.

The effect of xanthan is demonstrated in plots of peak frequency and bandwidth as a function of xanthan content (Figure 90). Peak frequency generally increased with an increase in xanthan content. At the low end of the xanhan concentration range (ratio of 0.0001), the values of peak frequency were smaller than those in pure sucrose; when xanthan increased to a level of 0.0005, the values were almost identical with those in sucrose; the frequency reached a plateau when xanthan content was 0.005. Bandwidth curve showed comparatively complicated behavior: the bandwidth decreased ~5% at low xanthan/sucrose ratio of 0.0001, and then increased at ratio of 0.0005 with values slightly lower than those in sucrose; with further increase in xanthan content, the bandwidth decreased again to some extent (not as significant as that at ratio of 0.0001); at a ratio of 0.005 and above, the values of bandwidth increased and remained the same as those at a ratio of 0.0005. The xanthan effect is more clearly illustrated in plots of relative peak frequency and bandwidth normalized to the values in pure sucrose film at temperature from 5 to 65°C (Figure 91).

The intensity ratio ln (I_{df}/I_p) was plotted as a van't Hoff plot versus 1/T and the slope obtained from the linear plot can be used to estimate the energy gap between the triplet and singlet states (Eq. 8 in Materials and Methods). In amorphous sucrose the values of ΔE_{TS} are 31.56±0.56 kJ mol^{-1}. In the presence of xanthan with weight ratio of 0.0001, 0.0005, 0.001, 0.002, 0.004, 0.005, and 0.01, the values of ΔE_{TS} were 31.92±0.19, 31.32±0.86, 31.64±0.16, 32.12±0.77, 31.13±0.55, 31.32±0.38, and

31.29±0.16 kJ mol^{-1}, respectively, indicating that addition of xanthan had an insignificant influence on the singlet-triplet energy gap.

The dipolar relaxation rates for sucrose and sucrose-xanthan films are plotted in an Arrhenius fashion in Figure 92 (Eq. 4 in Materials and Methods). These curves show upward curvature at high temperatures indicating the increased activation energy with increasing temperature. The curves in sucrose-xanthan films were almost identical with the curve of pure sucrose, indicating that addition of xanthan within the studied concentration range had an insignificant influence on the dipolar relaxation rate in sucrose matrix.

2. Phosphorescence decay kinetics

The phosphorescence intensity decays in sucrose-xanthan glass with different xanthan contents were measured over the temperature range from 5~100ºC. The stretched exponential lifetime and exponent β are plotted as a function of temperature (Figure 93). The lifetimes decreased biphasically with increasing temperature in all films, exhibiting a gradual linear decrease at low and a more dramatic decrease at high temperature. All the curves showed similar shape; however, the curve for film with xanthan/sucrose weight ratio of 0.0001 was below while those with xanthan/sucrose weight ratio higher than 0.0005 were above the curve for pure sucrose. The lifetimes increased with addition of xanthan, from 0.63 ms at 5°C in xanthan-sucrose film at weight ratio of 0.0005 to 0.69 ms in the film with a ratio of 0.004. With further increase in xanthan concentration, the lifetimes did not increase.

The exponent β in sucrose film showed biphasic behavior over the temperature range from 5 to 100ºC: β was almost constant at low temperature and decreased at high

temperature. The curves of β in sucrose-xanthan films were different from the curve in sucrose film, depending on the xanthan content. All the curves for films with xanthan/sucrose weight ratio from 0.0001 to 0.005 were above the curve for sucrose at low temperature. At 65°C and above, the curve for film with ratio of 0.0001 was below while those with ratios higher than 0.0005 were above the curve for sucrose. With increasing xanthan content, the decrease in exponent of β with temperature became less and the biphasic behavior disappeared at ratios above 0.002. The values of β at high ratios were almost constant over the whole temperature range. In sucrose film with ratio of 0.01, the curve was below at low temperature and above at high temperature the curve for sucrose. Similarly the values of β at a ratio of 0.01 did not change from 5 to 100°C. β reflects the distribution of lifetimes and thus the corresponding distribution of dynamically distinct probe environments with different values of k_{TS0} (Pravinata et al., 2005). The small increase in β with addition of xanthan indicated a significant decrease in the range of dynamically distinct probe environments both at low temperature (except at ratio of 0.01) and at high temperature (except at ratio of 0.0001).

The decrease in lifetime with temperature reflects an increase in the rate of non-radiative decay of the excited triplet state T_1 due to an increase in both the rate of non-radiative decay to the ground state S_0 (k_{TS0}) and reverse intersystem crossing to S_1 (k_{TS1}). Based on the maximum physically reasonable value of k_{TS1} (Pravinata et al., 2005), an estimate of the lower limits of k_{TS0} was calculated from Eq. 6 (Materials and Methods) and it is plotted as $\ln(k_{TS0})$ versus 1/T in Figure 94. The non-radiative quenching rate k_{TS0} was linear at low temperature and shot up at high temperature, which indicated that this rate is sensitive to the molecular mobility activated at the glass transition. Addition of

xanthan in sucrose at a ratio of 0.0005 decreased the quenching rate k_{TS0} over the whole temperature range. This constraining effect on mobility was more significant with increasing xanthan content, especially at high temperature. At a ratio of 0.0005, for instance, the value of k_{TS0} decreased by 3% at 5ºC and 8% at 95ºC compared to sucrose; upon increasing the ratio to 0.004, the value of k_{TS0} decreased by 13% at 5ºC and 36% at 95ºC. At a ratio of 0.0001, however, the quenching rate k_{TS0} increased by 4% at 5ºC and 50% at 100ºC.

Figure 95a shows the xanthan content-dependence of the collisional quenching rate k_{TS0} in sucrose films and Figure 95b is a plot of the relative rate normalized to the values in pure sucrose at temperatures from 5 to 65ºC. The rate constant k_{TS0} increased from ~5% at 5°C to ~20% at 55°C in the film with a weight ratio of 0.0001 while decreased at other xanthan contents over the same temperature range. k_{TS0} decreased with increasing xanthan content ($\geq$ 0.0005) until reached a minimum around a ratio of 0.004.

In the concentration range from 0.0001 to 0.002 weight ratio of xanthan/sucrose, at each xanthan content both the absolute and the relative quenching rate k_{TS0} increased with temperature. At ratios of 0.004 and above, the absolute rate increased but the relative rate decreased with increasing temperature.

3. Spectral heterogeneity

Phosphorescence intensity decays of Ery B in sucrose films with different xanthan contents were measured as a function of excitation and emission wavelength at 25°C. All decays were well analyzed using a stretched exponential model; lifetimes are plotted versus excitation and emission wavelength in Figure 96a. All lifetime curves showed a similar trend: the lifetime decreased with increasing wavelength across the emission

band. In sucrose, the lifetimes varied from a high of 0.65 ms at 640 nm to a low of 0.52 ms at 720 nm; lifetimes also decreased monotonically with increasing wavelength in sucrose-xanthan films. The values of the lifetime increased with increasing xanthan concentration. Lifetimes and lifetime variation were slightly reduced in the presence of a small amount of xanthan (ratio of 0.0001), with lifetimes ranging from 0.61 ms at 640 nm to 0.51 ms at 720 nm. At a ratio of 0.005 and above, lifetimes as well as lifetime variations increased with increasing xanthan content. Lifetimes also varied across the excitation band: lifetimes increased with increasing wavelength to a maximum at 520-540 nm and then decreased at higher wavelengths. The variation of lifetime within the excitation band showed similar trends as within the emission band.

The stretching exponent β also varied as a function of both excitation and emission wavelength (Figure 96b). In all films β values were lower at the blue edges in both emission and excitation bands, and increased with increasing wavelength to a maximum at 680-690 nm across the emission band and a maximum at 540-550 nm across the excitation band, then decreased slightly at the red edges. The values of β were generally higher in the presence of xanthan. The variation of β across the emission as well as excitation band in sucrose films was smaller in the presence of xanthan. At the high end of the xanthan content (ratio of 0.01), the values of β were lower but variation of β was larger than pure sucrose.

The calculated quenching rate k_{TS0} is plotted versus emission and excitation wavelength at various xanthan contents in Figure 97. k_{TS0} increased monotonically with increasing emission wavelength in all of the films. At low xanthan content (~0.0001) k_{TS0} was above, and at high xanthan content (≥ 0.0005) k_{TS0} was below that seen in pure

sucrose. The variation of k_{TS0} decreased with increasing xanthan content, except for the ratio of 0.01 (increased by ~10%). Across the excitation band, k_{TS0} curves showed minimum values around 530 nm and had the higher values at both the blue and red edge of the excitation band in all sucrose and sucrose-xanthan films. The quenching rate increased at low and decreased at high xanthan contents.

Discussion

1. Sample preparation and xanthan conformation

The behavior of xanthan in solution is complicated by its conformation and self-association. Xanthan shows weak gel properties under some specific conditions although it is considered as a non-gelling hydrocolloid (Giannouli and Morris, 2003). Xanthan is reported to be a semi-flexible molecule with a hydrodynamic length varying between 600 and 2000 nm and a hydrodynamic diameter of the order of 2 nm (Rodd et al., 2000). The light scattering data indicated that xanthan molecules have right hand double helix and a conformational transition from helix to coil occurs as temperature increases. The conformation of xanthan molecules are determined by concentration, ionic strength and temperature. At very low xanthan content, low ionic strength and high temperature, xanthan molecules exist as an individual random coil; while on cooling and/or increasing xanthan content and ionic strength (adding salts) the molecules tend to crosslink and exhibit a more ordered helix structure. Undoubtedly the conformational structure of macromolecules affects the properties of a matrix from a molecular level. To avoid these complications it is necessary to control the thermal history of xanthan samples. A true molecular dispersion thus appears important in studying the influence of xanthan on the

molecular mobility of amorphous sucrose solids. Heat treatment of the xanthan solutions has been reported to destroy the xanthan ordered structure in its native form (Milas et al., 1996). In the present work, heat treatment of a certain time was used before film casting to ensure that the xanthan molecules at all the studied levels were in the same disordered structure. Once the films were cast, fast drying was applied to remove the water and the consequently increased viscosity made it possible for the xanthan molecules to stay in the initial state.

2. Destabilization effect at low xanthan level

Phosphorescence data were collected in sucrose films at various xanthan contents at temperatures from 5 to 100°C. The phosphorescence emission wavelength and intensity of erythrosin B in amorphous sucrose and sucrose-xanthan mixtures are influenced by two kinds of molecular mobility: dipolar relaxation and collisional quenching. Our discussion of xanthan effect on molecular mobility in amorphous sucrose is based on the emission energy and lifetime data that are modulated by these two mobility motions.

In the xanthan concentration range from 0.0001 to 0.0005, xanthan showed a destabilization influence on sucrose matrix. The values of peak frequency were lower and the magnitude of dipolar relaxation (the total decrease in emission energy) larger than in pure sucrose. For instance, the peak frequency at 5°C in sucrose-xanthan at ratio of 0.0001 was 14600 cm^{-1} and the total decrease from 5 to 100°C in emission energy was 385 cm^{-1}, compared with 14700 cm^{-1} and 338 cm^{-1} in sucrose. With an increase in xanthan content, the peak frequency increased and became comparable with pure sucrose. Note that the decrease in emission energy from 5 to 65°C was larger (by 50-70%) in the

films with low xanthan content than in the sucrose film while the decreases from 65 to 100°C were quite similar in those films. Clearly greater intensity of localized mobility motions existed in the glassy matrix in the presence of a very small amount of xanthan. These enhanced localized motions were constrained when increasing xanthan content up to 0.001 and showed resistance to temperature to some extent.

The magnitude of k_{TS0} in the film with xanthan/sucrose ratio of 0.0001 was larger than that in sucrose over the whole temperature range. At this ratio k_{TS0} was 1600 s^{-1} and 4200 s^{-1} at 5 and 100°C, respectively, compared with 1550 s^{-1} at 5°C and 3000 s^{-1} at 100°C in sucrose. The mobility transition temperatures were calculated as 76.5°C in sucrose and 75.6°C in the sucrose-xanthan with ratio of 0.0001. The similar transition temperature indicated that addition of very low concentration of xanthan did not significantly change the glass transition temperature of the sucrose glass.

Addition of very small amounts of xanthan seemed not to influence the T_g of sucrose matrix significantly, however, the level was enough to make the matrix more mobile than pure sucrose over the whole temperature range. Fast dipolar relaxation (low emission energy) and high matrix mobility (short lifetime and high k_{TS0}) indicated a comparatively flexible sucrose matrix in the presence of the macromolecule xanthan. At this low level interactions between xanthan molecules may not exist, and the possible sucrose-xanthan interactions may not outweigh the sucrose-sucrose interactions, leading to a matrix with relatively weak structure. The semi-flexible xanthan molecule may also perturb the matrix through interfering the packing of sucrose molecules. This perturbing effect must propagate and influence the large numbers of sucrose molecules (~30000 sucrose molecules per xanthan penta-hexose repeating unit) so that the matrix was greatly

affected even at a very low concentration of xanthan. The relatively mobile matrix was a result of the movements of the side chains of xanthan molecules and the hydroxyl groups of sucrose molecules with more freedom due to the loosely packing within the whole matrix.

3. Stabilization effect at high xanthan level

Compared with sucrose, no changes have been observed in shape of the spectra collected from sucrose-xanthan mixtures, indicating that the probe molecules did not form probe aggregates with addition of xanthan. The phosphorescence characteristics of erythrosin B reflect the photophysical properties of local matrix environments.

Phosphorescence emission energy (peak frequency), the energy gap between T_1 and S_0, is primarily affected by the T_1 energy and thus the dipolar relaxation of hydroxyl groups around T_1 within the matrix (Pravinata et al., 2005). The emission energy increased with increasing xanthan content in sucrose. The increase in emission energy suggested a decrease in the dipolar relaxation rate due to the reduced mobility of polar groups around the excited probe molecules in the presence of xanthan.

All the curves of emission energy with temperature for erythrosin B showed similar trend: emission energy decreased gradually at low temperature and more dramatically at high temperature, reflecting a significant increase in the relaxation rate in the melt. The dipolar relaxation rate curves were very close to each other. In amorphous solid sugars, dipolar relaxation reflects mobility of the hydroxyl groups of sugars due either to localized motions in the glass or to large-scale α-relaxations associated with flow activated at T_g. In the presence of xanthan, the hydroxyl groups from sucrose molecules participated in specific interactions with polar groups such as carboxyl groups

from xanthan side chains, forming an intermolecular network. The strength of these interactions increased with increasing xanthan content. As a result the relaxation rate was restricted and resulted in increased emission energy due to the limited mobility of the dipolar groups.

The emission intensity and the lifetime are directly modulated by the rate of radiative emission k_{RP}, of reverse intersystem crossing to the excited triplet state k_{TS1} and of intersystem crossing to the ground state k_{TS0}. The rate of intersystem crossing k_{TS0}, which is modulated by the physical state of the amorphous matrix, reflects both the manner in which the excited T_1 state is vibrational coupled to the S_0 ground state as well as the manner in which the ground state vibrational energy can dissipate from the excited probe into the surrounding matrix. Since the efficiency of this vibrational dissipate is related to the overall mobility of the matrix, k_{TS0} provides a direct measure of matrix mobility.

Compared with sucrose, k_{TS0} in sucrose-xanthan (above xanthan/sucrose ratio of 0.001) decreased with increasing xanthan content, indicating more restricted mobility in xanthan-sucrose matrixes. All the curves of k_{TS0} versus temperature in sucrose films with various xanthan contents showed similar shape: k_{TS0} increased gradually and linearly up to a certain temperature, and then steeply at higher temperature. This temperature reflects the activation of α relaxation at T_g and can be calculated from the intersection of the trendlines at high and low temperature in Arrhenius plots of k_{TS0}. The calculated transition temperatures were 76.5°C in sucrose, and 81.4, 80.9, 80.4, 85.2, and 86.2°C in the sucrose-xanthan mixtures with xanthan/sucrose ratio of 0.001, 0.002, 0.004, 0.005 and 0.01, respectively. The significant increase in the transition temperature suggested

that addition of xanthan stretched the glassy state range of sucrose, keeping the probe in a rigid environment over a wider temperature range.

Lower dipolar relaxation (higher emission energy), lower matrix mobility (longer lifetime and lower k_{TS0}) and higher mobility transition temperature clearly suggested a stabilization (rigidification) effect in sucrose-xanthan mixtures, especially at high temperatures.

With addition of xanthan at ratio of 0.005 and above, both the emission energy and the lifetime did not increase, but slightly decreased instead. The magnitude of k_{TS0} increased within error in sucrose with ratios of 0.005 and 0.01. The increased mobility (but still much lower than sucrose) may be attributed to a change in the interactions. Xanthan molecules self-associate and tend to align along with the backbone in solutions (Rodd et al., 2000). At high xanthan levels, xanthan-xanthan interactions may become dominant in the sucrose-xanthan matrix. Hydration may facilitate the alignment of molecules, leading to formation of micro-aggregates or ordered structure. The anisotropic aggregation probably contributed to phase separation and/or fluctuation in packing degree.

4. Influence of xanthan on dynamic site heterogeneity

Supercooled liquids and amorphous polymers are dynamically heterogeneous spatially as well as temporally as reported by a variety of spectroscopic techniques (Ediger, 2000; Richert, 2002). This physical model is supported by more evidence from erythrosin B phosphorescence. Spectral heterogeneity in Ery B phosphorescence is observed in amorphous sugars and sugar alcohols (Pravinata, et al., 2005; Shirke and Ludescher, 2005; Shirke et al., 2006), and proteins (Nack and Ludescher, 2006; Lukasik

and Ludescher, 2006), indicating that the existence of dynamic site heterogeneity may be a characteristic feature of amorphous food materials and biomaterials.

The variation of lifetime with emission energy reflects variation in one or more of the rate constants for deexcitation of the triplet state. In amorphous sucrose matrix, the population of probes is distributed among the dynamically distinct sites with varied emission energy and matrix quenching rate (Pravinata et al., 2005). Pravinata et al. proposed a physical model for the origin of this site heterogeneity on the basis of emission energy and matrix quenching rate; that is, probes in local environments with less constrained packing have higher overall molecular mobility and thus shorter lifetime and have lower emission energy due to fast dipolar relaxation. When sucrose is mixed with xanthan, whether xanthan will change the local environments and further influence the site heterogeneity becomes one of our interests.

In comparison with sucrose, variations both in lifetime and in exponent β at 25°C of erythrosin B with emission wavelength were smaller in sucrose films containing xanthan except in sucrose-xanthan with ratio of 0.01 (Figure 96), indicating an increased ability within the sites to dynamically average out spectroscopic differences in the presence of xanthan. The variations in collisional quenching rate constant k_{TS0} with emission wavelength (Figure 97) were smaller in sucrose-xanthan mixtures than in sucrose, suggesting decreased heterogeneity in sucrose films with addition of xanthan. At a ratio of 0.01, the increased variation with emission and excitation wavelength in all the photophysical characteristics (lifetime, β and collisional quenching rate k_{TS0}) provided evidence of increased heterogeneity.

The temperature-dependence of the stretching exponent β (Figure 93b) shows that the values of β in the sucrose-xanthan films were larger than the value in pure sucrose at low temperature, suggesting diminished matrix heterogeneity with addition of xanthan. At ratio of 0.01 the value of β was lower at T≤ 65°C but higher at T>65°C indicating increased heterogeneity in the glass but reduced heterogeneity in the melt.

The emission bandwidth (Γ, FWHM) slightly decreased with xanthan content in sucrose-xanthan films (Figure 89b). The decrease in bandwidth indicated a corresponding decrease in the width of the distribution of energetically distinct matrix environments both in the glass and in the melt, probably a result of the formation of sucrose-xanthan network interactions with more uniform allocation of site energy.

Amorphous sucrose is considered structurally heterogeneous and consists of sucrose clusters (Molinero et al., 2003). Sucrose glass is also reported to have dynamically distinct sites with varied emission energy and matrix quenching rate (Pravinata et al., 2005). At xanthan/sucrose weight ratio below 0.0005, xanthan molecules were dispersed into sucrose matrix without xanthan-xanthan intermolecular interactions. The semi-flexible xanthan molecules may disrupt the sucrose clusters and/or disturb sucrose-sucrose interactions, making it possible to diminish the packing degree and average out the energies that are different in local environments. With increasing xanthan content, a strengthened xanthan-sucrose interaction network was formed throughout the matrix, making matrix more homogeneous. At ratio above 0.005 the matrix became heterogeneous probably because of the increased polymer-polymer interactions and the formation of micro-aggregates (phase separation).

The dynamic site heterogeneity changed with temperature (β variation in Figure 93b), indicating the different effect of heat on interactions existing in the matrix. The melt matrix showed more heterogeneity at low but more homogeneity at high xanthan content, suggesting that the matrix with little interactions was unable to resist temperature while the matrix with strong interactions (xanthan-sucrose, xanthan-xanthan) was insensitive to heat, showing homogeneity over the whole temperature range. At a ratio of 0.01 the aggregates formed upon cooling were destroyed by heat, and consequently heterogeneity decreased in the melt.

5. Xanthan change T_g of sucrose?

Khachatoorian et al. (2004) calculated the T_g of xanthan as 212°C based on its chemical structure and additive group-contributions using van Krevelen's method. DSC measurements showed that polysaccharides provided resistance to thermal deformation and increased viscosity above the T_g but did not influence the T_g and thermal properties of the sucrose solutions at subzero temperature (Goff et al., 1993). The T_g of sucrose-xanthan mixture can be estimated using Couchman and Karasz equation (Roos, 1995). Because the xanthan levels used in the sucrose-xanthan films are very low, the T_gs of mixtures were not significantly influenced.

Arrhenius plots of the collisional quenching rate k_{TS0} show biphasic behavior: $\ln(k_{TS0})$ increased linearly and gradually in the glass and more dramatically in the melt. The transition temperatures, calculated from the intersection of the linear fits to low and high temperature data, were estimated as 76.5°C for sucrose, and 72.7, 76.9, 81.4, 80.9, 80.4, 85.2, and 86.2°C in sucrose-xanthan matrix with xanthan/sucrose weight ratio of 0.0001, 0.0005, 0.001, 0.002, 0.004, 0.005 and 0.01, respectively. Compared with

sucrose, the transition temperature decreased at low (0.0001 to 0.0005) but increased at medium (0.001 to 0.004), and significantly increased at high xanthan content (≥0.005). These results clearly indicated that the T_g effect of xanthan is not a determined factor in influencing the sucrose matrix. The interactions distributed in the matrix along with xanthan conformation, rather than the T_g effect of xanthan, contribute to the molecular mobility map of sucrose-xanthan matrix.

Conclusion

Molecular mobility can be modulated by the composition of amorphous solid (such as polymers) and its environment (temperature). Phosphorescence of erythrosin B can report a detailed mobility map within amorphous sucrose film doped with xanthan ranging from 0.0001 to 0.01 (weight ratio). Based on the emission energy and lifetime of erythrosin B in sucrose and sucrose-xanthan films over the temperature range from 5°C to 100°C, we came to a conclusion that xanthan exerts a strong effect on amorphous sucrose and the effect is depended on the xanthan content. At xanthan/sucrose weight ratio below 0.0005, both emission energy and lifetime decreased and k_{TS0} increased, indicating a destabilization effect; at ratio above 0.001, xanthan exerts a stabilization effect: increasing emission energy, increasing lifetime and reducing mobility in the glassy state. The mobility reached a plateau in sucrose-xanthan mixtures at ratio of 0.005 and 0.01. The interactions existing in the sucrose-xanthan matrix, along with xanthan conformation, are considered as determining factors to influence the molecular mobility of sucrose-xanthan mixtures. The interactions vary with xanthan content, leading to different influence on mobility map of sucrose matrix. It is worthy of mapping out the

relationship between the xanthan concentration and the characteristics of the matrix since the matrix properties have implications for the processing and subsequent storage stability of biological materials and foods.

Dynamic site heterogeneities above and below the glass transition temperature may be a characteristic feature of amorphous food materials and biomaterials (Ediger, 2000; Richert, 2002), which has been supported by a series of techniques. Direct evidence is provided by Ery B phosphorescence in amorphous sucrose-xanthan films. Addition of xanthan influences the dynamic heterogeneity of amorphous sucrose matrix and this effect is depended on the xanthan content and temperature. Our data indicate that there are sites of different mobility within amorphous solid sucrose and reduced dynamic heterogeneity is seen in the presence of macromolecules such as xanthan. However, the dynamic heterogeneity can be enhanced by increasing xanthan content up to 0.01, probably due to the existence of micro-aggregates in sucrose-xanthan mixtures. Undoubtedly the ability to report dynamic heterogeneity using Ery B phosphorescence provides an insight into the complex dynamic properties of amorphous biomaterials.

References:

Carpenter, J.F., Prestrelski, S.J., and Arakawa, T. 1993. Separation of freezing- and drying-induced denaturation of lyophilized proteins using stress-specific stabilization. I. Enzyme activity and calorimetric studies. *Arch Biochem Biophys.* 303, 456-464.

Carpenter, J.F., and Crowe, J.H. 1989. An infrared spectroscopic study of the interactions of carbohydrates with dried proteins. *Biochem.* 28, 3916-3922.

Crowe, J.H., Crowe, L.M., and Carpenter, J.F. 1993. Preserving dry biomaterials: the water replacement hypothesis. Part 1. *BioPharm.* 6, 28-29, 32-33.

Chang, L., Shepherd, D., Sun, J., Ouellette, D., Grant, K.L., Tang, X., and Pikal, M.J. 2005. Mechanisms of protein stabilization by sugars during freeze-drying and storage:

native structure preservation, specific interaction, and/or immobilization in a glassy matrix? *J. Pharm. Sci.* 94(7), 1427-1444.

Duchowicz, R., Ferrer, M.L. and Acuna, A.U. 1998. Kinetic spectroscopy of erythrosin phosphorescence and delayed fluorescence in aqueous solution at room temperature. *Photochem. Photobiol.* 68, 494-501.

Ediger, M.D. 2000. Spatially heterogenous dynamics in supercooled liquids. *Annu. Rev. Phys. Chem.* 51, 99-128.

Franks, F., Hatley, R.H.M., and Mathias, S.F. 1991. Materials science and the production of shelf-stable biologicals. *BioPharm.* 4, 38, 40-42, 55.

Giannouli, P., and Morris, E.R. 2003. Cryogelation of xanthan. *Food Hydrocoll.* 17, 495-501.

Goff, H.D., Caldwell, K.B., Stanley, D.W., and Maurice, T.J. 1993. The influence of polysaccharides on the glass transition in frozen sucrose solutions and ice cream. *J. Dairy Sci.* 76, 1268-1277.

Kasapis, S., Mitchell, J., Abeysekera, R., and MacNaughtan, W. 2004. Rubber-to-glass transitions in high sugar/biopolymer mixtures. *Trends Food Sci. Technol.* 15, 298-304.

Kets, E.P.W., IJpelaar, P.J., Hoekstra, F.A., and Vromans, H. 2004. Citrate increases glass transition temperature of vitrified sucrose preparations. *Cryobiology*. 48, 46-54.

Khachatoorian, R., Petrisor, I.G., and Yen, T.F. 2004. Prediction of plugging effect of biopolymers using their glass transition temperatures. *J. Pet. Sci. Eng.* 41, 243-251.

Lakowicz, J.R. 1999. *Principles of fluorescence spectroscopy*. Plenum Press, NY

Lee, K.C.B., Siegel, J., Webb, S.E.D., Leveque-Fort, S., Cole, M.J., Jones, R., Dowling, K., Lever, M.J., and French, P.M.W. 2001. Application of the stretched exponential function to fluorescence lifetime imaging. *Biophys. J.* 81, 1265-1274.

Lukasik, K.V. and Ludescher, R.D. 2006. Effect of plasticizer on dynamic site heterogeneity in cold-cast gelatin films. *Food Hydrocoll.* 20, 88-95.

Maroncelli, M. and Fleming, G.R. 1987. Picosecond salvation dynamics of coumarin 153: the importance of molecular aspects of salvation. *J. Chem. Phys.* 86, 6221-6239.

Milas, M., Reed, W.F., and Printz, S. 1996. Conformation and flexibility of native and re-natured xanthan in aqueous solutions. *Int. J. Biol. Macaromol.* 18, 211-221.

Molinero, V., Cagin, T., and Goddard III, W.A. 2003. Sugar, water and free volume networks in concentrated sucrose solutions. *Chem. Phys. Lett.* 377, 469-474.

Nack, T.J, and Ludescher, R.D. 2006. Molecular mobility and oxygen permeability in amorphous bovine serum albumin films. *Food Biophys.* 1, 151-162.

Papp, S. and Vanderkooi, J.M. 1989. Tryptophan phosphorescence at room temperature as a tool to study protein structure and dynamics. *Photochem. Photobiol.* 49, 775-784.

Parker, C.A. 1968. *Photoluminescence of Solutions.* Elsevier, Amsterdam. Netherlands.

Pravinata, L.C., You, Y. and Ludescher, R.D. 2005. Erythrosin B phosphorescence monitors molecularmobility and dynamic site heterogeneity in amorphous sucrose. *Biophys. J.* 88(May), 3551-3561.

Ptaszek P., Lukasiewicz, M., Achremowicz, B., and Grzesik, M. 2007. Interaction of hydrocolloid networks with mono- and oligosaccharides. *Polymer Bulletin*. 58, 295-303.

Richert, R. 2000. Triplet state salvation dynamics: basics and applications. *J. Chem. Phys.* 113, 8404-8429.

Richert, R. 2002. Heterogeneous dynamics in liquids: fluctuations in space and time. *J. Phys. Condens. Matter.* 14, R738-R803.

Rodd, A.B., Dunstan, D.E., and Boger, D.V. 2000. Characterisation of xanthan gum solutions using dynamic light scattering and rheology. *Carbohydr. Polym.* 42, 159-174.

Roos, Y. 1995. *Phase Transitions in Foods.* Academic Press, San Diego, CA.

Ross-Murphy, S.B., Morris, V.J., and Morris, E.R. 1983. Molecular viscoelasticity of xanthan polysaccharide. *Faraday Symp. Chem. Soc.* 18, 115-129.

Shirke, S., and Ludescher, R.D. 2005. Dynamic site heterogeneity in amorphous maltose and maltitol from spectral heterogeneity in erythrosin B phosphorescence. *Carbohydr. Res.* 340, 2661-2669.

Shirke, S., Takhistov, P., and Ludescher, R.D. 2005. Molecular mobility in amorphous maltose and maltitol from phosphorescence of erythrosin B. *J. Phys. Chem. B.* 109, 16119-16126.

Shirke, S., You, Y., and Ludescher, R.D. 2006. Molecular mobility and dynamic site heterogeneity in amorphous lactose and lactitol from erythrosin B phosphorescence. *Biophys. Chem.* 123, 122-133.

Slade, L., and Levine, H. 1991. Beyond water activity: recent advances based on an alternative approach to the assessment of food quality and safety. *Crit. Rev. Food Sci. Nutr.* 30, 115-360.

You, Y., and Ludescher, R.D. 2006. Phosphorescence of erythrosin B as a robust probe of molecular mobility in amorphous solid sucrose. *Appl. Spectrosc.* 60, 813-819.

Zallen, R. 1983. *The physics of amorphous solids;* John Wiley & Sons: New York.

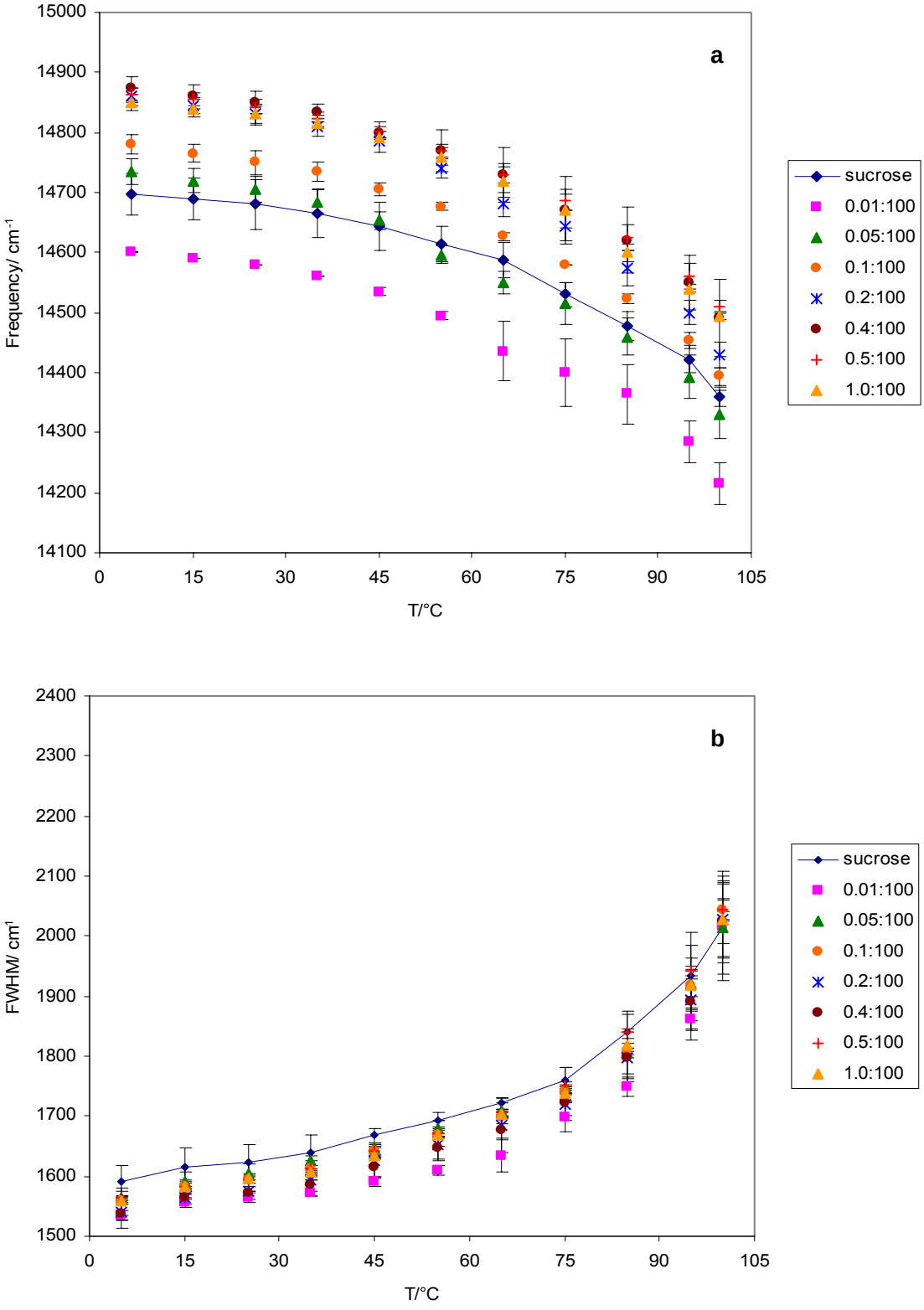

Figure 89: (a) Peak frequency (ν_p) and (b) bandwidth (full width at half maximum, FWHM) for phosphorescence emission from erythrosin B in amorphous sucrose-xanthan films plotted as a function of temperature. Delayed emission spectra collected as a function of temperature were analyzed using log-normal line shape function.

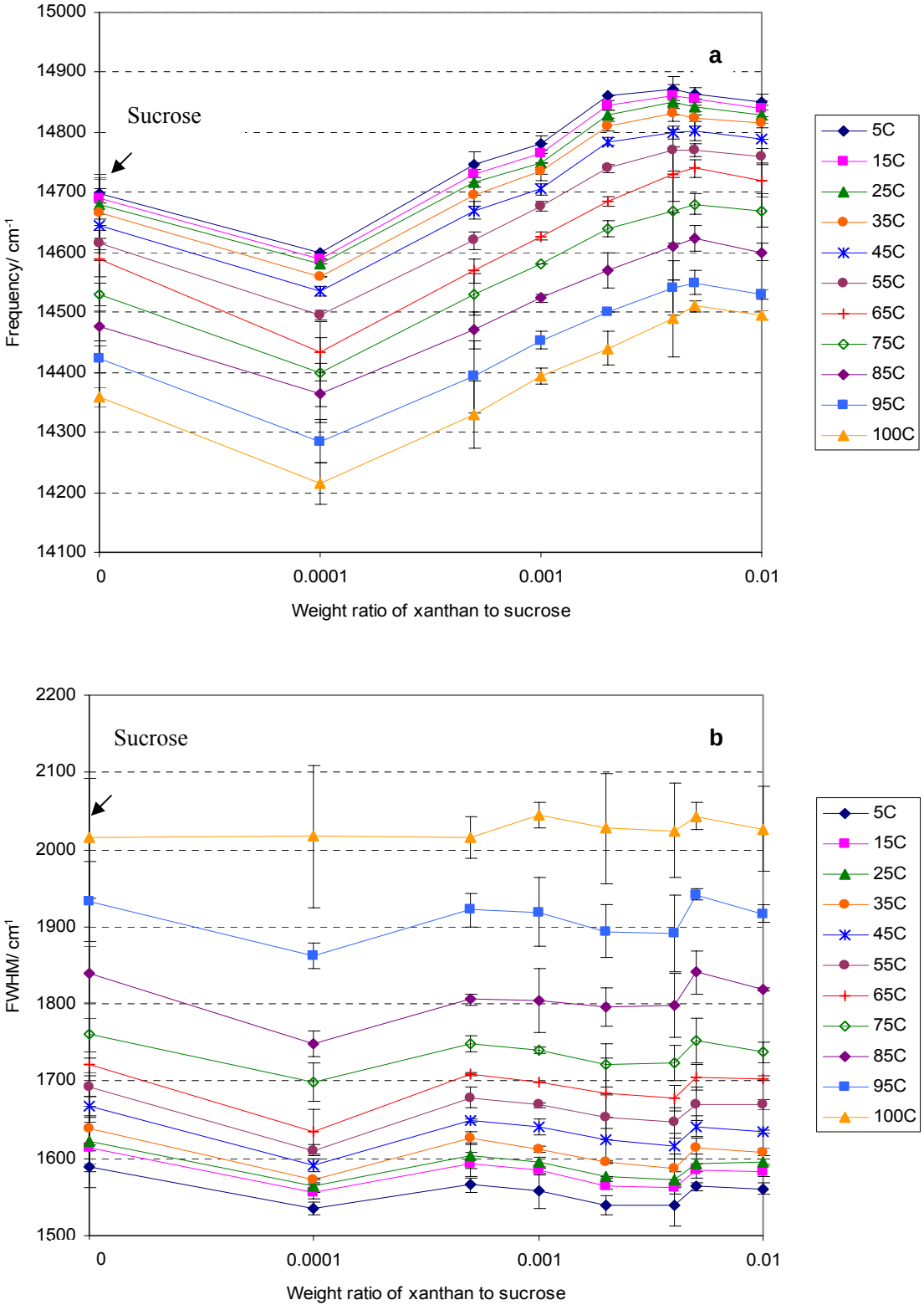

Figure 90: (a) Peak frequency (ν_p) and (b) bandwidth for phosphorescence emission from erythrosin B in amorphous sucrose-xanthan films as a function of weight ratio of xanthan/sucrose. Delayed emission spectra collected as a function of temperature were analyzed using log-normal line shape function.

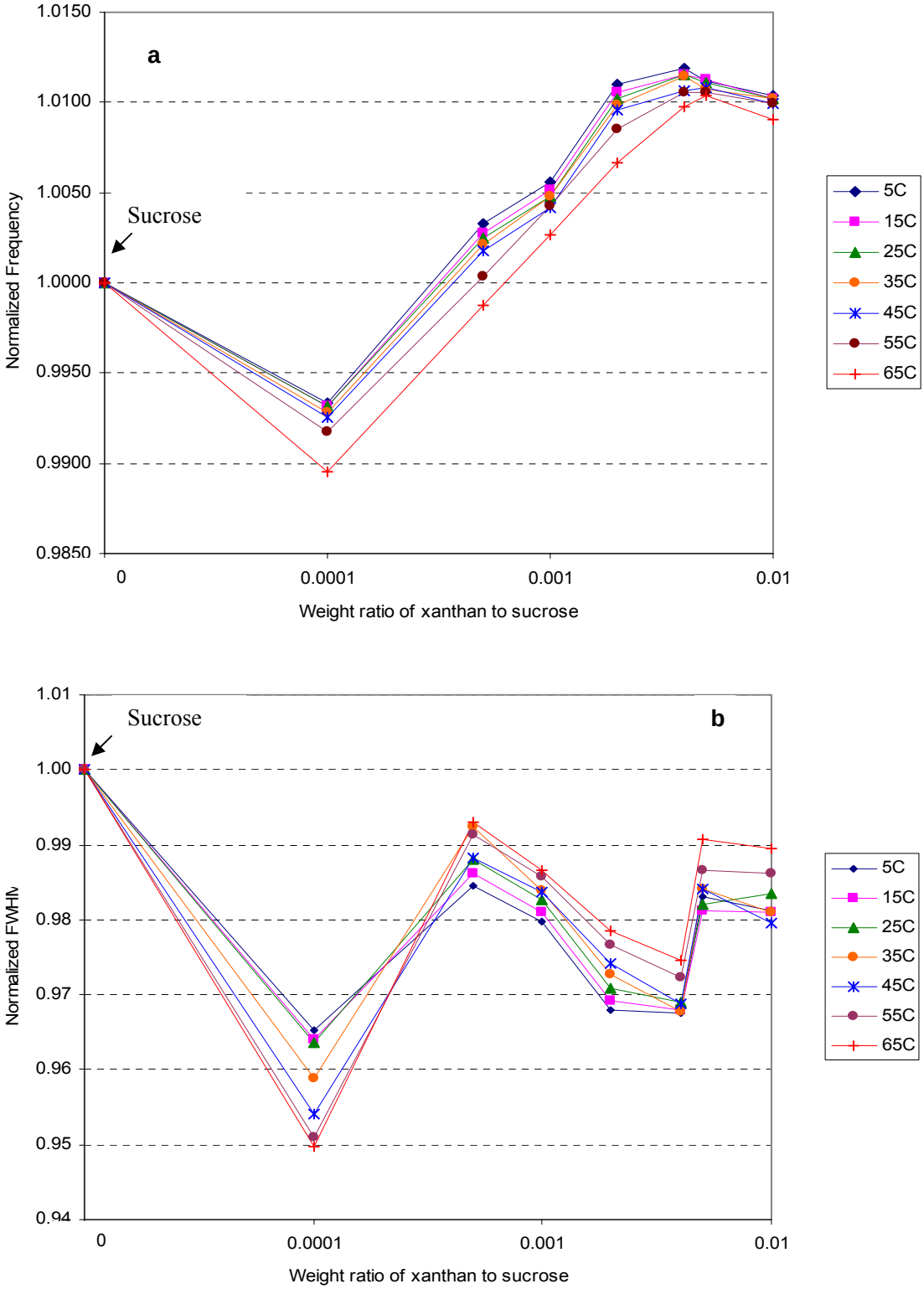

Figure 91: (a) Peak frequency and (b) bandwidth, normalized at each temperature to the value in pure sucrose, for erythrosin B phosphorescence in amorphous sucrose-xanthan films plotted as a function of weight ratio of xanthan/sucrose. Delayed emission spectra collected as a function of temperature were analyzed using a log-normal line shape function.

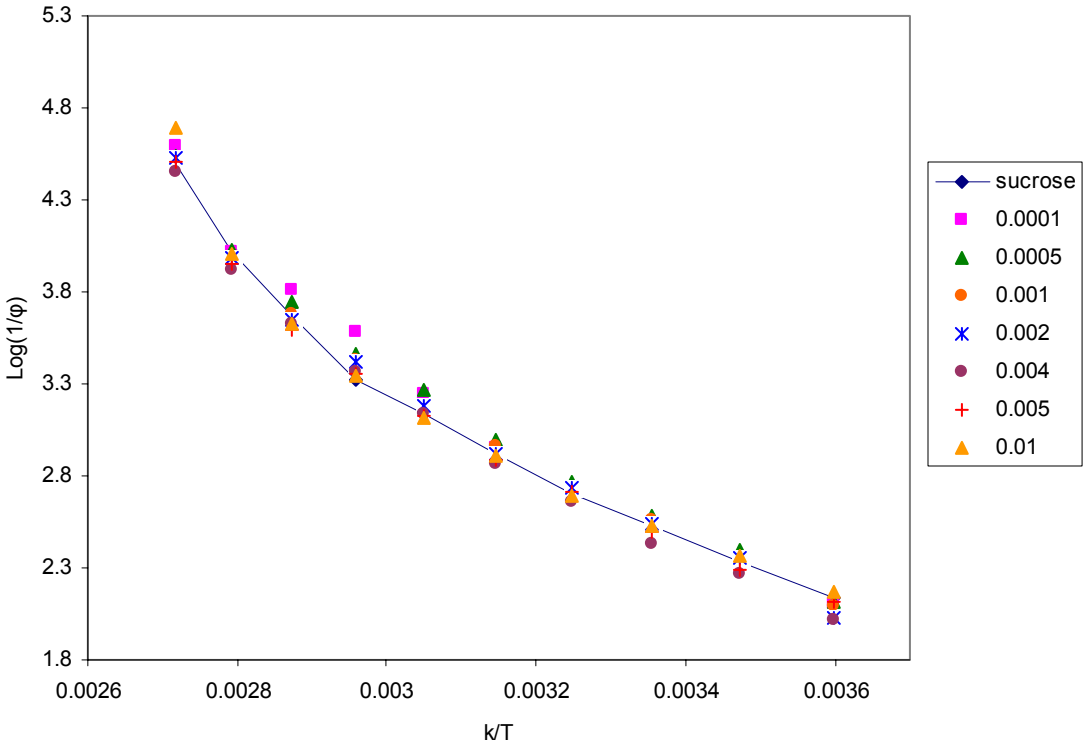

Figure 92: Arrhenius plot of the effect of temperature on the rate of matrix dipolar relaxation around the excited erythrosin B triplet state in sucrose films at various xanthan contents.

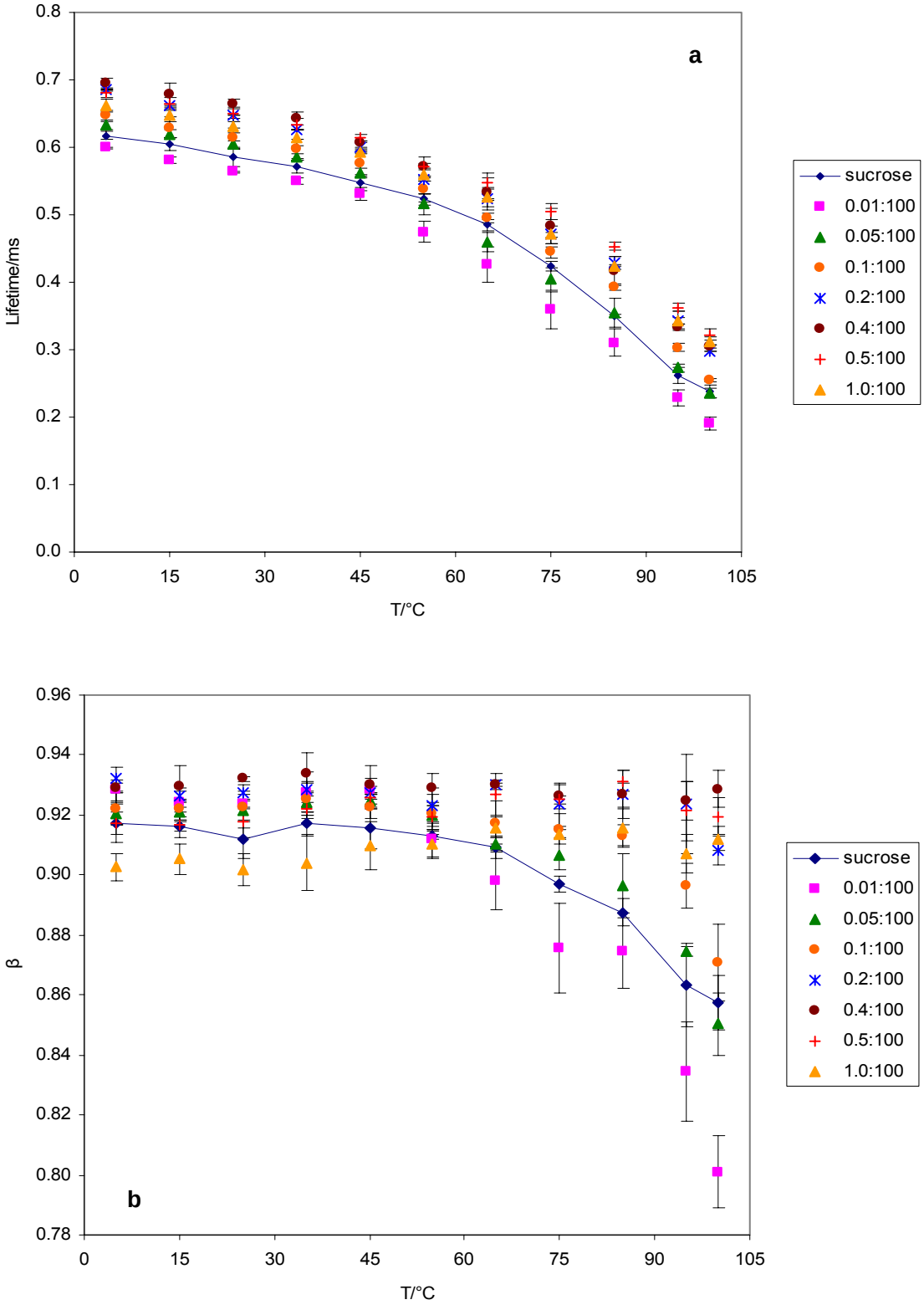

Figure 93: Temperature dependence of (a) lifetime and (b) stretching exponent β obtained from fits to a stretched exponential decay model of the intensity decay of erythrosin B in amorphous sucrose films with various xanthan/sucrose weight ratios.

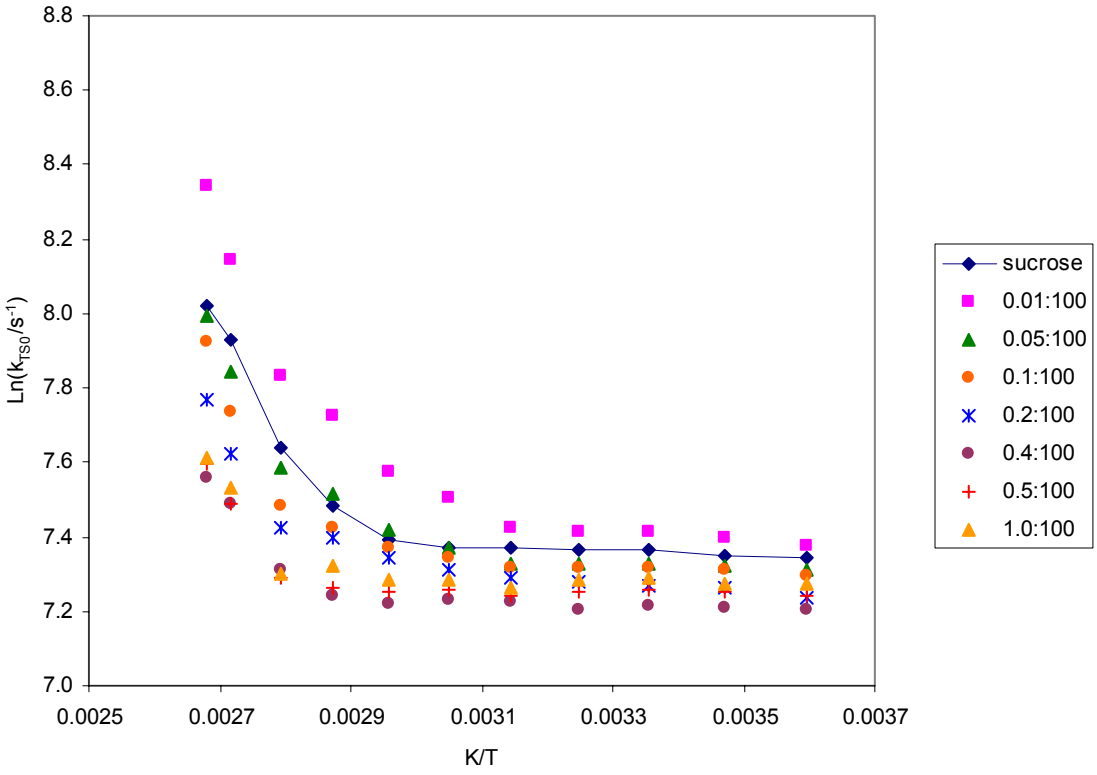

Figure 94: Arrhenius plot of the temperature effect on the rate constant for non-radiative decay of the triplet T_1 state to S_0 (k_{TS0}) in amorphous sucrose-xanthan films; data calculated from the lifetime data of Figure 5a; see text for additional details.

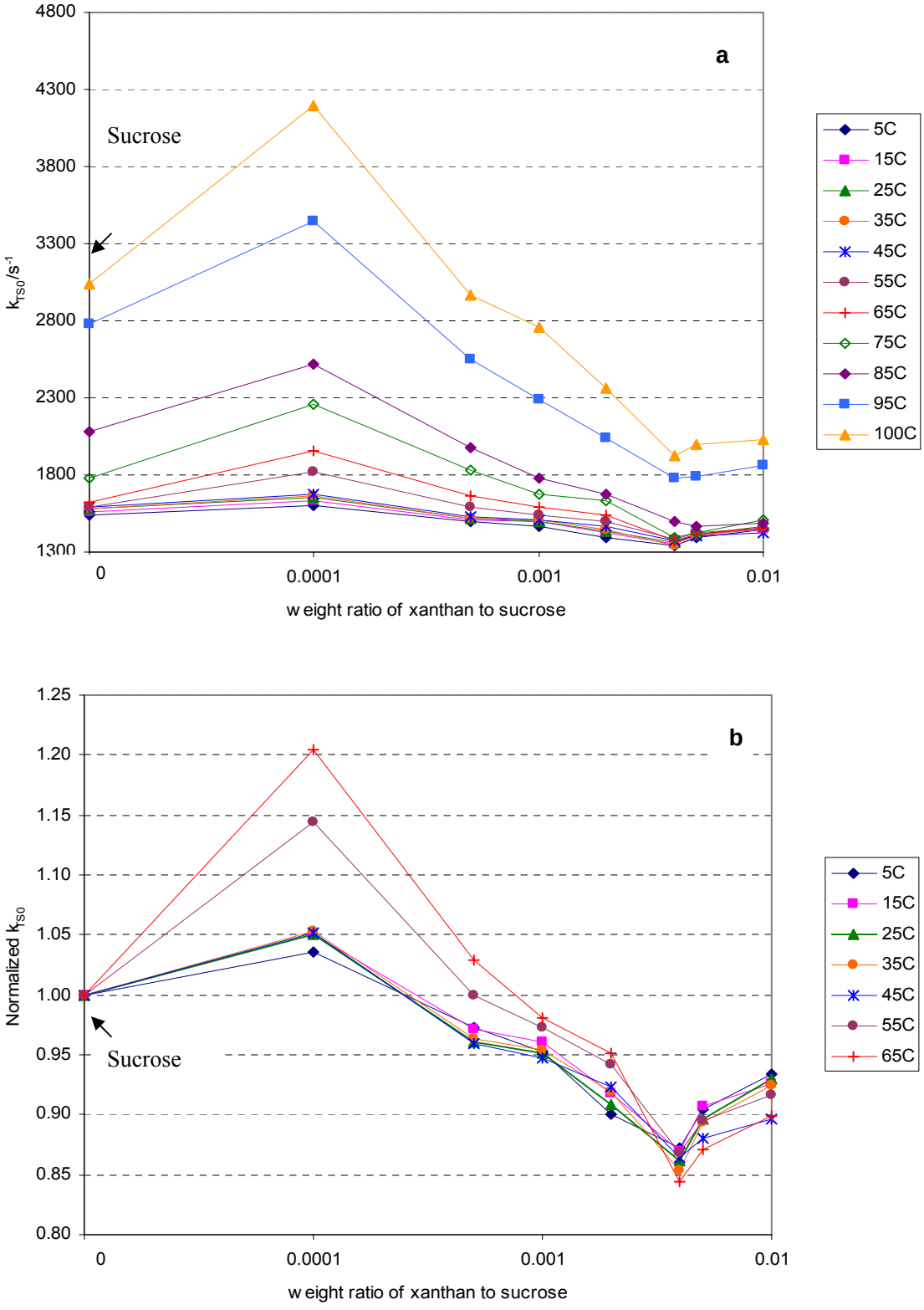

Figure 95: (a) The effect of xanthan on the rate constant for non-radiative decay of the triplet state to S_0 (k_{TS0}); data of Figure 6 were replotted as k_{TS0} versus xanthan/sucrose weight ratio. (b) Normalized rate constant for non-radiative decay of the triplet state to S_0 (k_{TS0}) as a function of xanthan/sucrose weight ratio at low xanthan contents.

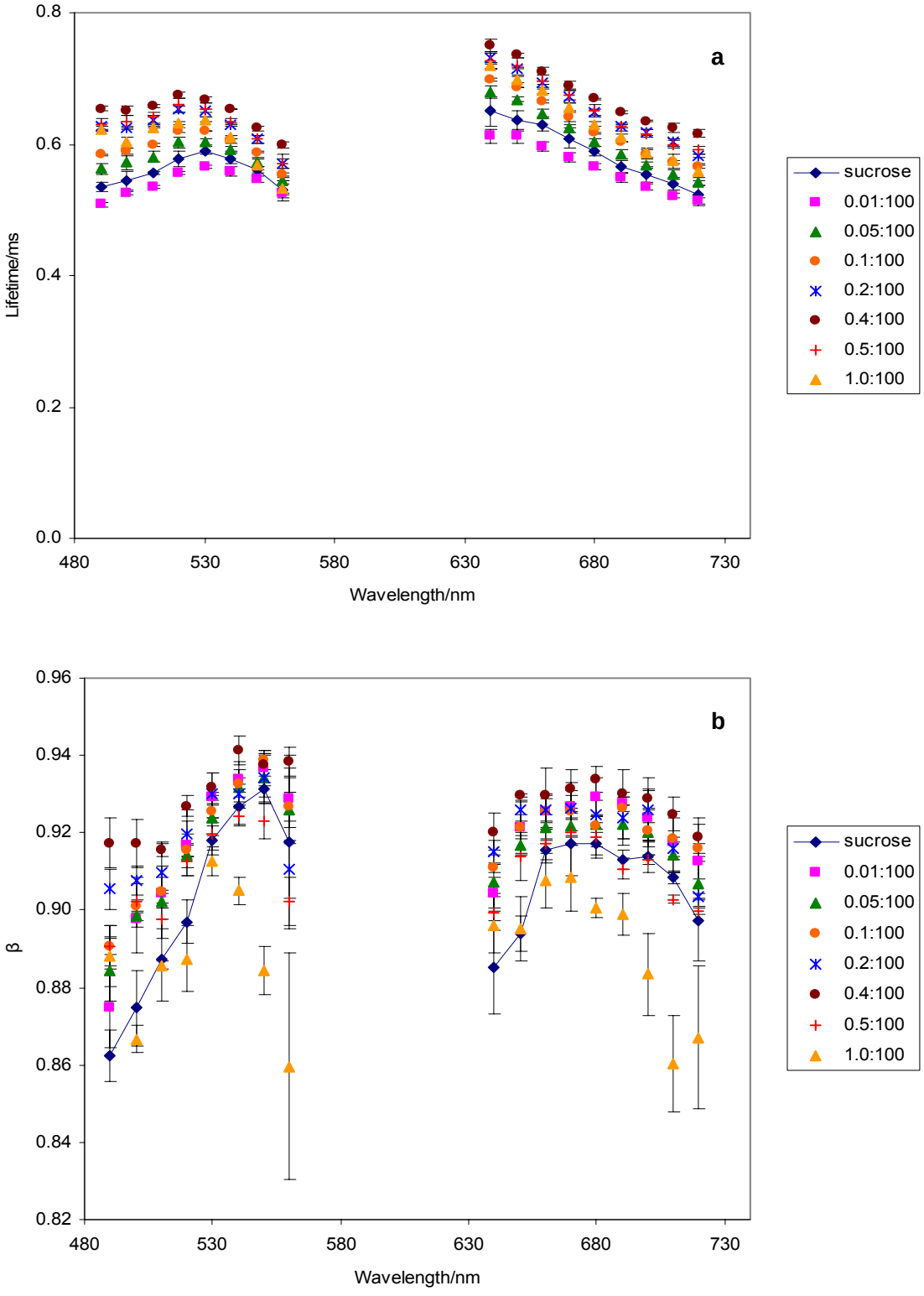

Figure 96: (a) The effect of excitation wavelength (with 680 nm emission) and emission wavelength (with 530 nm excitation) on the lifetimes (a) and stretching exponents β (b) from fits of erythrosin B phosphorescence intensity decays to the stretched exponential decay model. Data collected in sucrose films with various xanthan/sucrose weight ratios from 0.0001 to 0.01.

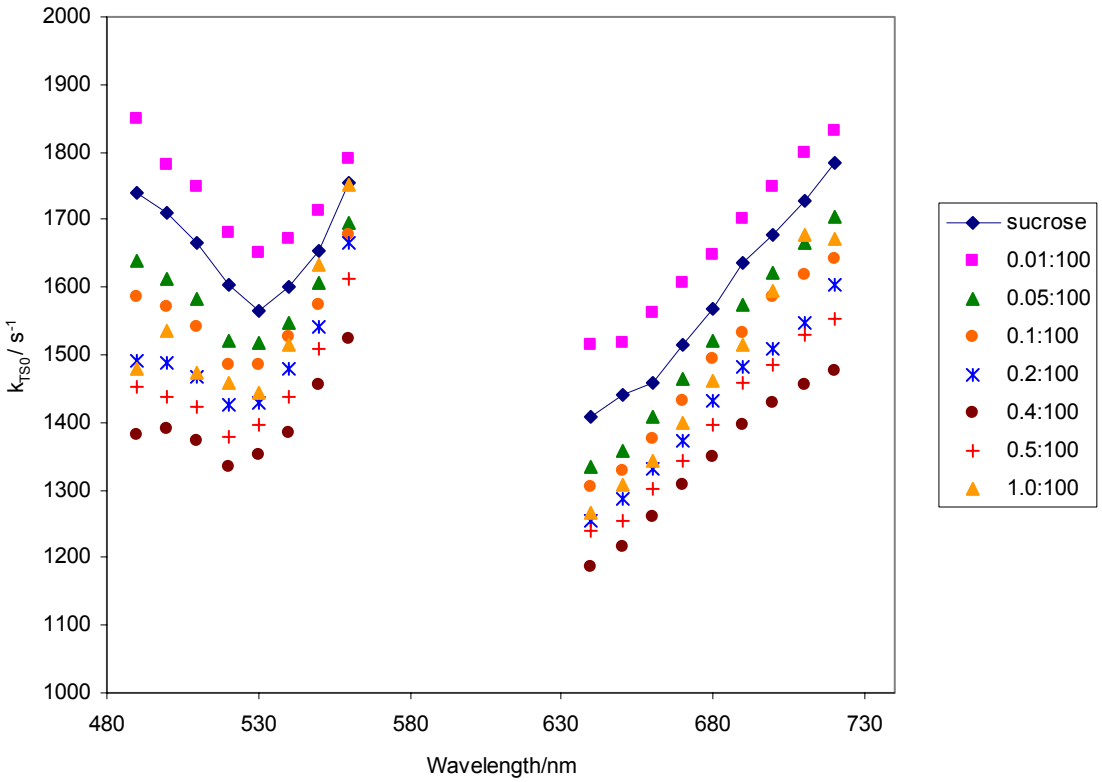

Figure 97: The rate constant for non-radiative decay of the triplet state to S_0 (k_{TS0}) plotted as a function of excitation wavelength (with 680 nm emission) and emission wavelength (with 530 nm excitation). Data collected from erythrosin B in sucrose films with xanthan/sucrose weight ratio from 0 to 0.01.

Chapter 10 Summary and future work

1. Summary

Luminescence from the triplet probe erythrosin B (tetra-iodo fluorescein; Ery B) provides spectroscopic characteristics such as lifetime and emission energy that are sensitive to molecular mobility of the local environment in amorphous solids. Measurements of emission energy and lifetime were made to investigate the temperature- and composition-dependence of molecular mobility in amorphous sucrose and sucrose-additive matrices. In amorphous sucrose film, the molecular mobility (both dipolar relaxation and collisional quenching) increased gradually below and dramatically above the T_g; the distribution of emission energy and lifetime, and the variation in lifetime with wavelength provided evidence of dynamic site heterogeneity in amorphous biomaterials.

In sucrose-based binary matrices, plasticizer (glycerol), salt (NaCl, $CaCl_2$, $MgCl_2$, Na-citrate, Na-acetate, Na-phosphates), maltodextrins (DE 5, 10, 15, and 18), protein (gelatin), and polysaccharides (xanthan and HYLON VII high amylose starch) were selected to investigate how variation in molecule nature influences the molecular mobility as well as dynamic site heterogeneity in amorphous sucrose matrix. The results are summarized in this chapter.

(a) Influence on T_g

Addition of a second molecule modulates the glass transition temperature T_g. However, different molecules influence the T_g in a different way. Due to their high T_g values, polymers normally increase the T_g of the matrix and the effect increases with increasing polymer content. For small molecules, the T_g effect is different depending on the molecule nature. Glycerol, as a plasticizer next to water, reduces the T_g and the

depression increases with an increase in glycerol content. Salts are believed to increase the T_g of the matrix; but the effect becomes complicated due to their nature of absorbing water (decreasing T_g). The overall effect is a result of competition of two opposite influences.

Phosphorescence can indirectly reflect the T_g effect by plotting the spectroscopic parameters as a function of temperature normalized to individual glass transition temperature (e.g. T- T_g or T_g/T). If the curves are identical, we can tell that the second molecule influences the matrix mainly through modulating the T_g; if the curves are parallel but not identical, other effects may exist in the sucrose matrix as well.

(b) Influence on molecular mobility

The primary effect of glycerol is to plasticize the sucrose matrix by increasing the matrix mobility (the rates for both dipolar relaxation and collisional quenching) and reducing T_g. At mole ratio glycerol/sucrose below 0.27 and at temperature below 45°C, glycerol slightly decreased both rates; displaying a phenomenon correlating with the so-called antiplasticization effect seen in polymers. On the contrary, all the polymers studied, displayed a 'plasticization' effect (increasing mobility without significant change in T_g) at very low concentration while a rigidification effect (decreasing mobility without significant increase in T_g) at high concentration. Maltodextrins, mixtures of molecules with a variety of molecular weight, increase the mobility although they have high T_g. Sodium chloride had a strong rigidification effect on sucrose matrix (increasing both kinds of mobility); however this effect was weakened at high content due to its strong ability to bind water. Other salts showed a similar effect as a result of a compromise of two opposite actions (decreasing mobility due to salt itself and increasing mobility due to

the absorbed moisture). These results reflect the complex effect of the additive molecules on the molecular mobility in hydrogen-bonded sugar matrix. The complexity mainly originates from the interactions existing in the sugar-additive molecule matrix, varying with molecular nature, conformation, concentration, physical state, etc. It is difficult to interpret these behaviors using traditional free volume theory or glass transition temperature. Molecular mobility measured from phosphorescence appears to be more accurate to describe the localized as well as the global microenvironment, providing a direct way to evaluate the physical stability of the matrix.

For all the molecules that decrease the mobility and increase the matrix rigidity, they show the maximum effect at different concentrations: NaCl 0.08, gelatin 0.073, xanthan 0.002 and starch at 0.01 weight ratio to sucrose. At each concentration, they exhibit a different rigidification effect. Figure 1 shows the influence of these additives on the nonradiative collisional quenching rate k_{TS0} in the sucrose matrix. It appears that molecules with larger molecular weight (xanthan and starch) have apparent influence at lower concentration; however, the influence is less effective than that with molecules with smaller molecular weight (gelatin and NaCl). In addition, NaCl and gelatin have a more significant effect on restricting the matrix mobility with temperature.

(c) Influence on dynamic site heterogeneity

Phosphorescence of erythrosin B has supported a model of dynamic sited heterogeneity that appears to be commonly present in all the biomaterials. From a molecular level, local regions with different packing and different mobility persist for times longer than the excited state lifetime of erythrosin (0.5 ms) and often exist in amorphous solids regardless of their chemical compositions. We proposed a reasonable

physical model for the origin of this site heterogeneity (Figure 99). The small circles stand for sucrose molecules and the faces stand for probe molecules. In sucrose glass, there is a wide range of sites with different energy and different mobility. Immobile sites consisting of the blue circles have lower overall molecular mobility (slower/less dipolar relaxation and collisional quenching) and higher activation energies. Mobile sites consisting of the red circles have higher overall mobility (faster/more dipolar relaxation and collisional quenching) and lower activation energies. We speculate that the different packing of molecules contributes to the local environments with different rigidity/flexibility. The presence of heterogeneity is proposed to be responsible to some extent for the chemical and physical changes in the glassy matrix. The measurement of dynamic heterogeneity thus provides another evidence of matrix stability.

Compared with amorphous sucrose solids, the plasticizer glycerol decreases while salt NaCl increases the heterogeneity. Polymers affect the site heterogeneity in a more complicated way. Maltodextrins are more heterogeneous than sucrose and they increase the heterogeneity in the sucrose matrix at high maltodextrin content (50:50 MD/S). Gelatin is more homogeneous than sucrose; however, it increases the heterogeneity in sucrose. Xanthan and high amylase starch are linear polymers, exhibiting opposite influences. Xanthan increases the homogeneity over a concentration range from 0.0001 to 0.005 (w/w) while starch decreases the homogeneity with contents varying from 0.001 to 0.1 (w/w). There is no obvious rule about the relationship between heterogeneity and added molecules. The dynamic site heterogeneity is associated with the packing degree of local regions in the matrix. Molecular conformation thus should be taken into

consideration along with other factors influencing the packing of molecules, which is more important in discussing the effects of polymer molecules on the sucrose matrix.

2. Future work

1. Molecular mobility varied with composition in amorphous sucrose matrix. The exact mechanism is still under investigation. One hypothesis is that the interactions between sucrose and added components and molecular conformation (especially for polymers) play an important role in modulating molecular mobility. Phosphorescence of erythrosin B is a novel tool to detect the mobility; however, it alone can not provide details about interactions such as hydrogen bonding. Other techniques including FTIR will be used to discover additional information.

2. In this project phosphorescence of erythrosin B was used to measure the molecular mobility as well as the variation in mobility within the amorphous sucrose matrix. Erythrosin B has many advantages as mentioned in INTRODUCTION. However, some of its properties limit the depth that the research can reach. Poor solubility, one of the limiting factors, makes it difficult to apply in water-soluble systems. Erythrosin B salt has improved solubility and reflects the similar results as Ery B free acid in single amorphous sucrose matrix (Figure 100-102). However, the presence of salt (normally sodium salt) increases the intensity signals significantly. Also the potential ion interactions may influence the matrix property. The data obtained from erythrosin B salt are probably artificial and difficult to interpret. Another disadvantage is the time scale of measurement. Erythrosin B has a lifetime around 0.6 ms at room temperature. Some mobility motions and related changes at low temperature may occur in a longer or shorter

time window, which cannot be captured by probe erythrosin B. Finding probes suitable for a certain purpose is another object in the future work.

3. Amorphous materials are commonly used for pharmaceutical application as excipients, offering protection for labile components such as enzymes and antibodies through lyophilization or spray drying. Recent years see the growing interests for developing solid state formulations. Studying the mechanisms of stabilization in solid state formulations thus becomes important to provide guidelines for designing formulations. As mentioned in some chapters, there are two major mechanisms (glass dynamics and specific interaction) about the stabilization of sensitive compounds, especially proteins. Most finished work has been done on the former mechanism, that is, exploring the role of sucrose and sucrose-based binary systems in stabilization during dehydration by measuring the molecular mobility, trying to correlate the mobility with the stability of the glass. However, in many cases, sucrose and sucrose-based matrix are used for protection not only due to its physical stability but also due to its ability to form specific interactions (hydrogen bonds) with target compounds. More work is needed to investigate the role of possible interactions in the stabilization. Basically, models will be established to study the physical and chemical properties of a specific compound in a specific matrix during dehydration and storage. In this part, molecular mobility of matrix, stability of target compound before and after processing and storage, and the potential interactions between matrix and target will be the focuses of study. The purpose is to find out any correlations between matrix materials and stability of targets.

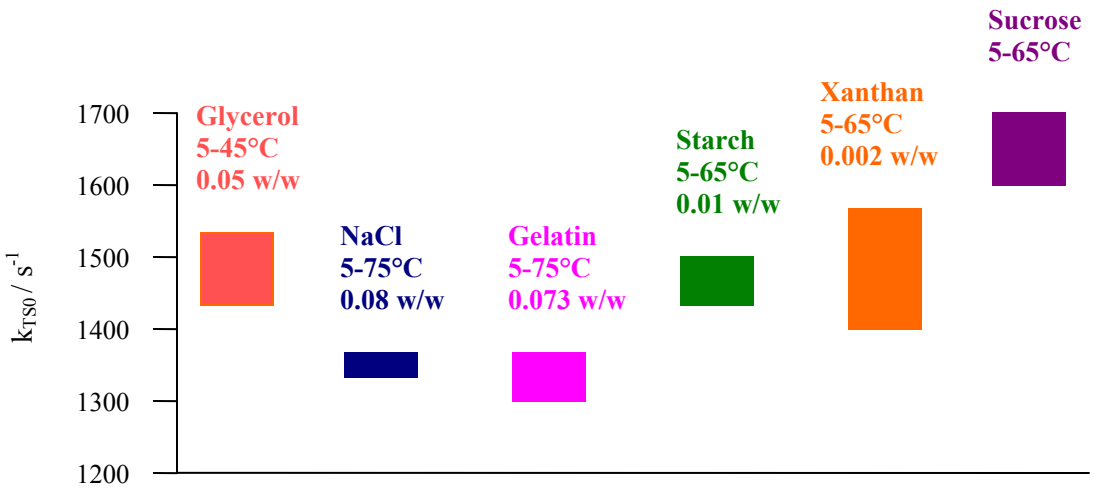

Figure 98: Influence of different molecules on nonradiative collisional quenching rate k_{TS0} in sucrose matrix at individual concentration that shows the maximum effect. The bottom line of the box refers to the rate at 5°C; the top line refers to the rate at 45°C (glycerol), 65°C (starch, xanthan and sucrose), or 75°C (NaCl and gelatin).

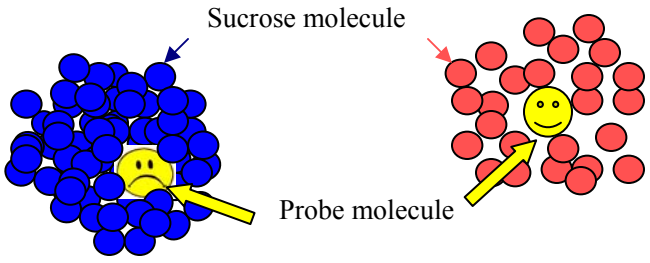

Rigid region (immobile sites):
Lower overall mobility
- Slower dipolar relaxation (higher ν_p)
- Slower collisional quenching (longer τ)

Higher activation energies
Tightly packed

Flexible region (mobile sites):
Higher overall mobility
- Faster dipolar relaxation (lower ν_p)
- Faster collisional quenching (shorter τ)

Lower activation energies
Loosely packed

Figure 99: Physical model for the origin of site heterogeneity in amorphous sucrose matrix.

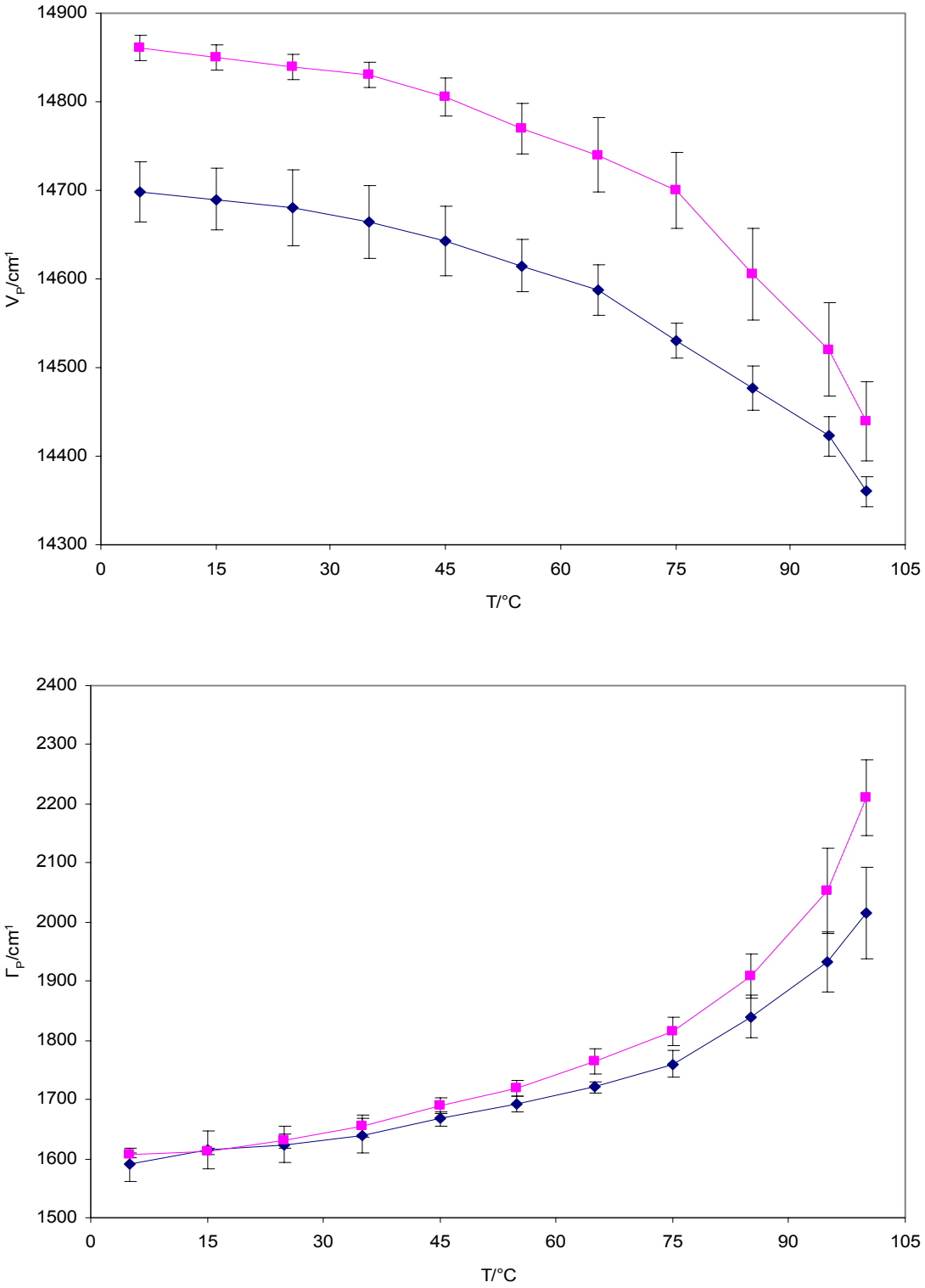

Figure 100: (a) Peak frequency (ν_p) and (b) bandwidth (full width at half maximum, FWHM) for phosphorescence emission from erythrosin B free acid (♦) and erythrosin B sodium salt (■) in amorphous sucrose films plotted as a function of temperature. Delayed emission spectra collected as a function of temperature were analyzed using log-normal line shape function.

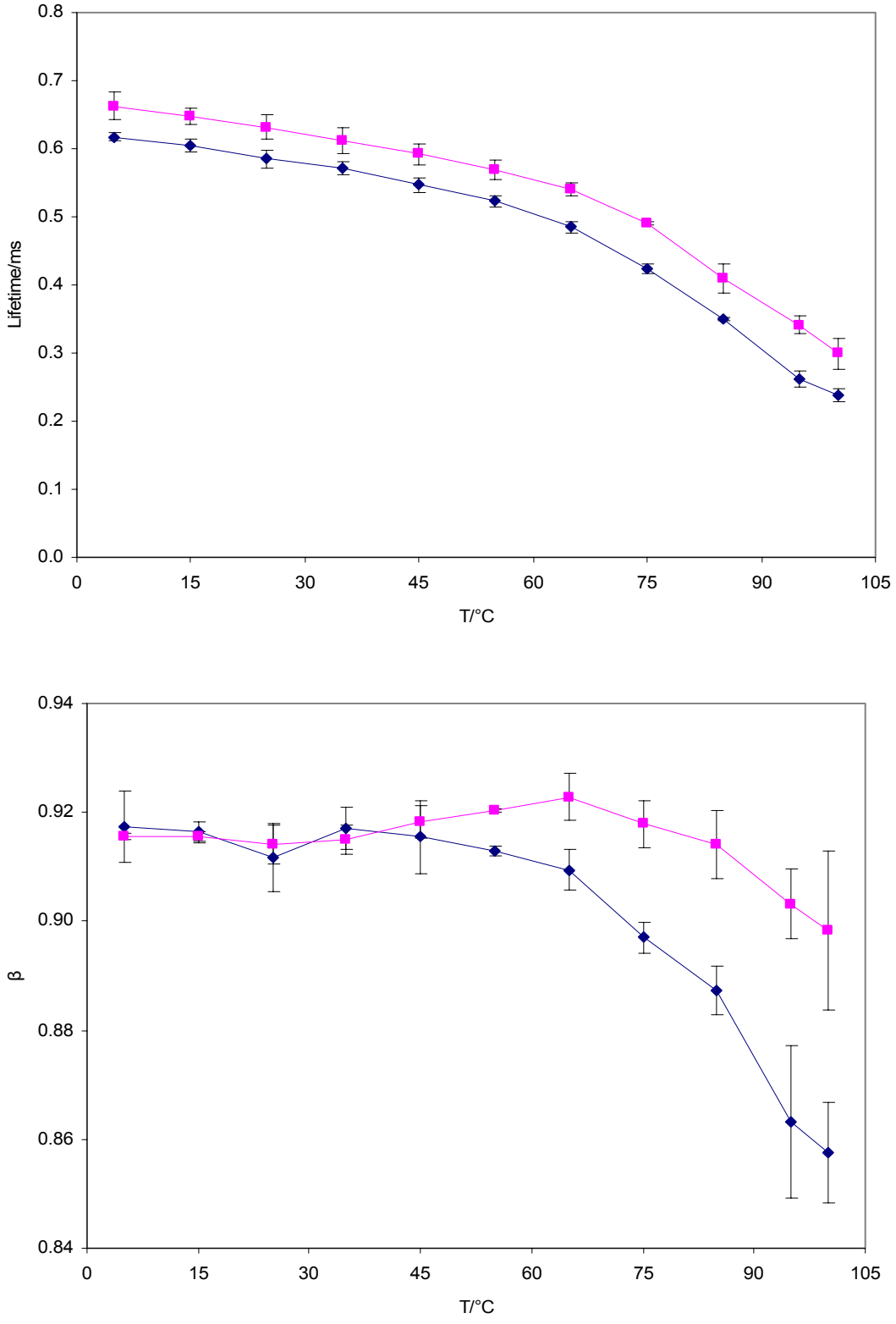

Figure 101: Temperature dependence of (a) lifetime and (b) stretching exponent β obtained from fits to a stretched exponential decay model of the intensity decay of erythrosin B free acid (♦) and erythrosin B sodium salt (■) in amorphous sucrose films.

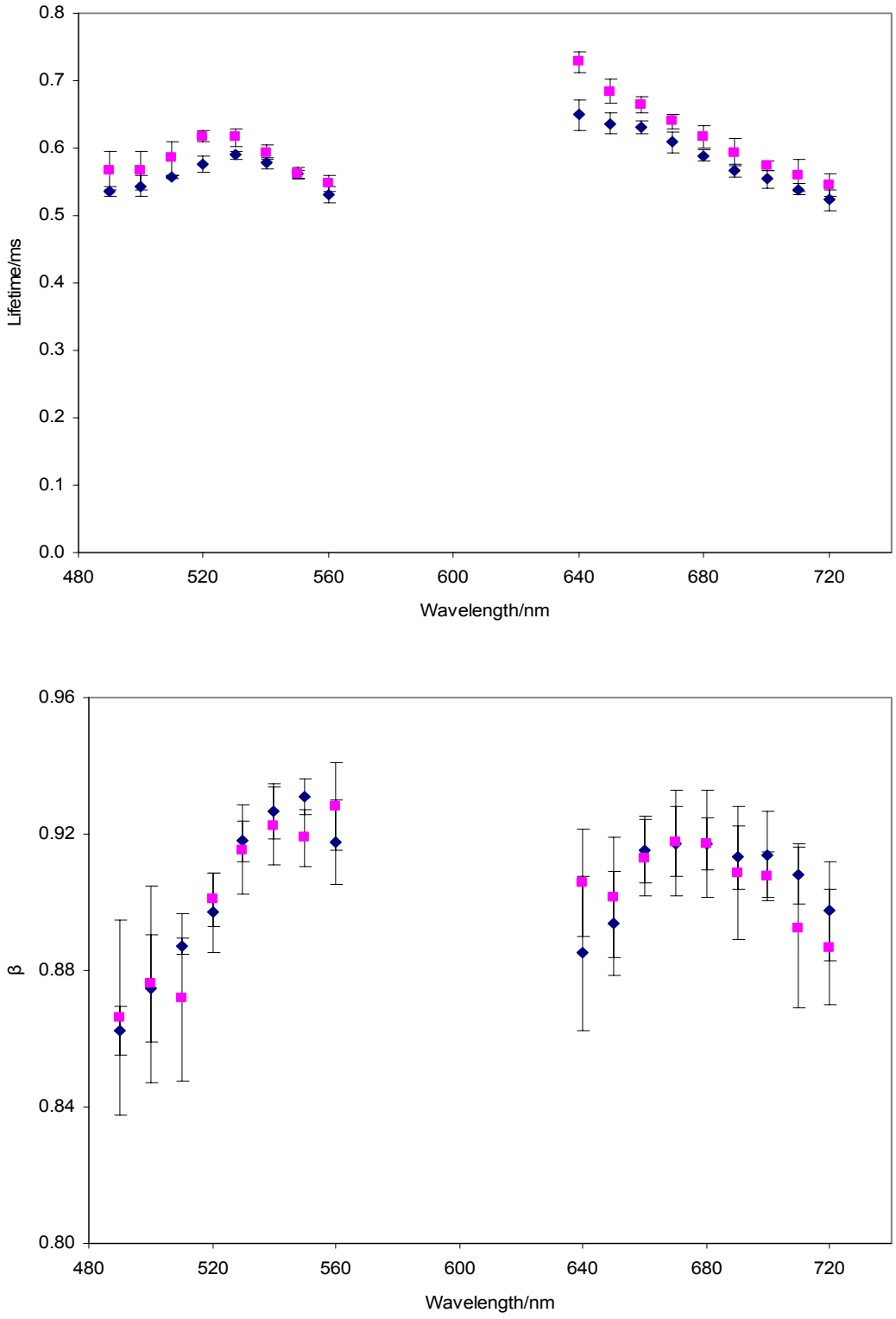

Figure 102: The effect of excitation wavelength (with 680 nm emission) and emission wavelength (with 530 nm excitation) on the lifetimes (a) and stretching exponents β (b) from fits of erythrosin B phosphorescence intensity decays to the stretched exponential decay model. Samples are erythrosin B free acid (♦) and erythrosin B sodium salt (■) in amorphous sucrose films.

Curriculum Vita

Yumin You

September 2003-Present	Rutgers, the State University of New Jersey Food Science Doctor of Philosophy
September 1993-December 1995	Wuxi University of Light Industry, Wuxi, China Food Science Master of Science
September 1989-July 1993	Wuhan College of Cereal Industry, Wuhan, P.R.China Food Science Bachelor of Science
September 2003-present	Graduate Assistant Department of Food Science Rutgers, the State University of New Jersey
February 1996–September 2002	Assistant Professor College of Food Science and Technology Shanghai Fisheries University, Shanghai, P.R.China

Publications

1. **Yumin You** and Richard D. Ludescher (2006). Phosphorescence of erythrosin B as a robust probe of molecular mobility in amorphous solid sucrose. *Applied Spectroscopy.* 60(7): 813-819.

2. Sonali Shirke, **Yumin You**, & Richard D. Ludescher (2006). Molecular mobility and dynamic site heterogeneity in amorphous lactose and lactitol from erythrosin B phosphorescence. *Biophysical Chemistry.* 123: 122-133.

3. Linda, Pravinata, **Yumin You** and Richard D. Ludescher (2005). Erythrosin B phosphorescence monitors molecular mobility and dynamic site heterogeneity in amorphous sucrose. *Biophysical Journal.* 88(May): 3551-3561.

4. **Yumin You** and Shiying Xu (2002) The extraction procedure of fucoidan from Sargassum fusiforme. *Journal of Wuxi University of Light Industry*. 21(3): 233-238.

5. Peigen Zhou, **Yumin You**, Ye Ni, Xiaoyu Qi, and Shuxia Tu (2002) Preparation and characterization of glucosamine sulfate. *Journal of Shanghai Fisheries University*. 11(2): 145-148.

6. **Yumin You** (2001) Review on thawing technology of frozen food. *Journal of Food Science (China).* 22(8): 87-90.

7. Hang Yuan, **Yumin You**, Zuoxian Gen and Peigen Zhou (2000) Application of enzyme preparations in the manufacturing of beer. *Journal of ZhengZhou Institute of Light Industry (Natural Science Bimonthly).* 15(1): 18-23.

8. Zuoxian Gen, **Yumin You**, Xiaoyu Qi, Ye Ni and Peigen Zhou. (2000) Preparation of D-glucosamine sulfate sodium and its properties. *Journal of Shanghai Fisheries University*. 9(2): 134-137.

9. Jinhong Gu and **Yumin You** (2000) Study on the equipment producing margarine. *China Oils and Fats*. 25(6): 96-101.

10. Peigen Zhou, **Yumin You**, Xiaoyu Qi, Zong'en Zhang, Zuoxian Gen, and Huiming Dai (2000) Preparation and some properties of D-glucosamine hydrochloride. *Journal of Fisheries of China*. 24(1): 76-80.

11. Jiao Zhao, Xiaoyu Qi, **Yumin You,** Jixiang Wang, and Peigen Zhou (1997) Study on some characteristics of polyphenoloxidase from Japanese prawn, *Penaeus Japonicus*. *Journal of Shanghai Fisheries University*. 6(3): 157-165.

12. Dayu Zhang, Peide Ni and **Yumin You** (1996) Extraction of raffinose from glandless cottonseed. *China Oils and Fats*. 21(5): 7-9.

13. **Yumin You**, Peide Ni, and Dayu Zhang (1996) Isolation of raffinose from glandless cottonseed. *Journal of the Chinese Cereals and Oils Association*. 11(6): 49-54.

14. **Yumin You** (1996) Study on stability of natural oligosaccharide—raffinose. *Cereals and Food Industry*. 3: 15-16.

15. **Yumin You** (1994) A new member of oil family: powder oil. *Jiangxi Cereals and Oils Scientific Technology*. 3-4: 57-59.

16. **Yumin You** (1993) Functional properties of soybean protein and its application in the food industry. *Food Research and Development*. 57(2): 1-10.

17. Dachuan Liu, Xiaohong Hu, **Yumin You**, Xiumin Ji, and Yongsheng Zhang (1993) Development of oilseed protein products rich-in-selenium. *China Oils and Fats*. 18(6): 4-8.